2017

STUDY OF MOLECULAR INTERACTIONS OF GLYCOSAMINOGLYCANS AND GLYCOSAMINOGLYCAN MIMETICS WITH THEIR PROTEIN TARGETS

Daniel K. Afosah
Virginia Commonwealth University

STUDY OF MOLECULAR INTERACTIONS OF GLYCOSAMINOGLYCANS AND GLYCOSAMINOGLYCAN MIMETICS WITH THEIR PROTEIN TARGETS

A dissertation submitted in partial fulfillment of the requirements for the degree of Doctor of Philosophy at Virginia Commonwealth University

by

DANIEL K. AFOSAH
MSc. Pharmaceutical Analysis and Quality Control, Kwame Nkrumah University of Science and Technology, Kumasi, Ghana, 2010
B Pharm., Kwame Nkrumah University of Science and Technology, Kumasi, Ghana, 2007

Director: UMESH R. DESAI
PROFESSOR, DEPARTMENT OF MEDICINAL CHEMISTRY

Virginia Commonwealth University
Richmond, Virginia
May 2017

Acknowledgement

I would like to start by expressing my profound gratitude to my advisor, Dr. Umesh R. Desai, for his wonderful mentorship and guidance, which has been an invaluable component of my five-year stay in this institution. The patience he has had for me is immeasurable, and not only has he contributed to my academic growth, he has also significantly enhanced my development as an individual. Dr. Desai, you have made this experience truly wonderful, and words cannot express how thankful I am.

I would also like to thank my committee members; Drs. Martin Safo, Glen E. Kellogg, H. Tonie Wright, Jurgen Venitz and Cynthia Kirkwood (Dean's Rep) for the time they have invested in my training. I would like to again acknowledge Drs. Safo and Kellogg for taking time out of their busy schedules to write recommendation letters for me.

My sincere gratitude also goes to all past and present members of the Desai laboratory. I would specifically like to acknowledge the immense contributions of Dr. Rami A. Al-Horani, and the unwavering support of Dr. Nehru Viji Sankaranarayan's. I would like to recognize Drs. Phil Mosier, Rajesh Karuturi, Rio Boothello, Stephen Verespy, Akul Mehta, Jyothi Sisthla and Balaji Nagarajan for their contribution to my graduate work. Additionally, I thank Drs. Mohini Ghatge and Faik Musayev of the Safo laboratory for their help.

Finally I would like to express my sincere gratitude to my family and friends. There is no way I could have gone through this without your support, encouragement and prayers. Akoma, Richard and Ken, I am forever grateful to you. Nkechi, you are truly an amazing person, and your support has been inconceivable.

Table of Contents

Acknowledgment…….....ii

List of Tables……...……x

List of Figures…….……xi

List of Schemes……..xv

List of Abbreviations……...…….xvi

Abstract……..…….xviii

1 INTRODUCTION 1

1.1 Glycosaminoglycans 1

1.1.1 GAG Biosynthesis 3

1.1.2 Biological Functions of GAGs..... 4

1.1.3 Interaction of GAGs and Their Binding Partners 5

1.2 GAG Binding Proteins 7

1.2.1 Serine Protease Inhibitors (Serpins)..... 7

1.2.2 GAG-Serpin Interactions 8

1.2.3 Serine Proteases 11

1.2.4 GAGs-Serine Protease Interactions 12

1.3 Glycosaminoglycan Mimetics..... 17

1.4 Non-Saccharide GAG Mimetics (NSGMs)..... 18

1.4.1 NGSMs in Hemostasis 19

1.4.2 NSGMs as Anticancer Agents 33

1.4.3 NSGMs as Regulators of Inflammation 37

1.4.4 NSGMs as Anti-Infective Agents 38

1.4.5 Summary of NSGMs 40

2 DESIGNING ALLOSTERIC THROMBIN INHIBITORS WITH SUBMAXIMAL INHIBITION OF THE PROTEASE 41

2.1 Introduction 41

2.1.1 The Coagulation Cascade 41

2.1.2 Hemostatic disorders 42

2.1.3 Anticoagulants 44

2.1.4 Thrombin 45

2.2 Rationale for Developing New Sulfated Benzofuran Dimers (SBDs). 47

2.3 Results And Discussion 48

2.3.1 Molecular Modeling Studies of SBD-Thrombin Interaction 48

2.3.2 Chemical Synthesis of Sulfated Benzofuran Molecules 49

2.3.3 Thrombin Inhibition by SBMs and SBDs. 57

2.3.4 Mechanisms of Thrombin Inhibition by **2c** And **2i**. 62

2.3.5 Thermodynamic Binding Affinity of **2c** and **2i** for Thrombin. 64

2.3.6 Binding Sites of **2c** and **2i** 66

2.3.7 Inhibition of Thrombin Mutants by **2c** And **2i**..... 68

2.3.8 Plasma Clotting Studies of **2c** And **2i**. 71

2.3.9 Inhibition of Thrombin's Cleavage of Fibrinogen by **2c** and **2i** 71

2.4 Conclusion..... 72

2.5 Experimental Section 74

2.5.1 General Methods..... 74

2.5.2 Molecular Modeling Studies..... 75

2.5.3 Chemical Characterization of Sulfated Benzofurans. 76

2.5.4 Purity Analysis of Synthesized Compounds..... 76

2.5.5 Synthetic Procedure and Spectral Characterization Data 77

2.5.6 Direct Enzyme Inhibition Studies Using Chromogenic Substrate Hydrolysis Assay 106

2.5.7 Mechanisms of Thrombin Inhibition by **2c** And **2i** 107

2.5.8 Thermodynamic Affinity of SBDs for Thrombin..... 107

2.5.9 Competitive Inhibition Studies of **2c** and **2i** 108

3 SULFATED DIFLAVONOIDS ARE POTENT AND SELECTIVE INHIBITORS OF PLASMIN..... 111

3.1 Introduction..... 111

3.1.1 Plasmin..... 111

3.1.2 Plasmin Inhibitors..... 113

3.2 Rational for the Development of Sulfated Diflavonoid Plasmin Inhibitors 115

3.3 Results and Discussion 116

3.3.1 Synthesis of Sulfated Diflavonoids 116

3.3.2 Plasmin Inhibition by Sulfated diflavonoids 119

3.3.3 Inhibition Studies of Thrombin, Factor IXa, Factor Xa, Factor XIa, Factor XIIa, Trypsin and Chymotrypsin 123

3.3.4 Mechanism of Plasmin Inhibition by Compound **23a** and Its Unsulfated Precursor **24j** 124

3.3.5 Binding Affinity of Sulfated Diflavonoids for Plasmin 127

3.3.6 Binding Site of Sulfated Diflavonoids on Plasmin 129

3.3.7 Salt Dependence of Plasmin Inhibition by Sulfated Diflavonoids 131

3.3.8 Reversibility of Inhibitory Activity of Sulfated Diflavonoids 132

3.3.9 Inhibition of Clot Lysis by Sulfated Diflavonoids 133

3.3.10 Molecular Modeling Studies of Sulfated Diflavonoids 134

3.4 Conclusion 136

3.5 Experimental Section 137

3.5.1 Chemicals, Reagents, Enzymes, and Substrates 137

3.5.2 Chemical Characterization of Synthesized Molecules 138

3.5.3 Purity Analysis of Synthesized Compounds 138

3.5.4 Synthetic Procedure and Spectral Characterization Data 139

3.5.5 Serine Protease Inhibition Assays 157

3.5.6 Michaelis-Menten Kinetics of Spectrozyme PL Hydrolysis. 158

3.5.7 Competition Studies with Heparin 159

3.5.8 Reversibility of Inhibitory Activity of Sulfated Diflavonoids 161

3.5.9 Inhibition of Clot Lysis 161

3.5.10 Fluorescence–Based Binding Affinity Determination 159

3.5.11 Preparation of Active Site Blocked Plasmin 159

3.5.12 Fluorescence–Based Binding Affinity of **23a** and **23l** for Active Site Blocked Plasmin 160

4 IDENTIFICATION OF SELECTIVE GAG OLIGOSACCHARIDES FOR HUMAN NETUTROPHIL ELASTASE 163

4.1 Introduction 163

4.1.1 Neutrophil Elastase 163

4.1.2 Functions of Neutrophil Elastase 164

4.1.3 Neutrophil Elastase as Drug Target 165

4.1.4 Inhibition of HNE by GAGs 166

4.2 Rational for Studies 167

4.3 Results and Discussion 167

4.3.1 Size Fractionation of ODSH 167

4.3.2 Enzymatic Depolymerization of ODSH 169

4.3.3 Preparation of ODSE. 170
4.3.4 Plasma Clotting Studies of ODSE 171
4.3.5 Inhibition of HNE by GAGs 172
4.3.6 Salt Dependent Studies 176
4.3.7 Mechanism of Inhibition of HNE by GAGs 180
4.3.8 Thermodynamic Binding Affinity GAGs for HNE 187
4.3.9 Computational Studies of GAG-HNE Interactions 188
4.4 Experimental Section 190
4.4.1 Size Fractionation of ODSH 190
4.4.2 Preparation of 2-O,3-O-Desulfated Enoxaparin (ODSE) 190
4.4.3 SEC HPLC of GAGs 191
4.4.4 Activated Partial Thromboplastin Time Assay 191
4.4.5 Direct Enzyme Inhibition Studies Using Chromogenic Substrate Hydrolysis Assay 192
4.4.6 Michaelis-Menten kinetics Study of GAG inhibition of HNE 193
4.4.7 Binding Affinity of GAGs for HNE 193
4.4.8 Computational Study of GAG-HNE interaction 194
4.5 Conclusion 195
5 SIGNIFICANCE AND FUTURE WORK 197
5.1 Sulfated Benzofuran Thrombin Inhibitors with Submaximal Protease Inhibition 197

5.2 Sulfated Diflavonoids as Potential Anti-Fibrinolytig Agents 197

5.3 GAG Oligosaccharides Targeting HNE 198

LITERATURE CITED……199

APPENDIX……..……220

List of Tables

Table 1. Properties of GAGs 2

Table 2. Therapeutic applications of GAGs 4

Table 3. AT activation by linear polyacrylic acids 23

Table 4. Inhibition of human thrombin by SBDs 59

Table 5. In vitro inhibition of human thrombin by SBMs 61

Table 6. Michaelis-Menten Kinetics of thrombin inhibition by **2c** and **2i** 64

Table 7. Binding affinity **2c** and **2i** for thrombin 65

Table 8. Inhibition of Human Thrombin by **2c** and **2i** in the Presence of UFH and HirP 68

Table 9. Inhibition of thrombin mutants by **2c** and **2i** 70

Table 10. In vitro inhibition of human plasmin by NSGMs 122

Table 11. Selectivity of NSGM **23a** and its precursor **24j** against a panel of related serine proteases 124

Table 12. Michaelis-Menten kinetics of human plasmin in the presence of **23a** or its precursor **24j** 127

Table 13. Dissociation equilibrium constants (K_D) and maximal fluorescence change (ΔF_{MAX}) for the interactions of NSGMs and UFH with human plasmin. 129

Table 14. Inhibition of human plasmin by **23a** in the presence of UFH 131

Table 15. Salt-Dependence of Plasmin Inhibition by **23a** 132

Table 16. Heparin lyase depolyremization of ODSH 170

Table 17. APTT assay for Enoxaparin and ODSE 171

Table 18. Inhibition of HNE by size fractionated ODSH 173

Table 19. Inhibition of HNE by GAGs and GAG oligosaccharides 179

Table 20. Michaelis-Menten kinetics of HNE inhibition by GAGs 183

Table 21. Michaelis-Menten kinetics of HNE inhibition by HO08 in buffers of different ionic strength..... 186

Table 22. Thermodynamic binding affinity GAGs for HNE 188

List of Figures

Figure 1. Disaccharide units of GAGs (A) heparin; (B) heparan sulfate; (C) dermatan sulfate; (D) chondroitin sulfate; (E) keratin sulfate; (F) hyaluronic acid. 1

Figure 2. Biosynthesis of heparan sulfate.[9] 3

Figure 3. Crystal structures of serine protease inhibitors showing GAG interacting residues (A) AT; (B) HCII; (C) PCI; (D)PAI. 10

Figure 4. Mechanism of serine protease hydrolysis. 12

Figure 5. Crystal structures of serine proteases showing GAG interacting residues (A) thrombin; (B) FXa; (C) FIXa; (D) FXIa. 16

Figure 6. Sulfated flavonoids with anticoagulant and antiplatelet aggregation effects. 20

Figure 7. Hybrid saccharide-NSGM compounds with anticoagulant properties. 22

Figure 8. General structure of linear polyacrylic acids 23

Figure 9. Sulfated LMWLs. 24

Figure 10. Structure of myo-inositol hexasulfate 26

Figure 11. Sulfated benzofuran compounds with anticoagulant potential. 28

Figure 12. Structure of SBO4L. 29

Figure 13. Sulfated coumarins with thrombin inhibitory potential. 30

Figure 14. Structure of SPGG. 31

Figure 15. Sulfated quinazolinones with FXIa inhibitory activity. 32

Figure 16. Tetrahydroisoquinoline compounds with AT activation activity. 33

Figure 17. NSGMs with anticancer potential. 34

Figure 18. NSGMs with anti-inflammatory properties. 37

Figure 19. NSGMs with anti-infective properties 39

Figure 20. The coagulation cascade. 42

Figure 21. Clinically used anticoagulants 44

Figure 22. Structure of thrombin..... 45

Figure 23. Development of sulfated benzofuran dimer thrombin inhibitors. 47

Figure 24. Projected interactions of SBD analogs with thrombin. 49

Figure 25. Inhibition of thrombin by SBDs. 58

Figure 26. Michaelis-Menten kinetics profiles of (A) **2c** and (B) **2i**. 63

Figure 27. Binding of SBDs to thrombin (A) fFPRCK-thrombin and (B) human plasma thrombin. 65

Figure 28. Competitive inhibition studies of **2c** and **2i** in the Presence of UFH and HirP. 67

Figure 29. Inhibition of thrombin mutants by (A) **2c** and (B) **2i**. 69

Figure 30. APTT assay for **2c**. 71

Figure 31. Inhibition of thrombin fibrinogen cleavage by **2c** and **2i.** (A) A representative PAGE (B) Semi-log plot of inhibition. 72

Figure 32. Structure of catalytic domain of human plasmin. 112

Figure 33. FDA approved plasmin inhibitors. 113

Figure 34. NSGMs with plasmin inhibitory activity. 115

Figure 35. Plasma inhibition profiles of sulfated di-flavonoids..... 120

Figure 36. Selectivity studies for compound **23a**. 123

Figure 37. Michealis-Menten kinetics profiles for **23a** and **24j**. 126

Figure 38. Binding affiinity of sulfated diflavonids for plasmin. (A) Native human plasmin (B) active-site-blocked plasmin. 129

Figure 39. UFH Competition studies of compound **23a**. 130

Figure 40. Salt dependence studies of 23a 131

Figure 41. Protamine reversibility of activity of sulfated diflavonoids. 132

Figure 42. Inhibition of clot lysis by compound **23a**. 133

Figure 43. Computational study of sulfated diflavonoid-human plasmin interaction. 135

Figure 44. Structure of human neutrophil elastase showing highly electropositive surface..... 163

Figure 45. SEC HPLC analysis of size-fractionated ODSH. 168

Figure 46. Inhibiton of HNE by clinically used GAGs and their 2-O,3-O-desulfate derivatives 172

Figure 47. Structures of GAG oligosaccharides. 174

Figure 48. Inhibition of HNE by GAG oligosaccharides..... 174

Figure 49. Salt dependence of HNE inhibition by GAGs..... 177

Figure 50. Salt dependence of HNE inhibition by GAG oligosaccharides..... 178

Figure 51. Michaelis-Menten kinetics of HNE inhibition by GAGs. 182

Figure 52. Michaelis-Menten kinetics of HNE inhibition by HO08 in buffers of different ionic strength..... 185

Figure 53. Affinity of GAG-HNE interaction..... 187

Figure 54. (A) Structure of HNE showing putatibe binding sites (B) Results from CVLS screening of ODSH sequences interacting with HNE. 189

List of Schemes

Scheme 1 Synthesis of benzofuran intermediates…….50

Scheme 2 Synthesis of benzofuran intermediates…….51

Scheme 3 Synthesis of benzofuran intermediates….....52

Scheme 4 Synthesis of benzofuran intermediates….....53

Scheme 5 Synthesis of benzofuran dimers…….....54

Scheme 6 Synthesis of benzofuran dimers.……...……55

Scheme 7 Synthesis of benzofuran monomers...……..…….56

Scheme 8 Chemical synthesis of sulfated diflavonoids.…….118

List of Abbreviations

APC	Activated protein C
APTT	Activated partial thromboplastin time
AT	Antithrombin III
ENOX	Enoxaparin
FIXa	Factor IXa
FVa	Factor Va
FVIIa	Factor VIIa
FXa	Factor Xa
FXIa	Factor XIa
FXIIA	Factor XIIa
GAG	Glycosaminoglycan
HCII	Heparin cofactor II
HNE	Human neutrophil elastase
LMWL	Low molecular weight lignin
NSGM	Non-saccharide glycosaminoglycan mimetic
ODSE	2-*O*,3-*O*-desulfated enoxaparin
ODSH	2-*O*,3-*O*-desulfated heparin
PAI	Plasminogen activator inhibitor
PCI	Protein C inhibitor
PT	Prothrombin time
SBD	Sulfated benzofuran dimer

SBM	Sulfated benzofuran monomer
SEC	Size exclusion chromatography
Serpin	Serine protease inhibitor
SPGG	Sulfated pentagalloylglucopyranoside
TEG	Thromboelastography
TT	Thrombin time
UFH	Unfractionated heparin

Abstract

STUDY OF MOLECULAR INTERACTIONS OF GLYCOSAMINOGLYCANS (GAGS) AND GAG MIMETICS WITH THEIR PROTEIN TARGETS

By Daniel K. Afosah, Ph.D.

A dissertation submitted in partial fulfillment of the requirements for the degree of Doctor of Philosophy at Virginia Commonwealth University

Virginia Commonwealth University, 2017

Director: Umesh R. Desai

Professor, Department of Medicinal Chemistry

Glycosaminoglycans (GAGs) are complex linear chain carbohydrate molecules found on virtually all animal cell surfaces. Owing to their negatively charged nature, GAGs interact with a number of different proteins. Thus, although they have great potential as therapeutic agents, their apparent promiscuous interactions increase their side effect risk. GAG mimetics, including GAG oligosaccharides and non-saccharide GAG mimetics (NSGMs) are viable approaches to address this. This work discusses sulfated benzofuran thrombin inhibitors with submaximal protease inhibition, sulfated diflavonoid inhibitors of plasmin and GAG oligosaccharides with selectivity for human neutrophil elastase (HNE).

Anticoagulants are very important for the treatment of thrombotic diseases. The adverse effects associated with current clinically used anticoagulants warrant the continuous search for new agents. Thrombin, being the central player in the coagulation cascade, remains a very important target for anticoagulant therapy, however drugs inhibiting its activity carry the risk of prolonged bleeding. Based on a previously identified sulfated benzofuran thrombin inhibitor, we have developed analogs with submaximal inhibition of the protease. These agents inhibit thrombin with efficacies approaching 50%, for both chromogenic and macromolecular

substrates, ensuring a basal level of thrombin activity even at saturating inhibitor concentrations. The most potent of these compounds had a potency of 1.8 μM, 2-3 fold better than the lead. Additionally, these compounds utilize an allosteric mechanism for thrombin inhibition. Further, studies have revealed structural features responsible for submaximal thrombin inhibition.

Fibrinolysis is an important part of hemostasis and plasmin is the most important fibrinolytic enzyme. Anti-plasmin agents are thus important for conditions such as hemophilia; however, there are no clinically used direct plasmin inhibitors. By structural modifications of a previously identified sulfated diflavonoid plasmin inhibitor, we have achieved a compound with 12-fold better potency (IC_{50} = 6.3 ± 0.4 μM), and a selectivity index of at least 22 over closely related serine proteases. We have shown that this compound inhibits plasmin mediated clot lysis, and further demonstrated that its activity is reversible using protamine sulfate, indicating its potential as a lead for the development of clinical anti-plasmin agents.

HNE, a serine protease associated with inflammatory diseases is known to be inhibited by GAGs. However, the interactions at the molecular level have remained elusive. Using biochemical methods, and by studying the inhibitory potency of different GAGs and GAG oligosaccharides, we have shown that an octasaccharide may be the ideal GAG length for the achievement of potent HNE inhibition. Under our assay conditions, the inhibition of HNE by an octasaccharide species was only 5-fold less than that of unfractionated heparin, whereas the hexasaccharide species was 30-fold less active. The data also suggests that the inhibition of HNE by GAGs is via an allosteric mechanism and using molecular modeling, we have identified putative GAG binding sites on HNE and further identified GAG species with potential selectivity for anti-HNE activity

1 INTRODUCTION

1.1 Glycosaminoglycans

Glycosaminoglycans (GAGs) are complex linear chain carbohydrate molecules with molecular weights of 10 – 100 kDa.[1–3] They are found on animal tissues/cell surfaces, usually covalently associated with proteins as proteoglycans.[3] GAGs are generally made up of repeating units of uronic acid (D-glucuronic/L-iduronic acid) and hexosamine (D-glucosamine/D-galactosamine) residues.[1] GAGs are highly charged molecules owing to negatively charged carboxylic acid units present in the uronic acid residues and sulfate groups present on most of the units. GAGs can be sulfated at various positions, which adds to their structural complexity and diversity.[4] That said, GAGs may be different from one another in the type of monomeric units, linkages between these monomeric units, position of sulfate groups and degree of sulfation and these features are used in differentiating one GAG from another.[3] The differences in GAGs arise from their biosynthesis and their complexity ensures that even a particular type/class of GAGs ends up as a complex heterogeneous mixtures of species having different molecular weights.

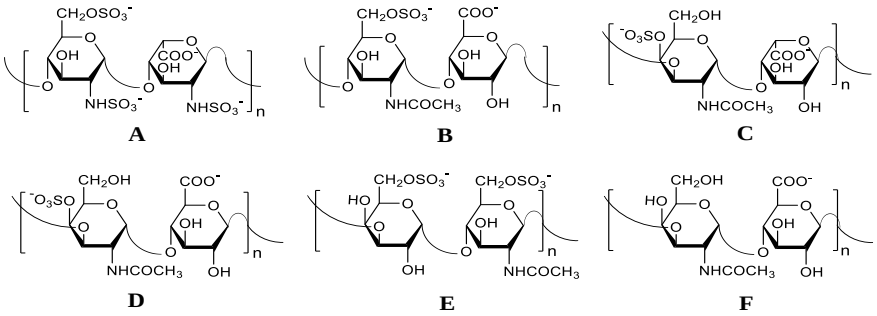

Figure 1. Disaccharide units of GAGs (A) heparin; (B) heparan sulfate; (C) dermatan sulfate; (D) chondroitin sulfate; (E) keratin sulfate; (F) hyaluronic acid.

Different groups have classified GAGs into a number of classes. One common classification is that there are four types of GAGs; namely: hyaluronic acid, chondroitin/dermatan sulfate, heparan sulfate/heparin and the keratan sulfate.[5] The structures of hyaluronic acid and chondroitin sulfate are simpler in comparison to dermatan sulfate, heparin and heparan sulfate in terms of number of units, orderliness of arrangements and types of sequences.[2] Hyaluronic acid is the only GAG that does not have sulfate moieties and

thus it owes its negative charge to carboxylate groups only.[6] This makes it the least charged of the GAGs and also the GAG with the least structural complexity. Though somewhat similar, heparin and heparan sulfate have significant structural differences. For instance, they have their saccharide units being either D-glucuronic acid and L-iduronic acid as the uronic acid unit and glucosamine as the hexosamine unit.[4] However, in heparin, l-iduronic acid is the predominant iduronic acid unit whereas D-glucuronic acid is the most abundant unit in heparan sulfate.[7] In addition, heparin is significantly more sulfated than heparan sulfate. In fact, heparin is the most highly charged and most acidic biomolecule known.[7]

Table 1. Properties of GAGs

GAG	**Properties**
Hyaluronic acid	4–8000 kDa Completely non-sulfated Not covalently bonded to proteins Present in synovial fluid, vitreous humor and ECM Lubricant properties
Heparin	5–25 kDa Most negatively charged bio macromolecule Present in mast cells
Heparan sulfate	Expressed and present in most mammalian cells Found on cells surfaces and ECM
Chondroitin sulfate	5–50 kDa Present in cartilage, tendons and ligaments Most abundant GAG Binds to proteins to form proteoglycan aggregates
Dermatan sulfate	15–40 kDa Present in skin, blood vessels and heart valves
Keratan sulfate	4–19 kDa Most heterogeneous GAG Present in the cornea and cartilage

1.1.1 GAG Biosynthesis

In nature, GAGs are synthesized enzymatically in a stepwise manner, initially with the assembly of monomeric sugar units sequentially from the non-reducing ends.[8] This is followed by enzymatic transformations, including epimerization and sulfation, to yield the different GAG types.[8] Most GAGs are produced and secreted covalently linked to proteins and are known as proteoglycans. Their saccharide units are linked to the protein via an intermediate trisaccharide unit made up of two galactose residues and a xylose residue, linked mostly to a serine residue of the protein using an O-glycosidic bond.[1] Hyaluronic acid, the only GAG not produced linked to proteins, interacts non-covalently with proteoglycans using hyaluronan binding motifs.[3] In the biosynthesis of heparan sulfate, for example (Fig. 2[9]), the process begins with the attachment of a linkage region of four monosaccharides to the core protein.[4] This is followed by the action of glycosyltransferases, which sequentially add disaccharide units composed of glucuronic acid and N-acetyl glucosamine.[4] Subsequent modifications to the chain are made by a series of enzymes beginning with N-deacetylase-N-sulfotransferase resulting in N-sulfation of some glucosamine

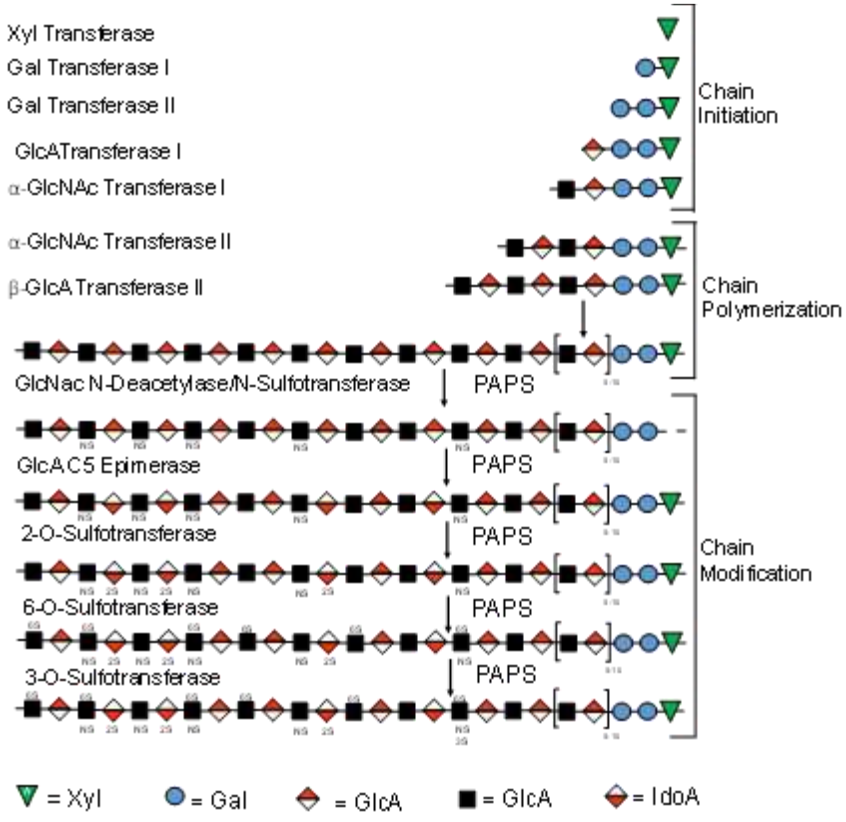

Figure 2. Biosynthesis of heparan sulfate.[9]

residues.[4,10] The action of epimerase then leads to the conversion of some glucuronic acid residues to iduronic acid. Finally, the 2-O, 3-O and the 6-O sulfotransferases act,resulting in variously sulfated species.[4,10]

1.1.2 Biological Functions of GAGs

GAGs have been found to have a plethora of functions. One striking function, due to their structure, is their role in maintaining the structural integrity of tissues.[2] In addition they are known to interact with a number of proteins and receptors, including cytokines, chemokines, growth factors, enzymes, and adhesion molecules,[5] and modulate a host of processes including coagulation, growth, infection, inflammation, angiogenesis, tumor progression and metastasis among others.[8,11–14] The use of GAGs for therapeutic purposes started with the use of heparin as an anticoagulant in 1935, following its discovery in 1916.[15] Since then, GAGs have been studied for potential therapeutic use in a number of conditions including cancer, wound healing, lung diseases, to name a few.[16–19]

Table 2. Therapeutic applications of GAGs

GAG	**(Potential) Therapeutic applications**
Hyaluronic acid	Wound healing, cancer, vascular disease, arthritis
Heparin	Thrombosis, cancer, infection, inflammation
Chondroitin sulfate	Osteoarthritis, cancer
Dermatan sulfate	Thrombosis, cancer

1.1.3 Interaction of GAGs and Their Binding Partners

To date, hundreds of GAG binding proteins have been identified and studied.[20] These include serine proteases, **se**rine **p**rotease **in**hibitor**s** (serpins), growth factors, lipolytic enzymes, extracellular matrix proteins, viral coat proteins and transcription factors.[21] GAG binding proteins usually have clusters of basic amino acid residues on their surface, a feature that has commonly been employed in the prediction of GAG binding proteins and the GAG binding sites on these proteins.[22] The clusters of the amino acids also determine the required GAG length for the interaction.[22] The basic amino acid clusters may be interspaced by hydrophobic patches and this feature introduces differences in the topology of GAG binding sites from one GAG binding protein to another, resulting in specificity of GAG-protein interactions. For instance, a protein surface with widely spaced cationic residues may have better interaction with GAG with lower sulfation level, such as heparan sulfate, than with a highly sulfated GAG like heparin and vice versa.[23]

Due to their highly charged nature, GAGs generally interact with a number of their binding partners using non-specific cooperating electrostatic binding, which is dependent on charge density of the GAGs.[2] These interactions are between the highly acidic sulfate groups and basic side chains of arginine and lysine, which are exposed on the surface of the protein.[23] In some instances, histidine residues are involved.[23] Of these basic amino acid residues, the electrostatic interaction with arginine residues is the strongest, approximately 2.5-fold greater than that for lysine.[24,25]

From studying GAG binding proteins and their interactions with GAGs, Cardin and Weintraub postulated the existence of a consensus sequence for GAG recognition in GAG binding proteins, further alluding to specificity of GAG-protein binding.[26] Their work identified two patterns of amino acid sequences of protein binding sites, XBBBXXBX and XBBXBX,

where B and X are basic and non-basic amino acids respectively. [26] Subsequently Sobel et al. identified another consensus sequence, XBBBXXBBBXXBBX.[27] Further, Margalit et al. suggested that a 20 Å separation between certain basic amino acid residues was important for the interaction of GAGs and their binding proteins.[28] Consensus peptides from AT were subsequently shown to bind specifically to the AT binding pentasaccharide, while disrupted and rearranged sequences lacked this binding specificity.[29] The contribution of these charged interactions to the overall binding energy of GAGs and their binding proteins varies greatly from one GAG-protein interaction to the other. For instance, in the binding of neutrophil elastase, a highly electropositive serine protease to GAGs, it has been shown that the interaction is significantly charge dependent with GAG species of higher charge density having better interactions.[30–34] In some cases, the contribution of ionic interactions to the total binding energy of GAG-protein interactions has been found to be as high as 85%.[35] It is however worth noting that other types of interactions including van der Waals forces, hydrogen bonding, and hydrophobic interactions also play a significant role in the interaction of GAGs with their binding partners.[1] These interactions arise from associations of the GAG backbone with neutral and non-positively charged amino acid groups, such as aspartic acid and glutamic acid. In fact, one study suggests that aromatic residues, especially tryptophan, are important in the binding of GAGs to proteins.[36] In certain instances, it has been shown that the binding contribution from these non-ionic interactions outweighs the contribution from ionic interactions by significant amounts, and are thus most important in binding of GAGs to some of their binding partners.[1] A typical example is the binding of brain natriuretic peptide to heparin, where the ionic component of the interaction was found to be only 6% of the total binding energy.[24] This however does not suggest that these GAG-protein interactions would be possible in the absence of the negatively

charged groups on the GAGs, as charge is important in steering the interactions. Overall, the variability in the contribution of various types of interactions to GAG-protein binding has contributed to our understanding of the specificity component of GAG protein interactions. Serine proteases and serpins are well studied binding partners of GAGs and their interactions shed more light on GAG-protein interactions.

1.2 GAG Binding Proteins

1.2.1 Serine Protease Inhibitors (Serpins)

Serpins are the natural inhibitors of serine proteases and include the prototypical serpin, α_1-antrypsin, antithrombin III (AT), heparin cofactor II (HCII) and protein C inhibitor (PCI) among many others.[37] Serpins play a vital role in maintaining homeostasis in a number of very important physiological processes including inflammation, coagulation and digestion. The mechanism of inhibition utilized by serpins is unique in that it involves a significant change in conformation.[38] Inhibition is initiated when the reactive site loop, a sequence of residues of the serpin, interacts with the active site serine of the protease, leading to a cleavage of the loop.[39] A subsequent conformational change results in a significant movement of the protease to the other end of the serpin and insertion of the cleaved loop into the protease, thus resulting in its irreversible inhibition.[38,39]

The serpin AT is a natural inhibitor of serine proteases of the coagulation cascade, including thrombin, factor Xa (FXa), factor IXa (FIXa), factor XIa (FXIa) and factor XIIa (FXIIa) and plasmin.[21] GAGs, including heparin, exert their anticoagulant activity by activating serpins, and thus accelerating their inhibition of proteases. For instance, on its own AT inhibits thrombin and FXa slowly, however, this is accelerated by up to >2000-fold in the presence of heparin.[40] Similarly the inhibition of thrombin by the thrombin-specific serpin HCII is also

accelerated in the presence of dermatan sulfate and heparin by >1000-fold.[41] The inhibition of activated protein C (APC) by protein C inhibitor is also increased in the presence of heparin.[42] These observations indicated interactions between GAGs with serpins and/or serine proteases and further studies pointed to certain peculiarities. In the case of FXa, a short heparin sequence of only five saccharide units is sufficient to bring about acceleration of its inhibition by AT,[43–45] whereas in the case of thrombin a longer sequence of about 18 monosaccharide units is required.[46] That this pentasaccharide does not accelerate the rate of thrombin inhibition by AT was vital in understanding the mechanism of inhibition. It was later shown that a bridging mechanism, where both AT and thrombin bind to the same heparin chain to facilitate the interaction, is required in the case in the case of thrombin, whereas in the case of FXa, the conformational change in the reactive center loop, which can be sufficiently induced by the pentasaccharide, is sufficient to accelerate the inhibition.[40,47,48]

1.2.2 GAG-Serpin Interactions

The most studied of GAG interactions is that of heparin and the serpin, AT. A key discovery in the understanding of the interaction with heparin was the identification of the pentasaccharide sequence, known as the heparin pentasaccharide, that bound with high affinity and specificity to AT and accelerates its inhibition of FXa.[49–52] This finding was very important in establishing the specificity element of GAG-protein interactions.

1.2.2.1 Antithrombin III (AT)

Following several studies spanning a period of over a decade,[53] the heparin binding site of AT was identified by Ersdal-Badju et al. using alanine scanning mutagenesis of basic residues previously shown to interact with heparin.[54] Their work revealed that important residues for binding to heparin were Lys11, Arg13, Arg24, Arg47, Lys125, Arg129 and Arg145, which lined

a channel on the protein surface.[54] Full length heparin was later shown to also engage the Lys136 residue.[55] Subsequently, a determination of the crystal structure of AT in complex with a variant of the heparin pentasaccharide, idraparinux, by Jin et al.,[56] showed additional interactions with the basic residues Arg129 and Arg46 and the non-basic Asn35 and Glu113. The crystal structure of the pentasaccharide complex, obtained a decade later, showed similar interactions as idraparinux, implicating Arg46, Arg47, Lys114, Lys125, and Arg129, of which Lys114 was deemed the most vital for the interaction.[47]

1.2.2.2 Heparin Cofactor II, Protein C Inhibitor and Plasminogen Activator Inhibitor

The GAG binding sites of other serpins have also been identified using methods including site directed mutagenesis. In HCII, heparin has been shown to interact with Lys 173 and Lys185,[57,58] whereas dermatan sulfate interacts with both Lys185 and Arg189.[57,59] Also, the heparin binding site in protein C inhibitor was found to span the residues 264 – 283 on the H-helix which is distinct from the heparin binding sites in the related AT and HCII.[60] Lys273, Arg269, Lys266 and Lys270, in order of decreasing importance, were found to be important, however, no single mutation severely affected heparin binding.[61,62] In plasminogen activator inhibitor (PAI), Lys65, Lys68, Arg76, Lys80 and Lys88 have been shown to be vital for the interaction with heparin.[63]

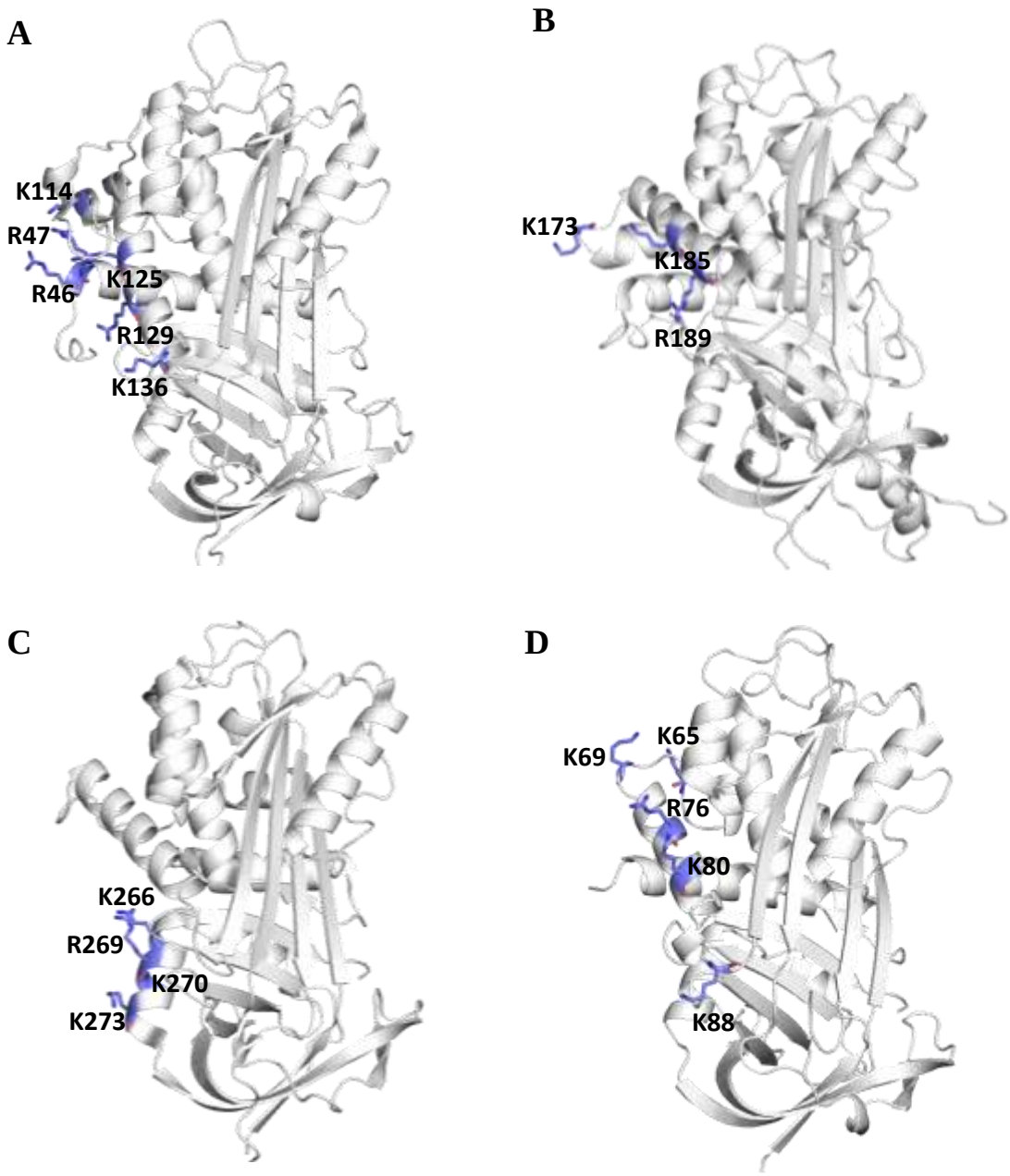

Figure 3. Crystal structures of serine protease inhibitors showing GAG interacting residues (A) AT; (B) HCII; (C) PCI; (D)PAI.

1.2.3 Serine Proteases

This family of enzymes derive their name from the nucleophilic serine residue present in the enzyme's active site.[64] Serine proteases account for over a third of known proteolytic enzymes, and are the most functionally diverse of this class of enzymes, having wide ranging presence among living organism.[64,65]. Serine proteases are grouped into thirteen clans which are further divided into a total of 52 families.[66] Of these, the most abundant in nature are the chymotrypsin-like serine proteases, which can be found in a range of organisms including eukaryotes, prokaryotes and viruses.[67] The functions of serine proteases include: digestion, hemostasis, immune response and apoptosis.[65]

The nucleophilicity of the serine residue is usually dependent on the catalytic triad of Asp, His and Ser.[64] Serine proteases with catalytic triads consisting of amino acid residues other than the typical Asp, His and Ser and even catalytic dyads have been discovered.[64] In achieving hydrolysis of bonds, there is an attack on the carbonyl carbon of the peptide substrate by the Ser195 with the aid of the His57 residue, acting as a general base, resulting in the formation of a tetrahedral intermediate.[68] The resulting protonated His57 is stabilized by Asp102 via a hydrogen bond interaction. The leaving group is subsequently expelled due to the collapse of the tetrahedral intermediate with the aid of the protonated His57, which assumes the role of a general acid, leading to formation of the acylenzyme intermediate.[68] A water molecule enters the active site and attacks the acyl enzyme, assisted by His57 forming another tetrahedral intermediate. Finally, the intermediate collapses releasing Ser195 and the cleaved carboxylic acid product.[68]

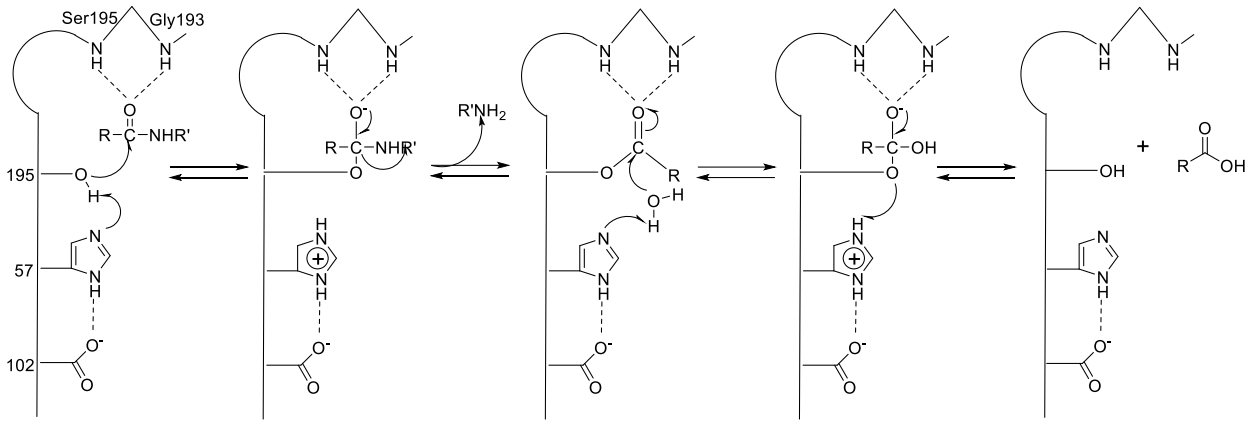

Figure 4. Mechanism of serine protease hydrolysis.

1.2.4 GAGs-Serine Protease Interactions

GAGs have been shown to interact with a number of serine proteases including thrombin, FXa, FXIa, FIXa, neutrophil elastase. A key feature of these serine proteases is the presence of a positively charged exosite.[69] It has been shown that the binding of GAGs at these exosites results in a conformational change at the active site.[70]

1.2.4.1 Thrombin

The heparin binding site of thrombin is the exosite II, which is located near the carboxy terminus.[71] Gan et al. were the first to identify important basic residues necessary for the interaction of thrombin with heparin using site directed mutagenesis. They showed that mutations to Arg175, Arg233, Lys 236 and Lys240 significantly reduced the heparin catalyzed AT inhibition of thrombin.[72] Sheehan et al. also confirmed that the interaction was at thrombin's exosite II by showing that mutations of the basic exosite II residues to glutamic acid affected the heparin mediated inactivation of thrombin by AT, while doing the same to exosite I residues had no effect.[71] Their work even indicated that not all basic exosite II residues were important in this interaction. Whereas decreases in the rate of inhibition and decreased affinity for a heparin

column were observed following mutations to Arg93, Arg233, Lys236 and Lys 240, those to Lys 174 and Lys 247 had no effect.[71]These two studies concluded the most important amino acid residues for thrombin's interaction with heparin are Arg233, Lys236 and Lys 240, and that thrombin binds to a groove formed by electropositive residues at the exosite II.[71,72] Following a number of high resolution crystal structures involving heparin and thrombin, a clearer understanding of the interaction has been reached at atomic level.[42, 48,73]

1.2.4.2 Factor Xa

In the closely related FXa, the heparin binding site has been found to include the residues Arg93, Lys96, Arg125, Arg165, Lys169, Lys236, and Arg240, with Lys236 and Lys240 contributing the most to the interaction.[74] Since thrombin and FXa are closely related, it is not surprising that these exoste II residues are rather conserved in both enzymes.

1.2.4.3 Factor IXa

Based on the knowledge of the heparin binding sites of thrombin and FXa it was easy to predict that the heparin binding site of the related enzyme, FIXa, would be similarly located. Using homology modeling Rezaie et al. identified 8 basic residues with the potential of interacting with heparin.[75] Subsequent mutagenesis of these residues, followed by rate and heparin binding experiments, led to the identification of five important residues, Arg233, Arg165, Lys230, Lys126 and Arg170, in order of decreasing contribution to binding, as being responsible for the interaction with heparin.[75] Subsequently, using the crystal structure of the FIXa-heparin-AT ternary complex, Johnson et al. revealed that the important contacts, which include salt bridges and hydrogen bonding interactions between FIXa and the heparin pentasaccharide, involved the residues identified by Reziaie et al.[76] In addition, residues 92, 101,

93, 236, 178, 179, 165, were seen to form salt bridges and/or hydrogen bonding interactions with the pentasaccharide.[76]

1.2.4.4 Factor XIa

FXIa is the only coagulation enzyme that exists as a homodimer, making it unique.[77] FXIa has been shown to have two different heparin binding sites, one located on the catalytic domain and the other on the Apple 3 (A3) domain.[78–80] After screening for heparin binding on all four apple domains of FXIa, Ho et al. came to the conclusion that only the A3 domain contained a heparin binding consensus sequence, of which two residues, Lys252 and Lys253, participated greatly in heparin binding [79] This same Apple domain plays a role in the interaction of FXIa with platelets. [79] It was also later shown that in addition to the previously identified A3 domain residues, Lys255 is important for the interaction with heparin. Results, however, suggested the possibility of another heparin binding site on FXIa, and subsequently the heparin binding site on the catalytic domain was identified.[80] The heparin binding region on the catalytic domain is described as a cysteine-constrained α-helix-containing loop,[80] and is a significantly higher affinity binding site (>100-fold) than the A3 heparin binding site.[80,81] The authors showed that Lys529, Arg530, Arg532, Lys535 (Chymotrypsin numbering: Lys170, Arg 171, Arg173, Lys 175) on the catalytic domain, are part of the high affinity heparin binding site on FXIa.[80]

1.2.4.5 Plasmin

Because it is the major enzyme in the degradation of fibrin clots, plasmin is an important enzyme in the maintenance of hemostasis.[82] AT inhibits plasmin activity, and in this case too, heparin has been shown to be an accelerant of the process.[83–85] Binding of heparin to plasmin has been shown to be in the nanomolar range, albeit at non physiological conditions.[86] The exact

heparin binding site on plasmin remains unknown, however, it is thought to be located on the catalytic domain.[87]

1.2.4.6 Human Neutrophil Elastase

Human neutrophil elastase (HNE) is a serine protease that has been identified to interact with heparin. A major difference of the interaction of GAG-neutrophil elastase from other heparin-serine protease interactions is that neutrophil elastase is inhibited directly by GAGs.[31–34] Although the binding of heparin to HNE has been shown, the exact binding site has not been established definitively.[88] Using molecular modeling, Spencer et al. proposed that full length heparin binds along a stretch made up of arginine residues, leading to the occlusion of the active site.[88]

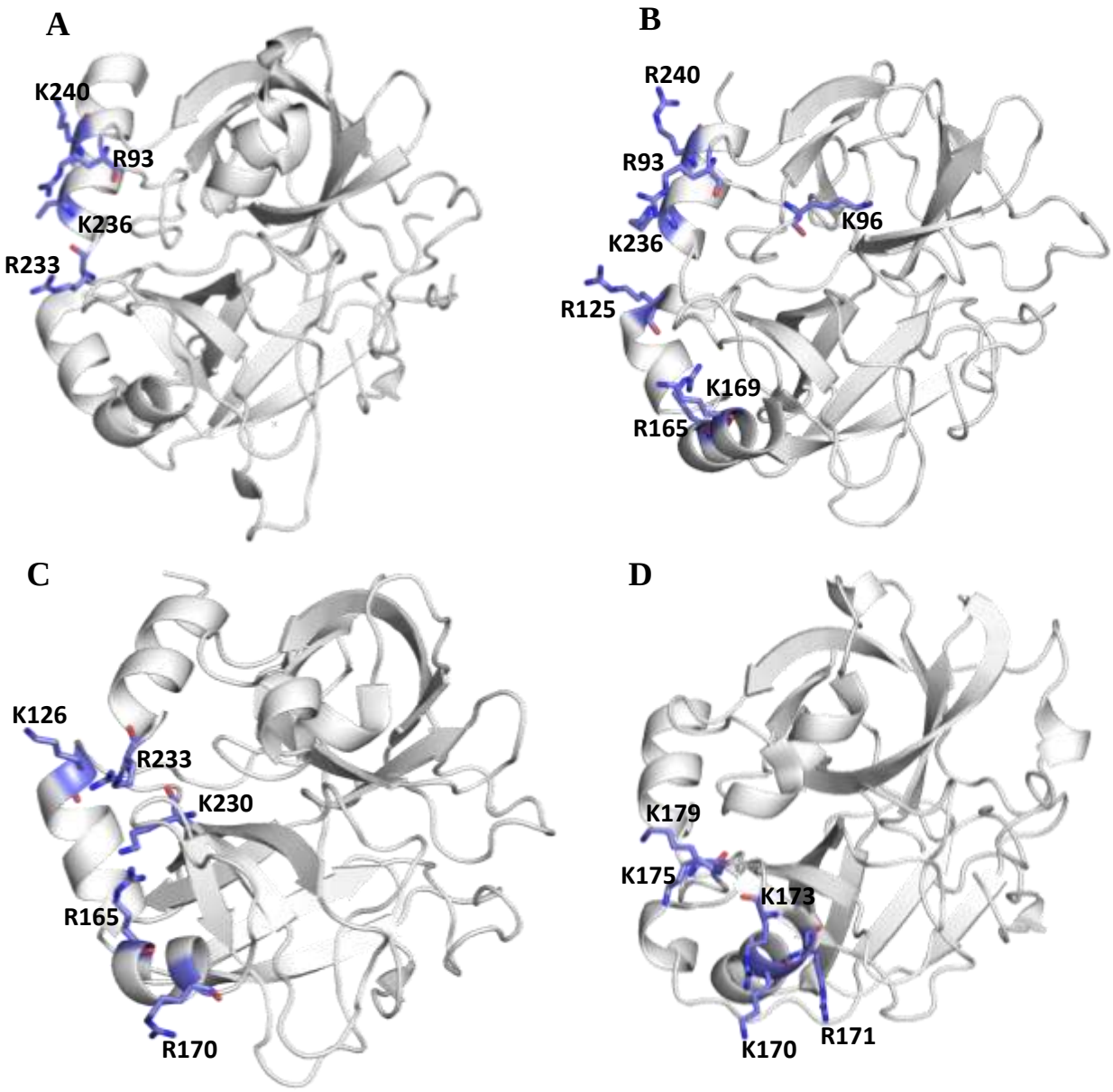

Figure 5. Crystal structures of serine proteases showing GAG interacting residues (A) thrombin; (B) FXa; (C) FIXa; (D) FXIa.

1.3 Glycosaminoglycan Mimetics

As noted, GAGs are complex heterogeneous compounds which interact with a multitude of proteins. Of these many interactions, only few specific ones have been clearly elucidated to date. Also, the source of most GAGs, which has been from animal sources, frequently adds to the variability of GAGs.[89,90] In addition, there is the possibility of impurities, including other GAGs and viruses and this has proven to have dire consequences.[91–95] These setbacks have thus necessitated the drive to derive GAGs from other sources including bacteria and mammalian cells.[96,97]

That said, GAG mimetics have an immeasurable advantage of overcoming some of these major setbacks with naturally derived GAGs. In addition to being devoid of contaminants, there is the possibility of obtaining structurally defined species that can achieve selectivity and specificity for particular binding partners and thus minimize off target effects. In addition, preferred pharmacokinetic properties can be achieved by the incorporation of different chemical moieties, such as hydrophobic groups, into GAG mimetics and by so doing arrive at properties that cannot be achieved by GAGs alone.[98,99]

Nonetheless, this is a challenging feat to achieve for a number of reasons. First, there is limited structural information on the interaction of GAGs with their protein targets.[100] Also, the study of GAG-protein interactions is still in an infant stage and the wide variety in GAG sequences makes it difficult to identify particular GAG sequences that will elicit a desired interaction, and thus an effect.[100] Researchers have utilized computational approaches in identifying GAG sequences that interact with proteins of interest and although this has achieved some level of success, there are still significant gaps that remain in the use of this approach.[101–105] The major factor that makes this approach tedious is the complexity of GAGs coupled with their flexibility.[100] The chemical synthesis of saccharide based GAG mimetics too is particularly

difficult to achieve, requiring multiple chemical reaction steps, often with very low yields.[106] In this regard, GAG mimetics not based on a saccharide scaffold, herein referred to as non-saccharide GAG mimetics (NSGMs), offer significant advantages.[107]

1.4 Non-Saccharide GAG Mimetics (NSGMs)

NSGMs are compounds that have a non-sugar backbone and sulfates, sulfonates, carboxylates and phosphates as the negatively charged groups. In fact, the study and development of non-saccharide GAG mimetics is still in its early stages.[107] However, this is a promising area for the development of compounds that regulate the activity of GAG binding proteins for a number of reasons. First, these molecules will be easier to synthesize and obtain as homogenous species in high yields and with high purity. Also, the synthetic ease will be helpful in developing structural analogs and hence chemical libraries that will aid in understanding the structure activity relationships of these compounds and their binding partners. Moreover, computational studies of these compounds will be easier to handle compared to GAGs as they have significantly fewer structural complexities and flexibilities. Another added advantage to these compounds has to do with their sites of interaction. Since GAGs bind to proteins at allosteric sites rather than the active sites, NSGMs are likely to possess this characteristic. Allostery presents a number of advantages over orthostery. Firstly, allosteric sites are less conserved than orthosteric sites, thus targeting allosteric sites is likely to result in more selective compounds.[108–110] Secondly, in orthosteric inhibition, there is total loss of activity, whereas in allosteric inhibition there can be submaximal inhibitor efficacy. Consequently, allosteric inhibitors can regulate rather than totally inhibit activity. NSGMs have been designed to target the coagulation cascade, inflammatory processes, cancer and infection among others, yielding some success and improving the understanding in this field. The focus of the remainder of this

chapter will be on discovered/designed NSGMs and their biological importance. A few saccharide-NSGM hybrid compounds, containing both saccharide and non-saccharide portions, have been studied and their biological importance will also be discussed.

1.4.1 NGSMs in Hemostasis

Heparins and the vitamin K antagonist, warfarin, remained the mainstay of anticoagulant therapy for several decades after their discovery.[111] These agents act via an indirect mechanism, including by activation cofactors such as AT or HCII, to bring about inhibition of a number of coagulation enzymes and thus coagulation. Their use remained beset with a number of side effects, including excessive bleeding risk and variability of patient response. In addition, constant monitoring was required, especially with warfarin, due to its narrow therapeutic window.[112] It was thought that direct inhibitors of these coagulation enzymes, which do not require a cofactor such as AT, would be better anticoagulants as they would act more specifically by targeting individual enzymes of the coagulation cascade. However, these agents still pose some bleeding risk among patients.[113] The search for new anticoagulants led to the search for different classes of compounds for use as anticoagulants. Since heparin, the most studied GAG, is widely known and used as anticoagulant, it is not surprising that coagulation is the common area where NSGMs have been targeted. Typically, NSGMs are initially screened for anticoagulant activity and a number of these have been discovered and designed to target coagulation cascade proteins, including AT, thrombin, factor Xa, factor XIa and plasmin, and their properties reported.

1.4.1.1 Anticoagulant and Anti-Platelet Aggregation Effects of Sulfated Flavonoids

Two naturally available sulfated flavonoids, quercetin 3-acetyl-7,3',4'-trisulfate **(1.1)** and quercetin 3,7,3',4'-tetrasulfate **(1.2),** isolated from *Flaveria bidentis,* were shown to possess anticoagulant activity, inferred from their significant prolongation of clotting in the activated partial thromboplastin time (APTT) assay at 1 mM concentration. [114] At the same concentration, their effect on prothrombin time (PT) was less, and there was no effect on thrombin time (TT).[114]

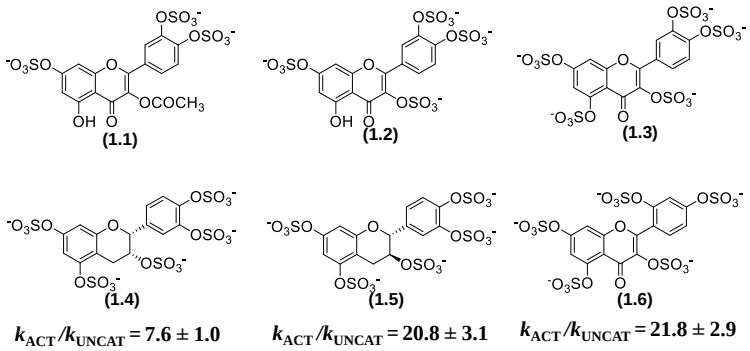

Figure 6. Sulfated flavonoids with anticoagulant and antiplatelet aggregation effects.

The effect of quercetin 3,7,3',4'-tetrasulfate was significantly higher than that of the trisulfate and it was demonstrated that these compounds had no direct effect on the coagulation enzymes, but rather, exerted their anticoagulant effects by the activation of heparin co-factor II at rates comparable to dermatan sulfate.[114] A subsequent study of the inhibition of platelet aggregation using both platelet rich plasma and washed human platelets, and a number of different platelet aggregation inducers revealed, that in addition to anticoagulant properties, quercetin 3-acetyl-7,3',4'-trisulphate (**1.1**) and quercetin 3,7,3',4'-tetrasulphate (**1.2**) possessed antiplatelet aggregation properties in a dose dependent manner.[114] Again, the effects the tetrasulfate was better at inhibiting platelet aggregation than the trisulfate.[114]

Gunnarson et al. used a computational based study of the interaction of heparin with AT to design the first non-sugar based compounds that bind AT and accelerate its inhibition of FXa.[115] Hydropathic Interactions (HINT) technique, a molecular modeling tool,[116] was used to study the

molecular interactions of heparin and AT and deduce the contribution of specific ligand-protein interactions at the residue level to the overall binding energy. A pharmacophore, deduced from these interactions, led to the discovery of (-)-epicatechin sulfate (ECS) (**1.4**), a sulfated flavonoid, as the first non-sugar small molecule activator of AT, with a 10-fold acceleration of AT activity.[115] This was followed by the development of other sulfated flavanoids and flavonoids that bound AT and accelerated its inhibition of FXa at better rates than the parent compound. Using computational studies and competition studies, it was demonstrated that these compounds interacted at the extended heparin binding site of AT.[117–119]

1.4.1.2 Anticoagulant Effects of Flavonoids with an Oligopolysulfated Moiety

Having established that sulfated flavonoids possess anticoagulant activity via activation of HCII and/or AT, Corriea-da-Silva et al. generated a chemical library containing 5 sulfated hybrid flavonoid-saccharide compounds as a potential new class of anticoagulants.[120] Four of these compounds showed anticoagulant activity in a dose dependent manner in the APTT assay with compound **1.10** being the most potent, requiring a concentration of 66 μM to double the clotting time. Clotting time in the PT assay required higher concentrations to achieve and again compound **1.10** was the most potent. [120] In the TT assay only two compounds, **1.9** and **1.10**, significantly extended the clotting time. [120] The authors concluded, based on their results, that there was a positive correlation between the number of sulfates and anticoagulant properties. Although none of the compounds had any direct or AT mediated indirect inhibitory effect on thrombin, compounds **1.9** and **1.10** directly inhibited FXa, while compounds **1.7** and **1.8** behaved similarly to heparin, inhibiting FXa in the presence of AT. [120]. Compounds **1.7** and **1.10** retained in vivo anticoagulant activity following intraperitoneal administration to mice and assessment of clotting using the APTT, PT and TT tests.[120]. Results from thromboelastography showed that

these compounds hindered both clot initiation and formation and also indicated an effect on platelets.[120]. In addition, preliminary toxicity studies based on the assessment of liver enzyme levels following the intraperitoneal administration of compounds **1.7** and **1.10** gave favorable results.[120]

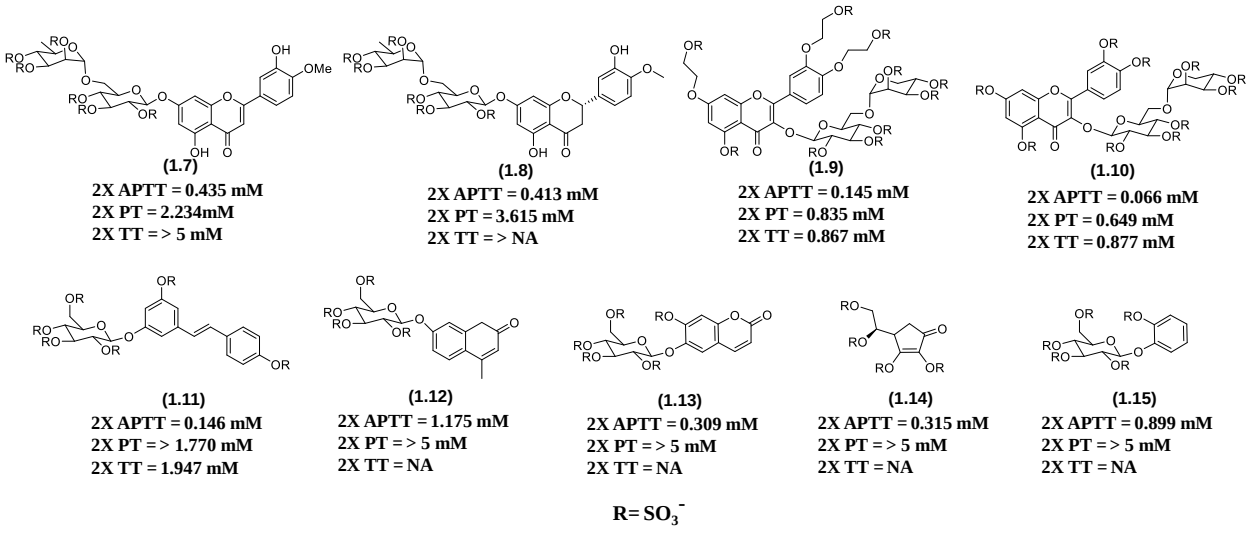

Figure 7. Hybrid saccharide-NSGM compounds with anticoagulant properties.

Following their initial study,[120] Correia-Da-Silva et al. studied another small library of sulfated saccharide-hybrid componds and discovered that they showed anticoagulant effects in a dose dependent manner.[120] Trans-Resveratrol 3-ß-D-glucopyranoside persulfate **(1.11)** proved to be the most potent compound in the APTT, PT and TT assays, requring 0.146, 1.770 and 1.947 µM to double the clotting times respectively.[120] Although 4-methyl 7-hydroxycoumarin 7-ß-D-glucopyranoside persulfate (**1.12**), esculin persulfate (**1.13**), ascorbic acid persulfate (**1.14**) and salicin persulfate (**1.15**) prolonged clotting in APTT assay (1.175, 0.309, 0.315, 0.899 µM respectively), they required greater than 5 µM to double clotting time in the PT assay and showed no effect on the TT at 5 µM.[120] Interestingly, none of these compounds exerted any inhibitory activity, direct or indirect, on thrombin and FXa, suggesting an alternative pathway for

their anticoagulant properties. A study on the effects on the protein C pathway revealed the possibility of interference of this pathway by compounds **1.9**, **1.10** and **1.11**, which decreased the levels of activated protein C to 40-60% at 1 μM concentrations, in addition to a significant reduction in prothrombin levels.[120] Thromboelastography and platelet aggreagation studies indicated that compounds **1.7-1.11** affected platelet function and thus possess both anticoagulant and antiplatelet activity. [120]

1.4.1.3 Linear Polyacrylic Acids Activate AT

Further work in the development of non-saccharide AT activators led to the discovery of linear poly(acrylic acid)s as AT activators, with AT rates of up to 284-fold for FXa inhibition and up to 1000-fold for thrombin inhibition. [121,122] Not surprisingly, AT activation was found to be significantly dependent on the chain length of the poly(acrylic acid)s, which was thought to lead to enhanced interactions.

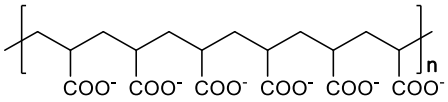

Figure 8. General structure of linear polyacrylic acids

Table 3. AT activation by linear polyacrylic acids

	M_R (kDa)	Monomers	k_{ACT}/k_{UNCAT}
1.16	0.8	~12	118
1.17	1.5	~21	114
1.18	2.3	~32	259
1.19	3.5	~48	579
1.20	6.2	~87	1109

1.4.1.4 Sulfated Low Molecular Weight Lignins Inhibit Coagulation Enzymes by a novel Direct Allosteric Inhibitory Mechanism

The earlier success achieved with the design of sulfated flavones as AT activators[115,117–119] drove the search for sulfated species with considerable hydrophobic character. A combination of these two characteristics was thought to be ideal for bringing about direct inhibition of coagulation enzymes. This resulted in the development of sulfated low molecular weight lignins (LMWLs), primarily because the lignin scaffold was hydrophobic in nature and also possessed hydroxyl groups that could be easily sulfated. These lignins, synthesized via chemo-enzymatic coupling of three 4-hydroxycinnamic acids, caffeic acid, ferulic acid, and sinapic acid employing horse-radish peroxidase, followed by a sulfation reaction, were named CDSO3 (**1.21**), FDSO3 (**1.22**) and SDSO3 (**1.23**) respectively.[123] An analysis of these compounds using SEC-HPLC revealed that they were heterogeneous polymers of about 4-15 monomer units having distinct differences based on the starting cinnamic acid. While CDSO3 and SDSO3 were found to be more heterogeneous with similar molecular weight distribution of about 3300 - 3500, FDSO3 had a higher molecular weight of about 4100 and was significantly less heterogeneous. [123,124] The level of sulfation for these compounds was calculated to be one sulfate group per 2-3 monomeric units. [123]

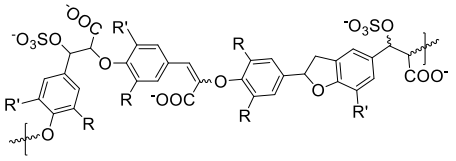

(1.21) CDSO3 R = OH; R' = H M_R = 3,320 Da
(1.22) FDSO3 R = OMe = OH; R' = H M_R = 4,120 Da
(1.23) SDSO3 R = OMe = OH; R' = OMe M_R = 3,550 Da

Figure 9. Sulfated LMWLs.

The sulfated LMWLs demonstrated similar potency to low molecular weight heparin in two plasma coagulation assays, the APTT and PTT assays. The unsulfated precursors also possessed anticoagulant activities, although with much lower potency. [123] Further studies revealed that these compounds directly target thrombin and FXa to bring about anticoagulation. The unsulfated precursors directly inhibited FXa at about 0.12 – 0.90 μM and thrombin at 0.06 – 0.32

μM whereas the sulfated species inhibited FXa at 0.03 – 0.25 μM and thrombin at 0.02 – 0.10 μM. [123] This difference in the inhibitory potencies of the sulfated and unsulfated species supports the hypothesis that both charged groups and hydrophobic groups are essential for inhibition of coagulation enzymes. Although there was only a slight selectivity for thrombin over FXa in comparison to FIXa and FVIIa nevertheless, the selectivity for thrombin was markedly high with 17-300 fold difference in potency over the two coagulation enzymes,[124] supporting the hypothesis that structural differences in the exosites of coagulation enzymes can be exploited in achieving selectivity. Mechanistic studies revealed that the sulfated lignins utilize a non-competitive allosteric mechanism for thrombin inhibition. Using known thrombin exosite I and exosite II binders and thrombin mutants, the sulfated LMWLs were shown to interact at or near thrombin's exosite II and interact with Arg93, Arg175, Arg165, Lys169, Arg173 and Arg233, with Arg93 and Arg175 having a higher contribution.[124,125] This very interesting result further emphasizes the role of hydrophobic groups present in the sulfated lignins, since the binding of heparin to exosite II of thrombin does not result in direct inhibition of enzymatic activity. Interestingly, the inhibitory activity of these compounds was totally reversed using protamine sulfate, an arginine-rich species employed as an antidote for heparin, further stressing that both hydrophobic and anionic interactions are vital.[126]

1.4.1.5 Sulfated Low Molecular Weight Lignins Bind to AT Primarily by Non-Ionic Interactions

A study of the AT mediated indirect inhibition of thrombin and FXa by sulfated LMWLs revealed a possible interaction of these compounds with AT, with a specific sulfated lignin showing a preference for this mechanism.[126] Consequently, the sulfated lignins were found to bind with high affinity to AT with close to 90% of the binding energy resulting from non-anionic

interactions, as determined by salt dependent studies.[126] Again, the binding site of the sulfated lignins was determined to include the pentasaccharide binding and extended heparin binding sites of AT showing the importance of the negatively charged moieties. [126].

1.4.1.6 Sulfated Low Molecular Weight Lignins are Potent Inhibitors of Plasmin Also

Heparin is known to interact with plasmin; however this interaction also does not result in the direct inhibition of enzymatic activity.[84,127] The sulfated lignins inhibited human plasmin with high nanomolar to low micromolar potencies. As in the case of thrombin and FXa, this inhibitory activity does not require AT, suggesting to a direct allosteric inhibition of the protease, which was confirmed using Michaelis-Menten kinetics.[128]

1.4.1.7 Sulfated Polyphenols Have Anticoagulant Properties

An analysis of the anticoagulant properties of persulfated derivatives of lignins performed by Krylov et al. revealed that myo-inositol hexasulfate, **1.24**, prolonged clotting time in the APTT assay, requiring a concentration of 23 mg/mL to double the clotting time. [129] The other compounds paled in comparison, requiring greater concentrations (> 120 mg/mL) to double the clotting time. Myoinositol hexasulfate was shown to exert its anticoagulant activity by activating AT, resulting in the inhibition of FXa..[129]

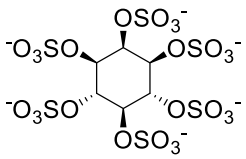

(1.24)

2X APTT = 23 mg/mL

Figure 10. Structure of myo-inositol hexasulfate.

1.4.1.8 Sulfated Benzofurans Display Interesting Inhibition Profiles for Thrombin and FXIa

The core structure of the sulfated benzofuran molecules is based on CDSO3,[130] the most potent sulfated lignin against thrombin and FXa, which also demonstrated good anticoagulant properties in plasma.[123] Structurally, CDSO3 contains a variety of linkages, including the β-5 type, and the

sulfated benzofuran compounds were designed to mimic this particular linkage type. Initially an enzyme mediated oxidative coupling of catechol and ethylacetoacetate was employed,[131] but later an oxidative Michael addition reaction was utilized.[132] Though biochemical screening of 17 sulfated benzofurans revealed only a weak inhibitory potency for both thrombin and FXa, the potential of developing more potent compounds based on this scaffold was thought to be high. The next generation of these compounds were a combination of dimers and monomers and displayed wide ranging inhibition for thrombin ranging from low to high μM IC_{50}s using a non-competitive allosteric mechanism. [133,134] The general observation was that sulfated benzofuran dimers were significantly more potent than monomers, which was not surprising considering that the parent compound, CDSO3, is oligomeric in nature. Also, the results point to the importance of both the charged group and the hydrophobic component of the molecules. Interestingly, these compounds lack any FXa inhibitory potential, which is a substantial deviation from the inhibitory profile of CDSO3. Prolongation of clotting time in the APTT and PT assays was also achieved with some of these compounds, albeit at high concentrations, indicating their potential as anticoagulants.[133,134] Competitive studies utilizing the exosite I binding hirudin peptide and exosite II binding unfractionated heparin, heparin octasaccharide and γ'-fibrinopeptide, point to the exosite of thrombin as the site of interaction. In studies using thrombin mutants, an interaction between a selected sulfated benzofuran dimer, **1.26**, and the Arg173 residue of thrombin was observed to be vital for inhibition. [134] Studies of sulfated benzofuran trimers and tetramers were very interesting and show a very complex structure activity relationship. The potencies of these compounds were varied with one trimer, **1.27**, having a submicromolar inhibitory potency of 670 nM for thrombin.[135] Increasing the length to a tetramer led to a drastic loss in inhibitory activity. [135] h the most potent of the tetramers was shown to interact at the

heparin binding site, mutant studies showed an interaction with the Arg233 residue, a marked difference from the interaction of the sulfated dimers. [135]. Further, a screen of a sulfated benozofuran compound library for FXIa discovered some inhibitors against this protease. An interesting discovery was allosteric inhibitors that did not compete with heparin for binding to thrombin, as observed with compound **1.28**, indicating the interaction with residues not utilized by heparin for binding to FXIa.[136]

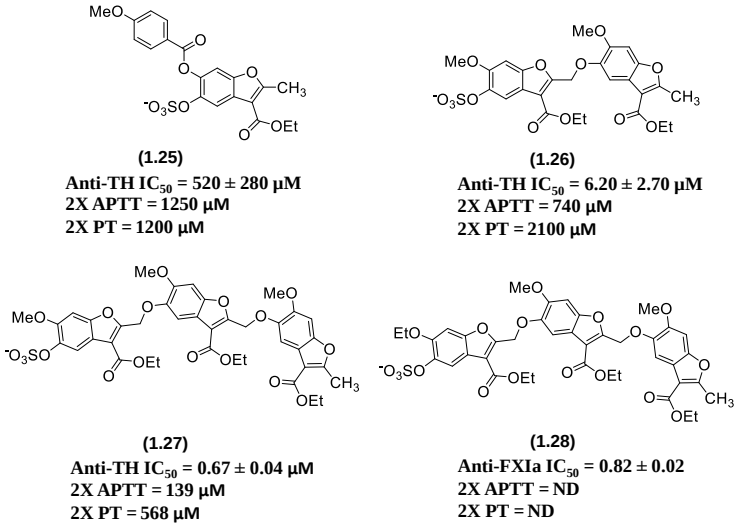

Figure 11. Sulfated benzofuran compounds with anticoagulant potential.

1.4.1.9 SbO4L is a Selective and Potent Inhibitor of Thrombin and Inhibitor of Platelet Aggregation

As a follow up to the sulfated LMWLs, SBO4L, **1.29**, a synthetic polymeric compound, was synthesized to mimic the sulfated tyrosine sequence in glycoprotein1bα (GPIbα).[137] Also polymeric and heterogeneous, SBO4L was fully chemically synthesized in only three steps, a marked advantage over the previously prepared sulfated LMWLs. In addition, it was a considerably more uniform species due to the presence of only one inter-monomer linkage type, the β−O4 linkage.[137] The inhibitory potency of SBO4L was skewed greatly to thrombin (IC_{50} of 0.17 µg/mL). With the exception of plasmin (IC_{50} of 0.38 µg/mL), the inhibitory potency for other serine proteases was weak. (> 81 µg/mL).[137] This was seen as a significant improvement over the non-selective sulfated LMWLs. SBO4L also inhibits thrombin via a non-competitive allosteric mechanism. (> 81 µg/mL)[137] and was found to compete with UFH and GPIbα. The use

of thrombin mutants indicated that SBO4L engages the exosite II residues: Arg233, Lys235, and Lys236, utilized by thrombin in interacting with both UFH and GPIbα.[137] As predicted, SBO4L functioned both as an anticoagulant and an anti-platelet agent, prolonging clotting time in the PT and APTT assays, and also impacting platelet aggregation and activation.[137,138] The potential of SBO4L as an anticoagulant has been further emphasized using whole blood experiments and animal mouse models, where it impacted clotting in the TEG assay and was potently antithrombotic in a mouse arterial thrombosis model among others.[138]

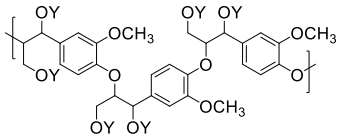

Y = H or SO3-

(1.29)

Anti-TH IC_{50} = 0.17 ± 0.01 µg/mL
2X APTT = 20 µg/mL
2X PT = 64 µg/mL

Figure 12. Structure of SBO4L.

1.4.1.10 Sulfated Coumarins Submaximally Inhibit Thrombin Activity

Following the studies on a chemical library of 36 singly and doubly sulfated coumarin monomers and dimers, Verespy et al. discovered that sulfated coumarins partially inhibited thrombin activity.[139] Three monomeric compounds and eight dimers were found to inhibit thrombin with IC_{50}s ranging from 0.2 to 50 µM, with the dimers having better inhibitory activity. An interesting finding was that 8 of these compounds had efficacies of less than 60% at saturating inhibitor concentrations.[139] Although partial inhibitors are known for receptors, this is the first report showing this phenomenon in a monomeric protease. A number of these compounds inhibited the closely related factors Xa and XIa, albeit with decreased activities and higher efficacies, especially for factor XIa.[139] Michaelis-Menten Kinetics of the most potent compound, **1.32**, indicated that it was an allosteric inhibitor and competition with unfractionated heparin suggested binding at thrombin's exosite II.[139] Further, the potency was unchanged in the

presence of AT, indicating a direct inhibition mechanism as the sole source of thrombin inhibition. [139] Further, they showed that compared to a benzofuran trimer, **1.27**, an allosteric thrombin inhibitor with >80% efficacy of thrombin inhibition, the conformational change at the active site was much reduced.[139] They concluded that partial inhibition is a result of restricted conformational change at the active site that permits small substrates to be cleaved by the protease.

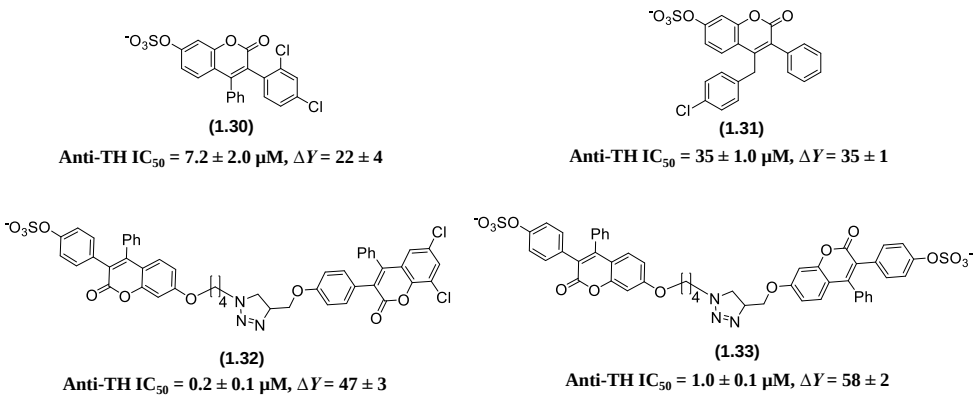

Figure 13. Sulfated coumarins with thrombin inhibitory potential.

1.4.1.11 SPGG and Its Analogs Inhibit FXIa via an Allosteric Mechanism

While most efforts toward the development of anticoagulants have focused on targeting thrombin and FXa, work on developing inhibitors for the intrinsic pathway enzyme, FXIa, has been minimal. Interestingly, new evidence suggests that FXIa inhibitors will have lower risk of bleeding complications, thus making FXIa an attractive target.[140,141] This is supported by the observation that bleeding disorders resulting from FXIa deficiency are mild compared to deficiencies in other coagulation enzymes.[142,143] In addition, elevated levels of FXIa increase the

risk of cardiovascular diseases in women.[144] From a biochemical screen of a focused library of sulfated compounds, SPGG (**1.34**) was discovered to potently inhibit FXIa via a non-competitive allosteric mechanisms with an IC_{50} of 551 nM and over 200-fold selectivity over closely related coagulation enzymes.[145] As an advantage, SPGG is easily synthesized via a three-step protocol in good yield, however the difficulty in achieving persulfation results in the final compound being a mixture and having between 7-12 sulfate groups per molecule.[145] A study of variant species of SPGG showed that the inhibitory potency of SPGG, as well as selectivity, varied mildly with sulfation levels, with highly sulfated species having improved potencies for FXIa, along with moderate losses in selectivity.[146] Surprisingly, it was demonstrated that the non-ionic interactions account for close to 90% of the binding energy of SPGG and FXIa.[146] SPGG was shown to bind at the heparin binding site on the catalytic domain of FXIa and interact with Lys529, Arg530 and Arg532 residues.[147] Marked prolongation of clotting time in the APTT assay but not the PT assay by SPGG further supports the notion that SPGG will have a better side effect profile over inhibitors that target enzymes of the common coagulation pathway.[145]. Another advantage is that SPGG binds to FXI, the zymogen of FXIa, making its use as antidote possible. [146] Also, SPGG inhibitory activity of FXIa was reversed to about 30% by protamine and almost completely by polybrene.[147]

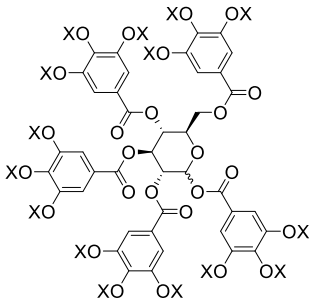

X = H or SO3-

(1.34)

Anti-TH IC_{50} = 551 ± 32 nM
2X APTT = 96 µg/mL
2X PT = 298 µg/mL

Figure 14. Structure of SPGG.

1.4.1.12 Sulfated Quianazolinones Inhibit FXIa

Following previous reports that the hydrophobic groups on non-saccharide GAG mimetics were important players in the interaction with proteins, Karuturi et al. hypothesized that it would be possible to develop compounds that specifically target hydrophobic patches

surrounding the heparin binding sites of proteins. [148] A biochemical screen of a library of 26 sulfated quinazolin-4(3F)-ones led to the discovery of direct allosteric FXIa inhibitors, with an interesting structure activity relationship.[148]

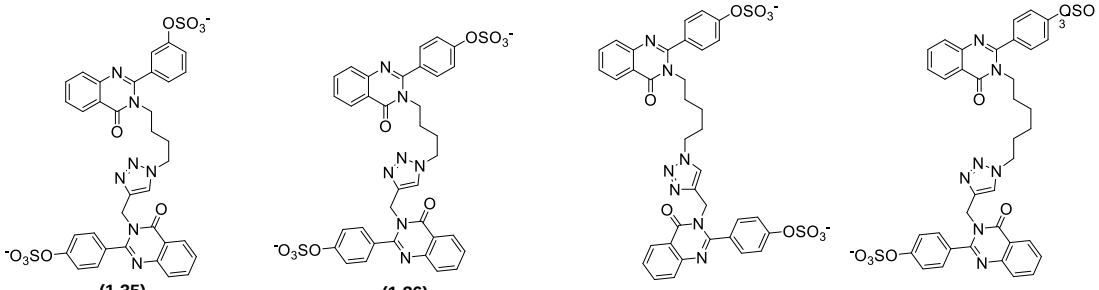

Figure 15. Sulfated quinazolinones with FXIa inhibitory activity.

These novel compounds, which were essentially sulfated quinazolin-4(3F)-one monomers and dimers, with inter-monomeric linkers of different lengths, had FXIa inhibitory potencies of 50 to >1000 µM and were selective over other coagulation cascade serine proteases.[148] The SAR revealed that only dimers bearing exactly one sulfate at the para positon of each monomer were most active.[148] The SAR also demonstrates an interesting influence of chain length on inhibitory activity, with longer linkers being favored. The anticoagulant potential of these compounds was also shown using plasma where the most active compounds prolonged clotting time both in the APPT assay and to a lesser extent the PT.[148] FXIa mutants indicated that these compounds bound at the heparin binding site on the catalytic domain and interacted with Lys529, Arg530, and Arg532 residues.[148]

1.4.1.13 Tetrahydroisoquinoline Compounds Activate AT for FXa inhibition

Raghuraman et al. designed a novel class of AT activators on the tetrahydroisoquinoline scaffold of which the IAS5 (**1.39**) was shown to accelerate FXa inhibition by 30 fold.[149] They utilized a three dimensional pharmacophore based approach by extracting known key interacting residues from the DEF trisaccharide, which subsequently revealed the tetrahydroisoquinoline scaffold as a suitable mimic.[149] Following this success, a focused virtual library based on IAS5 was designed. [150] The biochemical testing of synthesized compounds revealed a range of 7 to 80 fold acceleration of AT activation for FXa inhibition. [150] Three compounds activated the inhibition by rates 2-3 fold better than IAS5.[150]

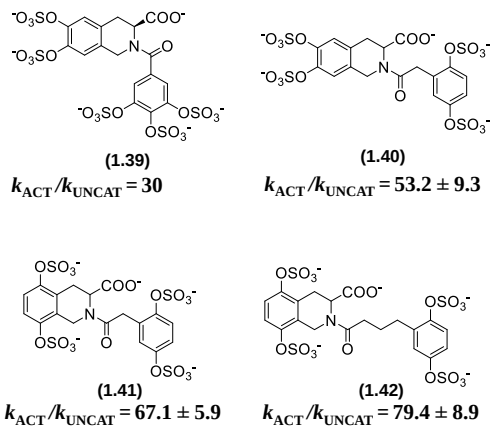

Figure 16. Tetrahydroisoquinoline compounds with AT activation activity.

1.4.2 NSGMs as Anticancer Agents

GAGs have been recognized as important players in cancer biology[13] and there is a concerted effort aimed at developing GAGs as cancer therapeutic agents.[19,151,152] Naturally, sulfated compounds have been documented to affect different targets involved in various stages of tumor growth and progression and a few of these are highlighted below. Using colon cancer cell lines, it was shown that two sulfated quercetin derivatives theograndin I (**1.43**) and II (**1.44**), inhibited two different colon cancer cell lines with IC_{50}s from 125 – 205 μM.[153] A high estrogen level is known to play a role in the development of some types of cancer, most notably breast and endometrial cancer,[154] and antiestrogens have thus been useful in the treatment of hormone dependent breast cancer. Aromatase, a cytochrome p450 family enzyme involved in the synthesis

of estrogen was shown to be weakly inhibited by sulfated resveratrol derivatives.[155] This was an important observation as anti-aromatase agents have been shown to be beneficial in breast cancer.[156] Also, steroid sulfatases are enzymes that hydrolyze sulfated steroids to their steroids. Since they are involved in the generation of steroids, including estrogen, they play a role in

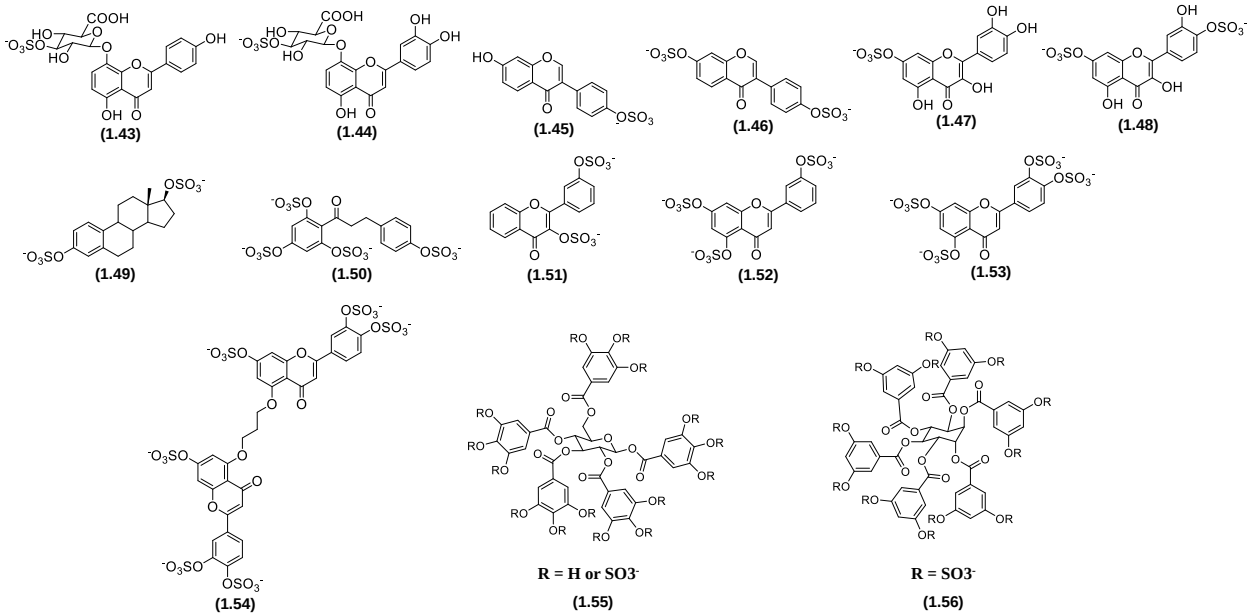

Figure 17. NSGMs with anticancer potential.

cancer, and thus their inhibitors may have use as anticancer agents.[157] Daidzein-4'-O-sulfate (**1.45**) and daidzein-7,4'-di-O-sulfate (**1.46**), two sulfoconjugates of the isoflavone, daidzein, were found to inhibit sterol sulfatase activity with IC_{50}s of 6 and 1.5μM respectively.[158] Interestingly, Daidzein was found to be completely inactive against the enzyme, indicating the importance of sulfation for this activity.[158] The phosphatidylinositol 3-kinase pathway, frequently activated in cancer, is vital for tumor progression and has also been shown to impact the development of resistance to anticancer agents.[159] This pathway also controls a number of important cell functions including cell metabolism, growth and angiogenesis.[160] The PI3-K pathway is thus an important target for cancer treatment with significant efforts applied in advancing PI3-K inhibitors for a number of different cancers including breast, endometrial, colon

and even in multidrug resistant cases [161–163]. Though flavonoids have been shown to possess inhibitory activity against PI3-K, their insolubility remains a critical limitation for their use. To improve this property, sulfation was performed on quercetin, yielding two derivatives, sodium quercetin-7-sulfate (**1.47**) and disodium quercetin-7,4'-disulfate (**1.48**). Biochemical studies indicated that these two sulfated compounds inhibited the recombinant human PI3-K p110β catalytic subunit in a dose dependent manner, with the monosulfated derivative having the better potency.[164] The authors mention that that the 3', 4' hydroxyl groups are required for activity, hence, the weaker potency of the disulfated derivative.[164]

Anti-angiogenic agents have been an important class of anticancer therapeutics for a number of decades. Data on the role of heparins in angiogenesis indicates that anti-angiogenic activity is dependent on size, with lower molecular weight heparins being inhibitors and longer chain heparins acting as promoters.[165,166] Low molecular weight heparan sulfate has been previously shown to reduce angiogenesis in rat corneas.[167] Additionally, it has been demonstrated that pro or anti-angiogenic properties of GAGs may be dependent on GAG sequence, that is very tedious to decipher.[168] This problem may, however, be averted with small molecule GAG mimetics which do not present with heterogeneity issues. After screening a chemical library of 18 sulfated non-saccharide compounds of different scaffolds, in an in vitro assay measuring tumor-associated angiogenesis, Raman et al. discovered that five of these compounds, **1.49-1.53**, abolished the formation of tubules.[169] Based on their results they reasoned that since the active compounds bore between 2 – 4 sulfate groups, activity required 2 sulfate groups that were 5 – 10 Å apart. [169]

A recent approach in cancer therapy is the targeting of cancer stem cells.[170] Cancer stems cells are resistant to most current anti-tumor agents and have the ability to self-renew and

generate the entire tumor.[171] Since GAGs, including heparan-sulfate and chondroitin sulfate, are regulators of stem cell proliferation, Patel et al. screened a 55 member diverse non-sugar sulfated compound library for anti-cancer stem cell activity using a dual screening strategy, which measured the ability of compounds to prevent self-renewal of colon cancer stem cells using two colon cancer lines HT-29 and HCT-116. [172] In this assay, the compounds that prevented growth under spheroid conditions and not monolayer conditions, and were able to inhibit this growth in both secondary and tertiary cultures, were deemed as possessing colon cancer stem cell inhibitory properties.[172] Three of the compounds screened, **1.54-1.56**, were found to satisfy this dual screen and the most potent one, a per sulfated di-quercetin compound (**1.54**) with an IC_{50} of about 58 μM was further studied.[172]. This lead compound was shown to reduce the expression of cancer stem cell markers in an in vitro assay and study of the mechanisms revealed that it acts by weakening the ability of cancer stem cells to self-renew.[172]. Studies using analogs of these compounds showed a strong dependence of activity on the length of the linker separating the two monomeric units. [172]

It is worth noting that the role of sulfated quercetins in cancer is yet to be fully understood. A study found that while quercetin and quercetin-3-glucuronide inhibited angiogenesis, quercetin-3'-sulfate promoted endothelial cell proliferation and angiogenesis.[173]

1.4.3 NSGMs as Regulators of Inflammation

Glycosaminoglycans are known to be very important in the inflammatory process.[174,175] GAGs including hyaluronic acid, heparin, heparan sulfate, and chondroitin sulfate have been shown to reduce inflammation in a number of different cell types by interacting with chemokines, selectins, cytokines, and proteases.[176–178] The benefits of this reduction in inflammation has also been demonstrated in conditions including asthma and ulcerative colitis.[179]

The possibility of developing GAG mimetics to modulate the inflammatory process is thus feasible and a number of such compounds with anti-inflammatory potential have been identified and/or developed. The sulfated quercetin metabolite, quercetin 3'- sulfate (**1.57**), was shown to inhibit the expression of COX-2 in lymphocytes[180] and also reduce the expression of COX-2 mRNA in colon cancer (Caco2) cells.[181] A study using chemically synthesized sulfated

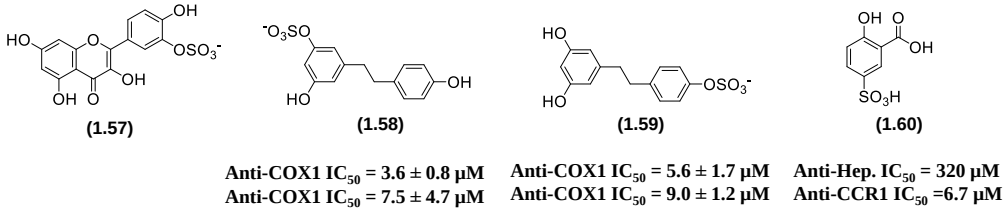

Figure 18. NSGMs with anti-inflammatory properties.

resveratrol derivatives showed that some of these compounds, including **1.58** and **1.59,** were equipotent with resveratrol in the inhibition of COX-1. In addition, they possessed anti-COX-2 activity albeit at weaker potencies than resveratrol.[155] In another study, over 200 small molecules bearing charged groups including sulfonates and carboxylates were screened for their ability to bind to CCL5, a well-studied pro-inflammatory chemokine[182] using an NMR-based screening approach.[183] In addition to having charged moieties, many of the compounds contained aromatic groups to introduce some hydrophobicity. This work resulted in the first small molecule **1.60** shown to inhibit the interaction of CCL5 with its receptor, and also with heparin, albeit at high to moderate potencies, respectively.[183] This compound also impeded leucocyte recruitment in

mouse models. Based on the results of this initial screen, a number analogs were obtained. However none had significant superior properties compared to the lead compound.[183]

Human neutrophil elastase, a hydrolytic enzyme produced by human neutrophils in response to infection and inflammation.[184,185] has been implicated in a number of lung diseases.[186–188]. GAGs are known to interact with human neutrophil elastase resulting in inhibition of enzymatic activity.[32, 34,88] The sulfated LMWLs described earlier strongly inhibit human neutrophil elastase with potencies ranging from 0.43 – 0.72 μM. Eddie-Hofstee plots for NE inhibition by a representative sulfated lignin point to a mixed inhibition mechanism.[189] In addition to anti-HNE activity, the sulfated lignins show strong anti-oxidative and anti-inflammatory activities making them potential anti-emphysema agents.[189]

1.4.4 NSGMs as Anti-Infective Agents

GAGs have been shown be involved in the pathogenesis of infectious diseases via their direct interaction with viruses, bacteria, fungi and parasites.[190,191] By interacting with these pathogens, GAGs facilitate invasion of cells as well as the spread of infection. Enveloped viruses in particular have been shown to attach to their target cells with the aid of heparan sulfate.[192,193] Other sulfated carbohydrates, including heparin, have been found to inhibit viruses including HSV and HIV due to their structural similarity to heparan sulfate.[194,195] Nature presents a good number of sulfated steroids, the majority of them isolated from marine sponges, and there are a number of documented results of these compounds possessing inhibitory activity against viruses, fungi, and bacteria. For instance, two weinbersterol disulfates, **1.61** and **1.62**, isolated from the marine sponge *Petrosia weinbergi*, were shown to have in vitro activity against feline leukemia virus and HIV.[196] Sulfated steroids from the ophiuroid, *Ophioplocus januarii*, **1.63** and **1.64**, were active in vitro against respiratory syncytial virus, polio virus and the Argentine

hemorrhagic fever-causing Junin virus. [197] Halistanol sulfate (24ε,25-dimethylcholestane-2β,3α,6α-triyl trisodium sulfate (**1.65**) isolated from the Okinawan sponge *Halichondria cf. moorei Bergquis*t also possesses antimicrobial properties against fungi and both gram negative and gram positive bacteria.[198] These reports confirm the potential of chemically synthesized non-saccharide GAG mimetics as potential anti-infective agents. In a bid to develop non-saccharide GAG mimetics, Raghuraman et al. discovered a biopolymer,that was confirmed to be a sulfated lignin, as possessing anti-HSV-1 activity.[199] Further studies on these sulfated lignins showed that they inhibit cellular entry of both HSV-1 and 2 with IC_{50}s of 0.017 – 1.45 μM and 0.32 – 5.0 μM, respectively, and also inhibited HIV-1 and prevented HIV-1 mediated cell fusion in a dose dependent manner.[200] A computational study indicated that some substructures in this polyomeric compound acted as heparan sulfate mimics, which could be their possible mechanism of viral inhibition.

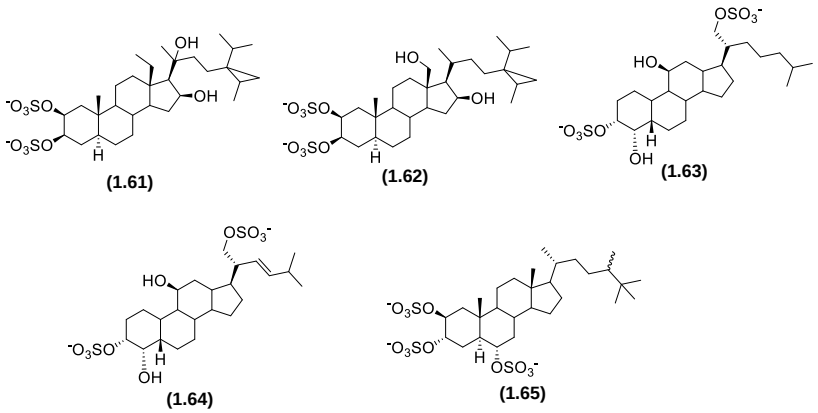

Figure 19. NSGMs with anti-infective properties

200

1.4.5 Summary of NSGMs

Overall, sulfated NSGMs are an important class of compounds with great potential. Their direct allosteric inhibitory mechanism for a number of serine proteases make them particularly attractive. The marked topographical difference in allosteric sites can be useful in achieving selective compounds. The broad activity of the sulfated lignins is not surprising due to their polymeric and heterogeneous nature that ensures the presence of multiple diverse species. To arrive at compounds with specificity for particular GAG binding proteins, teasing out and testing of particular species from this mixture is necessary.

2 DESIGNING ALLOSTERIC THROMBIN INHIBITORS WITH SUBMAXIMAL INHIBITION OF THE PROTEASE

2.1 Introduction

2.1.1 The Coagulation Cascade

Hemostasis, the balance between bleeding and thrombosis, is a highly regulated process in healthy individuals, with the balance in favor of the negative regulation of thrombus formation.[201,202] This is maintained by a rigorous regulation of the coagulation cascade, an intricate system involving several factors.[203] Numerous enzymes and co-factors play distinct and significant roles in the coagulation cascade. There are two related pathways that contribute to the regulation of coagulation. These are the intrinsic and extrinsic pathways, which converge into a common pathway.[201]

Contact of blood with hydrophilic pathways triggers the activation of the intrinsic pathway.[201] This sets up a cascade where coagulation enzymes are converted from their zymogen to active forms sequentially as shown in Figure 20. Specifically, FXII is converted to FXIIa, which in turn converts FXI to FXIa in the presence of calcium.[201,204] FXIa then catalyzes the conversion of FIX to FIXa, also in the presence of calcium. At this juncture, the common pathway is reached where FXa is activated from FX by FIXa in the presence of calcium.[201] FXa then, in combination with calcium and phosphatidylserine, catalyzes the conversion of prothrombin to thrombin, the central serine protease of the cascade.[201] Thrombin converts fibrinogen to fibrin, which is a key component of blood clots.[205] The extrinsic pathway on the other hand is initiated by vascular damage with the exposure of tissue factor to circulatory blood, and its subsequent binding to FVII.[201] The tissue factor forms a complex with FVIIa, leading to the activation of FIX and FX to FIXa and FXa respectively, and thus the common pathway.[201] It is important to note that the dissolution of the blood clot is an important part of hemostasis, and

the most important enzyme in this stage is plasmin.[206]

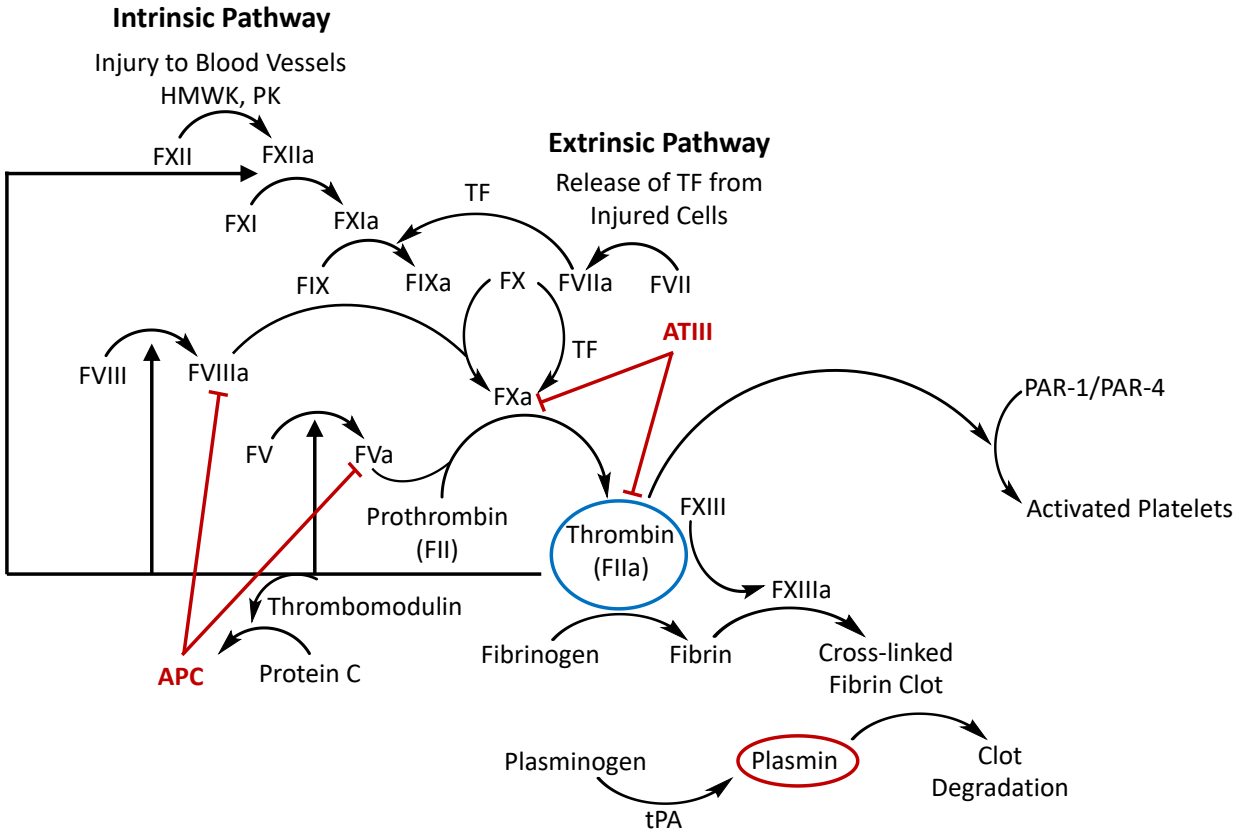

Figure 20. The coagulation cascade.

2.1.2 Hemostatic disorders

Deficiencies and/or mutations in one or more of the coagulation cascade enzymes result in bleeding disorders; however the severity depends on the specific enzyme affected, indicating that the involved enzymes do not contribute equally to maintaining hemostasis.[207,208] Hemophilia is a condition where the ability of blood to clot is impaired as a result of deficiencies in coagulation enzymes. The most common types of hemophilia, A and B, are X-linked genetic disorders occurring in 1:5000 and 1:30000 male births respectively.[209] Hemophilia A is a result of a deficiency in FVIII whereas hemophilia B is due to FIX deficiency. Prothrombin deficiency

on the other hand is very rare, occurring in 1 in 2,000,000.[210] The importance of thrombin for survival is emphasized by the fact that no living patient with undetectable prothrombin has ever been recorded. [210] Clinically, hemophilia is managed using platelet transfusion, coagulation factor replacement and the administration of antifibrinolytics.[211]

Hypercoagulable states, where the propensity of blood to clot is higher than normal, also exist, often resulting in a number of severe conditions. Thrombosis, which is the localized clotting of blood resulting in obstruction of blood flow, is the leading cause of death worldwide.[212] The two types of thrombosis are arterial (myocardial infarction, stroke) and venous thrombosis (venous thromboembolism, and pulmonary embolism).[213] The causes of thrombosis include genetic factors, medical conditions and medication. Congenital deficiencies in AT, protein C and protein S are known to be high risk factors for thrombotic events.[214] Other risk factors for thrombosis include factor V Leiden, the Prothrombin 20210A mutation, and elevated FVIII levels. [214] In factor V Leiden, there is a guanine to adenine substitution at nucleotide 1691 in the factor V gene and this results in the substitution of Arg506 of FVa with glutamine. [215] Consequently, FVa is rendered resistant to activated protein C, resulting in a 10-fold decrease in its inactivation and an increase in thrombin levels. [215] In Prothrombin 20210A, there is a guanine to adenine transition at the nucleotide position 202010, which results in increased prothrombin levels and thus an increased proclivity for blood coagulation.[216]

Medical conditions known to be risk factors for thrombosis include immobilization, surgery, trauma, pregnancy and malignant disease.[217] The use of chemotherapeutic agents and female hormones are also risk factors for thrombosis.[218,219] The management of thrombotic states requires the uses of antiplatelet and anticoagulant drugs. These agents are thus very important drugs, making up a large fraction of medication costs.[220]

2.1.3 Anticoagulants

Anticoagulants are agents that prevent the formation and growth of blood clots. Current estimates indicate that about 10% of all adults will receive an anticoagulant at least once in their lifetime. Currently, there are different classes of anti-coagulants in clinical use and thrombin and FXa are the main coagulation enzymes targeted by these agents.[220] The earliest class of anticoagulants to be used were the vitamin K antagonists, such as warfarin (**2.1**). Warfarin functions as an anticoagulant by disrupting the vitamin K cycle, resulting in decreased vitamin K levels, which in turn negatively impacts the activation of a number of clotting enzymes.[221,222] Though these agents are effective anticoagulants, their narrow therapeutic window, which results in the need for constant monitoring, presents a huge risk and limitation.[221] In addition, a number of drug-drug and drug-food interactions are known to occur with warfarin, resulting in an increase in its anticoagulant effect and thus the risk of bleeding with its use.[223] Heparin and low molecular weight heparin are also widely used anticoagulants, and they function in an indirect manner, accelerating the inhibition of FXa and thrombin by AT.[224] The risks associated with the use of heparin also include the risk of prolonged bleeding and heparin induced thrombocytopenia.[225] Fondaparinux **(2.2)** also accelerates the AT mediated inhibition of FXa. [224] More recently, direct FXa inhibitors, including rivaroxaban **(2.3**) and apixaban **(2.4)**, and direct thrombin inhibitors such as dabigatran **(2.5)**, and argatroban **(2.6),** have been approved for use

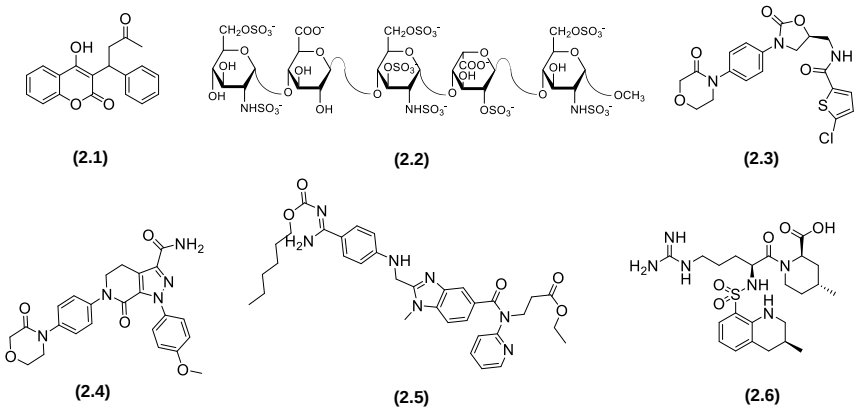

Figure 21. Clinically used anticoagulants

and although these agents have better side effect profiles, they still present with the risk of prolonged bleeding, making the search for new anticoagulant agents necessary.[226]

2.1.4 Thrombin

Thrombin is a 37 kDa monomeric serine protease made up of 308 amino acid residues. It is obtained after the proteolytic cleavage of prothrombin and occupies a central place in the coagulation cascade [227,228] Thrombin activity is necessary at several stages in blood clotting via its interactions with a number of substrates, which include protein substrates, receptors, co-factors and modulators.[229] The most notable are its interactions with fibrinogen, which it converts proteolytically to fibrin.[227] Thrombin also contributes to the maintenance of the fibrin network by its conversion of the zymogen FXIII to its active form, FXIIIa. FXIIIa in turn bolsters the integrity of the clot by crosslinking the α- and γ-chains of fibrin.[230] In addition, thrombin promotes its own generation by the activation factors required for its renewal and also stimulates platelet aggregation by interacting with protease activated receptors.[231]

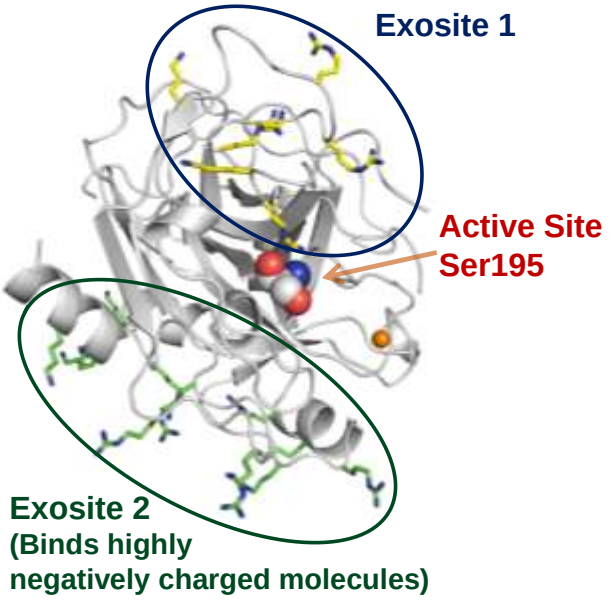

Figure 22. Structure of thrombin.

Interestingly, thrombin also plays a role in inhibiting coagulation: this is achieved through its interaction with protein C, in an interaction facilitated by thrombomodulin. [232] Like other serine proteases, thrombin cleaves peptide bonds after arginine residues, however, it is highly selective relative to other serine proteases like trypsin, and has been shown typically to

cleave peptides in the sequence X-Pro-Arg.[233] This selectivity for substrates is determined primarily by its insertion loops whose residues lead to n narrow and deep active site relative to other serine proteases.[229,234] Interaction of substrates with thrombin takes place through its active sites and exosites. Endogenous ligands known to regulate thrombin activity include AT, alpha-2 macroglobulin, alpha-1-antitrypsin and heparin cofactor II, and these promote inhibition via both covalent and non-covalent complex formation with thrombin.[235]

The important role of thrombin in the coagulation cascade has maintained its importance as a target for anticoagulant therapy.[228,236,237] A good number of the clinically available anticoagulants impact thrombin activity in bringing about coagulation. The anticoagulant agents with the longest use, heparin and warfarin, both affect thrombin. In recent years, a number of direct thrombin inhibitors have been developed and approved for clinical use,[238–240] and although these agents have improved side effect profiles over the earlier agents, they still carry some risk of prolonged bleeding.[241]

In order to advance new anticoagulants with even more improved side effect profiles, our lab has developed a number of direct allosteric inhibitors of thrombin with different core structures.[123, 133,134, 137,139] This is particularly promising for a number of reasons. First, allosteric sites are less conserved compared to active sites: thus, selective inhibitors are more likely to be achieved. Also, inhibitor efficacy can be modulated, hence, inhibitors that do not totally eliminate thrombin activity can be achieved and are thus thrombin inhibitors with reduced bleeding risk. This is not the case with orthosteric inhibitors which result in total elimination of enzymatic activity.

2.2 Rationale for Developing New Sulfated Benzofuran Dimers (SBDs).

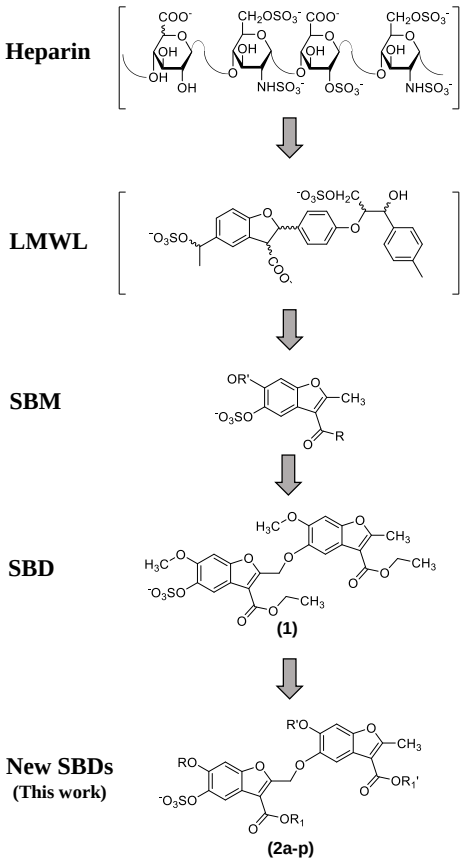

Figure 23. Development of sulfated benzofuran dimer thrombin inhibitors.

The first discovered direct allosteric thrombin inhibitors were the sulfated LMWLs, a heterogeneous and polymeric species which lacked selectivity and inhibited other enzymes including FXa, plasmin, and human neutrophil elastase.[126, 189,242] Based on the sulfated LMWLs, the sulfated benzofuran monomers (SBMs), which inhibited both thrombin and FXa with weak potency, were developed.[130] Dimerization of these monomeric units led to the discovery of sulfated benzofuran dimers (SBDs) with low micromolar potency and selectivity for thrombin over other coagulation serine proteases.[134] A more important finding was that some of these inhibitors exerted submaximal thrombin inhibition, even at saturating inhibitor concentration. One specific SBD **(1)** had an IC_{50} of 6.7 μM and displayed about 75% inhibition efficacy (ΔY) at saturating conditions.[134] We reasoned that the submaximal inhibition at saturating inhibitor concentrations would be an avenue for the development of anticoagulants with lower risk of bleeding, providing an improvement over current thrombin inhibitors. Interestingly, mechanistic studies indicated that this compound utilized a non-competitive, allosteric mechanism of thrombin inhibition, with the exosite II Arg173 residue identified as an interacting residue.[134] Based on this, we reasoned that more potent analogs with a better regulation capability of about 50% should be possible to achieve. Also, a recent report from our lab put forward the first allosteric partial inhibitor of thrombin, a sulfated coumarin, which inhibited thrombin's cleavage of the chromogenic

substrate by only 50% at saturating inhibitor concentrations[139]. Although the partial inhibitory property of the lead molecule was lost with fibrinogen, thrombin's natural substrate, we thought partial inhibition could be possible with a different scaffold, such as the benzofurans. We opted to use computational tools alongside data from our previous studies, with thrombin mutants, to design an advanced generation of benzofuran dimers to achieve our goal.

2.3 Results And Discussion

2.3.1 Molecular Modeling Studies of SBD-Thrombin Interaction

We created a diverse virtual library of about 100 SBDs based on the previously published SBD prototype (**1**), as shown in figure 23. Molecular members of this library were docked onto exosite II of human thrombin and scored using GOLD, as reported earlier.[134] The modifications made to the scaffold took into consideration a number of factors, including the synthetic ease of the modeled structures as well as their potential hydrophobicity. Specifically, we introduced bulky hydrophobic groups including alkyl, cycloalkyl, and substituted and unsubstituted aromatic groups at the R, R', R_1 and R_1' positions (Fig. 23). Also, additional sulfate groups attached to aromatic groups or straight chains were introduced. The introduction of hydrophobic groups including aromatic rings was to target hydrophobic pockets surrounding the positively charged residues of exosite II, specifically Arg173. The introduction of an extra sulfate group was to foster an additional ionic interaction with the positively charged residues around exosite II of thrombin.

Results from the docking and scoring suggested that the presence of aromatic groups at the R' encouraged better interaction between thrombin and the inhibitors via an added pi-pi

interaction with a tryptophan residue in the thrombin S4 pocket. We thus thought that this modification would result in enhanced potency. Modeling also suggested that the presence of an aromatic group at the R_1' position would result in inhibitors targeting the S1 pocket of thrombin, and thus have improved potency. We also reasoned that targeting the S1 pocket would result in compounds exhibiting different inhibition mechanisms from that of the prototype. The introduction of a sulfate at the R_1 positon was also expected to result in an additional ionic interaction with the Arg221A residue of thrombin. Modifications at the R position, however, did not seem to yield any interesting results in the computational study nevertheless, we selected a few of these compounds for chemical synthesis to aid in our understanding of the SBD structure activity relationship. Figure 24 summarizes the protein ligand interactions observed in the computational study.

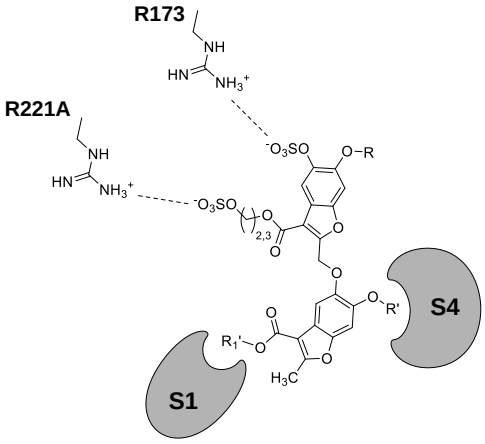

Figure 24. Projected interactions of SBD analogs with thrombin.

Based on the data, a total of 16 SBDs, 13 monosulfated (**2a-m**) and 3 disulfated (**2n-p**), were then selected for chemical synthesis. In addition, 12 mono and di-sulfated SBMs (**21a-l**) were also selected for synthesis.

2.3.2 Chemical Synthesis of Sulfated Benzofuran Molecules

Synthesis of sulfated benzofuran monomers and dimers was achieved in 3 – 14 steps culminating with a microwave assisted sulfation reaction. The benzofuran precursor **3**, was synthesized as previously described.[133] Unsulfated precursors were obtained using a number of chemical reactions including protection and deprotection strategies, S_N2 substitution reactions, DCC coupling, ester hydrolysis and radical bromination. Dimerization of monomeric units was

achieved using an S_N2 reaction. The schemes for the reactions are given below and detailed experimental procedure are available in the experimental section.

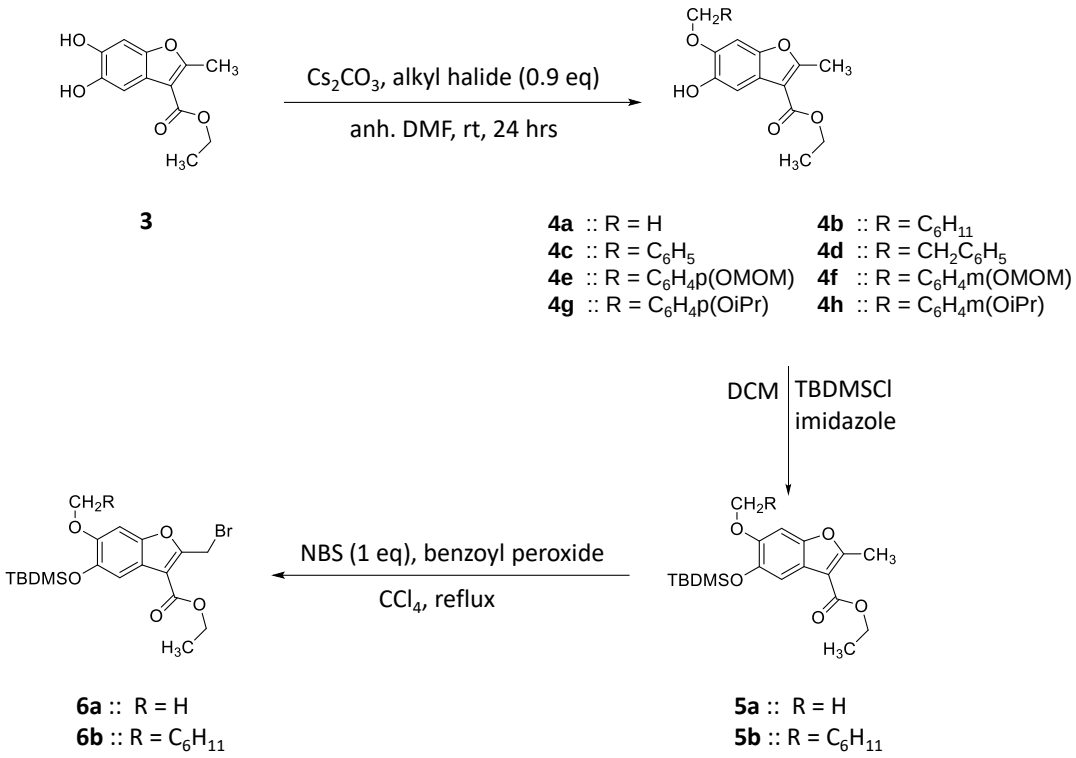

Scheme 1. Synthesis of benzofuran intermediates

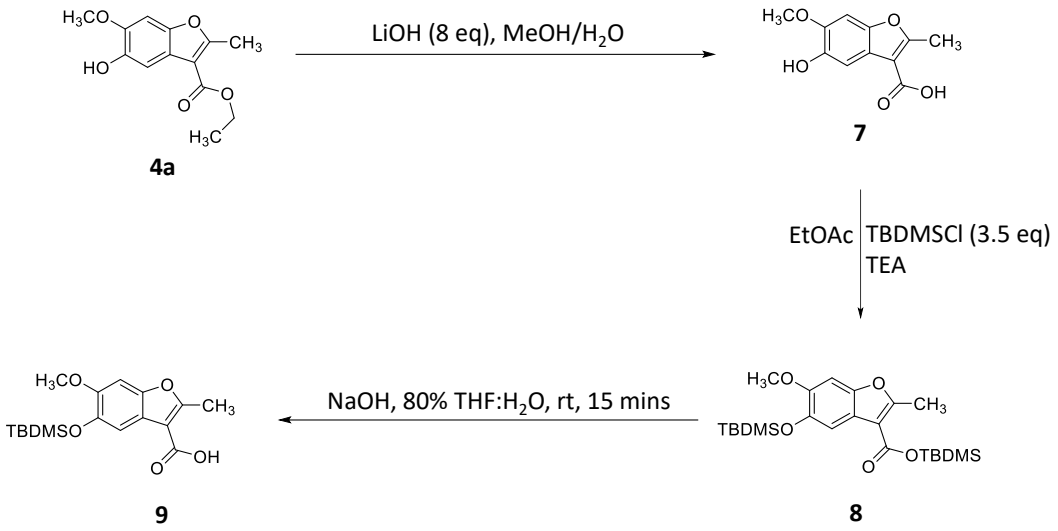

Scheme 2. Synthesis of benzofuran intermediates

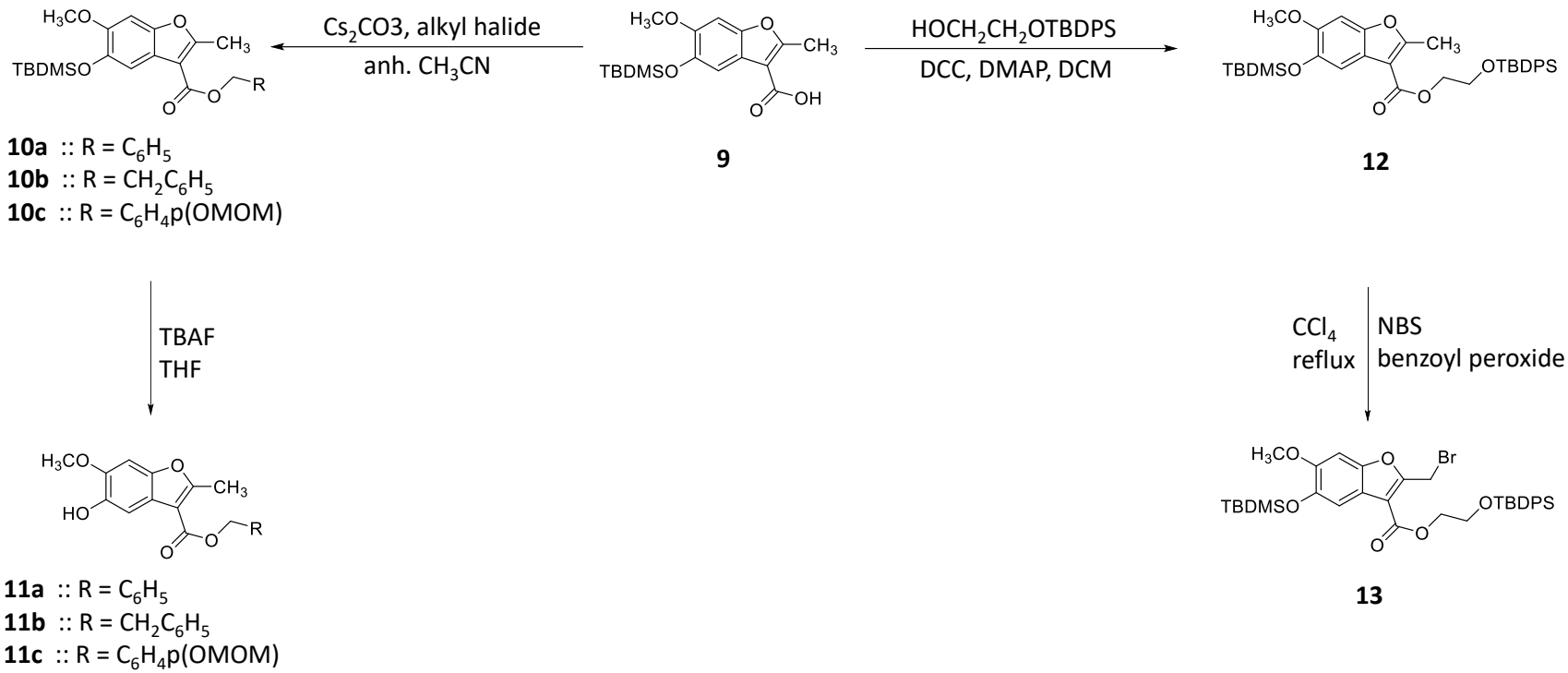

Scheme 3. Synthesis of benzofuran intermediates

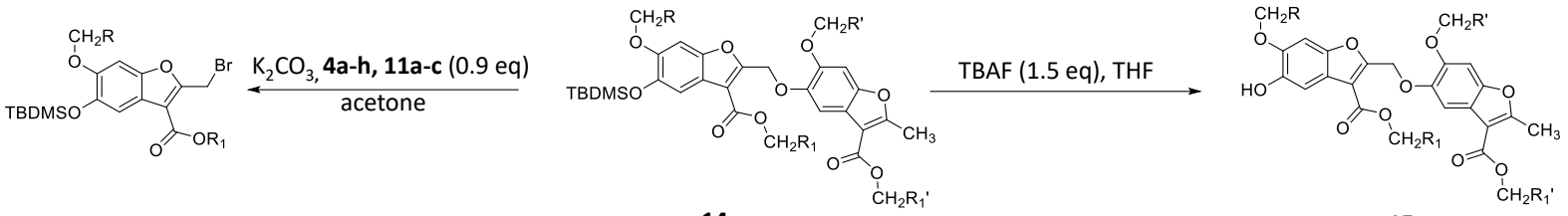

6a, **6b**, **13** **14a-n** **15a-n**

14a :: R = H, R' = C_6H_{11}, $R_1 = R_1' = CH_3$
14b :: R = H, R' = C_6H_5, $R_1 = R_1' = CH_3$
14c :: R = H, R' = $CH_2C_6H_5$, $R_1 = R_1' = CH_3$
14d :: R = H, R' = C_6H_4p(OMOM), $R_1 = R_1' = CH_3$
14e :: R = H, R' = C_6H_4m(OMOM), $R_1 = R_1' = CH_3$
14f :: R = H, R' = C_6H_4p(OiPr), $R_1 = R_1' = CH$
14g :: R = H, R' = C_6H_4m(OiPr), $R_1 = R_1' = CH_3$
14h :: R = R' = C_6H_{11}, $R_1 = R_1' = CH_3$
14i :: R = C_6H_{11}, R' = C_6H_5, $R_1 = R_1' = CH_3$
14j :: R = C_6H_{11}, R' = H, $R_1 = R_1' = CH_3$
14k :: R = R' = H, $R_1 = CH_3$, $R_1' = C_6H_5$
14l :: R = R' = H, $R_1 = CH_3$, $R_1' = CH_2C_6H_5$
14m :: R = R' = H, $R_1 = CH_3$, $R_1' = C_6H_5$p(OMOM)
14n :: R = H, R' = C_6H_5, $R_1 = CH_2$OTBS, $R_1' = CH_3$

15a :: R = H, R' = C_6H_{11}, $R_1 = R_1' = CH_3$
15b :: R = H, R' = C_6H_5, $R_1 = R_1' = CH_3$
15c :: R = H, R' = $CH_2C_6H_5$, $R_1 = R_1' = CH_3$
15d :: R = H, R' = C_6H_4p(OMOM), $R_1 = R_1' = CH_3$
15e :: R = H, R' = C_6H_4m(OMOM), $R_1 = R_1' = CH_3$
15f :: R = H, R' = C_6H_4p(OiPr), $R_1 = R_1' = CH_3$
15g :: R = H, R' = C_6H_4m(OiPr), $R_1 = R_1' = CH_3$
15h :: R = R' = C_6H_{11}, $R_1 = R_1' = CH_3$
15i :: R = C_6H_{11}, R' = C_6H_5, $R_1 = R_1' = CH_3$
15j :: R = C_6H_{11}, R' = H, $R_1 = R_1' = CH_3$
15k :: R = R' = H, $R_1 = C_2H_5$, $R_1' = C_6H_5$
15l :: R = R' H, $R_1 = C_2H_5$, $R_1' = CH_2C_6H_5$
15m :: R = R' = H, $R_1 = C_2H_5$, $R_1' = C_6H_5$p(OMOM)
15n :: R = H, R' = C_6H_5, $R_1 = CH_2$OH, $R_1' = CH_3$

Scheme 4. Synthesis of benzofuran intermediates

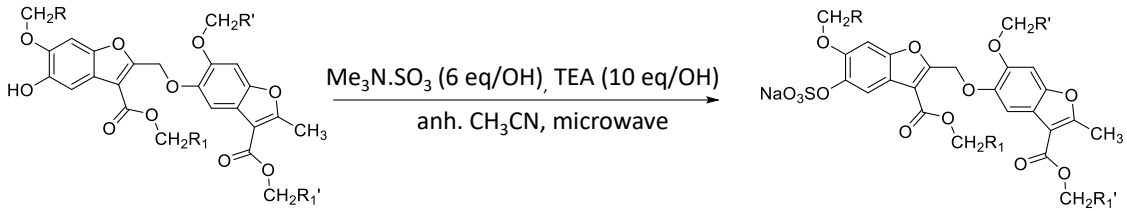

15a-n **2a-n**

15a :: R = H, R' = C_6H_{11}, $R_1 = R_1' = CH_3$
15b :: R = H, R' = C_6H_5, $R_1 = R_1' = CH_3$
15c :: R = H, R' = $CH_2C_6H_5$, $R_1 = R_1' = CH_3$
15d :: R = H, R' = C_6H_4p(OMOM), $R_1 = R_1' = CH_3$
15e :: R = H, R' = C_6H_4m(OMOM), $R_1 = R_1' = CH_3$
15f :: R = H, R' = C_6H_4p(OiPr), $R_1 = R_1' = CH_3$
15g :: R = H, R' = C_6H_4m(OiPr), $R_1 = R_1' = CH_3$
15h :: R = R' = C_6H_{11}, $R_1 = R_1' = CH_3$
15i :: R = C_6H_{11}, R' = C_6H_5, $R_1 = R_1' = CH_3$
15j :: R = C_6H_{11}, R' = H, $R_1 = R_1' = CH_3$
15k :: R = R' = H, $R_1 = C_2H_5$, $R_1' = C_6H_5$
15l :: R = H, $R_1 = C_2H_5$, $R_1' = CH_2C_6H_5$
15m :: R = R' = H, $R_1 = C_2H_5$, $R_1' = C_6H_5$p(OMOM)
15n :: R = H, R' = C_6H_5, $R_1 = CH_2OH$, $R_1' = CH_3$

2a :: R = H, R' = C_6H_{11}, $R_1 = R_1' = CH_3$
2b :: R = H, R' = C_6H_5, $R_1 = R_1' = CH_3$
2c :: R = H, R' = $CH_2C_6H_5$, $R_1 = R_1' = CH_3$
2d :: R = H, R' = C_6H_4p(OMOM), $R_1 = R_1' = CH_3$
2e :: R = H, R' = C_6H_4m(OMOM), $R_1 = R_1' = CH_3$
2f :: R = H, R' = C_6H_4p(OiPr), $R_1 = R_1' = CH_3$
2g :: R = H, R' = C_6H_4m(OiPr), $R_1 = R_1' = CH_3$
2h :: R = R' = C_6H_{11}, $R_1 = R_1' = CH_3$
2i :: R = C_6H_{11}, R' = C_6H_5, $R_1 = R_1' = CH_3$
2j :: R = C_6H_{11}, R' = H, $R_1 = R_1' = CH_3$
2k :: R = R' = H, $R_1 = C_2H_5$, $R_1' = C_6H_5$
2l :: R = H, $R_1 = C_2H_5$, $R_1' = CH_2C_6H_5$
2m :: R = R' = H, $R_1 = C_2H_5$, $R_1' = C_6H_5$p(OMOM)
2n :: R = H, R' = C_6H_5, $R_1 = CH_2OSO_3Na$, $R_1' = CH_3$

Scheme 5. Synthesis of sulfated benzofuran dimers

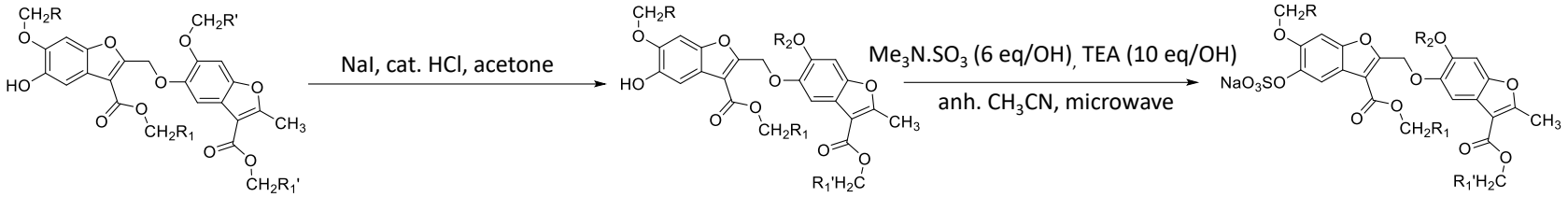

15d :: R = H, R' = C_6H_4p(OMOM), $R_1 = R_1' = CH_3$
15e :: R = H, R' = C_6H_4m(OMOM), $R_1 = R_1' = CH_3$

16a :: R = H, $R_1 = R_1' = CH_3$, $R_2 = C_6H_4$m(OH)
16b :: R = H, $R_1 = R_1' = CH_3$, R_2 = H

2o :: R = H, $R_1 = R_1' = CH_3$, $R_2 = C_6H_4$m(OSO_3Na)
2p :: R = H, $R_1 = R_1' = CH_3$, $R_2 = SO_3Na$

Scheme 6. Synthesis of sulfated benzofuran dimers

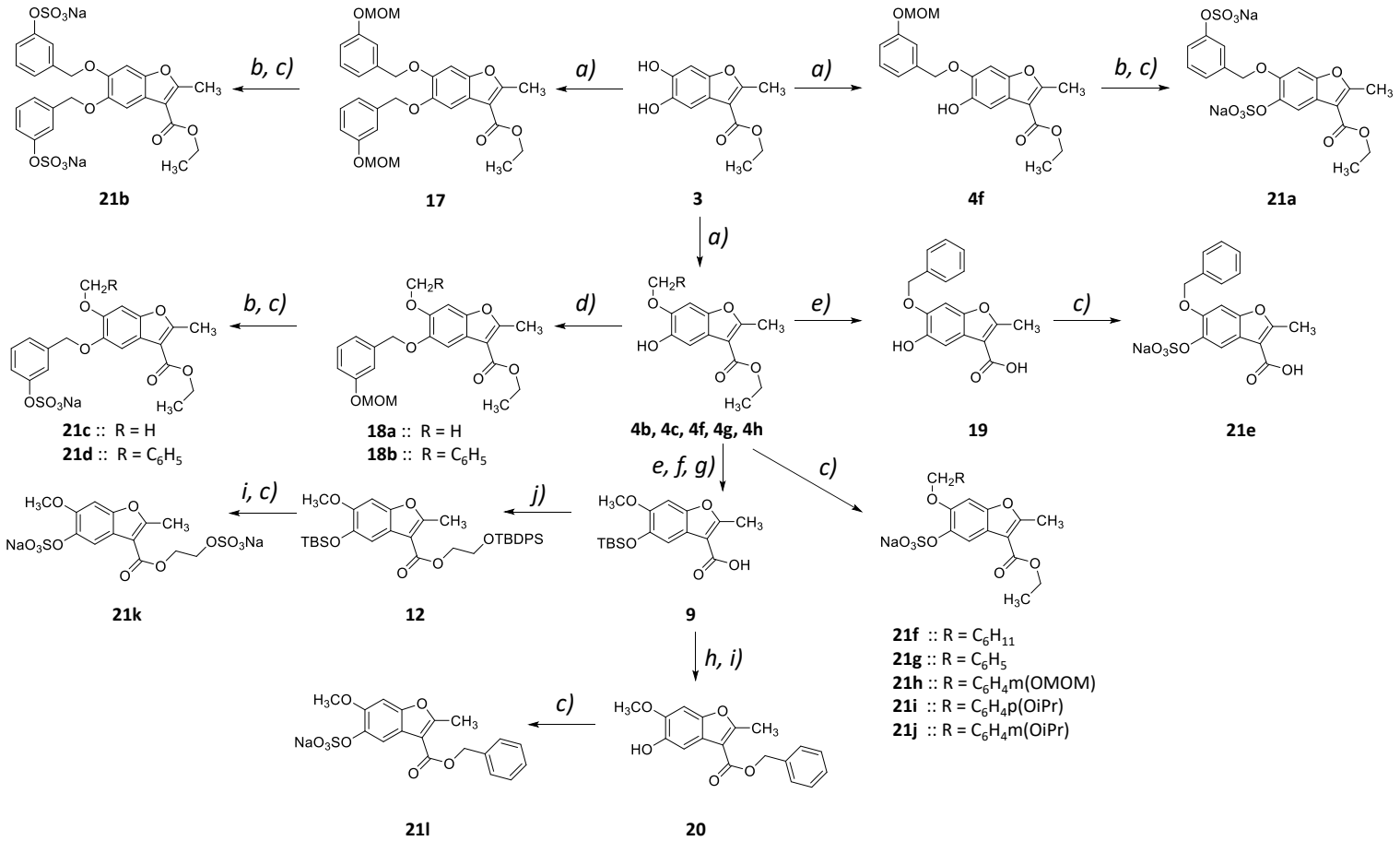

Scheme 7. Synthesis of sulfated benzofuran monomers

Conditions**.** *a)* Cs_2CO_3, alkyl halide, anh. DMF; *b)* NaI, cat. HCl, acetone; *c)* $Me_3N.SO_3$ (6 eq/OH), anh. CH_3CN, TEA (10 eq/OH), microwave; *d)* K_2CO_3, akyl halide (1.5 eq), acetone; *e)* LiOH (8 eq), $MeOH/H_2O$; *f)* TBDMSCl, TEA, EtOAc; *g)* NaOH, THF/H_2O; *h)* Cs_2CO_3, BnBr(1.5 eq), anh. CH_3CN; *i)* TBAF (1.5 eq), THF; *j)* DCC, DMAP, $HOCH_2CH_2OTBDPS$.

2.3.3 Thrombin Inhibition by SBMs and SBDs.

A chromogenic substrate hydrolysis assay utilizing spectrozyme TH was used to determine the thrombin inhibitory potential of the synthesized compounds in a 20 mM Tris buffer pH 7.4, containing 100 mM NaCl, 2.5 mM $CaCl_2$, and 0.1% polyethylene glycol (PEG) 8000 at 25 °C using a microplate reader (FlexStation III, Molecular Devices) as previously reported.[133] The assay measures the decrease in the initial rate of hydrolysis in the presence of inhibitor to determine the inhibitory potency of potential inhibitors. After an initial screening at a concentration of 300 μM for SBDs and 500 μM for SBMs, compounds that resulted in > 50% reproducible inhibition of coagulation enzyme had their IC_{50} values determined. For IC_{50} determination, stocks of the compounds were serially diluted to give about 24 different aliquots in the wells with final concentrations ranging from 200 – 0.02 μM. Nonlinear curve fitting resulted in IC_{50}, ΔY (efficacy) and HS values.

Of the SBDs, all the monosulfated compounds demonstrated reasonable thrombin inhibition ranging from 2 to 9 μM. Importantly, 11 of the analogs were 2-3 fold more potent than the prototype. Based on our modeling studies, we were expecting more potent compounds, but this was not achieved. However, the results demonstrate that structural modifications to this scaffold can result in compounds with improved potency. Also, the results suggest that structural modifications resulted in compounds that interacted with thrombin in an essentially different manner compared to the prototype. Regarding the level of sulfation, only one of the three disulfated analogs inhibited thrombin, albeit at about 2 fold lower than the prototype. The remaining two analogs were inactive at the highest concentration tested (200 μM). This agrees

with our earlier observation that an additional sulfate group on the benzofuran dimer scaffold is detrimental to thrombin inhibition potential and that hydrophobicity is a key factor in the thrombin inhibition by SBDs. The most striking observation with these new analogs was that, though some of these inhibitors had similar potencies, there were significant differences in their efficacies (ΔY values). Some compounds demonstrated 50 - 60 % thrombin inhibition at saturating inhibitor concentrations, whilst others showed almost 100% thrombin inhibition. This result confirmed our hypothesis that we could achieve inhibitors that resulted in regulation of thrombin activity, rather than total inhibition. An analysis of the structural differences revealed an interesting structure activity relationship. Compounds **2b-g** which had an aromatic group at the R' position and a methyl at the R position exhibited submaximal thrombin inhibition of about 60%. However, the presence of a cyclohexylmethyl group at R position, compounds **2h-j**, resulted in a significant increase in the inhibitory efficacy to greater than 85%. Altogether, these results demonstrate that structural changes can be taken advantage of in improving and fine-tuning the activity of this class of thrombin inhibitors.

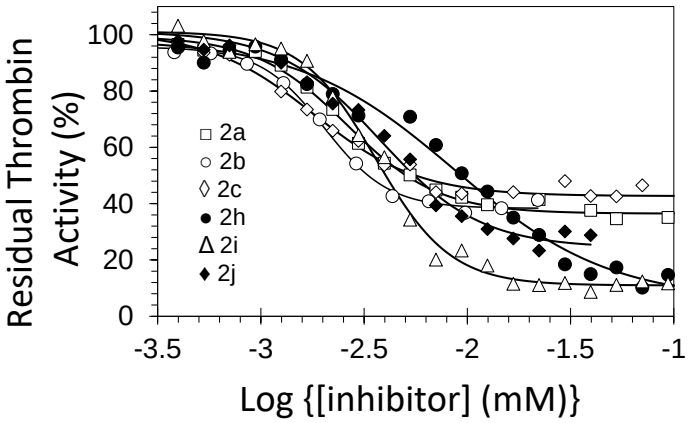

Figure 25. Inhibition of thrombin by SBDs.

Table 4. Inhibition of human thrombin by SBDs

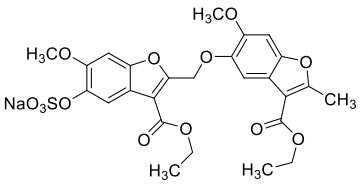

1

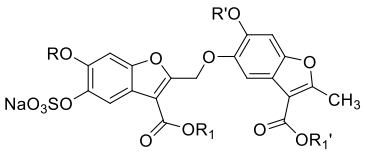

2a-p

	R	R’	R_1	R_1’	IC_{50} (μM)	ΔY (%)
1	Me	Me	Et	Et	6.2±2.7	75±1
2a	Me	$C_6H_{11}CH_2$	Et	Et	2.6±0.1	63±1
2b	Me	$C_6H_5CH_2$	Et	Et	2.0±0.1	57±1
2c	Me	$C_6H_5CH_2CH_2$	Et	Et	1.8±0.1	58±1
2d	Me	*p*-OMOM-$C_6H_5CH_2$	Et	Et	3.3±0.2	61±2
2e	Me	*m*-OMOM-$C_6H_5CH_2$	Et	Et	4.0±0.5	59±5
2f	Me	*p*-O-*i*Pr-$C_6H_5CH_2$	Et	Et	2.3±0.1	74±3
2g	Me	*m*-O-*i*Pr-$C_6H_5CH_2$	Et	Et	2.6±0.1	57±1
2h	$C_6H_{11}CH_2$	$C_6H_{11}CH_2$	Et	Et	8.7±0.8	93±4
2i	$C_6H_{11}CH_2$	$C_6H_5CH_2$	Et	Et	3.6±0.1	90±2
2j	$C_6H_{11}CH_2$	Me	Et	Et	3.8±0.3	77±3
2k	Me	Me	Et	$C_6H_5CH_2$	4.9±0.2	68±2
2l	Me	Me	Et	$C_6H_5CH_2CH_2$	3.2±0.2	58±3
2m	Me	Me	Et	*p*-OMOM-$C_6H_5CH_2$	2.6±0.1	66±2
2n	Me	$CH_2CH_2OSO_3Na$	$C_6H_5CH_2$	Et	14±0.5	74±2
2o	Me	*m*-OSO_3Na-$C_6H_5CH_2$	Et	Et	>300	ND
2p	Me	OSO_3Na	Et	Et	>300	ND

It is worth noting that these compounds were specific for thrombin inhibition and did not inhibit the proteolytic activity of the closely related FX and FXIa at the highest concentrations tested of 200 μM. To further understand the differences in thrombin inhibition observed, the two most potent compounds belonging to each group of the inhibitors showing variable efficacy, **2c** and **2i**, were selected for further biochemical studies.

Of the 12 SBMs, four monosulfated compounds exhibited a potencies that were an improvement over our SBM prototype that had an IC_{50} of 520 μM, [133] (Table 5) although not in the range of the dimers. The active compounds had IC_{50} values ranging from 134 to 229 μM. The structural difference between the SBM prototype and the best among the new SBMs, is the substitution of the *p*-methoxybenzoyl group with a benzyl group at the R position, which indicates that a more hydrophobic moiety is preferred. The only tolerable substitution on the aromatic group at the R position was a meta position OMOM group. All other substitutions on the aromatic ring led to compounds with $IC_{50} > 500$ μM. This shows that the presence of an unsubstituted aromatic group at this position is vital for the thrombin inhibitory activity of the SBMs. The other active SBMs had benzyl groups at the R' and R positions, thus highlighting the usefulness of hydrophobic groups for anti-thrombin activity. It is worth noting that none of the disulfated SBMs were active against thrombin at the highest concentration tested.

Table 5. In vitro inhibition of human thrombin by SBMs

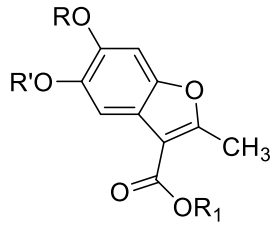

Comp.	R	R'	R_1	IC_{50} (μM)	ΔY (%)	HS
Prot.	*p*OMe-Bz [b]	SO_3Na	Et	520±280[c]	54 [c]	NA[d]
21a	*m*OSO_3Na-Bn[e]	SO_3Na	Et	>500	ND	ND[f]
21b	*m*OSO_3Na-Bn	*m*OSO_3Na-Bn	Me	>500	ND	ND
21c	Me	*m*OSO_3Na-Bn	Et	134±28	101±29	3.4±1.5
21d	Bn	*m*OSO_3Na-Bn	Et	> 500	ND	ND
21e	Bn	SO_3Na	Na	> 500	ND	ND
21f	$C_6H_{11}CH_2$	SO_3Na	Et	> 500	ND[c]	ND
21g	Bn	SO_3Na	Et	134±5	72.0±3.9	5.3±1.7
21h	*m*OMOM-Bn	SO_3Na	Et	229±37	75.9±11.4	2.6±0.7
21i	*p*O-*i*Pr-Bn	SO_3Na	Et	> 500	ND	ND
21j	*m*O-*i*Pr-Bn	SO_3Na	Et	> 500	ND	ND
21k	Me	SO_3Na	$CH_2CH_2OSO_3Na$	> 500	ND	ND
21l	Me	SO_3Na	Bn	168±18	95±33	3.7±1.3

2.3.4 Mechanisms of Thrombin Inhibition by 2c and 2i.

To determine the mechanism of thrombin inhibition by these thrombin inhibitors, Michaelis-Menten kinetics was performed. In this experiment, two parameters the, V_{MAX} and the $K_{M,}$ are determined from the hyperbolic profile obtained after measuring the initial rate of the hydrolysis of chromogenic substrate at different concentrations, both in the presence and absence of inhibitor. The data was fitted by the Michaelis-Menten equation to obtain the K_M and V_{MAX}. The values of the K_M and V_{MAX} at different inhibitor concentrations give an indication of the mechanism of inhibition. A constant V_{MAX} and an increase with increasing inhibitor concentration is suggestive of orthosteric inhibition where the substrate and the inhibitor compete for the same binding site. In classical non-competitive inhibition, the K_M remains unchanged whereas the V_{MAX} decreases with increasing inhibitor amounts. Other inhibition mechanisms include the mixed inhibition mechanism, where the K_M increases with a decrease in V_{MAX}, and the uncompetitive inhibition mechanism that presents with a decrease in the both K_M and V_{MAX} with increasing concentration of the inhibitor. The results from this experiment revealed an interesting difference between the two compounds.

For **2c**, in the absence of the inhibitor, the K_M and V_{MAX} for spectrozyme TH were 51.0± 2.8 mAU/min and 9.3± 2.8 μM, respectively. In the presence of 1, 2, 10 and 40 μM of the inhibitor, the V_{MAX} decreased consistently with values of 44.1 ± 2.7, 41.0 ± 2.6, 30.9 ± 1.2 and 23.7 ± 1.3 mAU/min respectively. $K_{M,}$ on the other hand, remained fairly unchanged having values of 9.3 ± 2.8, 8.3 ± 2.1, 9.2 ± 2.4, 7.4 ± 1.2 and 6.8 ± 1.6 μM. This is characteristic of a non-competitive allosteric mechanism where binding of the inhibitor does not increase or decrease binding affinity of the chromogenic substrate for the enzyme. This is the mechanism that was observed with our prototype SBD.

Similarly, in the presence of 1, 2, 10 and 40 µM of **2i**, the V_{MAX} values obtained were 43.8 ± 2.4, 38.7 ± 1.5, 32.5 ± 2.8 and 26.5 ± 1.8 mAU/min, respectively, indicating a decrease upon increasing inhibitor concentrations. In contrast to **2c,** however, the values of K_M in the presence of the same concentrations of **2i** gradually increased with values of 8.8 ± 2.0, 10.7 ± 1.0, 29.7 ± 8.1 and 61.0 ± 10.9 µM, respectively. This demonstrates that the binding of **2i** to thrombin affects the binding of the chromogenic substrate to the catalytic site of the enzyme. This mechanism is known as mixed inhibition and could be the reason for the close to total thrombin inhibition observed with **2i**. These results are very interesting and demonstrate that structural changes to the scaffold can result in compounds that interact in very different ways with thrombin.

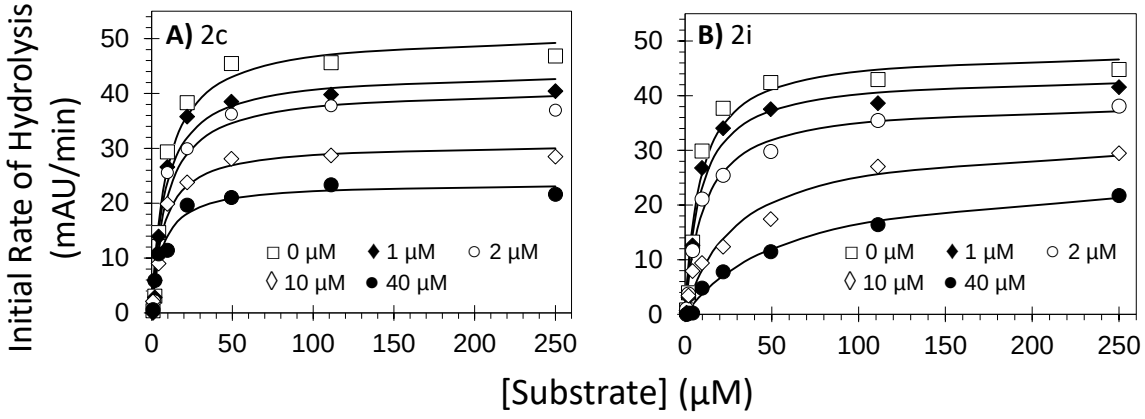

Figure 26. Michaelis-Menten kinetics profiles of (A) **2c** and (B) **2i**.

Table 6. Michaelis-Menten Kinetics of thrombin inhibition by **2c** and **2i**

Conc. (μM**)**	V_{MAX} (mAU/min)	K_M (μM)
2c		
0	51.0 ± 2.8	9.3 ± 2.8
1	44.1 ± 2.7	8.3 ± 2.1
2	41.0 ± 2.6	9.2 ± 2.4
10	30.9 ± 1.2	7.4 ± 1.2
40	23.7 ± 1.3	6.8 ± 1.6
2i		
0	48.2 ± 2.8	8.6 ± 2.8
1	43.8 ± 2.4	8.8 ± 2.0
2	38.7 ± 1.5	10.7 ± 1.
10	32.5 ± 2.8	29.7 ± 8.1
40	26.5 ± 1.8	61.0 ± 10.9

2.3.5 Thermodynamic Binding Affinity of 2c and 2i for Thrombin.

The binding of thrombin to the inhibitors was determined using a fluorimetric method, where the changes in fluorescence of fluorescein labeled thrombin and unmodified human thrombin were monitored as a function of inhibitor concentrations in a 20 mM Tris Buffer pH 7.4 containing 100 mM NaCl, 2.5 mM $CaCl_2$, and 0.1% PEG 8000 at 25 °C, as previously described. There was a gradual decrease in the fluorescence to a saturation point on increasing inhibitor concentrations. The data when fitted to a quadratic curve, gave binding affinities of 3.7 ± 0.3 and 1.0 ± 0.1 μM for **2c** and **2i,** respectively, for fluorescein labeled thrombin and 2.8 ± 0.3

for **2c** for unmodified human thrombin. These values are in agreement with their inhibitory potencies.

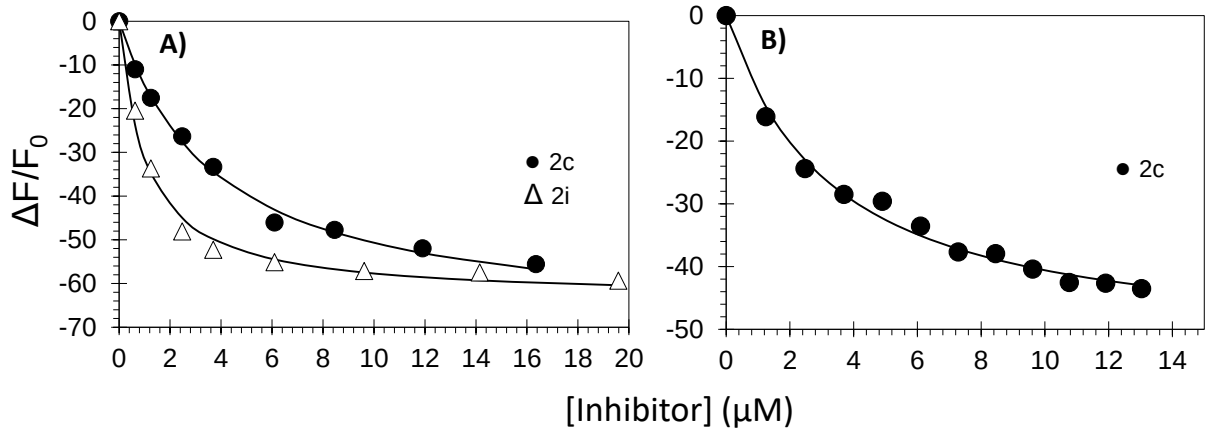

Figure 27. Binding of SBDs to thrombin (A) fFPRCK-thrombin and (B) human plasma thrombin.

Table 7. Binding affinity **2c** and **2i** for thrombin

Cpd.	KD (μM)	DFmax
f FPRCK-thrombin		
2c	3.7 ± 0.3	-69.8 ± 1.8
2i	1.0 ± 1	-63.4 ± 1.5
Human plasma thrombin		
2c	2.8 ± 0.3	-57.9 ± 1.8

2.3.6 Binding Sites of 2c and 2i

It is well documented that thrombin possesses allosteric sites in addition to its active site.[243,244] Two electropositive anion binding sites, designated exosites I and II, have been well studied.[245,246] Fibrinogen, a major substrate for thrombin, binds at exosite I. In addition, hirudin the naturally occurring peptide obtained from leeches, binds to this exosite.[246] The exosite II of thrombin is known to be the site of thrombin interaction with unfractionated heparin.[246] To identify the thrombin binding sites of these two inhibitors, competition studies with hirudin peptide and unfractionated heparin were performed. This involved determining the potencies of the inhibitors in increasing concentrations of the known thrombin binders. Significant changes in potency are indicative of competition for thrombin binding at specific exosites.

The presence of increasing concentrations of hirudin peptide had no effect on the IC_{50} values of both **2c** and **2i.** This implies that both of these compounds do not utilize exosite I of thrombin for interaction and achieving inhibition.

In terms of binding at exosite II, the observations are different for the two inhibitors. The potency of **2c** was significantly affected by the presence of UFH, with an 11 fold decrease in potency observed in the presence of 50 μM of heparin. This indicates a competition with the UFH binding site, exosite II. In contrast, the presence of similar concentrations of UFH had no effect on the inhibitory potency of **2i**. This is interesting for a number of reasons. Firstly, it indicates that these two compounds interact differently with thrombin and supports the observation that the two compounds utilize different mechanisms for thrombin inhibition. In addition, it further indicates that **2i** interacts with thrombin residues other than the ones utilized primarily by both hirudin peptide and UFH for interacting with thrombin. This is an interesting result that is worth pursuing, as it may shed more light on the SAR of these compounds.

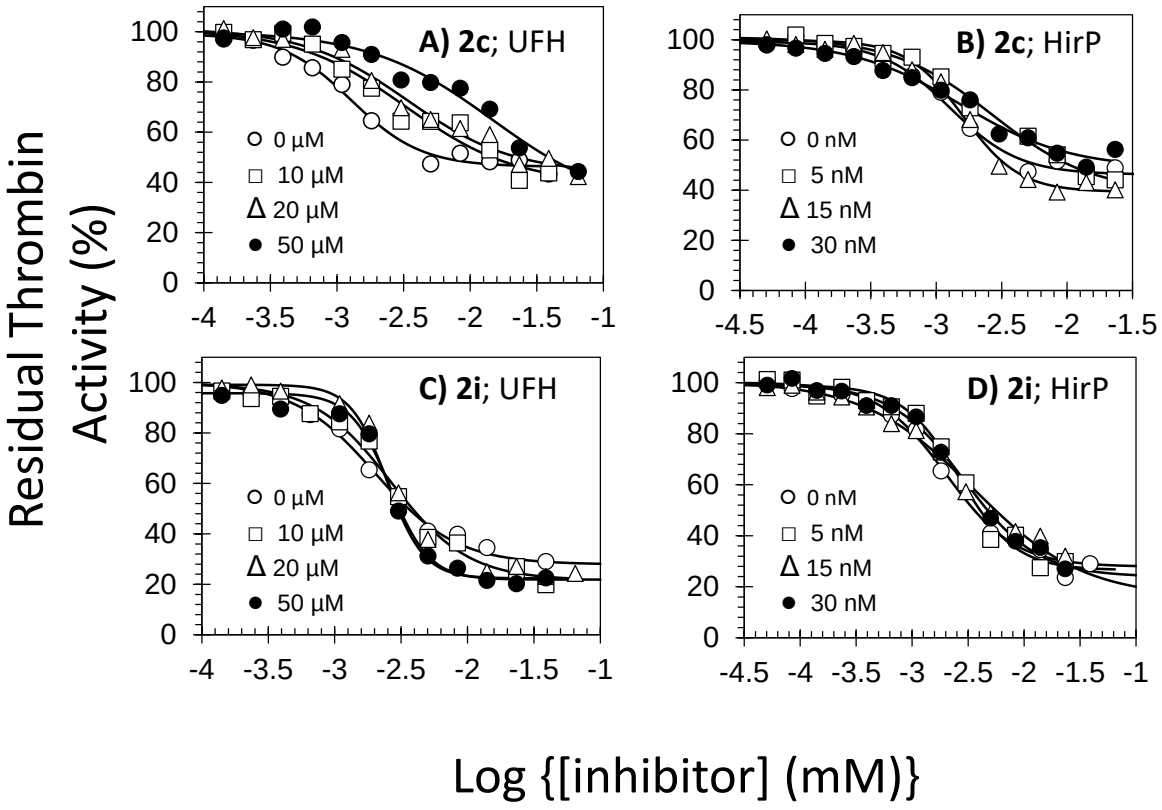

Figure 28. Competitive inhibition studies of **2c** and **2i** in the Presence of UFH and HirP.

Table 8. Inhibition of Human Thrombin by **2c** and **2i** in the Presence of UFH and HirP

	$IC_{50,\ app}$ (μM)	
[UFH] (μM)	**2c**	**2i**
0	1.3 ± 0.1	2.0 ± 0.2
10	3.3 ± 0.7	2.7 ± 0.2
20	3.4 ± 0.5	2.8 ± 0.1
50	14.5 ± 4.9	2.6 ± 0.1
[HirP] (nM)		
0	1.3 ± 0.1	2.0 ± 0.2 [b]
5	2.7 ± 0.4	2.6 ± 0.2
15	1.6 ± 0.1	3.6 ± 0.4
30	1.5 ± 0.3	2.9 ± 0.2

2.3.7 Inhibition of Thrombin Mutants by 2c and 2i.

Studies utilizing thrombin mutants carried out to further elucidate the binding site of these molecules on thrombin revealed interesting results. The mutants utilized were obtained from the Rezaie lab and had most exosite II Arg and Lys residues mutated to Ala.[247] These mutants permit the study of ionic interaction with our sulfated compounds and allow the identification of residues contributing most to the interaction with the molecules, giving an indication of the binding sites. The IC_{50} of benzofuran compounds against recombinant mutants of thrombin was measured using the chromogenic hydrolysis, as previously described in a 96-well format, and the differences from those of the mutants compared to the wild type enzyme.

For **2c**, there were virtually no differences observed between the wild type and the mutants with the exception of two residues, R233 and K235, which demonstrated subtle changes

in potency upon mutation (Figure 29). This observation is significantly different from what was observed from the prototypical compound, which was demonstrated to be interacting with thrombin around the Arg173 residue and explains why the two compounds may have different efficacies for thrombin inhibition. This is, however, not surprising, as our earlier work has shown that benzofuran compounds may utilize different thrombin exosite II sites for interaction.[135] Also, the results indicate that our discovery is serendipitous as the mutant studies do not support our molecular model for the SBD-thrombin interaction. However, it does supports our hypothesis that hydrophobic groups play a crucial role in thrombin inhibition by **2c**. The lack of any inhibitory activity of the unsulfated phenolic precursor of **2i** continues to emphasize the importance of the sulfate group.

2i on the other hand showed about two fold differences in potency observed in a number of mutants. This indicates the possibility of a different number of binding modes for the compound and may explain the reason behind it demonstrating a mixed inhibition mechanism. Thus, again, studies on the benzofuran scaffold indicate that subtle structural changes can significantly affect the inhibition potential and mechanism for thrombin inhibition.

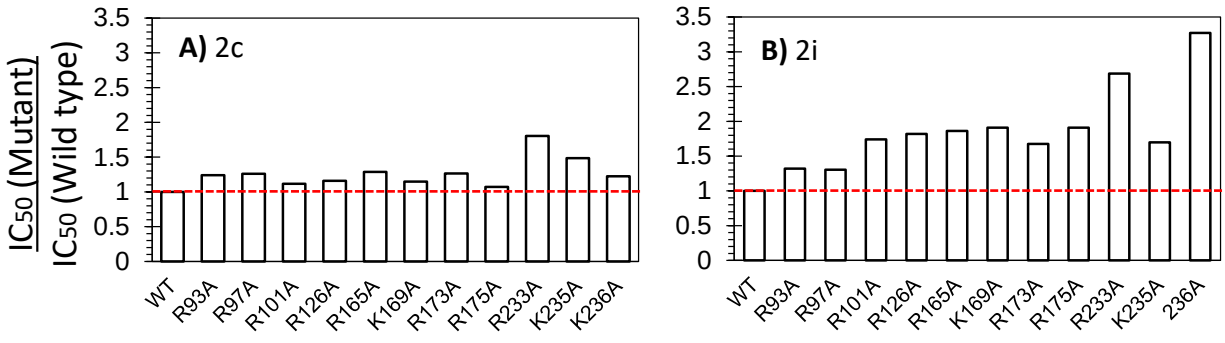

Figure 29. Inhibition of thrombin mutants by (A) **2c** and (B) **2i**.

Table 9. Inhibition of thrombin mutants by **2c** and **2i**

Mutant	IC50	IC50 – Mutant / IC50 - Wildtype
2c		
WT	0.94 ± 0.05	1.00
R93A	1.16 ± 0.05	1.24
R97A	1.18 ± 0.06	1.26
R101A	1.05 ± 0.07	1.12
R126A	1.09 ± 0.1	1.16
R165A	1.21 ± 0.04	1.29
K169A	1.07 ± 0.02	1.15
R173A	1.18 ± 0.11	1.26
R175A	1.00 ± 0.09	1.07
R233A	1.69 ± 0.09	1.80
K235A	1.39 ± 0.1	1.48
K236A	1.15 ± 0.04	1.22
2i		
WT	3.32 ± 0.39	1.00
R93A	4.38 ± 0.5	1.32
R97A	4.33 ± 1.1	1.30
R101A	5.78 ± 0.33	1.74
R126A	6.04 ± 3.09	1.82
R165A	6.18 ± 0.78	1.86
K169A	6.34 ± 3.18	1.91
R173A	5.56 ± 0.57	1.67
R175A	6.34 ± 0.38	1.91
R233A	8.92 ± 1.45	2.69
K235A	5.64 ± 0.43	1.70
K236A	10.86 ± 0.92	3.27

2.3.8 Plasma Clotting Studies of 2c And 2i.

The activated partial thromboplastin time and prothrombin time tests are plasma clotting assays employed to determine the anticoagulant properties of potential anticoagulants.[248] The APTT assay assesses the effect on the intrinsic coagulation pathway, whereas the PT assay is for the extrinsic pathway. These assays are routinely performed and provide vital information on the possible use of inhibitors as anticoagulants. In both assays, the times to double the APTT and PT were determined as previously reported.[133] The concentration of **2c** required to double the APTT was 580 µM and that for **2i** was > 660 µM. These values appear to be higher than expected, and are possibly due to interaction of the inhibitor with plasma proteins including albumin. Interestingly, at the highest concentrations tested, none of the inhibitors doubled the PT. Again, binding to plasma proteins may play a role in this.

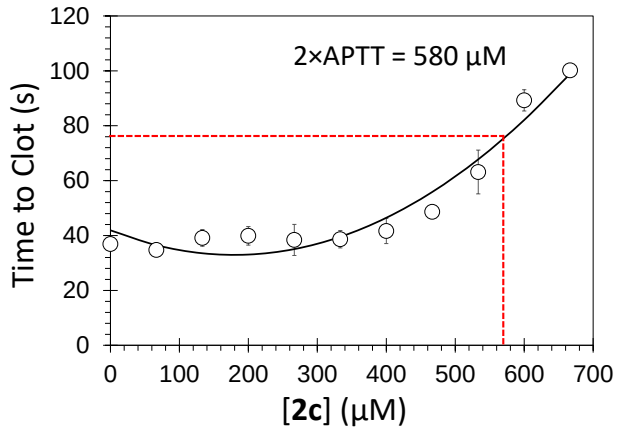

Figure 30. APTT assay for **2c**.

2.3.9 Inhibition of Thrombin's Cleavage of Fibrinogen by 2c and 2i

In order to demonstrate whether the partial inhibitory effect shown by **2c** with the chromogenic substrate would be reproducible with fibrinogen, an in vivo thrombin substrate, we utilized gel electrophoresis. With this, we measured the cleavage of fibrinogen by thrombin in the presence and absence of increasing and saturating concentrations of the two thrombin inhibitors using densitometric analysis of the bands at 320 KDa . A dose dependent inhibition of fibrinogen cleavage by thrombin was observed for both **2c** and **2i.** As in the case of the chromogenic

substrate, a significant difference in the efficacy of inhibition was observed. At saturating levels of **2c**, inhibition of fibrinogen cleavage reached a maximum of about 70±8 % whereas in the presence of inhibitor **2i**, inhibition was found to be greater than 90%. The IC50s calculated based on these PAGE profiles were 8.8 and 17.1 µM for **2c** and **2i**, respectively. These numbers are higher than the corresponding IC_{50}s measured using chromogenic substrate hydrolysis assays. It is possible that macromolecular fibrinogen in the milieu sequesters some proportion of the two small allosteric SBDs, which reduces their free concentration responsible for inhibitory action. These results support the idea that partial protease inhibition may be useful in reducing the side effect of prolonged bleeding associated with current anticoagulants.

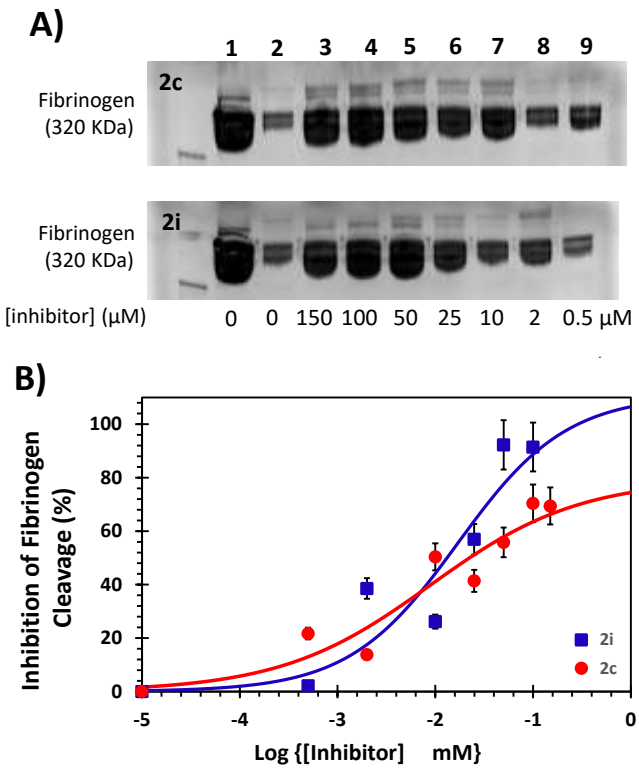

Figure 31. Inhibition of thrombin fibrinogen cleavage by **2c** and **2i.** (A) A representative PAGE (B) Semi-log plot of inhibition.

2.4 Conclusion

The importance of thrombin in coagulation is one that cannot be overemphasized. Its role has made it an important target in the development of anticoagulants. Though the clinically approved direct thrombin inhibitors have improved therapeutic profiles over the vitamin K antagonists and heparin, the associated bleeding risk calls for a continuous search for the ideal anticoagulant.

Computational screening of a virtual library of SBDs, based on a prototypical SBD showing submaximal thrombin inhibition at saturating conditions, led to development of a new generation of sulfated benzofuran compounds. These compounds were synthesized in pure forms, employing protection and deprotection strategies, S_N2 substitution reactions, DCC coupling, ester hydrolysis and radical bromination among others. Biochemical studies revealed compounds that bind to and inhibit thrombin with even lower efficacies than the prototype. Michaelis-Menten kinetics, competitive binding studies using allosteric site binders, and studies using thrombin mutants point to an allosteric inhibition mechanism.

Finally, studies using fibrinogen, a physiological macromolecular substrate of thrombin show the maintenance of this phenomenon with the substrate. This work thus puts forward compound **2c** as the first small molecule allosteric thrombin inhibitor that shows submaximal inhibition of protease cleavage of a macromolecular substrate and provides support for the concept that inhibitors showing submaximal thrombin inhibition may yield safer anticoagulants. Studies using animal models will be important in ascertaining the benefits of submaximal inhibition in vivo.

2.5 Experimental Section

2.5.1 General Methods

2.5.1.1 Computational Tools

SYBYL-X2.1 (Cetera) and GOLD v5.2 (Cambridge Crystallographic Data Centre, Cambridge, U.K.) were used in computational study of sulfated benzofuran-thrombin interaction.

2.5.1.2 Chemicals, Reagents, Enzymes, and Substrates

Anhydrous organic solvents were obtained from Fisher (Pittsburgh, PA) or Sigma-Aldrich (Milwaukee, WI). Acetone-d_6, $CDCl_3$, and DMSO-d_6 for NMR were purchased from Sigma Aldrich. Other chemicals used were of reagent grade or higher. Analytical TLC was performed using UNIPLATE^{TM} silica gel GHLF 250 μm pre-coated plates (ANALTECH, Newark, DE). Flash chromatography was performed using Teledyne ISCO (Lincoln, NE) with mobile phase gradients of ethyl acetate/hexanes and CH_2Cl_2/CH_3OH at flow rates ranging from 18 to 35 ml/min. Silica gel (200-400 mesh, 60 Å) was from Sigma-Aldrich. Air or moisture sensitive reactions were performed under nitrogen atmosphere in well-dried glassware. Human thrombin, fluorescein-labeled (f FPRCK-) thrombin, factor Xa, and factor XIa were obtained from Haematologic Technologies (Essex Junction, VT). Stock solutions of serine proteases (thrombin, factor Xa, and factor XIa) were prepared in 20 mM TrisHCl buffer, pH 7.4, containing 100 mM NaCl, 2.5 mM $CaCl_2$ and 0.1% PEG8000. Chromogenic substrates of thrombin (Spectrozyme TH) and factor Xa (Spectrozyme FXa) were obtained from Sekisui Diagnostics (Lexington, MA). The chromogenic substrate of factor XIa (Chromogenix S-2366) was from DiaPharma (West Chester, OH). Bovine unfractionated heparin was from Sigma Aldrich, hirudin peptide (HirP, [5F]-Hir-(54–65)-(SO_3^-)) was from Anaspec (Fremont, CA) and human plasma fibrinogen was from EMD Millipore (Darmstadt, Germany).

2.5.2 Molecular Modeling Studies

The crystal structure of thrombin bound to hirugen, its exosite I ligand, was obtained from the protein data bank (3EQ0). The protein structure was prepared in Sybyl, using the Biopolymer structure preparation tool as previously described.[134] Briefly, hirugen, and other substructures including water molecules were extracted from the crystal structure. Next, side chains were fixed, followed by the setting of protonation types of charged residues to their physiological relevant states. Hydrogen atoms were then added, followed by minimization, using the Tripos Force Field and Gasteiger Hückel charges. (Dielectric constant ε = 4; gradient = 0.05 kcal/ (mol ×Å); number of iterations = 1×10^5).

A virtual benzofuran library, containing about 100 molecules was also generated in Sybyl, ensuring assignment of appropriate atom types to all atoms. For sulfate groups, sulfur atom = S.o2; terminal oxygen atoms = O.co2. Hydrogen atoms were subsequently added and the resulting virtual compounds were energy minimized using the Tripos Force Field as for the protein.

Docking and scoring of the sulfated benzofuran dimer prototype was done using GOLD v5.2 (Cambridge Crystallographic Data Centre, Cambridge, U.K.), as previously reported.[134] The putative binding site defined to include all atoms in a radius of 22 Å around the alpha carbon atom of thrombin's Arg173 residue. A hydrogen bonding constraint was set to promote hydrogen bonding between the ligands and the guanidinium hydrogens of the Arg173 residue and a penalty of 10 was enforced in the absence of such an interaction. The number of GA runs per ligand was set to 100 to enable comprehensive docking of the ligands. Early termination was disallowed to allow the generation of all docked solutions. To enable a comprehensive analysis of the docking and scoring, solutions within 1.5 and 2.5 Å of each other were grouped into clusters. All

remaining parameters were kept at their default values. ChemPLP scoring was employed as the primary scoring function, and rescoring of docked solutions was done using GoldScores.

The following were taking into consideration in the docking and scoring of the ligands. Interaction of the Arg173 residue and the sulfate group of the ligand, the number of different clusters identified, the number of solutions per cluster and the ChemPLP scores and GoldScores. Further, a manual inspection of the docked poses was performed to analyze and identify interesting protein ligand interactions.

2.5.3 Chemical Characterization of Sulfated Benzofurans.

A Bruker-400 MHz spectrometer was used to record the ^{1}H and ^{13}C NMR of compounds in $CDCl_3$, acetone-d_6 or DMSO-d_6. Signals, in part per million (ppm), are relative to the residual peak of the solvent. The NMR data are reported as chemical shift (ppm), integration, multiplicity of signal (s= singlet, d= doublet, t= triplet, q= quartet, dd= doublet of doublet, m= multiplet), and coupling constants (Hz). A Waters Acquity TQD MS spectrometer was used in recording ESI-MS of compounds. MS of intermediate compounds was determined in positive ion mode and final products in negative ion mode. Samples, dissolved in methanol, were infused at rates of approximately 20 – 40 μL/min, and ionization conditions optimized for each sample to maximize ionization.

2.5.4 Purity Analysis of Synthesized Compounds

Sulfated benzofuran compounds were analyzed by UPLC with a Waters Acquity H-class UPLC system equipped with a photodiode array detector and triple quadrupole mass spectrometer. A reversed-phase Waters BEH C18 column of particle size 1.7 μm and 2.1 mm × 50 mm dimensions at 30±2 °C was used. All final compounds were obtained with purity of

>95% purity. Spectral data are provided below. Representative ^{1}H NMR, ^{13}C NMR, and MS profiles of the final products are also provided.

2.5.5 Synthetic Procedure and Spectral Characterization Data

2.5.5.1 Synthesis of 4a-f

To a solution of **3** (500 mg, 2.12 mmol, 1.0 equiv.) in DMF were added cesium carbonate (345mg, 1.06 mmol, 0.5 equiv.) and benzyl/alkyl halide (1.91 mmol, 0.9 equiv.). The reaction mixture was stirred under an atmosphere nitrogen for 18 hours. The reaction was quenched with 2N HCl and extracted with ethyl acetate. The organic layer was dried using Na_2SO_4 and evaporated to dryness. The residue was purified on silica gel (5 – 20% EtOAc in Hexanes) and dried under vacuum to give **4a-h** in 45-55% yield.

4a. ^{1}H NMR (400 MHz, $CDCl_3$): 7.40 (s, 1H), 6.91 (s, 1H), 5.50 (s, 1H), 4.33 (q, *J* = 7.1 Hz, 3H), 3.88 (s, 3H), 2.67 (s, 3H), 1.38 (t, *J* = 7.1 Hz, 2H).

4b. ^{1}H NMR (400 MHz, $CDCl_3$): 7.39 (s, 1H), 6.88 (s, 1H), 5.52 (s, 2H), 4.32 (q, *J* = 7.1 Hz, 2H), 3.80 (d, *J* = 6.0 Hz, 2H), 2.66 1.84 – 1.65 (m, 6H), 1.38 (t, *J* = 7.1 Hz, 3H), 1.30 – 1.02 (m, 5H). ^{13}C NMR (100 MHz, Acetone-d_6): 164.75, 162.74, 148.54, 146.56, 146.50, 145.32, 145.22, 119.49, 109.63, 106.75, 106.67, 96.37, 75.45, 60.61, 38.42, 27.18, 26.54, 14.69, 14.30.

4c. ^{1}H NMR (400 MHz, $CDCl_3$): 7.47 – 7.35 (m, 6H), 7.02 (s, 1H), 5.60 (s, 1H), 5.15 (s, 2H), 4.40 (q, *J* = 8.0 Hz, 2H), 2.71 (s, 3H), 1.43 (t, J = 8.0 Hz, 3H). ^{13}C NMR (100 MHz, Acetone-d_6):164.71, 163.03, 148.38, 145.99, 145.58, 137.91, 129.28, 128.80, 128.77, 120.09, 109.62, 107.15, 97.50, 71.89, 60.64, 14.68, 14.30.

4d. ^{1}H NMR (400 MHz, $CDCl_3$): 7.20 (s, 1H), 7.15 – 7.10 (m, 2H), 7.07 – 7.03 (s, 3H), 6.7 (s, 1H), 5.23 (s, 1H), 4.15 (q (t, J = 7.1 Hz, 2H), 2H), 4.07 (q, *J* = 6.8 Hz, 2H), 2.93 (t, *J* = 6.8 Hz, 2H), 2.48 (s, 3H), 1.20 (t, *J* = 7.1 Hz, 3H).

4e. ^{1}H NMR (400 MHz, Acetone-d_6): 7.60 (s, 1H), 7.48 – 7.46 (m, 2H), 7.40 (s, 1H), 7.25 (s, 1H), 7.08 – 7.06 (m, 2H), 5.22 (s, 2H), 5.17 (s, 2H), 4.37 (q, J = 7.1 Hz, 2H), 3.45 (s, 3H), 2.70 (s, 3H), 1.42 (t, J = 7.1 Hz, 3H). ^{13}C NMR (100 MHz, Acetone-d_6): 164.73, 163.00, 158.22, 148.38, 146.01, 145.64, 145.54, 130.96, 130.49, 128.77, 119.97, 117.01, 116.86, 109.62, 107.09, 107.00, 97.42, 95.06, 71.57, 60.65, 56.02, 14.69, 14.31.

4f. ^{1}H NMR (400 MHz, Acetone-d_6): 7.96 (s, 1H), 7.41 – 7.13 (m, 5H), 7.00 – 6.98 (m, 1H), 5.21 (s, 2H), 5.14 (s, 2H), 4.39 – 4.33 (m, 2H), 3.43 (s, 3H), 2.68 (s, 3H), 1.44 – 1.36 (m, 3H). ^{13}C NMR (100 MHz, Acetone-d_6): 164.71, 163.04, 158.54, 148.37, 145.98, 145.63, 139.48, 130.33, 121.95, 121.61, 120.13, 116.63, 116.56, 109.62, 107.22, 107.14, 97.53, 95.14, 71.71, 60.64, 14.68, 14.31.

4g. ^{1}H NMR (400 MHz, Acetone-d_6): 7.54 (s, 1H), 7.43 – 7.41 (m, 2H), 7.38 (s, 1H), 7.22 (s, 1H), 6.94 – 6.90 (m, 2H), 5.13 (s, 2H), 4.67 – 4.58 (m, 1H), 4.36 (q, J = 8.0 Hz, 2H), 2.68 (s, 3H), 1.40 (t, J = 8.0 Hz, 3H), 1.30 – 1.29 (m, 6H).^{13}C NMR (100 MHz, Acetone-d_6): 164.73, 162.96, 158.93, 148.40, 146.07, 145.68, 130.57, 129.55, 120.00, 116.49, 109.64, 107.07, 97.52, 71.78, 70.36, 60.63, 22.29, 14.68, 14.30.

4h. ^{1}H NMR (400 MHz, Acetone-d_6): 7.39 (s, 1H), 7.29 – 7.24 (m, 1H), 7.20 (s, 1H), 7.08 – 7.03 (m, 2H), 6.87 – 6.84 (m, 1H), 5.19 (s, 2H), 4.66 – 4.60 (m, 1H), 4.34 (q, J = 8.0 Hz, 2H), 2.66 (s, 3H), 1.40 (t, J = 8.0 Hz, 3H), 1.29– 1.29 (m, 6H). ^{13}C NMR (100 MHz, Acetone-d_6): 164.71, 163.02, 159.15, 148.37, 145.96, 145.90, 145.64, 145.54, 139.44, 130.33, 120.59, 120.08, 116.08, 116.04, 109.62, 107.19, 107.11, 97.49, 71.76, 70.24, 60.64, 22.28, 14.68, 14.30.

2.5.5.2 Synthesis of 5a-b

To a solution of **4a/b** (380 mg, 1.71 mmol, 1 equiv.) in DCM were added TBSCl (2.57 mmol, 1.5 equiv.) and imidazole (2.57 mmol, 1.5 equiv.) and the reaction stirred for 12 hours. The

reaction was quenched by adding H_20 and extracted with EtOAc. The organic extract was dried over Na_2SO_4, concentrated and purified on silica gel (0 – 10% EtoAc in hexanes) to give the product in 90% yield.

5a. ^{1}H NMR (400 MHz, $CDCl_3$): 7.32 (s, 1H), 6.86 (s, 1H), 4.30 (q, *J* = 7.1 Hz, 3H), 3.76 (s, 3H), 2.63 (s, 3H), 1.38 (t, *J* = 7.1 Hz, 2H), 0.95 (s, 9H), 0.09 (s, 6H). ^{13}C NMR (100 MHz, $CDCl_3$): 164.61 162.34, 149.60, 148.79, 118.62, 112.29, 108.93, 95.13, 60.07, 55.89, 25.77. 18.48, 14.31, -4.73.

5b. ^{1}H NMR (400 MHz, *Acetone-d_6*): 7.40 (s, 1H), 7.11 (s, 1H), 4.35 (q, *J* = 8.0 Hz, 2H), 3.84 (d, *J* = 8.0 Hz, 2H), 2.68 (s, 3H), 1.95 – 1.68 (m, 6H), 1.41 (t, *J* = 8.0 Hz, 3H), 1.32 – 1.08 (m, 5H), 1.05 (s, 9H), 0.20 (s, 6H). ^{13}C NMR (100 MHz, *Acetone-d_6*): 164.66, 162.87, 150.39, 149.79, 143.55, 119.08, 112.63, 109.60, 96.93, 75.13, 60.66, 38.79, 27.20, 26.53, 26.18, 18.98, 14.64, 14.23, -4.43.

2.5.5.3 Synthesis of 6a/b

Briefly, to a solution of **5a/b** in CCl_4 was added 1 equivalent of NBS and 0.1 equivalent of benzoylperoxide. The reaction was refluxed for 1.5 hrs and extracted with DCM. The DCM extract was dried in vacuo to obtain the bromominated precursors 6a/b in quantitative yield.

6a. ^{1}H NMR (400 MHz, $CDCl_3$): 7.35 (s, 1H), 6.90 (s, 1H), 4.87 (s, 2H), 4.34 (q, *J* = 7.1 Hz, 3H), 3.77 (s, 3H), 1.38 (t, *J* = 7.1 Hz, 2H), 0.94 (s, 9H), 0.09 (s, 6H).

6b. ^{1}H NMR (400 MHz, *Acetone-d_6*): 7.45 (s, 1H), 7.21 (s, 1H), 5.07 (s, 2H), 4.42 (q, *J* = 8.0 Hz, 2H), 3.89 (d, *J* = 8.0 Hz, 2H), 2.68 (s, 3H), 1.87 – 1.64 (m, 6H), 1.45 (t, *J* = 8.0 Hz, 3H), 1.30 – 1.0 (m, 5H), 1.06 (s, 9H), 0.22 (s, 6H). ^{13}C NMR (100 MHz, *Acetone-d_6*): 164.65, 164.60, 163.18, 162.88, 150.39, 149.70, 143.85, 143.51, 137.98, 129.23, 128.90, 128.80, 119.04, 112.84,

112.62, 109.59, 97.86, 96.89, 75.09, 71.74, 60.70, 60.67, 38.78, 27.19, 26.53, 26.17, 26.14, 18.98, 14.63, 14.24. -4.44.

2.5.5.4 Synthesis of 7 and 19

To a solution of **4a/c,** (450 mg, 1.80 mmol, 1 equiv.) in 80% (MeOH:H_2O) was added lithium hydroxide (14.40 mmol, 8 equiv.) and stirred for 24 hours. The reaction was quenched by the addition 2N HCl and extracted with EtOAc. The organic extract was dried with Na_2SO_4, concentrated and purified on silica gel (20 – 40% hexanes to give 4 in 60% yield.

7. ^{1}H NMR (400 MHz, *Acetone-d_6*): 7.40 (s, 1H), 7.15 (s, 1H), 3.91 (s, 3H), 2.70 (s, 3H).

19. ^{1}H NMR (400 MHz, *Acetone-d_6*): 8.52 (s, 1H), 6.95 – 6.85 (m, 4H), 6.78 (s, 1H), 7.25 (s, 1H), 4.69 (s, 2H), 2.18 (s, 3H). ^{13}C NMR (100 MHz, *Acetone-d_6*): 165.13, 161.53, 146.71, 145.12, 144.73, 137.01, 128.29, 127.71, 12.69, 118.91, 108.72, 106.29, 97.57, 70.36, 13.98.

2.5.5.5 Synthesis of 8

To a solution of **7** (380 mg, 1.71 mmol, 1 equiv.) in EtOAc were added TBSCl (902 mg, 5.98 mmol, 3.5 equiv.) and trimethylamine (0.83 ml, 5.98 mmol, 3.5 equiv.) and the reaction stirred for 12 hours. The reaction was quenched by adding H_20 and extracted with EtOAc. The organic extract was dried over Na_2SO_4, concentrated and purified on silica gel (0 – 10% EtoAc in hexanes) to give the product in 90% yield.

8. ^{1}H NMR (400 MHz, *DMSO-d_6*): 7.30 (s, 1H), 7.27 (s, 1H), 3.82 (s, 3H), 2.70 (s, 3H), 1.02 (s, 9H), 0.99 (s, 9H), 0.38 (s, 6H), 0.12 (s, 6H). ^{13}C NMR (100 MHz, *DMSO-d_6*): 164.50, 149.49, 148.75, 142.64, 112.34, 94.97, 55.73, 25.90, 25.80, 18.47, 17.91, 14.57, -4.39, -4.72.

2.5.5.6 Synthesis of 9

To a solution of **8** (580 mg, 1.29 mmol, 1 equiv.) in 80% THF:H_2O was added NaOH (51 mg, 1.29 mmol, 1 equiv.). The reaction was stirred for 15 minutes, quenched using 2N HCl and extracted using EtOAc. The organic extract was dried over Na_2SO_4, concentrated and purified on silica gel (0 – 40 % EtoAc in hexanes) to give the product in 90% yield.

9: ^{1}H NMR (400 MHz, *DMSO-d_6*): 7.29 (s, 1H), 7.27 (s, 1H), 3.82 (s, 3H), 2.54 (s, 3H), 1.00 (s, 9H), 0.14 (s, 6H). MS (ESI) calculated for $C_{17}H_{24}O_5Si$ $[(M+Na)]^+$, m/z 359.1291, found for $[(M+Na)]^+$, m/z 359.2057.

2.5.5.7 Synthesis of 10a-c

To a solution of **9** (400 mg, 1.24 mmol, 1 equiv.) in acetonitrile were added alkyl halide (1.86 mmol, 1.5 equiv.) and cesium carbonate (604 mg, 1.86 mmol, 1.5 equiv.). The reaction was stirred for 12 hours under nitrogen gas. The reaction was quenched using 2N HCl and extracted using EtOAc. The organic layer was dried over Na_2SO_4 and purified on silica gel (0 – 10 % EtOAc in hexanes) to give the product in 80 - 85% yield.

10a. ^{1}H NMR (400 MHz, Acetone-*d_6*): 7.55 – 7.52 (m, 2H), 7.45 – 7.36 (m, 3H), 7.32 (s, 1H), 7.15 (s, 1H), 5.37 (s, 2H), 3.86 (s, 3H), 2.70 (s, 3H), 0.98 (s, 9H), 0.10 (s, 6H). ^{13}C NMR (100 MHz, Acetone-*d_6*): 164.51, 163.45, 150.75, 149.77, 143.60, 137.39, 129.50, 129.26, 129.05, 119.14, 112.70, 109.37, 96.19, 66.69, 56.24, 26.13, 19.02, 14.30, -4.55.

10b. ^{1}H NMR (400 MHz, Acetone-*d_6*): 7.37 – 7.29 (m, 5H) 7.24 – 7.20 (m, 1H), 7.15 (s, 1H), 4.56 (t, *J* = 6.9 Hz, 2H), 3.87 (s, 3H), 3.13 (t, *J* = 6.8 Hz, 2H), 2.62 (s, 3H), 1.03 (s, 9H), 0.16 (s, 6H). ^{13}C NMR (100 MHz, Acetone-*d_6*): 164.59, 163.07, 150.71, 149.76, 143.58, 139.21, 129.72, 129.34, 127.32, 119.33, 112.69, 109.48, 96.13, 65.45, 56.22, 35.78, 26.16, 19.06, 14.37, -4.48.

10c. ^{1}H NMR (400 MHz, $CDCl_3$): 7.40 – 7.33 (m, 3H), 7.25 (s, 1H), 7.00 (d, *J* = 8.0, 2H), 6.87 (s, 1H), 5.24 (s, 2H), 5.14 (s, 2H), 3.77 (s, 3H), 3.44 (s, 3H), 2.66 (s, 3H), 0.92 (s, 9H), 0.04 (s, 6H). ^{13}C NMR (100 MHz, $CDCl_3$): 164.47, 162.75, 157.32, 149.59, 148.76, 142.66, 132.97, 130.06, 129.98, 129.69, 129.37, 128.35, 116.38, 112.28, 108.73, 95.06, 94.06, 65.87, 56.01, 55.86, 25.75, 18.45, 14.41, -4.79.

2.5.5.8 Synthesis of 11a-c

To **10a-c** in THF were added 1.5 equivalents of TBAF in THF. The reaction was stirred for 3 hours, quenched with 2N HCl and extracted with EtOAc. The EtOAc extract was purified using combiflash RF system in 30% EtOAc/Hexanes, and dried in vacuo to obtain the phenolic precursors in 75% yield.

11a. ^{1}H NMR (400 MHz, Acetone-d_6): 7.55 – 7.52 (m, 2H), 7.46 – 7.36 (m, 5H), 7.15 (s, 1H), 5.40 (s, 2H), 3.90 (s, 3H), 2.69 (s, 3H). ^{13}C NMR (100 MHz, Acetone-d_6): 164.61, 163.21, 148.56, 147.30, 145.35, 1137.65, 129.43, 129.10, 128.96, 119.55, 109.42, 106.81, 95.77, 66.42, 56.73, 14.41.

11b. ^{1}H NMR (400 MHz, Acetone-d_6): 7.45 (s, 1H), 7.39 – 7.29 (m, 5H) 7.24 – 7.20 (m, 1H), 7.13 (s, 1H), 4.56 (t, *J* = 6.9 Hz, 2H), 3.90 (s, 3H), 3.13 (t, *J* = 8.8 Hz, 2H), 2.61 (s, 3H). ^{13}C NMR (100 MHz, Acetone-d_6): 164.70, 162.90, 148.51, 147.25, 145.30, 139.28, 129.81, 129.34, 127.30, 119.64, 109.52, 106.89, 95.69, 65.47, 56.73, 35.82, 14.37.

11c. ^{1}H NMR (400 MHz, $CDCl_3$): 7.37 – 7.33 (m, 3H), 7.21 (s, 1H), 7.01 – 6.99 (m, 2H), 6.90 (s, 1H), 5.49 (s, 1H), 5.27 (s, 2H), 5.14 (s, 2H), 3.87 (s, 3H), 3.44 (s, 3H), 2.65 (s, 3H). ^{13}C NMR (100 MHz, $CDCl_3$): 164.43, 162.89, 157.24, 147.65, 145.01, 143.20, 129.97, 129.57, 118.92, 116.34, 108.88, 105.84, 94.41, 94.12, 65.71, 56.32, 14.51.

2.5.5.9 Synthesis of 12

To a solution of **9** (400mg, 1.24 mmol, 1 equiv.) in DCM were added DMAP (227 mg, 1.86 mmol, 1.5 equiv.), DCC (384 mg, 1.86 mmol, 1.5 equiv.) and $HOCH_2CH_2OTBDPS$ (559 mg, 1.86 mmol, 1.5 equiv.). The reaction was stirred for 24 hours, quenched by adding 2N HCl, and extracted using using EtOAc. The organic layer was dried over Na_2SO_4 and purified on silica gel (0 – 20 % EtoAc in hexanes) to give the product in 75% yield.

12. ^{1}H NMR (400 MHz, Acetone-d_6): 7.72 – 7.60 (m, 4H) 7.46 – 7.34 (m, 7H), 7.17 (s, 1H), 4.51 – 4.48 (m, 2H), 4.08 – 4.06 (m, 2H), 3.89 (s, 3H), 2.70 (s, 3H), 1.05 (s, 9H), 1.01 (s, 9H), 0.15 (s, 6H). ^{13}C NMR (100 MHz, Acetone-d_6): 164.58, 163.06, 150.77, 149.83, 143.67, 136.29, 134.24, 130.65, 128.63, 119.48, 112.81, 109.65, 96.19, 65.79, 63.31, 56.26, 56.12, 35.71, 27.20, 26.17, 25.21, 19.73, 19.05, 14.47, -4.43.

2.5.5.10 Synthesis of 13

*See synthesis of **6a/b**

13. ^{1}H NMR (400 MHz, *Acetone-d_6*): 7.72 – 7.68 (m, 4H) 7.50 – 7.34 (m, 8H), 5.08 (s, 2H), 4.55 – 4.51 (m, 2H), 4.10– 4.06 (m, 2H), 3.89 (s, 3H), 1.04 (s, 9H), 1.01 (s, 9H), 0.15 (s, 6H). ^{13}C NMR (100 MHz, Acetone-d_6): 164.58, 163.07, 150.74, 149.82, 143.63, 136.29, 134.20, 130.67, 129.23, 128.90, 128.65, 119.43, 112.86, 112.81, 109.63, 97.85, 96.14, 71.75, 65.80, 63.30, 60.70, 56.23, 27.20, 26.18, 26.16, 19.73, 19.06, 14.49, -4.23.

2.5.5.11 Synthesis of 14a-n

To a solution each of **6a-b, 13** in acetone was added 1.5 equivalents of K_2CO_3 and 1.1 equivalents of **4a-h and 11a-c** and the reaction was stirred under an atmosphere of nitrogen for 24 hours. The reaction was quenched with 2N HCl, extracted with EtOAc, dried with Na_2SO_4 and concentrated in vacuo. Purification was done using a combiflash RF system using

Hexanes/EtOAc (75/25) and the corresponding fractions pooled and concentrated to obtain the compounds 14a-n in 60 – 75% yield.

1**4a.** ^{1}H NMR (400 MHz, $CDCl_3$): 7.57 (s, 1H), 7.46 (s, 1H), 6.99 (m, 2H), 5.55 (s, 2H), 4.38 – 4.32 (m, 4H), 3.84 (s, 3H) 3.81 – 3.79 (m, 2H), 2.71 (s, 3H), 1.90 – 1.66 (m, 6H), 1.37 – 1.02 (m, 20H), 0.17 (s, 6H). ^{13}C NMR (100 MHz, $CDCl_3$): 163.64, 162.47, 158.42, 150.64, 149.82, 149.49, 146.42, 143.09, 118.60, 118.09, 112.53, 111.53, 109.96, 97.25, 95.29, 75.30, 64.98, 60.42, 60.06, 55.79, 37.62, 30.84, 29.89, 26.53, 25.82, 25.75, 18.48, 14.37, 14.20

14b. ^{1}H NMR (400 MHz, $CDCl_3$): 7.57 (s, 1H), 7.42 – 7.34 (m, 3H) 7.29 – 7.21 (m, 3H), 6.95 (s, 1H), 6.92 (s, 1H), 5.56 (s, 2H), 5.10 (s, 2H), 4.34 – 4.26 (m, 4H), 3.79 (s, 3H), 2.64 (s, 3H), 1..34 – 1.30 (m, 6H), 0.97 (s, 9H), 0.12 (s, 6H). ^{13}C NMR (100 MHz, $CDCl_3$): 164.36, 163. 63, 158.11, 150.70, 149.87, 149.02, 147.96, 146.72, 143.12, 137.03, 128.79, 128.45, 127.77, 127.32, 119.45, 118.02, 112.54, 111.79, 109.15, 109.07, 98.77, 95.31, 71.96, 64.49, 60.47, 60.10, 55.79, 29.67, 25.75, 18.49, 14.38, 14.19, -4.72.

14c. ^{1}H NMR (400 MHz, $CDCl_3$): 7.53 (s, 1H), 7.42 (s, 1H), 7.28 – 7.14 (m, 5H), 6.94 (s, 1H), 6.92 (s, 1H), 5.48 (s, 2H), 4.34 – 4.26 (m, 4H), 4.17 (t, J = 8.0, 2H), 3.78 (s, 3H), 3.12 – 3.06 (m, 2H), 2.65 (s, 3H), 1.33 – 1.29 (m, 6H), 0.97 (s, 9H), 0.12 (s, 6H). ^{13}C NMR (100 MHz, $CDCl_3$): 164.42, 163.65, 162.62, 158.18, 150.71, 149.87, 149.21, 148.25, 146.34, 143.12, 138.17, 129.13, 128.85, 128.75, 128.42, 126.82, 126.44, 118.98, 118.01, 112.55, 111.69, 109.13, 97.40, 95.29, 70.52, 64.44, 61.65, 60.48, 60.11, 55.79, 35.77, 35.65, 25.76, 25.68, 18.49, 14.37, 14.20, -4.71

14d. ^{1}H NMR (400 MHz, $CDCl_3$): 7.41 (s, 1H), 7.46 – 7.43 (m, 3H), 7.26 (s, 1H), 7.22 (s, 1H), 7.04 – 7.00 (m, 2H), 5.63 (s, 2H), 5.18 (s, 2H), 5.11 (s, 2H), 4.38 – 4.30 (m, 4H), 3.91 (s, 3H), 3.41 (s, 3H), 2.63 (s, 3H), 1.38 – 1.33 (m, 6H), 1.03 (, 9H), 0.18 (s, 6H).^{13}C NMR (100

MHz, $CDCl_3$) δ 164.47, 163.93, 163.32, 159.22, 158.10, 151.86, 150.72, 149.98, 149.27, 147.48, 144.00, 131.33, 130.05, 119.80, 118.64, 116.99, 112.97, 112.63, 109.76, 109.71, 99.20, 96.27, 95.13, 71.85, 64.70, 61.24, 60.71, 56.25, 56.02, 26.12, 19.07, 14.69, 14.51, 14.31, -4.52

14e. ^{1}H NMR (400 MHz, *Acetone-d_6*): 7.60 (s, 1H), 7.44 (s, 1H), 7.48 (s, 1H), 7.30 – 7.13 (m, 5H), 6.99 – 6.96 (m, 2H), 5.64 (s, 2H), 5.18 – 5.17 (m, 2H), 4.38 – 4.31 (m, 4H), 3.90 (s, 3H), 3.40 (s, 3H), 2.68 (s, 3H), 1.38 – 1.33 (m, 6H), 1.03 (s, 9H), 0.18 (s, 6H). ^{13}C NMR(400 MHz, *Acetone-d_6*): 164.47, 163.94, 163.37, 159.20, 158.57, 151.88, 150.76, 150.01, 149.25, 147.51, 144.04, 139.88, 130.27, 121.60, 119.98, 118.72, 116.52, 116.23, 112.97, 112.69, 109.84, 99.26, 96.35, 95.18, 71.96, 64.78, 61.21, 60.71, 56.28, 56.03, 26.12, 19.05, 14.67, 14.50, 14.28, -4.51

14f. ^{1}H NMR H NMR (400 MHz, *Acetone-d_6*): 7.59 (s, 1H), 7.47 (s, 1H), 7.41 (s, 1H), 7.39 (s, 1H), 7.25 (s, 1H), 7.21 (s, 1H), 6.89 – 6.86 (m, 2H), 5.62 (s, 2H), 5.11 (s, 2H), 4.63 – 4.57 (m, 1), 4.37 – 4.31 (m, 4H), 3.91 (s, 3H), 2.68 (s, 3H), 1.35 (t, *J* = 8.0 Hz, 6H), 1.28 (d, *J* = 8.0 Hz, 6H), 1.03 (s, 9H), 0.18 (s,6H). ^{13}C NMR (100 MHz, *Acetone-d_6*) δ 164.49, 163.94, 163.31, 159.25, 158.75, 151.86, 150.73, 150.01, 149.35, 147.54, 144.01, 136.37, 130.59, 130.23, 129.88, 128.61, 119.78, 118.67, 116.44, 112.97, 112.63, 109.78, 109.72, 99.26, 96.30, 72.02, 70.30, 64.72, 61.23, 60.71, 56.26, 26.12, 25.81, 23.26, 22.30, 20.89, 19.06, 14.69, 15.50, 14.31, -4.51

14g. ^{1}H NMR (400 MHz, $CDCl_3$): 7.61 (s, 1H), 7.46 (s, 1H), 7.23 – 7.19 (m, 1H), 7.00 – 6.98 (m, 4H), 6.81 – 6.79 (m, 1H), 5.62 (s, 2H), 5.13 (s, 2H), 4.54 – 4.48 (m, 1H), 4.40 – 4.33 (m, 4H), 3.84 (s, 3H), 2.69 (s, 3H), 1.39 – 1.33 (m, 6H), 1.28 – 1.27 (m, 6H), 1.03 (s, 9H), 0.17 (s, 6H). ^{13}C NMR (100 MHz, $CDCl_3$):164.37, 163.63, 162.69, 158.14, 158.08, 150.69, 149.87, 148.99, 147.89, 146.61, 143.10, 138.58, 129.50, 119.34, 119.26, 117.98, 115.49, 114.50, 112.52,

111.78, 109.12, 108.82, 98.60, 95.31, 71.77, 69.83, 64.36, 60.49, 60.10, 55.78, 25.76, 22.01, 18.49, 14.38, 14.20, -4.71

14h. ^{1}H NMR (400 MHz, *Acetone-d_6*): 7.56 (s, 1H), 7.46 (s, 1H), 7.18 (d, *J* = 8.0 Hz, 2H), 5.58 (s, 2H), 4.34 (m, 4H), 3.86 (m, 4H), 2.68 (s, 3H), 1.77 – 1.45 (m, 10H), 1.30 – 1.10 (m, 18 H), 1.05 (s, 9H), 0.21 (s, 6H). ^{13}C NMR (400 MHz, *Acetone-d_6*): 164.53, 163.94, 163.12, 159.36, 151.49, 150.71, 150.37, 150.27, 147.26, 143.91, 119.24, 118.38, 112.88, 112.44, 110.56, 109.75, 98.06, 96.90, 75.64, 75.05, 65.22, 61.17, 60.70, 38.70, 38.57, 18.99, 14.70, 14.53, 14.31, -4.45.

14i. ^{1}H NMR (400 MHz, *Acetone-d_6*): 7.60 (s, 1H), 7.52 – 7.50 (m, 2H), 7.46 (s, 1H), 7.37 – 7.30 (m, 3H), 7.25 (s, 1H), 7.17 (s, 1H), 5.63 (s, 2H), 5.20 (s, 2H), 4.33 (q, *J* = 8.0 Hz, 4H), 3.86 (d, *J* = 8.0 Hz, 2H), 2.67 (s, 3H), 1.96 – 1.69 (m, 6H), 1.37 – 1.15 (m, 11H), 1.05 (s, 9H), 0.21 (s, 6H)**.** ^{13}C NMR (400 MHz, *Acetone-d_6*): 164.51, 163.98, 163.40, 159.15, 151.54, 150.77, 149.99, 149.28, 147.48, 143.96, 138.27, 129.24, 128.60, 128.43, 119.89, 118.33, 112.87, 112.64, 109.85, 109.78, 99.21, 96.98, 75.08, 72.12, 64.78, 61.23, 60.74, 38.71, 27.18, 26.51, 26.16, 18.99, 14.69, 14.51, 14.30, -4.44.

14j. ^{1}H NMR (400 MHz, *Acetone-d_6*): 7.55 (s, 1H), 7.42 (s, 1H), 7.20 (s, 1H), 7.19 (s, 1H), 5.57 (s, 2H), 3.94 – 3.93 (m, 2H), 3.87 (s, 3H), 2.68 (s, 3H), 1.95 – 1.74 (m, 6H), 1.33 – 1.11 (m, 11H).

14k. ^{1}H NMR (400 MHz, *Acetone-d_6*): 7.60 (s, 1H), 7.55 (s, 1H), 7.42 (s, 1H), 7.22 (s, 1H), 7.19 (s, 1H), 5.53 (s, 2H), 5.39 (s, 2H), 4.34 (q, *J* = 8 Hz, 2H), 3.91 (s, 3H), 3.86 (s, 3H), 2.77 (s, 3H), 1.34 (t, *J* = 8.0 Hz. 3H), 1.04 (s, 9H), 0.19 (s, 6H). ^{13}C NMR (100 MHz, *Acetone-d_6*): 163.93, 163.37, 158.96, 151.95, 150.77, 150.35, 150.07, 147.00, 144.05, 137.60, 129.42,

129.01, 128.92, 119.03, 118.66, 113.01, 112.73, 109.58, 108.49, 96.70, 96.34, 66.53, 64.09, 61.26, 56.63, 56.28, 26.12, 19.07, 14.48, 14.37, -4.51.

14l. ^{1}H NMR (400 MHz, *Acetone-d_6*): 7.48 (m, 2H), 7.37 – 7.18 (m, 7H), 5.49 (s, 2H), 4.56 (t, *J* = 8 Hz, 2H), 4.34 (q, *J* = 8.0 Hz, 2H), 3.89 (s, 2H), 3.10 (t, *J* = 8.0 Hz, 2H), 2.63 (s, 3H), 1.35 (t, J = 8 Hz, 3H) 1.03 (s, 9H), 0.17 (s, 6H). ^{13}C NMR (400 MHz, *Acetone-d_6*) δ 164.52, 163.93, 163.18, 159.01, 151.92, 150.75, 150.32, 150.02, 146.89, 144.01, 139.21, 129.80, 129.73, 129.34, 127.28, 118.94, 118.63, 112.99, 112.72, 109.64, 108.61, 96.57, 96.29, 65.31, 64.24, 61.27, 56.57, 56.24, 35.70, 19.07, 14.49, 14.33, -4.52

14m. ^{1}H NMR (400 MHz, $CDCl_3$): 7.61 (s, 1H), 7.46 (s, 1H), 7.42 – 7.35 (m, 2H), 7.04 – 6.95 (m, 4H), 5.53 (s, 2H), 5.30 (s, 2H), 5.12 (s, 2H), 4.36 (q, *J* = 7.1 Hz, 2H), 3.85 (s, 3H), 3.84 (s, 3H), 3.42 (s, 3H), 2.70 (s, 3H), 1.37 (t, *J* = 7.1 Hz, 3H), 1.02 (s, 9H), 0.17 (s, 6H). ^{13}C NMR (100 MHz, CDCl3): 164.20, 163.66, 162.53, 157.62, 157.21, 150.72, 149.95, 148.93, 148.69, 145.83, 143.04, 129.82, 129.57, 118.34, 117.93, 116.31, 112.57, 111.98, 108.97, 107.05, 99.98, 95.27, 94.35, 65.70, 63.53, 60.57, 56.31, 55.96, 55.77, 29.72, 25.77, 18.51, 14.52, 14.20, -4.71.

14n. ^{1}H NMR (400 MHz, $CDCl_3$): ^{1}H NMR (400 MHz, *Acetone-d_6*) δ 7.68 – 7.65 (m, 4H), 7.57 (s, 1H), 7.52 (s, 1H), 7.42 – 7.32 (m, 6H), 7.24 – 7.28 (m, 5H), 6.97 (s, 2H), 5.58 (s, 2H), 5.14 (s, 2H), 4.49 – 4.42 (m, 2H), 4.35 (q, *J* = 7.1 Hz, 2H), 4.05 – 4.03 (m, 2H), 3.92 (s, 3H), 1.43 – 1.33 (m, 3H), 1.00 (d, *J* = 3.4 Hz, 18H), 0.15 (s, 6H).

2.5.5.12 Synthesis of 15a-n

To the products, **14a-n**, obtained in THF were added 1.5 equivalents of TBAF in THF. The reaction was stirred for 3 hours, quenched with 2N HCl and extracted with EtOAc. The EtOAc extract was purified using combiflash RF system in 30% EtOAc/Hexanes, and dried in

vacuo to obtain the phenolic/alcoholic precursors in 70 – 80% yield. Spectral data are given below.

15a. ^{1}H NMR (400 MHz, $CDCl_3$): 7.50 (s, 1H), 7.46 (s, 1H), 6.97 (s,1), 6.93 (s, 1H), 5.51 (s, 2H), 4.34 – 4.26 (m, 4H), 3.89 (s, 3H) 3.76 – 3.75 (m, 2H), 2.65 (s, 3H), 1.85 – 1.49 (m, 6H), 1.38 – 1.02 (m, 11H). ^{13}C NMR (100 MHz, $CDCl_3$): 164.44, 163.61, 162.47, 158.71, 149.49, 149.06, 148.72, 146.31, 146.01, 143.56, 118.57, 118.55, 111.64, 109.94, 109.14, 106.12, 97.16, 94.40, 64.95, 60.50, 60.07, 56.30, 37.60, 29.90, 29.70, 26.53, 25.82, 14.35, 14.29.

15b. ^{1}H NMR (400 MHz, $CDCl_3$): 7.54 (s, 1H), 7.43 (s, 1H) 7.38 – 7.35 (m, 2H), 7.28 – 7.20 (m, 3H), 6.93 (s, 1H), 6.91 (s, 1H), 5.56 (s, 2H), 5.51 (s, 1H), 5.08 (s, 2H), 4.28 (q, J = 8.0, 4H), 3.86 (s, 3H), 2.62 (s, 3H), 1..32 – 1.28 (m, 6H). ^{13}C NMR (100 MHz, $CDCl_3$): 164.35, 163.61, 162.73, 158.42, 149.05, 148.75, 147.98, 146.64, 146.06, 143.59, 137.01, 128.44, 127.77, 127.32, 119.44, 118.49, 111.88, 109.16, 98.70, 94.44, 71.93, 64.52, 60.55, 60.10, 56.31, 14.35, 14.27.

15c. ^{1}H NMR (400 MHz, $CDCl_3$): 7.50 (s, 1H), 7.44 (s, 1H), 7.24 – 7.10 (m, 5H), 6.94 (s, 1H), 6.90 (s, 1H), 5.53 (s, 1H), 5.47 (s, 2H), 4.32 – 4.24 (m, 4H), 4.14 (t, J = 8.0, 2H), 3.85 (s, 3H), 3.06 (t, J = 8.0, 2H), 2.63 (s, 3H), 1..33 – 1.27 (m, 6H). ^{13}C NMR (100 MHz, $CDCl_3$) δ 164.41, 163.63, 162.62, 158.47, 149.22, 148.75, 148.24, 146.26, 146.07, 143.60, 138.16, 129.12, 128.43, 126.45, 118.99, 118.48, 111.80, 109.18, 109.13, 106.13, 97.39, 94.44, 70.53, 64.47, 60.57, 60.12, 56.32, 35.77, 14.37, 14.30.

15d. ^{1}H NMR (400 MHz, $CDCl_3$): 7.59 (s, 1H), 7.50 (s, 1H), 7.36 – 7.34 (m, 2H), 7.00 – 6.97 (m, 4H), 5.62 (s, 2H), 5.15 (s, 2H), 5.08 (s, 2H), 4.38 – 4.32 (m, 4H), 3.94 (s, 3H), 3.47 (s, 3H), 2.69 (s, 3H), 1.40 – 1.35 (m, 6H). ^{13}C NMR (100 MHz, $CDCl_3$) δ 164.40, 163.65, 162.73, 158.41, 156.95, 148.98, 148.73, 147.84, 146.58, 146.03, 143.53, 130.28, 128.94, 119.30, 118.39,

116.22, 111.84, 109.10, 108.91, 106.09, 98.69, 94.43, 94.41, 71.59, 64.41, 60.60, 60.14, 56.30, 55.99, 14.41, 14.38, 14.31.

15e. ^{1}H NMR (400 MHz, Acetone-d_6): 7.60 (s, 1H), 7.44 (s, 1H), 7.48 (s, 1H), 7.30 – 7.13 (m, 5H), 6.99 – 6.96 (m, 2H), 5.64 (s, 2H), 5.19 (s, 2H), 5.18 (s, 2H), 4.38 – 4.31 (m, 4H), 3.93 (s, 3H), 3.40 (s, 3H), 2.68 (s, 3H), 1.38 – 1.33 (m, 6H). ^{13}C NMR (100 MHz, Acetone-d_6) δ 163.36, 162.93, 162.57, 159.28, 159.04, 155.52, 155.03, 153.97, 153.83, 149.97, 147.52, 146.42, 141.98, 135.83, 130.13, 126.75, 120.00, 107.07, 99.34, 96.03, 93.95, 71.95, 64.82, 61.26, 60.07, 57.02, 56.13, 19.04, 14.67, 14.53, 14.27

15f. ^{1}H NMR (400 MHz, *Acetone-d_6*): 7.97 (s, 4H), 7.59 (s, 1H), 7.43 – 7.39 (m, 3H), 7.25 (s, 1H), 7.21 (s, 1H), 6.89 – 6.86 (m, 2H), 5.62 (s, 2H), 5.11 (s, 2H), 4.63 – 4.57 (m, 1H), 4.37 – 4.31 (m, 4H), 3.93 (s, 3H), 2.68 (s, 3H), 1.37 – 1.33 (m, 6H), 1.28 (d, *J* = 8.0 Hz, 6H). ^{13}C NMR (100 MHz, *Acetone-d_6*): 7.58 (s, 1H), 7.50 (s, 1H), 7.33 – 7.31 (m, 2H), 7.26 (s, 1H), 7.01 (s, 1H), 6.98 (s, 1H), 6.83 – 6.81 (m, 2H), 5.61 (s, 2H), 5.06 (s, 2H), 4.54 – 4.48 (m, 1H), 4.38 – 4.32 (m, 2H), 3.93 (s, 3H), 2.69 (s, 3H), 1.39 – 1.33 (m, 6H), 1.31 (d, J = 8 Hz, 2H).

15g. 1H NMR (400 MHz, *Acetone-d_6*): 7.60 (m, 2H), 7.43 (s, 1H), 7.27 – 7.20 (m, 3H), 7.09 – 7.04 (m, 2H), 6.85 – 6.82 (m, 1H), 5.64 (s, 2H), 5.18 (s, 2H), 4.59 – 4.56 (m, 1H), 4.38 – 4.31 (m, 4H), 3.89 (s, 3H), 2.69 (s, 3H), 1.37 – 1.34 (m, 6H), 1.25 – 1.24 (m, 6H). ^{13}C NMR (100 MHz, *Acetone-d_6*) δ 164.48, 164.05, 163.32, 159.13, 159.03, 149.95, 149.55, 149.19, 148.44, 147.45, 145.72, 139.78, 130.29, 120.24, 119.85, 118.99, 116.17, 115.49, 112.73, 109.79, 109.65, 107.05, 99.12, 95.86, 71.95, 70.26, 64.72, 61.17, 60.72, 56.72, 22.26, 14.66, 14.56, 14.29.

15h. ^{1}H NMR (400 MHz, *Acetone-d_6*): 7.57 (s, 1H), 7.42 (s, 1H), 7.20 (s, 1H), 7.17 (s, 1H), 5.57 (s, 2H), 4.36 – 4.30 (m, 4H), 3.93 (d, *J* = 8.0 Hz, 2H), 3.85 (d, J = 8 Hz, 2H) 2.68 (s, 3H), 1.92 – 1.66 (m,10 H), 1.37 – 1.09 (m, 18H). ^{13}C NMR (100 MHz, *Acetone-d_6*) δ 164.53,

164.04, 163.09, 159.22, 150.39, 150.32, 149.52, 147.75, 147.29, 145.75, 119.29, 118.91, 112.53, 110.66, 109.78, 106.98, 98.10, 96.45, 75.70, 75.46, 65.30, 61.09, 60.69, 38.58, 38.35, 14.67, 14.56, 14.28.

15i. ^{1}H NMR (400 MHz, *Acetone-d_6*): 7.60 (s, 1H), 7.53 – 7.49 (m, 2H), 7.41 (s, 1H), 7.38 – 7.30 (m, 3H), 7.25 (s, 1H), 7.18 (s, 1H), 5.63 (s, 2H), 5.21 (s, 2H), 4.37 – 4.31 (m, 4H), 3.93 – 3.92 (m, 2H), 2.76 (s, 3H), 1.90 – 1.68 (m, 6H), 1.37 – 1.11 (m, 11H). ^{13}C NMR (100 MHz, *Acetone-d_6*) δ 164.47, 164.06, 163.34, 159.00, 149.98, 149.55, 149.30, 147.77, 147.50, 145.74, 145.65, 138.28, 129.23, 128.58, 128.42, 119.91, 118.83, 112.70, 109.91, 109.79, 106.96, 99.22, 96.47, 75.45, 72.14, 64.85, 61.15, 60.72, 38.36, 27.17, 26.53, 14.67, 14.55, 14.29.

15j. ^{1}H NMR (400 MHz, *Acetone-d_6*): 7.55 (s, 1H), 7.42 (s, 1H), 7.20 (s, 1H), 7.19 (s, 1H), 5.57 (s, 2H), 3.94 – 3.93 (m, 2H), 3.87 (s, 3H), 2.68 (s, 3H), 1.95 – 1.74 (m, 6H), 1.33 – 1.11 (m, 11H). ^{13}C NMR (100 MHz, *Acetone-d_6*) δ 164.55, 164.08, 162. 99, 158.93, 150.44, 150.12, 149.57, 147.82, 146.83, 145.76, 119.08, 118.78, 112.71, 109.79, 109.03, 106.95, 96.62, 96.46, 75.42, 64.39, 61.17, 60.71, 56.62, 38.35, 36.12, 27.17, 26.53, 14.67, 14.55, 14.29.

15k. ^{1}H NMR (400 MHz, *Acetone-d_6*): 7.68 (s, 1H), 7.59 (s, 1H), 7.52 – 7.50 (m, 2H), 7.44 (s, 1H), 7.40 – 7.31 (m, 3H), 7.22 (s, 1H), 7.20 (s, 1H), 5.52 (s, 2H), 5.38 (s, 2H), 4.34 (q, *J* = 8.0 Hz, 2H), 3.93 (s, 3H), 3.86 (s, 3H), 2.69 (s, 3H), 1.34 (t, *J* = 8.0 Hz. 3H). ^{13}C NMR (100 MHz, *J Acetone-d_6*) δ 164.36, 164.05, 163.34, 158.79, 150.31, 150.03, 149.55, 148.49, 146.96, 145.73, 137.58, 129.41, 129.03, 128.92, 118.97, 118.93, 112.74, 109.55, 108.42, 107.05, 96.64, 95.85, 66.52, 64.09, 61.21, 56.70, 56.60, 14.54, 14.38.

15l. ^{1}H NMR (400 MHz, *Acetone-d_6*): 7.47 (s, 1H), 7.44 (s, 1H), 7.36 – 7.13 (m, 8H), 5.49 (s, 2H), 4.56 (t, J = 8.0 Hz, 2H), 4.35 (q, *J* = 8.0 Hz, 2H), 3.92 (t, *J* = 8.0 Hz, 2H), 3.85 (s, 2H), 3.09 (t, J = 8 Hz, 2H), 2.63 (s, 3H), 1.34 (t, = 8.0 Hz, 3H). ^{13}C NMR (100 MHz, *Acetone-d_6*)

δ 164.52, 164.04, 163.17, 158.87, 150.40, 150.06, 149.56, 146.95, 139.21, 129.71, 129.32, 127.26, 119.00, 112.77, 109.67, 108.86, 107.05, 96.64, 95.86, 65.29, 64.39, 61.18, 56.70, 56.62, 35.70, 14.53, 14.30.

15m. ^{1}H NMR (400 MHz, $CDCl_3$) 7.60 (s, 1H), 7.51 (s, 1H), 7.37 – 7.35 (m, 2H), 7.03 – 6.96 (m, 4H), 5.56 (s, 2H), 5.29 (s, 2H), 5.13 (s, 2H), 4.37 (q, *J* = 7.2 Hz, 2H), 3.93 (s, 3H), 3.87 (s, 3H), 3.43 (s, 3H), 2.69 (s, 3H), 1.37 (t, *J* = 7.1 Hz, 3H). ^{13}C NMR (100 MHz, $CDCl_3$) δ 164.15, 163.63, 162.58, 158.04, 157.17, 148.98, 148.82, 148.74, 146.11, 145.77, 143.56, 129.75, 129.62, 118.40, 118.36, 116.30, 112.02, 108.97, 107.35, 106.15, 95.32, 94.50, 94.34, 65.64, 63.66, 60.63, 56.34, 56.30, 55.94, 14.48, 14.29.

15n. ^{1}H NMR (400 MHz, $CDCl_3$) δ 7.64 (s, 1H), 7.52 (s, 1H), 7.42 – 7.40 (m, 2H), 7.36 – 7.27 (m, 3H), 6.97 (s, 2H), 5.62 (s, 2H), 5.14 (s, 2H), 4.49 – 4.42 (m, 2H), 4.35 (q, *J* = 7.1 Hz, 2H), 3.92 (s, 3H), 3.91 – 3.89 (m, 2H), 2.67 (s, 3H), 1.43 – 1.33 (m, 3H). ^{13}C NMR (100 MHz, $CDCl_3$) δ 164.47, 163.62, 162.65, 158.45, 149.00, 148.70, 147.82, 146.33, 146.19, 143.75, 136.86, 128.49, 127.85, 127.36, 119.52, 118.57, 111.82, 109.07, 108.84, 105.93, 98.66, 94.42, 71.94, 66.30, 64.57, 61.20, 60.26, 56.30, 14.48, 14.36.

2.5.5.13 Synthesis of 16a/b

To a solution of **15d/e** (0.17 mmol, 1 equiv.) in acetone was added NaI (0.21 mmol, 1.2 equiv.) and a drop of conc. HCl. After 24 hours of stirring, the reaction was quenched by adding water and extracted using using EtOAc. The organic layer was dried over Na_2SO_4 and purified on silica gel (0 – 20 % EtoAc in hexanes) to give the product in 80% yield.

16a. ^{1}H NMR (400 MHz, Acetone-d_6): 7.59 (s, 1H), 7.53 (s, 1H), 7.42 (s, 1H), 7.48 (s, 1H), 7.29 – 7.13 (m, 5H), 6.98 – 6.95 (m, 2H), 5.18 (s, 2H), 5.17 (s, 2H), 4.37 – 4.31 (m, 4H), 3.93 (s, 3H), 2.67 (s, 3H), 1.38 – 1.33 (m, 6H).

16b. ^{1}H NMR (400 MHz, *Acetone-d_6*): 8.08 (s, 1H), 7.79 (s, 0.68H), 7.61 (s, 1H), 7.41 (s, 1H), 7.23 (s, 1H), 7.01 (s, 1H), 5.61 (s, 2H), 4.41 – 4.32 (m, 4H), 3.94 (s, 3H), 2.68 (s, 3H), 1.40 – 1.35 (m, 6H). ^{13}C NMR (100 MHz, *Acetone-d_6*) δ 164.60, 164.15, 162.69, 158.52, 150.07, 149.50, 148.54, 147.07, 145.79, 145.68, 145.28, 130.06, 129.04, 118.92, 118.59, 116.97, 115.74, 112.89, 109.77, 107.22, 106.97, 106.89, 98.79, 98.71, 95.83, 95.80, 64.56, 64.34, 61.32, 60.73, 60.70, 60.53, 56.71, 14.69, 14.54, 14.50, 14.31.

2.5.5.14 Synthesis of 2a-p

A CEM-Discover synthesizer was used for microwave based sulfation reactions in 10 mL vessels at 90 ºC as previously described.[145] Briefly, to solution of the precursor in CH_3CN (~3 mL) in a 10ml vessel were added Et_3N (10 eq/-OH group) and SO_3/Me_3N complex (6 eq/-OH). The reaction vessel was sealed and microwaved at 90 ºC for 1-2 hrs. The reaction mixture was cooled, concentrated and purified on a combiflash RF system using CH_2Cl_2/CH_3OH (7:3). The fractions corresponding to the final compounds were pooled together and concentrated *in vacuo*. Cation exchange chromatography was performed using Sephadex C-25 column for sodium exchange. This was followed by lyophilization of pooled fractions to obtain final compounds in a white to cream fluffy powder as previously reported.[133] High yields of >70% were obtained for final compounds. Spectral details of compounds are available below.

2a. Sodium 2-(((6-(cyclohexylmethoxy)-3-(ethoxycarbonyl)-2-methylbenzofuran-5-yl)oxy)methyl)-3-(ethoxycarbonyl)-6-methoxybenzofuran-5-yl sulfate. ^{1}H NMR (400 MHz, *DMSO-d_6*): 8.04 (s, 1H), 7.39 (s, 1H), 7.28 (m, 2H), 5.52 (s, 2H), 4.29 – 4.24 (m, 4H), 3.81 – 3.79 (m, 5H), 2.66 (s, 3H), 1.82 – 1.62 (m, 6H), 1.28 – 1.02 (m, 11H). ^{13}C NMR (100 MHz, *DMSO-d_6*) δ 163.31, 162.70, 162.36, 157.71, 150.13, 150.07, 148.44, 147.60, 145.65, 141.29, 136.83, 128.35, 127,77, 127.56, 118.03, 116.53, 113.37, 111.50, 108.30, 107.98, 98.14, 96.79,

74.12, 70.53, 63.53, 60.37, 59.92, 52.74, 37.02, 29.22, 26.08, 25.26, 14.07, 14.00, 13.88. HRMS calculated for $C_{32}H_{35}NaO_{13}S$ [(M-Na)]$^-$, m/z 659.18039, found for [(M-Na)]$^-$, 659.1785.

2b. Sodium 2-(((6-(benzyloxy)-3-(ethoxycarbonyl)-2-methylbenzofuran-5-yl)oxy)methyl)-3-(ethoxycarbonyl)-6-methoxybenzofuran-5-yl sulfate. ^{1}H NMR (400 MHz, *DMSO-d$_6$*): 8.06 (s, 1H), 7.49 – 7.44 (m, 3H), 7.41 – 7.28 (m, 5H), 5.58 (s, 2H), 5.17 (s, 2H), 4.28 (q, *J* = 8.0, 4H), 3.80 (s, 3H), 2.67 (s, 3H), 1.30 – 1.25 (m, 6H). ^{13}C NMR (100 MHz, *DMSO-d$_6$*): 163.31, 162.28, 162.39, 157.74, 150.75, 148.45, 147.63, 145.69, 140.99, 136.82, 128.36, 127.79, 127.55, 118.07, 116.55, 113.29, 111.53, 108.33, 108.04, 98.21, 95.73, 70.59, 63.56, 60.38, 59.94, 56.08, 14.08, 14.01, 13.88. MS (ESI) calculated for $C_{32}H_{29}NaO_{13}S$ [(M-Na)]$^-$, m/z 653.13344, found for [(M-Na)]$^-$, 653.1081.

2c. Sodium 3-(ethoxycarbonyl)-2-(((3-(ethoxycarbonyl)-2-methyl-6-phenethoxybenzofuran-5-yl)oxy)methyl)-6-methoxybenzofuran-5-yl sulfate. ^{1}H NMR (400 MHz, *DMSO-d$_6$*): 8.07 (s, 1H), 7.40 (s, 1H), 7.36 – 7.30 (m, 4H), 7.29 – 7.18 (m, 3H), 5.49 (s, 2H), 4.32 – 4.20 (m, 6H), 3.80 (s, 3H), 3.05 (t, *J* = 8.0, 2H), 2.67 (s, 3H), 1.30 – 1.25 (m, 6H). ^{13}C NMR (100 MHz, *DMSO-d$_6$*): 163.34, 162.67, 162.43, 157.78, 150.13, 148.64, 147.92, 145.44, 140.94, 138.25, 129.05, 128.17, 126.21, 117.75, 116.57, 113.24, 111.46, 108.29, 108.02, 97.46, 95.70, 69.61, 63.47, 60.37, 59.94, 56.08, 34.93, 14.07, 14.02, 13.88. HRMS calculated for $C_{33}H_{31}NaO_{13}S$ [(M-Na)]$^-$, m/z 667.14909, found for [(M-Na)]$^-$, 667.1516.

2d. Sodium 3-(ethoxycarbonyl)-2-(((3-(ethoxycarbonyl)-6-((4-(methoxymethoxy)benzyl)oxy)-2-methylbenzofuran-5-yl)oxy)methyl)-6-methoxybenzofuran-5-yl sulfate. ^{1}H NMR (400 MHz, *DMSO-d$_6$*): 8.05 (s, 1H), 7.44 – 7.39 (m, 4H), 7.30 (s, 1H), 7.03 – 7.01 (m, 2H), 5.57 (s, 2H), 5.19 (s, 2H), 5.09 (s, 2H), 4.33 – 4.25 (m, 4H), 3.80 (s, 3H), 3.37 (s, 3H), 2.67 (s, 3H), 1.30 – 1.26 (m, 6H). ^{13}C NMR (100 MHz, *DMSO-*

d$_6$) δ 163.32, 162.69, 162.35, 157.76, 156.48, 150.70, 150.11, 148.41, 147.55, 145.57, 140.85, 129.85, 129.33, 117.86, 116.44, 116.01, 113.18, 111.49, 108.28, 107.75, 98.07, 95.64, 93.80, 70.17, 63.37, 60.41, 59.95, 55.98, 55.52, 14.07, 14.04, 13.80. HRMS calculated for $C_{34}H_{33}NaO_{15}S$ $[(M-Na)]^-$, m/z 713.15457, found for $[(M-Na)]^-$, 713.1511.

2e. Sodium 3-(ethoxycarbonyl)-2-(((3-(ethoxycarbonyl)-6-((3-(methoxymethoxy)benzyl)oxy)-2-methylbenzofuran-5-yl)oxy)methyl)-6-methoxybenzofuran-5-yl sulfate. ^{1}H NMR (400 MHz, *DMSO-d*$_6$): 8.04 (s, 1H), 7.44 (s, 1H), 7.38 (s, 1H), 7.30 – 7.26 (m, 2H), 7.14 – 6.95 (m, 3H), 5.57 (s, 2H), 5.15 – 5.11 (m, 4H), 4.30 – 4.25 (m, 4H), 3.79 (s, 3H), 3.33 (s, 3H), 2.66 (s, 3H), 1.33 – 1.23 (m, 6H). ^{13}C NMR (100 MHz, *DMSO-d*$_6$) δ 163.31, 162.90, 162.68, 162.40, 157.70, 157.50, 156.90, 150.74, 150.13, 148.41, 147.51, 145.65, 140.95, 138.46, 129.48, 120.71, 118.07, 116.55, 115.53, 115.23, 113.24, 111.56, 108.32, 107.86, 98.16, 95.69, 93.84, 70.32, 63.45, 60.38, 59.95, 56.05, 55.49, 14.07, 14.02, 13.94, 13.87. HRMS calculated for $C_{34}H_{33}NaO_{15}S$ $[(M-Na)]^-$, m/z 713.1540, found for $[(M-Na)]^-$, 713.1568.

2f. Sodium 3-(ethoxycarbonyl)-2-(((3-(ethoxycarbonyl)-6-((4-isopropoxybenzyl)oxy)-2-methylbenzofuran-5-yl)oxy)methyl)-6-methoxybenzofuran-5-yl sulfate ^{1}H NMR (400 MHz, *DMSO-d*$_6$): 8.03 (s, 1H), 7.41 (s, 1H), 7.38 (s, 1H), 7.35 (s, 1H), 7.32 (s, 1H), 7.28 (s, 1H), 6.88 (s, 1H), 6.86 (s, 1H), 5.54 (s, 2H), 5.04 (s, 2H), 4.61 – 4.55 (m, 1), 4.29 – 4.23 (m, 4H), 3.77 (s, 3H), 2.65 (s, 3H), 1.27 – 1.23 (m, 12H). ^{13}C NMR (100 MHz, *DMSO-d*$_6$) δ 163.33, 162.69, 162.34, 157.77, 157.20, 150.70, 150.10, 148.43, 147.62, 145.62, 140.86, 129.51, 128.33, 117.83, 116.46, 115.35, 113.18, 11.48, 108.28, 107.75, 98.10, 95.66, 70.34, 60.09, 63.38, 60.41, 59.95, 55.99, 21.78, 14.08, 13.87. HRMS calculated for $C_{35}H_{35}NaO_{14}S$ $[(M-Na)]^-$, m/z 711.17531, found for $[(M-Na)]^-$, 711.1753.

2g. Sodium 3-(ethoxycarbonyl)-2-(((3-(ethoxycarbonyl)-6-((3-isopropoxybenzyl)oxy)-2-methylbenzofuran-5-yl)oxy)methyl)-6-methoxybenzofuran-5-yl sulfate. ^{1}H NMR (400 MHz, *DMSO-d_6*): 8.04 (s, 1H), 7.43 (s, 1H), 7.36 (s, 1H), 7.27 – 7.202 (m, 2H), 7.00 – 6.97 (m, 2H), 6.84 – 6.82 (m, 1H), 5.57 (s, 2H), 5.13 (s, 2H), 4.57 – 4.51 (m, 1H), 4.30 – 4.24 (m, 4H), 3.78 (s, 3H), 2.65 (s, 3H), 1.29 – 1.24 (m, 6H), 1.21 – 1.20 (m, 6H). ^{13}C NMR (100 MHz, *DMSO-d_6*) δ 164.51, 163.26, 162.43, 157.73, 150.22, 148.56, 147.80, 145.96, 141.47, 138.61, 130.87, 129.49, 119.42, 115.28, 114.74, 108.42, 98.55, 95.98, 83.36, 76.20, 69.30, 60.33, 21.81, 14.10, 14.02. HRMS calculated for $C_{35}H_{35}NaO_{14}S$ [(M-Na)]$^{-}$, m/z 711.17531, found for [(M-Na)]$^{-}$, 711.1766.

2h. Sodium 6-(cyclohexylmethoxy)-2-(((6-(cyclohexylmethoxy)-3-(ethoxycarbonyl)-2-methylbenzofuran-5-yl)oxy)methyl)-3-(ethoxycarbonyl)benzofuran-5-yl sulfate. ^{1}H NMR (400 MHz, *DMSO-d_6*): 8.04 (s, 1H), 7.40 (s, 1H), 7.32 (s, 1H), 7.25 (s, 1H), , 5.52 (s, 2H), 4.30-4.25 (m, 4H), 3.80 (m, 4H), 3.85 (d, J = 8 Hz, 2H) 2.68 (s, 3H), 1.88 – 1.63 (m, 10H), 1.30 – 1.04 (m, 18H). ^{13}C NMR (100 MHz, *DMSO-d_6*) δ 162.66, 162.20, 157.85, 150.08, 148.81, 148.54, 145.45, 141.22, 117.50, 116.55, 113.36, 108.66, 108.27, 97.35, 96.70, 74.16, 74.09, 63.89, 60.32, 59.93, 36.99, 36.87, 29.21, 26.08, 26.02, 25.25, 14.07, 14.02, 13.88. HRMS calculated for $C_{38}H_{45}NaO_{13}S$ [(M-Na)]$^{-}$, m/z 741.25864, found for [(M-Na)]$^{-}$, 741.2564.

2i. Sodium 2-(((6-(benzyloxy)-3-(ethoxycarbonyl)-2-methylbenzofuran-5-yl)oxy)methyl)-6-(cyclohexylmethoxy)-3-(ethoxycarbonyl)benzofuran-5-yl sulfate. ^{1}H NMR (400 MHz, *DMSO-d_6*): 8.05 (s, 1H), 7.44 – 7.22 (m, 8H), 5.57 (s, 2H), 5.16 (s, 2H), 4.37 – 4.31 (q, *J* = 8.0 Hz, 4H), 3.79 (d, *J* = 8.0 Hz, 2H), 2.66 (s, 3H), 1.92 – 1.64 (m, 6H), 1.29 – 1.00 (m, 11H). ^{13}C NMR (100 MHz, *DMSO-d_6*): 163.82, 163.21, 162.89, 158.21, 150.59, 150.57, 148.89, 148.03, 146.05, 141.67, 137.29, 128.88, 128.30, 128.10, 118.41, 116.92, 113.82, 111.98, 108.77,

108.28, 98.53, 97.18, 74.50, 70.92, 63.92, 60.90, 60.47, 37.37, 29.71, 26.58, 25.77, 14.59, 14.55, 14.39. HRMS (ESI) calculated for $C_{38}H_{39}NaO_{13}S$ $[(M-Na)]^-$, m/z 735.21169, found for $[(M-Na)]^-$, 735.2119.

2j. Sodium 6-(cyclohexylmethoxy)-3-(ethoxycarbonyl)-2-(((3-(ethoxycarbonyl)-6-methoxy-2-methylbenzofuran-5-yl)oxy)methyl)benzofuran-5-yl sulfate. ^{1}H NMR (400 MHz, *DMSO-d*$_6$): 8.04 (s, 1H), 7.41 (s, 1H), 7.31 (s, 1H), 7.29 (s, 1H), 5.52 (s, 2H), 4.32 – 4.25 (m, 2H), 3.80 – 3.79 (m, 4H), 2.67 (s, 3H), 1.87 – 1.61 (m, 6H), 1.30 – 1.00 (m, 14H). ^{13}C NMR (100 MHz, *DMSO-d*$_6$,) δ 163.40, 162.70, 162.06, 157.62, 150.08, 148.90, 145.33, 141.58, 130.68, 128.90, 113.42, 111.59, 107.42, 98.26, 96.28, 74.33, 60.37, 59.91, 56.20, 36.99, 29.23, 26.09, 25.27, 14.09, 14.00, 13.90. HRMS calculated for $C_{32}H_{35}NaO_{13}S$ $[(M-Na)]^-$, m/z 659.18039, found for $[(M-Na)]^-$, 659.1770.

2k. Sodium 2-(((3-((benzyloxy)carbonyl)-6-methoxy-2-methylbenzofuran-5-yl)oxy)methyl)-3-(ethoxycarbonyl)-6-methoxybenzofuran-5-yl sulfate. ^{1}H NMR (400 MHz, *DMSO-d*$_6$): 8.07 (s, 1H), 7.47 – 7.31 (m, 8H), 5.46 (s, 2H), 5.34 (s, 2H), 4.27 (q, *J* = 8.0 Hz, 2H), 3.81 – 3.79 (m, 5H), 2.68 (s, 3H), 1.25 (t, *J* = 8.0 Hz. 3H). ^{13}C NMR (100 MHz, *DMSO-d*$_6$) δ 163.16, 162.66, 162.38, 157.34, 150.79, 150.15, 148.55, 148.46, 145.25, 140.93, 136.19, 128.50, 128.07, 127.96, 117.34, 116.46, 113.22, 116.63, 113.22, 111.63, 96.14, 95.75, 65.59, 62.68, 60.45, 56.07, 14.11, 13.86. HRMS calculated for $C_{31}H_{27}NaO_{13}S$ $[(M-Na)]^-$, m/z 639.11779, found for $[(M-Na)]^-$, 639.1143.

2l. Sodium 3-(ethoxycarbonyl)-6-methoxy-2-(((6-methoxy-2-methyl-3-(phenethoxycarbonyl)benzofuran-5-yl)oxy)methyl)benzofuran-5-yl sulfate. ^{1}H NMR (400 MHz, *DMSO-d*$_6$): 8.08 (s, 1H), 7.35 – 7.26 (m, 7H), 7.19 – 7.15 (m, 1H), 5.48 (s, 2H), 4.53 (t, *J* = 8.0 Hz, 2H), 4.30 (q, *J* = 8.0 Hz, 2H), 3.79 (s, 6H), 3.07 (t, J = 8 Hz, 2H), 2.61 (s, 3H), 1.27 (t,

J = 8.0 Hz, 3H). ^{13}C NMR (100 MHz, *DMSO-d*$_6$) δ 163.36, 162.66, 162.19, 157.36, 150.79, 150.15, 148.50, 148.40, 145.22, 140.90, 138.07, 128.68, 128.34, 126.30, 117.26, 116.44, 113.32, 111.66, 108.20, 106.322, 96.05, 95.71, 64.31, 62.80, 60.45, 56.03, 34.22, 14.02, 13.87. HRMS calculated for $C_{32}H_{29}NaO_{13}S$ $[(M-Na)]^-$, m/z 653.13344, found for $[(M-Na)]^-$, 653.1299.

2m. Sodium 3-(ethoxycarbonyl)-6-methoxy-2-(((6-methoxy-3-(((4-(methoxymethoxy)benzyl)oxy)carbonyl)-2-methylbenzofuran-5-yl)oxy)methyl)benzofuran-5-yl sulfate. ^{1}H NMR (400 MHz, DMSO-*d*$_6$) δ 8.08 (s, 1H), 7.48 – 7.40 (m, 3H), 7.33 (d, *J* = 4.8 Hz, 2H), 7.05 – 6.99 (m, 2H), 5.47 (s, 2H), 5.28 (s, 2H), 5.15 (s, 2H), 4.30 (q, *J* = 7.1 Hz, 2H), 3.80 (s, 6H), 3.33 (s, 3H), 2.68 (s, 3H), 1.27 (t, *J* = 7.1 Hz, 3H). ^{13}C NMR (100 MHz, DMSO): 163.18, 162.66, 162.25, 157.32, 156.65, 150.77, 150.13, 148.45, 148.38, 145.20, 140.90, 129.83, 129.29, 117.32, 116.42, 116.07, 113.17, 111.63, 108.15, 106.11, 96.09, 95.70, 93.75, 65.32, 62.58, 60.47, 56.03, 55.47, 14.10, 13.86. HRMS calculated for $C_{33}H_{31}NaO_{15}S$ $[(M-Na)]^-$, m/z 699.13892, found for $[(M-Na)]^-$, 699.1366.

2n. Sodium 2-(((6-(benzyloxy)-3-(ethoxycarbonyl)-2-methylbenzofuran-5-yl)oxy)methyl)-6-methoxy-3-((2-(sulfonatooxy)ethoxy)carbonyl)benzofuran-5-yl sulfate. ^{1}H NMR (400 MHz, *DMSO-d*$_6$): 8.02 (s, 1H), 7.52 – 7.34 (m, 6H), 7.37 – 7.24 (m, 2H), 5.60 (s, 2H), 5.19 (s, 2H), 4.40 – 4.38 (m, 2H), 4.28 (q, *J* = 7.1 Hz, 2H), 4.03 – 3.99 (m, 2H), 3.79 (s, 3H), 2.66 (s, 3H), 1.27 (t, *J* = 7.1 Hz, 3H). ^{13}C NMR (101 MHz, *DMSO-d*$_6$) δ 163.32, 162.46, 162.30, 157.95, 150.76, 150.14, 148.35, 147.52, 145.59, 140.88, 136.84, 128.36, 127.76, 127.64, 117.97, 116.65, 113.19, 111.06, 108.35, 107.79, 98.10, 95.70, 70.53, 63.66, 63.44, 63.31, 59.98, 56.03, 14.09, 14.02. HRMS (ESI) calculated for $C_{32}H_{28}Na_2O_{17}S_2$ $[(M-Na)]^-$, m/z 771.06712 found for $[(M-Na)]^-$, 771.0656.

2o. Sodium 3-(ethoxycarbonyl)-2-(((3-(ethoxycarbonyl)-2-methyl-6-((3-(sulfonatooxy)benzyl)oxy)benzofuran-5-yl)oxy)methyl)-6-methoxybenzofuran-5-yl sulfate. ^{1}H NMR (400 MHz, *DMSO-d_6*): 8.02 (s, 1H), 7.40 – 7.26 (m, 5H), 7.17 – 7.15 (m, 2H), 5.59 (s, 2H), 5.14 (s, 2H), 4.31 – 4.22 (m, 4H), 3.78 (s, 3H), 2.65 (s, 3H), 1.29 – 1.23 (m, 6H). ^{13}C NMR (100 MHz, DMSO): 163.81, 163.22, 162.89, 158.33, 154.14, 151.17, 150.69, 148.90, 148.04, 145.88, 141.25, 138.11, 129.31, 122.58, 120.38, 120.11, 118.32, 116.89, 113.58, 111.93, 108.74, 108.25, 98.47, 96.26, 70.75, 63.83, 60.94, 60.43, 56.50, 53.29, 42.00, 14.56, 14.54, 14.41, 14.04. HRMS calculated for $C_{32}H_{28}Na_2O_{17}S_2$ $[(M-Na)]^-$, m/z 771.06712 found for $[(M-Na)]^-$, 374.1971.

2p. Sodium 3-(ethoxycarbonyl)-5-((3-(ethoxycarbonyl)-6-methoxy-5-(sulfonatooxy)benzofuran-2-yl)methoxy)-2-methylbenzofuran-6-yl sulfate. ^{1}H NMR (400 MHz, *DMSO-d_6*): 8.07 (s, 1H), 7.72 (s, 1H), 7.40 (s, 1H), 7.36 (s, 1H), 5.56 (s, 2H), 4.37 – 4.24 (m, 4H), 3.79 (s, 3H), 2.69 (s, 3H), 1.35 – 1.25 (m, 6H). ^{13}C NMR (100 MHz, DMSO): 163.83, 163.62, 163.25, 158.46, 151.13, 150.63, 148.18, 147.20, 142.60, 141.27, 127.46, 120.61, 120.25, 116.98, 113.63, 111.77, 108.72, 107.58, 103.99, 96.28, 63.92, 60.97, 60.46, 42.00, 14.63, 14.56, 14.43, 14.04. MS (ESI) calculated for $C_{25}H_{22}Na_2O_{16}S_2$ $[(M-Na)]^-$, m/z 665.02525, found for $[(M-Na)]^-$, 665.0271.

2.5.5.15 Synthesis of 4f*

To a solution of **4f** (0.17 mmol, 1 equiv.) in acetone was added NaI (0.21 mmol, 1.2 equiv.) and a drop of conc. HCl. After 24 hours of stirring, the reaction was quenched by adding water and extracted using using EtOAc. The organic layer was dried over Na_2SO_4 and purified on silica gel (0 – 20 % EtoAc in hexanes) to give the product in 80% yield.

4f *. ^{1}H NMR (*Acetone-d_6* 400 MHz): 9.42 (s, 1H), 9.05 (s, 2H), 7.31 – 7.29 (m. 1H), 7.22 – 7.15 (m, 2H), 6.89 – 6.88 (m, 2H), 6.72 – 6.69 (m, 1H), 5.07 (s, 2H), 4.34 – 4.26 (m, 2H), 2.66 (s,

3H), 1.37 – 1.25 (m, 3H). ^{13}C NMR (*Acetone-d_6* 400 MHz): 163.61, 161.18, 157.37, 146.72, 145.30, 144.79, 138.45, 118.13, 117.83, 114.66, 115.40, 108.74, 106.12, 97.40, 70.16, 59.85, 14.19, 14.05.

2.5.5.16 Synthesis of 12a*

12a*. ^{1}H NMR (400 MHz, *Acetone-d_6*): 7.41 (s, 1H), 7.15 (s, 1H), 4.41 – 4.38 (m, 2H), 3.94 – 3.89 (m, 5H), 2.70 (s, 3H).

2.5.5.17 Synthesis of 17

To a solution of **3** (500 mg, 2.12 mmol, 1.0 equiv.) in DMF were added cesium carbonate (1.73 g, 5.30 mmol, 2.5 equiv.) and 1-(bromomethyl)-3-(methoxymethoxy)benzene (5.30 mmol, 2.5 equiv.) with stirring for 18 hours under an atmosphere of nitrogen.The reaction was quenched with 2N HCl and extracted with ethyl acetate. The organic layer was dried using Na_2SO_4 and evaporated to dryness. The residue was purified on silica gel (5 – 20% EtOAc in Hexanes) and dried under vacuum to give **17** in 70% yield.

17. ^{1}H NMR (400 MHz, *Acetone-d_6*): 7.57 (s, 1H), 7.32 – 7.15 (m, 7H), 7.02 – 6.99 (m, 2H), 5.22 – 5.19 (m, 8H), 4.40 – 3.34 (m, 2H), 3.43 (s, 6H), 2.70 (s, 3H), 1.43 – 1.39 (m, 3H). ^{13}C NMR (100 MHz, Acetone-d_6):164.58, 163.17, 158.55, 149.38, 148.74, 147.88, 140.34, 139.94, 130.33, 130.31, 130.24, 121.60, 119.89, 116.47, 116.33, 116.21, 116.19, 109.78, 108.00, 99.05, 95.14, 72.22, 71.83, 60.74, 56.04, 14.68, 14.32

2.5.5.18 Synthesis of 17a*

*Same as synthesis of **4f***, but with 2 equiv. of NaI

17a*. ^{1}H NMR (400 MHz, *Acetone-d_6*): 8.29 – 9.27 (m, 1H), 7.53 (s, 1H), 7.22 – 7.18 (m, 3H), 7.04 – 6.99 (m, 4H), 6.79 – 6.76 (m, 2H), 5.17 (s, 2H), 5.15 (s, 2H), 4.35 (q, J = 8.0,

2H), 2.67 (s, 3H), 1.39 (t, J = 8.0, 3H). ^{13}C NMR (100 MHz, Acetone-d_6): 164.59, 163.11, 158.46, 158.44, 149.30, 148.44, 147.91, 140.31, 139.92, 130.36, 130.28, 119.75, 119.36, 119.34, 115.60, 115.40, 115.18, 115.15, 115.07, 109.76, 107.93, 99.00, 72.24, 71.85, 60.72, 14.67, 14.29.

2.5.5.19 Synthesis of 18a-b

To a solution of **4a/c** (1.0 mmol, 1.0 equiv.) in DMF were added cesium carbonate (1.5 mmol, 1.5 equiv.) and 1-(bromomethyl)-3-(methoxymethoxy)benzene (1.5 mmol, 1.5 equiv.). The reaction mixture was stirred under an atmosphere nitrogen for 18 hours. The reaction was quenched with 2N HCl, extracted with ethyl acetate and the organic layer evaporated to dryness. The residue was purified on silica gel (5 – 20% EtOAc in Hexanes) and dried under vacuum to give **2a-h** in 70-80% yield.

18a. 1H NMR (*Acetone-d_6* 400 MHz): 7.36 (s, 1H), 7.08 – 7.04 (m, 2H), 6.88 – 6.80 (m, 2H), 6.66 – 6.63 (m, 1H), 5.19(s, 2H), 5.10 (s, 2H), 4.21 (q, *J* = 8.0 Hz, 2H), 3.87 (s, 3H), 2.80 (s, 3H), 2.66 (s, 3H), 1.26 (t, *J* = 8.0 Hz, 3H)

18b. 1H NMR (400 MHz, $CDCl_3$): 7.55 (s, 1H) 7.49 – 7.15 (m, 8H), 7.06 – 7.00 (m, 2H), 5.21 – 5.17 (m, 6H), 4.40 (q, *J* = 8.0 Hz, 2H), 2.88 (s, 3H), 2.73 (s, 3H), 1.43 (t, *J* = 8.0 Hz, 3H). ^{13}C NMR (100 MHz, Acetone-d_6): 164.58, 163.16, 158.56, 149.38, 148.80, 147.91, 140.34, 138.37, 130.22, 129.27, 129.25, 128.79, 128.76, 128.61, 128.43, 121.58, 119.89, 116.33, 116.21, 109.78, 108.00, 99.09, 95.16, 72.21, 72.08, 60.73, 56.04, 14.68, 14.31.

2.5.5.20 Synthesis of 18a* and 18b*

*See synthsis of **4f***

18a*. ^{1}H NMR (400 MHz, *Acetone-d_6*): 8.32 (s, 1H), 7.50 (s, 1H), 7.22 – 7.28 (m, 2H), 7.01 – 6.96 (m, 2H), 6.80 – 6.87 (m, 1H), 5.10 (s, 2H), 4.35 (q, *J* = 8.0 Hz, 2H), 3.90 (s, 3H),

2.74 (s, 3H), 1.39 (t, *J* = 8.0 Hz, 3H).^{13}C NMR (100 MHz, *Acetone-d_6*): 164.63, 162.80, 158.46, 150.07, 149.50, 147.46, 140.26, 130.23, 119.37, 119.15, 115.51, 115.42, 115.26, 109.80, 107.42, 96.69, 72.13, 60.69, 56.72, 14.67, 14.28.

18b*. ^{1}H NMR (400 MHz, *Acetone-d_6*): 8.17 (s, 1H), 7.55 – 7.54 (m, 3H) 7.39 – 7.18 (m, 5H), 7.04 – 6.99 (m, 2H), 6.80 – 6.78 (m, 2H), 5.23 (s, 2H), 5.15 (s, 2H), 4.35 (q, *J* = 8 Hz, 2H), 2.68 (s, 3H), 1.43 (t, J = 8 Hz, 3H). ^{13}C NMR (100 MHz, *Acetone-d_6*): 164.59, 163.16, 149.30, 148.74, 148.03, 140.30, 138.40, 130.26, 129.26, 128.59, 128.41, 119.35, 115.50, 115.41, 115.21, 115.12, 107.89, 99.21, 72.27, 72.21, 60.73, 14.68, 14.30.

2.5.5.21 Synthesis of 21a

*See synthsis of **2a-p**

21a. Sodium 3-(ethoxycarbonyl)-2-methyl-6-((3-(sulfonatooxy)benzyl)oxy)benzofuran-5-yl sulfate ^{1}H NMR (400 MHz, *DMSO-d_6*): 8.04 (s, 1H), 7.23 – 7.13 (m, 5H), 5.11 (s, 2H), 4.30 (q, *J* = 8 Hz, 2H), 2.68 (s, 3H), 1.35 (t, J = 8 Hz, 3H). ^{13}C NMR (100 MHz, *DMSO-d_6*): 163.43, 162.18, 153.49, 149.07, 148.45, 141.03, 138.04, 128.65, 122.01, 119.55, 119.27, 117.95, 113.60, 108.37, 98.07, 70.49, 59.93, 52.81, 14.13, 14.07, 13.54. MS (ESI) calculated for $C_{19}H_{16}Na_2O_{12}S_2$ $[(M-2Na)/2]^{2-}$, m/z 250.0047, found for $[(M-2Na)/2]^{2-}$, m/z 250.0573.

2.5.5.22 Synthesis of 21b

*See synthsis of **2a-p**

21b. Sodium (((3-(ethoxycarbonyl)-2-methylbenzofuran-5,6-diyl)bis(oxy))bis(methylene))bis(3,1-phenylene) bis(sulfate) ^{1}H NMR (400 MHz, *DMSO-d_6*): 7.40 (s, 1H), 7.34 (s, 1H), 7.32 – 7.25 (m, 4H), 7.20 – 7.12 (m, 4H), 5.17 (s, 2H), 5.14 (s, 2H),

4.30 (q, *J* = 8.0 Hz, 2H), 2.66 (s, 3H), 1.33 (t, *J* = 8.0 Hz, 3H).^{13}C NMR (100 MHz, *DMSO-d$_6$)*: 163.46, 162.18, 153.64, 153.60, 147.71, 147.03, 146.22, 138.16, 137.78, 128.87, 128.78, 121.99, 119.74, 119.68, 119.25, 117.95, 108.33, 106.16, 98.13, 70.69, 70.32, 59.98, 52.80, 41.55, 15.156, 14.00, 13.55. HRMS calculated for $C_{26}H_{22}Na_2O_{13}S_2$ [(M-Na)]$^-$, m/z 629.04050, found for [(M-Na)]$^-$, m/z 629.0394.

2.5.5.23 Synthesis of 21c/d

*See synthsis of **2a-p**

21c. Sodium 3-(((3-(ethoxycarbonyl)-6-methoxy-2-methylbenzofuran-5-yl)oxy)methyl)phenyl sulfate. ^{1}H NMR (400 MHz, *DMSO-d$_6$*): 7.41 (s, 1H), 7.32 – 7.25 (m, 3H), 7.17 – 7.13 (m, 2H), 5.09 (s, 2H), 4.32 (q, *J* = 8.0 Hz, 2H), 3.84 (s, 3H), 2.69 (s, 3H), 1.35 (t, *J* = 8.0 Hz, 3H). ^{13}C NMR (100 MHz, *DMSO-d$_6$*): 163.50, 161.83, 153.67, 148.27, 147.89, 145.81, 137.98, 128.69, 122.19, 119.87, 119.62, 117.37, 108.35, 105.28, 95.98, 70.50, 59.98, 56.10, 14.15, 14.02. HRMS calculated for $C_{20}H_{19}NaO_9S$ [(M-Na)]$^-$, m/z 435.07553, found for [(M-Na)]$^-$, m/z 435.0734.

21d. Sodium 3-(((6-(benzyloxy)-3-(ethoxycarbonyl)-2-methylbenzofuran-5-yl)oxy)methyl)phenyl sulfate. ^{1}H NMR (400 MHz, *DMSO-d$_6$*): 7.50 – 7.49 (m, 2H), 7.42 – 7.37 (m, 4H), 7.33 – 7.25 (m, 3H), 7.16 – 7.14 (m, 2H), 5.20 (s, 2H), 5.13 (s, 2H), 4.31 (q, *J* = 7.1 Hz, 2H), 2.67 (s, 3H), 1.33 (t, J = 7.1 Hz, 3H). ^{13}C NMR (100 MHz, *DMSO-d$_6$*): 163.45, 162.15, 153.75. 147.72, 147.03, 146.29, 138.10, 136.95, 128.64, 128.43, 127.73, 127.58, 121.85, 119.76, 119.36, 117.98, 108.35, 70.65, 70.49, 60.00, 14.16, 14.03. HRMS calculated for $C_{26}H_{23}NaO_9S$ [(M-Na)]$^-$, m/z 511.10683, found for [(M-Na)]$^-$, m/z 511.1052.

2.5.5.24 Synthesis of 21e

*See synthsis of **2a-p**

21e. Sodium 6-(benzyloxy)-3-carboxy-2-methylbenzofuran-5-yl sulfate. ^{1}H NMR (400 MHz, *DMSO-d_6*): 8.52 (s, 1H), 7.37 – 7.22 (m, 5H), 7.01 (s, 1H), 7.25 (s, 1H), 5.10 (s, 2H), 2.62 (s, 3H). HRMS calculated for $C_{17}H_{12}NaO_8S$ $[(M-Na)]^-$, m/z 377.03366, found for $[(M-Na)]^-$, m/z 377.0341.

2.5.5.25 Synthesis of 21f-j

*See synthsis of **2a-p**

21f. Sodium 6-(cyclohexylmethoxy)-3-(ethoxycarbonyl)-2-methylbenzofuran-5-yl sulfate. ^{1}H NMR (400 MHz, *DMSO-d_6*): 7.97 (s, 1H), 7.18 (s, 1H), 4.31 (q, *J*= 8.0 Hz, 2H), 3.78 (d, *J* = 8.0 Hz, 2H), 2.68 (s, 3H), 1.87 – 1.64 (m, 6H), 1.34 (t, *J* = 8.0 Hz, 3H), 1.30 – 1.0 (m, 5H). HRMS calculated for $C_{19}H_{23}NaO_8S$ $[(M-Na)]^-$, m/z 411.11191, found for $[(M-Na)]^-$, m/z 411.1139.

21g. Sodium 6-(benzyloxy)-3-(ethoxycarbonyl)-2-methylbenzofuran-5-yl sulfate. ^{1}H NMR (400 MHz, *DMSO-d_6*): 7.99 (s, 1H), 7.53 – 7.52 (m, 2H), 7.40 – 7.31 (m, 3H), 7.25 (s, 1H), 5.16 (s, 2H), 4.32 (q, *J* = 8.0 Hz, 2H), 2.69 (s, 3H), 1.36 (t, *J* = 8.0 Hz, 3H). ^{13}C NMR (100 MHz, *DMSO-d_6*):163.42, 162.11, 149.09, 148.52, 141.06, 137.21, 128.21, 127.56, 127.54, 117.91, 113.65, 109.40, 97.86, 70.55, 59.92, 14.12, 14.05. MS (ESI) calculated for $C_{19}H_{17}NaO_8S$ $[(M-Na)]^-$, m/z 405.06496, found for $[(M-Na)]^-$, m/z 405.1115.

21h. Sodium 3-(ethoxycarbonyl)-6-((3-(methoxymethoxy)benzyl)oxy)-2-methylbenzofuran-5-yl sulfate. ^{1}H NMR (400 MHz, *DMSO-d_6*): 7.56 (s, 1H), 7.26 – 7.12 (m, 4H), 6.96 – 6.93 (m, 1H), 5.19 (s, 2H), 5.12 (s, 2H), 4.31 (q, *J* = 8.0 Hz, 2H), 3.37 (s, 3H), 2.68 (s, 3H), 1.35 (t, *J* = 8.0 Hz, 3H). ^{13}C NMR (100 MHz, *DMSO-d_6*): 163.42, 162.13, 156.83,

149.11, 148.53, 141.05, 138.85, 129.29, 120.70, 117.96, 115.39, 115.23, 113.75, 108.41, 97.88, 93.90, 70.35, 59.92, 55.57, 52.76, 14.12, 14.04. HRMS calculated for $C_{22}H_{23}NaO_{10}S$ [(M-Na)]$^-$, m/z 465.08610, found for [(M-Na)]$^-$, m/z 465.0870.

21i. Sodium 3-(ethoxycarbonyl)-6-((4-isopropoxybenzyl)oxy)-2-methylbenzofuran-5-yl sulfate. ^{1}H NMR (400 MHz, *DMSO-d$_6$*): 7.98 (s, 1H), 7.42 – 7.40 (m, 2H), 7.25 (s, 1H), 6.91 – 6.89 (m, 2H), 5.04 (s, 2H), 4.65 – 4.59 (m, 1H), 4.32 (q, *J* = 8.0 Hz, 2H), 2.69 (s, 3H), 1.35 (t, *J* = 8.0 Hz, 3H), 1.27 – 1.26 (m, 6H). ^{13}C NMR (100 MHz, *DMSO-d$_6$*): 163.49, 162.06, 157.05, 149.13, 148.54, 141.08, 129.38, 115.31, 113.48, 108.39, 98.04, 70.39, 69.09, 59.93, 21.83, 14.12, 14.06. MS (ESI) calculated for $C_{22}H_{23}NaO_9S$ [(M-Na)]$^-$, m/z 463.10683, found for [(M-Na)]$^-$, m/z 462.9859.

2.5.5.26 Synthesis of 21k

*See synthsis of **2a-p**

21k. Sodium 6-methoxy-2-methyl-3-((2-(sulfonatooxy)ethoxy)carbonyl)benzofuran-5-yl sulfate. ^{1}H NMR (400 MHz, *DMSO-d$_6$*): 7.95 (s, 1H), 7.23 (s, 1H), 4.42 – 4.39 (m, 2H), 4.06 – 4.03 (m, 2H) 3.78 (s, 3H), 2.70 (s, 3H). ^{13}C NMR (100 MHz, *DMSO-d$_6$*): 163.21, 161.86, 149.79, 149.36, 140.46, 117.54, 112.98, 108.26, 95.74, 63.67, 63.05, 56.14, 14.37. HRMS calculated for $C_{13}H_{12}Na_2O_{12}S2$ [(M-Na)]$^-$, m/z 446.96734, found for [(M-Na)]$^-$, m/z 446.9680.

2.5.5.27 Synthesis of 21l

21l. Sodium 3-((benzyloxy)carbonyl)-6-methoxy-2-methylbenzofuran-5-yl sulfate. ^{1}H NMR (400 MHz, *DMSO-d$_6$*): 8.06 (s, 1H), 7.51 – 7.50 (m, 2H), 7.42 – 7.32 (m, 3H), 7.24 (s, 1H), 5.38 (s, 2H), 3.77 (s, 3H), 2.69 (s, 3H). ^{13}C NMR (100 MHz, *DMSO-d$_6$)*: 163.26, 162.22, 149.80, 149.31, 140.52, 136.16, 128.54, 127.91, 127.81, 117.15, 113.00, 108.19, 95.72, 65.43,

56.11, 14.22. MS (ESI) calculated for $C_{18}H_{15}NaO_8S$ $[(M-Na)]^-$, m/z 391.04932, found for $[(M-Na)]^-$, m/z 391.0032.

2.5.6 Direct Enzyme Inhibition Studies Using Chromogenic Substrate Hydrolysis Assay

Direct thrombin inhibition was measured using a chromogenic substrate hydrolysis assay using a microplate reader (FlexStation III, Molecular Devices) as previously described.[133] The buffer utilized in this assay was a 20 mM Tris buffer pH 7.4, containing 100 mM NaCl, 2.5 mM $CaCl_2$, and 0.1% polyethylene glycol (PEG) 8000, with the experiment performed at 25 °C.

Briefly, 189 μL of pH 7.4 buffer was added to the wells and 5 μL of potential thrombin inhibitor (or DMSO) and 4 μL of thrombin (6 nM final concentration) were sequentially added. After a 10 min incubation, 2 μL of thrombin substrate (125 μM) was rapidly added and the residual thrombin activity was measured from the initial rate of increase in absorbance at 405 nm. Relative residual thrombin activity at each concentration of the inhibitor was calculated from the ratio of thrombin activity in the presence and absence of inhibitor. Logistic equation 1 was used to fit the dose dependence of residual protease activity to obtain the potency (IC_{50}) and efficacy (ΔY) of inhibition.

$$Y = Y_0 + \frac{Y_M - Y_0}{1 + 10^{(\log [\text{Inhibitor}]_0 - \log \text{IC}_{50})(\text{HS})}} \qquad (1)$$

In this equation, Y is the ratio of residual thrombin activity in the presence of inhibitor to that in its absence (fractional residual activity), Y_M and Y_0 are the maximum and minimum possible values of the fractional residual proteinase activity respectively, IC50 is the concentration of the inhibitor that results in 50% inhibition of enzyme activity and HS is the Hill slope. Likewise, compounds were screened for direct FXa and FXIa activity employing FXa and FXIa at 1.09 nM and 0.75 nM and using spectrozyme FXa and S-2366 respectively as chromogenic substrates.

2.5.7 Mechanisms of Thrombin Inhibition by 2c and 2i

The initial rate of substrate hydrolysis by 6 nM Thrombin was monitored from the linear increase in absorbance at 405 nm corresponding to less than 10% consumption of the chromogenic substrate, as earlier described.[133] The initial rate was measured as a function of various concentrations of the substrate (0.85 – 250 μM) in the absence and presence of fixed concentrations of inhibitor (0, 1, 2, 10, and 40 μM), following a 10-minute incubation in a 20 mM Tris buffer pH 7.4 containing 100 mM NaCl, 2.5 mM $CaCl_2$, and 0.1% PEG 8000. The data were fitted by the Michaelis-Menten equation 2 to determine $K_{M,app}$ and V_{MAX}.

$$V_I = \frac{V_{MAX}[S]}{K_M + [S]} \quad (2)$$

2.5.8 Thermodynamic Affinity of SBDs for Thrombin

The thrombin – benzofuran dissociation constant was obtained by measuring the change in fluorescence emission of fluorescein labeled thrombin as a function of the concentration of benzofuran dimer in 20 mM Tris Buffer pH 7.4, containing 100 mM NaCl, 2.5 mM $CaCl_2$, and 0.1% PEG 8000 at 25 °C in a quartz microcuvette using a QM4 fluorimeter (Photon Technology International, Birmingham, NJ). Solutions of the compounds were titrated into a 200 μL solution of Fluorescein labeled thrombin (100 nM) and the change in the fluorescence at 520 nm (λEX = 490 nm) monitored. The excitation and emission slit width were set to 1.0 mm. Using the quadratic equilibrium binding equation 3, the saturable change in the fluorescence signal was fitted to obtain the K_D of interaction. In this equation, ΔF represents the change in fluorescence at a fixed concentration of thrombin, [P] from the initial fluorescence F_O, and ΔF_{MAX} represents

the maximal change in fluorescence following saturation. [L] is the concentration of the benzofuran dimer.

$$\frac{\Delta F}{F_0} = \frac{\Delta F_{max}}{[P]_0} \times \left\{ \frac{([P]_0 + [L]_0 + K_D) - \sqrt{(([P]_0 + [L]_0 + K_D)^2 - 4[P]_0[L]_0)}}{2} \right\} \quad (3)$$

2.5.9 Competitive Inhibition Studies of 2c and 2i

Thrombin inhibition by benzofuran compounds was studied in the presence of the exosite 1 competitor hirudine peptide (HirP) and exosite 2 competitor unfractionated heparin (UFH), in a manner similar to that described for direct thrombin inhibition. Briefly, to a solution of thrombin (6 nM final concentration) in 20 mM TrisHCl buffer, pH 7.4, containing 100 mM NaCl, 2.5 mM $CaCl_2$, and 0.1% PEG 8000 at 25 °C was added HirP (0 − 30 nM) or UFH (0 − 50 μM). After a 10 minute incubation period, different concentrations of inhibitor (final concentration 200 – 0.03 μM) were added and further incubated for 10 minutes. Following the incubation, the residual thrombin activity was measured through Spectrozyme TH hydrolysis assay. The dose dependence of the fractional residual thrombin activity at each concentration of inhibitor was fitted using equation 1 to obtain the apparent IC_{50}, HS, Y_O, and Y_M.

2.5.9.1 Inhibition of Thrombin Mutants by SBDs

In general, benzofuran compounds (200 – 0.02 μM**)** were incubated with individual mutants of thrombin (6 nM) in a 20 mM TrisHCl buffer containing 100 mM NaCl, 2.5 mM CaCl2, 0.1% PEG 8000 at a pH 7.4 for 10 min. Following this, substrate Spectrozyme TH (100 μM) was added to the mixture and the initial rate of increase in absorbance at 405 nm was measured. The rate of initial hydrolysis was used to calculate residual thrombin activity, which was used to calculate the IC_{50} from equation 1.

2.5.9.2 PT and APTT Tests for 2c and 2i

Clotting time was measured in a standard one-stage recalcification assay with a BBL Fibrosystem fibrometer (BectonDickinson, Sparles, MD), as described previously.[133] For the APTT assay, 10 µL of benzofuran was mixed with 90 µL of citrated human plasma and 100 µL of prewarmed APTT reagent (0.2% ellagic acid). After incubation for 4 min at 37 °C, clotting was initiated by adding 100 µL of prewarmed 25 mM $CaCl_2$ and time to clot noted. For PT assays, thromboplastin was reconstituted according to manufacturer's directions and warmed to 37 °C. A 10 µL sample of the sulfated benzofuran, to give the desired concentration, was brought up to 100 µL with citrated human plasma, incubated for 30 s at 37 °C followed by addition of 200 µL prewarmed thromboplastin. The time to clot was again noted. The data were fit to a quadratic trend line, which was used to determine the concentration of the inhibitor necessary to double the clotting time. Clotting time in the absence of an anticoagulant was determined in a similar fashion using 10 µL of deionized water and/or appropriate organic vehicle and was found to be 42.0 s and 19.0s for APTT and AP respectively.

2.5.9.3 Inhibition of Thrombin Mediated Fibrinogen Cleavage by 2c and 2i

83 µL of a 20 mM Tris Buffer pH 7.4, containing 100 mM NaCl, 2.5 mM $CaCl_2$, and 0.1% PEG8000 was added to 9 centrifuge tubes. Thrombin was added to tubes 2 – 9 at a final concentration of 6 nM. Inhibitor was added to tubes 3 – 9 and well mixed resulting in final concentrations from 150, 100, 50, 20, 10, 2, and 0.5 µM, and incubated for 10 minutes. 15 µL of a 10 mg/mL fibrinogen solution was added to the tubes (final concentration, 1.5 mg/mL) and mixed. After allowing to stand for 1 minute, 5 µL of a 300 nM PPACK solution was added and the tubes were centrifuged at 10000 RPM for 10 minutes. 20 µL of the resulting supernatant solution were mixed with 20 µL of lamella dye, loaded onto a 7.5% SDS PAGE gel and run.

Detection was by means of coomassie blue dye and analysis of the gel was performed on GE imager and Quantity One software from Bio-Rad. Multiple PAGE images were averaged to deduce standard errors (~15%) and plotted on a semi-log plot to estimate inhibition potency and efficacy of fibrinogen cleavage using non-linear sigmoidal regression.

3 SULFATED DIFLAVONOIDS ARE POTENT AND SELECTIVE INHIBITORS OF PLASMIN

3.1 Introduction

An important part of maintaining hemostasis is fibrinolysis, which involves the dissolution of blood clots[249–251] This process is necessary to ensure the correct resumption of blood flow following clot formation. Fibrinolysis is controlled by various cofactors and inhibitors, and among these, plasmin is the most important fibrinolytic agent.[252]

3.1.1 Plasmin

Plasmin is a trypsin like serine protease obtained from the proenzyme, plasminogen, an 810 amino acid residue single chain polypeptide, by the action of tissue plasminogen activator (tPa) or urokinase (uPA).[206] It is also known that the complex of fibrinogen and some bacterial proteins catalyzes the conversion of plasminogen to plasmin.[252] An initial cleavage of a 19 residue peptide from plasminogen leads to its release into plasma and further cleavage at the Arg561–Val562 peptide bond results in the single chain plasminogen being converted to plasmin, a two chain protein held together by disulfide bonds.[249,253] Mechanistically, the generation of plasmin from plasminogen requires fibrin, to which both plasminogen and tissue plasminogen activator bind. This binding to fibrin increases the rate of conversion of plasminogen to plasmin.[254] It is important to note that plasmin promotes its own generation via the conversion of tPA and uPA into two-chain proteases, possessing higher proteolytic activity.[254] The heavy chain of plasmin forms the five kringle domains of plasmin, which are

known to be critical for plasmin's numerous interactions, including the ones with fibrin and its primary inhibitor, α2-antiplasmin.[252] The light chain makes up the serine protease domain, bearing the His-Asp-Ser catalytic triad.[252,255] The serine-protease domain of plasmin bears structural resemblance to other members of the trypsin serine-family of serine proteases[256] and has dimensions of about 40Å×45 Å×50 Å.[255] A notable difference between plasmin and the other serine proteases is that plasmin lacks the group of residues (95-100, chymotrypsinogen numbering) that form a beta hairpin. This makes the active site of plasmin more open than other serine proteases,[257] making the enzyme less specific.[258]

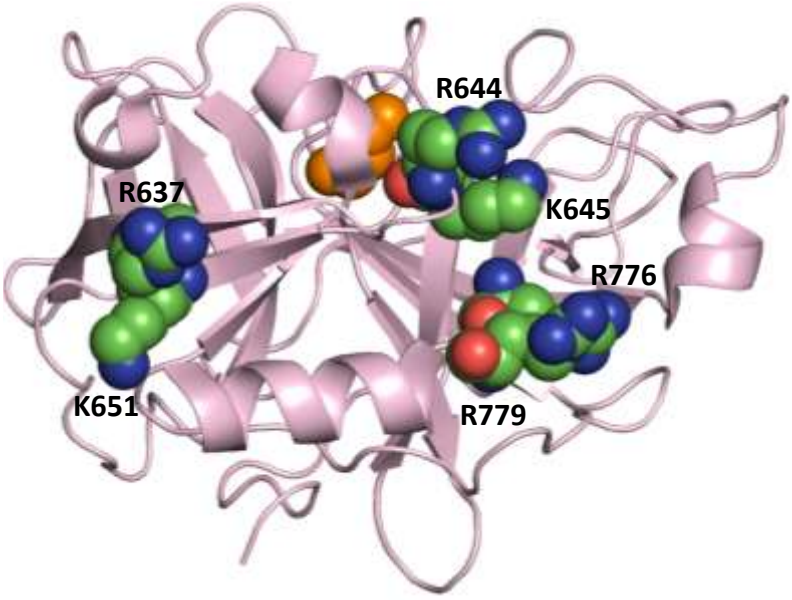

Figure 32. Structure of catalytic domain of human plasmin.

Following its formation, plasmin remains bound to the fibrin surface where it exerts its action by cleaving the fibrin network holding the clot together, leading to the restoration of blood flow.[259] Thus plasmin has a very important role in the coagulation process and its regulation in the body is thus very important. Beyond its role in maintaining hemostasis, plasmin has other functions including the activation of metalloproteinases and has been shown to be important in the wound healing process, pathogen invasion, cancer invasion and metastasis.[87,257] The role of plasmin in a number of cancers including prostate cancer has been shown.[260,261] Plasmin is also

known to be a pro-inflammatory cell activator.[87,259] These diverse roles highlight the vast physiological importance of plasmin.

Since it is a highly non-specific protease, it is important that plasmin activity is tightly regulated to prevent detrimental effects. By being localized to the site where its activity is required, the fibrin surface, its activity is highly regulated. In addition, the activity of plasmin is regulated by endogenous inhibitors, a major one being α_2-antiplasmin, which is found in plasma at high concentrations.[254] It is important to note that binding of plasmin to fibrin renders it inaccessible to α_2-antiplasmin and thus its inhibition by the anti-protease is not possible.[262] This again emphasizes the tight regulatory processes in place for plasmin.

3.1.2 Plasmin Inhibitors

In a number of conditions including haemophilia, disseminated intravascular coagulation, chronic hepatic disease, and von Willenbrand disease, the downregulation of plasmin activity may be necessary to prevent the occurrence of bleeding incidents. In addition, the regulation of plasmin in surgery to prevent excessive blood loss is also important.[263] Also, plasmin regulation may be of significant benefit in inflammatory conditions and cancer.[87,259]

Although these scenarios call for plasmin inhibitors, only two plasmin inhibitors, ε-aminocaproic acid **(3.1)** and tranexamic acid **(3.2)**, have been approved for clinical use as anti-fibrinolytics.[87] Both of these agents are lysine-analogs that do not directly interact with plasmin, but rather interact with the lysine binding sites in the kringle domain of plasminogen and hinder plasmin generation.[87] These agents are also known to bind to gamma aminobutyric acid (GABA) receptors, leading to severe

(3.1) **(3.2)**

K_i = 9 µM K_i = 1.1 µM

Figure 33. FDA approved plasmin inhibitors.

undesirable effects such as convulsions and renal damage.[264,265] Aprotinin, a Kunitz -type direct plasmin inhibitor initially approved by the FDA, was later withdrawn from clinical use because it carries the risk of increased mortality and morbidity.[266] The lack of clinical anti-plasmin agents and the immense therapeutic potential of plasmin inhibitors has driven the search for new agents that target plasmin. Considerable effort in the search for anti-plasmin agents has resulted in a number of plasmin inhibitors, some with subnanomolar inhibitory activity.[87] These agents target the active site, taking advantage of the difference in the active site with other serine proteases.[267–274] The fact that none of these agents has resulted in a clinical candidate calls for the use of a new strategy for the development of plasmin inhibitors.

In a bid to identify a new class of plasmin inhibitors, Al-Horani et al. screened a chemical library of 55 NSGMs.[275] The rationale for this screen was the knowledge that heparin binds to plasmin.[87] In addition, there had been previous reports of non-saccharide GAG mimetics inhibiting serine proteases and this indicated the possibility of identifying one such agent with plasmin inhibitory activity. Also, since non-saccharide GAG mimetics have been shown to be allosteric inhibitors of serine proteases, chances were high that any such non-saccharide GAG mimetic would behave similarly. This would result in a structurally and mechanistically novel inhibitor. The biochemical screen led to the discovery of NSGMs that inhibited plasmin and an important class was the sulfated diflavonoid compound that inhibited plasmin via an uncompetitive inhibitory mechanism.[275]

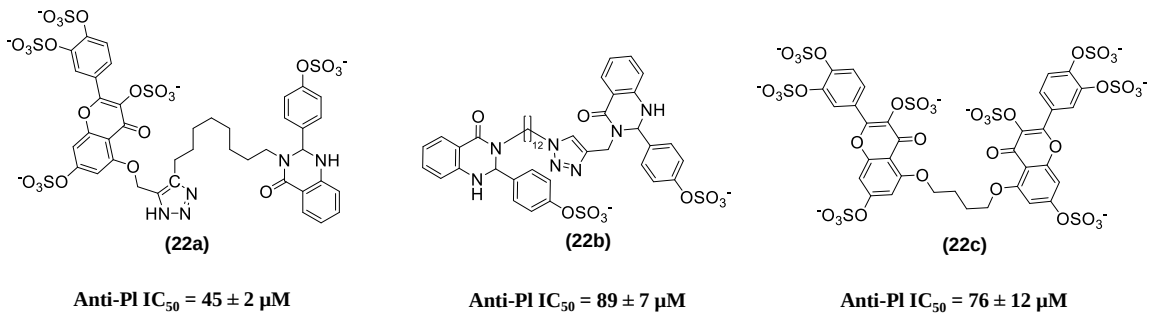

Figure 34. NSGMs with plasmin inhibitory activity.

3.2 Rational for the Development of Sulfated Diflavonoid Plasmin Inhibitors

The discovery of sulfated diflavonoid compounds as plasmin inhibitors[275] led us to develop a focused library of this class of compounds with the aim of identifying more potent inhibitors and also increasing our understanding of the structure activity relationship of this interaction. The previous work showed that inhibitory activity was severely dependent on the intermonomer linker separating the two quercetin units.[275] It was shown that a 4-atom linker connecting two quercetin moieties, each with sulfate groups at positions 3, 7, 3', and 4', was ideal for plasmin inhibition. This compound, **22c**, had an IC_{50} for plasmin inhibition of 75 µM and a 5-fold selectivity over thrombin.[275] The strong dependence of activity on the length of the linker led us to study a different set of compounds with an aromatic linkers, **23a-e**, as opposed to the straight chain linkers earlier studied. In addition, to identify the contribution of sulfate groups on the compound, sulfated diflavonoids from apigenin, **25a**, which has 2 less phenolic groups than quercetin, **24a**, (3, and -4' positions only) were synthesized, resulting in compounds with 4 sulfate groups (**23f-n**). A heterodimer made from quercetin and apigenin with 6 sulfate moieties was also synthesized, **23o**. In this regard the compounds in this chemical library were different from each other in the type of linker, aromatic or non-aromatic, and the number of sulfate

groups. Five of these compounds were sulfated diquercertins with an aromatic linker, four were sulfated di-apegin compounds with non-aromatic linkers and **5** were sulfated di-apigenin compounds with aromatic linkers. One compound was a heterodimer of quercetin and apigenin having a para xylene linker.

3.3 Results and Discussion

3.3.1 Synthesis of Sulfated Diflavonoids

The synthesis of the sulfated diflavonoids was achieved in four steps that ended with a microwave assisted sulfation reaction to achieve the persulfated flavonoid dimers. The first step was the selective protection of the flavonoids with methoxy-O-methyl groups with diisopropyl ethyl amine as the base. The stoichiometries of the reagents were regulated to keep the 5-position OH free to enable subsequent dimerization. This phenolic group is the least reactive of all the phenolic groups due to intramolecular hydrogen boding. Thus, for apigenin, 2 equivalents of the protecting group were used whereas 4 equivalents were used for quercetin. The products which were quercetin with MOM protection at the 3, 7, 3', and 4' positions (**24b**) and apigenin protected with MOM groups at the 7 and 4' position (**25b**), were obtained in good yield. The next step was the dimerization of the selectively protected flavonoid units with appropriate di-bromo linker via S_N2 reactions employing K_2CO_3 as a base. This reaction yielded the MOM protected flavonoid dimers with 30-50% yield (**24c–24h, 25c–25f**). The heterodimer, **26a**, on the other hand required an additional step. First, the linker was reacted with quercetin and the resulting product reacted with apigenin.

The third step involved the removal of the MOM groups resulting in polyphenolic compounds. Previously, this reaction was done with p-toluenesulfonic acid; however, in this case a TMS-Br based deprotection strategy was employed. This resulted in the deprotected

compounds with yields of 70 – 90% (**24i–24n, 25l–25o, 26b**). The sulfation step was carried out using microwave assisted reaction in CH_3CN using triethyl amine and SO_3/Me_3N at 90 – 100 ºC as previously described.[275] We used 6 and 10 equivalents respectively for SO_3/Me_3N and triethyl amine respectively were used and the reaction time was kept at an hour per phenolic group resulting in reaction time of 4 – 8 hours per compound. The reaction resulted in quantitative yields of persulfated diflavonoid compounds (**22c, 23a–23o**).

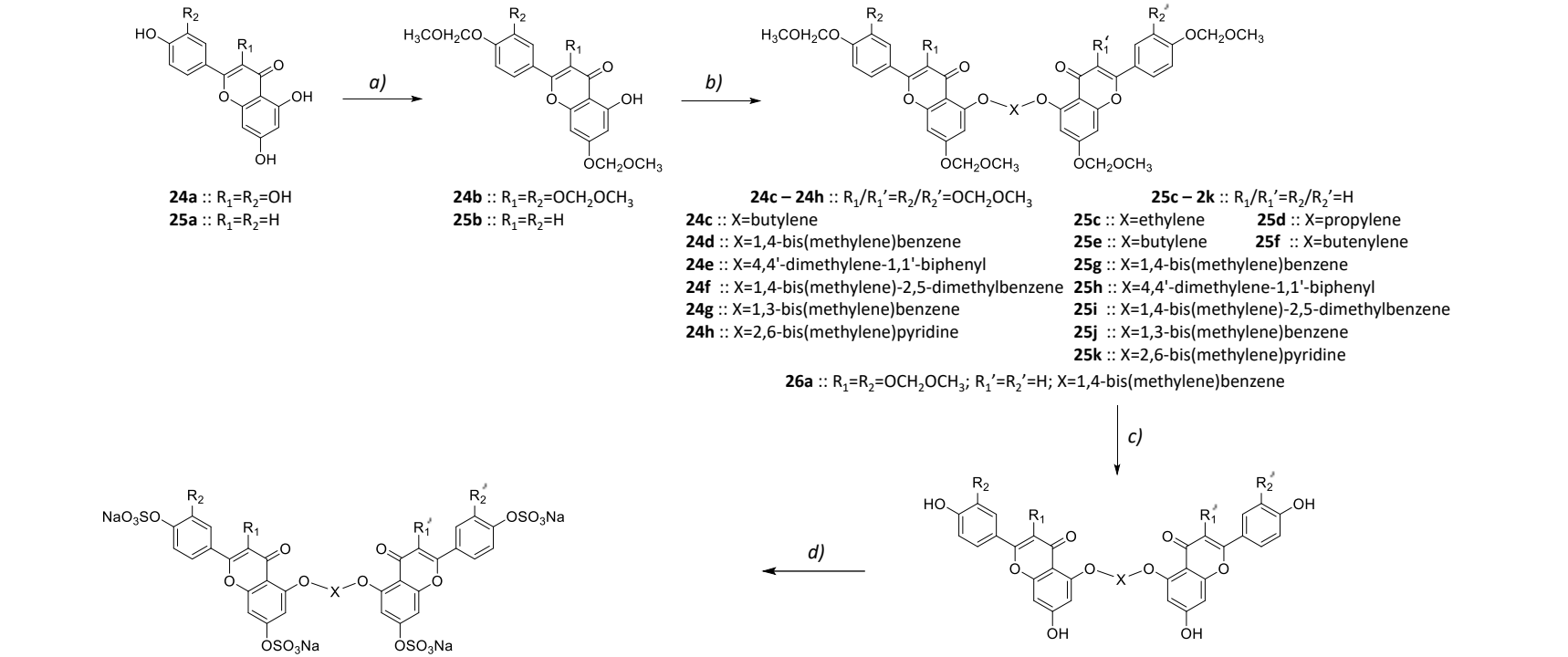

24a :: R_1=R_2=OH
25a :: R_1=R_2=H

24b :: R_1=R_2=OCH_2OCH_3
25b :: R_1=R_2=H

24c – 24h :: R_1/R_1'=R_2/R_2'=OCH_2OCH_3

24c :: X=butylene
24d :: X=1,4-bis(methylene)benzene
24e :: X=4,4'-dimethylene-1,1'-biphenyl
24f :: X=1,4-bis(methylene)-2,5-dimethylbenzene
24g :: X=1,3-bis(methylene)benzene
24h :: X=2,6-bis(methylene)pyridine

25c – 2k :: R_1/R_1'=R_2/R_2'=H

25c :: X=ethylene **25d** :: X=propylene
25e :: X=butylene **25f** :: X=butenylene
25g :: X=1,4-bis(methylene)benzene
25h :: X=4,4'-dimethylene-1,1'-biphenyl
25i :: X=1,4-bis(methylene)-2,5-dimethylbenzene
25j :: X=1,3-bis(methylene)benzene
25k :: X=2,6-bis(methylene)pyridine

26a :: R_1=R_2=OCH_2OCH_3; R_1'=R_2'=H; X=1,4-bis(methylene)benzene

22c, 23a – 23e :: R_1/R_1'=R_2/R_2'=OSO_3Na

22c :: X=butylene
23a :: X=1,4-bis(methylene)benzene
23b :: X=4,4'-dimethylene-1,1'-biphenyl
23c :: X=1,4-bis(methylene)-2,5-dimethylbenzene
23d :: X=1,3-bis(methylene)benzene
23e :: X=2,6-bis(methylene)pyridine

23f – 23n :: R_1/R_1'=R_2/R_2'= H

23f :: X=ethylene **23h** :: X=propylene
23g :: X=butylene **23i** :: X=butenylene
23j :: X=1,4-bis(methylene)benzene
23k :: X=4,4'-dimethylene-1,1'-biphenyl
23l :: X=1,4-bis(methylene)-2,5-dimethylbenzene
23m :: X=1,3-bis(methylene)benzene
23n :: X=2,6-bis(methylene)pyridine

23o :: R_1=R_2=OSO_3Na; R_1'=R_2'=H; X=1,4-bis(methylene)benzene

1i – 1n :: R_1/R_1'=R_2/R_2'=OH

24i :: X=butylene
24j :: X=1,4-bis(methylene)benzene
24k :: X=4,4'-dimethylene-1,1'-biphenyl
24l :: X=1,4-bis(methylene)-2,5-dimethylbenzene
24m :: X=1,3-bis(methylene)benzene
24n :: X=2,6-bis(methylene)pyridine

2k – 2t :: R_1/R_1'=R_2/R_2'=H

25l :: X=ethylene **25m** :: X=propylene
225n :: X=butylene **25o** :: X=butenylene
25p :: X=1,4-bis(methylene)benzene
25q :: X=4,4'-dimethylene-1,1'-biphenyl
25r :: X=1,4-bis(methylene)-2,5-dimethylbenzene
25s :: X=1,3-bis(methylene)benzene
25t :: X=2,6-bis(methylene)pyridine

26b :: R_1=R_2=OH; R_1'=R_2'=H; X=1,4-bis(methylene)benzene

Scheme 8. Chemical synthesis of sulfated diflavonoids. *a)* MOM-Cl (2 or 4 eq), DIPEA, DCM, rt, 12 hrs, 50 – 60%; *b)* K_2CO_3 (2 eq), dibromo-linker derivative (1 eq), DMF, rt, 12 hrs, 30 – 50%; *c)* TMS-Br, CH_2Cl_2, -30, 1hr then 0ºC, 12–24 hrs, 70 – 90%; *d)* SO_3/Me_3N (6 eq/-OH), Et_3N (10 eq/-OH), CH_3CN, microwave, 90–100 °C, 4–8 hrs, 60 – 90%.

3.3.2 Plasmin Inhibition by Sulfated diflavonoids

The inhibition of human plasmin by the sulfated diflavonoids and a polyphenol precursor were measured using a chromogenic substrate hydrolysis assay as previously described [275] In this assay the direct relationship between the initial rate of substrate hydrolysis and catalytic activity of a protease is utilized and the fractional decrease in initial rate of hydrolysis in the presence of an inhibitor is analyzed using a dose-response equation to calculate the potency (IC_{50}, HS) and efficacy (ΔY*)* parameters (refer to previous equation).

The sulfated diflavonoids varied significantly in their inhibition of plasmin. This observation was not surprising, as a similar trend was observed in the sulfate diflavonoid compounds studied previously[275] and the results further emphasize the dependence of plasmin inhibitory activity on the fine structure of the molecules. The type and length of linker proved to be a key determinant of inhibitory activity. The IC_{50}s of these compounds range from 6 µM to >1 mM. The efficacy of the compounds were, however, similar, being > 80%.

3.3.2.1 Quercetin Series

The new quercetin series of compounds had their IC_{50}s ranging from 6.3 – 231 µM. This was a marked improvement over the previous series having the non-aromatic straight chain linkers. Interestingly, there was striking variation in potency depending on the length of the aromatic linker as well as the position of the substituents. The most potent of these compounds, with IC_{50}s of ~6 µM and a 12-fold improvement over the previously identified inhibitor **(22c)**, had *p-xylenic* linkers (**23a, 23c**). The marked improvement in potency over the compounds with the non-aromatic linker suggests a possible important interaction of the aromatic group with plasmin. Replacement with a *m-xylenic* linker (**23d**) led to an 11-fold drop in activity, suggesting that an optimal orientation was important for inhibition. Changing the linker to a 2,6

dimethylpyridine linker (**23e**) resulted in a further drop of potency to 231 µM, suggesting possible unfavorable interactions arising from the heteroatom. There was also a 6-fold drop in potency with a 4,4'-dimethyl-1,1'-biphenyl linker (**23b**). Altogether, the results indicate the importance of the type of linker, its length and substitution on the potency.

3.3.2.2 Apigenin Series

The IC_{50}s of these compounds ranged from 20 to > 1 mM. The general trend observed with the quercetin series, where compounds with aromatic linkers were better inhibitors than the non-aromatic straight chain linkers, was also observed with the apigenin series. Furthermore, as with the quercetin compounds, the most potent of this series had a *p-xylenic* linker (**23l**).

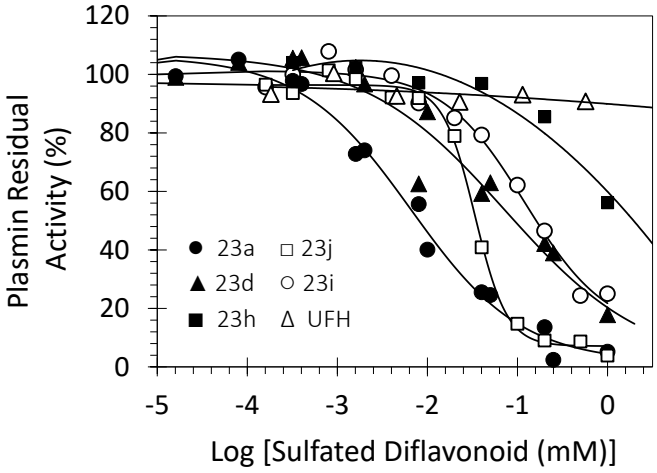

Figure 35. Plasma inhibition profiles of sulfated di-flavonoids.

Interestingly, substitution with a meta linker was not detrimental to inhibitory activity as was observed with the quercetin compounds and replacement with a 2,6-dimethylpyridine or 4,4'-dimethyl-1,1'-biphenyl linker also led to only a 2-fold drop in potency. These results suggest that the interaction of these two classes of compounds with plasmin may be different.

The potency of the *p-xylene*-linked apigenin-quercetin dimer (**23**o) was 14 µM, approximately the average of the two *p-xylene* linked homodimers of apigenin and quercetin.

Overall, the structure activity relationship suggests that aromatic linkers are preferred over non-aromatic linkers, with *p-xylenic* linkers being preferred. This suggests that a particular

three-dimensional and distance relationship between the two monomeric moieties is important for plasmin recognition. The trends in the potency of the two series of compounds also suggest that for preferred linkers, higher sulfation density is better, while for less preferred linkers, sulfation does not guarantee better inhibitory activity.

The inhibitory potency of the unsulfated polyphenol precursor of the most potent inhibitor was also determined to demonstrate the importance of the sulfate groups for plasmin inhibitory potency. The results showed that the unsulfated precursor of the most potent inhibitor (**24j**) was 116 μM, which is almost 20 fold less potent than that for the sulfated compound, showing the important role of the negatively charged sulfate groups for plasmin inhibitory activity.

Table 10. In vitro inhibition of human plasmin by NSGMs

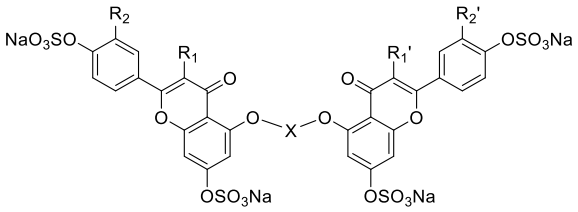

Inhibitor	R_1/ R_1`	R_2/ R_2`	X	IC_{50} (μM)	HS	Δ Y (%)
22c	OSO_3Na	OSO_3Na	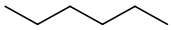	76 ± 12[b]	1.0 ± 0.2	72 ± 9
23a	OSO_3Na	OSO_3Na	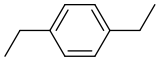	6.3 ± 0.4	0.7 ± 0.1	93 ± 4
23b	OSO_3Na	OSO_3Na	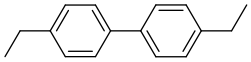	37 ± 7	0.8 ± 0.2	80 ± 11
23c	OSO_3Na	OSO_3Na	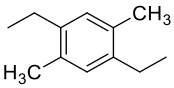	6.5 ± 0.7	0.7 ± 0.1	104 ± 7
23d	OSO_3Na	OSO_3Na	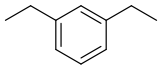	73 ± 11	0.6 ± 0.1	107 ± 7
23e	OSO_3Na	OSO_3Na	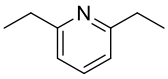	231 ± 27	0.8 ± 0.2	90 ± 5
23f	H	H		71 ± 2	2.4 ± 0.3	79 ± 3
23g	H	H	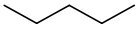	>1000	*ND*[c]	*ND*
23h	H	H	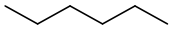	282 ± 17	1.8 ± 0.3	90 ± 8
23i	H	H	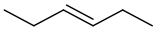	121 ± 18	0.9 ± 0.2	90 ± 11
23j	H	H	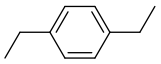	34 ± 1	2.4 ± 0.3	89 ± 2
23k	H	H	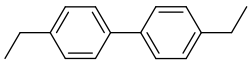	47 ± 2	1.1 ± 0.1	79 ± 3
23l	H	H	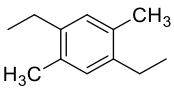	20 ± 1	2.0 ± 0.1	94 ± 2
23m	H	H	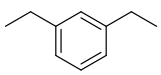	34 ± 2	2.3 ± 0.5	86 ± 4
23n	H	H	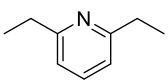	42 ± 3	1.2 ± 0.2	63 ± 4
23o	H/OSO_3Na	H/OSO_3Na	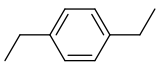	14 ± 1	0.9 ± 0.1	109 ± 6

3.3.3 Inhibition Studies of Thrombin, Factor IXa, Factor Xa, Factor XIa, Factor XIIa, Trypsin and Chymotrypsin

The inhibitory effects of the most potent sulfated diflavonoid on the serine proteases thrombin, FIXa, FXa, FXIa, FXIIa, trypsin and chymotrypsin were also studied using a chromogenic substrate assay employing appropriate small peptide-based chromogenic substrates for these enzymes.

The results from screening our most potent inhibitor against a large panel of coagulation and digestive serine proteases confirmed our hypothesis that targeting the less conserved allosteric sites was an effective way of achieving selectivity among a family of enzymes. There was vast variation in inhibitory potency of the inhibitor on the different enzymes, showing a clear selectivity for plasmin.

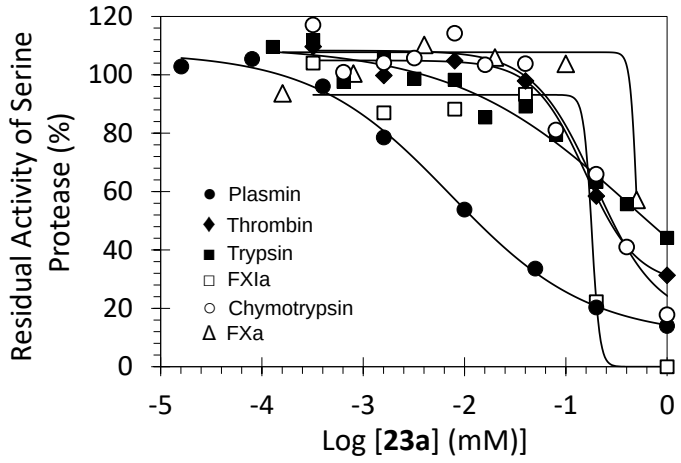

Figure 36. Selectivity studies for compound **23a**.

Of the serine proteases screened, thrombin was the most potently inhibited with an IC_{50} of 156 µM, a 22-fold difference in inhibitory activity relative to plasmin. The selectivity indices of the inhibitor against Xa, XIa, IXa, XIIa, trypsin and chymotrypsin were 70-, 26-, >277-, >138-, >61-, and 27-fold respectively, indicating a marked selectivity for plasmin. On the other hand the selectivity index for the unsulfated precursor against thrombin, FXa and FXIa, was only 2-fold. Thus, the unsulfated precursor does not differentiate among these serine proteases and most likely interacts at a site common to all these enzymes.

Table 11. Selectivity of NSGM **23a** and its precursor **24j** against a panel of related serine proteases

Inhibitor	Enzyme	IC_{50} (μM)	ΔY (%)	SI
23a	Plasmin	7.2 ± 0.6	98 ± 5	-
	Thrombin	156 ± 14	77 ± 8	22
	FXa	~505	*ND*[c]	70
	FXIa	180 ± 20	93 ± 11	26
	FIXa	>2000	*ND*	>277
	FXIIa	>1000	*ND*	>138
	Trypsin	>440	*ND*	>61
	Chymotrypsin	196 ± 39	92 ± 9	27
24j	Plasmin	116 ± 9	111 ± 8	-
	Thrombin	267 ± 28	91 ± 11	2
	FXa	212 ± 30	104 ± 17	2
	FXIa	208 ± 32	109 ± 16	2

3.3.4 Mechanism of Plasmin Inhibition by Compound 23a and Its Unsulfated Precursor 24j

In order to understand the mechanism of inhibition of the sulfated flavonoid, we performed Michaelis-Menten kinetics studies on the most potent inhibitor discovered, **23a**. This study was important in confirming whether the inhibitor bound at an allosteric site as we had proposed. This assay measures the V_{MAX} and K_M of the enzyme in the presence and absence of the inhibitors. The experiment was conducted at 37 ºC in a pH 7.4 Tris buffer containing 100 mM NaCl, 2.5 mM $CaCl_2$, 0.1% PEG8000, and 0.02% Tween80. The data were fitted to the Michaelis-Menten equation to determine $K_{M,}$ and V_{MAX}:

The same studies were performed using the unsulfated precursor of **23a, 24j**, which had shown moderate inhibitory activity towards plasmin and other serine proteases. A plot of the initial velocity with increasing concentrations of the substrate revealed a hyperbolic relationship in the absence and presence of **23a** and its unsulfated precursor, **24j**. The trends in the V_{MAX} and K_M values from the presence of the two inhibitors revealed a key difference in their mechanism of plasmin inhibition.

In the case of compound **23a**, there was decrease in the V_{MAX} with increasing concentrations of the inhibitor. A V_{MAX} of 42.2 ± 2.3 mAU/min was recorded in the absence of the inhibitor and this dropped gradually with increasing inhibitor concentrations to a significant 4-fold drop in the presence of 200 μM to 10.4 ± 0.5 mAU/min. This result is in agreement with a non-competitive inhibition mechanism. The Michaelis constant K_M also experienced a substantial gradual drop in value from 0.050 ± 0.001 mM in the absence of the inhibitor to 0.004 ± 0.001 mM, in the presence of 200 μM, representing a 12.5 fold decrease. The decrease in both V_{MAX} and K_M values in the presence of increasing inhibitor concentrations show that the inhibitor utilizes an uncompetitive inhibition mechanism.

The results obtained for the unsulfated precursor, **24j**, are totally different. There is no change in V_{MAX} with increasing inhibitor concentrations; however an increase in the K_M is observed. This result suggests competition between the substrate and the inhibitor for binding with plasmin at the active site of the enzyme. Thus, the unsulfated precursor is an orthosteric inhibitor. Considering the conserved nature of the active sites of serine proteases, this result explains the lack of selectivity observed with the unsulfated precursor.

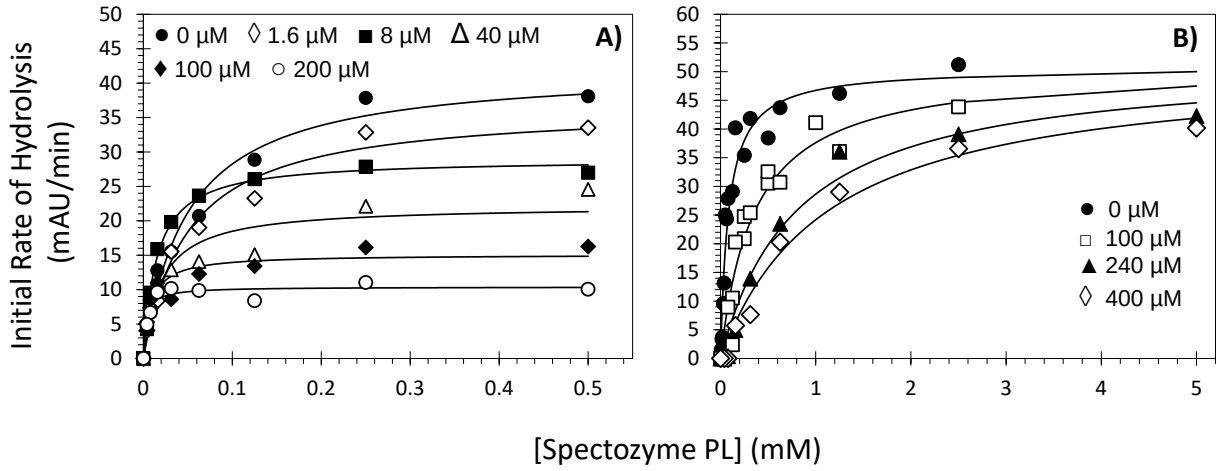

Figure 37. Michealis-Menten kinetics profiles for **23a** and **24j**.

Table 12. Michaelis-Menten kinetics of human plasmin in the presence of **23a** or its precursor **24j**

	[Inhibitor] (μM)	K_M (mM)	V_{MAX} (mAU/min)
23a	0	0.050 ± 0.001	42.2 ± 2.3
	1.6	0.050 ± 0.001	36.3 ± 2.0
	8	0.020 ± 0.001	29.0 ± 0.6
	40	0.020 ± 0.007	22.1 ± 1.9
	100	0.008 ± 0.003	15.1 ± 1.0
	200	0.004 ± 0.001	10.4 ± 0.5
24j	0	0.083 ± 0.014	50.6 ± 2.4
	100	0.357 ± 0.082	51.0 ± 4.6
	240	0.807 ± 0.180	51.7 ± 3.9
	400	1.122 ± 0.233	51.3 ± 4.0

3.3.5 Binding Affinity of Sulfated Diflavonoids for Plasmin

The thermodynamic binding affinity (K_D) of ligands to proteins is an important parameter in the study of their interactions. The thermodynamic binding affinity of the sulfated diflavonoids with both free plasmin and active-site blocked plasmin was studied by fluorescence experiments performed using a QM4 spectrofluorometer (Photon Technology International, Birmingham, NJ) in 20 mM TrisHCl buffer, pH 7.4, containing 100 mM NaCl, 2.5 mM $CaCl_2$, and 0.1% PEG8000 at 37 °C. In the determination of thermodynamic binding affinity, the inhibitors were titrated against a fixed concentration of plasmin and the change in intrinsic fluorescence, due to tryptophan (λ_{EM} =348 nm, λ_{EX} = 280 nm) was monitored as a function of inhibitor concentration. A saturating decrease in intrinsic fluorescence was observed for both free and active site blocked plasmin, ranging from 90-108%.

The binding affinities determined for compounds **23a**, **23b**, **23i**, and **23l** were 0.7±0.1 μM, 1.0±0.1 μM, 3.6±0.6 μM, and 1.9±0.2 μM, respectively, indicating a high affinity for plasmin. However, there are significant differences between the K_D and the IC_{50}s. The uncompetitive nature of the interaction may play a role in this observed difference. In this mechanism, the inhibitor binds to both the free enzyme (E) and the enzyme – substrate complex (E:S) with affinities that are different, which forms the basis for observed K_D to be less than the IC_{50}. This is also especially true because the substrate concentration used in the inhibition experiment was below the K_M. Thus, active site blocked plasmin was prepared for binding studies.

The affinity of sulfated diflavonoids for active site blocked plasmin, representing the plasmin-substrate complex, was also determined as above. The K_Ds calculated using the quadratic binding equation were 4.4±0.4 μM and 5.4±0.3 μM for **23a** and **23l**, respectively. These values, especially for **23a**, are significantly different from the affinity of ~700 nM measured for free plasmin–**23a** complex, but very similar to the observed IC_{50} of 6.3 μM. The results are in line with the expectation from the mechanistic basis of different conformational states of the free E and E:S complex and imply that NSGMs bind to plasmin at a site other than the active site.

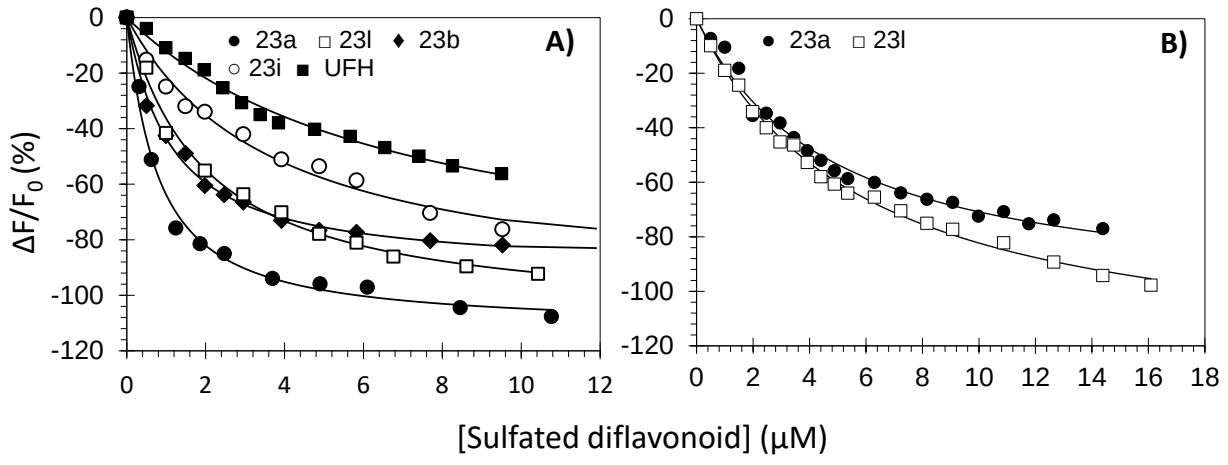

Figure 38. Binding affiinity of sulfated diflavonids for plasmin. (A) Native human plasmin (B) active-site-blocked plasmin.

Table 13. Dissociation equilibrium constants (K_D) and maximal fluorescence change (ΔF_{MAX}) for the interactions of NSGMs and UFH with human plasmin.

Inhibitor	K_D (μM)	ΔF_{MAX} (%)
Human plasmin		
23a	0.7 ± 0.1	-112 ± 3
23b	1.0 ± 0.1	-90 ± 2
23i	3.6 ± 0.6	-101 ± 7
23l	1.9 ± 0.2	-108 ± 3
UFH	6.7 ± 0.8	-97 ± 7
Active-site-blocked human plasmin		
23a	4.4 ± 0.4[b]	-103 ± 4
23l	5.4 ± 0.3	-128 ± 3

3.3.6 Binding Site of Sulfated Diflavonoids on Plasmin

Unfractionated heparin has been shown to bind to plasmin with high affinity in the nanomolar range, however the exact binding site is yet to be identified. The binding of heparin to plasmin does not result in inhibition of enzymatic activity. To confirm that the sulfated

flavonoids mimic heparin in regard to their sites of interaction with plasmin, we measured the potencies of the compound in the presence of increasing concentrations of UFH in pH 7.4 Tris buffer containing 0 or 100 mM NaCl, 2.5 mM $CaCl_2$, 0.1% PEG8000, and 0.02% Tween80 at 37 °C, using a microplate reader. A decrease in inhibitor potency with increasing UFH concentrations indicates a possible competition between the two compounds for plasmin interaction. The results obtained in both the NaCl-free and NaCl-containing buffer reveal the same trend. In both instances there is a gradual drop in inhibitor potency with increasing concentrations of UFH. In the NaCl-free buffer, the IC_{50} of plasmin inhibition by **23a** increased from 2.8 to 10.4 μM as the concentration of UFH increased from 0 to 285 μM.

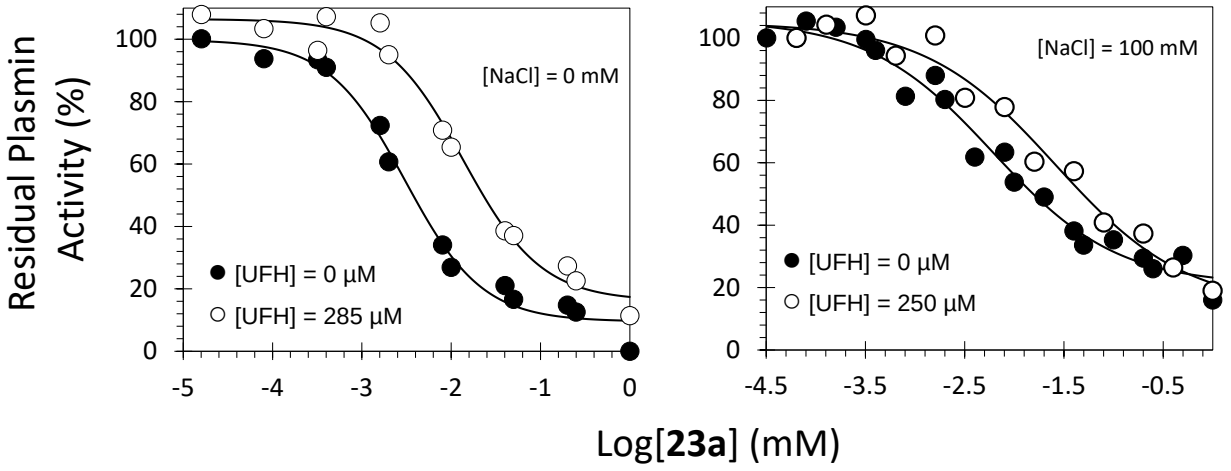

Figure 39. UFH Competition studies of compound **23a**.

Similarly in the buffer containing 100 mM NaCl, the IC_{50} increased from 6.1 to 25.9 μM with increasing UFH concentration from 0 to 250 μM. This drop in potency suggests competition of the inhibitor with UFH, possibly by binding the same site, though these data cannot entirely confirm this supposition..

Table 14. Inhibition of human plasmin by **23a** in the presence of UFH

[NaCl] (mM)	[UFH] (μM)	IC_{50} (μM)	HS	ΔY (%)
0	0	2.8 ± 0.3	1.0 ± 0.3	90 ± 7
	15	3.6 ± 0.3	1.3 ± 0.3	82 ± 5
	50	4.6 ± 0.7	0.8 ± 0.1	93 ± 13
	285	10.4 ± 1.2	1.0 ± 0.2	93 ± 7
100	0	6.1 ± 0.6	0.7 ± 0.1	85 ± 5
	50	14.1 ± 1.4	1.0 ± 0.2	81 ± 6
	250	25.9 ± 4.6	0.7 ± 0.1	91 ± 11

3.3.7 Salt Dependence of Plasmin Inhibition by Sulfated Diflavonoids

To assess the ionic contributions to the interaction between compound **23a** and plasmin, we assessed the inhibitory potency of **23a** in buffers containing different concentrations of NaCl (0, 100 and 200 mM) As can be seen from the results (Figure 40, Table 15), the potency of compound 2 decreases by a factor of about 2-fold for each 100 mM increase in NaCl concentration of the buffer. This indicates that ionic contributions contribute to the binding of compound **23a** to plasmin, which is not surprising due to the highly negatively charged nature of compound. Thus, the negatively charged sulfate groups possibly form ionic interactions with basic amino acid residues on the enzyme. That the effect on the potency is not marked suggests that

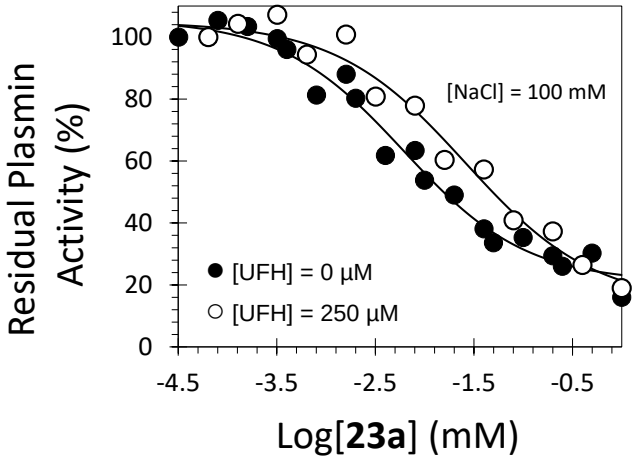

Figure 40. Salt dependence studies of 23a

the non-ionic interactions, possibly with the hydrophobic aromatic core of the compound, contribute significantly to the interaction.

Table 15. Salt-Dependence of Plasmin Inhibition by **23a**

[NaCl] (mM)	IC_{50} (μM)	HS	ΔY (%)
0	2.8 ± 0.3	1.0 ± 0.3	90 ± 7
100	6.3 ± 0.4	0.7 ± 0.1	93 ± 4
200	17.1 ± 2.7	0.8 ± 0.2	71 ± 7

3.3.8 Reversibility of Inhibitory Activity of Sulfated Diflavonoids

Considering the sensitive balance of coagulation, an important consideration in the development of coagulation altering drugs is the availability of antidotes in the event of drug overdose. Following the determination that ionic interactions contribute to the interaction compound **23a** and plasmin, we hypothesized that protamine, a known antidote for heparin, can reverse the inhibitory activity of compound **23a** on plasmin. Protamine is an arginine-rich polypeptide that functions by mopping up negatively charged species, such as heparin, and thus reduces their effective concentration in blood.[276] We thus monitored the in vitro reversibility of plasmin inhibition by measuring enzymatic activity in the presence of a saturating concentration

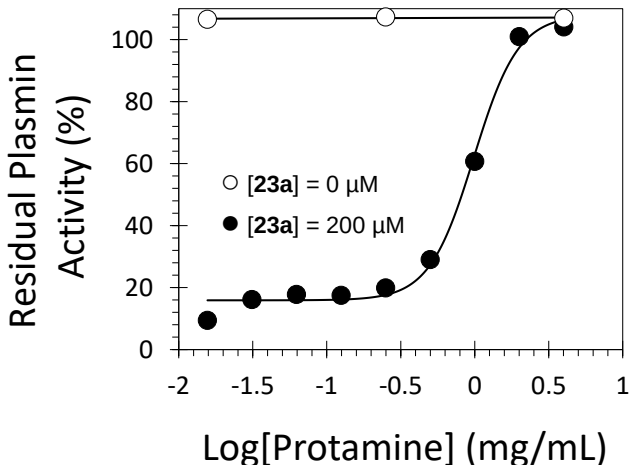

Figure 41. Protamine reversibility of activity of sulfated diflavonoids.

of the inhibitor, and increasing concentrations of protamine spectrophotometrically by measuring spectrozyme PL hydrolysis.

The results indicate that the inhibitory effect of **23a** is totally reversed by protamine sulfate with an efficacy of almost 100 %. The concentration of protamine required to restore enzymatic activity to 50% (EC_{50}) was 19.9 ± 0.8 mg/mL. These results, together with results from salt dependence studies, confirm the contribution of ionic interactions to the interaction of the sulfated diflavonoids with plasmin.

3.3.9 Inhibition of Clot Lysis by Sulfated Diflavonoids

Following demonstration of inhibition of hydrolysis of a small peptide chromogenic substrate by compound **23a**, the ability of the compound to inhibit plasmin mediated clot lysis was studies. This was done using in an in vitro assay by generating a fibrin rich clot through the action of thrombin on fibrinogen and subsequent addition of FXIIIa. The inhibition of clot lysis by plasmin in the presence of different inhibitor concentrations was monitored spectrophotometrically. The results clearly show that plasmin's lysis of the fibrin clot is inhibited by compound **23a** in a dose dependent manner.

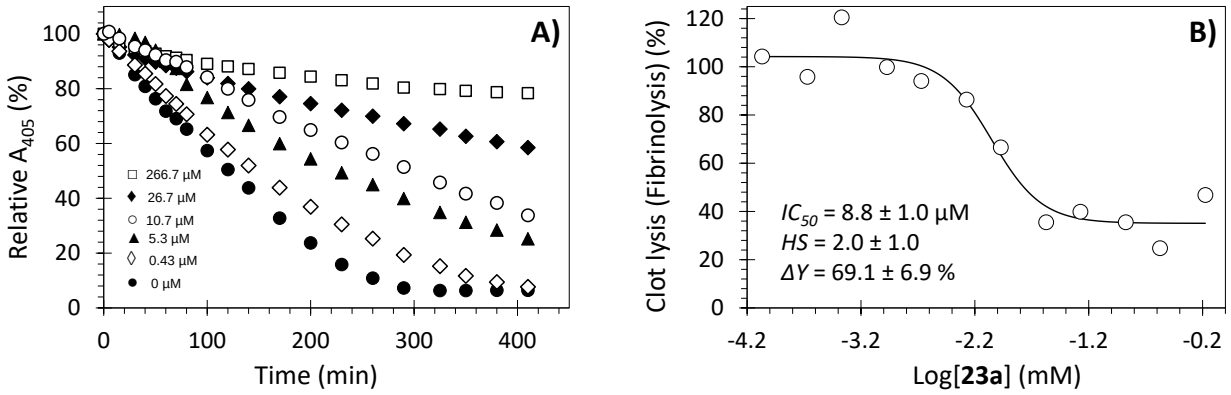

Figure 42. Inhibition of clot lysis by compound **23a**.

Under the study conditions, the clot is lysed in about 300 minutes in the absence of **23a**, however this is inhibited markedly by compound 2 in a dose dependent manner. Fitting the data obtained (the rate of clot lysis versus concentration of compound **23a**, results in a semilog sigmoidal plot (Figure 42B) from which the potency (IC_{50}), efficacy (ΔY) and Hill slope (HS) of inhibition can be obtained. The calculated IC_{50} for the inhibition was 8.8±1.0 μM and the efficacy of inhibition of clot lysis was 69.1±6.9%. The ability of the compound to inhibit plasmin mediated clot lysis is an important property of **23a** and indicates its promise as a lead antifibrinolysis agent.

3.3.10 Molecular Modeling Studies of Sulfated Diflavonoids

To study the interaction of sulfated diflavonoid compounds with plasmin, computational tools were employed. This was done with the aim of identifying key molecular interactions responsible for the inhibitory activity of the compounds. We reasoned that this exercise would shed more light on the structure activity relationship of the sulfated diflavonoid plasmin interaction. A GOLD-based docking and scoring of a selected group of sulfated diflavonoids covering the different structural variations was thus performed using our earlier methodology of GAGs and GAG mimetics docking to proteins.[102, 134,136]

The results clearly show that the sulfated diflavonoids **23a**, **23b**, **23c**, **23h**, **23i** and **23j** interact well with the allosteric site, whereas the unsulfated inhibitor **24j** preferentially binds in the active site. A detailed look at the proposed interaction between compound **23a** and plasmin revealed ionic interactions between Arg637, Arg779 and Arg664 and sulfate groups present on the compound. Similar interactions were observed with compound **23c**, which is equipotent with compound **23a**. The unsulfated precursor aligned itself in the active site of plasmin. A logIC_{50} vs GOLDSCORE plot for the six allosteric NSGMs docked onto plasmin shows a good correlation between the GOLDSCORE and the inhibition potency (R^2 = 0.92). These plots show that the

allosteric NSGMs interact with about the same group of electropositive residues in the heparin-binding site and differences in potency arise from different levels of hydrogen bonding interactions made by each inhibitor.

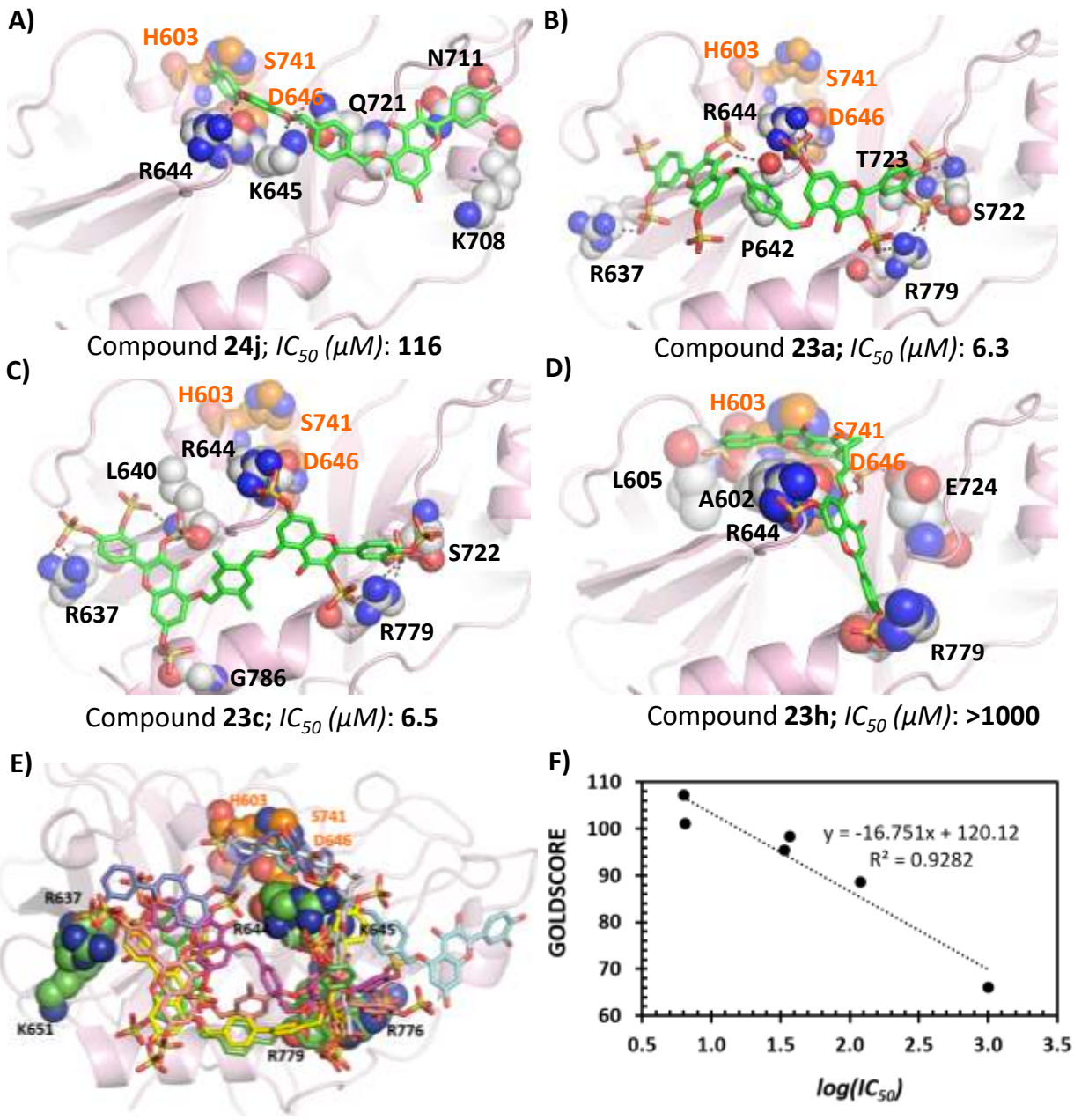

Figure 43. Computational study of sulfated diflavonoid-human plasmin interaction.

3.4 Conclusion

Plasmin is a very important serine protease whose regulation is necessary to normal physiological functioning.

This work has demonstrated that non-saccharide glycosaminoglycans have the potential to inhibit plasmin activity with moderate to high potency and is thus a significant addition to the search of anti-plasmin agents. The sulfated diflavonoids inhibit plasmin activity via an allosteric mechanism and do not interact at the active site, which is conserved among the serine proteases; accounting for the high selectivity for plasmin over other serine proteases.

The ability of these compounds to inhibit plasmin-mediated clot lysis also emphasizes the potential of this class of compounds as anti-fibrinolytic agents. Also, the highly charged nature of these compounds greatly increases their likelihood of crossing the blood-brain barrier and thus will be devoid of CNS effects, a major side effect of the current clinically used anti-fibrinolytic agents. Also, the fact that the anti-plasmin potential of this class of compounds was totally reversed by plasmin is an added advantage. However, it will be necessary to study these compounds in advanced pharmacological models before advancing their clinical importance.

Overall, this work has put forward sulfated di-flavonoid compounds as potent and selective anti-plasmin agents of which compound **23a** represents the best and most inspiring lead compound.

3.5 Experimental Section

3.5.1 Chemicals, Reagents, Enzymes, and Substrates

All anhydrous organic solvents were purchased from Sigma-Aldrich (Milwaukee, WI) or Fisher (Pittsburgh, PA) and used as such. Other solvents used were of reagent gradient and used as purchased. Analytical TLC was performed using UNIPLATE^{TM} silica gel GHLF 250 μm pre-coated plates (ANALTECH, Newark, DE). Silica gel (200-400 mesh, 60 Å), fibrinogen, and UFH were from Sigma-Aldrich. Chemical reactions sensitive to air or moisture were carried out under nitrogen atmosphere in oven-dried glassware. Reagent solutions, unless otherwise noted, were handled under a nitrogen atmosphere using syringe techniques. Flash chromatography was performed using Teledyne ISCO (Lincoln, NE). Combiflash RF was performed using disposable normal silica cartridges of 30–50 μ particle size, 230–400 mesh size and 60 Å pore size. The flow rate of the mobile phase was in the range of 18 to 35 mL/min and mobile phase gradients of ethyl acetate/hexanes and CH_2Cl_2/CH_3OH were used to elute compounds. Human plasmin, thrombin, factor Xa, and factor XIa were obtained from Haematologic Technologies (Essex Junction, VT). Stock solutions of serine proteases (plasmin, thrombin, factor Xa, and factor XIa) was prepared in 20 mM TrisHCl buffer, pH 7.4, containing 100 mM NaCl, 2.5 mM $CaCl_2$, 0.1% PEG8000, and 0.02% Tween80. Chromogenic substrates of thrombin (Spectrozyme TH), plasmin (Spectrozyme PL), and factor Xa (Spectrozyme FXa) were obtained from Sekisui Diagnostics (Lexington, MA). The chromogenic substrate of factor XIa (Chromogenix S-2366) was from DiaPharma (West Chester, OH).

3.5.2 Chemical Characterization of Synthesized Molecules

A Bruker-400 MHz spectrometer was used to record the ^{1}H and ^{13}C NMR of compounds in $CDCl_3$, acetone-d_6 or DMSO-d_6. Signals, in part per million (ppm), are either relative to the residual peak of the solvent or to the internal standard of TMS. The NMR data are reported as chemical shift (ppm), integration, multiplicity of signal (s= singlet, d= doublet, t= triplet, q= quartet, dd= doublet of doublet, m= multiplet), and coupling constants (Hz). A Waters Acquity TQD MS spectrometer was used in recording ESI-MS of compounds. MS of intermediate compounds was determined in positive ion mode and final products in negative ion mode. Samples were dissolved in methanol and infused at a rate of approximately 20 μL/min. Ionization conditions were optimized for each intermediate and final persulfated product to maximize the ionization of the parent ion.

3.5.3 Purity Analysis of Synthesized Compounds

Sulfated diflavonoid compounds were analyzed by UPLC with a Waters Acquity H-class UPLC system equipped with a photodiode array detector and triple quadrupole mass spectrometer. A reversed-phase Waters BEH C18 column of particle size 1.7 μm and 2.1 mm × 50 mm dimensions at 30±2 °C was used. Solvents A and B consisted of 25 mM n-hexylamine in water containing 0.1% (v/v) formic acid and 25 mM n-hexylamine in acetonitrile−water mixture (3:1 v/v) containing 0.1% (v/v) formic acid, respectively. A linear gradient of 3% solvent B per min over 20 min (initial solvent B proportion was 20% v/v) at a flow rate of 500 μL/min was used. The sample was monitored for absorbance in the range of 190−400 nm and then directly introduced into the mass spectrometer, with ESI-MS detection performed in positive ion mode. The following parameters were used; capillary voltage, 4 kV; cone voltage, 20 V; desolvation

temperature, 350 °C.; nitrogen gas flow, 650 L/h. Mass scans were collected in the range of 250−1500 amu within 0.25 s and several of these were added to enhanced signal-to-noise ratio.

3.5.4 Synthetic Procedure and Spectral Characterization Data

3.5.4.1 General Procedure for Flavonoid Monomers Protection by Methoxymethyl (MOM) Chloride

MOM protection of quercetin and apigenin molecules was achieved using MOM-Cl as previously reported.[172,275] Briefly, to a solution of quercetin or apigenin (1 eq) in DCM, *N*, *N*-diisopropylethylamine (DIPEA) (4-8 eq) and MOM chloride (4 eq for quercetin and 2 eq for apigenin) were added under nitrogen atmosphere. The reaction was stirred at 0 °C for 1 h, and the reaction mixture allowed to warm to room temperature over 2 h. The reaction was allowed to continue for a 12 h period. The reaction was quenched by diluting with water and the resulting mixture was extracted with ethylacetate (200 mL). The organic layer was then dried using Na_2SO_4, concentrated under reduced pressure, and purified by flash column chromatography using hexanes and ethyl acetate to obtain the tetraprotected quercetin **24b** as a yellow solid in yields of 50 – 55% and the diprotected apigenin **25b** as a cream solid in yields of 52 – 60%. Spectral characteristics of purified MOM protected flavonoid monomers are given below:

2-(3,4-bis(methoxymethoxy)phenyl)-5-hydroxy-3,7-bis(methoxymethoxy)-4H-chromen-4-one (24b). ^{1}H NMR (400 MHz, $CDCl_3$) δ 12.47 (s, 1H), 7.84 (d, *J* = 2.1 Hz, 1H), 7.64 (dd, *J* = 8.7, 2.1 Hz, 1H), 7.25 – 7.11 (m, 1H), 6.54 (d, *J* = 2.2 Hz, 1H), 6.39 (d, *J* = 2.1 Hz, 1H), 5.24 (d, *J* = 7.4 Hz, 4H), 5.17 (s, 2H), 5.11 (s, 2H), 3.47 (d, *J* = 4.6 Hz, 6H), 3.42 (s, 3H), 3.17 (s, 3H). ^{13}C NMR (100 MHz, $CDCl_3$) δ 178.60, 162.94, 161.91, 156.67, 156.49, 149.65, 146.60, 135.63, 124.42, 123.92, 117.74, 115.66, 106.63, 99.70, 97.81, 95.64, 95.10, 94.22, 94.14,

57.72, 56.41, 56.35. MS (ESI) calculated for $C_{23}H_{26}O_{11}$ $[(M+H)]^+$, m/z 478.15, found for $[(M+H)]^+$, m/z 478.907.

5-hydroxy-7-(methoxymethoxy)-2-(4-(methoxymethoxy)phenyl)-4H-chromen-4-one (25b). ^{1}H NMR (400 MHz, $CDCl_3$) δ 12.70 (s, 1H), 7.81 – 7.77 (m, 2H), 7.13 – 7.08 (m, 2H), 6.61 (d, J = 2.2 Hz, 1H), 6.54 (s, 1H), 6.43 (d, J = 2.2 Hz, 1H), 5.20 (d, J = 3.0 Hz, 4H), 3.46 (d, J = 1.2 Hz, 6H). ^{13}C NMR (100 MHz, $CDCl_3$) δ 182.48, 164.01, 163.00, 162.15, 160.27, 157.61, 127.99, 124.69, 116.61, 104.72, 100.10, 94.37, 94.30, 56.34, 56.21. MS (ESI) calculated for $C_{19}H_{18}O_7$ $[(M+Na)]^+$, m/z 359.11, found for $[(M+H)]^+$, m/z 359.171.

3.5.4.2 General Procedure for Flavonoid Dimerization by SN_2 Reaction.

Coupling of the quercetin- and apigenin-based monomers was achieved under basic conditions using different dibromo-linkers as reported earlier.[172,275] Briefly, to a solution of tetraprotected quercetin or dibrotected apigenin (1 eq) in *N, N*-dimethylformamide (DMF) was added K_2CO_3 (2.5 eq) and stirred for two minutes. 0.5 eq of the appropriate dibromo linker was added and the reaction stirred for 12 h at room temperature. The reaction was monitored be TLC and after reaching completion, it was quenched using 2N HCl. The mixture was diluted with a 50 mL, 50:50 mixture of ethylacetate:H_2O (50 mL; 1:1 mixture). The organic layer was then separated and the aqueous phase was further extracted with ethylacetate (2 × 25 mL). The organic layer was subsequently washed with saturated NaCl solution (25 mL). The resulting organic layers were combined, dried over anhydrous Na_2SO_4 and concentrated under reduced pressure to afford the crude intermediates **24c–26a**, that were further purified using flash chromatography on silica gel (70-85% ethyl acetate in hexanes). The pure intermediates were obtained as white to cream solids in yields of 30 - 50 %. Spectral characteristics of intermediate

1c matched earlier reports.[172,275] Spectral characteristics of the new purified intermediates are as follows:

5,5'-((1,4-phenylenebis(methylene))bis(oxy))bis(2-(3,4-bis(methoxymethoxy)phenyl)-3,7-bis(methoxymethoxy)-4H-chromen-4-one) (24d). ^{1}H NMR (400 MHz, $CDCl_3$) δ 7.97 (s, 1H), 7.86 (s, 2H), 7.62 (dd, *J* = 29.3, 8.9 Hz, 5H), 7.40 (t, *J* = 7.8 Hz, 1H), 7.16 (s, 1H), 6.65 (d, *J* = 2.4 Hz, 2H), 6.44 (s, 2H), 5.38 – 5.10 (m, 20H), 3.49 (d, *J* = 5.2 Hz, 12H), 3.43 (s, 6H), 3.19 (s, 6H). ^{13}C NMR (100 MHz, $CDCl_3$) δ 173.63, 161.28, 159.75, 158.56, 153.34, 149.19, 146.58, 137.96, 135.89, 127.03, 125.02, 123.71, 117.85, 115.78, 110.47, 98.64, 97.81, 95.88, 95.73, 95.18, 94.39, 77.32, 77.00, 76.68, 70.73, 57.65, 57.60, 56.41, 56.33. MS (ESI) calculated for $C_{54}H_{58}O_{22}$ $[(M+K)]^+$, m/z 1097.44, found for $[(M+K)]^+$, m/z 1097.373.

5,5'-(([1,1'-biphenyl]-4,4'-diylbis(methylene))bis(oxy))bis(2-(3,4-bis(methoxymethoxy) phenyl)-3,7-bis(methoxymethoxy)-4H-chromen-4-one) (24e). ^{1}H NMR (400 MHz, $CDCl_3$) δ 7.84 (d, *J* = 2.1 Hz, 2H), 7.68 – 7.51 (m, 11H), 7.20 (d, *J* = 4.6 Hz, 1H), 6.64 (d, *J* = 2.2 Hz, 2H), 6.44 (d, *J* = 2.2 Hz, 2H), 5.26 – 5.22 (m, 12H), 5.17 (s, 4H), 5.15 (s, 4H), 3.47 (d, *J* = 6.1 Hz, 12H), 3.41 (s, 6H), 3.17 (s, 6H). ^{13}C NMR (100 MHz, $CDCl_3$) δ 173.61, 161.26, 159.82, 158.58, 153.36, 149.22, 146.61, 140.29, 137.98, 135.49, 127.41, 127.35, 127.31, 127.29, 127.27, 125.04, 123.72, 117.92, 115.84, 110.56, 98.70, 97.82, 95.98, 95.76, 95.21, 94.40, 70.77, 57.59, 56.41, 56.39, 56.31. MS (ESI) calculated for $C_{60}H_{62}O_{22}$ $[(M+K)]^+$, m/z 1173.47, found for $[(M+K)]^+$, m/z 1173.046.

5,5'-(((2,5-dimethyl-1,4-phenylene)bis(methylene))bis(oxy))bis(2-(3,4-bis(methoxy-methoxy)phenyl)-3,7-bis(methoxymethoxy)-4H-chromen-4-one) (24f). ^{1}H NMR (400 MHz, $CDCl_3$) δ 7.87 (d, *J* = 2.1 Hz, 2H), 7.68 (d, *J* = 2.1 Hz, 1H), 7.66 (d, *J* = 2.1 Hz, 1H), 7.49 (s, 2H), 7.23 (d, *J* = 2.7 Hz, 2H), 6.67 (d, *J* = 2.2 Hz, 2H), 6.46 (d, *J* = 2.2 Hz, 2H), 5.26 (d, *J* = 4.3

Hz, 8H), 5.24 – 5.03 (m, 12H), 3.51 (d, *J* = 4.8 Hz, 12H), 3.46 (s, 6H), 3.20 (s, 6H), 2.36 (s, 6H). ^{13}C NMR (100 MHz, $CDCl_3$) δ 173.47, 161.28, 159.94, 158.59, 153.22, 149.18, 146.60, 137.93, 133.59, 133.34, 129.86, 125.07, 123.67, 117.90, 115.84, 110.52, 98.50, 97.77, 95.82, 95.75, 95.21, 94.42, 69.43, 57.56, 56.40, 56.31, 18.60. MS (ESI) calculated for $C_{56}H_{62}O_{22}$ $[(M+K)]^+$, m/z 1125.34, found for $[(M+K)]^+$, m/z 1125.026.

5,5'-((1,3-phenylenebis(methylene))bis(oxy))bis(2-(3,4-bis(methoxymethoxy)phenyl)-3,7-bis(methoxymethoxy)-4H-chromen-4-one) (24g). ^{1}H NMR (400 MHz, $CDCl_3$) δ 7.87 (d, *J* = 2.1 Hz, 2H), 7.70 – 7.55 (m, 5H), 7.42 (t, *J* = 7.6 Hz, 1H), 7.23 (d, *J* = 1.9 Hz, 2H), 6.66 (d, *J* = 2.1 Hz, 2H), 6.45 (d, *J* = 2.2 Hz, 2H), 5.26 (d, *J* = 4.0 Hz, 12H), 5.20 (s, 4H), 5.17 (s, 4H), 3.50 (d, *J* = 5.3 Hz, 12H), 3.44 (s, 6H), 3.20 (s, 6H). ^{13}C NMR (100 MHz, $CDCl_3$) δ 173.64, 162.49, 161.29, 159.74, 158.55, 153.36, 149.17, 146.55, 137.92, 136.71, 129.21, 126.15, 124.98, 124.57, 123.70, 117.80, 115.74, 110.43, 98.62, 97.79, 95.86, 95.70, 95.16, 94.36, 70.80, 57.60, 56.42, 56.34, 56.32. MS (ESI) calculated for $C_{54}H_{58}O_{22}$ $[(M+K)]^+$, m/z 1097.44, found for $[(M+K)]^+$, m/z 1097.337.

5,5'-((pyridine-2,6-diylbis(methylene))bis(oxy))bis(2-(3,4-bis(methoxymethoxy)phenyl)-3,7-bis(methoxymethoxy)-4H-chromen-4-one) (24h). ^{1}H NMR (400 MHz, $CDCl_3$) δ 8.89 – 8.80 (m, 2H), 8.53 – 8.47 (m, 1H), 7.84 (d, *J* = 2.1 Hz, 2H), 7.66 (d, *J* = 2.1 Hz, 1H), 7.64 (d, *J* = 2.1 Hz, 1H), 7.19 (d, *J* = 2.0 Hz, 2H), 6.75 (d, *J* = 2.0 Hz, 2H), 6.62 (d, *J* = 2.1 Hz, 2H), 5.70 (s, 4H), 5.26 – 5.22 (m, 8H), 5.21 (s, 4H), 5.15 (s, 4H), 3.49 (s, 6H), 3.47 (s, 6H), 3.45 (s, 6H), 3.15 (s, 6H). ^{13}C NMR (100 MHz, $CDCl_3$) δ 173.72, 161.59, 158.57, 157.78, 154.25, 149.44, 146.65, 137.88, 124.70, 123.82, 117.93, 115.83, 110.02, 99.20, 97.80, 96.84, 95.75, 95.19, 94.32, 66.12, 57.68, 56.57, 56.36, 56.33. MS (ESI) calculated for $C_{53}H_{57}NO_{22}$ $[(M+H)]^+$, m/z 1060.34, found for $[(M+H)]^+$, m/z 1060.072.

5,5'-(ethane-1,2-diylbis(oxy))bis(7-(methoxymethoxy)-2-(4-(methoxymethoxy)phenyl)-4H-chromen-4-one) (25c). ^{1}H NMR (400 MHz, $CDCl_3$) δ 7.85 – 7.76 (m, 5H), 7.38 – 6.82 (m, 5H), 6.78 (s, 2H), 6.65 (s, 2H), 5.18 (s, 8H), 4.54 (s, 4H), 3.80 – 3.26 (m, 12H). ^{13}C NMR (100 MHz, $CDCl_3$) δ 177.50, 162.49, 159.84, 159.52, 128.08, 116.57, 100.23, 96.63, 94.47, 94.25, 68.32, 56.58, 56.26. MS (ESI) calculated for $C_{40}H_{38}O_{14}$ $[(M+Na)]^+$, m/z 765.13, found for $[(M+Na)]^+$, m/z 765.393.

5,5'-(propane-1,3-diylbis(oxy))bis(7-(methoxymethoxy)-2-(4-(methoxymethoxy)phenyl)-4H-chromen-4-one) (25d). ^{1}H NMR (400 MHz, $CDCl_3$) δ 7.76 – 7.63 (m, 4H), 7.11 – 6.97 (m, 4H), 6.63 (d, J = 2.2 Hz, 2H), 6.50 (d, J = 2.2 Hz, 2H), 6.43 (s, 2H), 5.18 – 5.13 (m, 8H), 4.38 (t, J = 5.7 Hz, 4H), 3.42 (t, J = 1.7 Hz, 12H), 2.53 – 2.36 (m, 2H). ^{13}C NMR (100 MHz, $CDCl_3$) δ 177.39, 161.47, 160.45, 160.40, 159.59, 159.38, 127.55, 125.11, 116.43, 110.04, 107.89, 98.43, 95.51, 94.27, 65.72, 56.38, 56.17. MS (ESI) calculated for $C_{41}H_{40}O_{14}$ $[(M+Na)]^+$, m/z 779.14, found for $[(M+Na)]^+$, m/z 779.400.

5,5'-(butane-1,4-diylbis(oxy))bis(7-(methoxymethoxy)-2-(4-(methoxymethoxy)phenyl)-4H-chromen-4-one) (25e). ^{1}H NMR (400 MHz, $CDCl_3$) δ 7.73 (d, *J* = 8.7 Hz, 4H), 7.06 (d, *J* = 8.7 Hz, 4H), 6.59 (d, *J* = 2.1 Hz, 2H), 6.49 – 6.36 (m, 4H), 5.17 (d, *J* = 7.6 Hz, 8H), 4.28 – 4.10 (m, 4H), 3.43 (d, *J* = 2.6 Hz, 12H), 2.25 – 2.17 (m, 4H). ^{13}C NMR (100 MHz, $CDCl_3$) δ 177.27, 161.39, 160.39, 160.35, 159.61, 159.37, 127.64, 127.53, 125.16, 116.45, 109.97, 107.91, 98.03, 95.43, 94.35, 94.30, 69.12, 56.38, 56.16, 25.84. MS (ESI) calculated for $C_{42}H_{42}O_{14}$ $[(M+Na)]^+$, m/z 793.16, found for $[(M+Na)]^+$, m/z 793.442.

(E)-5,5'-(but-2-ene-1,4-diylbis(oxy))bis(7-(methoxymethoxy)-2-(4-(methoxymethoxy) phenyl)-4H-chromen-4-one) (25f). ^{1}H NMR (400 MHz, $CDCl_3$) δ 7.77 (d, *J* = 8.9 Hz, 4H), 7.09 (d, *J* = 8.9 Hz, 4H), 6.72 (d, *J* = 2.2 Hz, 2H), 6.52 (s, 2H), 6.48 – 6.42 (m, 4H), 5.20 (d, *J* = 6.4

Hz, 8H), 4.76 – 4.65 (m, 4H), 3.46 (d, *J* = 9.1 Hz, 12H). ^{13}C NMR (100 MHz, $CDCl_3$) δ 177.38, 161.42, 159.81, 159.66, 159.52, 127.61, 126.47, 125.06, 116.46, 107.95, 99.99, 95.86, 94.43, 94.28, 68.88, 56.44, 56.17. MS (ESI) calculated for $C_{42}H_{40}O_{14}$ $[(M+Na)]^+$, m/z 791.14, found for $[(M+Na)]^+$, m/z 791.150.

5,5'-((1,4-phenylenebis(methylene))bis(oxy))bis(7-(methoxymethoxy)-2-(4-(methoxy-methoxy)phenyl)-4H-chromen-4-one) (25g). ^{1}H NMR (400 MHz, $CDCl_3$) δ 7.79 – 7.72 (m, 4H), 7.58 (s, 4H), 7.11 – 7.03 (m, 4H), 6.70 (d, *J* = 2.2 Hz, 2H), 6.52 (s, 2H), 6.44 (d, *J* = 2.2 Hz, 2H), 5.23 – 5.13 (m, 12H), 3.43 (s, 12H). ^{13}C NMR (100 MHz, $CDCl_3$) δ 177.36, 161.32, 160.65, 159.65, 159.50, 135.91, 127.62, 126.94, 125.04, 116.54, 116.44, 110.37, 107.96, 99.02, 96.11, 94.40, 94.25, 70.71, 56.43, 56.20. MS (ESI) calculated for $C_{46}H_{42}O_{14}$ $[(M+Na)]^+$, m/z 841.16, found for $[(M+Na)]^+$, m/z 841.574.

5,5'-(([1,1'-biphenyl]-4,4'-diylbis(methylene))bis(oxy))bis(7-(methoxymethoxy)-2-(4-(methoxymethoxy)phenyl)-4H-chromen-4-one) (25h). ^{1}H NMR (400 MHz, $CDCl_3$) δ 7.91 – 7.79 (m, 5H), 7.64 – 7.51 (m, 7H), 7.16 – 7.04 (m, 6H), 6.89 – 6.73 (m, 2H), 6.60 – 6.46 (m, 2H), 5.32 – 5.10 (m, 12H), 3.49 – 3.43 (m, 12H). ^{13}C NMR (100 MHz, $CDCl_3$) δ 177.59, 159.78, 159.68, 140.30, 135.16, 128.19, 127.29, 127.27, 116.59, 99.42, 96.15, 94.52, 94.25, 70.85, 56.55, 56.27. MS (ESI) calculated for $C_{52}H_{46}O_{14}$ $[(M+Na)]^+$, m/z 917.19, found for $[(M+Na)]^+$, m/z 917.522.

5,5'-(((2,5-dimethyl-1,4-phenylene)bis(methylene))bis(oxy))bis(7-(methoxymethoxy)-2-(4-(methoxymethoxy)phenyl)-4H-chromen-4-one) (25i). ^{1}H NMR (400 MHz, $CDCl_3$) δ 7.96 – 7.65 (m, 4H), 7.57 (s, 2H), 7.20 – 7.01 (m, 6H), 6.81 (d, *J* = 2.1 Hz, 2H), 6.55 (d, *J* = 2.2 Hz, 2H), 5.32 – 5.02 (m, 12H), 3.55 – 3.31 (m, 12H), 2.36 (s, 6H). ^{13}C NMR (100 MHz, $CDCl_3$) δ 177.43, 159.86, 159.64, 133.44, 133.06, 129.48, 127.87, 116.52, 98.97, 95.98, 94.50, 94.25,

69.31, 56.52, 56.23, 18.60. MS (ESI) calculated for $C_{48}H_{46}O_{14}$ [(M+Na)] $^{+}$, m/z 869.19, found for [(M+Na)] $^{+}$, m/z 869.488.

5,5'-((1,3-phenylenebis(methylene))bis(oxy))bis(7-(methoxymethoxy)-2-(4-(methoxy-methoxy)phenyl)-4H-chromen-4-one) (25j). ^{1}H NMR (400 MHz, $CDCl_3$) δ 7.94 – 7.80 (m, 4H), 7.75 (s, 1H), 7.60 – 7.48 (m, 2H), 7.44 – 7.35 (m, 1H), 7.24 (s, 2H), 7.14 – 6.99 (m, 4H), 6.79 (d, *J* = 2.1 Hz, 2H), 6.64 – 6.51 (m, 2H), 5.31 – 5.14 (m, 12H), 3.55 – 3.31 (m, 12H). ^{13}C NMR (100 MHz, $CDCl_3$) δ 177.60, 162.43, 160.29, 159.74, 159.65, 136.48, 129.10, 128.12, 126.10, 124.65, 116.57, 99.32, 96.09, 94.51, 94.25, 70.89, 56.55, 56.26. MS (ESI) calculated for $C_{52}H_{46}O_{14}$ [(M+Na)]$^{+}$, m/z 841.16, found for [(M+Na)]$^{+}$, m/z 841.510.

5,5'-((pyridine-2,6-diylbis(methylene))bis(oxy))bis(7-(methoxymethoxy)-2-(4-(methoxy-methoxy)phenyl)-4H-chromen-4-one) (25k). ^{1}H NMR (400 MHz, $CDCl_3$) δ 8.73 (s, 2H), 8.38 (s, 1H), 7.92 – 7.57 (m, 4H), 7.17 – 6.98 (m, 4H), 6.82 (d, *J* = 2.1 Hz, 2H), 6.63 (d, *J* = 2.2 Hz, 2H), 6.55 (s, 2H), 5.62 (s, 4H), 5.40 – 5.01 (m, 8H), 3.63 – 3.25 (m, 12H). ^{13}C NMR (100 MHz, $CDCl_3$) δ 177.43, 161.77, 161.63, 159.99, 159.52, 157.70, 151.80, 130.89, 127.80, 124.58, 116.56, 109.77, 107.56, 99.79, 97.13, 94.38, 94.26, 66.22, 56.60, 56.23. MS (ESI) calculated for $C_{45}H_{41}O_{14}$ [(M+Na)]$^{+}$, m/z 842.15, found for [(M+Na)]$^{+}$, m/z 842.48.

2-(3,4-bis(methoxymethoxy)phenyl)-3,7-bis(methoxymethoxy)-5-((4-(((7-(methoxy-methoxy)-2-(4-(methoxymethoxy)phenyl)-4-oxo-4H-chromen-5-yl)oxy)methyl)benzyl)oxy)-4H-chromen-4-one (26a). ^{1}H NMR (400 MHz, $CDCl_3$) δ 7.88 – 7.81 (m, 3H), 7.66 (dd, *J* = 8.7, 2.1 Hz, 1H), 7.61 – 7.55 (m, 3H), 7.25 – 7.16 (m, 2H), 7.14 – 7.05 (m, 3H), 6.78 (d, *J* = 2.2 Hz, 1H), 6.65 (d, *J* = 2.2 Hz, 1H), 6.51 (d, *J* = 2.2 Hz, 1H), 6.44 (d, *J* = 2.3 Hz, 1H), 5.28 – 5.13 (m, 16H), 3.54 – 3.39 (m, 16H), 3.19 (s, 2H). ^{13}C NMR (100 MHz, $CDCl_3$) δ 177.50, 173.63, 161.30, 159.74, 158.55, 153.35, 149.19, 146.58, 137.95, 127.88, 127.03, 127.00, 125.01, 123.71, 117.85,

116.52, 115.78, 110.44, 98.64, 97.82, 96.10, 95.87, 95.73, 95.18, 94.39, 94.24, 84.54, 77.32, 77.00, 76.68, 70.71, 57.64, 57.60, 56.51, 56.42, 56.32, 56.24. MS (ESI) calculated for $C_{50}H_{50}O_{18}$, $[(M+Na)]^+$, m/z 961.29, found for $[(M+Na)]^+$, m/z 961.45.

3.5.4.3 General Procedure for Preparation of Polyphenolic Flavonoid Dimers by MOM Deprotection.

Complete deprotection of MOM groups was achieved using bromotrimethylsilane (TMS-Br). Briefly, to a solution of MOM-protected coupled produce in dry CH_2Cl_2, TMS-Br (6 eq per MOM group) was added. The reaction mixture was stirred at -30ºC for 1 h and then at 0 ºC for 12 – 24 h. The deprotection was monitored using MS until no MOM-protected products could be detected. Subsequently, ethylacetate was added to precipitate the polyphenol product from the reaction mixture. The precipitate was filtered, washed with excess ethylacetate to remove the excess TMS-Br, and dried to obtain pure polyphenols **24i–26b** as yellow to orange solid which were used in subsequent reactions without further purification. Spectral characteristics of intermediate **1i** matched earlier reports.[172,275] Spectral characteristics of the resulting new polyphenols are as follows:

5,5'-((1,4-phenylenebis(methylene))bis(oxy))bis(2-(3,4-dihydroxyphenyl)-3,7-dihydroxy-4H-chromen-4-one) (24j). ^{1}H NMR (400 MHz, DMSO-d_6) δ 10.73 (s, 2H), 9.34 (bs, 1H), 8.81 (s, 1H), 7.73 (s, 4H), 7.67 (d, *J* = 2.2 Hz, 2H), 7.51 (dd, *J* = 8.4, 2.2 Hz, 2H), 6.89 (d, *J* = 8.5 Hz, 2H), 6.54 – 6.46 (m, 4H), 5.25 (s, 4H). ^{13}C NMR (100 MHz, DMSO-d_6) δ 171.07, 162.36, 159.20, 157.89, 146.94, 145.03, 142.02, 137.24, 136.08, 126.54, 125.47, 122.28, 119.12, 115.58, 114.53, 105.45, 97.13, 94.86, 69.49. MS (ESI) calculated for $C_{36}H_{26}O_{14}$ $[(M+H)]^+$, m/z 707.13, found for $[(M+H)]^+$, m/z 706.892.

5,5'-(([1,1'-biphenyl]-4,4'-diylbis(methylene))bis(oxy))bis(2-(3,4-dihydroxyphenyl)-3,7-dihydroxy-4H-chromen-4-one) (24k). ^{1}H NMR (400 MHz, DMSO-d_6) δ 10.84 (s, 4H), 9.22 (bs, 2H), 7.77 (q, *J* = 8.5 Hz, 9H), 7.67 (d, *J* = 2.2 Hz, 2H), 7.54 – 7.52 (m, 1H), 7.50 (d, *J* = 2.2 Hz, 1H), 6.89 (d, *J* = 8.4 Hz, 3H), 6.51 (s, 4H), 5.29 (s, 4H). ^{13}C NMR (100 MHz, DMSO-d_6) δ 171.07, 162.35, 159.20, 157.89, 146.93, 145.02, 142.01, 139.06, 137.26, 136.17, 127.21, 126.51, 122.29, 119.13, 115.57, 115.04, 114.52, 105.48, 97.17, 69.41. MS (ESI) calculated for $C_{44}H_{40}O_{14}$ $[(M+H)]^+$, m/z 783.16, found for $[(M+H)]^+$, m/z 783.113.

5,5'-(((2,5-dimethyl-1,4-phenylene)bis(methylene))bis(oxy))bis(2-(3,4-dihydroxyphenyl)-3,7-dihydroxy-4H-chromen-4-one) (24l). ^{1}H NMR (400 MHz, DMSO-d_6) δ 10.79 (bs, 2H), 7.63 (d, *J* = 2.2 Hz, 2H), 7.57 (s, 2H), 7.48 (dd, *J* = 8.5, 2.2 Hz, 2H), 6.86 (d, *J* = 8.5 Hz, 2H), 6.53 (d, *J* = 2.1 Hz, 2H), 6.48 (d, *J* = 2.0 Hz, 2H), 5.14 (s, 4H), 2.37 (s, 6H). ^{13}C NMR (100 MHz, DMSO-d_6) δ 170.94, 162.34, 159.38, 157.91, 146.91, 145.02, 141.91, 137.14, 133.99, 133.23, 129.79, 122.28, 119.10, 115.57, 114.50, 105.42, 97.07, 94.78, 68.56. MS (ESI) calculated for $C_{40}H_{30}O_{14}$ $[(M+H)]^+$, m/z 735.17, found for $[(M+H)]^+$, m/z 734.960.

5,5'-((1,3-phenylenebis(methylene))bis(oxy))bis(2-(3,4-dihydroxyphenyl)-3,7-dihydroxy-4H-chromen-4-one) (24m). ^{1}H NMR (400 MHz, DMSO-d_6) δ 10.81 (bs, 6H), 7.65 (dd, *J* = 8.8, 2.2 Hz, 5H), 7.55 – 7.47 (m, 3H), 6.87 (dd, *J* = 8.5, 3.0 Hz, 2H), 6.49 (t, *J* = 1.9 Hz, 2H), 6.40 (d, *J* = 2.0 Hz, 1H), 6.17 (d, *J* = 2.0 Hz, 1H), 5.23 (s, 4H). ^{13}C NMR (100 MHz, DMSO-d_6) δ 175.79, 171.04, 163.84, 162.35, 160.67, 159.22, 157.88, 156.09, 147.66, 146.92, 145.02, 137.24, 136.85, 135.68, 122.28, 121.91, 119.94, 119.14, 115.58, 115.03, 114.50, 105.46, 102.98, 98.15, 93.32, 69.82. MS (ESI) calculated for $C_{36}H_{26}O_{14}$ $[(M+H)]^+$, m/z 707.13, found for $[(M+H)]^+$, m/z 706.960.

5,5'-((pyridine-2,6-diylbis(methylene))bis(oxy))bis(2-(3,4-dihydroxyphenyl)-3,7-dihydroxy-4H-chromen-4-one) (24n). ^{1}H NMR (400 MHz, DMSO-d_6) δ 10.77 (bs, 2H), 8.28 – 8.12 (m, 3H), 7.68 (d, J = 2.2 Hz, 2H), 7.53 (dd, J = 8.5, 2.2 Hz, 2H), 6.90 (d, J = 8.5 Hz, 2H), 6.62 – 6.45 (m, 4H), 5.40 (s, 4H). ^{13}C NMR (100 MHz, DMSO-d_6) δ 171.19, 162.46, 158.58, 157.81, 155.47, 147.03, 145.04, 142.42, 137.30, 122.20, 120.52, 119.23, 115.59, 114.58, 105.42, 97.46, 95.30, 69.88. MS (ESI) calculated for $C_{37}H_{25}NO_{14}$ $[(M+H)]^+$, m/z 708.14, found for $[(M+H)]^+$, m/z 707.920.

5,5'-(ethane-1,2-diylbis(oxy))bis(7-hydroxy-2-(4-hydroxyphenyl)-4H-chromen-4-one) (25l). ^{1}H NMR (400 MHz, DMSO-d_6) δ 10.67 (s, 2H), 10.16 (s, 2H), 7.84 (d, J = 8.8 Hz, 4H), 6.97 – 6.79 (m, 4H), 6.59 – 6.53 (m, 4H), 6.49 (s, 2H), 4.38 (s, 4H). ^{13}C NMR (100 MHz, DMSO-d_6) δ 175.50, 162.27, 160.39, 159.94, 159.50, 158.98, 127.96, 127.76, 125.49, 121.47, 115.81, 107.68, 105.93, 95.95, 68.01. MS (ESI) calculated for $C_{32}H_{22}O_{10}$ $[(M+H)]^+$, m/z 566.12, found for $[(M+H)]^+$, m/z 567.103.

5,5'-(propane-1,3-diylbis(oxy))bis(7-hydroxy-2-(4-hydroxyphenyl)-4H-chromen-4-one) (25m). ^{1}H NMR (400 MHz, DMSO-d_6) δ 11.52 (s, 2H), 7.93 (d, J = 8.1 Hz, 2H), 7.83 (dd, J = 8.8, 2.8 Hz, 2H), 6.92 (dd, J = 12.1, 8.4 Hz, 5H), 6.77 – 6.39 (m, 5H), 4.33 – 4.23 (m, 4H), 2.31 – 2.18 (m, 2H). ^{13}C NMR (100 MHz, DMSO-d_6) δ 175.66, 162.36, 160.37, 159.88, 159.80, 158.99, 137.62, 131.37, 128.02, 127.72, 125.46, 121.48, 116.59, 115.80, 107.24, 105.93, 97.11, 95.18, 64.88, 20.74. MS (ESI) calculated for $C_{33}H_{24}O_{10}$ $[(M+H)]^+$, m/z 581.14, found for $[(M+H)]^+$, m/z 581.273.

5,5'-(butane-1,4-diylbis(oxy))bis(7-hydroxy-2-(4-hydroxyphenyl)-4H-chromen-4-one) (25n). ^{1}H NMR (400 MHz, DMSO-d_6) δ 11.35 (s, 2H), 10.24 (bs, 2H), 8.29 – 7.69 (m, 5H), 7.01 – 6.87 (m, 4H), 6.75 – 6.22 (m, 5H), 4.80 – 3.87 (m, 4H), 2.44 – 1.61 (m, 4H). ^{13}C NMR

(100 MHz, DMSO-d_6) δ 175.50, 162.30, 160.34, 159.91, 158.94, 145.52, 137.69, 128.04, 127.69, 127.60, 125.46, 121.53, 116.59, 115.80, 107.26, 105.94, 95.06, 60.03, 48.57, 20.74. MS (ESI) calculated for $C_{34}H_{26}O_{10}$ $[(M+H)]^+$, m/z 595.15, found for $[(M+H)]^+$, m/z 595.952.

(E)-5,5'-(but-2-ene-1,4-diylbis(oxy))bis(7-hydroxy-2-(4-hydroxyphenyl)-4H-chromen-4-one) (25o). ^{1}H NMR (400 MHz, DMSO-d_6) δ 10.61 (s, 2H), 10.09 (s, 2H), 7.76 (d, *J* = 8.8 Hz, 4H), 6.82 (d, *J* = 8.7 Hz, 4H), 6.45 (d, *J* = 2.1 Hz, 2H), 6.41 (s, 2H), 6.33 (d, *J* = 2.2 Hz, 2H), 6.28 (s, 2H), 4.58 (s, 4H). ^{13}C NMR (100 MHz, DMSO-d_6) δ 175.27, 162.26, 160.63, 160.35, 159.84, 159.17, 154.90, 127.84, 127.72, 121.51, 121.22, 115.95, 115.81, 108.35, 107.37, 106.00, 105.80, 88.69, 68.18. MS (ESI) calculated for $C_{34}H_{24}O_{10}$ $[(M+H)]^+$, m/z 593.14, found for $[(M+H)]^+$, m/z 593.032.

5,5'-((1,4-phenylenebis(methylene))bis(oxy))bis(7-hydroxy-2-(4-hydroxyphenyl)-4H-chromen-4-one) (25p). ^{1}H NMR (400 MHz, DMSO-d_6) δ 11.48 (s, 2H), 10.32 (s, 2H), 8.17 – 7.79 (m, 5H), 7.64 (s, 3H), 7.01 – 6.84 (m, 5H), 6.66 (d, *J* = 8.4 Hz, 3H), 6.58 – 6.40 (m, 2H), 5.21 (s, 4H). ^{13}C NMR (100 MHz, DMSO-d_6) δ 175.30, 160.65, 159.90, 159.13, 158.00, 154.93, 135.90, 127.85, 127.73, 126.88, 126.81, 121.23, 116.09, 115.96, 115.82, 108.57, 105.82, 98.00, 88.96, 69.77. MS (ESI) calculated for $C_{38}H_{26}O_{10}$ $[(M+H)]^+$, m/z 643.15, found for $[(M+H)]^+$, m/z 642.978.

5,5'-(([1,1'-biphenyl]-4,4'-diylbis(methylene))bis(oxy))bis(7-hydroxy-2-(4-hydroxyphenyl)-4H-chromen-4-one) (25q). ^{1}H NMR (400 MHz, DMSO-d_6) δ 11.47 (s, 2H), 10.28 (bs, 2H), 7.94 (d, *J* = 8.8 Hz, 2H), 7.84 (d, *J* = 8.8 Hz, 2H), 7.78 – 7.58 (m, 8H), 7.44 – 7.23 (m, 2H), 7.12 – 6.83 (m, 4H), 6.77 – 6.59 (m, 2H), 6.59 – 6.41 (m, 2H), 5.24 (s, 4H). ^{13}C NMR (100 MHz, DMSO-d_6) δ 175.31, 160.66, 160.38, 159.91, 159.14, 158.01, 154.94, 128.61, 128.50, 127.86, 127.74, 127.51, 127.42, 127.00, 126.97, 126.56, 126.43, 126.30, 121.23, 116.10,

115.96, 115.83, 108.57, 105.84, 88.96, 69.66. MS (ESI) calculated for $C_{44}H_{30}O_{10}$ $[(M+H)]^+$, m/z 719.19, found for $[(M+H)]^+$, m/z 719.021.

5,5'-(((2,5-dimethyl-1,4-phenylene)bis(methylene))bis(oxy))bis(7-hydroxy-2-(4-hydroxyphenyl)-4H-chromen-4-one) (25r). ^{1}H NMR (400 MHz, DMSO-d_6) δ 11.46 (s, 2H), 10.30 (bs, 2H), 7.93 (d, *J* = 8.8 Hz, 3H), 7.87 – 7.76 (m, 1H), 7.68 – 7.55 (m, 2H), 7.00 – 6.86 (m, 5H), 6.71 (s, 2H), 6.65 (s, 1H), 6.56 – 6.50 (m, 2H), 5.12 (s, 4H), 2.33 (s, 6H). ^{13}C NMR (100 MHz, DMSO-d_6) δ 175.27, 160.64, 159.86, 159.14, 158.09, 154.94, 133.69, 132.89, 129.49, 127.84, 127.71, 121.26, 115.95, 115.82, 108.51, 105.83, 97.74, 88.79, 68.49, 18.13. MS (ESI) calculated for $C_{40}H_{30}O_{10}$ $[(M+H)]^+$, m/z 671.18, found for $[(M+H)]^+$, m/z 670.831.

5,5'-((1,3-phenylenebis(methylene))bis(oxy))bis(7-hydroxy-2-(4-hydroxyphenyl)-4H-chromen-4-one) (25s). ^{1}H NMR (400 MHz, DMSO-d_6) δ 10.71 (bs, 4H), 7.96 – 7.91 (m, 1H), 7.87 – 7.82 (m, 3H), 7.77 (s, 1H), 7.62 (dd, *J* = 7.6, 1.6 Hz, 1H), 7.54 – 7.35 (m, 2H), 6.92 (dd, *J* = 8.8, 6.8 Hz, 4H), 6.78 (s, 1H), 6.56 (d, *J* = 2.1 Hz, 1H), 6.53 (s, 1H), 6.50 – 6.48 (m, 2H), 6.20 (d, *J* = 2.1 Hz, 1H), 5.22 (s, 4H). ^{13}C NMR (100 MHz, DMSO-d_6) δ 181.69, 175.59, 164.09, 162.26, 161.42, 161.13, 160.39, 159.95, 159.29, 159.00, 157.28, 136.93, 128.42, 127.84, 127.74, 126.06, 121.17, 115.94, 115.83, 107.56, 105.98, 102.83, 95.61, 93.93, 69.85. MS (ESI) calculated for $C_{38}H_{26}O_{10}$ $[(M+H)]^+$, m/z 643.16, found for $[(M+H)]^+$, m/z 643.148.

5,5'-((pyridine-2,6-diylbis(methylene))bis(oxy))bis(7-hydroxy-2-(4-hydroxyphenyl)-4H-chromen-4-one) (25t). ^{1}H NMR (400 MHz, DMSO-d_6) δ 10.83 (s, 2H), 10.23 (s, 2H), 8.11 – 8.01 (m, 3H), 7.86 (d, *J* = 8.8 Hz, 4H), 6.93 (d, *J* = 8.8 Hz, 4H), 6.61 (d, *J* = 2.0 Hz, 2H), 6.56 (s, 2H), 6.54 – 6.43 (m, 2H), 5.28 (s, 4H). ^{13}C NMR (100 MHz, DMSO-d_6) δ 175.72, 162.39, 160.46, 160.15, 158.98, 158.84, 155.80, 138.48, 127.78, 121.44, 120.28, 115.84, 107.44, 106.01,

98.04, 95.88, 70.29. MS (ESI) calculated for $C_{37}H_{25}NO_{10}$ $[(M+H)]^+$, m/z 644.15, found for $[(M+H)]^+$, m/z 643.922.

2-(3,4-dihydroxyphenyl)-3,7-dihydroxy-5-((4-(((7-hydroxy-2-(4-hydroxyphenyl)-4-oxo-4H-chromen-5-yl)oxy)methyl)benzyl)oxy)-4H-chromen-4-one (26b). ^{1}H NMR (400 MHz, DMSO-d_6) δ 10.66 (s, 3H), 7.85 – 7.76 (m, 2H), 7.70 (d, J = 8.2 Hz, 2H), 7.64 – 7.58 (m, 2H), 7.55 – 7.37 (m, 2H), 6.91 – 6.77 (m, 3H), 6.56 – 6.35 (m, 5H), 5.21 – 5.14 (m, 4H). ^{13}C NMR (100 MHz, DMSO-d_6) δ 175.65, 162.29, 160.42, 159.26, 159.00, 157.87, 146.90, 145.02, 137.34, 136.10, 128.42, 127.77, 126.57, 126.47, 126.36, 122.32, 121.47, 115.94, 115.83, 115.57, 107.51, 105.99, 105.45, 95.53, 69.47. MS (ESI) calculated for $C_{38}H_{26}O_{12}$ $[(M+H)]^+$, m/z 675.15, found for $[(M+Na)]^+$, m/z 675.23.

3.5.4.4 General procedure for chemical sulfation of polyphenols

Microwave-assisted chemical protocol, as described earlier, was performed to yield persulfated diflavonoids.[172,275] Briefly, to a stirred solution of polyphenol in anhydrous CH_3CN (~3 mL) at room temperature, Et_3N (10 eq/-OH group) and SO_3/Me_3N complex (6 eq/-OH) were added. The reaction vessel was sealed and microwaved (CEM Discover, Cary, NC) for 4–8 h at 90-100 ºC. The reaction mixture was cooled and concentrated *in vacuo* at temperature <30°C. The reaction mixture was then purified on Combiflash RF system using CH_2Cl_2/CH_3OH mobile system (6:4) to obtain the persulfated molecules. The fractions containing the desired molecule were pooled together, concentrated *in vacuo*, and re-loaded onto a SP Sephadex C-25 column for sodium exchange. Fractions containing sodium salts of the per-sulfated molecules were pooled and lyophilized to obtain a fluffy white/off white powder. All sulfation reactions were quantitative with >65% yield. Spectral characteristics of sulfated diflavonoid **22c** matched earlier reports.[172,275] Spectral characteristics of the new final per-sulfated products are as follows:

Sodium 4-(5-((4-(((2-(3,4-bis(sulfonatooxy)phenyl)-4-oxo-3,7-bis(sulfonatooxy)-4H-chromen-5-yl)oxy)methyl)benzyl)oxy)-4-oxo-3,7-bis(sulfonatooxy)-4H-chromen-2-yl)-1,2-phenylene bis(sulfate) (23a). ^{1}H NMR (400 MHz, DMSO-d_6) δ 8.15 (d, J = 2.3 Hz, 2H), 8.09 (d, J = 2.3 Hz, 1H), 8.08 (d, J = 2.3 Hz, 1H), 7.76 (s, 4H), 7.65 (d, J = 8.9 Hz, 2H), 7.11 (d, J = 2.0 Hz, 2H), 6.82 (d, J = 2.2 Hz, 2H), 5.25 (s, 4H). ^{13}C NMR (100 MHz, DMSO-d_6) δ 172.98, 158.73, 158.34, 157.10, 153.49, 146.53, 142.95, 135.72, 135.32, 126.82, 124.50, 123.58, 119.89.03, 118.80, 109.56, 100.72, 99.38, 70.15.MS (ESI) calculated for $C_{38}H_{18}Na_8O_{38}S_8$ [(M-2Na)/2]$^{2-}$, m/z 737.8314, found for [(M- 2Na)/2]$^{2-}$, m/z 738.2780.

Sodium 4-(5-((4'-(((2-(3,4-bis(sulfonatooxy)phenyl)-4-oxo-3,7-bis(sulfonatooxy)-4H-chromen-5-yl)oxy)methyl)-[1,1'-biphenyl]-4-yl)methoxy)-4-oxo-3,7-bis(sulfonatooxy)-4H-chromen-2-yl)-1,2-phenylene bis(sulfate) (23b). ^{1}H NMR (400 MHz, DMSO-d_6) δ 8.13 (dd, J = 4.6, 2.3 Hz, 2H), 8.10 – 8.03 (m, 2H), 7.76 (s, 8H), 7.64 (dd, J = 8.9, 3.7 Hz, 2H), 7.07 (dd, J = 3.8, 2.0 Hz, 2H), 6.79 (d, J = 2.3 Hz, 2H), 5.26 (s, 4H). ^{13}C NMR (100 MHz, DMSO-d_6) δ 172.47, 158.61, 158.10, 157.02, 153.12, 146.35, 142.89, 139.19, 135.93, 135.29, 127.52, 126.65, 123.87, 119.98, 118.80, 109.80, 100.83, 69.86. MS (ESI) calculated for $C_{44}H_{22}Na_8O_{38}S_8$ [(M-2Na)/2]$^{2-}$, m/z 775.8471, found for [(M- 2Na)/2]$^{2-}$, m/z 776.6650

Sodium 4-(5-((4-(((2-(3,4-bis(sulfonatooxy)phenyl)-4-oxo-3,7-bis(sulfonatooxy)-4H-chromen-5-yl)oxy)methyl)-2,5-dimethylbenzyl)oxy)-4-oxo-3,7-bis(sulfonatooxy)-4H-chromen-2-yl)-1,2-phenylene bis(sulfate) (23c). ^{1}H NMR (400 MHz, DMSO-d_6) δ 8.14 (d, J = 2.4 Hz, 2H), 8.05 (dd, J = 8.9, 2.4 Hz, 2H), 7.63 (d, J = 8.9 Hz, 2H), 7.55 (s, 2H), 7.11 (d, J = 2.0 Hz, 2H), 6.83 (d, J = 2.1 Hz, 2H), 5.14 (s, 4H), 2.38 (s, 6H). ^{13}C NMR (100 MHz, DMSO-d_6) δ 172.68, 158.91, 158.18, 157.07, 153.22, 146.42, 142.90, 135.19, 133.85, 133.62, 130.20, 124.48,

123.80, 120.05, 118.84, 109.68, 100.63, 99.25, 69.10, 18.30. MS (ESI) calculated for $C_{40}H_{22}Na_8O_{38}S_8$ [(M- 2Na)/2]$^{2-}$, m/z 751.8471, found for [(M- 2Na)/2]$^{2-}$, m/z 751.7020.

Sodium 4-(5-((3-(((2-(3,4-bis(sulfonatooxy)phenyl)-4-oxo-3,7-bis(sulfonatooxy)-4H-chromen-5-yl)oxy)methyl)benzyl)oxy)-4-oxo-3,7-bis(sulfonatooxy)-4H-chromen-2-yl)-1,2-phenylene bis(sulfate) (23d). ^{1}H NMR (400 MHz, DMSO-d_6) δ 8.13 (dd, J = 6.3, 2.4 Hz, 2H), 8.03 – 7.97 (m, 2H), 7.67 – 7.40 (m, 6H), 7.17 (d, J = 2.0 Hz, 2H), 6.76 (d, J = 2.1 Hz, 2H), 5.28 (s, 4H). ^{13}C NMR (100 MHz, DMSO-d_6) δ 172.75, 158.71, 158.17, 157.05, 153.27, 146.42, 142.91, 136.74, 135.28, 128.64, 126.35, 124.52, 123.76, 119.99, 118.83, 109.69, 100.84, 99.30, 70.28. MS (ESI) calculated for $C_{38}H_{18}Na_8O_{38}S_8$ [(M- 2Na)/2]$^{2-}$, m/z 737.8314, found for [(M-2Na)/2]$^{2-}$, m/z 737.6929.

Sodium 4-(5-((6-(((2-(3,4-bis(sulfonatooxy)phenyl)-4-oxo-3,7-bis(sulfonatooxy)-4H-chromen-5-yl)oxy)methyl)pyridin-2-yl)methoxy)-4-oxo-3,7-bis(sulfonatooxy)-4H-chromen-2-yl)-1,2-phenylene bis(sulfate) (23e). ^{1}H NMR (400 MHz, DMSO-d_6) δ 8.15 – 8.05 (m, 7H), 7.65 (d, J = 8.9 Hz, 2H), 7.15 (d, J = 2.0 Hz, 2H), 6.78 (d, J = 2.2 Hz, 2H), 5.31 (s, 4H). ^{13}C NMR (100 MHz, DMSO-d_6) δ 172.62, 158.19, 157.04, 155.89, 153.35, 146.41, 142.89, 135.29, 124.48, 123.80, 120.27, 119.95, 118.74, 109.61, 99.43, 70.76. MS (ESI) calculated for $C_{37}H_{17}NNa_8O_{38}S_8$ [(M- 2Na)/2]$^{2-}$, m/z 738.3290, found for [(M- 2Na)/2]$^{2-}$, m/z 738.7981.

Sodium 4-oxo-5-(2-((4-oxo-7-(sulfonatooxy)-2-(4-(sulfonatooxy)phenyl)-4H-chromen-5-yl)oxy)ethoxy)-2-(4-(sulfonatooxy)phenyl)-4H-chromen-7-yl sulfate (23f). ^{1}H NMR (400 MHz, DMSO-d_6) δ 8.06 – 8.00 (m, 5H), 7.47 (s, 2H), 7.41 – 7.20 (m, 5H), 6.92 – 6.66 (m, 2H), 4.41 (s, 4H). ^{13}C NMR (100 MHz, DMSO-d_6) δ 175.78, 160.06, 157.54, 156.67, 155.59, 154.17, 127.21, 124. 68, 120.13, 110.67, 107.01, 101.69, 93.82, 67.92. MS (ESI)

calculated for $C_{32}H_{18}Na_4O_{22}S_4$ $[(M-2Na)/2]^{2-}$, m/z 463.9484, found for $[(M-2Na)/2]^{2-}$, m/z 464.0431.

Sodium 4-oxo-5-(3-((4-oxo-7-(sulfonatooxy)-2-(4-(sulfonatooxy)phenyl)-4H-chromen-5-yl)oxy)propoxy)-2-(4-(sulfonatooxy)phenyl)-4H-chromen-7-yl sulfate (23g). ^{1}H NMR (400 MHz, DMSO-d_6) δ 7.97 – 7.94 (m, 4H), 7.32 – 7.30 (m, 4H), 7.17 (d, J = 2.2 Hz, 2H), 6.71 – 6.70 (m, 4H), 4.35 – 4.28 (m, 4H), 2.30 – 2.23 (m, 2H). ^{13}C NMR (100 MHz, DMSO-d_6) δ 175.87, 159.82, 158.99, 158.17, 158.08, 156.26, 127.02, 125.09, 120.10, 109.54, 107.33, 100.23, 99.50, 65.27 MS (ESI) calculated for $C_{33}H_{20}Na_4O_{22}S_4$ $[(M-2Na)/2]^{2-}$, m/z 470.9562, found for $[(M-2Na)/2]^{2-}$, m/z 471.1272.

Sodium 4-oxo-5-(4-((4-oxo-7-(sulfonatooxy)-2-(4-(sulfonatooxy)phenyl)-4H-chromen-5-yl)oxy)butoxy)-2-(4-(sulfonatooxy)phenyl)-4H-chromen-7-yl sulfate (23h). ^{1}H NMR (400 MHz, DMSO-d_6) δ 7.97 – 7.94 (m, 4H), 7.33 (dd, J = 8.9, 1.2 Hz, 4H), 7.17 (d, J = 1.9 Hz, 2H), 6.73 (t, J = 1.7 Hz, 2H), 6.66 (d, J = 0.9 Hz, 2H), 4.22 – 4.03 (m, 4H), 2.09 – 1.99 (m, 4H). ^{13}C NMR (100 MHz, DMSO-d_6) δ 175.80, 175.49, 159.80, 159.71, 159.15, 158.17, 158.11, 157.98, 156.54, 156.30, 155.49, 154.15, 127.1, 127.00, 125.11, 124.86, 120.15, 110.55, 109.54, 107.31, 107.12, 101.10, 100.51, 99.45, 93.05, 68.65, 25.52, 25.31, 25.13. MS (ESI) calculated for $C_{34}H_{22}Na_4O_{22}S_4$ $[(M-2Na)/2]^{2-}$, m/z 477.9641, found for $[(M-2Na)/2]^{2-}$, m/z 478.2439.

Sodium (E)-4-oxo-5-((4-((4-oxo-7-(sulfonatooxy)-2-(4-(sulfonatooxy)phenyl)-4H-chromen-5-yl)oxy)but-2-en-1-yl)oxy)-2-(4-(sulfonatooxy)phenyl)-4H-chromen-7-yl sulfate (23i). ^{1}H NMR (400 MHz, DMSO-d_6) δ 7.99 – 7.93 (m, 4H), 7.35 – 7.31 (m, 4H), 7.21 (d, J = 2.0 Hz, 2H), 6.72 (d, J = 2.2 Hz, 2H), 6.68 (s, 2H), 6.40 (s, 2H), 4.69 (s, 4H). ^{13}C NMR (100 MHz, DMSO-d_6) δ 175.74, 159.88, 158.57, 158.20, 158.13, 156.36, 127.00, 126.89, 125.03,

120.11, 109.54, 107.30, 99.63, 68.34. MS (ESI) calculated for $C_{34}H_{20}Na_4O_{22}S_4$ $[(M-2Na)/2]^{2-}$, m/z 476.9562, found for $[(M-2Na)/2]^{2-}$, m/z 477.1390.

Sodium 4-oxo-5-((4-(((4-oxo-7-(sulfonatooxy)-2-(4-(sulfonatooxy)phenyl)-4H-chromen-5-yl)oxy)methyl)benzyl)oxy)-2-(4-(sulfonatooxy)phenyl)-4H-chromen-7-yl sulfate (23j). ^{1}H NMR (400 MHz, DMSO-d_6) δ 7.92 – 7.79 (m, 4H), 7.59 (s, 4H), 7.28 – 7.21 (m, 4H), 7.13 (d, *J* = 2.1 Hz, 2H), 6.71 (d, *J* = 2.2 Hz, 2H), 6.61 (s, 2H), 5.14 (s, 4H). ^{13}C NMR (100 MHz, DMSO-d_6) δ 175.80, 159.99, 158.54, 158.23, 158.12, 156.39, 136.08, 127.03, 126.82, 125.05, 120.14, 109.77, 107.33, 101.09, 99.89, 69.91. MS (ESI) calculated for $C_{38}H_{22}Na_4O_{22}S_4$ $[(M-2Na)/2]^{2-}$, m/z 501.9641, found for $[(M-2Na)/2]^{2-}$, m/z 502.2589.

Sodium 4-oxo-5-((4'-(((4-oxo-7-(sulfonatooxy)-2-(4-(sulfonatooxy)phenyl)-4H-chromen-5-yl)oxy)methyl)-[1,1'-biphenyl]-4-yl)methoxy)-2-(4-(sulfonatooxy)phenyl)-4H-chromen-7-yl sulfate (23k). ^{1}H NMR (400 MHz, DMSO-d_6) δ 8.00 – 7.87 (m, 4H), 7.84 – 7.58 (m, 8H), 7.34 (d, *J* = 8.9 Hz, 4H), 7.23 (d, *J* = 2.1 Hz, 2H), 6.82 (d, *J* = 2.2 Hz, 2H), 6.72 (s, 2H), 5.27 (s, 4H). ^{13}C NMR (100 MHz, DMSO-d_6) δ 175.81, 160.00. 158.53, 158.23, 158.12, 156.39, 139.14, 136.04, 127.50, 127.05, 126.58, 125.04, 120.14, 109.76, 107.32, 101.07, 99.91, 69.75. MS (ESI) calculated for $C_{40}H_{26}Na_4O_{22}S_4$ $[(M-2Na)/2]^{2-}$, m/z 540.07, found for $[(M-2Na)/2]^{-}$, m/z 539.761.

Sodium 5-((2,5-dimethyl-4-(((4-oxo-7-(sulfonatooxy)-2-(4-(sulfonatooxy)phenyl)-4H-chromen-5-yl)oxy)methyl)benzyl)oxy)-4-oxo-2-(4-(sulfonatooxy)phenyl)-4H-chromen-7-yl sulfate (23l). ^{1}H NMR (400 MHz, DMSO-d_6) δ 7.99 (d, *J* = 8.9 Hz, 4H), 7.69 (s, 2H), 7.34 (d, *J* = 8.9 Hz, 4H), 7.25 (d, *J* = 2.1 Hz, 2H), 6.87 (d, *J* = 2.2 Hz, 2H), 6.74 (s, 2H), 5.14 (s, 4H), 2.37 (s, 6H). ^{13}C NMR (100 MHz, DMSO-d_6) δ 175.77, 159.90, 158.66, 158.23, 158.13, 156.34, 133.87, 132.96, 129.61, 127.01, 125.08, 120.13, 109.69, 107.32, 100.86, 99.73, 68.72, 18.16. MS

(ESI) calculated for $C_{40}H_{26}Na_4O_{22}S_4$ $[(M-2Na)/2]^{2-}$, m/z 515.9797, found for $[(M-2Na)/2]^{2-}$, m/z 515.8131.

Sodium 4-oxo-5-((3-(((4-oxo-7-(sulfonatooxy)-2-(4-(sulfonatooxy)phenyl)-4H-chromen-5-yl)oxy)methyl)benzyl)oxy)-2-(4-(sulfonatooxy)phenyl)-4H-chromen-7-yl sulfate (23m). ^{1}H NMR (400 MHz, DMSO-d_6) δ 7.98 – 7.83 (m, 4H), 7.71 (s, 1H), 7.61 (dd, *J* = 7.6, 1.6 Hz, 2H), 7.41 (t, *J* = 7.6 Hz, 1H), 7.26 (d, *J* = 8.9 Hz, 4H), 7.23 (d, *J* = 2.1 Hz, 2H), 6.79 (d, *J* = 2.2 Hz, 2H), 6.71 (s, 2H), 5.23 (s, 4H). ^{13}C NMR (100 MHz, DMSO-d_6) δ 175.82, 159.97, 158.54, 158.22, 158.12, 156.38, 136.84, 128.37, 127.03, 126.15, 125.31, 125.05, 120.13, 109.76, 107.32, 101.10, 99.90, 70.09. MS (ESI) calculated for $C_{38}H_{22}Na_4O_{22}S_4$ $[(M-2Na)/2]^{2-}$, m/z 501.9641, found for $[(M-2Na)/2]^{2-}$, m/z 502.2365.

Sodium 4-oxo-5-((6-(((4-oxo-7-(sulfonatooxy)-2-(4-(sulfonatooxy)phenyl)-4H-chromen-5-yl)oxy)methyl)pyridin-2-yl)methoxy)-2-(4-(sulfonatooxy)phenyl)-4H-chromen-7-yl sulfate (23n). ^{1}H NMR (400 MHz, DMSO-d_6) δ 8.08 – 7.92 (m, 7H), 7.36 (d, *J* = 8.9 Hz, 4H), 7.29 (d, *J* = 2.0 Hz, 2H), 6.80 (d, *J* = 2.2 Hz, 2H), 6.75 (s, 2H), 5.29 (s, 4H). ^{13}C NMR (100 MHz, DMSO-d_6) δ 175.94, 160.15, 158.23, 158.20, 158.08, 156.42, 156.09, 137.84, 127.08, 124.99, 120.15, 119.98, 109.58, 107.33, 100.81, 99.95, 99.49, 70.65. MS (ESI) calculated for $C_{37}H_{21}NNa_4O_{22}S_4$ $[(M-2Na)/2]^{2-}$, m/z 502.4617, found for $[(M-2Na)/2]^{2-}$, m/z 502.3524.

Sodium 4-(4-oxo-5-((4-(((4-oxo-7-(sulfonatooxy)-2-(4-(sulfonatooxy)phenyl)-4H-chromen-5-yl)oxy)methyl)benzyl)oxy)-3,7-bis(sulfonatooxy)-4H-chromen-2-yl)-1,2-phenylene bis(sulfate) (23o). ^{1}H NMR (400 MHz, DMSO-d_6) δ 8.07 (d, *J* = 2.4 Hz, 1H), 7.99 (dd, *J* = 8.9, 2.3 Hz, 1H), 7.96 – 7.79 (m, 2H), 7.66 – 7.49 (m, 5H), 7.27 (dd, *J* = 9.0, 2.2 Hz, 2H), 7.22 – 7.09 (m, 1H), 7.01 (d, *J* = 2.0 Hz, 1H), 6.79 – 6.54 (m, 3H), 5.16 (d, *J* = 5.5 Hz, 4H). ^{13}C NMR (100 MHz, DMSO-d_6) δ 176.35, 173.11, 160.43, 159.10, 158.71, 158.56, 157.48,

156.82, 153.60, 146.83, 143.33, 136.51, 135.76, 127.56, 127.45, 125.56, 124.28, 120.63, 120.40, 119.19, 110.22, 107.84, 101.55, 100.36, 99.72, 70.43. MS (ESI) calculated for $C_{38}H_{20}Na_6O_{30}S_6$ $[(M- 2Na)/2]^{2-}$, m/z 619.8977, found for $[(M- 2Na)/2]^{2-}$, m/z 620.4034.

3.5.5 Serine Protease Inhibition Assays

Direct inhibition of human plasmin was measured using a chromogenic substrate hydrolysis assay on a microplate reader (FlexStation III, Molecular Devices, Sunnyvale, CA, USA), as reported earlier. 85 μL of 20 mM TrisHCl buffer, pH 7.4, containing 100 mM NaCl, 2.5 mM $CaCl_2$, 0.1% PEG8000, and 0.02% Tween80 was added to each well of a 96-well plate. This was followed by the addition of 5 μL of stock plasma to achieve a final plasma concentration of 25 nM. Subsequently 5 μL of sulfated diflavonoids, yielding final concentrations of 0-1 mM, was added to the wells. After a 10 minute incubation period, 5 μL of 1 mM Spectrozyme PL was rapidly added and the residual enzyme activity was measured from the initial rate of increase in A405. The Relative residual enzyme activity (*Y*) as a function of the concentration of sulfated molecule was fitted using logistic equation 1 to obtain the potency (IC_{50}), efficacy (ΔY) and Hill slope (*HS*) of inhibition.

$$Y = Y_0 + \frac{Y_M - Y_0}{1 + 10^{(log[Inhibitor]_0 - logIC_{50})(HS)}} \quad (1)$$

In this equation, *Y* is fractional residual activity, the ratio of residual plasmin activity in the presence of inhibitor to that in its absence. Y_M and Y_0 are the maximum and minimum possible values of the fractional residual protease activity respectively, which are used in evaluating the efficacy of enzymatic activity. IC_{50} is the concentration of the inhibitor that results in 50% inhibition of enzyme activity and it is used to evaluate the inhibitor's potency.

Direct inhibition of thrombin, factor IXa, factor Xa, factor XIa, factor XIIa, trypsin and chymotrypsin by inhibitor **23a** was measured using a chromogenic substrate hydrolysis assay on

a microplate reader (FlexStation III, Molecular Devices), as reported earlier. Briefly, to each well of a 96-well microplate containing 85–185 μL of 20 mM TrisHCl buffer, pH 7.4, containing 100 mM NaCl, 2.5 mM $CaCl_2$, 0.1% PEG8000, and 0.02% Tween80 at either 25 °C (thrombin) or 37 °C (factor IXa, factor Xa, factor XIa, factor XIIa, trypsin and chymotrypsin) or 20 mM TrisHCl buffer, pH 7.4, containing 100 mM NaCl, 2.5 mM $CaCl_2$, 0.1% PEG8000, 0.02% Tween80 and 33% Ethylene glycol at 37 37 °C (factor IXa) was added 5 μL of inhibitor **2** (0 – 20 mM) or vehicle and 5 μL of the enzyme. The final concentrations of the enzymes were 6 nM (thrombin), 250 nM (factor IXa), 1.09 nM (factor Xa), 0.75 nM (factor XIa), 10 nM (factor XIIa), 0.145 μg/mL (trypsin), and 0.5 mg/mL (chymotrypsin). After 5 min incubation, 5 μL of 1.0 mM Spectrozyme TH, 10.0 mM Spectrozyme FIXa, 2.5 mM Spectrozyme FXa, 6.9 mM S-2366, 5.0 mM Spectrozyme FXIIa, 3.2 mM SS-2222 or 5.0 mM Spectrozyme Cty was rapidly added and the residual enzyme activity was measured from the initial rate of increase in absorbance at 405 nm. Relative residual enzyme activity (Y, activity in the presence of inhibitor to that in its absence) as a function of inhibitor **23a** concentrations was fitted using logistic equation 1 to obtain the IC_{50}, ΔY, and *HS* of inhibition. The studies were repeated using the unsulfated precursor of **23a, 24j.**

3.5.6 Michaelis-Menten Kinetics of Spectrozyme PL Hydrolysis.

The initial rate of Spectrozyme PL hydrolysis by human plasmin (~25 nM) was monitored from the linear increase in absorbance at 405 nm corresponding to less than 10% consumption of the substrate. The initial rate was measured as a function of various concentrations of the substrate (0–2 mM) in the presence of fixed concentration of inhibitor **23a** (0–200 μM) or inhibitor **24j** (0 – 400 μM) in 20 mM TrisHCl buffer, pH 7.4, containing 100 mM

NaCl, 2.5 mM $CaCl_2$, 0.1% PEG8000, and 0.02% Tween80 at 37 °C. The data were fitted by Michaelis-Menten equation 2 to determine $K_{M,}$ and V_{MAX}:

$$V_i = \frac{V_{MAX} \times [S]}{K_M + [S]} \qquad (2)$$

3.5.7 Fluorescence–Based Binding Affinity Determination

Fluorescence experiments were performed using a QM4 spectrofluorometer (Photon Technology International, Birmingham, NJ) in 20 mM TrisHCl buffer, pH 7.4, containing 100 mM NaCl, 2.5 mM $CaCl_2$, and 0.1% PEG8000 at 37 °C. To determine the thermodynamic affinity of compounds **23a**, **23c**, **23j**, and **23l** for free plasmin, the titrations were performed by adding aliquots of 250 μM aqueous solution of inhibitors to 200 μL solution of plasmin (160 nM) and monitoring the fluorescence intensity at λ_{EM} =348 nm. The excitation and emission slits were set to 1.0 mm. The observed change in fluorescence (ΔF) relative to initial fluorescence (F_o) was fitted using equation 3 to obtain the dissociation constant (K_D) and the maximal change in fluorescence (ΔF_{MAX}) at saturation. Each measurement was performed three times.

$$\frac{\Delta F}{F_0} = \frac{\Delta F_{MAX}}{F_0} \times \frac{([P]_0 + [L]_0 + K_D) - \sqrt{([P]_0 + [L]_0 + K_D)^2 - 4[P]_0[L]_0}}{2\,[P]_0} \qquad (3)$$

3.5.8 Preparation of Active Site Blocked Plasmin

Active site blocked plasmin was prepared using 1,5-dansyl-EGR-cmk as previously described.[277] Human plasmin (25 μM) was treated with 1,5-dansyl-EGR-cmk (1 mM) in phosphate buffered saline (PBS) at 37 °C for 2 hours. At the end of the incubation, the activity of

the treated enzyme was determined using the chromogenic substrate hydrolysis to confirm active site blockage. Excess 1,5-dansyl-EGR-cmk was removed by overnight dialysis against PBS.

3.5.9 Fluorescence–Based Binding Affinity of 23a and 23l for Active Site Blocked Plasmin

Affinity of compounds **23a** and **23l** for active site blocked plasmin were determined using the changes in intrinsic tryptophan fluorescence (λ_{EM} =348 nm, λ_{EX} = 280 nm) at varying inhibitor concentrations. The buffer used was a 20 mM TrisHCl buffer, pH 7.4, containing 100 mM NaCl, 2.5 mM $CaCl_2$, and 0.1% PEG8000 at 37 °C. The titrations were performed as with free plasmin, but with a concentration of active-site-blocked plasmin of 500 nM. The data so obtained was fitted using equation 3 to obtain the dissociation constant (K_D) and the maximal change in fluorescence (ΔF_{MAX}) at saturation. Each measurement was performed three times.

3.5.10 Competition Studies with Heparin

A chromogenic substrate hydrolysis assay on a microplate reader (FlexStation III, Molecular Devices, Sunnyvale, CA, USA) was used in this studiy. To each well of a 96-well microplate containing 80 µL of the buffer was added 5 µL enzyme (stock of 500 nM, effective concentration in the well is ~25 nM) and 5 µL of UFH, final concentration 0 – 285 µM. After an incubation period of 5 minutes, 5 uL of potential plasmin inhibitor (0–20 mM aqueous solution) or vehicle alone was added. 5 µL of 1 mM Spectrozyme PL was rapidly added after incubating for 5 mins and the residual enzyme activity was measured from the initial rate of increase in A405. The results were then fitted to the logistic equation 1 to obtain the potency (IC_{50}), efficacy (ΔY) and Hill slope (HS) of inhibition.

3.5.11 Reversibility of Inhibitory Activity of Sulfated Diflavonoids

Generally, to each well of the 96-well microplate containing 86 µL of 20 mM Tris-HCl buffer of pH 7.4 containing 100 mM NaCl, 2.5 mM $CaCl_2$, 0.02% Tweeen80 and 0.1% PEG8000 was added 1 µL of inhibitor **2** (20 mM) or vehicle, 3 µL of plasmin (stock of 1.6 µM), and 5 µL of protamine sulfate (0 – 80 mg/mL; effective concentrations were 0 – 4 mg/mL) in a sequential manner. 5 µL of Spectrozyme PL (1 mM) was rapidly added after a 5 min incubation period, and the restored plasmin activity was measured from the initial rate of increase in absorbance at 405 nm over the time period of 20–120 sec. Stock of protamine sulfate was serially diluted to give 9 different aliquots in the wells. Relative restored plasmin activity at each concentration of protamine was calculated from the ratio of plasmin activity in the presence and absence of the reversing agent. Equation 4 was used to fit the dose dependence of restored protease activity to obtain the effective concentration of reversing agent required to restore 50% of enzyme activity at specific inhibitor concentration (EC_{50}) and the efficacy (ΔY) of reversing process.

$$Y = Y_0 + \frac{Y_M - Y_0}{1 + 10^{(log[protamine]_0 - logEC_{50})(-HS)}} \qquad (4)$$

3.5.12 Inhibition of Clot Lysis

The experiment was performed using a 96-well plate reader.The clot was generated by the addition of 80 µL of a solution of thrombin (2.5 µg/mL) in 20 mM TrisHCl containing 10 mM $CaCl_2$ to 60 µL of a solution of fibrinogen (10 mg/mL) and factor XIIIa (2 µg/mL) in 20 mM TrisHCl containing 10 mM $CaCl_2$. The resulting clot was stabilized for 15 min at 37 ºC. The absorbance was then measured at 405 nm and was about 0.91 across all 16 wells. Afterward, 5 µL compound 2 (or vehicle) (effective concentrations in the well were 0 – 666 µM) was added to each well resulting in no significant change in the A405 of the corresponding wells. Finally, 5 µL of human plasmin (stock of 1.6 µM) in 20 mM TrisHCl buffer of pH 7.4 containing 2.5 mM

$CaCl_2$ and 100 mM NaCl was added to each well and the A405 of each well was recorded over more than 400 min at various time intervals. In this assay, clost lysis results in a decrease in the A405. By semilog plotting the rate of clot lysis (fibrinolysis) over the time period of 50–200 min versus the corresponding concentrations of inhibitor **23a** using the logistic equation 1, the IC_{50} of fibrinolysis inhibition by this inhibitor and its efficacy were determined.

3.5.12.1 Molecular Modeling Studies.

The 3D coordinates of plasmin were extracted from protein databank (PDB ID: 3UIR). Molecular modeling studies were performed using protein preparation tools in Tripos Sybyl-X v2.2 (www.tripos.com/sybyl). Hydrogen atoms were added and minimized keeping all heavy atoms as aggregates. Potential site of binding was identified by analyzing the proteins electrostatic potential (Figure 1A) using APBS tool in PyMOL Molecular Graphics System, v1.5.0.4 (Schrödinger, New York, NY). The potential binding site included residues R637, R644, K645, K651, R776 and R779 and all residues within 18 Å of centroid were identified as part of the binding site. Inhibitors **24j**, **23a**, 2**3b**, **23c**, **23h**, **23j** and **23l** were modeled in Sybyl and docked into the structure using GOLD v5.2, as described earlier.[102] For each inhibitor, 300 genetic algorithm run, 100,000 iterations were employed in which the early termination option was disabled. Each docked pose was scored using GOLDSCORE and all poses were retained.

***Contributions**

1. Most biochemical assays for this work were performed by Dr. Rami A. Al-Horani
2. Molecular modeling experiments were performed by Dr. Nehru Viji Sankaranarayanan.

4 IDENTIFICATION OF SELECTIVE GAG OLIGOSACCHARIDES FOR HUMAN NETUTROPHIL ELASTASE

4.1 Introduction

4.1.1 Human Neutrophil Elastase

Human neutrophil elastase is the most potent among the hydrolytic enzymes produced by human neutrophils in response to infection and inflammation.[184,185] Others include cathepsin G, and proteinase 3.[278]. These enzymes belong to the serine protease family and are known as neutrophil serine proteases.[279] Neutrophil elastase, and to a lesser extent cathepsin G and proteinase 3, are known to degrade macromolecules including elastin, collagen, proteoglycan, fibrinogen and fibrin.[280,281] Structurally, human neutrophil elastase is a 218 amino acid residue single-chain polypeptide linked by four intramolecular disulfide bonds.[280]. The HNE sequence folds into two β-barrels that are each composed of six anti-parallel β-sheets.[30] HNE has an abundance of arginine residues making it highly basic, with an isoelectric point near 10. This abundance of basic amino acid residues ensures that most of its surface is highly positively charged.[30] Electrostatic interactions are thus very important in the interaction of human neutrophil elastase with other macromolecules including other proteins and glycosaminoglycans. [30–34]

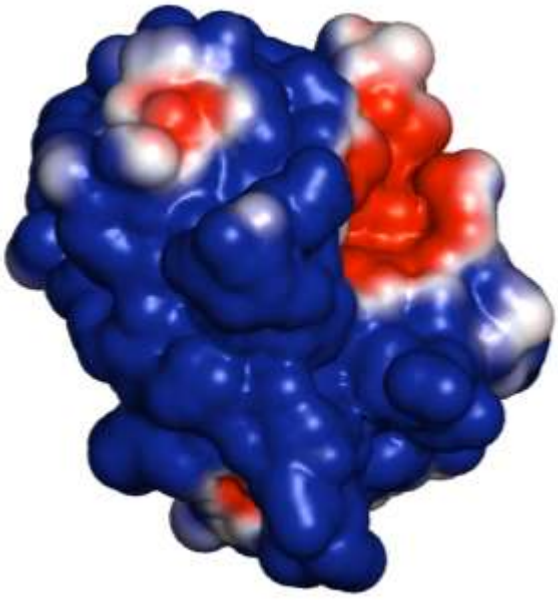

Figure 44. Structure of human neutrophil elastase showing highly electropositive surface.

4.1.2 Functions of Human Neutrophil Elastase

Human neutrophil elastase is known to play a key role in the human defense against infection. HNE and the other neutrophil serine proteases are important in the non-oxidative pathway of intracellular and extracellular pathogen destruction, and together with microbicidal peptides and reactive oxygen species, degrade engulfed microbes inside phagolysosomes.[282] The antimicrobial activity of HNE on gram positive bacteria results from cleavage of the outer membrane proteins and virulence factors by the enzyme.[283–286] However studies also indicate that the antimicrobial property of HNE is not solely a result of its proteolytic activity and that binding of HNE to the microbe alone is enough to affect its ability to cause infection.[282] Interestingly, there is data that shows that in some instances neutrophil elastase facilitates infection, as in the case of reovirus infection in U937 cells. [287] A wide range of matrix proteins, including elastin, collagen, fibronectin, laminin and proteoglycans, are known to be broken down by HNE, and by this activity it is important in the maintenance of tissue homeostasis.[288] Another role played by HNE is in the regulation of the inflammatory process.[289]This function is a result of regulation of the activities of a variety of proteins including chemokines, cytokines, growth factors, and cell surface receptors via proteolysis.[282] By activating lymphocytes and by lysis of apoptotic and adhesion molecules, HNE demonstrates both pro- and anti-inflammatory activities, hence its regulation of the immune response.[289]

In addition, HNE has been shown to be involved in cell apoptosis.[290–292] As with other proteases, HNE activity requires tight regulation to prevent damage resulting from excessive proteolysis and a number of physiological HNE inhibitors that regulate HNE activity are known. The most notable of these inhibitors is α-1 antitrypsin which is found in high concentrations in the blood. Peptidase inhibitor 3 and secretory leucocyte protease inhibitors are also HNE

inhibitors produced by epithelial cells. These form part of a defense mechanism to limit damage from HNE.[293]

4.1.3 Human Neutrophil Elastase as Drug Target

A balance of proteases and anti-proteases is required for normal physiology with an excess of HNE been shown to be detrimental.[294] HNE has been implicated in a number of inflammatory lung conditions including COPD, cystic fibrosis, acute lung injury and acute respiratory syndrome. HNE levels and activity are grossly elevated in these conditions and HNE's broad hydrolytic property results in the degradation of elastin, which is the elastic component of lung tissue, and other components of lung matrix. [282,295] Further, HNE induces the release of pro-inflammatory cytokines including interleukin 6 and interleukin 8.[186]. Houghton et al. have also shown that, via its degradation of insulin receptor substrate-1, HNE directly promotes the growth of tumor cells in both human and mouse adenocarcinomas.[296] HNE has also been implicated in rheumatoid arthritis (RA) and it is thought that it potentiates the damage to tissues due to its hydrolytic activity on structural components of cartilage.[297,298] The concentrations of elastase-inhibitor complex have been found to be elevated in plasma of rheumatoid arthritis and systemic lupus erythematosus (SLE) patients, further pointing to the role of this protease in these conditions.[299] Therapeutic strategies towards minimizing HNE levels, and thus their deleterious effects, will be beneficial in these disease conditions.[282] Key amongst these is targeting excess HNE using inhibitors.

It has been demonstrated that regulation of the HNE levels leads to improvement of chronic lung diseases such as COPD,[288] emphysema,[300–302] as well as acute lung injury.[303,304] Also elastase inhibitors drastically increased survival in rats with pulmonary hypertension.[305] The same can be said for arthritis and Kakimoto et al. have demonstrated that a neutrophil

elastase inhibitor diminished the occurrence and severity of arthritis in both mouse and rat models.[306] Despite these studies indicating the immense benefit to be derived from HNE inhibitors, no HNE inhibitor has been approved for clinical use to date, but there are a number these in clinical studies. [307] Major limitations to the development of these agents include achieving potency, selectivity and stability.[307] The majority of these agents developed are small molecule active site inhibitors, with a number of high molecular weight peptide inhibitors also identified.[295] Glycosaminoglycans are also another class of macromolecules that inhibit HNE activity. [32, 34, 88,308]

4.1.4 Inhibition of HNE by GAGs

GAGs, including heparin and heparan sulfate, chondroitin sulfate and dermatan sulfate have been shown to be potent inhibitors of HNE.[32, 34, 88,308] Electrostatic interactions between the negatively charged sulfates and carboxylates on GAGs and the positively charged arginine residues on the GAGs are known to be important in this interaction.[33] Studies have shown that GAG chain length is important for HNE inhibition and although the required chain length for inhibition remains unknown, reports indicate that GAG molecular weight of greater than about 2 KDa is required for activity.[33] Additionally, Spencer et al. mention that a dodeca- or tetradeca-saccharide is minimally needed to achieve HNE inhibition.[88] GAG sulfation levels and patterns have also been demonstrated to be important for HNE inhibition.[32,309] For instance, it has been demonstrated that 6-O and N-sulfates are the most important heparin sulfate groups required for HNE inhibition, with 2-O and 3-O sulfates being less important. The mechanism of inhibition of HNE by GAGs remains controversial. Whereas earlier reports indicate that it is via an allosteric mechanism,[32] a recent publication by Spencer et al mention that it is a competitive mechanism.[88]

4.2 Rationale for Studies

Though GAGs, including heparin, are potent inhibitors of HNE, their anticoagulant and other effects limit their usefulness in conditions where the inhibition of HNE activity may be useful. For instance, in the case of inflammatory lung conditions, there is the possibility of associated bleeding with the use of heparin as an inflammatory modulator and HNE inhibiting agent. The discovery of 2-O,3-O desulfated heparin (ODSH), a modified heparin was a significant improvement in this regard, as ODSH maintains GAG anti-HNE activity with loss of anticoagulant effects.[310] It has also been demonstrated that ODSH further maintains anti-inflammatory activity via its interaction with p300 histone acetyl transferase and possibly high mobility group box protein 1 (HMGB1).[311] ODSH, however, also has a major limitation in that it is highly polymeric, heterogeneous and structurally undefined. These are serious limitations that may present challenges in its use as a therapeutic agent. Based on previous results that suggest that GAGs with shorter chain length may retain anti-HNE activity, we reasoned that it should be possible to identity a GAG oligosaccharide, with defined structure, having potent anti-NE activity. This GAG would be selective for HNE and thus have fewer unwanted effects. We decided to use a combination of biochemical and computational methods to arrive at GAG oligosaccharide sequences with potent anti-HNE activity. We also sought to further elucidate the mechanism by which HNE is inhibited by GAGs.

4.3 Results and Discussion

4.3.1 Size Fractionation of ODSH

Our initial efforts at obtaining oligosaccharides from ODSH employed the use of molecular weight cut-off filters. Two molecular cut-off filters with exclusion limits of 10 kDa and 3 kDa were employed, and by using these, three fractions were obtained. These were;

fractions with molecular weight less than 3 kDa, greater than 3 kDa but less than 10 kDa, and greater than 10 kDa. The anti-HNE potentials of these fractions were subsequently determined.

Further, preparative size exclusion chromatography (SEC) was employed to yield well separated size fractions of poly- and oligo- saccharides from ODSH. The use of SEC in the separation has been widely reported in literature and has been shown to yield different sized species, from an initial heterogeneous species. Preparative SEC of ODSH was performed on a G75 matrix and the fractions collected were frozen and lyophilized to dryness. Subsequently, the analytical SEC-HPLC was performed to assess the different fractions and assess for shorter chain oligosaccharides. The results indicated that the size fractionation was successful, with ODSH species of different molecular weights obtained. However, GAGs with molecular weights less than that of enoxaparin (4.5 kDa) were not achieved. While disappointing, this is not surprising as the preparation of ODSH requires desalting using SEC, which can lead to the loss of smaller molecular weight species.

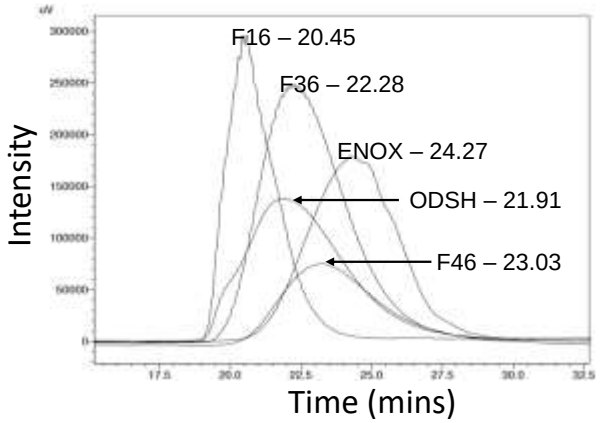

Figure 45. SEC HPLC analysis of size-fractionated ODSH.

4.3.2 Enzymatic Depolymerization of ODSH

Since our bid to obtain lower molecular weight oligosaccharides from ODSH by SEC of the heterogeneous polymeric mixture was not successful, we tried to use enzymatic methods to depolymerize ODSH into smaller sized oligosaccharides. To achieve this we tried a number of GAG lyases, including heparanase and heparin lyase I, II, and III. These enzymes have previously been used to obtain oligosaccharides from heparan sulfate and heparin. In this technique, preparative SEC is employed to obtain GAG oligosaccharides of different molecular weights following enzymatic digestion of ODSH.

For heparanase depolymerization, ODSH was dissolved in MES buffer, followed by the addition of heparanase and incubation at 37 ºC, with the enzymatic reaction being monitored at different time intervals for oligosaccharide formation using SEC HPLC for up to 48 hours. The analysis indicated that depolymerization of ODSH using heparanase was not achieved as no oligosaccharides were detected. These result indicate that ODSH is not a suitable substrate for heparanase, an are not surprising as these enzyme are known to require particular saccharide units and sulfation patterns for cleavage of GAGs.

Employing heparin lyase I, III and II for the depolymerization process, however, yielded very different results. The study of ODSH polymerization using heparin lyases was done on µg scale in a pH 7.4 PBS buffer at 25 ºC and monitored using UPLC MS for a period of 1 -24 hours. The results indicate that the heparin lyases differ greatly in their digestion of ODSH. The digestion of ODSH by heparin lyases I and II resulted in mostly smaller fragments of ODSH, with disaccharide species accounting for about 85%. Tetrasaccharide, pentasaccharide and hexasaccharide species made up the rest of the oligosaccharides with 0.5-1% only being octasaccharide species. Heparin lyase III on the other hand did not lead to the depolymerization

of ODSH and no oligosaccharide fragements were observed. These results, while again disappointing, can be attributed to the difference in structure of ODSH from the naturally available GAGs, heparan sulfate and heparin, and the differences in depolymerization capabilities of the different enzymes.

Table 16. Heparin lyase depolymerization of ODSH

	% of Oligosaccharide Species		
	HEP I	**HEP II**	**HEP III**
dp2	84	87	No digestion
dp4	1.36	1.5	
dp5	8.6	5.4	
dp6	4.6	4.6	
dp8	1	0.5	
dp10	0	0	

4.3.3 Preparation of ODSE.

2-O,3-O-desulfated enoxaparin was obtained by the alkaline hydrolysis of enoxaparin using NaOH. This is the same method employed in the preparation of 2-O,3-O-desulfated heparin as detailed in the patent by Holme et al.[312] Alkaline treatment leads to a loss of sulfates as the 2 positon of iduronic acid and 3 position of glucosamine. Since the 3-O sulfate is vital for anticoagulant activity, these GAG derivatives of heparin and enoxaparin are rendered non-anticoagulant. Treatment of ODSH with NaOH followed by lyophilization resulted in a yellow-brown residue. Neutralization of the alkali and lyophilization resulted in a powder that was desalted using a G10 SEC column to obtain the desired product at about 40% yield. The product was characterized by NMR.

4.3.4 Plasma Clotting Studies of ODSE

The activated partial thromboplastin time assay was used in the assessment of anti-coagulant properties of ODSE, using enoxaparin as a positive control. The APTT assay targets the intrinsic coagulation pathway and can be used in determining the anticoagulant properties of potential anticoagulants. In this case, the test was employed to confirm that the 2-O and 3-O sulfate groups, and thus anticoagulant properties of enoxaparin, had been lost following alkaline hydrolysis. The effects of two saturating concentrations of enoxaparin and ODSE (17 and 33 µg/mL) were used. In the absence of any of the agents, the time to clot was found to be 29.6. At both concentrations of enoxaparin tested, clotting was not observed at 180 minutes indicating strong anticoagulant properties. However in the presence of 17 µg/mL of ODSE, the time to clot was 46.8 ± 0.7 s and in the presence of 33 µg/mL a clotting time of 49.4 ± 2.5 s. These results clearly demonstrate that ODSE lacks the potent anticoagulant effect of enoxaparin confirming that the desulfation process was successful.

Table 17. APTT assay for Enoxaparin and ODSE

	Time to clot (s)		
Species	**1**	**2**	**Average**
Blank	29.7	29.5	29.6
ENOX			
33 µg/mL	>200	>200	ND
17 µg/mL	>200	>200	ND
ODSE			
33 µg/mL	47.6	51.1	49.4
17 µg/mL)	47.3	46.3	46.8

4.3.5 Inhibition of HNE by GAGs

The inhibition of NE by GAGs was measured using a chromogenic substrate hydrolysis assay using N-succinyl-Ala-Ala-Val p-nitroanilide in a 125 mM HEPES buffer, pH 7.4 containing different concentrations of Na^+ ranging from 62.5 mM to 365 mM at 37 °C using a microplate reader (FlexStation III, Molecular Devices). In this assay the decrease in the initial rate of hydrolysis in the presence of the inhibitors is employed in the determination of potency.

4.3.5.1 Commercially Available GAGS and Their 2-O, 3-O-Desulfated Derivatives

The NE inhibitory potency of unfractionated heparin, 2-O,3-O-desulfated heparin, enoxaparin, 2-O,3-O-desulfated enoxaparin and fondaparinux were determined in a 125 mM HEPES buffer (62.5 mM Na+), pH 7.4 containing 0.125 M triton-X100. The IC_{50}s for NE inhibition obtained for these different species were 7.5 ± 0.4, 13.6 ± 0.6, 17.6 ± 0.6, 24.7 ± 3.6 and 1180 ± 260 nM, respectively. These results clearly emphasize the fact GAG chain length plays an important role in HNE inhibitory potency, with the pentasaccharide being too short to elicit HNE inhibition comparable to the other GAGs. The similarity of potency of the other samples gives the indication that beyond a particular chain length there is no significant benefit in GAG chain length. In addition the lack of a loss in activity following 2-O,3-O desulfation of enoxaparin indicates the non-importance of these two sulfate groups for HNE inhibition. It is worth

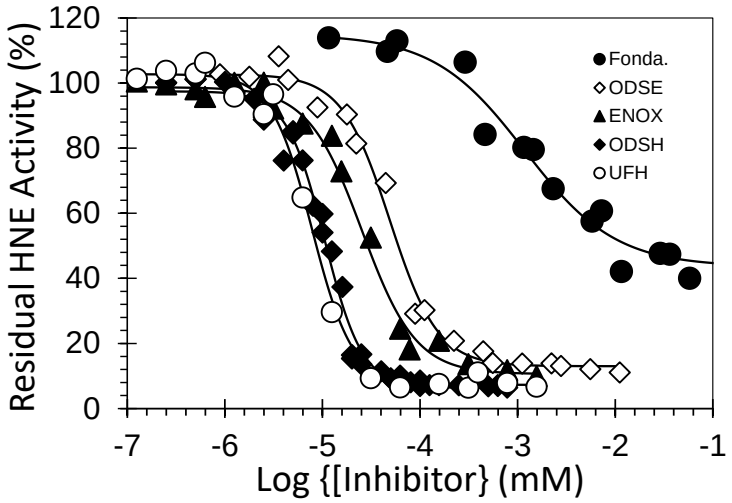

Figure 46. Inhibiton of HNE by clinically used GAGs and their 2-*O*,3-*O*-desulfate derivatives

mentioning that fondaparinux is also a structurally defined molecule, unlike the other samples, which are essentially mixtures and thus there is the possibility that it lacks the particular sulfation pattern for NE inhibitory potency, that may be present in the mixtures. We thus decided to study oligosaccharides obtained by size fractionation of ODSH.

4.3.5.2 Oligosaccharides from Size Fractionation of ODSH

The NE inhibitory potency of size fractionated ODSH indicated that samples were equipotent with unfractionated ODSH. The samples obtained using molecular weight cut-off filters had approximate IC_{50}s of 40 nM, 25 nM and 10 nM for fractions >3 KDa, 3 KDa<x<10 KDa and >10 KDa, respectively. Similarly, the samples obtained using SEC separation all ranged from 12 – 20 nM potency for HNE inhibition. These results further confirm that there is no benefit to having a longer GAG chain length beyond a threshold and that above a lower limit of chain length, lower molecular weight species may be equally as potent as longer chain lengths.

Table 18. Inhibition of HNE by size fractionated ODSH

ODSH fraction	IC_{50} (nM)	ΔY (%)	HS
Molecular Weight Cut-Off Filters			
<3kDa	40	89.4±2.2	2.2±0.2
<3kDa<x<10kDa	25	92.1±2.4	1.9±0.9
>10kDa	10	88.7±2.4	2.1±0.2
Size Exclusion Chromatography			
F 45-50	20.2	87.7±3.4	1.5±0.2
F 34-36	14.4	90.9±2.7	2.0±0.2
F 10-15	19.5	87.7±3.1	1.9±0.2

4.3.5.3 Heparin Oligosaccharides.

The results from studying HNE inhibitory potency of size fractions of ODSH thus prompted study of the NE inhibitory potency of heparin derived oligosaccharides. The oligosaccharides have the general formula ΔHexA,2S - GlcNS,6S– (IdoUA,2S – GlcNS,6S)n as shown in figure 47 and are non-anticoagulant due to the absence of the 3-O sulfate on the glucosamine unit. This was necessary to decipher the required GAG chain length for satisfactory HNE inhibition under our assay conditions, 125 mM HEPES buffer ($[Na^+]$ = 62.5 mM), pH 7.4, at 37 °C. The HNE inhibitory potency of the GAG oligosaccharides was determined as for the polysaccharides and the results obtained in this assay generally confirm earlier reports that GAG chain length is an important factor in HNE inhibition, with GAGs with longer chain lengths being better inhibitors. At this ionic strength, the HNE inhibitory potency was fairly well maintained throughout GAG species of 8 sugar units and above. The potencies recorded for these GAGs were heparin derived dodecasaccharide, 19.2 ± 2.0 nM; heparin derived

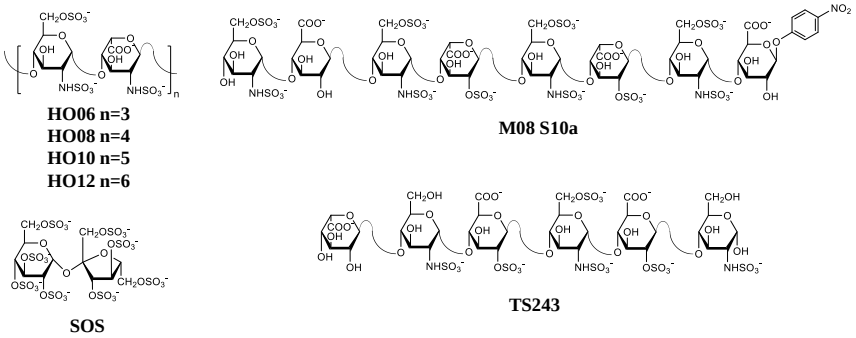

Figure 47. Structures of GAG oligosaccharides.

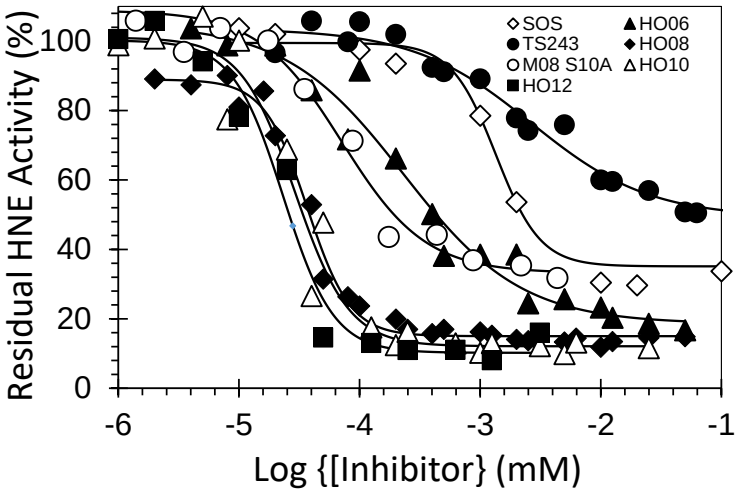

Figure 48. Inhibition of HNE by GAG oligosaccharides.

decasaccharide, 29.2 ± 4.0 nM, heparin derived octasaccharide, 33.1 ± 1.5 nM, heparin derived hexasaccharide, 230 ± 52, and sucrose octasulfate 1349 ± 161 nM. These inhibitory potencies do not differ significantly from longer chain GAGs, which range from about 7.5 – 40 nM. This is particularly interesting considering that the molecular weights of these species are very wide ranging. Clearly, below the size of the oligosaccharide, there is a noticeable drop in potency with the hexasaccharide showing a 15-fold drop in potency compared to ODSH. Nevertheless, the hexasaccharide is 4-8 fold more potent than fondparinux (IC_{50} = 1180 ± 260). These results suggest that the octasaccharide may be the minimal length required to achieve satisfactory HNE inhibition.

A structurally defined octasaccharide MO8 S10a and a structurally defined hexasaccharide TS243 were studied and found to have potencies of 70.9 ± 8.9 and 2648 ± 526 nM respectively. Both MO8 S10a and TS243 3 lack sulfation at the 3-O sulfate position and in turn are not fully sulfated at the 6-O and N positions. The fact that MO8 S10a is only about 2-fold less potent than the heparin derived octasaccharide, although it lacks full 6-O and N-sulfation shows that not all 6-O and N-sulfates contribute equally to HNE inhibition. TS243, like MO8 S10a, is not fully sulfated at the 6-O position; however, unlike MO8 S10a, it is about 10-fold less potent than the heparin derived hexasaccharide. These results indicate that correlation of sulfation levels with potency is more pronounced in shorter chain species. An important difference between the TS243 and HO06 is the type of hexuronic acid residues. HO06 has as its hexuronic acid residues iduronic acid, whereas in the case of TS243, this residue is glucuronic acid. The 10-fold difference in potency suggests that iduronic acid is preferred over glucuronic acid for HNE inhibition.

4.3.6 Salt Dependent Studies

The study of different concentrations of salt was important in identifying the contributions of ionic interactions for GAG inhibition of HNE. Also, this was necessary as our initial studies were conducted in a buffer with a slightly lower ionic strength than physiological conditions. The inhibitory potency of selected GAGs was studied in buffers of higher ionic strength, which were the same as our initial buffer but with added NaCl. These buffer solutions had [Na^+] of 112.5, 162.5, 262.5 and 362.5 mM. The results generally show a decrease in inhibitory potency and efficacy with increasing buffer ionic strength, supporting the importance of ionic interactions with the effect felt less with high molecular weight GAG species. In the case of UFH, the potency remained virtually unchanged at about 7 nM up to [Na^+] of 162.5 mM. However, at Na^+ of 362.5, there was a 5-fold drop in potency. For ODSH, the potency was maintained at about 14 nM at both 62.5 and 112.5 mM Na^+ and experienced only a 2-fold drop at 162.5 mM Na^+. The IC50 at 262.5 mM was however 261 nM, a 20-fold drop in potency compared to lower ionic strengths. The differences in potency trends of these two high molecular weight GAGs is not surprising as their sulfation levels are considerably different. The IC_{50} of enoxaparin was about 20 nM in the two buffers with the lowest ionic strength and increased 3-fold to approximately 70 nM at 162.5 mM Na^+. This HNE inhibitory potency was lost at greater than physiological ionic strengths. A trend similar to that observed with UFH and ODSH was observed with ODSE and Enoxaparin. The IC_{50} of ODSE increased in higher proportions compared to enoxaparin with increasing buffer ionic strength. At 62.5 mM Na^+, the IC_{50} for NE inhibition recorded for ODSE was 24.7 nM and this experienced a 2.6-fold and 10-fold increase in value at 112.5 and 162.5 mM Na^+ respectively, indicating a higher salt effect on the species with lower sulfation levels.

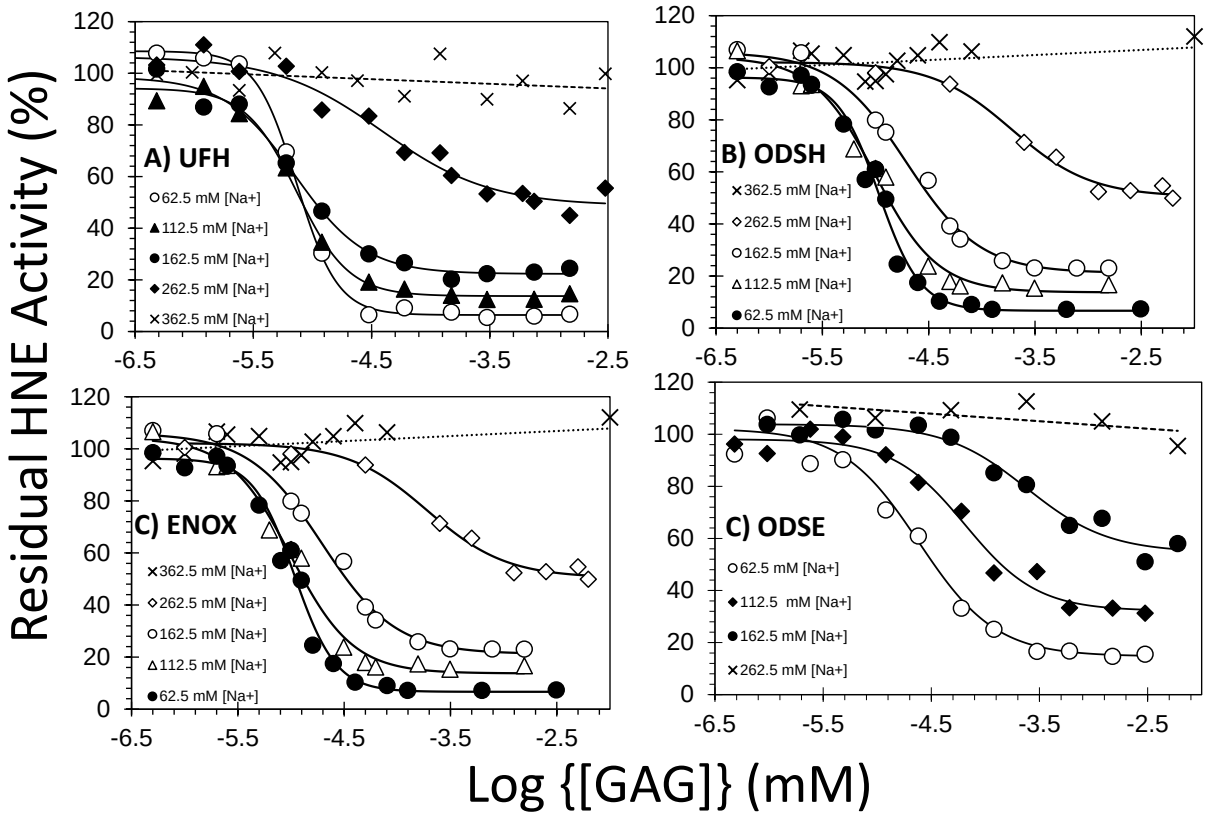

Figure 49. Salt dependence of HNE inhibition by GAGs

The ionic strength effect was felt more on the heparin derived oligosaccharides. At 112.5 mM Na+, the potency of the dodecassacharide remained unchanged. The decasaccharide and the octasaccharide, however, experienced 2.7-fold and 12.5-fold drops in potency, respectively. At 162.5 mM Na^+ the potency of dodecasaccharide, decasaccharide and the octasaccharide dropped by 15 to 23-fold compared to the values at the lowest ionic strength. Altogether, these results indicate that the interaction between GAGs and HNE involves ionic interactions.

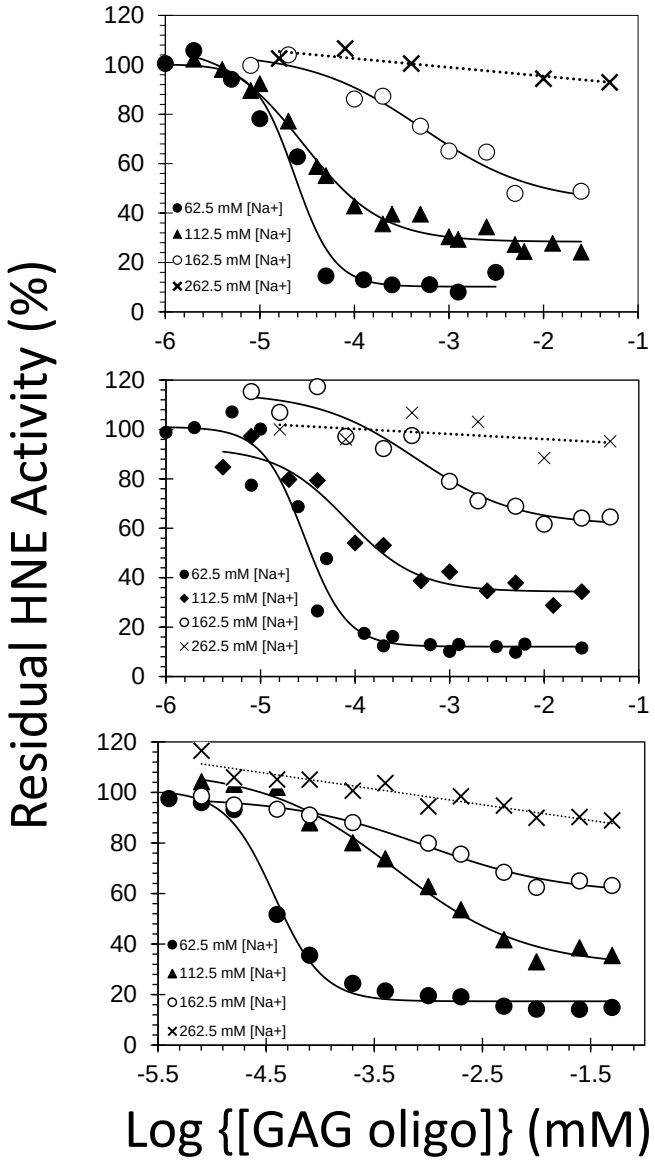

Figure 50. Salt dependence of HNE inhibition by GAG oligosaccharides

These results give an indication that both specific and non-specific interactions may be responsible for HNE inhibition by GAGs. Thus, at higher ionic strengths, though there is loss of specific interactions between particular residues, this is then compensated for by non-specific interactions of longer chain or higher sulfated GAGs.

Table 19. Inhibition of HNE by GAGs and GAG oligosaccharides

[Na^+]	IC_{50} (nM)	IC_{50}-app /IC_{50}-62.5 mM	HS	ΔY (%)
		UFH		
62.5	7.3 ± 0.2	1.0	2.5 ± 0.2	102.2 ± 1.2
112.5	7.4 ± 0.4	1.0	2.0 ± 0.2	80.5 ± 1.9
162.5	7.1 ± 0.7	1.0	1.5 ± 0.2	76.3 ± 3.0
262.5	38.9 ± 9.2	5.3	1.0 ± 0.2	57.8 ± 4.9
362.5	> 50000	ND	ND	ND
		ODSH		
62.5	14.1 ± 0.9	1.0	2.1 ± 0.4	91.0 ± 6.2
112.5	13.5 ± 1.1	1.0	1.5 ± 0.2	90.4 ± 5.0
162.5	26.7 ± 2.2	1.9	1.3 ± 0.2	84.8 ± 4.1
262.5	261 ± 33	18.4	1.2 ± 0.2	51.7 ± 4.1
362.5	> 50000	ND	ND	ND
		ENOX		
62.5	17.6 ± 0.6	1.0	2.5 ± 0.2	86.4 ± 1.6
112.5	22.2 ± 3.1	1.3	1.2 ± 0.2	71.9 ± 3.8
162.5	68.1 ± 9.9	3.9	1.1 ± 0.20	63.4 ± 3.4
262.5	> 50000	ND	ND	ND
		ODSE		
62.5	24.7 ± 3.6	1.0	1.2 ± 0.2	83.9 ± 4.5
112.5	65 ± 11	2.6	1.3 ± 0.3	65.9 ± 4.1
162.5	241± 58	9.8	1.45 ± 0.20	49.3 ± 4.8
262.5	> 50000	ND	ND	ND
		HO12		
62.5	23.3 ± 3.5	1	2.1 ± 0.6	90.0 ± 6.3
112.5	28.5 ± 4.7	1.2	1.0 ± 0.2	79.6 ± 5.4
162.5	520 ± 210.0	22.2	0.7 ± 0.3	60.9 ± 11.6
262.5	> 50000	ND	ND	ND
		HO10		
62.5	29.1 ± 4.2	1	1.9 ± 0.6	88.9 ± 4.2
112.5	82 ± 23	2.8	1.2 ± 0.4	58.4 ± 7.0
162.5	440± 170	15.3	0.8 ± 0.4	53.6 ± 8.7
262.5	> 50000	ND	ND	ND
		HO08		
62.5	37.7 ± 3.7	1	1.9 ± 0.3	83.5 ± 4.0
112.5	490 ± 110	12.9	0.7 ± 0.2	77.7 ± 6.5
162.5	950 ± 270	26.6	0.7 ± 0.2	38.1 ± 4.1
262.5	> 50000	ND	ND	ND
		M08 S10a		
62.5	70.9 ± 8.9	-	1.3 ± 0.4	79.1± 3.7
		HO06		
62.5	230 ± 52	-	0.9 ± 0.2	86.4 ± 7.3
		TS243		

62.5	2600± 500	-	0.9 ± 0.2	54.3 ± 3.9
		SOS		
62.5	1350± 160	-	2.4 ± 0.8	64.5 ± 3.5

4.3.7 Mechanism of Inhibition of HNE by GAGs

The mechanism of GAG inhibition of HNE remains controversial. Earlier reports indicate a non-competitive allosteric mechanism for inhibition.[32] Kostoulas et al. reported that there was an additional competitive component in the inhibition of HNE by GAGs resulting in a mixed type inhibition mechanism.[31] They reported that this competitive-inhibition component, which is felt at low ionic strengths and is lost with increasing ionic strength, is a result of the interaction with Arg217A of the enzyme, that is close to the substrate binding site.[31] They hypothesize that at high ionic strengths, Arg217A is shielded by ions and thus prevented from interacting with GAGs; hence the loss in the competitive component.[31] The latest contribution to this field by Spencer et al., however, is totally different from the previous reports and rather makes mention of a totally competitive mechanism of inhibition.[88] Thus, we thought it would be necessary to investigate this further. In addition to clarifying the issue, the results obtained will aid our computational study of GAG-HNE interactions.

Michaelis-Menten kinetics of GAG inhibition of HNE were studied for a number of GAGs in our study buffer. The V_{MAX} and K_M were obtained from the hyperbolic profile obtained from measuring the initial rate of hydrolysis of chromogenic substrate in the absence, as well as at different concentrations, of the GAGs. The GAGs studied were UFH, ODSH, heparin-derived octasaccharide and sucrose octasulfate. For all the GAGs studied, with the exception of sucrose octasulfate, a common trend was observed. There was as decrease in V_{MAX} with increasing concentrations of all GAGs. For UFH, the V_{MAX} was 46.7± 1.1 mAU/min in the absence of the inhibitor, and this decreased to 41.1±1.0, 34.3±1.0, 25.9 ±0.6, 19.3 ±1.6 and 12.0 ±0.5 mAU/min

in the presence of 5, 7.5, 12.5, 17.5 and 25 nM of UFH, respectively. This is indicative of an allosteric mechanism as the V_{MAX} in the presence of UFH never approaches that in its absence. The trend in the K_M was however very interesting. The K_M remained fairly constant at 0.50 mM across concentrations ranging from 0 – 12.5 nM of the inhibitor, but further increases in the concentration of UFH resulted in doubling of the K_M. For ODSH, the V_{MAX} in the absence of the inhibitor was 42.3±0.7 mAU/min and decreased gradually, reaching 9.9±0.7 mAU/min at 20 nM concentration of the inhibitor. The trend in K_M was also the same as observed for UFH, being fairly constant at lower inhibitor concentrations and doubling at higher concentrations. For heparin derived octasaccharide, the V_{MAX} in the absence of the inhibitor was 47.8±1.5 mAU/min and this decreased, gradually reaching 14.4±1.25 mAU/min at 200 nM. Again, the K_M remained fairly constant at lower concentrations and doubled at higher concentrations of the octasaccharide. These gradual decrease in V_{MAX} across the board indicate an allosteric inhibition mechanism for inhibition of HNE by GAGs. The interesting K_M trend on the other hand suggests the possibility of both specific and non-specific interactions contributing to the inhibition of HNE by GAGs. At lower concentration, GAGs interact with high specificity at an allosteric binding site whereas at high concentration some non-specific binding, possibly close to the active site may take place. The K_M trend could also mean that is a competitive component in this mechanism, as reported by Kostoulas et al.[31]

The trend observed with sucrose octasulfate is more supportive of the mixed-inhibition mechanism. The V_{MAX} values were 42.0±0.7 , 42.0±1.9, 33.5±2.3, 29.6±1.6 and 24.3±1.5 mAU/min at concentrations of 0, 1, 5, 10 and 100 µM, respectively. At the same concentrations, the K_M values were 0.32 ± 0.02, 0.78 ± 0.10, 1.37 ± 0.19, 1.59 ± 0.16 and 1.33 ± 0.16 mM, respectively. However, the small size of sucrose ocatasulfate in relation to the other

oligosaccharides could account for the difference in the interaction, and hence the mechanism of inhibition.

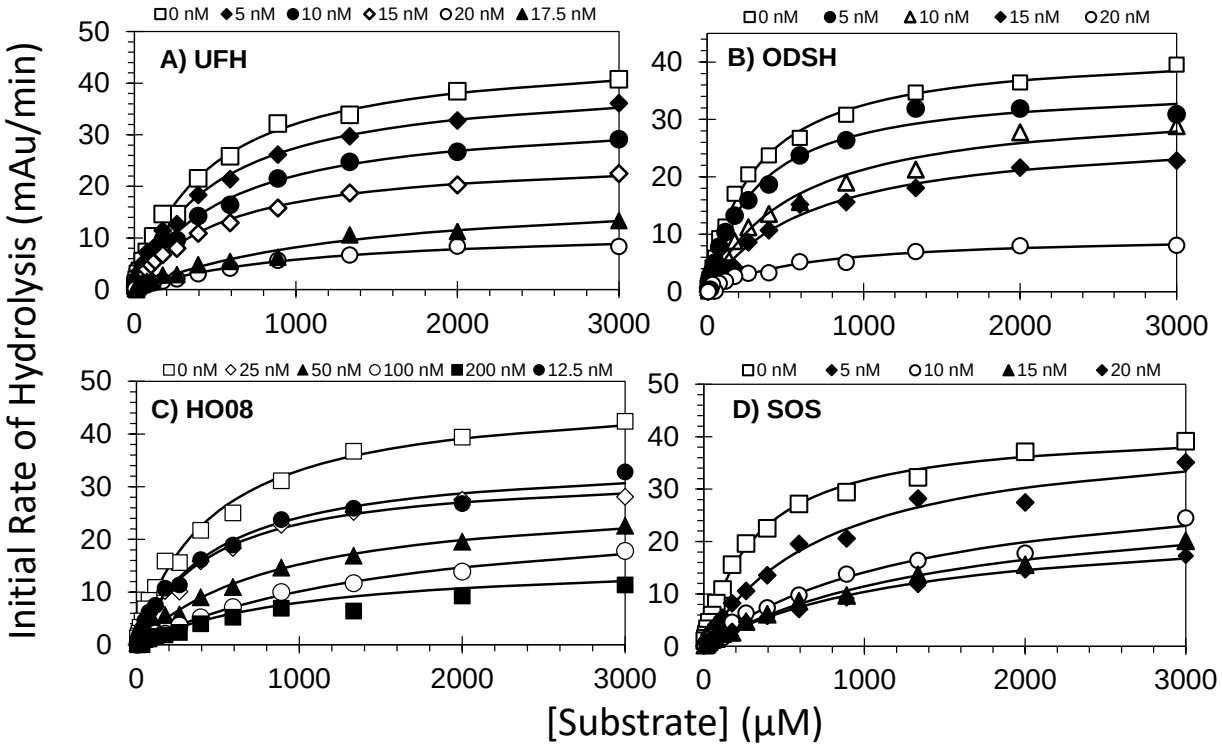

Figure 51. Michaelis-Menten kinetics of HNE inhibition by GAGs.

Table 20. Michaelis-Menten kinetics of HNE inhibition by GAGs

Conc. [nM]	Vmax (mAU/min)	Km (mM)
	UFH	
0.00	46.7 ± 1.1	0.45 ± 0.03
5.00	41.1 ± 1.0	0.50 ± 0.04
7.50	34.3 ± 1.0	0.55 ± 0.04
12.50	25.9 ± 0.6	0.53 ± 0.3
17.50	19.3 ± 1.6	1.36 ± 0.2
25.00	12.0 ± 0.5	1.07 ± 0.1
	ODSH	
0.0	42.3 ± 0.1	0.30 ± 0.02
5.0	36.1± 0.1	0.31 ± 0.03
10.0	33.1 ± 1.5	0.55 ± 0.66
15.0	28.1 ± 1.1	0.66 ± 0.67
20.0	9.9 ± 0.6	0.61 ± 0.92
	HO08	
0.0	47.8 ± 1.5	0.45 ± 0.04
12.5	35.5 ± 1.2	0.47 ± 0.04
25.0	32.9 ± 0.9	0.44 ± 0.03
50.0	28.5 ± 1.0	0.87 ± 0.07
100.0	26.6 ± 1.2	1.62 ± 0.15
200.0	15.4 ± 1.3	1.30 ± 0.22
	SOS	
0.00	42.0 ± 0.7	0.32 ± 0.02
1000	42.0 ± 1.9	0.78 ± 0.09
5000	33.5 ± 2.3	1.37 ± 0.19
10000	29.6 ± 1.6	1.59 ± 0.16
100000	24.2 ± 1.5	1.33 ± 0.16

To further study the mechanism of this inhibition, further Michaelis-Menten kinetics studies were performed using the heparin derived octasaccharide in pH 7.4, 20 mM tris buffer containing $CaCl_2$, 0.1% PEG8000 and Tween 20 and having varying ionic strengths owing to different concentrations of NaCl. In the NaCl free buffer, the V_{MAX} in the absence of the inhibitor was 53.5 ± 1.4 which decreased gradually with values of 41.7 ± 1.2, 20.2 ± 0.1 and 17.3 ± 0.1 mAU/min at 25, 100 and 200 nM concentrations of octasaccharide. The K_M followed the same trend as in the case of the HEPES buffer being maintained at 0.30 mM both in the absence of and in the presence of 25 nM of the octasaccharide. Increasing the concentration of the octasaccharide led to about 2-fold increase in the K_M.

At higher ionic strengths (25 mM NaCl and above) only a decrease in V_{MAX} was observed with the K_M remaining unchanged. At 25 mM NaCl, the V_{MAX} drops from 46.1 ± 0.8 mAU/min in the absence of the octasaccharide to 22. 2 ±1.2 mAU/min at a concentration of 400 nM of the octasaccharide but the K_M remained fairly the same. Similarly, at 50 mM NaCl, the value of the V_{MAX} is 49.7 ± 1.1 mAU/min in the absence of the octasaccharide but 26.0 ± 1.3 mAU/min in the presence of 1 µM of the octasaccharide. However, the corresponding values for the K_M are 0.45 ± 0.02 and 0.41 ± 0.05 mAU/min. Finally, in the buffer containing 100 mM NaCl, the V_{MAX} drops from 41.2 ± 1.2 mAU/min in the absence of inhibitor to 34.2 ± 1.8 mAU/min in the presence of 1 µM with no change in the K_M.

These observations are in agreement with the report by Kostoulas et al., but the change in K_M at high inhibitor concentrations also suggests that binding with Arg217A is a non-specific interaction and only occurs at high GAG concentrations. More importantly, however, the interaction between the GAGs studied here and HNE is via a non-competitive allosteric mechanism. By binding to Arg and other residues, GAGs induce a conformational change at the

active site of HNE, thus halting its hydrolytic activity.

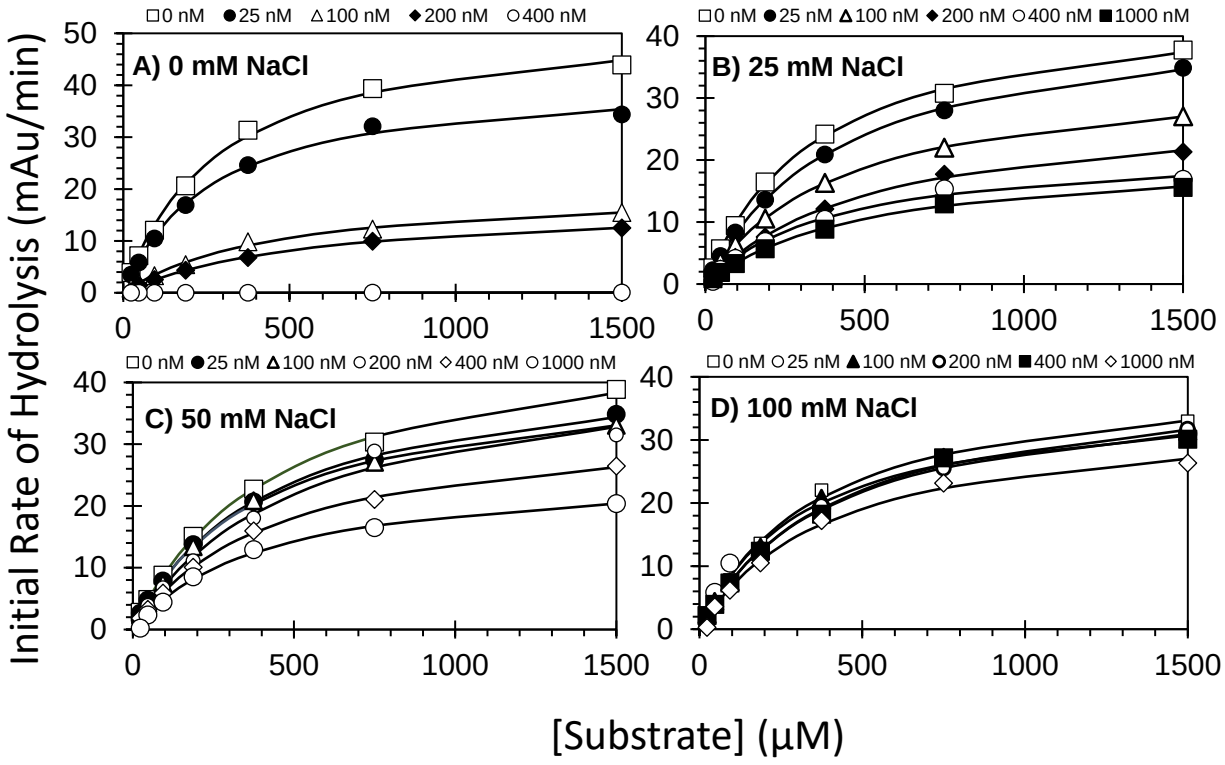

Figure 52. Michaelis-Menten kinetics of HNE inhibition by HO08 in buffers of different ionic strength.

Table 21. Michaelis-Menten kinetics of HNE inhibition by HO08 in buffers of different ionic strength

Conc. [nM]	Vmax	Km (mM)
	0 mM NaCl	
0.0	53.5 ± 1.4	0.29 ± 0.02
25.0	41.7 ± 1.2	0.27 ± 0.02
100.0	20.2 ± 0.1	0.46 ± 0.05
200.0	17.3 ± 0.1	0.56 ± 0.04
	25 mM NaCl	
0.0	46.1 ± 0.8	0.35 ± 0.02
25.0	44.5 ± 0.5	0.43 ± 0.01
100.0	34.7 ± 0.5	0.43 ± 0.01
200.0	29.0 ± 0.7	0.52 ± 0.03
400.0	22.2 ± 1.2	0.41 ± 0.06
1000.0	21.0 ± 0.5	0.50 ± 0.03
	50 mM NaCl	
0.0	49.7 ± 1.1	0.45 ± 0.02
25.0	44.2 ± 0.9	0.40 ± 0.02
100.0	41.9 ± 0.7	0.43 ± 0.01
200.0	43.9 ± 3.6	0.51 ± 0.10
400.0	34.0 ± 0.5	0.44 ± 0.02
1000.0	26.0 ± 1.3	0.41 ± 0.05
	100 mM NaCl	
0.0	41.2 ± 1.2	0.37 ± 0.03
25.0	37.4 ± 2.6	0.33 ± 0.06
100.0	39.7 ± 1.0	0.37 ± 0.02
200.0	40.5 ± 1.5	0.42 ± 0.03
400.0	39.2 ± 1.7	0.40 ± 0.04
1000.0	34.2 ± 1.8	0.40 ± 0.05

4.3.8 Thermodynamic Binding Affinity GAGs for HNE

The thermodynamic binding affinity of GAGs for HNE was studied using fluorescein isothiocyanate (FITC) tagged HNE and monitoring the change in fluorescence upon titrating with the GAGs in a HEPES buffer containing 0.125 M Triton-x100 due to fluorescein (λ_{EM} = 520 nm, λ_{EX} = 490 nm). A saturating sigmoidal increase in fluorescence was observed upon titrating of the GAGs and this was used in the determination of the K_D using the 3-parameter Hill equation for cooperative binding. Five different GAG species, UFH, enoxaparin, heparin derived octasaccharide, heparin derived hexasaccharide and sucrose octasulfate were studied and their apparent binding affinities to HNE in the assay conditions were 186 ± 5, 116 ± 7, 118 ± 4, 17500 ±1000, and 8403 ±300 nM respectively. These K_D values are significantly higher than the IC_{50} values obtained in the same conditions. The reason for this difference is not apparent, but could be due to the availability of more than one binding GAG site on HNE, a lower affinity site and higher affinity site, with the lower affinity binding site being the one that requires binding to elicit the observed change in fluorescence.

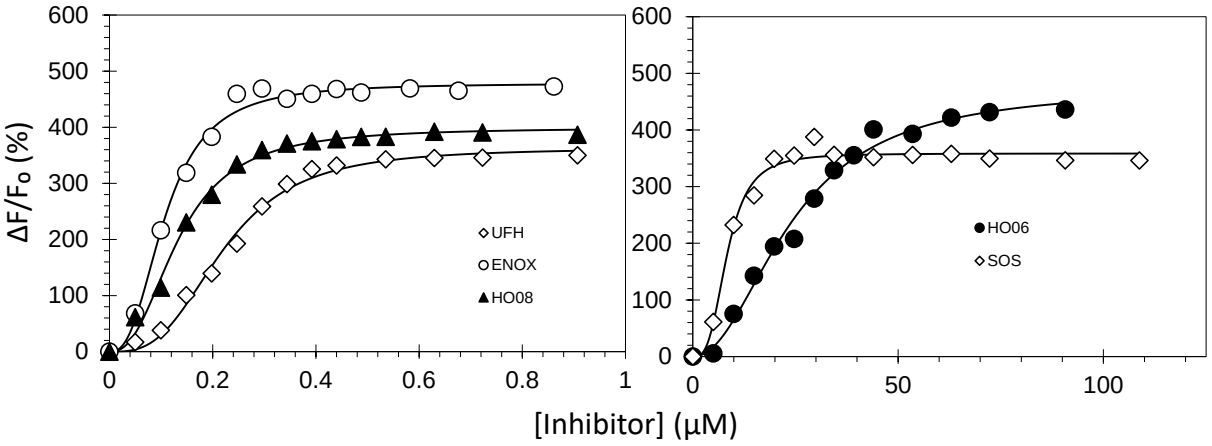

Figure 53. Affinity of GAG-HNE interaction.

Table 22. Thermodynamic binding affinity of GAGs for HNE

Species	KD (nM)	HS	$\Delta F/F_0$
UFH	186 ± 5	2.6 ± 0.2	416 ± 8
ENOX	116 ± 7	2.3 ± 0.2	473 ± 15
HO08	118 ± 4	2.1 ± 0.1	303 ± 4
HO06	17500 ±1000	1.6 ± 0.1	566 ± 21
SOS	8403 ±300	2.8 ± 0.2	392 ± 5

4.3.9 Computational Studies of GAG-HNE Interactions

To study the GAG-HNE interaction, computational studies were conducted using a crystal structure of HNE (PDB ID: 1HNE; 1.84 Å resolution) obtained from the PDB and subsequently prepared for modeling using SYBYL-X, v2.1. The highly electropositive nature of HNE presented a significant challenge in identifying and defining of binding sites. To circumvent this problem, a simple method of binding site identification was employed. This involved selecting various sites surrounding four arginine residues, Arg75, Arg87, Arg178 and Arg187. These resulted in four segments named BS1, BS2, BS3 and BS4, respectively. The combinatorial virtual library screening technique, previously used in the study of GAG-protein interactions, was then employed to identify the putative binding sites and also identify specific ODSH sequences for HNE. The interaction of the virtual library of 3,456 GAG hexasaccharide sequences with 3-O-desulfation around all four sites within a 16Å radius around the central residue, was screened using GOLD. The GOLDSCORES following docking and scoring revealed that sites BS1 and BS4 were higher affinity GAG binding sites in that they had higher scores (>70) than BS2 and BS3 (<40). This results point to the possibility of more than one GAG binding site on HNE, where the interaction of GAGs and HNE will be of high affinity. Further

comprehensive docking and scoring of the 50 highest ODSH hexasaccharide sequences from each library on these two putative high affinity sites, BS1 and BS3, resulted in the identification of 23 GAG hexasaccharide sequences that bound with high affinity and high specificity to BS1 and 20 GAG hexasaccharide sequences that did same for BS3. These sequences interacted with HNE with high GOLDSCORES and RMSD <2.5Å. Further analysis of these sequences was carried out using UCSF Chimera[313] individually. This analysis indicated that multiple hydrogen bonding interactions existed between the GAG sequences and HNE at both sites. These interactions were specifically with Gln34, His40, Leu73,Ser74, Arg76, Glu77, Arg80, Val82 and Ser153 of BS1 and Gly18, Gly19, Arg20, Arg21, Gln135, Arg149, Asn159 and Arg187 of BS4 (Figure 54). The results suggested that longer GAG sequences could simultaneously engage both sites. Thus, computational molecular modeling predicted strong interaction between HNE and GAG sequences.

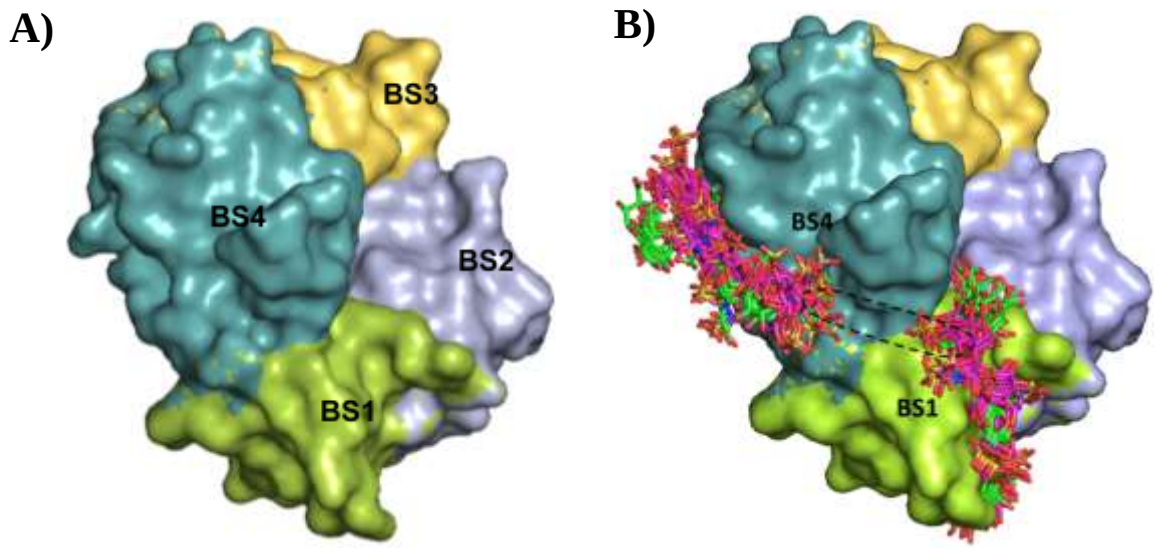

Figure 54. (A) Structure of HNE showing putatibe binding sites (B) Results from CVLS screening of ODSH sequences interacting with HNE.

4.4 Experimental Section

4.4.1 Size Fractionation of ODSH

4.4.1.1 Using Molecular Weight Cut-Off Filters

Two molecular weight cut-off filters, 3 kDa and 10 kDa, were employed. 50 mg of ODSH was dissolved in about 200 µL of high purity water and transferred into the 10 kDa molecular weight cut-off filter and centrifuged at 10000G. The filtrate thus contains fragments of molecular weight less than 10 kDa and the residue contains fragments 10 kDa and above. The filtrate was then transferred to a 3 kDa molecular weight cut-off filter and treated similarly as for the 10 kDa filter yielding a fraction with molecular weght less than 3 kDa and a fraction with molecular weight greater than 3 kDa and less than 10 kDa.

4.4.1.2 Using Size Exclusion Chromatography

Separation of ODSH into different sized fractions was done using G75 matrix. The matrix was swollen in high purity water overnight and packed into a glass column with dimensions 7 cm 2 × 45 cm. This was allowed to stand overnight to ensure adequate packing of the material in the column. 500 mg of ODSH was dissolved in about 1 mL and applied on the column employing water as the eluent. 1 mL fractions of the eluate were collected, totaling 100 mL. The collected fractions were frozen and lyophilized.

4.4.2 Preparation of 2-O,3-O-Desulfated Enoxaparin (ODSE)

ODSE was prepared by alkaline treatment of enoxaparin using NaOH as detailed in the patent by Holme et al.[312] Briefly, a volume of Enoxaparin solution, corresponding to 100 mg of Enoxaparin was lyophilized to dryness. This was then dissolved in 18 mL of water. 2 mL of 1M NaOH was then added, well mixed, frozen and lyophilized to dryness. The yellow-brown residue obtained was then dissolved in 5 mL of water, and the pH adjusted to 6-7 with 20% acetic acid.

This was followed by addition of $NaHCO_3$ to bring the pH of the solution to 8-9. The resulting solution was then frozen and lyophilized to dryness. The resulting white-cream powder contains both desulfated enoxaparin and salts from the desulfation process. This powder is taken through a two-step desalting process using a G10 column, leading to pure ODSE in about 30-40% yield. The ODSE obtained was characterized by NMR spectroscopy.

4.4.3 SEC HPLC of GAGs

The SEC HPLC analysis of GAGs was performed on a Shimadzu HPLC system equipped with a UV/Vis detector capable of monitoring at two different wavelengths. A Shodex Asahipak GS-320 HQ size exclusion column was used employing 0.1M NaCl at a rate of 0.3 mL/min as the mobile phase. The detectors were set to 206 nm and 232 nm. An injection volume of 10 μL of GAGs (about 1 mg/mL) was employed. The elution time for the different GAGs was recorded.

4.4.4 Activated Partial Thromboplastin Time Assay

The effect of Enoxaparin and ODSE on clotting was determined in a standard one-stage recalcification assay with a BBL Fibrosystem fibrometer (BectonDickinson, Sparles, MD), as described previously.[133] 10 μL of enoxaparin or ODSE was mixed with 90 μL of citrated human plasma and 100 μL of prewarmed APTT reagent (0.2% ellagic acid). After an incubation period of 4 min at 37 °C, clotting was initiated by adding 100 μL of prewarmed 25 mM $CaCl_2$ and time to clot noted. The times to clot were noted and compared to that obtained in the absence of each of the agents (10 μL of water), determined in similar fashion.

4.4.5 Direct Enzyme Inhibition Studies Using Chromogenic Substrate Hydrolysis Assay

The determination of direct HNE inhibition by the GAGs was done using a chromogenic substrate hydrolysis assay employing a microplate reader (FlexStation III, Molecular Devices) as previously described. [133]The buffer utilized in this assay was a pH 7.4, 125 mM Hepes buffer containing 0.125 M Triton-X100. 2 μM of HNE was prepared by diluting a 340 μM stock of the enzyme in the assay buffer. A 25 mM concentration of the chromogenic substrate (N-succinyl-Ala-Ala-Val *p*-nitroanilide) was prepared in DMSO. Appropriate solutions of GAG in water were prepared and serially diluted.

Briefly, 88 μL of the buffer was added to the wells and 4 μL of NE (80 nM final concentration) was added. 5 μL of GAG solution (or water) was added and an incubation period of 10 minutes was allowed. After the incubation, 3 μL of elastase substrate was rapidly added, followed by mixing and the residual NE activity was measured from the initial rate of increase in absorbance at 405 nm. Relative residual NE activity at each concentration of the GAGs was calculated from the ratio of NE activity in the presence and absence of GAGs. The dose dependence of residual protease activity was fitted using logistic equation 1 to obtain the potency (IC_{50}), Hill slope (HS) and efficacy (ΔY) of inhibition.

$$Y = Y_0 + \frac{Y_M - Y_0}{1 + 10^{(\log [\text{Inhibitor}]_0 - \log IC_{50})(HS)}} \qquad (1)$$

In this equation, Y is the ratio of residual HNE activity in the presence of inhibitor to that in its absence (fractional residual activity), Y_M and Y_0 are the maximum and minimum possible values of the fractional residual proteinase activity respectively, IC_{50} is the concentration of the inhibitor that results in 50% inhibition of enzyme activity and HS is the Hill slope.

4.4.6 Michaelis-Menten kinetics Study of GAG inhibition of HNE

The initial rate of substrate hydrolysis by 80 nM NE was monitored from the linear. Increase in absorbance at 405 nm corresponding to less than 10% consumption of the chromogenic substrate, as earlier described.[133] The initial rate was measured as a function of various concentrations of the substrate (0.85 – 3 mM) in the absence and presence of fixed concentrations of selected GAGs following a 10-minute incubation in a 125 mM HEPEs buffer containing 0.125 M of triton-X. GAG concentrations ranged from 0-25 nM for UFH, 0-20 nM for ODSH, 0-400 nM for heparin derived octasaccharide and 1000-100000 nM for sucrose octasulfate. The data were fitted by the Michaelis-Menten equation 2 to determine $K_{M,app}$ and V_{MAX}.

$$V_I = \frac{V_{MAX}[S]}{K_M + [S]} \quad (2)$$

The procedure was repeated for selected GAGs in 20 mM Tris buffer pH 7.4 containing, 2.5 mM $CaCl_2$, 0.1% PEG 8000 and 0.025% Tween 20 containing different amounts of NaCl.

4.4.7 Binding Affinity of GAGs for HNE

The thermodynamic binding affinity of GAGs to HNE was studied using fluorescence spectroscopy. The change in the fluorescence emission of fluoresceinamine isothiocyanate labeled NE as a function of GAG concentration was measured in 125 mM HEPES buffer containing 0.125M Triton X . Solutions of GAGs were titrated into a 200 μL solution of the labelled NE and the change in fluorescence at 520 nm ((λEX = 490 nm) monitored. The excitation and emission slit widths were set to 1.0 mm. The data was fitted to the sigmoidal curve (Hill 3 Parameter) to obtain the K_D and the Hill slope. ΔF represents the change in fluorescence of the labeled HNE.

$$\frac{\Delta F}{F_O} = \Delta F_{max} \times \frac{[ODSH]^n}{(K_{D,app})^n + [ODSH]^n} \quad (3)$$

4.4.8 Computational Study of GAG-HNE interaction

The crystal structure of NE was obtained from the RCSB Protein Data Bank (PDB ID: 1HNE; 1.84 Å resolution),[314] and prepared for modeling with SYBYL-X, v2.1 (Certara,St. Louis, MO) as follows. Water molecules were removed and protonation states of amino acids were adjusted to physiological states. Hydrogen atoms were then added, followed by Powell minimization. Potential sites of GAG binding were identified by analyzing the electrostatic potential of the protein (Figure. 54A), which resulted in four different sites, centered on residues Arg75, Arg87, Arg178 and Arg187 respectively. A radius of 16 Å around the identified Arg residues was defined as the binding site for molecular docking. To identify the site with highest GAG binding potential, a small library of GAG sequences were docked using GOLD v5.2 (Cambridge Crystallographic Data Centre, Cambridge, UK)[315] and the site that had the highest GOLDSCORE and specificity of binding from multiple docking runs was selected for further study. The coordinates for GAG sequences was taken from the CVLS library previously generated in our lab.[102] which incuded 3,456 GAG hexasaccharide sequences with 3-O-desulfation in the library, including both reducing and non-reducing end combinations. Molecular docking of each GAG sequence at the predicted binding site was performed with GOLD v5.2 by using a previously described dual filter strategy. [102] Best sequences were identified as those with the highest GOLDScore and the lowest root-mean-square deviation between top six solutions derived from a triplicate docking run.

4.5 Conclusion

The inhibition of HNE has great therapeutic potential in the management and treatment of inflammatory conditions. Thus, the lack of clinical anti-HNE agents requires great attention.

Using the APTT assay we showed that the 2-*O*,3-*O* desulfated species of glycosaminoglycans were devoid of anti-coagulant properties. Also, the lack of a difference between HNE inhibitory potencies of GAGs and their respective 2-*O*,3-*O* desulfated analogs indicates that 2 and 3 position sulfates are not crucial for HNE inhibition. The heparin hexasaccharide was five-fold more potent than the pentasaccharide, which confirms the dependence of HNE inhibitory activity on GAG chain length. The octasaccharide was 7-fold more potent than the hexasaccharide; however, the potencies of the deca- and dodeca- saccharide were not significantly different from the octasaccharide. These results suggest that the octasaccharide is the ideal GAG chain length for HNE inhibition. The inhibitory potencies of the two hexasaccharides also show that a higher degree of iduronic acid residues results in better HNE inhibitory potency.

Furthermore, the results indicate that long and short chain species utilize a non-competitive allosteric mechanism for inhibition of HNE activity, in which ionic interactions contribute significantly. Molecular modeling studies have helped to identify putative GAG binding sites on HNE and results suggest that an electropositive domain comprising Arg75, Arg87, Arg178 and Arg187 residues is the putative GAG binding. Additionally, we have identified GAG hexasaccharide sequences with potential selectivity for HNE inhibitory activity. This work demonstrates that the heparin octasaccharide is the ideal chain length for HNE inhibition and provides a structural foundation for the development of distinct chemically-defined heparin oligosaccharides that selectively inhibit HNE.

***Contributions**

Molecular modeling experiments were performed by Dr. Nehru Viji Sankaranarayanan.

5 SIGNIFICANCE AND FUTURE WORK

5.1 Sulfated Benzofuran Thrombin Inhibitors with Submaximal Protease Inhibition

Though direct thrombin and FXa inhibitors have lower risk of side effects compared to earlier agents, prolonged bleeding is still a side effect observed among some patients. In this vein agents that do not completely inhibit protease activity, but maintain a basal level of enzymatic activity, will be advantageous.

Our work has demonstrated the viability of such an approach in regard to the inhibition of thrombin. We have developed agents that demonstrate submaximal thrombin cleavage of both a chromogenic substrate and a macromolecular substrate. This is the first report of an agent that results in partial inhibition of a monomeric protease for the cleavage of a macromolecular substrate, and provides evidence that this is a feasible strategy towards the development of the ideal anticoagulant with a significantly reduced side effect profile. The work further emphasizs the advantage of targeting allosteric sites versus orthosteric sites. Work is on-going to study the effects of these agents in whole blood, which will be followed by in vivo studies using mice.

5.2 Sulfated Diflavonoids as Potential Anti-Fibrinolytic Agents

Targeting plasmin with inhibitors has potential therapeutic benefit in a number of conditions including hemophilia, cancer and inflammation. The lack of clinical plasmin inhibitors stems from the difficulty in reaching a balance between selectivity and potency.

This work demonstrates the benefit of allostery as a strategy for the development of target-selective compounds. Not only did sulfation improve the potency, it also markedly

increased selectivity for plasmin over other serine proteases. The ability to prevent clot lysis by plasmin also demonstrates the potential anti-fibrinolytic characteristics of these agents. Also, the ability of protamine sulfate to totally reverse anti-plasmin activity is an added advantage possessed by these agents. Future work will be focused on testing these agents on in vivo models to assess their potential.

5.3 GAG Oligosaccharides Targeting HNE

HNE has been implicated in disease conditions where inflammation plays a role and thus HNE inhibitors will be of benefit. There are, however, no HNE inhibitors in clincal use, an issue that requires addressing.

This work reveals certain fine details of the GAG-HNE interaction. The results indicate that particular GAG sequences will have selectivity for HNE over other serine proteases, and thus be devoid of side effects associated with GAGs. The results show that an octasaccharide may be minimally needed for potent anti-HNE activity. Also, the results confirm that N and 6-O sulfates are most important for HNE inhibition by GAGs. Additonally, it shows that iduronic acid is a preferred sugar unit for HNE inbibitory potential. Currently, X-ray crystallography is ongoing to obtain a co-crystal of HNE bound to GAGs to aid in drug discovery efforts.

LITERATURE CITED

1. Gandhi, N. S.; Mancera, R. L. The structure of glycosaminoglycans and their interactions with proteins. *Chem. Biol. Drug Des.* **2008**, *72*, 455–482.

2. Lindahl, U.; Hook, M. Glycosaminoglycans and their binding to biologial macromolecules. *Ann. Rev. Biochem.* **1978**, *47*, 385–417.

3. Esko, J. D.; Kimata, K.; Lindahl, U. Proteoglycans and sulfated glycosaminoglycans. In Essentials of Glycobiology; 2nd ed.; Varki, A.; Cummings, R. D.; Esko, J. D., Freeze, H. H.; Stanley, P.; Bertozzi, C. R.; Hart, G. W.; Etzler, M. E.; Eds.; Cold Spring Harbor Laboratory Press: New York, 2009; pp 229–248.

4. Sasisekharan, R.; Venkataraman, G. Heparin and heparan sulfate: Biosynthesis, structure and function. *Curr. Opin. Chem. Biol.* **2000**, *4*, 626–631.

5. Imberty, A.; Lortat-Jacob, H.; Pérez, S. Structural view of glycosaminoglycan-protein interactions. *Carbohydr. Res.* **2007**, *342*, 430–439.

6. Spicer, A. P.; Tien, J. L.; Joo, A.; Bowling, R. A. Investigation of hyaluronan function in the mouse through targeted mutagenesis. *Glycoconj. J.* **2003**, *19*, 341–345.

7. Capila, I.; Linhardt, R. J. Heparin-protein interactions. *Angew. Chem. Int. Ed. Engl.* **2002**, *41*, 391–412.

8. Sugahara, K.; Kitagawa, H. Recent advances in the study of the biosynthesis and functions of sulfated glycosaminoglycans. *Curr. Opin. Struct. Biol.* **2000**, *10*, 518–527.

9. Esko, J. D.; Lindahl, U. Molecular diversity of heparan sulfate. *J. Clin. Invest.* **2001**, *108*, 169–173.

10. Lindahl, U.; Kusche-Gullberg, M.; Kjellen, L. Regulated diversity of heparan sulfate. *J. Biol. Chem.* **1998**, *273*, 24979–24982.

11. Iozzo, R. V. Heparan sulfate proteoglycans: Intricate molecules with intriguing functions. *J. Clin. Invest.* **2001**, *108*, 165–167.

12. Aquino, R. S.; Lee, E. S.; Park, P. W. Diverse functions of glycosaminoglycans in infectious diseases. *Prog. Mol. Biol. Transl. Sci.* **2010**, *93*, 373–394.

13. Sasisekharan, R.; Shriver, Z.; Venkataraman, G.; Narayanasami, U. Roles of heparan-sulphate glycosaminoglycans in cancer. *Nat. Rev. Cancer* **2002**, *2*, 521–528.

14. Li, J. P.; Vlodavsky, I. Heparin, heparan sulfate and heparanase in inflammatory reactions. In *Thrombosis and Haemostasis*; 2009; Vol. 102, pp 823–828.

15. Rabenstein, D. L. Heparin and heparan sulfate: structure and function. *Nat. Prod. Rep.* **2002**, *19*, 312–331.

16. Volpi, N. Therapeutic applications of glycosaminoglycans. *Curr. Med. Chem.* **2006**, *13*, 1799–1810.

17. Yamada, S.; Sugahara, K. Potential therapeutic application of chondroitin

sulfate/dermatan sulfate. *Curr Drug Discov Technol* **2008**, *5*, 289–301.

18. Gervais, F.; Chalifour, R.; Garceau, D.; Kong, X.; Laurin, J.; Mclaughlin, R.; Morissette, C.; Paquette, J. Glycosaminoglycan mimetics: a therapeutic approach to cerebral amyloid angiopathy. *Amyloid* **2001**, *8 Suppl 1*, 28–35.

19. Yip, G. W.; Smollich, M.; Götte, M. Therapeutic value of glycosaminoglycans in cancer. *Mol. Cancer Ther.* **2006**, *5*, 2139–2148.

20. Zhang, L. Glycosaminoglycan (GAG) biosynthesis and GAG-binding proteins. *Prog. Mol. Biol. Transl. Sci.* **2010**, *93*, 1–17.

21. Jackson, R. L.; Busch, S. J.; Cardin, A D. Glycosaminoglycans: molecular properties, protein interactions, and role in physiological processes. *Physiol. Rev.* **1991**, *71*, 481–539.

22. Hileman, R. E.; Fromm, J. R.; Weiler, J. M.; Linhardt, R. J. Glycosaminoglycan-protein interactions: Definition of consensus sites in glycosaminoglycan binding proteins. *BioEssays* **1998**, *20*, 156–167.

23. J. R. Fromm, R. E. Hileman, E. E. Caldwell, J. M.; Linhardt, W. and R. J. Pattern and spacing of basic amino acids in heparin binding sites. **1997**, *343*, 343, 92–100.

24. Hileman, R. E.; Jennings, R. N.; Linhardt, R. J. Thermodynamic analysis of the heparin interaction with a basic cyclic peptide using isothermal titration calorimetry. *Biochemistry* **1998**, *37*, 15231–15237.

25. Fromm, J. R.; Hileman, R. E.; Caldwell, E. E. O.; Weiler, J. M.; Linhardt, R. J. Differences in the Interaction of Heparin with Arginine and Lysine and the Importance of these Basic Amino Acids in the Binding of Heparin to Acidic Fibroblast Growth Factor. *Arch. Biochem. Biophys.* **1995**, *323*, 279–287.

26. Cardin, A. D.; Weintraub, H. J. Molecular modeling of protein-glycosaminoglycan interactions. *Arteriosclerosis* **1989**, *9*, 21–32.

27. Sobel, M.; Soler, D. F.; Kermode, J. C.; Harris, R. B. Localization and characterization of a heparin binding domain peptide of human von Willebrand factor. *J. Biol. Chem.* **1992**, *267*, 8857–8862.

28. Margalit, H.; Fischer, N.; Ben-Sasson, S. A. Comparative analysis of structurally defined heparin binding sequences reveals a distinct spatial distribution of basic residues. *J. Biol. Chem.* **1993**, *268*, 19228–19231.

29. Bae, J.; Desai, U. R.; Pervin, A.; Caldwell, E. E.; Weiler, J. M.; Linhardt, R. J. Interaction of heparin with synthetic antithrombin III peptide analogues. *Biochem. J.* **1994**, *301*, 121–129.

30. Hajjar, E.; Broemstrup, T.; Kantari, C.; Witko-Sarsat, V.; Reuter, N. Structures of human proteinase 3 and neutrophil elastase--so similar yet so different. *FEBS J.* **2010**, *277*, 2238–2254.

31. Kostoulas, G.; Hörler, D.; Naggi, A.; Casu, B.; Baici, A. Electrostatic interactions between human leukocyte elastase and sulfated glycosaminoglycans: physiological implications.

Biol. Chem. **1997**, *378*, 1481–1489.

32. Redini Francois, Tixier Jean_Michel, Petitou Maurice, Choay Jean, Robert Ladislas, H. W. Inhibition of leucocyte elastase by heparin and its derivatives. *Biochem J* **1988**, *252*, 515–519.

33. Volpi, N. Inhibition of human leukocyte elastase activity by chondroitin sulfates. *Chem. Biol. Interact.* **1997**, *105*, 157–167.

34. Walsh, R. L.; Dillon, T. J.; Scicchitano, R.; McLennan, G. Heparin and heparan sulphate are inhibitors of human leucocyte elastase. *Clin. Sci.* **1991**, *81*, 341–346.

35. Fath, M. A.; Wu, X.; Hileman, R. E.; Linhardt, R. J.; Kashem, M. A.; Nelson, R. M.; Wright, C. D.; Abraham, W. M. Interaction of secretory leukocyte protease inhibitor with heparin inhibits proteases involved in asthma. *J. Biol. Chem.* **1998**, *273*, 13563–13569.

36. Malik, A.; Ahmad, S. Sequence and structural features of carbohydrate binding in proteins and assessment of predictability using a neural network. *BMC Struct. Biol.* **2007**, *7*, 1.

37. Pratt, C. W. General features of the heparin-binding serpins antithrombin, heparin cofactor II and protein C inhibitor. *Blood Coagul. Fibrinolysis* **1997**, *4*, 479–490.

38. Huntington, J. A.; Read, R. J.; Carrell, R. W. Structure of a serpin-protease complex shows inhibition by deformation. *Nature* **2000**, *407*, 923–926.

39. Gettins, P. G. W. Serpin structure, mechanism, and function. *Chem. Rev.* **2002**, *102*, 4751–4803.

40. Desai, U. R. New Antithrombin-Based Anticoagulants. *Med. Res. Rev.* **2004**, *24*, 151–181.

41. Tollefsen, D. M.; Pestka, C. A.; Monafo, W. J. Activation of heparin cofactor II by dermatan sulfate. *J. Biol. Chem.* **1983**, *258*, 6713–6716.

42. Li, W.; Adams, T. E. T. E.; Nangalia, J.; Esmon, C. T. C. T.; Huntington, J. A. J. A. Molecular basis of thrombin recognition by protein C inhibitor revealed by the 1.6-A structure of the heparin-bridged complex. *Proc. Natl. Acad. Sci. U. S. A.* **2008**, *105*, 4661–4666.

43. Laurent, T. C.; Tengblad, a; Thunberg, L.; Höök, M.; Lindahl, U. The molecular-weight-dependence of the anti-coagulant activity of heparin. *Biochem. J.* **1978**, *175*, 691–701.

44. Choay, J.; Petitou, M.; Lormeau, J. C.; Sinaÿ, P.; Casu, B.; Gatti, G. Structure-activity relationship in heparin: A synthetic pentasaccharide with high affinity for antithrombin III and eliciting high anti-factor Xa activity. *Biochem. Biophys. Res. Commun.* **1983**, *116*, 492–499.

45. Bray, B.; Lane, D. A.; Freyssinet, J. M.; Pejler, G.; Lindahl, U. Anti-thrombin activities of heparin. Effect of saccharide chain length on thrombin inhibition by heparin cofactor II and by antithrombin. *Biochem. J.* **1989**, *262*, 225–232.

46. L Thunberg, U Lindahl, A Tengblad, T C Laurent, C. M. J. On the Molecular-Weight-Dependence of the Anticoagulant Activity of Heparin. *Biochem. J.* **1979**, *181*, 241–243.

47. Johnson, D. J. D.; Li, W.; Adams, T. E.; Huntington, J. a. Antithrombin-S195A factor Xa-heparin structure reveals the allosteric mechanism of antithrombin activation. *EMBO J.* **2006**, *25*, 2029–2037.

48. Li, W.; Johnson, D. J. D.; Esmon, C. T.; Huntington, J. a. Structure of the antithrombin-thrombin-heparin ternary complex reveals the antithrombotic mechanism of heparin. *Nat. Struct. Mol. Biol.* **2004**, *11*, 857–862.

49. Choay, J.; Lormeau, J.; Petitou, M.; Sinay, P.; Fareed, J. Structural studies on a biologically active hexasaccharide obtained. **1981**, 644–649.

50. Thunberg, L.; Bäckström, G.; Lindahl, U. Further characterization of the antithrombin-binding sequence in heparin. *Carbohydr. Res.* **1982**, *100*, 393–410.

51. Petitou, M.; Duchaussoy, P.; Lederman, I.; Choay, J.; Sinaÿ, P.; Jacquinet, J. C.; Torri, G. Synthesis of heparin fragments. A chemical synthesis of the pentasaccharide. *Carbohydr. Res.* **1986**, *147*, 221–236.

52. Duchaussoy, P.; Lei, P. S.; Petitou, M.; Sinaÿ, P.; Lormeau, J. C.; Choay, J. The first total synthesis of the antithrombin III binding site of porcine mucosa heparin. *Bioorg. Med. Chem. Lett.* **1991**, *1*, 99–102.

53. Petitou, M.; Casu, B.; Lindahl, U. 1976-1983, a critical period in the history of heparin: The iscovery of the antithrombin binding site. *Biochimie* **2003**, *85*, 83–89.

54. Ersdal-Badju, E.; Lu, A.; Zuo, Y.; Picard, V.; Bock, S. C. Identification of the antithrombin III heparin binding site. *J. Biol. Chem.* **1997**, *272*, 19393–19400.

55. Arocas, V.; Turk, B.; Bock, S. C.; Olson, S. T.; Björk, I. The region of antithrombin interacting with full-length heparin chains outside the high-affinity pentasaccharide sequence extends to LYS136 but not to Lys139. *Biochemistry* **2000**, *39*, 8512–8518.

56. Jin, L.; Abrahams, J. P.; Skinner, R.; Petitou, M.; Pike, R. N.; Carrell, R. W. The anticoagulant activation of antithrombin by heparin. *Med. Sci.* **1997**, *94*, 14683–14688.

57. Blinder, M. A.; Tollefsen, D. M. Site-directed mutagenesis of arginine 103 and lysine 185 in the proposed glycosaminoglycan-binding site of heparin cofactor II. *J. Biol. Chem.* **1990**, *265*, 286–291.

58. Whinna, H. C.; Blinder, M. A.; Szewczyk, M.; Tollefsen, D. M.; Church, F. C. Role of lysine 173 in heparin binding to heparin cofactor II. *J. Biol. Chem.* **1991**, *266*, 8129–8135.

59. Blinder, M. A.; Anderssonq, T. R.; Abildgaardll, U.; Tollefsensii, D. M. Heparin Cofactor II. *J. Biol. Chem.* **1989**, *264*, 5128–5133.

60. Pratt, C. W.; Church, F. C. Heparin binding to protein C inhibitor. *J. Biol. Chem.* **1992**, *267*, 8789–8794.

61. Shirk, R. a; Elisen, M. G.; Meijers, J. C.; Church, F. C. Role of the H helix in heparin binding to protein C inhibitor. *J. Biol. Chem.* **1994**, *269*, 28690–28695.

62. Protease-dependent, I.; Li, W.; Huntington, J. A. The Heparin Binding Site of Protein C Inhibitor. **2008**, *283*, 36039–36045.

63. Ehrlich, H. J.; Gebbink, R. K.; Keijer, J.; Pannekoek, H. Elucidation of structural requirements on plasminogen activator inhibitor 1 for binding to heparin. *J. Biol. Chem.* **1992**, *267*, 11606–11611.

64. Hedstrom, L. Serine protease mechanism and specificity. *Chem. Rev.* **2002**, *102*, 4501–4523.

65. Di Cera, E. Serine proteases. *IUBMB Life* **2009**, *61*, 510–515.

66. Rawlings, N. D.; Barrett, A. J.; Finn, R. Twenty years of the MEROPS database of proteolytic enzymes, their substrates and inhibitors. *Nucleic Acids Res.* **2016**, *44*, D343–D350.

67. Page, M. J.; Di Cera, E. Serine peptidases: Classification, structure and function. *Cell. Mol. Life Sci.* **2008**, *65*, 1220–1236.

68. Perona, J. J.; Craik, C. S. Structural basis of substrate specificity in the serine proteases. *Protein Sci.* **1995**, *4*, 337–360.

69. Bock, P. E.; Panizzi, P.; Verhamme, I. M. A. Exosites in the substrate specificity of blood coagulation reactions. *J. Thromb. Haemost.* **2007**, *5*, 81–94.

70. O'Brien, L. A.; Stafford, A. R.; Fredenburgh, J. C.; Weitz, J. I. Glycosaminoglycans Bind Factor Xa in a Ca2+-Dependent Fashion and Modulate Its Catalytic Activity. *Biochemistry* **2003**, *42*, 13091–13098.

71. Sheehan, J. P.; Sadler, J. E. Molecular mapping of the heparin-binding exosite of thrombin (antithrombin III/serine proteases). *Biochemistry* **1994**, *91*, 5518–5522.

72. Gan, Z. R.; Li, Y.; Chen, Z.; Lewis, S. D.; Shafer, J. A. Identification of basic amino acid residues in thrombin essential for heparin-catalyzed inactivation by antithrombin III. *J. Biol. Chem.* **1994**, *269*, 1301–1305.

73. Carter, W. J.; Cama, E.; Huntington, J. A. Crystal structure of thrombin bound to heparin. *J. Biol. Chem.* **2005**, *280*, 2745–2749.

74. Rezaie, A. R. Identification of basic residues in the heparin-binding exosite of factor Xa critical for heparin and factor Va binding. *J. Biol. Chem.* **2000**, *275*, 3320–3327.

75. Yang, L.; Manithody, C.; Rezaie, A. R. Localization of the heparin binding exosite of factor IXa. *J. Biol. Chem.* **2002**, *277*, 50756–50760.

76. Johnson, D. J. D.; Langdown, J.; Huntington, J. a. Molecular basis of factor IXa recognition by heparin-activated antithrombin revealed by a 1.7-A structure of the ternary complex. *Proc. Natl. Acad. Sci. U. S. A.* **2010**, *107*, 645–650.

77. Emsley, J.; McEwan, P. a.; Gailani, D. Structure and function of factor XI. *Blood* **2010**, *115*, 2569.

78. Zhao, M.; Abdel-Razek, T.; Sun, M. F.; Gailani, D. Characterization of a heparin binding site on the heavy chain of factor XI. *J. Biol. Chem.* **1998**, *273*, 31153–31159.

79. Ho, D. H.; Badellino, K.; Baglia, F. A.; Walsh, P. N. A Binding Site for Heparin in the

Apple 3 Domain of Factor XI. *J. Biol. Chem.* **1998**, *273*, 16382–16390.

80. Badellino, K. O.; Walsh, P. N. Localization of a heparin binding site in the catalytic domain of factor XIa. *Biochemistry* **2001**, *40*, 7569–7580.

81. Sinha, D.; Badellino, K. O.; Marcinkiewicz, M.; Walsh, P. N. Allosteric modification of factor XIa functional activity upon binding to polyanions. *Biochemistry* **2004**, *43*, 7593–7600.

82. Castellino, F. J.; Ploplis, V. A. Structure and function of the plasminogen/plasmin system. *Thromb. Haemost.* **2005**, *93*, 647–654.

83. Chander, A.; Atkinson, H. M.; Stevic, I.; Berry, L. R.; Kim, P. Y.; Chan, A. K. C. Interactions of heparin and a covalently-linked antithrombin-heparin complex with components of the fibrinolytic system. *Thromb. Haemost.* **2013**, *110*, 1180–1188.

84. Bauer, P. I.; Pozsgay, M.; Machovich, R.; Elödi, P.; Horváth, I. The interaction of heparin with human plasmin. *Int. J. Biochem.* **1983**, *15*, 871–874.

85. Andrade-Gordon, P.; Strickland, S. Interaction of heparin with plasminogen activators and plasminogen: effects on the activation of plasminogen. *Biochemistry* **1986**, *25*, 4033–4040.

86. Robert E. Jordan, Gary M. Oosta, William T. Gardner, and R. D. R. The Binding of Low Molecular Weight Heparin to Hemostatic Enzymes. *J. Biol. Chem.* **1980**, *255*, 10073–10080.

87. Al-Horani, R. A.; Desai, U. R. Recent Advances on Plasmin Inhibitors for the Treatment of Fibrinolysis-Related Disorders. *Med. Res. Rev.* **2014**, *34*, 1168–1216.

88. Spencer, J. L.; Stone, P. J.; Nugent, M. A. New insights into the inhibition of human neutrophil elastase by heparin. *Biochemistry* **2006**, *45*, 9104–9120.

89. Linhardt, A. P. C. G. K. A. J. X.-J. H. R. J. Preparation and structural characterization of large heparin-derived oligosaccharides. *Glycobiology* **1995**, *5*, 83–95.

90. Linhardt, R. J.; Rice, K. G.; Kim, Y. S.; Lohse, D. L.; Wang, H. M.; Loganathan, D. Mapping and quantification of the major oligosaccharide components of heparin. *Biochem. J.* **1988**, *254*, 781–787.

91. Pan, J.; Qian, Y.; Zhou, X.; Pazandak, A.; Frazier, S. B.; Weiser, P.; Lu, H.; Zhang, L. Oversulfated chondroitin sulfate is not the sole contaminant in heparin. *Nat. Biotechnol.* **2010**, *28*, 203-207-211.

92. Guerrini, M.; Beccati, D.; Shriver, Z.; Naggi, A.; Viswanathan, K.; Bisio, A.; Capila, I.; Lansing, J. C.; Guglieri, S.; Fraser, B.; Al-Hakim, A.; Gunay, N. S.; Zhang, Z.; Robinson, L.; Buhse, L.; Nasr, M.; Woodcock, J.; Langer, R.; Venkataraman, G.; Linhardt, R. J.; Casu, B.; Torri, G.; Sasisekharan, R. Oversulfated chondroitin sulfate is a contaminant in heparin associated with adverse clinical events. *Nat. Biotechnol.* **2008**, *26*, 669–675.

93. Blossom, D. B.; Kallen, A. J.; Patel, P. R.; Elward, A.; Robinson, L.; Gao, G.; Langer, R.; Perkins, K. M.; Jaeger, J. L.; Kurkjian, K. M.; Jones, M.; Schillie, S. F.; Shehab, N.;

Ketterer, D.; Venkataraman, G.; Kishimoto, T. K.; Shriver, Z.; McMahon, A. W.; Austen, K. F.; Kozlowski, S.; Srinivasan, A.; Turabelidze, G.; Gould, C. V; Arduino, M. J.; Sasisekharan, R. Outbreak of adverse reactions associated with contaminated heparin. *N. Engl. J. Med.* **2008**, *359*, 2674–2684.

94. Kishimoto, T. K.; Viswanathan, K.; Ganguly, T.; Elankumaran, S.; Smith, S.; Pelzer, K.; Lansing, J. C.; Sriranganathan, N.; Zhao, G.; Galcheva-Gargova, Z.; Al-Hakim, A.; Bailey, G. S.; Fraser, B.; Roy, S.; Rogers-Cotrone, T.; Buhse, L.; Whary, M.; Fox, J.; Nasr, M.; Dal Pan, G. J.; Shriver, Z.; Langer, R. S.; Venkataraman, G.; Austen, K. F.; Woodcock, J.; Sasisekharan, R. Contaminated heparin associated with adverse clinical events and activation of the contact system. *N. Engl. J. Med.* **2008**, *358*, 2457–2467.

95. Liu, H.; Zhang, Z.; Linhardt, R. J. Lessons learned from the contamination of heparin. *Nat. Prod. Rep.* **2009**, *26*, 313–321.

96. DeAngelis, P. L. Glycosaminoglycan polysaccharide biosynthesis and production: Today and tomorrow. *Appl. Microbiol. Biotechnol.* **2012**, *94*, 295–305.

97. Oduah, E. I.; Linhardt, R. J.; Sharfstein, S. T. Heparin: Past, present, and future. *Pharmaceuticals* **2016**, *9*, 1–12.

98. Ernst, B.; Magnani, J. L. From carbohydrate leads to glycomimetic drugs. *Nat. Rev. Drug Discov.* **2009**, *8*, 661–677.

99. Magnani, J. L.; Ernst, B. Glycomimetic drugs--a new source of therapeutic opportunities 2. *Discov.Med.* **2009**, *8*, 247–252.

100. Samsonov, S. A.; Pisabarro, M. T. Computational analysis of interactions in structurally available protein-glycosaminoglycan complexes. *Glycobiology* **2016**, *26*, 850–861.

101. Sankaranarayanan, N. V.; Sarkar, A.; Desai, U. R.; Mosier, P. D. Designing "high-affinity, high-specificity" glycosaminoglycan sequences through computerized modeling. In *Methods in Molecular Biology*; Series Ed.; Balagurunathan, K., Nakato, H., Desai, U. R., Eds.; Springer New York: New York, 2015; pp 289–314.

102. Sankaranarayanan, N. V.; Desai, U. R. Toward a robust computational screening strategy for identifying glycosaminoglycan sequences that display high specificity for target proteins. *Glycobiology* **2014**, *24*, 1323–1333.

103. Raghuraman, A.; Mosier, P. D.; Desai, U. R. Finding a Needle in a Haystack: Development of a Combinatorial Virtual Screening Approach for Identifying High Specificity Heparin/Heparan Sulfate Sequence(s). *J. Med. Chem.* **2006**, *49*, 3553–3562.

104. Sarkar, A.; Desai, U. R. A simple method for discovering druggable, specific glycosaminoglycan-protein systems. Elucidation of key principles from heparin/heparan sulfate-binding proteins. *PLoS One* **2015**, *10*, 1–18.

105. Agostino, M.; Gandhi, N. S.; Mancera, R. L. Development and application of site mapping methods for the design of glycosaminoglycans. *Glycobiology* **2014**, *24*, 840–851.

106. Koester, D. C.; Holkenbrink, A.; Werz, D. B. Recent advances in the synthesis of carbohydrate mimetics. *Synthesis (Stuttg).* **2010**, No. 19, 3217–3242.

107. Desai, U. R. The promise of sulfated synthetic small molecules as modulators of glycosaminoglycan function. *Future Med. Chem.* **2013**, *5*, 1363–1366.

108. Shen, A. Allosteric regulation of protease activity by small molecules. *Mol. Biosyst.* **2010**, *6*, 1431.

109. Merdanovic, M.; Mönig, T.; Ehrmann, M.; Kaiser, M. Diversity of allosteric regulation in proteases. *ACS Chem. Biol.* **2013**, *8*, 19–26.

110. Hauske, P.; Ottmann, C.; Meltzer, M.; Ehrmann, M.; Kaiser, M. Allosteric regulation of proteases. *Chembiochem* **2008**, *9*, 2920–2928.

111. Adams, R. L. C.; Bird, R. J. Review article: Coagulation cascade and therapeutics update: Relevance to nephrology. Part 1: Overview of coagulation, thrombophilias and history of anticoagulants. *Nephrology* **2009**, *14*, 462–470.

112. Gage, B. F.; Fihn, S. D.; White, R. H. Management and dosing of warfarin therapy. *Am. J. Med.* **2000**, *109*, 481–488.

113. Ruff, C. T.; Giugliano, R. P.; Braunwald, E.; Hoffman, E. B.; Deenadayalu, N.; Ezekowitz, M. D.; Camm, A. J.; Weitz, J. I.; Lewis, B. S.; Parkhomenko, A.; Yamashita, T.; Antman, E. M. Comparison of the efficacy and safety of new oral anticoagulants with warfarin in patients with atrial fibrillation: A meta-analysis of randomised trials. *Lancet* **2014**, *383*, 955–962.

114. Guglielmone, H. A.; Agnese, A. M.; N??ez Montoya, S. C.; Cabrera, J. L. Anticoagulant effect and action mechanism of sulphated flavonoids from Flaveria bidentis. *Thromb. Res.* **2002**, *105*, 183–188.

115. Gunnarsson, G. T.; Desai, U. R. Designing small, nonsugar activators of antithrombin using hydropathic interaction analyses. *J. Med. Chem.* **2002**, *45*, 1233–1243.

116. Kellogg, G. E.; Semus, S. F.; Abraham, D. J. HINT: A new method of empirical hydrophobic field calculation for CoMFA. *J. Comput. Aided. Mol. Des.* **1991**, *5*, 545–552.

117. Gunnarsson, G. T.; Desai, U. R. Interaction of designed sulfated flavanoids with antithrombin: Lessons on the design of organic activators. *J. Med. Chem.* **2002**, *45*, 4460–4470.

118. Gunnarsson, G. T.; Desai, U. R. Exploring new non-sugar sulfated molecules as activators of antithrombin. *Bioorganic Med. Chem. Lett.* **2003**, *13*, 679–683.

119. Gunnarsson, G. T.; Riaz, M.; Adams, J.; Desai, U. R. Synthesis of per-sulfated flavonoids using 2,2,2-trichloro ethyl protecting group and their factor Xa inhibition potential. *Bioorganic Med. Chem.* **2005**, *13*, 1783–1789.

120. Correia-Da-Silva, M.; Sousa, E.; Duarte, B.; Marques, F.; Carvalho, F.; Cunha-Ribeiro, L. M.; Pinto, M. M. M. Flavonoids with an oligopolysulfated moiety: A new class of anticoagulant agents. *J. Med. Chem.* **2011**, *54*, 95–106.

121. Monien, B. H.; Desai, U. R. Antithrombin activation by nonsulfated, non-polysaccharide organic polymer. *J. Med. Chem.* **2005**, *48*, 1269–1273.

122. Monien, B. H.; Cheang, K. I.; Desai, U. R. Mechanism of poly(acrylic acid) acceleration of antithrombin inhibition of thrombin: Implications for the design of novel heparin mimics. *J. Med. Chem.* **2005**, *48*, 5360–5368.

123. Monien, B. H.; Henry, B. L.; Raghuraman, A.; Hindle, M.; Desai, U. R. Novel chemo-enzymatic oligomers of cinnamic acids as direct and indirect inhibitors of coagulation proteinases. *Bioorganic Med. Chem.* **2006**, *14*, 7988–7998.

124. Henry, B. L.; Monien, B. H.; Bock, P. E.; Desai, U. R. A novel allosteric pathway of thrombin inhibition: Exosite II mediated potent inhibition of thrombin by chemo-enzymatic, sulfated dehydropolymers of 4-hydroxycinnamic acids. *J. Biol. Chem.* **2007**, *282*, 31891–31899.

125. Abdel Aziz, M. H.; Mosier, P. D.; Desai, U. R. Identification of the site of binding of sulfated, low molecular weight lignins on thrombin. *Biochem. Biophys. Res. Commun.* **2011**, *413*, 348–352.

126. Henry, B. L.; Connell, J.; Liang, A.; Krishnasamy, C.; Desai, U. R. Interaction of antithrombin with sulfated, low molecular weight lignins. Opportunities for potent, selective modulation of antithrombin function. *J. Biol. Chem.* **2009**, *284*, 20897–20908.

127. Machovich, R.; Bauer, P. I.; Arányi, P.; Kecskés, E.; Büki, K. G.; Horváth, I. Kinetic analysis of the heparin-enhanced plasmin--antithrombin III reaction. Apparent catalytic role of heparin. *Biochem. J.* **1981**, *199*, 521–526.

128. Henry, B. L.; Aziz, M. A.; Zhou, Q.; Desai, U. R. Sulfated, low-molecular-weight lignins are potent inhibitors of plasmin, in addition to thrombin and factor Xa: Novel opportunity for controlling complex pathologies. *Thromb. Haemost.* **2010**, *103*, 507–515.

129. Krylov, V. B.; Ushakova, N. A.; Ustyuzhanina, N. E.; Preobrazhenskaya, M. E.; Yashunsky, D. V.; Menshov, V. M.; Tsvetkov, D. E.; Sharma, G. V. M.; Krishna, P. R.; Nifantiev, N. E. Study of sulfated derivatives of polyhydroxy compounds as inhibitors of blood coagulation. *Russ. Chem. Bull.* **2010**, *59*, 232–235.

130. Verghese, J.; Liang, A.; Sidhu, P. P. S.; Hindle, M.; Zhou, Q.; Desai, U. R. First steps in the direction of synthetic, allosteric, direct inhibitors of thrombin and factor Xa. *Bioorg. Med. Chem. Lett.* **2009**, *19*, 4126–4129.

131. Witayakran, S.; Gelbaum, L.; Ragauskas, A. J. Cascade synthesis of benzofuran derivatives via laccase oxidation-Michael addition. *Tetrahedron* **2007**, *63*, 10958–10962.

132. Pei, L. X.; Li, Y. M.; Bu, X. Z.; Gu, L. Q.; Chan, A. S. C. One-pot synthesis of 5,6-dihydroxylated benzo[b]furan derivatives. *Tetrahedron Lett.* **2006**, *47*, 2615–2618.

133. Sidhu, P. S.; Liang, A.; Mehta, A. Y.; Abdel Aziz, M. H.; Zhou, Q.; Desai, U. R. Rational design of potent, small, synthetic allosteric inhibitors of thrombin. *J. Med. Chem.* **2011**, *54*, 5522–5531.

134. Abdel Aziz, M. H.; Sidhu, P. S.; Liang, A.; Kim, J. Y.; Mosier, P. D.; Zhou, Q.; Farrell, D. H.; Desai, U. R. Designing allosteric regulators of thrombin. Monosulfated benzofuran dimers selectively interact with Arg173 of exosite 2 to induce inhibition. *J. Med. Chem.* **2012**, *55*, 6888–6897.

135. Sidhu, P. S.; Abdel Aziz, M. H.; Sarkar, A.; Mehta, A. Y.; Zhou, Q.; Desai, U. R. Designing allosteric regulators of thrombin. Exosite 2 features multiple subsites that can be targeted by sulfated small molecules for inducing inhibition. *J. Med. Chem.* **2013**, *56*, 5059–5070.

136. Argade, M. D.; Mehta, A. Y.; Sarkar, A.; Desai, U. R. Allosteric inhibition of human factor XIa: Discovery of monosulfated benzofurans as a class of promising inhibitors. *J. Med. Chem.* **2014**, *57*, 3559–3569.

137. Mehta, A. Y.; Thakkar, J. N.; Mohammed, B. M.; Martin, E. J.; Brophy, D. F.; Kishimoto, T.; Desai, U. R. Targeting the GPIbα binding site of thrombin to simultaneously induce dual anticoagulant and antiplatelet effects. *J. Med. Chem.* **2014**, *57*, 3030–3039.

138. Mehta, A. Y.; Mohammed, B. M.; Martin, E. J.; Brophy, D. F.; Gailani, D.; Desai, U. R. Allosterism-based simultaneous, dual anticoagulant and antiplatelet action: Allosteric inhibitor targeting the glycoprotein Ibα-binding and heparin-binding site of thrombin. *J. Thromb. Haemost.* **2016**, *14*, 828–838.

139. Verespy, S.; Mehta, A. Y.; Afosah, D.; Al-Horani, R. A.; Desai, U. R. Allosteric Partial Inhibition of Monomeric Proteases. Sulfated Coumarins Induce Regulation, not just Inhibition, of Thrombin. *Sci. Rep.* **2016**, *6*, 24043.

140. Löwenberg, E. C.; Meijers, J. C. M.; Monia, B. P.; Levi, M. Coagulation factor XI as a novel target for antithrombotic treatment. *J. Thromb. Haemost.* **2010**, *8*, 2349–2357.

141. Schumacher, W. A.; Luettgen, J. M.; Quan, M. L.; Seiffert, D. A. Inhibition of factor XIa as a new approach to anticoagulation. *Arterioscler. Thromb. Vasc. Biol.* **2010**, *30*, 388–392.

142. Gomez, K.; Bolton-Maggs, P. Factor XI deficiency. *Haemophilia* **2008**, *14*, 1183–1189.

143. Seligsohn, U. Factor XI deficiency in humans. *J. Thromb. Haemost.* **2009**, *7*, 84–87.

144. Berliner, J. I.; Rybicki, A. C.; Kaplan, R. C.; Monrad, E. S.; Freeman, R.; Billett, H. H. Elevated levels of Factor XI are associated with cardiovascular disease in women. *Thromb. Res.* **2002**, *107*, 55–60.

145. Al-Horani, R. A.; Ponnusamy, P.; Mehta, A. Y.; Gailani, D.; Desai, U. R. Sulfated pentagalloylglucoside is a potent, allosteric, and selective inhibitor of factor XIa. *J. Med. Chem.* **2013**, *56*, 867–878.

146. Al-Horani, R. A.; Desai, U. R. Designing allosteric inhibitors of factor XIa. Lessons from the interactions of sulfated pentagalloylglucopyranosides. *J. Med. Chem.* **2014**, *57*, 4805–4818.

147. Al-Horani, R. A.; Gailani, D.; Desai, U. R. Allosteric inhibition of factor XIa. Sulfated non-saccharide glycosaminoglycan mimetics as promising anticoagulants. *Thromb. Res.* **2015**, *136*, 379–387.

148. Karuturi, R.; Al-Horani, R. A.; Mehta, S. C.; Gailani, D.; Desai, U. R. Discovery of allosteric modulators of factor XIa by targeting hydrophobic domains adjacent to its heparin-binding site. *J. Med. Chem.* **2013**, *56*, 2415–2428.

149. Raghuraman, A.; Liang, A.; Krishnasamy, C.; Lauck, T.; Gunnarsson, G. T.; Desai, U. R. On designing non-saccharide, allosteric activators of antithrombin. *Eur. J. Med. Chem.* **2009**, *44*, 2626–2631.

150. Al-Horani, R. A.; Liang, A.; Desai, U. R. Designing nonsaccharide, allosteric activators of antithrombin for accelerated inhibition of factor Xa. *J. Med. Chem.* **2011**, *54*, 6125–6138.

151. Belting, M. Glycosaminoglycans in cancer treatment. *Thromb. Res.* **2014**, *133*, S95–S101.

152. Afratis, N.; Gialeli, C.; Nikitovic, D.; Tsegenidis, T.; Karousou, E.; Theocharis, A. D.; Pavão, M. S.; Tzanakakis, G. N.; Karamanos, N. K. Glycosaminoglycans: Key players in cancer cell biology and treatment. *FEBS J.* **2012**, *279*, 1177–1197.

153. Yang, H.; Protiva, P.; Cui, B.; Ma, C.; Baggett, S.; Hequet, V.; Mori, S.; Weinstein, I. B.; Kennelly, E. J. New bioactive polyphenols from Theobroma grandiflorum ("cupuaçu"). *J. Nat. Prod.* **2003**, *66*, 1501–1504.

154. Liang, J.; Shang, Y. Estrogen and Cancer. *Annu. Rev. Physiol.* **2013**, *75*, 225–240.

155. Hoshino, J.; Park, E.; Kondratyuk, T. P.; Marler, L.; Pezzuto, J. M.; Breemen, R. B. Van; Mo, S.; Li, Y.; Cushman, M. Selective Synthesis and Biological Evaluation of Sulfate-Conjugated Resveratrol Metabolites. **2010**, 5033–5043.

156. Smith, I. E.; Dowsett, M. Aromatase Inhibitors in Breast Cancer. *N. Engl. J. Med.* **2003**, *348*, 2431–2442.

157. Suzuki, T.; Nakata, T.; Miki, Y.; Kaneko, C.; Moriya, T.; Ishida, T.; Akinaga, S.; Hirakawa, H.; Kimura, M.; Sasano, H. Estrogen sulfotransferase and steroid sulfatase in human breast carcinoma. *Cancer Res.* **2003**, *63*, 2762–2770.

158. Ec, S. Daidzein Sulfoconjugates Are Potent Inhibitors. *Biochem. Biophys. Res. Commun.* **1997**, *583*, 579–583.

159. Courtney, K. D.; Corcoran, R. B.; Engelman, J. A. The PI3K pathway as drug target in human cancer. *J. Clin. Oncol.* **2010**, *28*, 1075–1083.

160. Rodon, J.; Dienstmann, R.; Serra, V.; Tabernero, J. Development of PI3K inhibitors: lessons learned from early clinical trials. *Nat Rev Clin Oncol* **2013**, *10*, 143–153.

161. Miller, T. W.; Rexer, B. N.; Garrett, J. T.; Arteaga, C. L. Mutations in the phosphatidylinositol 3-kinase pathway: role in tumor progression and therapeutic implications in breast cancer. *Breast Cancer Res.* **2011**, *13*, 224.

162. Abdul-Ghani, R.; Serra, V.; Györffy, B.; Jürchott, K.; Solf, a; Dietel, M.; Schäfer, R. The PI3K inhibitor LY294002 blocks drug export from resistant colon carcinoma cells overexpressing MRP1. *Oncogene* **2006**, *25*, 1743–1752.

163. Weigelt, B.; Warne, P. H.; Lambros, M. B.; Reis-Filho, J. S.; Downward, J. PI3K pathway dependencies in endometrioid endometrial cancer cell lines. *Clin. Cancer Res.* **2013**, *19*, 3533–3544.

164. Nian-Ci, L. W. and L. Effect of semi-synthesized sodium quercetin.pdf. *Acta Pharmacol. Sin.* **2002**, *23*, 339–342.

165. Norrby, K. Heparin and angiogenesis: a low-molecular-weight fraction inhibits and a high-molecular-weight fraction stimulates angiogenesis systemically. *Haemostasis* **1993**, *23 Suppl 1*, 141–149.

166. Khorana, A. A.; Sahni, A.; Altland, O. D.; Francis, C. W. Heparin Inhibition of Endothelial Cell Proliferation and Organization is Dependent on Molecular Weight. *Arterioscler. Thromb. Vasc. Biol.* **2003**, *23*, 2110–2115.

167. Lepri, A.; Benelli, U.; Bernardini, N.; Bianchi, F.; Lupetti, M.; Danesi, R.; Del Tacca, M.; Nardi, M. Effect of low molecular weight heparan sulphate on angiogenesis in the rat cornea after chemical cauterization. *J. Ocul. Pharmacol.* **1994**, *10*, 273–280.

168. Liu, D.; Shriver, Z.; Venkataraman, G.; El Shabrawi, Y.; Sasisekharan, R. Tumor cell surface heparan sulfate as cryptic promoters or inhibitors of tumor growth and metastasis. *Proc. Natl. Acad. Sci. U. S. A.* **2002**, *99*, 568–573.

169. Raman, K.; Karuturi, R.; Swarup, V. P.; Desai, U. R.; Kuberan, B. Discovery of novel sulfonated small molecules that inhibit vascular tube formation. *Bioorg. Med. Chem. Lett.* **2012**, *22*, 4467–4470.

170. J. Prud'homme, G. Cancer Stem Cells and Novel Targets for Antitumor Strategies. *Curr. Pharm. Des.* **2012**, *18*, 2838–2849.

171. Reya, T.; Morrison, S. J.; Clarke, M. F.; Weissman, I. L. Stem cells, cancer, and cancer stem cells. *Nature* **2001**, *414*, 105–111.

172. Patel, N. J.; Karuturi, R.; Al-Horani, R. A.; Baranwal, S.; Patel, J.; Desai, U. R.; Patel, B. B. Synthetic, non-saccharide, glycosaminoglycan mimetics selectively target colon cancer stem cells. *ACS Chem. Biol.* **2014**, *9*, 1826–1833.

173. Donnini, S.; Finetti, F.; Lusini, L.; Morbidelli, L.; Cheynier, V.; Barron, D.; Williamson, G.; Waltenberger, J.; Ziche, M. Divergent effects of quercetin conjugates on angiogenesis. *Br. J. Nutr.* **2006**, *95*, 1016–1023.

174. Lever, R.; Smailbegovic, A.; Page, C. Role of glycosaminoglycans in inflammation. *Inflammopharmacology* **2001**, *9*, 165–169.

175. Gozzo, A. J.; Nunes, V. A.; Carmona, A. K.; Nader, H. B.; Von Dietrich, C. P.; Silveira, V. L. F.; Shimamoto, K.; Ura, N.; Sampaio, M. U.; Sampaio, C. A. M.; Araújo, M. S. Glycosaminoglycans affect the action of human plasma kallikrein on kininogen hydrolysis and inflammation. *Int. Immunopharmacol.* **2002**, *2*, 1861–1865.

176. Holzmann, J.; N, B.; Zemann, A.; Schabus, R.; Marlovits, S.; Cowburn, R.; Huettinger, M. Assorted effects of TGF b and chondroitinsulfate on p38 and ERK1/2 activation levels in human articular chondrocytes stimulated with LPS. *OsteroArthritis Cartil.* **2006**, *14*, 519–525.

177. Yasuda, T. Hyaluronan inhibits cytokine production by lipopolysaccharide-stimulated U937 macrophages through down-regulation of NF-κB via ICAM-1. *Inflamm. Res.* **2007**, *56*, 246–253.

178. Nelson, B. R. M.; Cecconi, O.; Roberts, W. G.; Aruffo, A.; Linhardt, R. J.; Bevilacqua, M.

P. Heparin Oligosaccharides Bind L- and P-Selectin and Inhibit Acute Inflammation. *Blood* **1993**, *82*, 3253–3258.

179. Young, E. The anti-inflammatory effects of heparin and related compounds. **2008**, 743–752.

180. Pascual-teresa, S. De; Johnston, K. L.; Dupont, M. S.; Leary, K. A. O.; Needs, P. W.; Morgan, L. M.; Clifford, M. N.; Bao, Y. Quercetin metabolites downregulate cyclooxygenase-2 transcription in human lymphocytes ex vivo but not in vivo. *J. Nutr.* **2004**, No. 134, 552–557.

181. Leary, K. A. O.; Pascual-tereasa, S. De; Needs, P. W.; Bao, Y.; Brien, N. M. O.; Williamson, G. Effect of flavonoids and Vitamin E on cyclooxygenase-2 (COX-2) transcription. **2004**, *551*, 245–254.

182. Nonaggregating, C. O. F.; Mutants, N. R.; Appay, V.; Brown, A.; Cribbes, S.; Randle, E.; Czaplewski, L. G. Aggregation of RANTES Is Responsible for. **1999**, *274*, 27505–27512.

183. Severin, I. C.; Soares, A.; Hantson, J.; Teixeira, M.; Sachs, D.; Valognes, D.; Scheer, A.; Schwarz, M. K.; Wells, T. N. C.; Proudfoot, A. E. I.; Shaw, J. Glycosaminoglycan analogs as a novel anti-inflammatory strategy. *Front. Immunol.* **2012**, *3*, 1–12.

184. Bardoel, B. W.; Kenny, E. F.; Sollberger, G.; Zychlinsky, A. The balancing act of neutrophils. *Cell Host Microbe*. 2014, pp 526–536.

185. Smith, J. a. Neutrophils, host defense, and inflammation: a double-edged sword. *J. Leukoc. Biol.* **1994**, *56*, 672–686.

186. Kawabata, K.; Hagio, T.; Matsuoka, S. The role of neutrophil elastase in acute lung injury. *Eur J Pharmacol* **2002**, *451*, 1–10.

187. Sandhaus, R. A.; Turino, G. Neutrophil Elastase-Mediated Lung Disease. *COPD J. Chronic Obstr. Pulm. Dis.* **2013**, *10*, 60–63.

188. Carden, D.; Xiao, F.; Moak, C.; Willis, B. H.; Robinson-Jackson, S.; Alexander, S. Neutrophil elastase promotes lung microvascular injury and proteolysis of endothelial cadherins. *Am. J. Physiol.* **1998**, *275*, H385–H392.

189. Saluja, B.; Thakkar, J. N.; Li, H.; Desai, U. R.; Sakagami, M. Novel low molecular weight lignins as potential anti-emphysema agents: In vitro triple inhibitory activity against elastase, oxidation and inflammation. *Pulm. Pharmacol. Ther.* **2013**, *26*, 296–304.

190. Jinno, A.; Park, P. W. Role of glycosaminoglycans in infectious disease. In *Methods in Molecular Biology*; Series Ed.; Balagurunathan, K., Nakato, H., Desai, U. R., Eds.; Springer New York: New York, 2015; pp 567–585.

191. Aquino, R. S.; Park, P. W. Glycosaminoglycans and infection. *Front. Biosci. (Landmark Ed.)* **2016**, *21*, 1260–1277.

192. Tiwari, V.; O'Donnell, C.; Copeland, R. J.; Scarlett, T.; Liu, J.; Shukla, D. Soluble 3-O-sulfated heparan sulfate can trigger herpes simplex virus type 1 entry into resistant Chinese hamster ovary (CHO-K1) cells. *J. Gen. Virol.* **2007**, *88*, 1075–1079.

193. Choudhary, S.; Marquez, M.; Alencastro, F.; Spors, F.; Zhao, Y.; Tiwari, V. Herpes simplex virus type-1 (HSV-1) entry into human mesenchymal stem cells is heavily dependent on heparan sulfate. *J. Biomed. Biotechnol.* **2011**, *2011*, 264350.

194. Witvrouw, M.; De Clercq, E. Sulfated polysaccharides extracted from sea algae as potential antiviral drugs. *Gen. Pharmacol*. 1997, pp 497–511.

195. Kim, M.; Yim, J. H.; Kim, S. Y.; Kim, H. S.; Lee, W. G.; Kim, S. J.; Kang, P. S.; Lee, C. K. In vitro inhibition of influenza A virus infection by marine microalga-derived sulfated polysaccharide p-KG03. *Antiviral Res.* **2012**, *93*, 253–259.

196. Sun, H. H.; Gross, S. S.; Gunasekera, M.; Koehn, F. E. Weinbersterol disulfates A and B, antiviral steroid sulfates from the sponge petrosia weinbergi. *Tetrahedron* **1991**, *47*, 1185–1190.

197. Roccatagliata, A. J.; Maier, M. S.; Seldes, A. M.; Pujol, C. A.; Damonte, E. B. Antiviral sulfated steroids from the ophiuroid Ophioplocus januarii. *J. Nat. Prod.* **1996**, *59*, 887–889.

198. Fusetani, N.; Matsunaga, S.; Konosu, S. Bioactive marine metabolites II. Halistanol sulfate, an antimicrobial novel steroid sulfate from the marine sponge halichondria cf. moorei bergquist. *Tetrahedron Lett.* **1981**, *22*, 1985–1988.

199. Raghuraman, A.; Tiwari, V.; Thakkar, J. N.; Gunnarsson, G. T.; Shukla, D.; Hindle, M.; Desai, U. R. Structural characterization of a serendipitously discovered bioactive macromolecule, lignin sulfate. *Biomacromolecules* **2005**, *6*, 2822–2832.

200. Raghuraman, A.; Tiwari, V.; Zhao, Q.; Shukla, D.; Debnath, A. K.; Desai, U. R. Viral inhibition studies on sulfated lignin, a chemically modified biopolymer and a potential mimic heparan sulfate. *Biomacromolecules* **2007**, *8*, 1759–1763.

201. Versteeg, H. H.; Heemskerk, J. W. M.; Levi, M.; Reitsma, P. H. New fundamentals in hemostasis. *Physiol. Rev.* **2013**, *93*, 327–358.

202. Gale, A. J. Continuing education course #2: current understanding of hemostasis. *Toxicol. Pathol.* **2011**, *39*, 273–280.

203. Green, D. Coagulation cascade. *Hemodial. Int.* **2014**, *10*, S2–S4.

204. Gale, A. J. Current understanding of hemostasis. *Toxicol. Pathol.* **2011**, *39*, 273–280.

205. Schenone, M.; Furie, B. C.; Furie, B. The blood coagulation cascade. *Curr. Opin. Hematol.* **2004**, *11*, 272–277.

206. Chapin, J. C.; Hajjar, K. A. Fibrinolysis and the control of blood coagulation. *Blood Reviews*. 2015, pp 17–24.

207. Zimmerman, B.; Valentino, L. A. Hemophilia : In Review Hemophilia : In Review. **2016**, *34*,.

208. McDonald, V.; Scully, M. Disorders of haemostasis and thrombosis. *Medicine (Baltimore).* **2009**, *37*, 149–154.

209. Zimmerman, B.; Valentino, L. A. Hemophilia : In Review. *Pediatr. Rev.* **2016**, *34*, 289–295.

210. Lancellotti, S.; Basso, M.; Cristofaro, R. De. Congenital Prothrombin Deficiency: An Update. *Semin. Thromb. Hemost.* **2013**, *39*, 596–606.

211. Kruse-Jarres, R.; Singleton, T. C.; Leissinger, C. a. Identification and Basic Management of Bleeding Disorders in Adults. *J. Am. Board Fam. Med.* **2014**, *27*, 549–564.

212. Foy, P.; Moll, S. Thrombophilia : 2009 Update. *Curr. Treat. Options Cardiovasc. Med.* **2009**, *11*, 114–128.

213. Mackman, N. Triggers, targets and treatments for thrombosis. *Nature* **2008**, *451*, 914–918.

214. Makris, M. Thrombophilia: Grading the risk. *Blood* **2009**, *113*, 5038–5039.

215. Kujovich, J. L. Factor V Leiden thrombophilia. *Genet. Med.* **2011**, *13*, 1–16.

216. Rosendaal, F. R.; Reitsma, P. H. Genetics of venous thrombosis. *J. Thromb. Haemost.* **2009**, *7*, 301–304.

217. Rosendaal, F. R. Venous thrombosis: A multicausal disease. *Lancet* **1999**, *353*, 1167–1173.

218. Haddad, T. C.; Greeno, E. W. Chemotherapy-induced thrombosis. *Thromb. Res.* **2006**, *118*, 555–568.

219. F.R. Rosendaal, F.M. Helmerhorst, J. P. V. Female Hormones and Thrombosis. *Arterioscler. Thromb. Vasc. Biol.* **2002**, *22*, 201–210.

220. Melnikova, I. The anticoagulants market. *Nat. Rev. Drug Discov.* **2009**, *8*, 353–354.

221. Wadelius, M.; Pirmohamed, M. Pharmacogenetics of warfarin: current status and future challenges. *Pharmacogenomics J.* **2007**, *7*, 99–111.

222. Bell, R. G.; Sadowski, J. a; Matschiner, J. T. Mechanism of action of warfarin. Warfarin and metabolism of vitamin K 1 . *Biochemistry* **1972**, *11*, 1959–1961.

223. Wells, P. S.; Holbrook, A. M.; Crowther, N. R.; Hirsh, J. Interactions of warfarain with drugs and food. *Am. Coll. Pysicians* **1994**, *121*, 676–682.

224. Desai, U. R. New Antithrombin-Based Anticoagulants. *Med. Res. Rev.* **2004**, *24*, 151–181.

225. Bick, R. L.; Frenkel, E. P. Clinical aspects of heparin-induced thrombocytopenia and thrombosis and other side effects of heparin therapy. *Clin. Appl. Thromb.* **1999**, *5*, S7–S15.

226. Katherine Harter, MD Michael Levine, MD Sean O. Henderson, M. Anticoagulation Drug Therapy: A Review. *West. J. Emerg.* **2015**, *16*, 11–17.

227. Earl W. Davie, Ph.D., and John D. Kulman, P. D. An Overview of the Structure and Function of Thrombin. *Semin. Thromb. Hemost.* **2006**, *32*, 3–15.

228. Fenton, J. W., Ofosu, F. A., Moon, D. G., and Maraganore, J. M. Thrombin structure and

function-why thrombin is the primary target for antithrombotics.pdf. *Blood Coagul. Fibrinolysis* **1991**, *2*, 69–75.

229. Bode, W. Structure and interaction modes of thrombin. *Blood Cells, Mol. Dis.* **2006**, *36*, 122–130.

230. Kanaide, H.; Shainoff, J. R. Cross-linking of fibrinogen and fibrin by fibrin-stablizing factor (factor XIIIa). *J. Lab. Clin. Med.* **1975**, *85*, 574–597.

231. Coughlin, S. R. Protease-activated receptors in hemostasis, thrombosis and vascular biology. *J Thromb Haemost* **2005**, *3*, 1800–1814.

232. Esmon, C. T. The roles of protein C and thrombomodulin in the regulation of blood coagulation. *J. Biol. Chem.* **1989**, *264*, 4743–4746.

233. Becker, R. C.; Spencer, F. A. Thrombin: Structure, biochemistry, measurement, and status in clinical medicine. *J. Thromb. Thrombolysis* **1998**, *5*, 215–229.

234. Bode, W.; Turk, D.; Karshikov, A. The refined 1.9-A X-ray crystal structure of D-Phe-Pro-Arg chloromethylketone-inhibited human alpha-thrombin: structure analysis, overall structure, electrostatic properties, detailed active-site geometry, and structure-function relationships. *Protein Sci.* **1992**, *1*, 426–471.

235. Huntington, J. A. Natural inhibitors of thrombin. *Thromb. Haemost.* **2014**, *111*, 583–589.

236. Mann, K. G.; Brummel, K.; Butenas, S. What is all that thrombin for? *J. Thromb. Haemost.* **2003**, *1*, 1504–1514.

237. Weitz, J. I. Factor Xa or thrombin: Is FXa a better target? *J. Thromb. Haemost.* **2007**, *5*, 60–64.

238. Weitz, J. I.; Crowther, M. Direct thrombin inhibitors. *Thromb. Res.* **2002**, *106*,.

239. Marcello, D. N.; Saskia, M.; Büller, H. R. Direct Thrombin Inhibitors. *N. Engl. J. Med.* **2005**, *353*, 1028–1040.

240. Mega, J. L.; Simon, T. Pharmacology of antithrombotic drugs: An assessment of oral antiplatelet and anticoagulant treatments. *Lancet* **2015**, *386*, 281–291.

241. Ruff, C. T.; Giugliano, R. P.; Braunwald, E.; Hoffman, E. B.; Deenadayalu, N.; Ezekowitz, M. D.; Camm, a J.; Weitz, J. I.; Lewis, B. S.; Parkhomenko, A.; Yamashita, T.; Antman, E. M. Comparison of the efficacy and safety of new oral anticoagulants with warfarin in patients with atrial fibrillation: a meta-analysis of randomised trials. *Lancet* **2014**, *383*, 955–962.

242. Henry, B. L.; Thakkar, J. N.; Liang, A.; Desai, U. R. Sulfated, low molecular weight lignins inhibit a select group of heparin-binding serine proteases. *Biochem. Biophys. Res. Commun.* **2012**, *417*, 382–386.

243. Di Cera, E.; Page, M. J.; Bah, A.; Bush-Pelc, L. A.; Garvey, L. C. Thrombin allostery. *Phys. Chem. Chem. Phys.* **2007**, *9*, 1291–1306.

244. Lechtenberg, B. C.; Freund, S. M. V; Huntington, J. A. An ensemble view of thrombin

allostery. In *Biological Chemistry*; 2012; Vol. 393, pp 889–898.

245. Huntington, J. A. Molecular recognition mechanisms of thrombin. *J. Thromb. Haemost.* **2005**, *3*, 1861–1872.

246. Bode, W. The structure of thrombin: A Janus-headed proteinase. *Semin. Thromb. Hemost.* **2006**, *32*, 16–31.

247. He, X.; Ye, J.; Esmon, C. T.; Rezaie, A. R. Influence of arginines 93, 97, and 101 of thrombin to its functional specificity. *Biochemistry* **1997**, *36*, 8969–8976.

248. Hayward, C. P. M.; Moffat, K. a; Liu, Y. Laboratory investigations for bleeding disorders. *Semin. Thromb. Hemost.* **2012**, *38*, 742–752.

249. Collen, D.; Lijnen, H. R. Basic and clinical aspects of fibrinolysis and thrombolysis. *Blood* **1991**, *78*, 3114–3124.

250. Rijken, D. C.; Lijnen, H. R. New insights into the molecular mechanisms of the fibrinolytic system. *J. Thromb. Haemost.* **2009**, *7*, 4–13.

251. Rau, J. C.; Beaulieu, L. M.; Huntington, J. A.; Church, F. C. Serpins in thrombosis, hemostasis and fibrinolysis. *J. Thromb. Haemost.* **2007**, *5*, 102–115.

252. Novokhatny, V. Structure and activity of plasmin and other direct thrombolytic agents. *Thromb. Res.* **2008**, *122*, 1–6.

253. Syrovets, T.; Lunov, O.; Simmet, T. Plasmin as a proinflammatory cell activator. *J. Leukoc. Biol.* **2012**, *92*, 509–519.

254. Cesarman-Maus, G.; Hajjar, K. A. Molecular mechanisms of fibrinolysis. *Br. J. Haematol.* **2005**, *129*, 307–321.

255. Wang, X. Crystal Structure of the Catalytic Domain of Human Plasmin Complexed with Streptokinase. *Science.* **1998**, *281*, 1662–1665.

256. Perona, J. J.; Craik, C. S. Structural basis of substrate specificity in the serine proteases. *Protein Sci.* **1995**, *4*, 337–360.

257. Parry, M. a; Fernandez-Catalan, C.; Bergner, a; Huber, R.; Hopfner, K. P.; Schlott, B.; Gührs, K. H.; Bode, W. The ternary microplasmin-staphylokinase-microplasmin complex is a proteinase-cofactor-substrate complex in action. *Nat. Struct. Biol.* **1998**, *5*, 917–923.

258. Hervio, L. S.; Coombs, G. S.; Bergstrom, R. C.; Trivedi, K.; Corey, D. R.; Madison, E. L. Negative selectivity and the evolution of protease cascades: The specificity of plasmin for peptide and protein substrates. *Chem. Biol.* **2000**, *7*, 443–453.

259. Swedberg, J. E.; Harris, J. M. Natural and engineered plasmin inhibitors: Applications and design strategies. *ChemBioChem* **2012**, *13*, 336–348.

260. Deryugina, E. I.; Quigley, J. P. Cell surface remodeling by plasmin: A new function for an old enzyme. *J. Biomed. Biotechnol.* **2012**, *2012*, 564259.

261. Munakata, S.; Tashiro, Y.; Nishida, C.; Sato, A.; Komiyama, H.; Shimazu, H.; Dhahri, D.; Salama, Y.; Eiamboonsert, S.; Takeda, K.; Yagita, H.; Tsuda, Y.; Okada, Y.; Nakauchi,

H.; Sakamoto, K.; Heissig, B.; Hattori, K. Inhibition of plasmin protects against colitis in mice by suppressing matrix metalloproteinase 9-mediated cytokine release from myeloid cells. *Gastroenterology* **2015**, *148*, 565–578.

262. Yang, C.-D.; Hwang, K.-K.; Yan, W.; Gallagher, K.; FitzGerald, J.; Grossman, J. M.; Hahn, B. H.; Chen, P. P. Identification of anti-plasmin antibodies in the antiphospholipid syndrome that inhibit degradation of fibrin. *J. Immunol.* **2004**, *172*, 5765–5773.

263. Royston, D. Blood-sparing drugs: aprotinin, tranexamic acid, and epsilon-aminocaproic acid. *Int. Anesth. Clinics*. 1995, pp 155–179.

264. Dhir, A. Antifibrinolytics in cardiac surgery. *Ann. Card. Anaesth.* **2013**, *16*, 117–125.

265. Lecker, I.; Wang, D.; Romaschin, A. D.; Peterson, M.; Mazer, C. D.; Orser, B. A. Tranexamic acid concentrations associated with human seizures inhibit glycine receptors. *J. Clin. Invest.* **2012**, *122*, 4654–4666.

266. Mangano, D. T.; Tudor, I. C.; Dietzel, C. The risk associated with aprotinin in cardiac surgery. *N Engl J Med* **2006**, *354*, 353–365.

267. Hidaka, K.; Gohda, K.; Teno, N.; Wanaka, K.; Tsuda, Y. Active site-directed plasmin inhibitors: Extension on the P2 residue. *Bioorganic Med. Chem.* **2016**, *24*, 545–553.

268. Cheng, L.; Pettersen, D.; Ohlsson, B.; Schell, P.; Karle, M.; Evertsson, E.; Pahl??n, S.; Jonforsen, M.; Plowright, A. T.; Bostr??m, J.; Fex, T.; Thelin, A.; Hilgendorf, C.; Xue, Y.; Wahlund, G.; Lindberg, W.; Larsson, L. O.; Gustafsson, D. Discovery of the fibrinolysis inhibitor AZD6564, acting via interference of a protein-protein interaction. *ACS Med. Chem. Lett.* **2014**, *5*, 538–543.

269. Teno, N.; Gohda, K.; Wanaka, K.; Tsuda, Y.; Akagawa, M.; Akiduki, E.; Araki, M.; Masuda, A.; Otsubo, T.; Yamashita, Y. Novel type of plasmin inhibitors: Providing insight into P4 moiety and alternative scaffold to pyrrolopyrimidine. *Bioorganic Med. Chem.* **2015**, *23*, 3696–3704.

270. Teno, N.; Gohda, K.; Yamashita, Y.; Otsubo, T.; Yamaguchi, M.; Wanaka, K.; Tsuda, Y. Plasmin inhibitors with hydrophobic amino acid-based linker between hydantoin moiety and benzimidazole scaffold enhance inhibitory activity. *Bioorganic Med. Chem. Lett.* **2016**, *26*, 2259–2261.

271. Teno, N.; Gohda, K.; Wanaka, K.; Tsuda, Y.; Sueda, T.; Yamashita, Y.; Otsubo, T. Pyrrolopyrimidine-inhibitors with hydantoin moiety as spacer can explore P4/S4 interaction on plasmin. *Bioorganic Med. Chem.* **2014**, *22*, 2339–2352.

272. Saupe, S. M.; Leubner, S.; Betz, M.; Klebe, G.; Steinmetzer, T. Development of new cyclic plasmin inhibitors with excellent potency and selectivity. *J. Med. Chem.* **2013**, *56*, 820–831.

273. Saupe, S. M.; Steinmetzer, T. A new strategy for the development of highly potent and selective plasmin inhibitors. *J. Med. Chem.* **2012**, *55*, 1171–1180.

274. Hinkes, S.; Wuttke, A.; Saupe, S. M.; Ivanova, T.; Wagner, S.; Kn??rlein, A.; Heine, A.; Klebe, G.; Steinmetzer, T. Optimization of Cyclic Plasmin Inhibitors: From Benzamidines

to Benzylamines. *J. Med. Chem.* **2016**, *59*, 6370–6386.

275. Al-Horani, R. A.; Karuturi, R.; White, D. T.; Desai, U. R. Plasmin regulation through allosteric, sulfated, small molecules. *Molecules* **2015**, *20*, 608–624.

276. Van Ryn-McKenna; Cai, L.; Ofosu, F. A.; Hirsh, J.; Buchanan, M. R. Neutralization of enoxaparine-induced bleeding by protamine sulfate. *Thromb. Haemost.* **1990**, *63*, 271–274.

277. Bøtkjær, K. A.; Byszuk, A. A.; Andersen, L. M.; Christensen, A.; Andreasen, P. A.; Blouse, G. E. Nonproteolytic induction of catalytic activity into the single-chain form of urokinase-type plasminogen activator by dipeptides. *Biochemistry* **2009**, *48*, 9606–9617.

278. Segal, A. W. How neutrophils kill microbes. *Annu. Rev. Immunol.* **2005**, *23*, 197–223.

279. Pham, C. T. N. Neutrophil serine proteases: specific regulators of inflammation. *Nat. Rev. Immunol.* **2006**, *6*, 541–550.

280. Sinha, S.; Watorek, W.; Karr, S.; Giles, J.; Bode, W.; Travis, J. Primary structure of human neutrophil elastase. *Proc. Natl. Acad. Sci. U. S. A.* **1987**, *84*, 2228–2232.

281. Bode, W.; Wei, A. Z.; Huber, R.; Meyer, E.; Travis, J.; Neumann, S. X-ray crystal structure of the complex of human leukocyte elastase (PMN elastase) and the third domain of the turkey ovomucoid inhibitor. *EMBO J.* **1986**, *5*, 2453–2458.

282. Korkmaz, B.; Horwitz, M. S.; Jenne, D. E.; Gauthier, F. Neutrophil elastase, proteinase 3, and cathepsin G as therapeutic targets in human diseases. *Pharmacol. Rev.* **2010**, *62*, 726–759.

283. Belaaouaj, A.; Kim, K. S.; Shapiro, S. D. Degradation of Outer Membrane Protein A in Escherichia coli Killing by Neutrophil Elastase. *Science* **2000**, *289*, 1185–1187.

284. Weinrauch, Y.; Drujan, D.; Shapiro, S. D.; Weiss, J.; Zychlinsky, A. Neutrophil elastase targets virulence factors of enterobacteria. *Nature* **2002**, *417*, 91–94.

285. Johansson, A.; Claesson, R.; Hänström, L.; Sandström, G.; Kalfas, S. Polymorphonuclear leukocyte degranulation induced by leukotoxin from Actinobacillus actinomycetemcomitans. *J. Periodontal Res.* **2000**, *35*, 85–92.

286. Lopez-Boado, Y. S.; Espinola, M.; Bahr, S.; Belaaouaj, A. Neutrophil Serine Proteinases Cleave Bacterial Flagellin, Abrogating Its Host Response-Inducing Activity. *J. Immunol.* **2003**, *172*, 509–515.

287. Golden, J. W.; Schiff, L. A. Neutrophil elastase, an acid-independent serine protease, facilitates reovirus uncoating and infection in U937 promonocyte cells. *Virol. J.* **2005**, *2*, 48.

288. Ohbayashi, H. Neutrophil elastase inhibitors as treatment for COPD. *Expert Opin. Investig. Drugs* **2002**, *11*, 965–980.

289. Pham, C. T. N. Neutrophil serine proteases fine-tune the inflammatory response. *Int. J. Biochem. Cell Biol.* **2008**, *40*, 1317–1333.

290. Ginzberg, H. H.; Shannon, P. T.; Suzuki, T.; Hong, O.; Vachon, E.; Moraes, T.; Abreu, M. T. H.; Cherepanov, V.; Wang, X.; Chow, C.-W.; Downey, G. P. Leukocyte elastase induces epithelial apoptosis: role of mitochondial permeability changes and Akt. *Am. J. Physiol. Gastrointest. Liver Physiol.* **2004**, *287*, G286–G298.

291. Suzuki, T.; Moraes, T. J.; Vachon, E.; Ginzberg, H. H.; Huang, T. T.; Matthay, M. A.; Hollenberg, M. D.; Marshall, J.; McCulloch, C. A. G.; Abreu, M. T. H.; Chow, C. W.; Downey, G. P. Proteinase-activated receptor-1 mediates elastase-induced apoptosis of human lung epithelial cells. *Am. J. Respir. Cell Mol. Biol.* **2005**, *33*, 231–247.

292. Yang, J. J.; Kettritz, R.; Falk, R. J.; Jennette, J. C.; Gaido, M. L. Apoptosis of endothelial cells induced by the neutrophil serine proteases proteinase 3 and elastase. *Am. J. Pathol.* **1996**, *149*, 1617–1626.

293. Henriksen, P. A.; Sallenave, J. M. Human neutrophil elastase: Mediator and therapeutic target in atherosclerosis. *Int. J. Biochem. Cell Biol.* **2008**, *40*, 1095–1100.

294. Stockley, R. A. Neutrophils and protease/antiprotease imbalance. *Am. J. Respir. Crit. Care Med.* **1999**, *160*, S49–S52.

295. William C. Groutas, Dengfeng Dou, and K. R. A. Neutrophil Elastase Inhibitors. **2012**, *21*, 339–354.

296. Houghton, A. M.; Rzymkiewicz, D. M.; Ji, H.; Gregory, A. D.; Egea, E. E.; Metz, H. E.; Stolz, D. B.; Land, S. R.; Marconcini, L. A.; Kliment, C. R.; Jenkins, K. M.; Beaulieu, K. A.; Mouded, M.; Frank, S. J.; Wong, K. K.; Shapiro, S. D. Neutrophil elastase-mediated degradation of IRS-1 accelerates lung tumor growth. *Nat. Med.* **2010**, *16*, 219–223.

297. Wipke, B. T.; Allen, P. M. Essential Role of Neutrophils in the Initiation and Progression of a Murine Model of Rheumatoid Arthritis. *J. Immunol.* **2001**, *167*, 1601–1608.

298. Barrett, A. J. The possible role of neutrophil proteinases in damage to articular cartilage. *Agents Actions* **1994**, *43*, 194–201.

299. Adeyemi, E. O.; Hull, R. G.; Chadwick, V. S.; H.J.F., H. Circulating human leucocyte elastase in rheumatoid arthritis. **1986**, *6*, 57–60.

300. Powers, J. C. Synthetic Elastase Inhibitors: Prospects for Use in the Treatment of Emphysema 13. *Am. Rev. Respir. Dis.* **1983**, *127*, S54-658.

301. Eriksson, S. The potential role of elastase inhibitors in emphysema treatment. *Eur. Respir. J.* **1991**, *4*, 1041–1043.

302. Kuraki, T.; Ishibashi, M.; Takayama, M.; Shiraishi, M.; Yoshida, M. A novel oral neutrophil elastase inhibitor (ONO-6818) inhibits human neutrophil elastase-induced emphysema in rats. *Am. J. Respir. Crit. Care Med.* **2002**, *166*, 496–500.

303. Nishina, K.; Mikawa, K.; Takao, Y.; Maekawa, N.; Shiga, M.; Obara, H. ONO-5046, an elastase inhibitor, attenuates endotoxin-induced acute lung injury in rabbits. *Anesth Analg* **1997**, *84*, 1097–1103.

304. Zeiher, B. G.; Matsuoka, S.; Kawabata, K.; Repine, J. E. Neutrophil elastase and acute

lung injury: prospects for sivelestat and other neutrophil elastase inhibitors as therapeutics. *Crit. Care Med.* **2002**, *30*, S281-7.

305. Cowan, K. N.; Heilbut, A.; Humpl, T.; Lam, C.; Ito, S.; Rabinovitch, M. Complete reversal of fatal pulmonary hypertension in rats by a serine elastase inhibitor. *Nat. Med.* **2000**, *6*, 698–702.

306. Kakimoto, K.; Matsukawa, A.; Yoshinaga, M.; Nakamura, H. Suppressive effect of a neutrophil elastase inhibitor on the development of collagen-induced arthritis. *Cell. Immunol.* **1995**, *165*, 26–32.

307. Von Nussbaum, F.; Li, V. M. J. Neutrophil elastase inhibitors for the treatment of (cardio)pulmonary diseases: Into clinical testing with pre-adaptive pharmacophores. *Bioorganic Med. Chem. Lett.* **2015**, *25*, 4370–4381.

308. Bartolucci, C.; Cellai, L.; Iannelli, M. A.; Lamba, D.; Liverani, L.; Mascellani, G.; Perola, E. Inhibition of human leukocyte elastase by chemically and naturally oversulfated galactosaminoglycans. *Carbohydr. Res.* **1995**, *276*, 401–408.

309. Volpi, N. Inhibition of human leukocyte elastase activity by heparins: influence of charge density. *Biochim. Biophys. Acta - Gen. Subj.* **1996**, *1290*, 299.

310. Fryer, a; Huang, Y. C.; Rao, G.; Jacoby, D.; Mancilla, E.; Whorton, R.; Piantadosi, C. a; Kennedy, T.; Hoidal, J. Selective O-desulfation produces nonanticoagulant heparin that retains pharmacological activity in the lung. *J. Pharmacol. Exp. Ther.* **1997**, *282*, 208–219.

311. Zheng, S.; Kummarapurugu, A. B.; Afosah, D. K.; Sankaranarayanan, N. V.; Boothello, R. S.; Desai, U. R.; Kennedy, T.; Voynow, J. A. 2-O, 3-O Desulfated Heparin Blocks HMGB1 Release by Inhibition of p300 Acetyltransferase Activity. *Am. J. Respir. Cell Mol. Biol.* **2016**.

312. Holme, K. R.; Liang, W.; Shaklee, P. N. Method for controlling O-desulfation of heparin and compositions produced thereby. US5696100 A, December 9, 1997..

313. Pettersen, E. F.; Goddard, T. D.; Huang, C. C.; Couch, G. S.; Greenblatt, D. M.; Meng, E. C.; Ferrin, T. E. UCSF Chimera—A visualization system for exploratory research and analysis. *J. Comput. Chem.* **2004**, *25*, 1605–1612.

314. Navia, M. A.; McKeever, B. M.; Springer, J. P.; Lin, T. Y.; Williams, H. R.; Fluder, E. M.; Dorn, C. P.; Hoogsteen, K. Structure of human neutrophil elastase in complex with a peptide chloromethyl ketone inhibitor at 1.84-A resolution. *Proc. Natl. Acad. Sci. U. S. A.* **1989**, *86*, 7–11.

315. Jones, G.; Willett, P.; Glen, R. C.; Leach, A. R.; Taylor, R. Development and validation of a genetic algorithm for flexible docking. *J. Mol. Biol.* **1997**, *267*, 727–748.

APPENDIX

*1) UV/Vis spectra of **2c** in assay buffer*

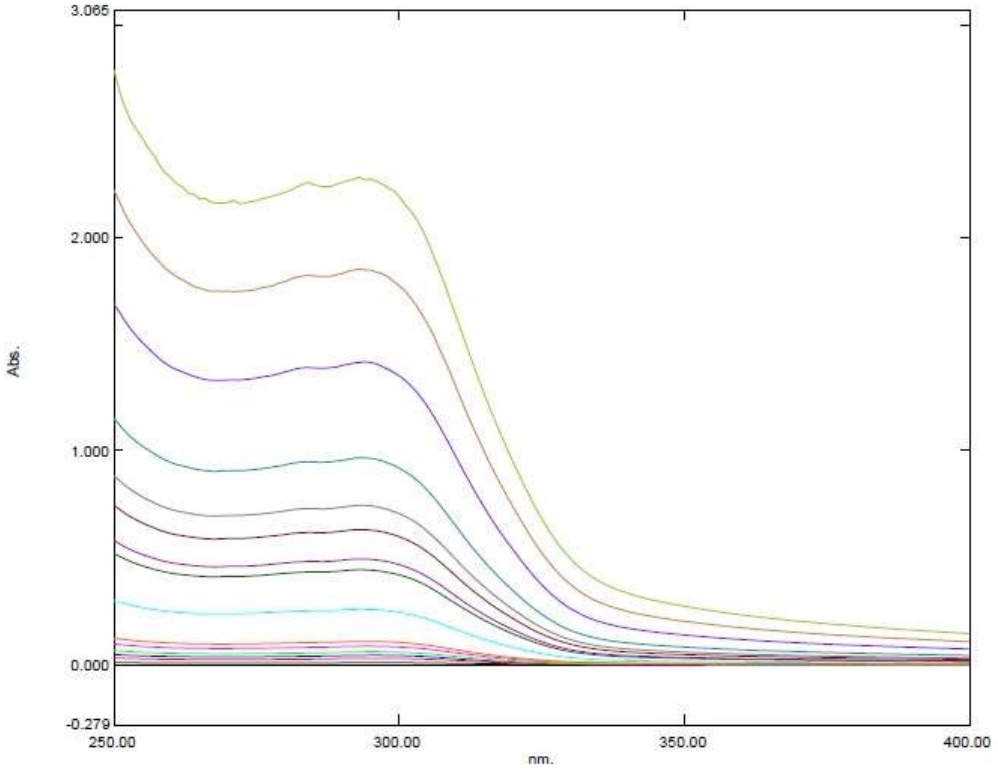

UV profile of 2c (up to 200 µM)

λ_{MAX} = 294.00 nM

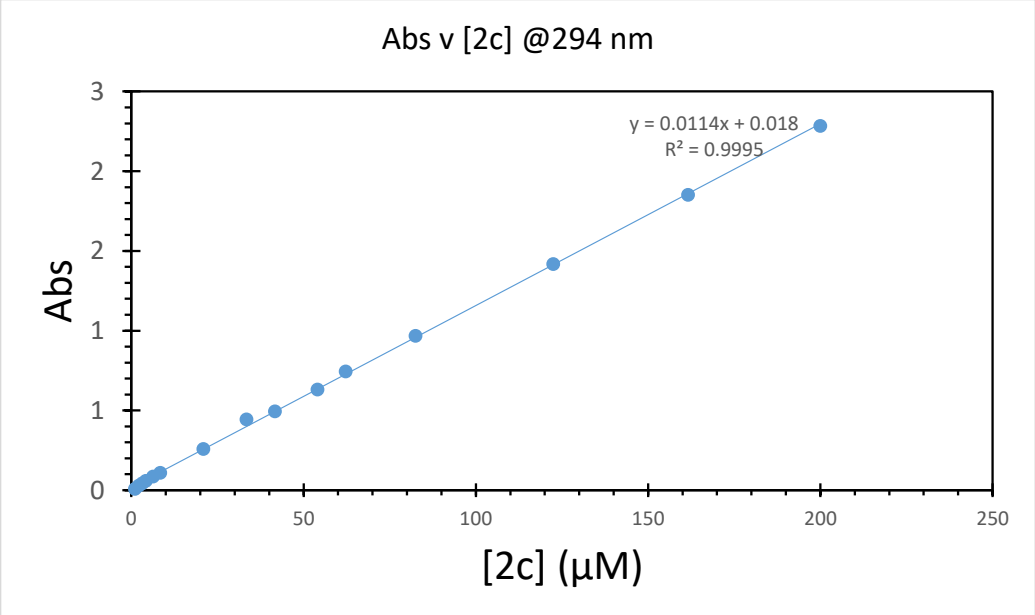

2) *UV/Vis spectra of **2i** in assay buffer*

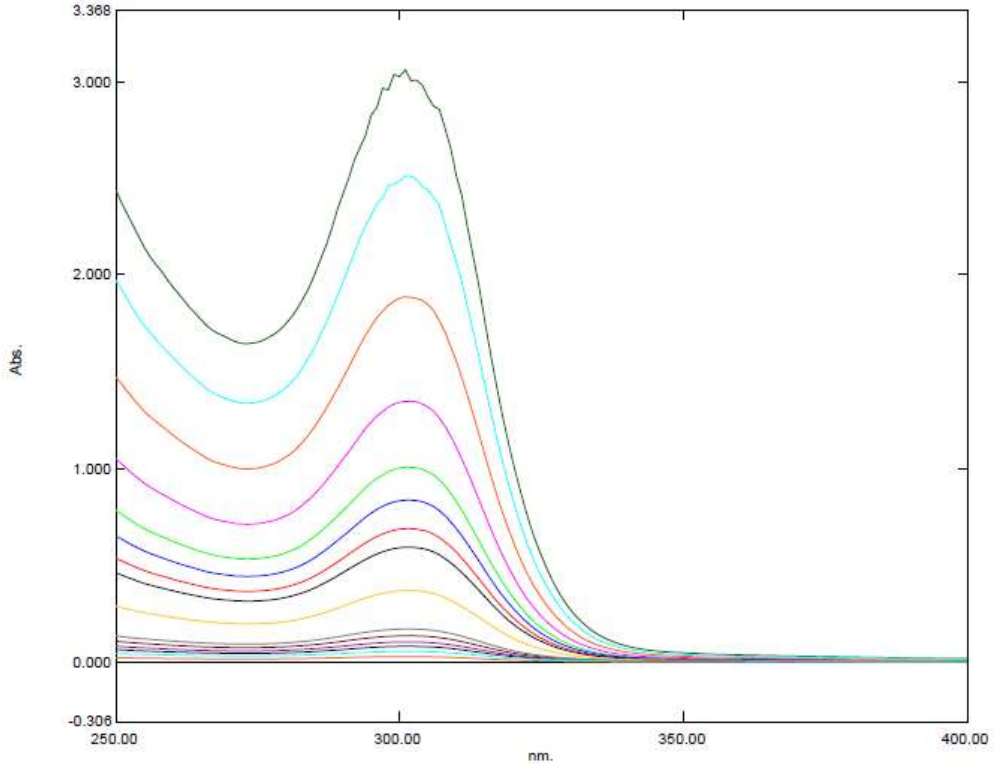

UV profile of 2i (up to 200 µM)

λ_{MAX} = 302.00 nM

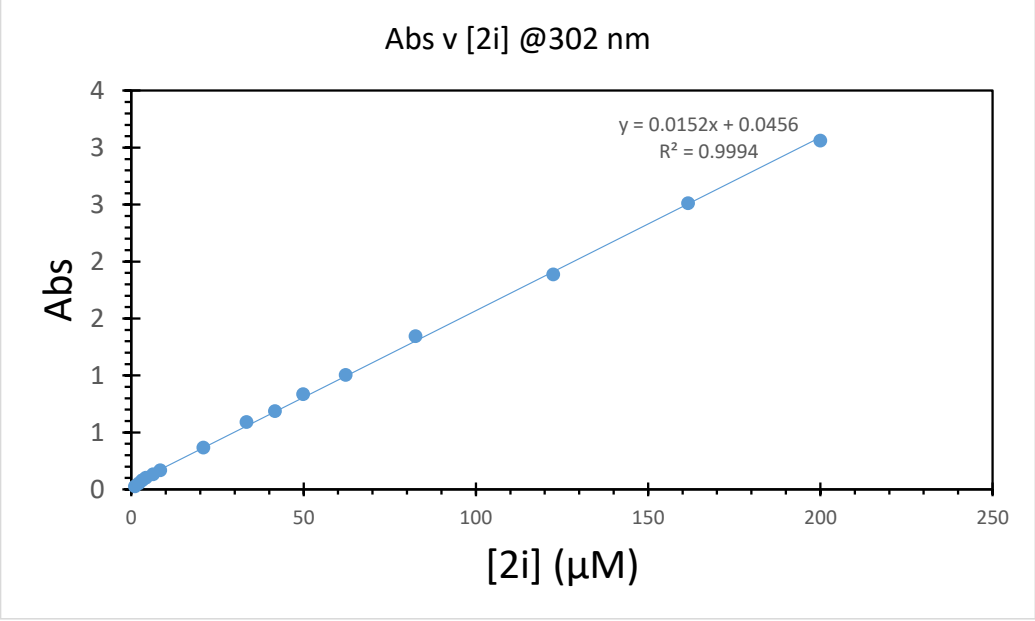

3) Spectral Profiles for SBDs and SBMs

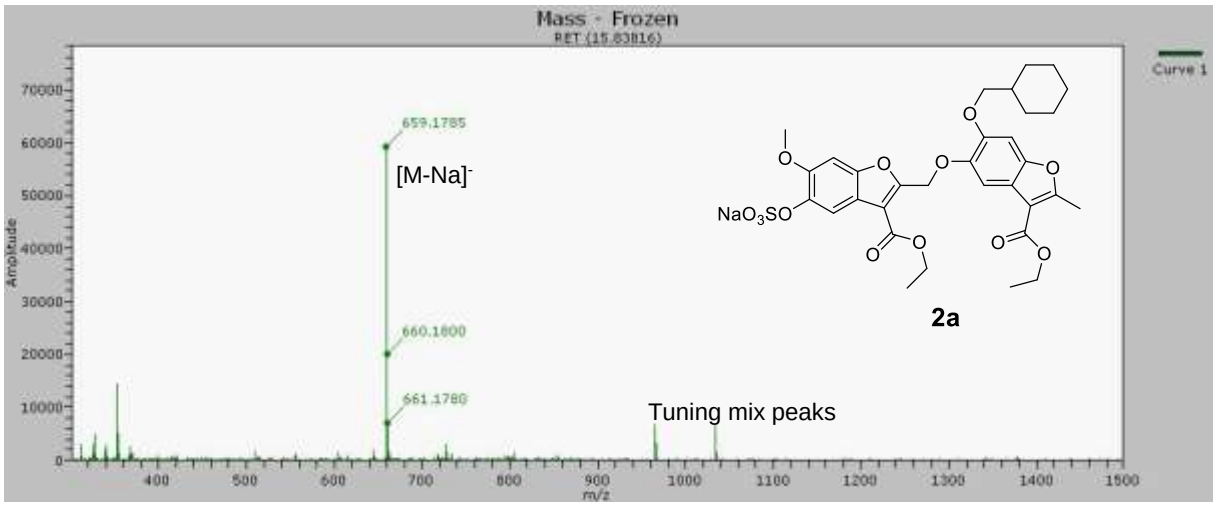

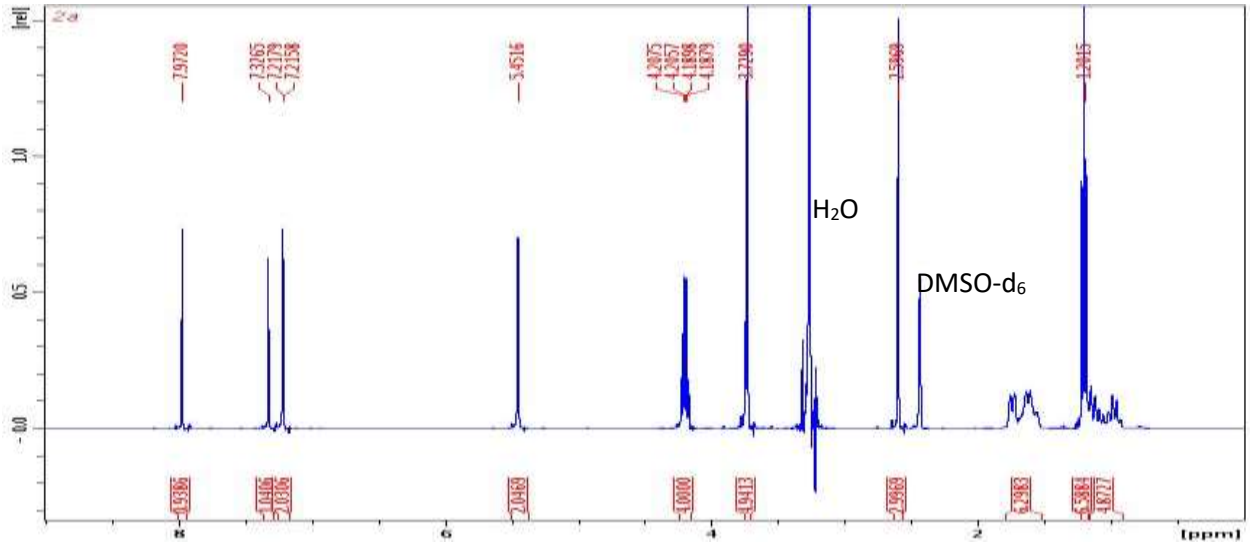

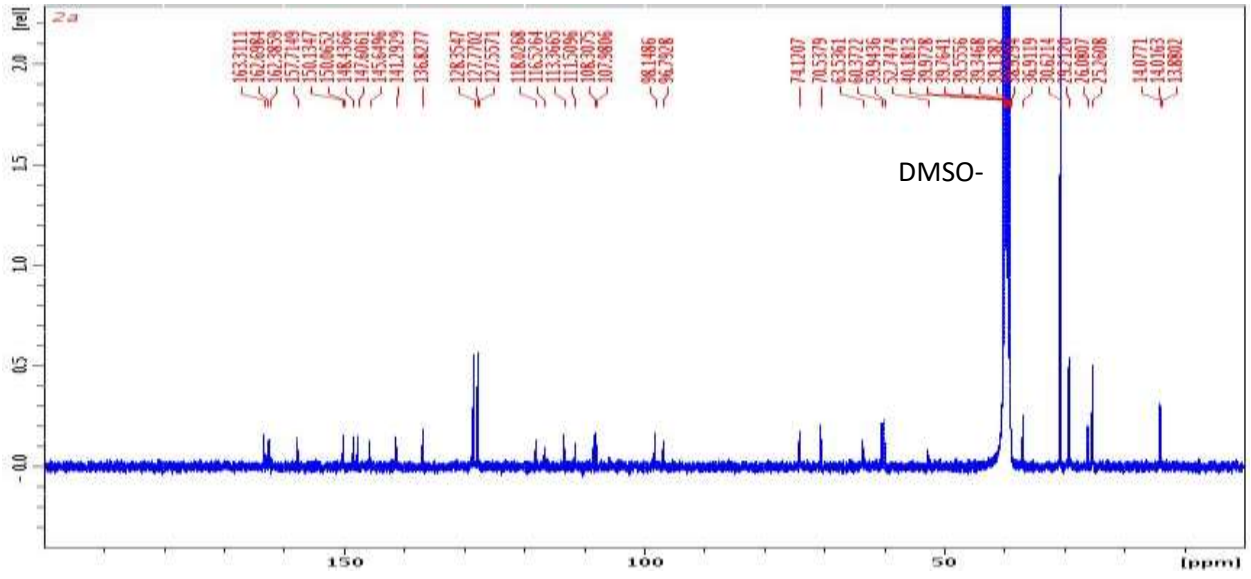

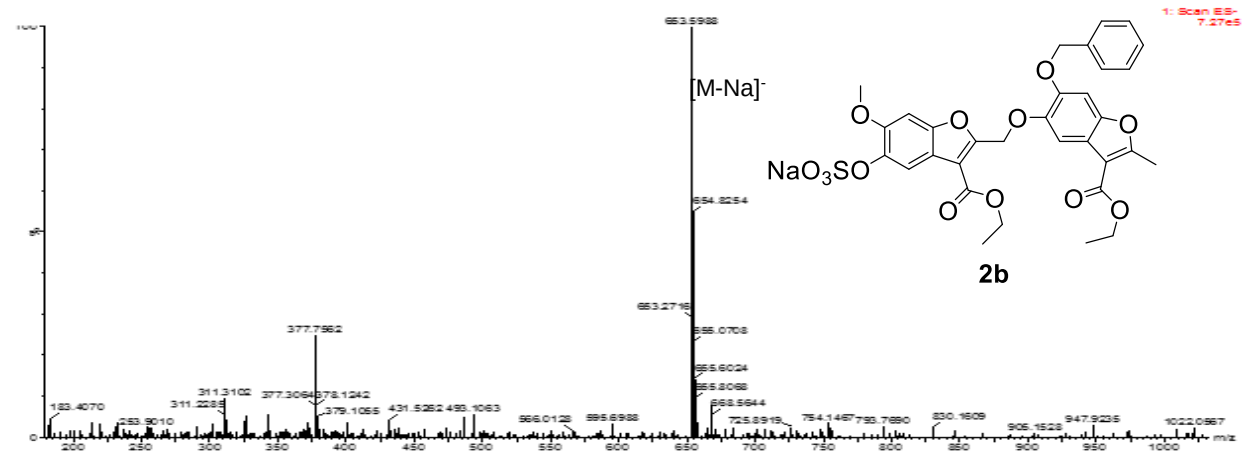
[M-Na]-
NaO3SO
2b

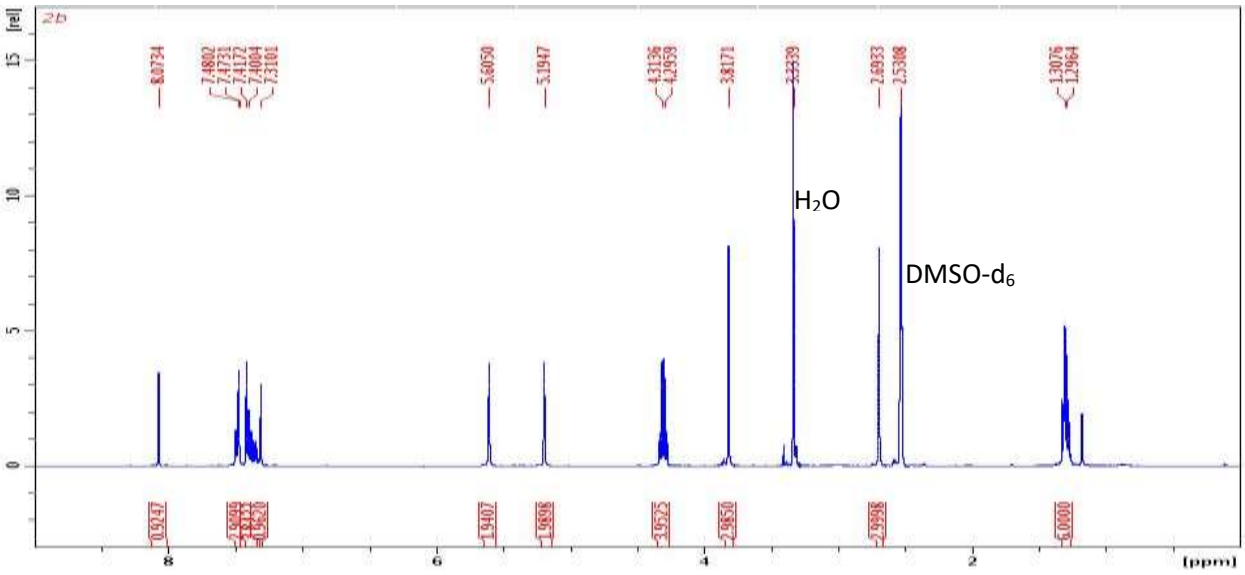
2b
H2O
DMSO-d6
[ppm]

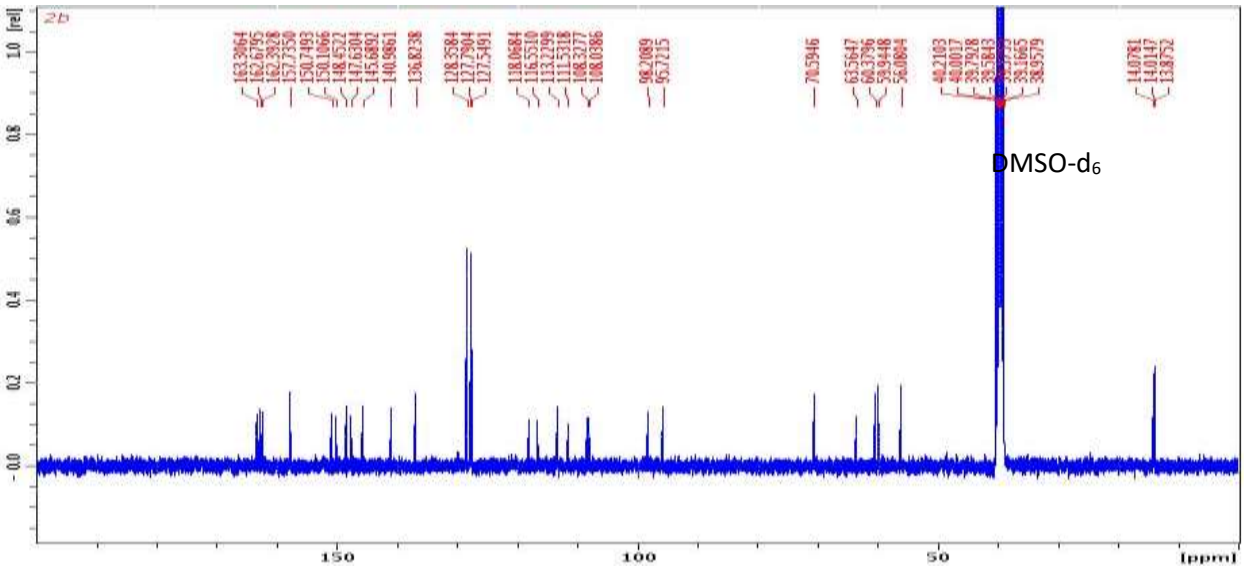
2b
DMSO-d6
[ppm]

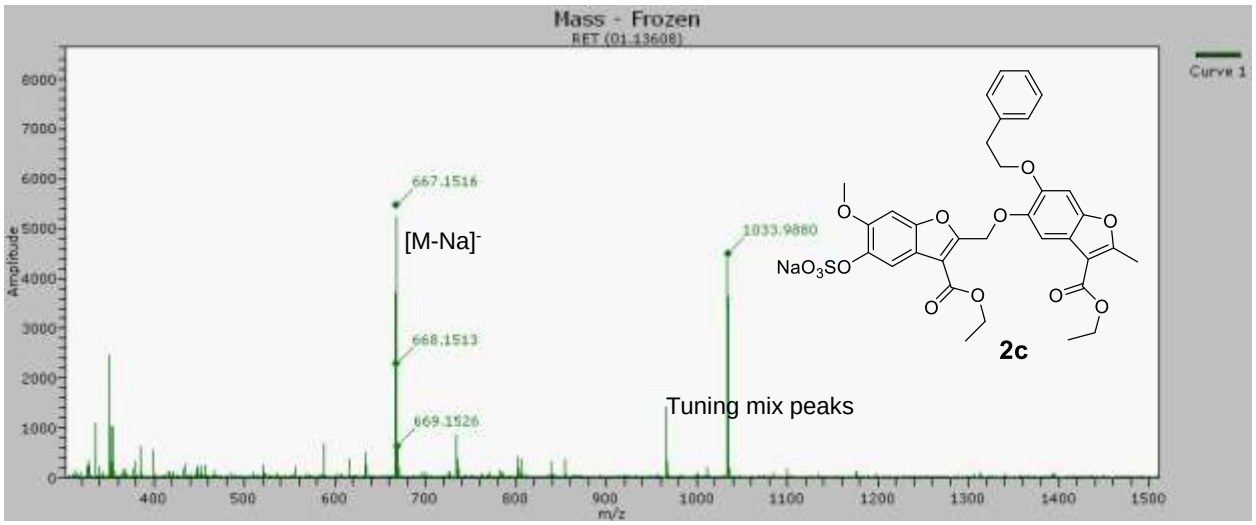
Mass - Frozen
RET (01.13608)
Curve 1
667.1516
[M-Na]-
668.1513
669.1526
1033.9880
Tuning mix peaks
NaO3SO
2c
Amplitude
m/z

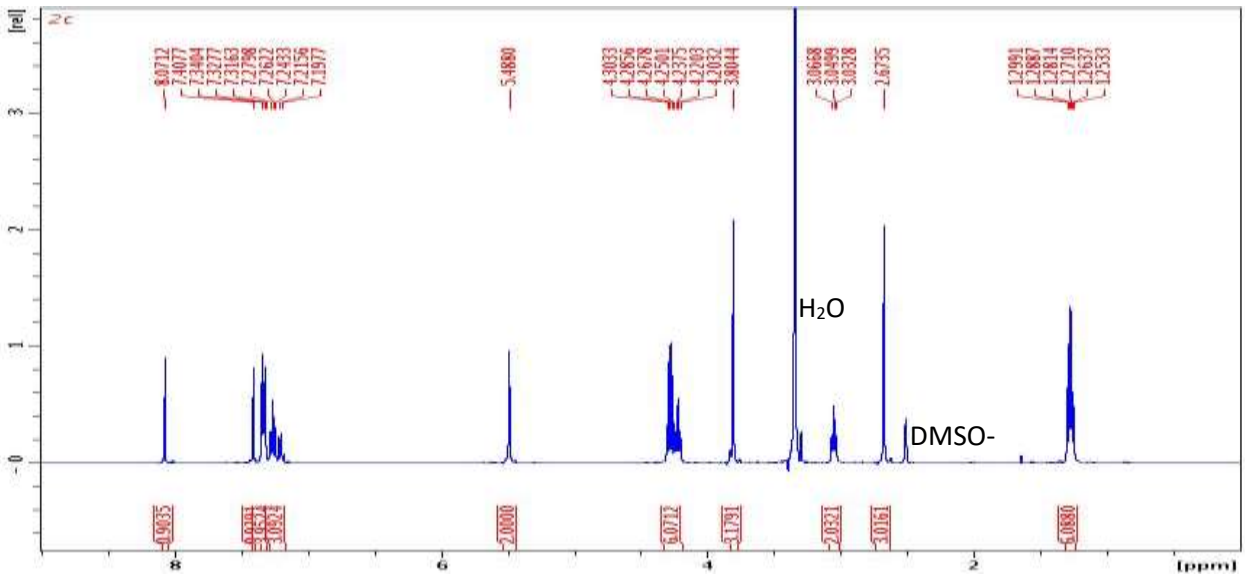
2c
H2O
DMSO-
[ppm]

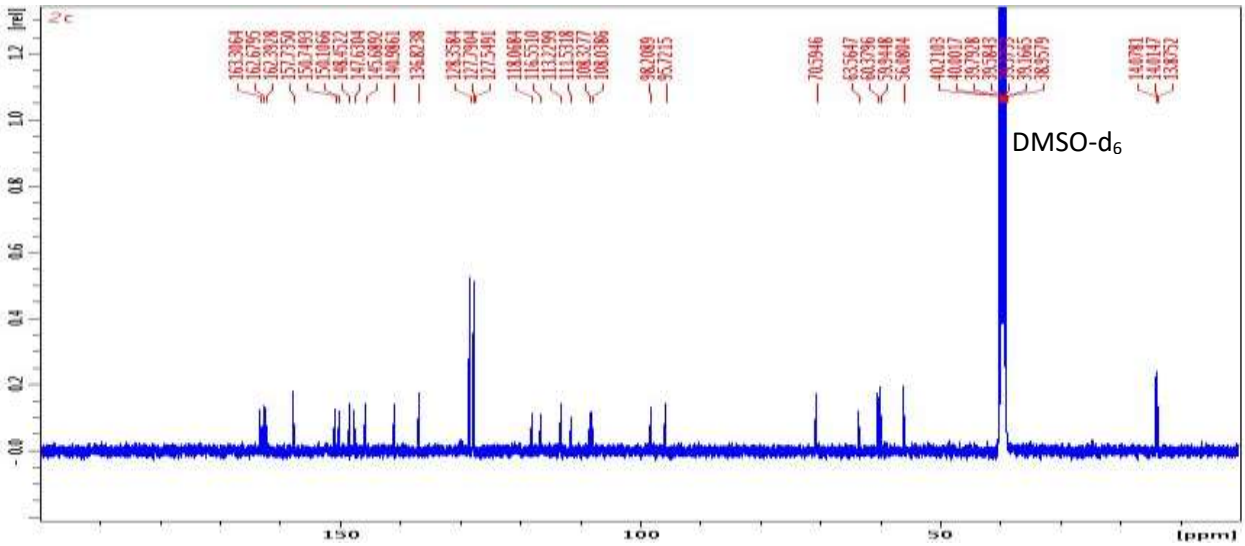
2c
DMSO-d6
[ppm]

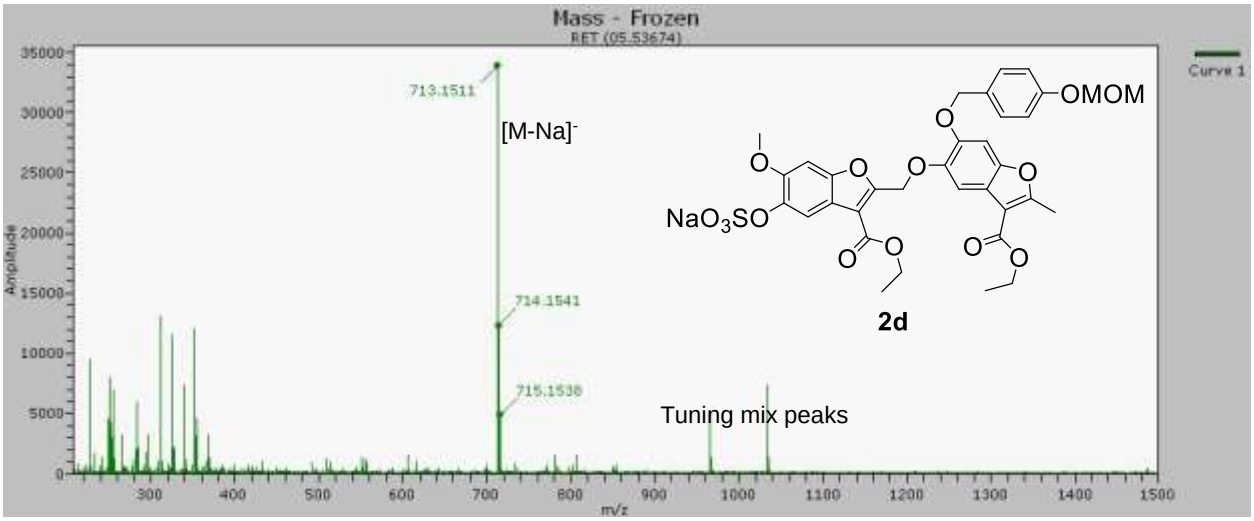
Mass - Frozen
RET (05.53674)
713.1511
[M-Na]-
714.1541
715.1538
Tuning mix peaks
OMOM
NaO3SO
2d
Amplitude
m/z
Curve 1

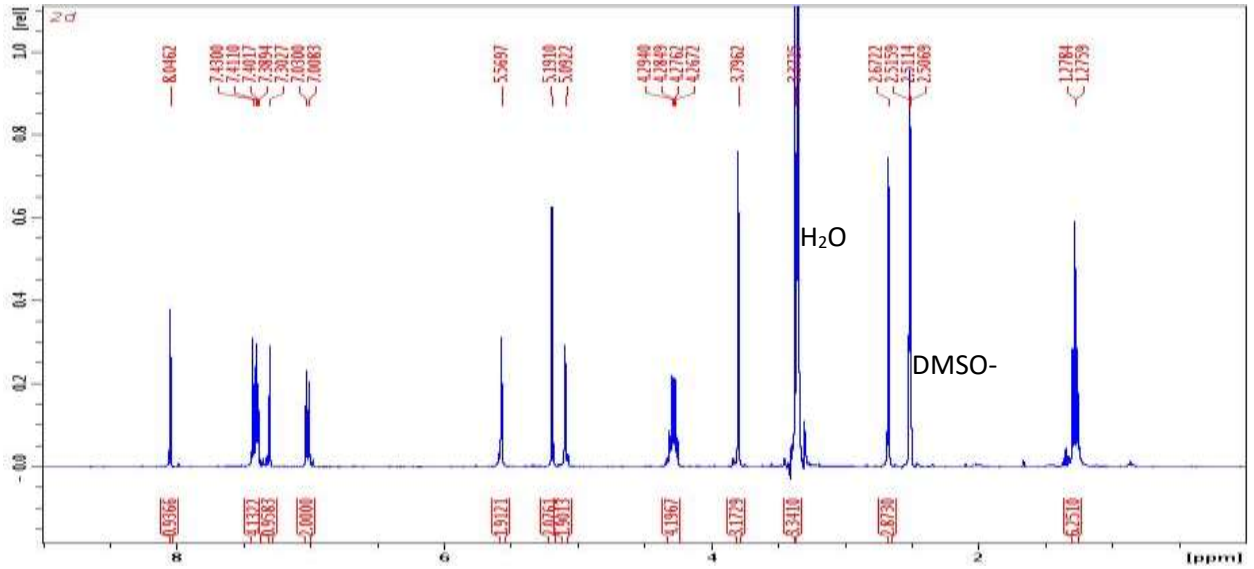
2d
H2O
DMSO-
[ppm]

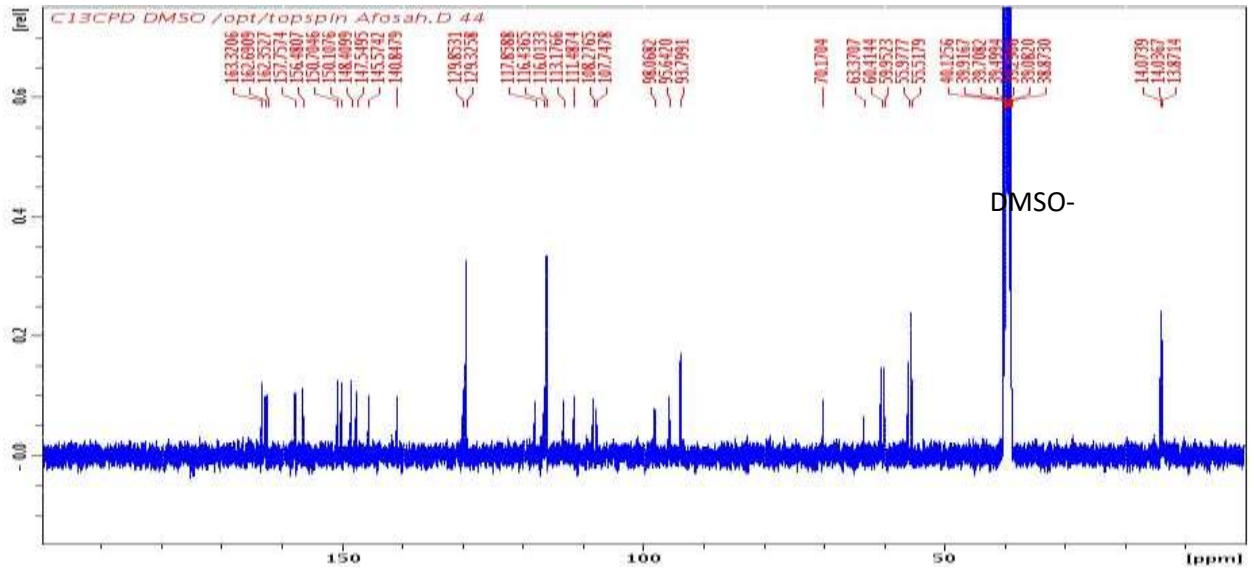
C13CPD DMSO /opt/topspin Afosah.D 44
DMSO-
[ppm]

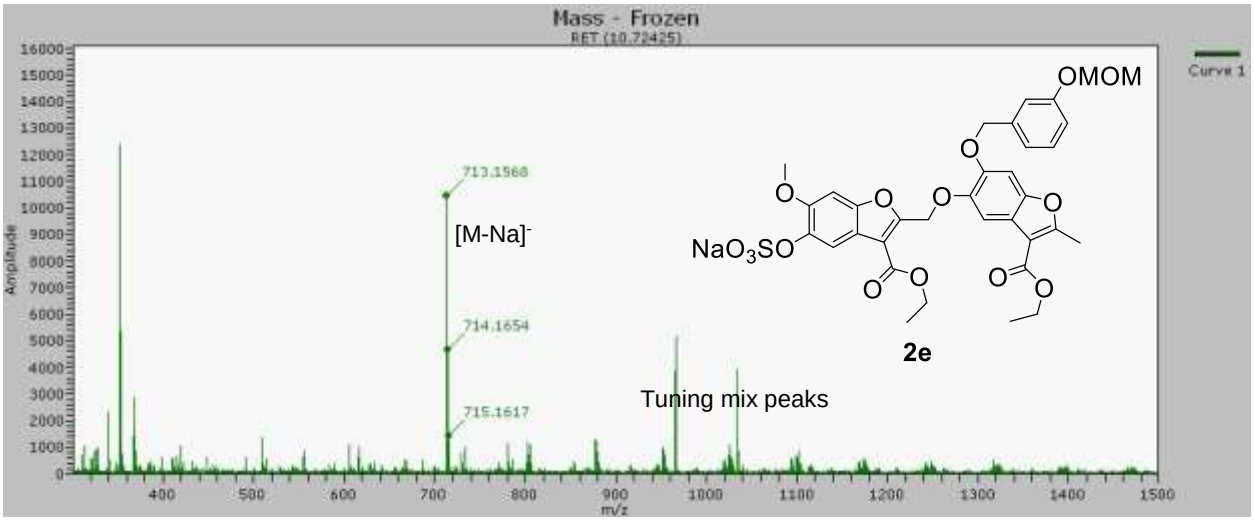
Mass - Frozen
RET (10.72425)
Curve 1
Amplitude
m/z
713.1568
[M-Na]-
714.1654
715.1617
Tuning mix peaks
OMOM
NaO3SO
2e

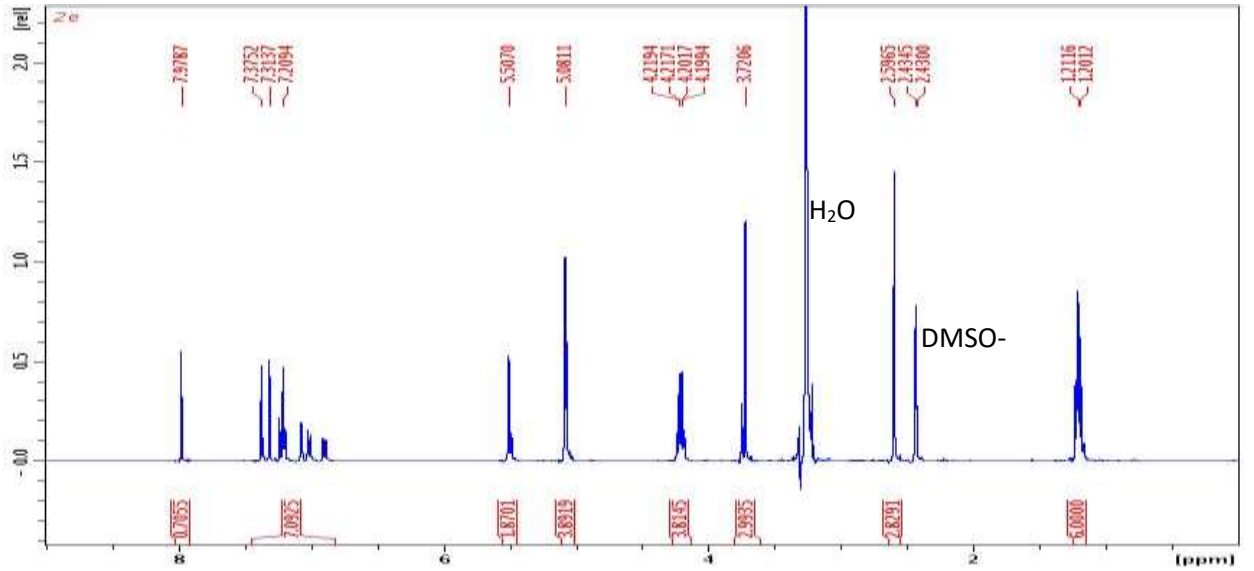
H2O
DMSO-
[ppm]

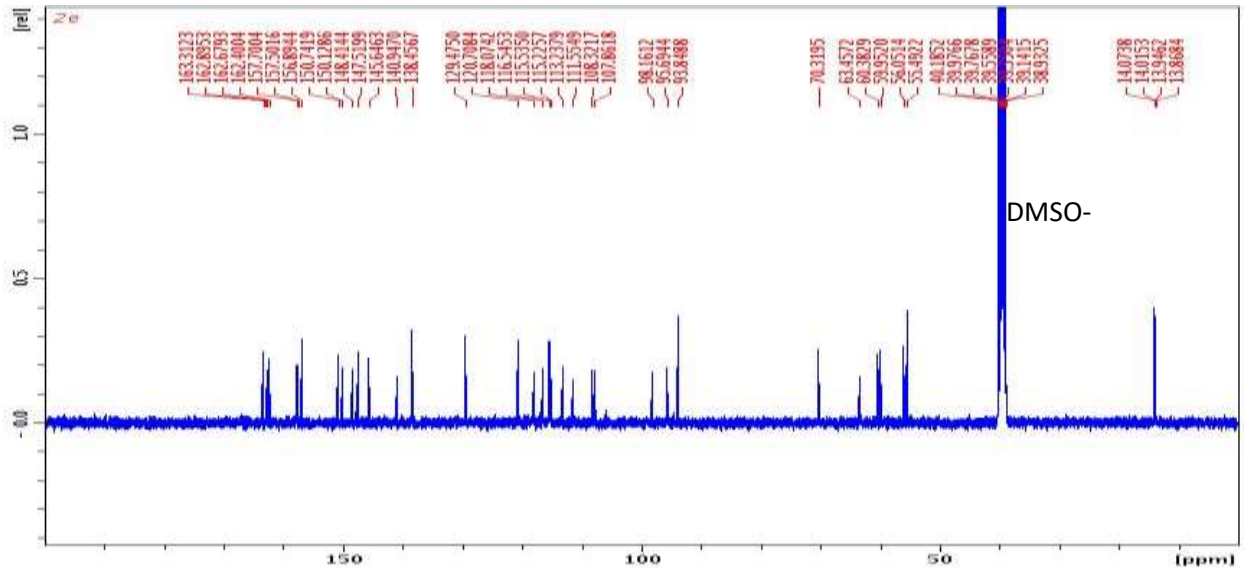
DMSO-
[ppm]

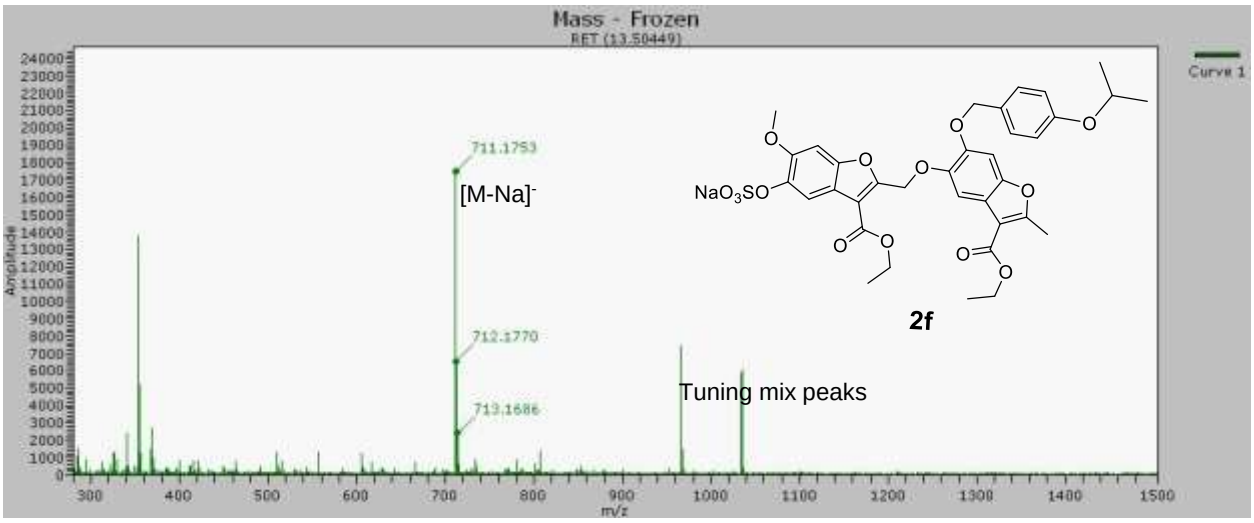
Mass - Frozen
RET (13.50449)
Curve 1
711.1753
[M-Na]-
712.1770
713.1686
Tuning mix peaks
NaO3SO
2f
Amplitude
m/z

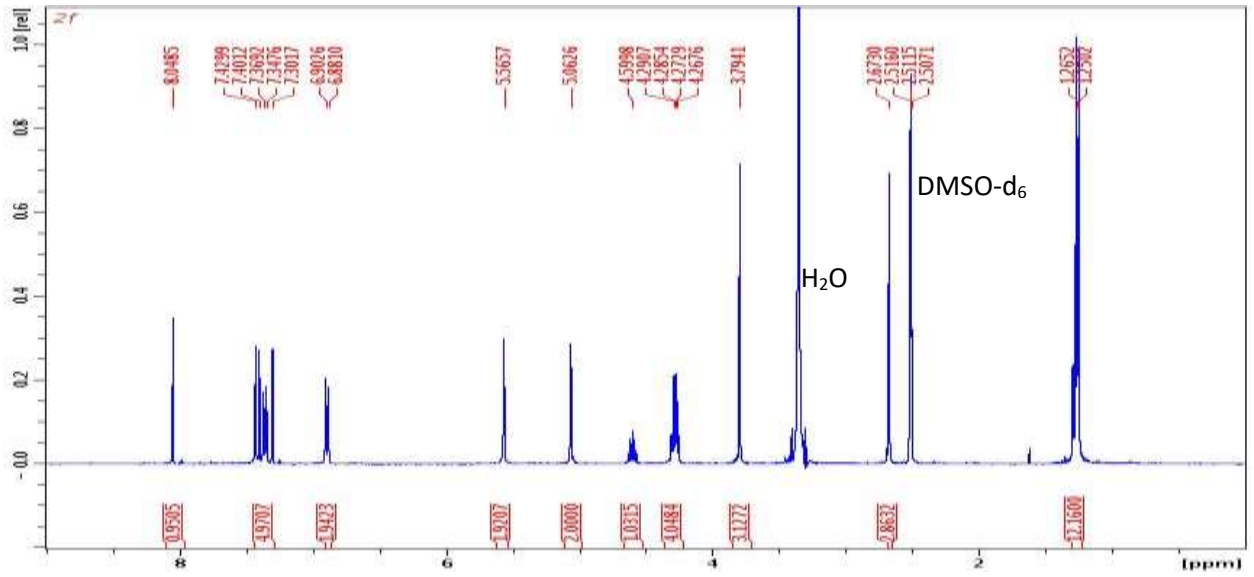
2f
DMSO-d6
H2O
[ppm]

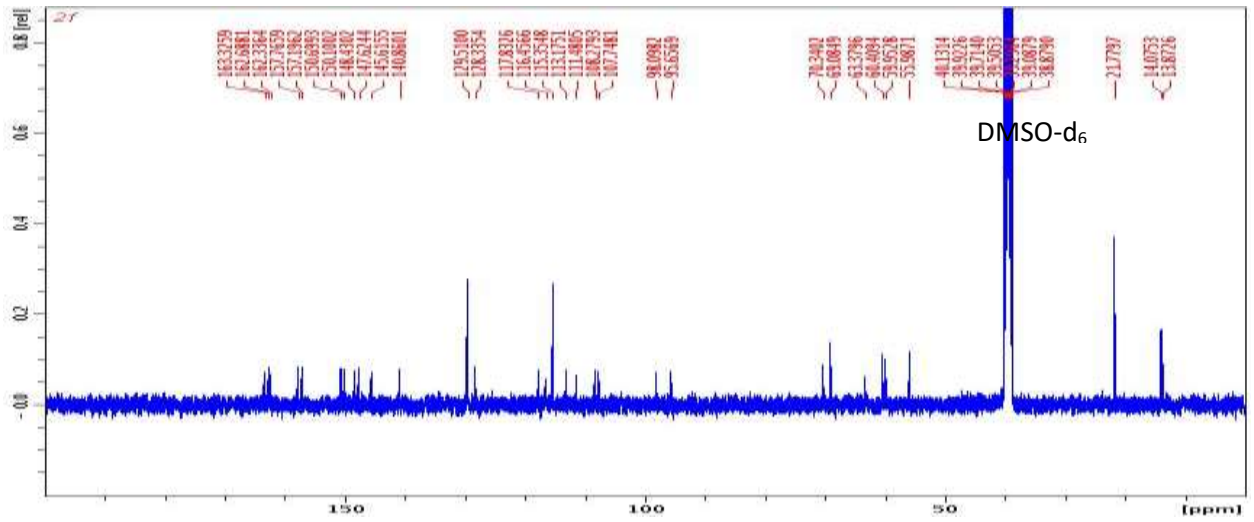
2f
DMSO-d6
[ppm]

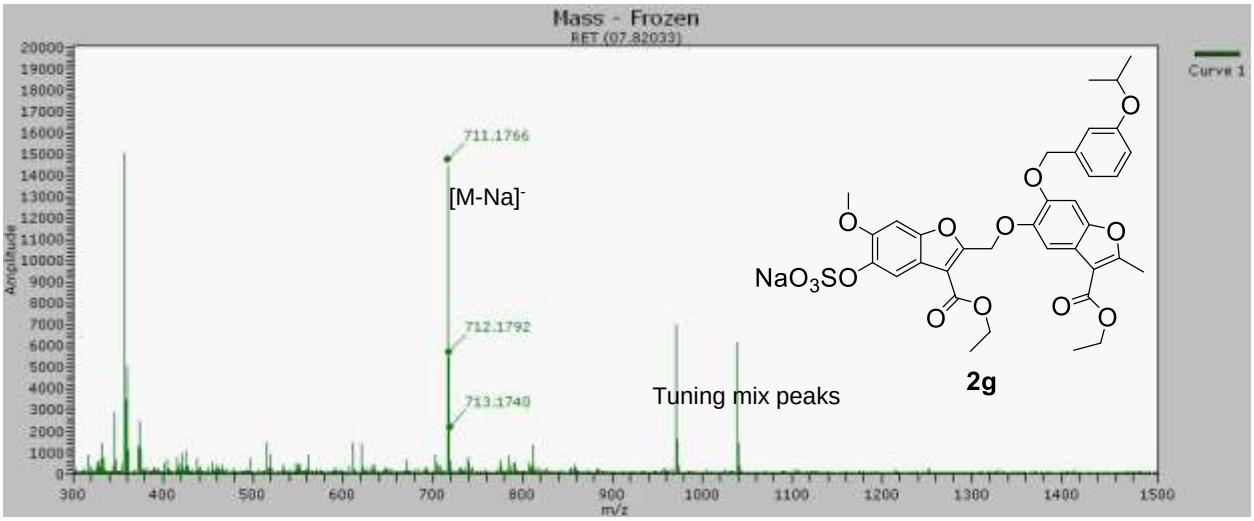
Mass - Frozen
RET (07.82033)
Curve 1
711.1766
[M-Na]-
712.1792
713.1740
Tuning mix peaks
NaO3SO
2g
Amplitude
m/z

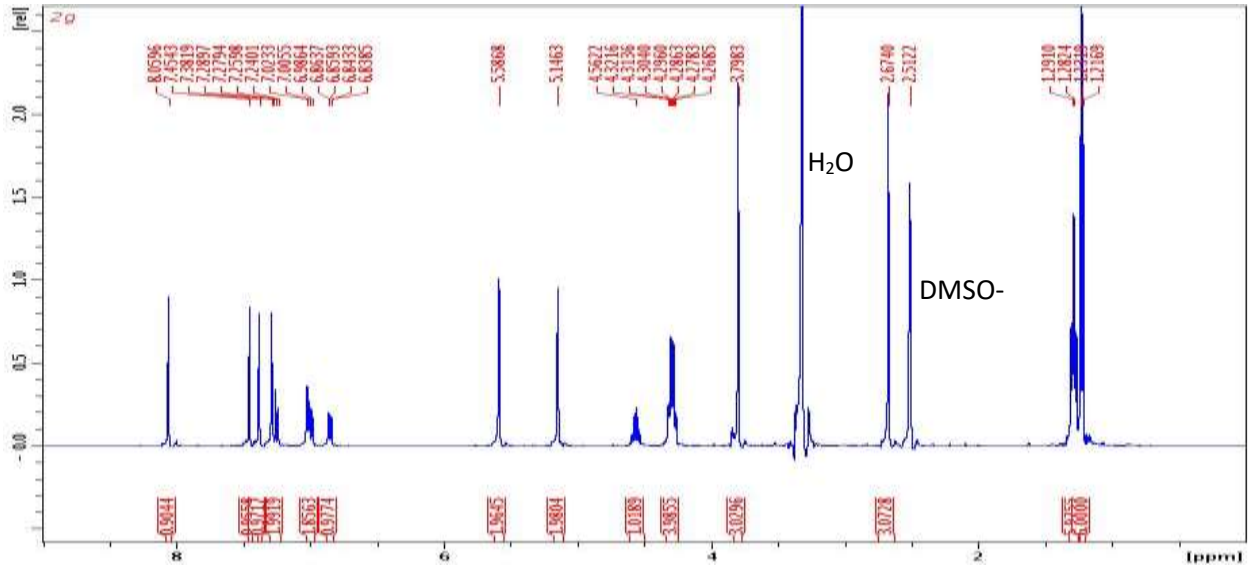
H2O
DMSO-
[ppm]

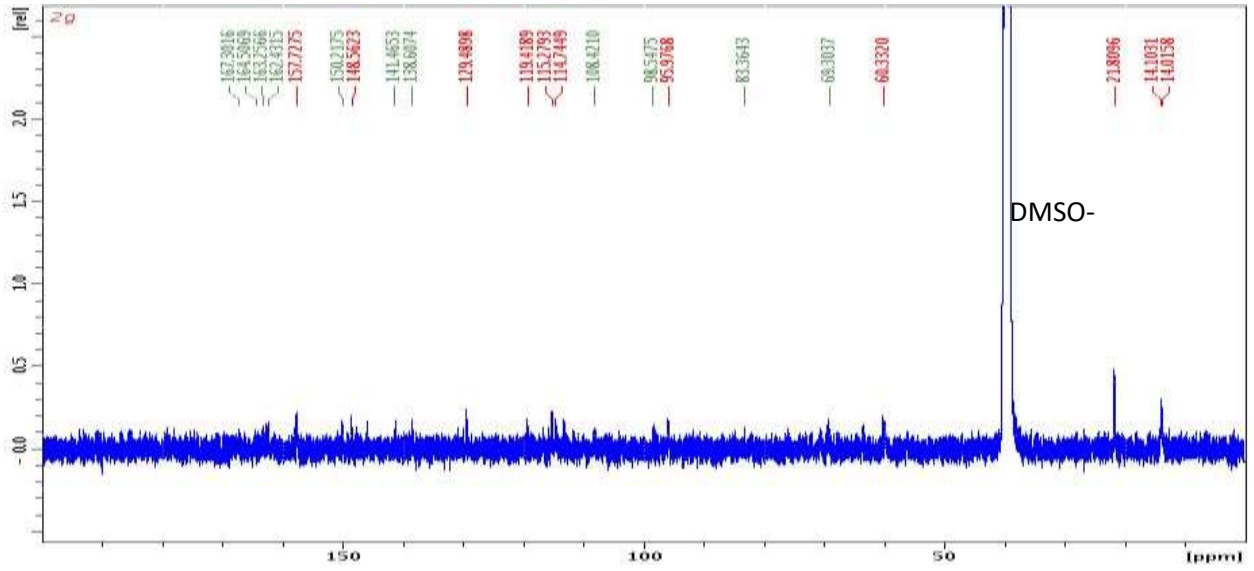
DMSO-
[ppm]

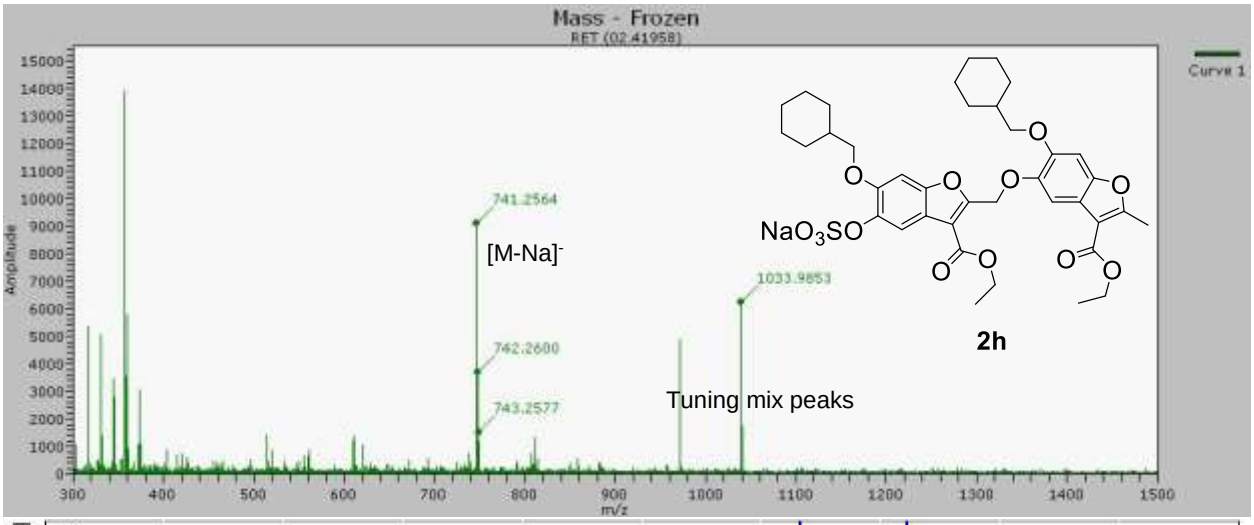
Mass - Frozen
RET (02.41958)
Curve 1
Amplitude
m/z
741.2564
[M-Na]-
742.2600
743.2577
1033.9853
Tuning mix peaks
NaO3SO
2h

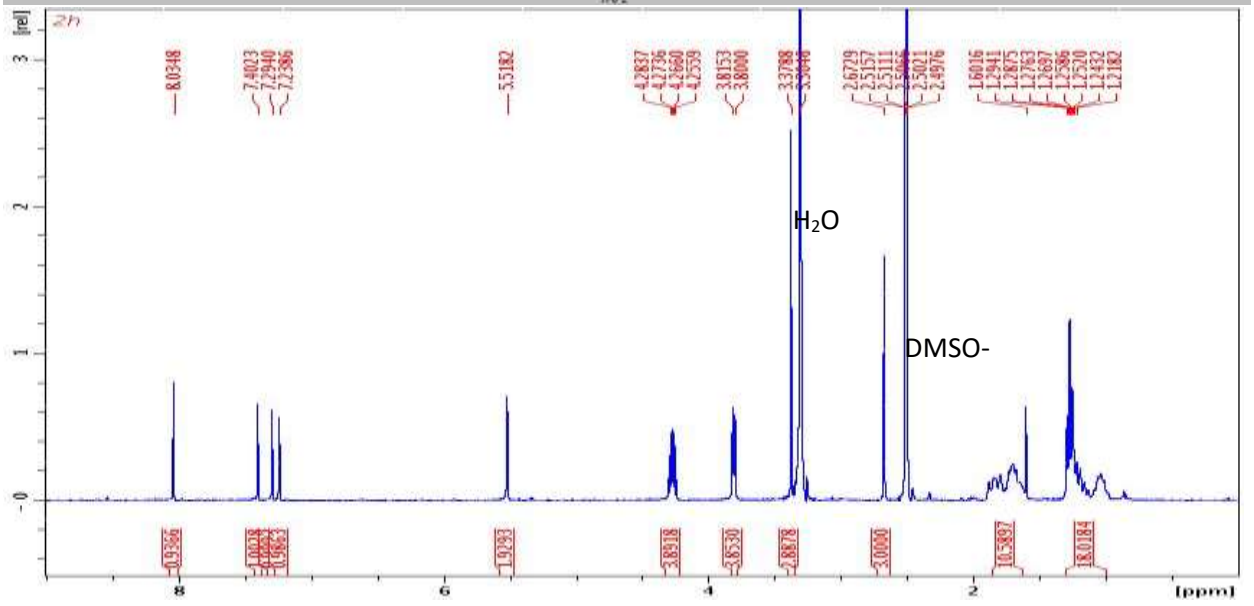
2h
[rel]
H2O
DMSO-
[ppm]

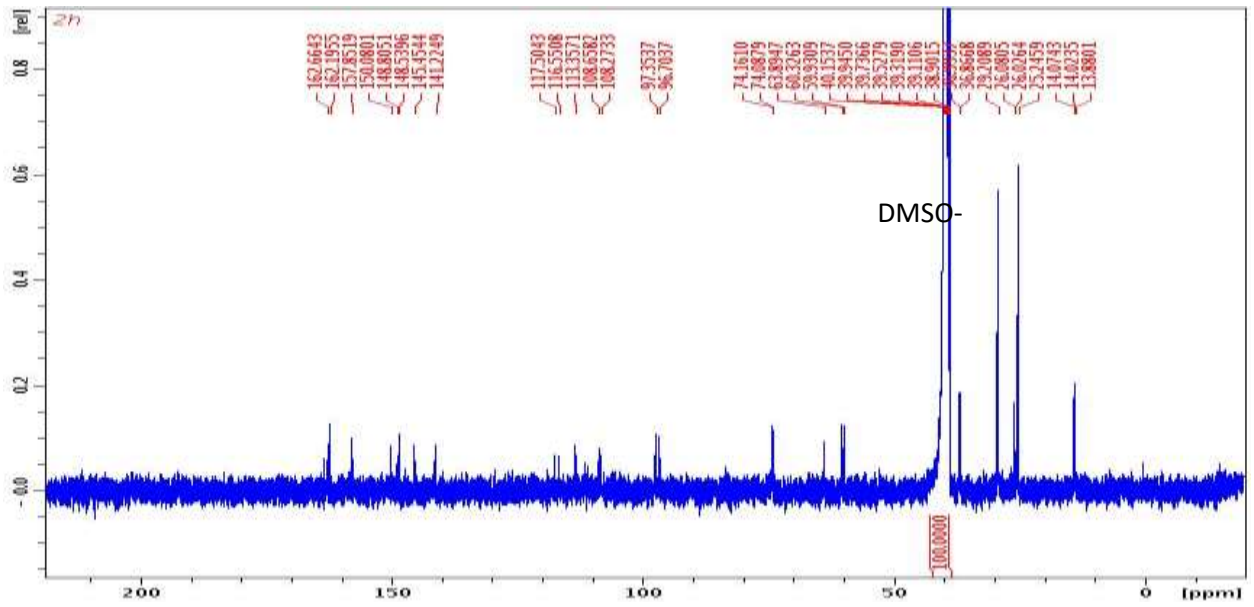
2h
[rel]
DMSO-
[ppm]

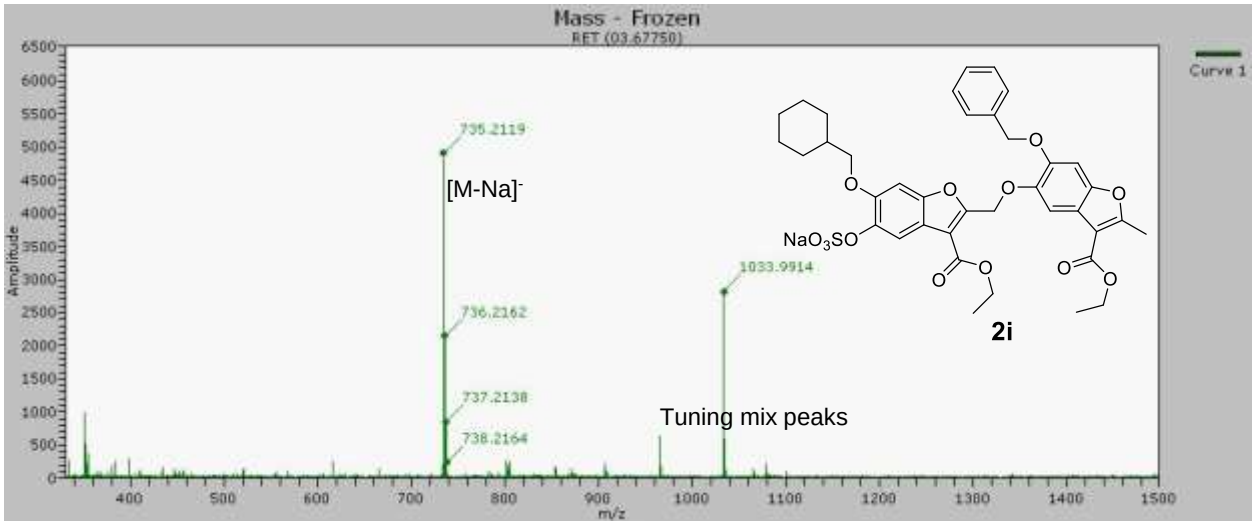
Mass - Frozen
RET (03.67750)
Curve 1
Amplitude
m/z
735.2119
[M-Na]-
736.2162
737.2138
738.2164
1033.9914
Tuning mix peaks
NaO3SO
2i

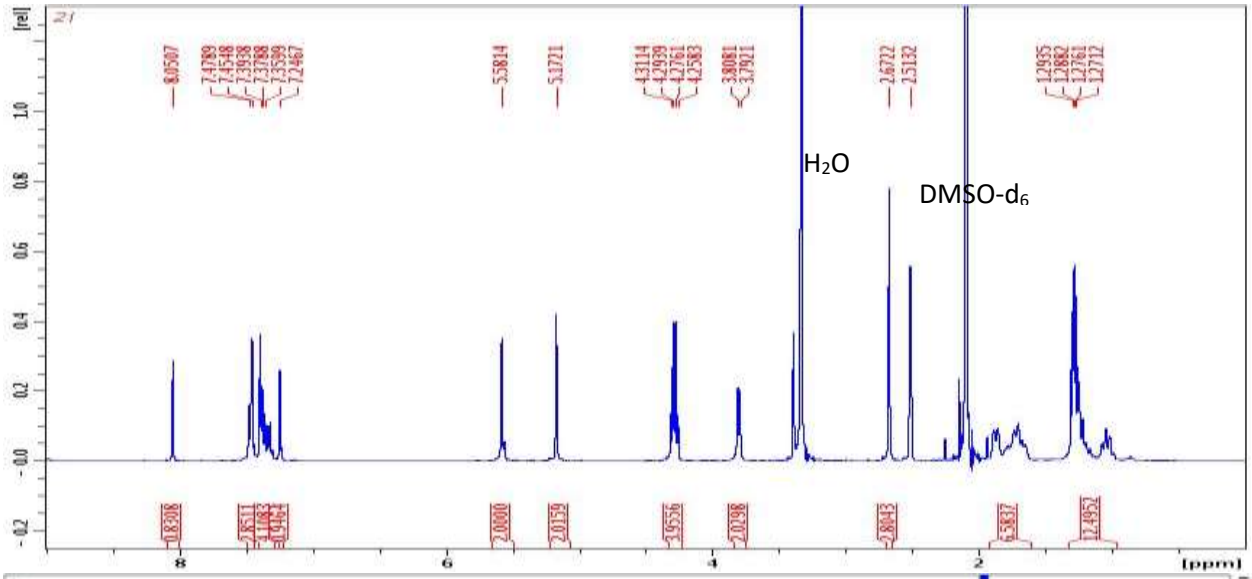
H2O
DMSO-d6
(ppm)

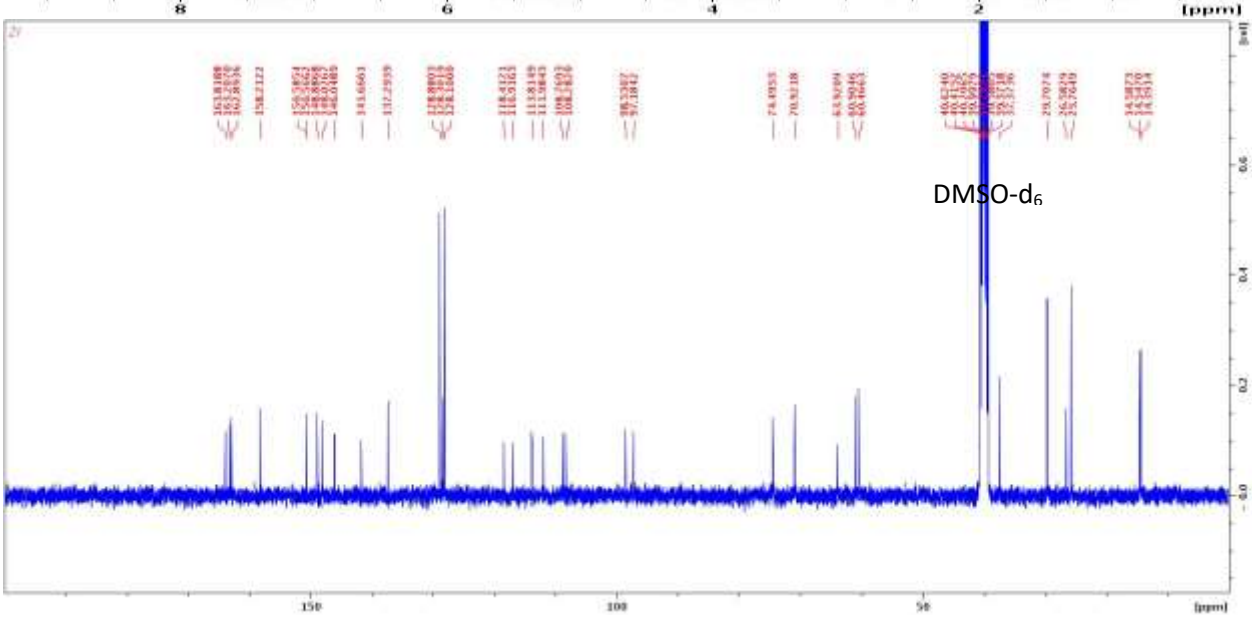
DMSO-d6
(ppm)

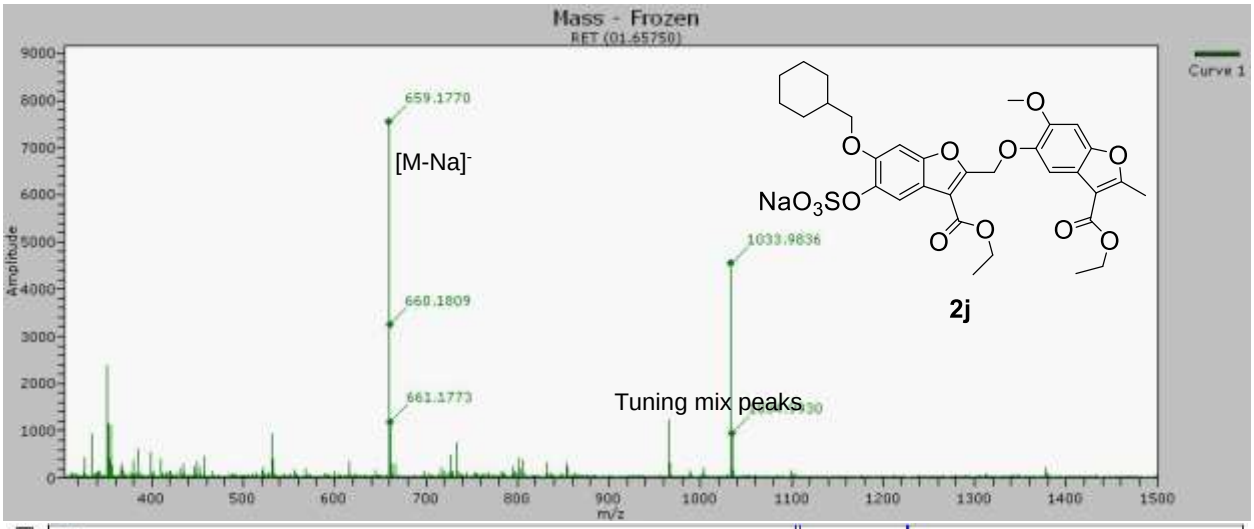
Mass - Frozen
RET (01.65750)
Curve 1
659.1770
[M-Na]-
660.1809
661.1773
1033.9836
Tuning mix peaks
Amplitude
m/z
NaO3SO
2j

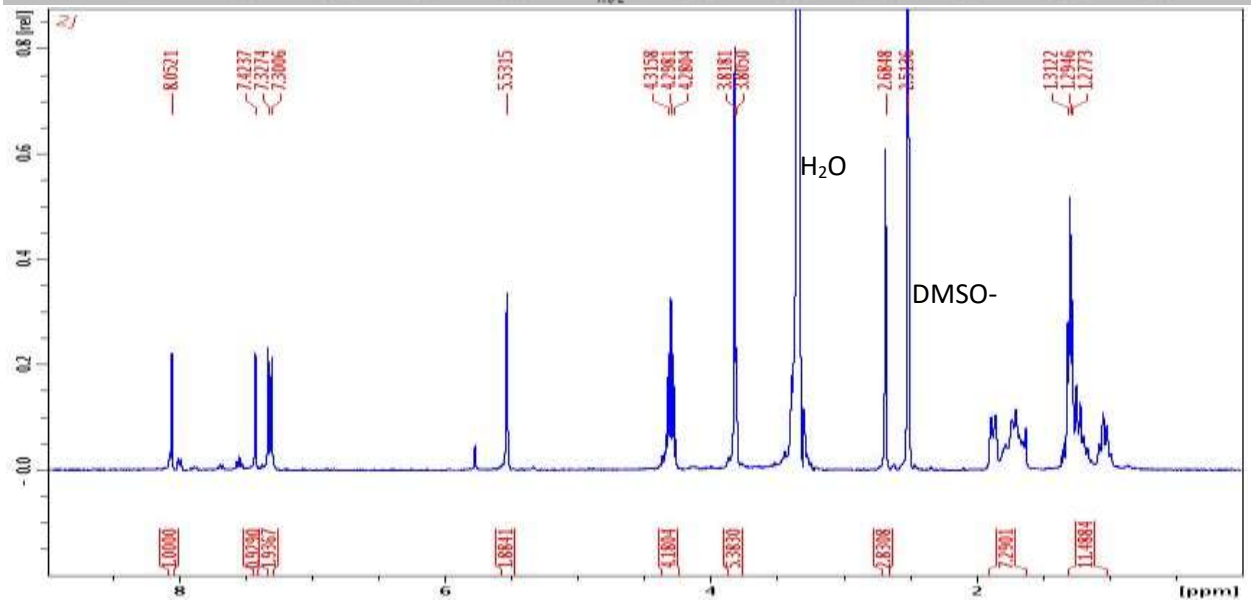
H2O
DMSO-
[ppm]

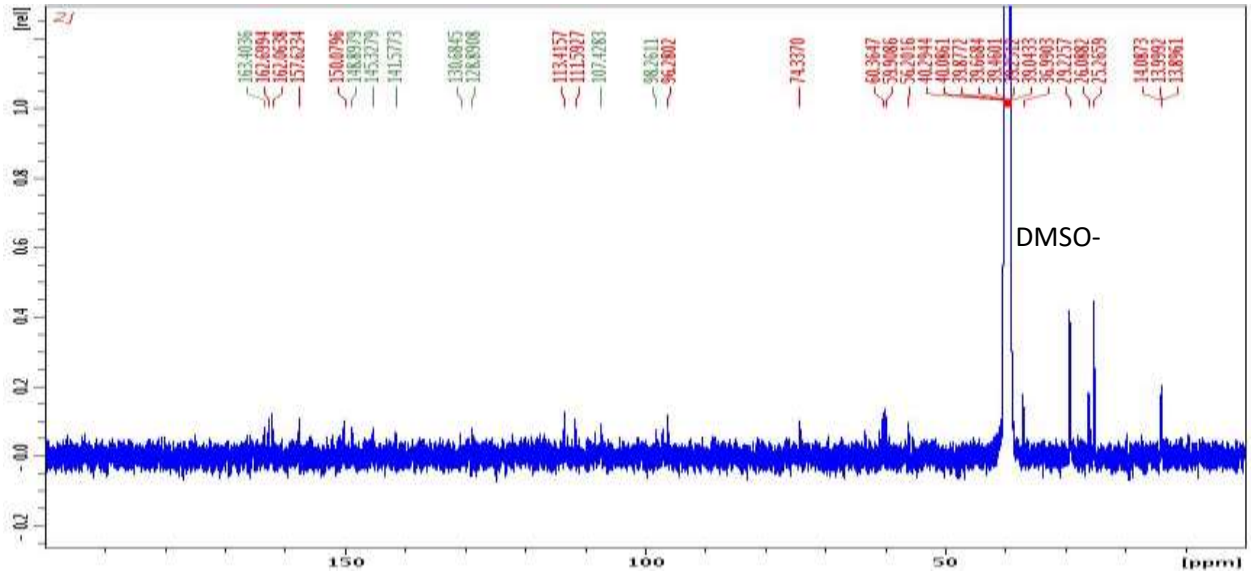
DMSO-
[ppm]

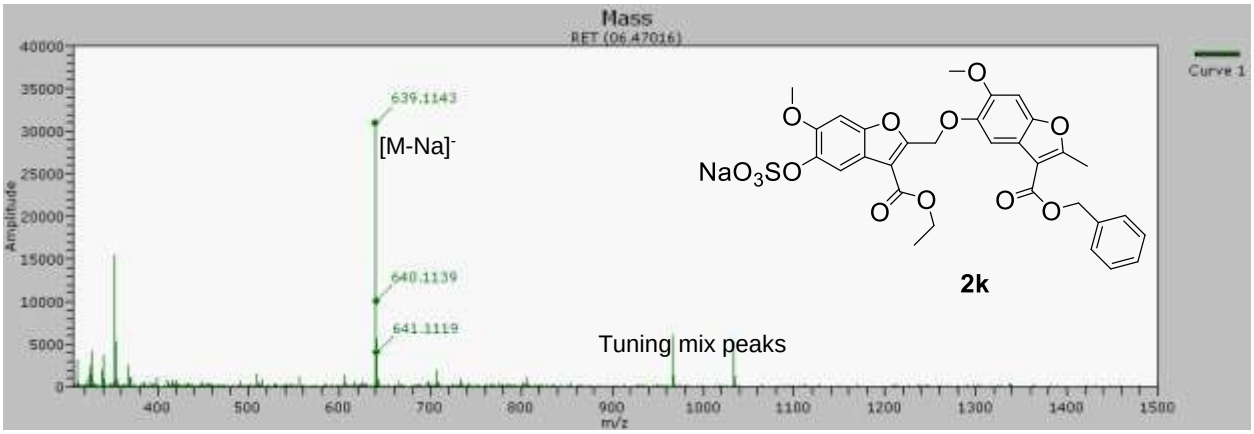
Mass
RET (06.47016)
Curve 1
Amplitude
m/z
639.1143
[M-Na]-
640.1139
641.1119
Tuning mix peaks
NaO3SO
2k

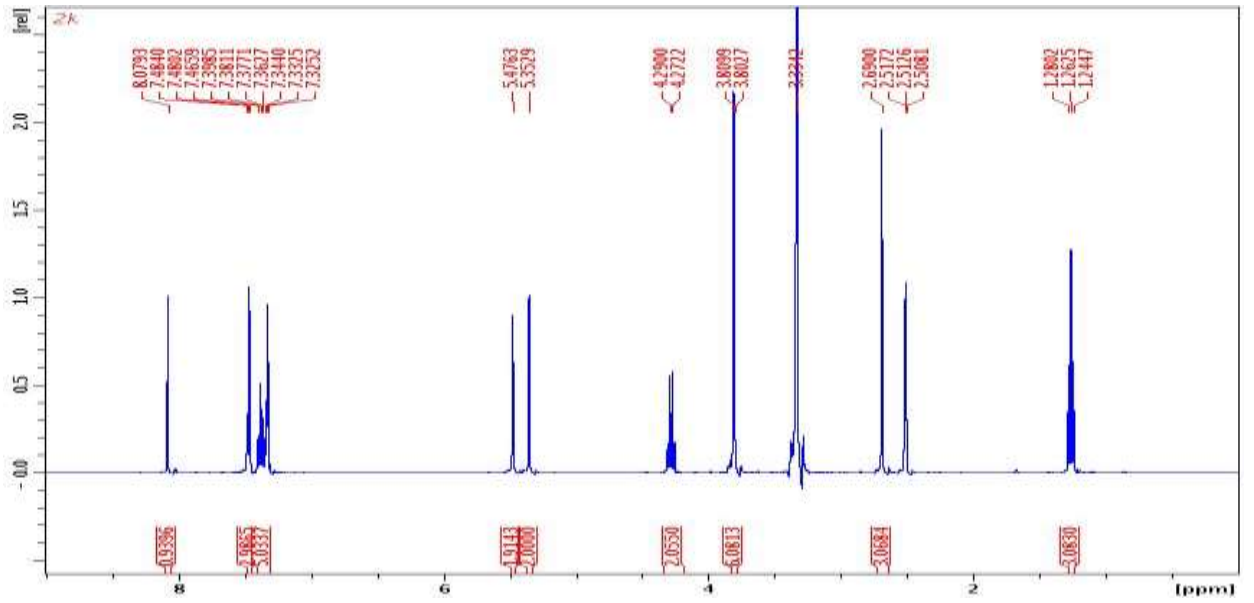
2k
[rel]
[ppm]

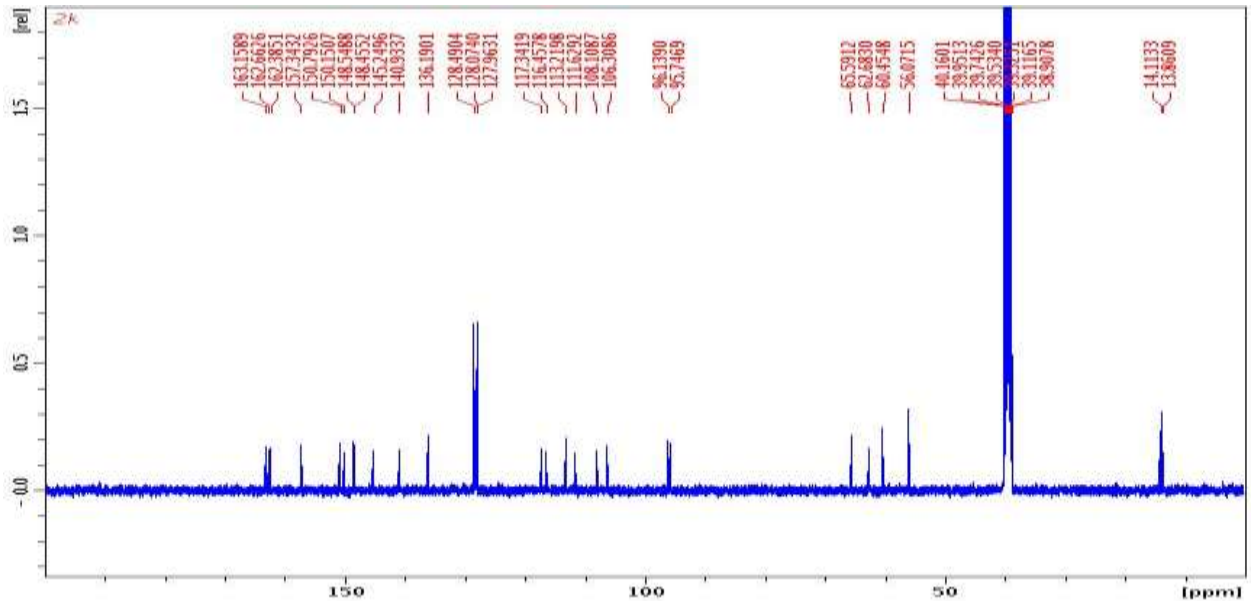
2k
[rel]
[ppm]

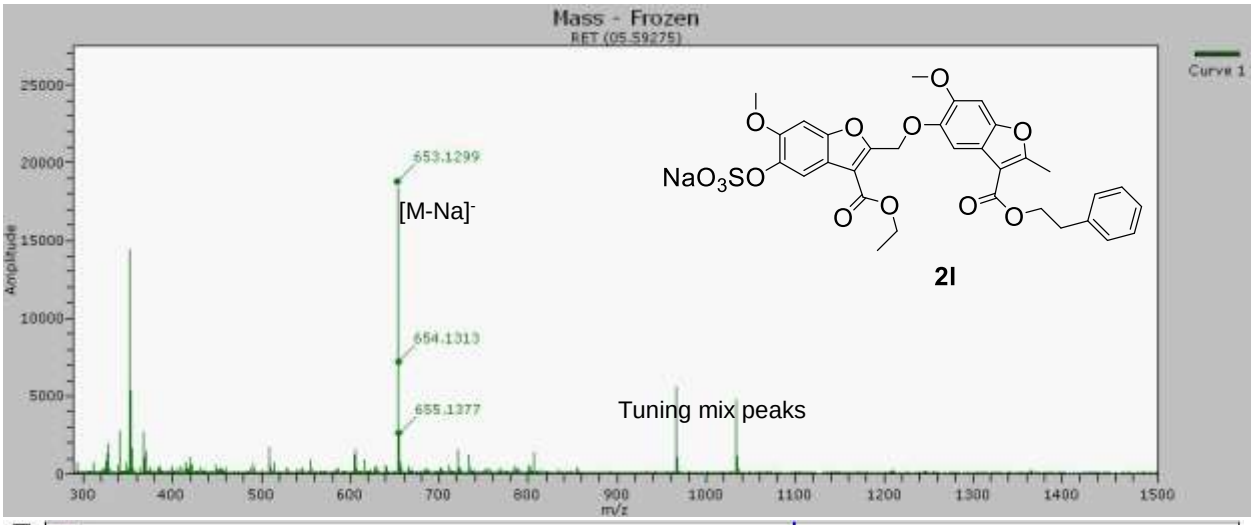
Mass - Frozen
RET (05.59275)
Curve 1
Amplitude
m/z
653.1299
654.1313
655.1377
[M-Na]-
Tuning mix peaks
NaO3SO
2l

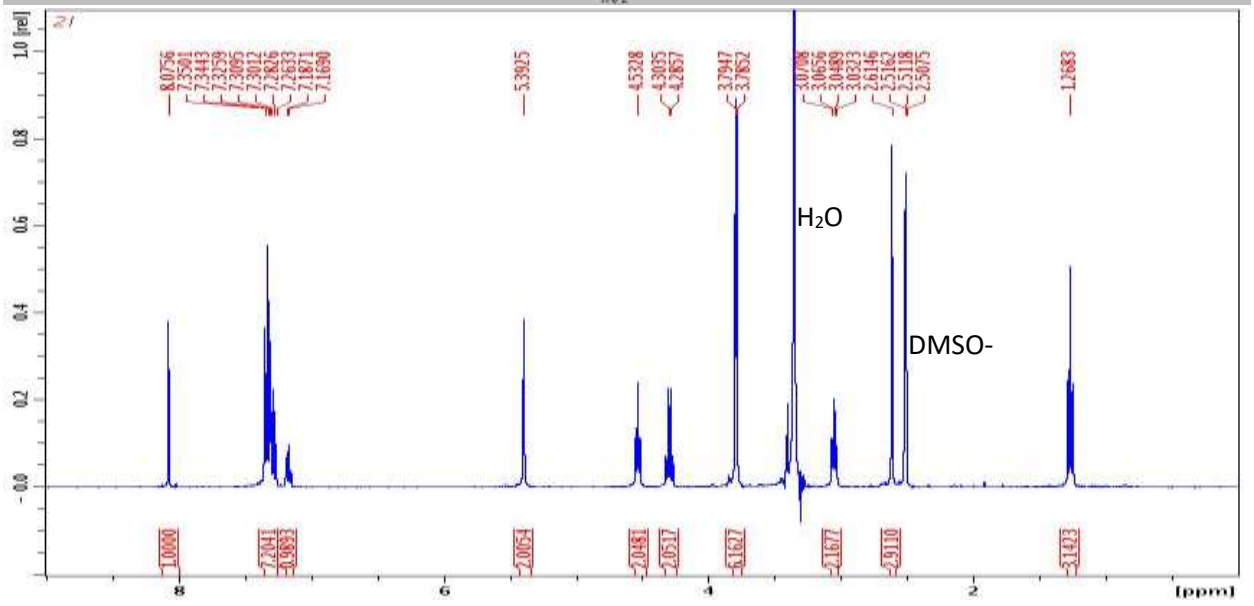
H2O
DMSO-
[ppm]

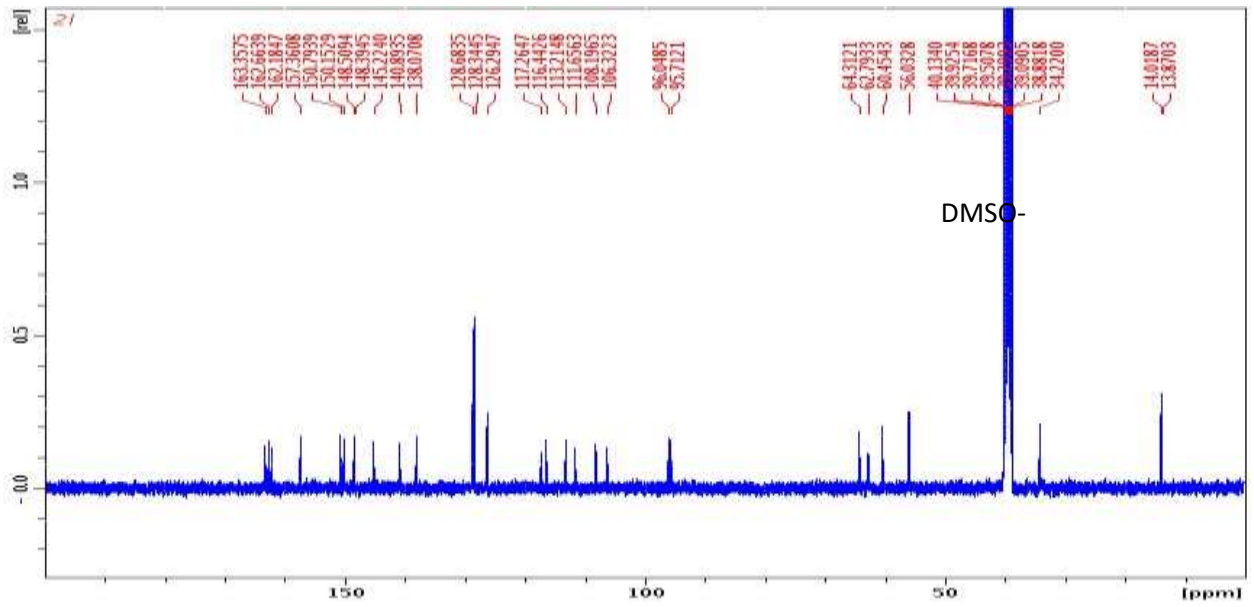
DMSO-
[ppm]

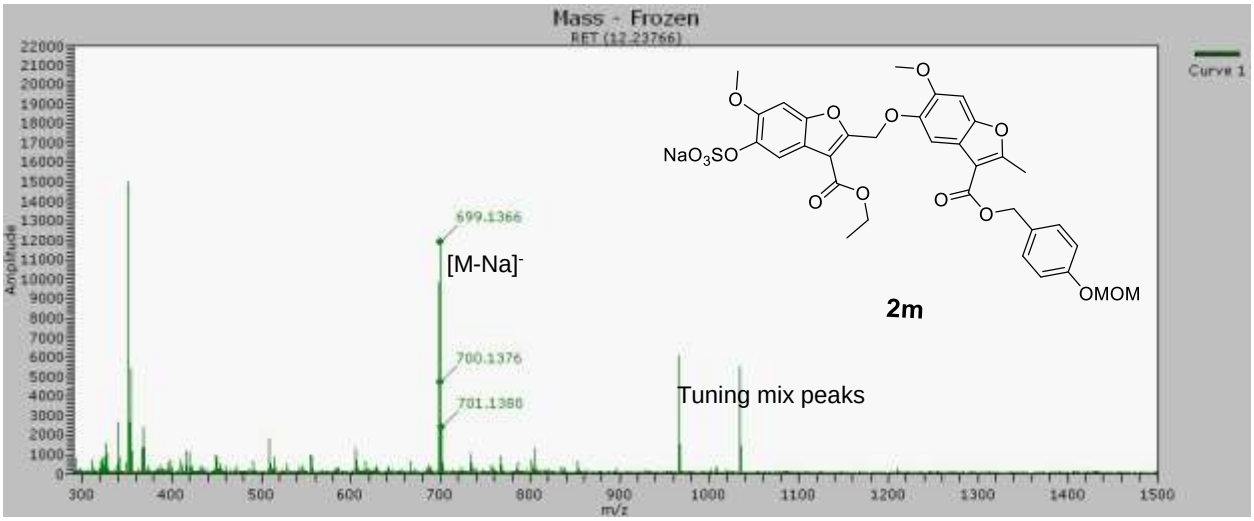
Mass - Frozen
RET (12.23766)
Curve 1
Amplitude
m/z
699.1366
[M-Na]-
700.1376
701.1380
Tuning mix peaks
NaO3SO
OMOM
2m

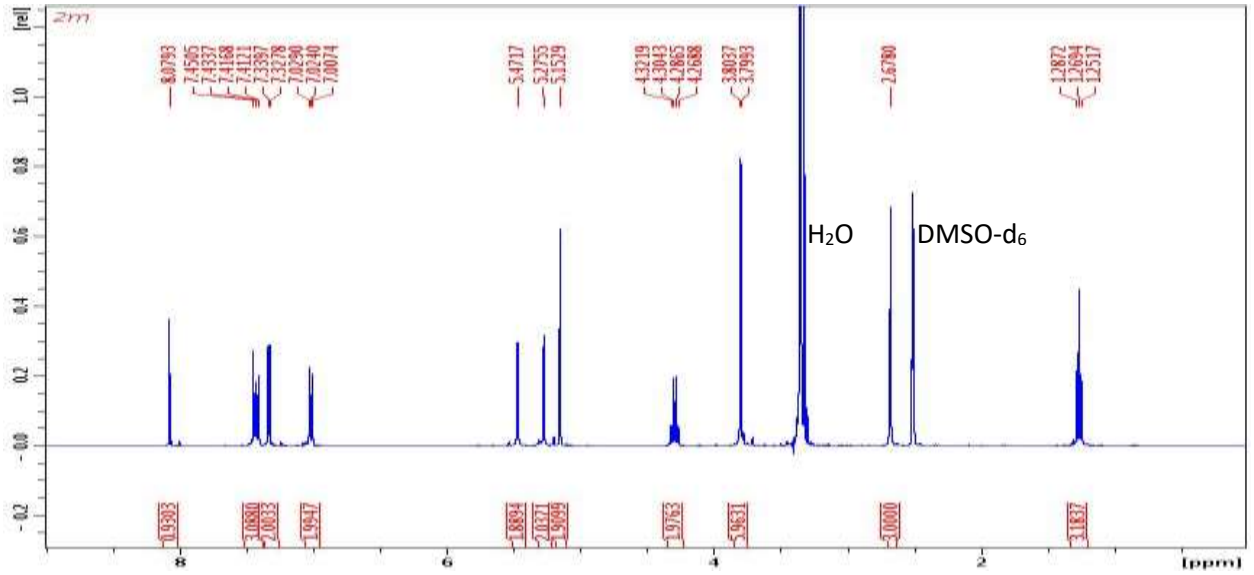
2m
[rel]
H2O
DMSO-d6
[ppm]

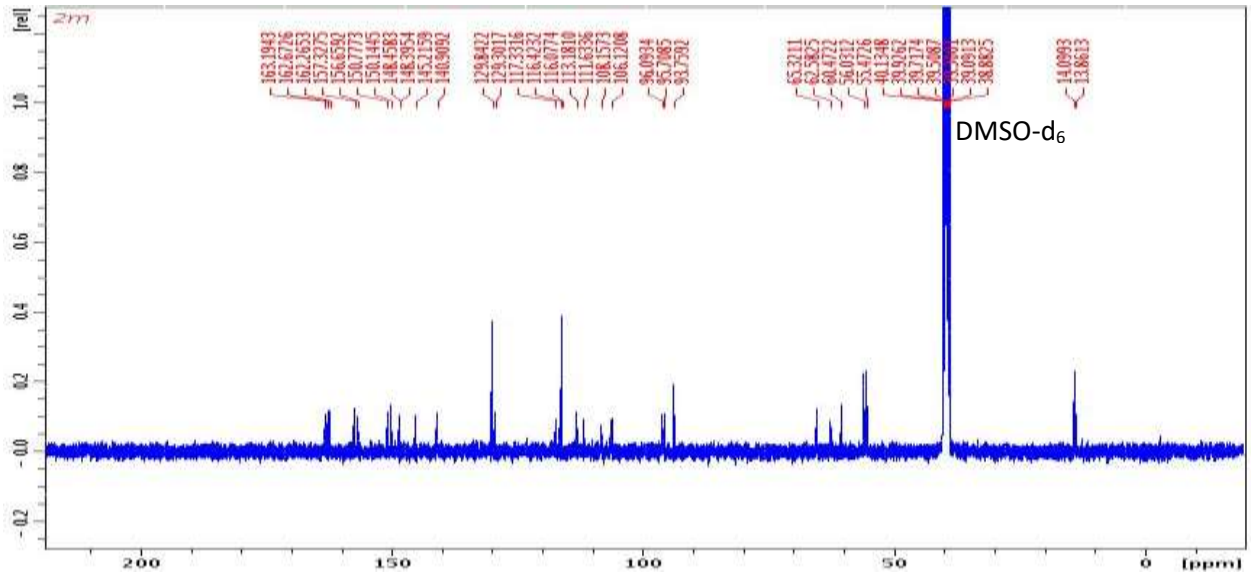
2m
[rel]
DMSO-d6
[ppm]

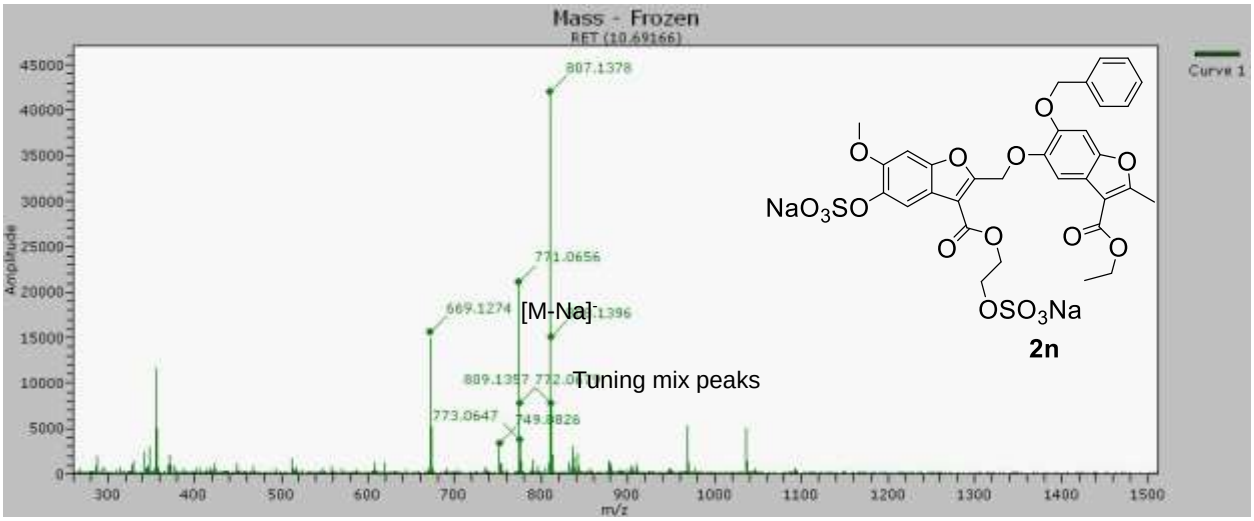
Mass - Frozen
RET (10.69166)
807.1378
771.0656
669.1274
[M-Na]
Tuning mix peaks
773.0647
749.0826
Curve 1
Amplitude
m/z
NaO3SO
OSO3Na
2n

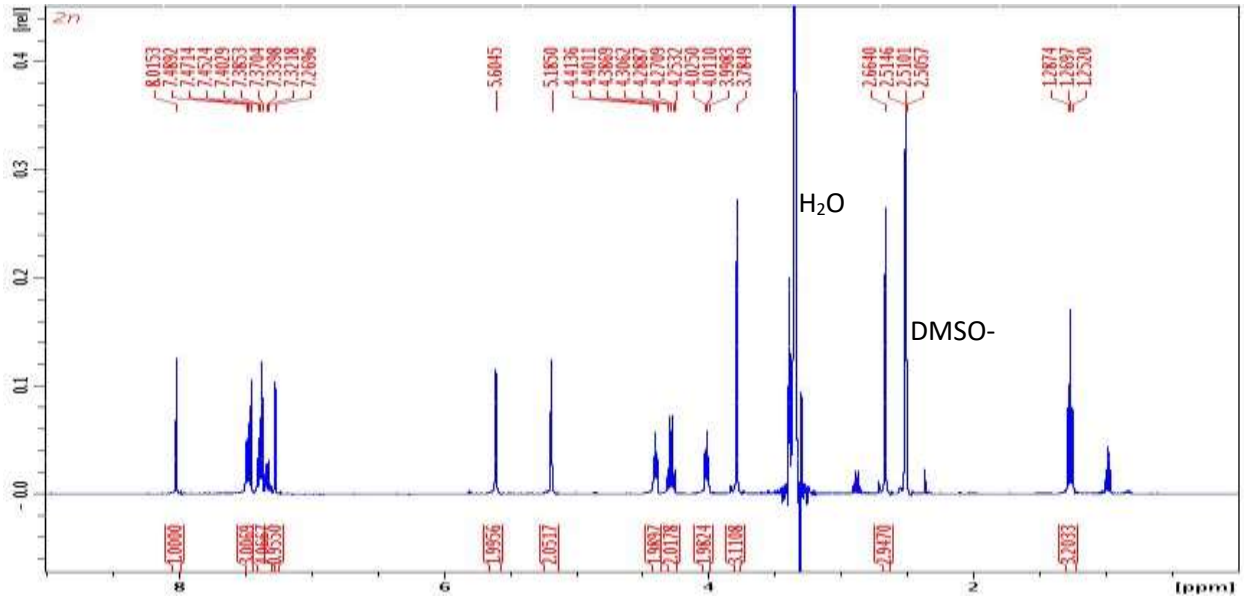
2n
H2O
DMSO-
[ppm]

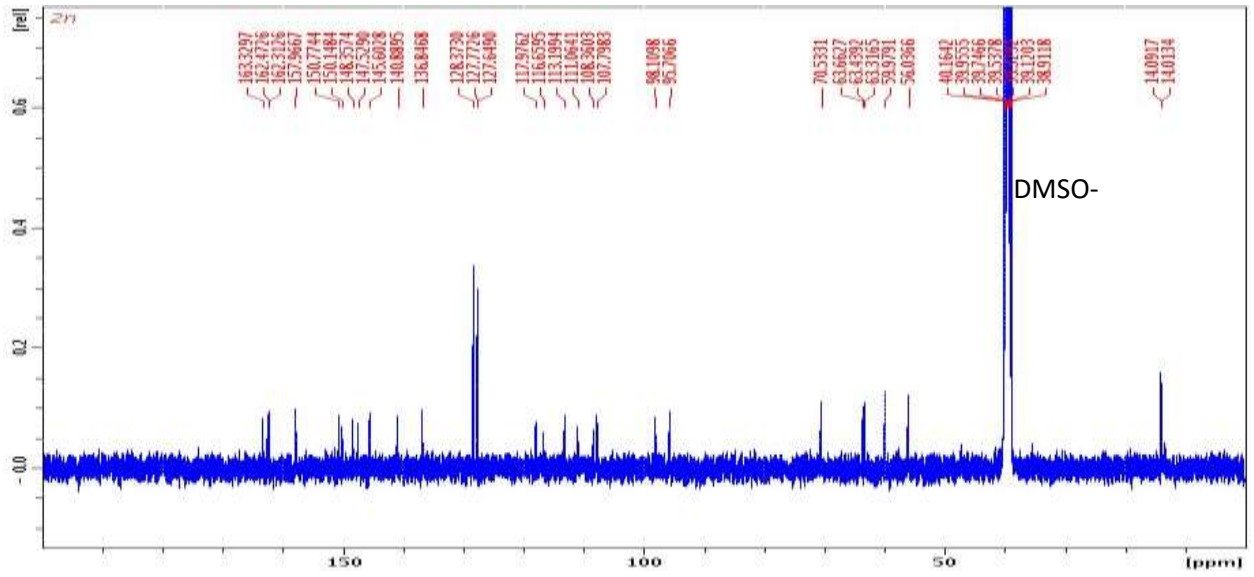
2n
DMSO-
[ppm]

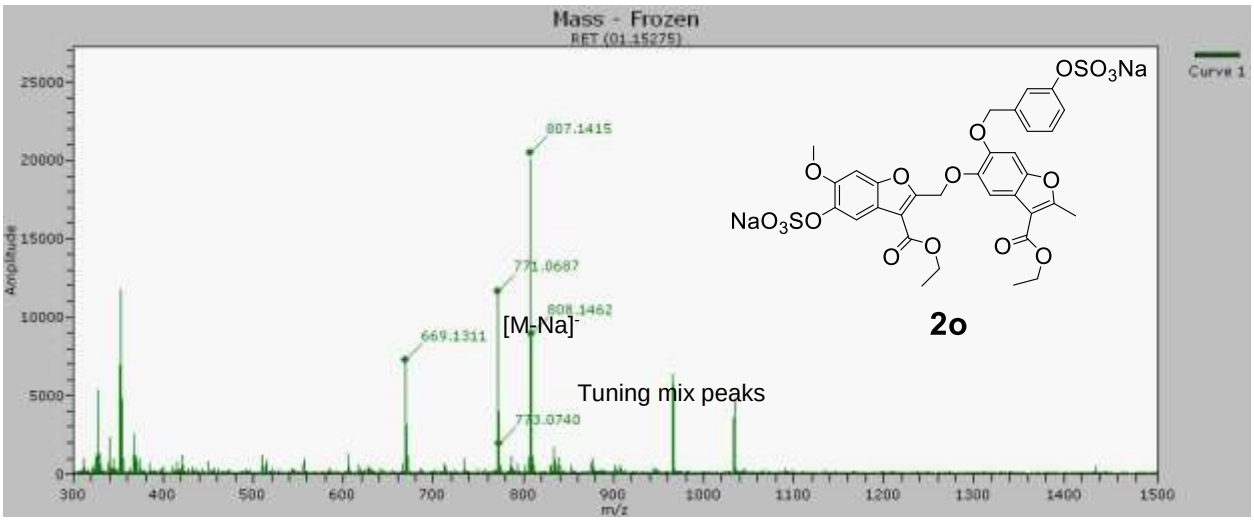
Mass - Frozen
RET (01.15275)
Curve 1
Amplitude
m/z
807.1415
771.0687
808.1462
669.1311
773.0740
[M-Na]-
Tuning mix peaks
OSO3Na
NaO3SO
2o

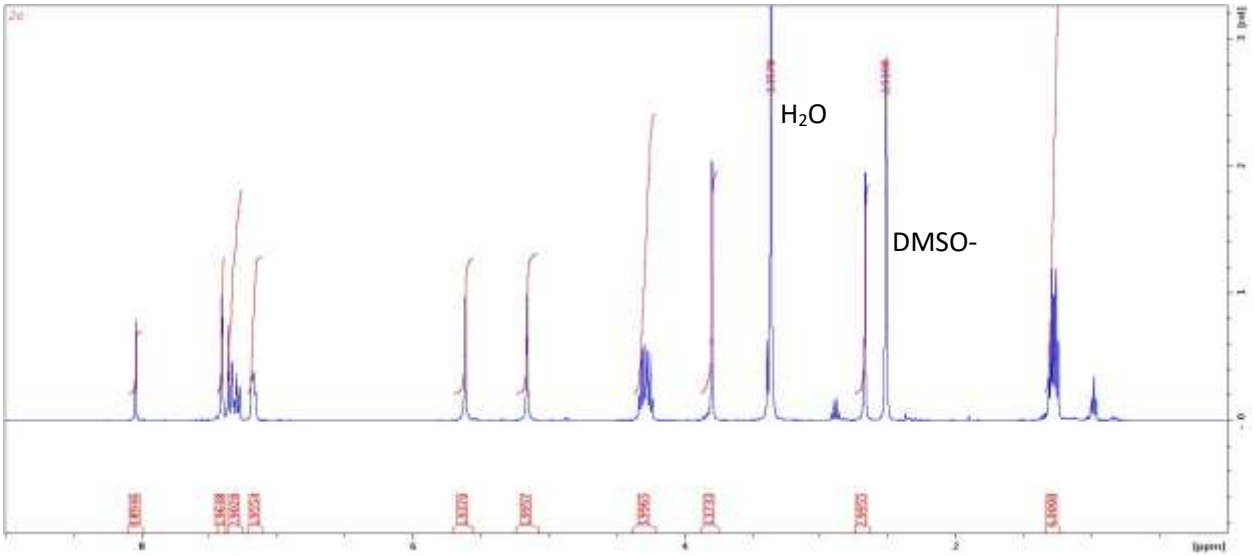
H2O
DMSO-

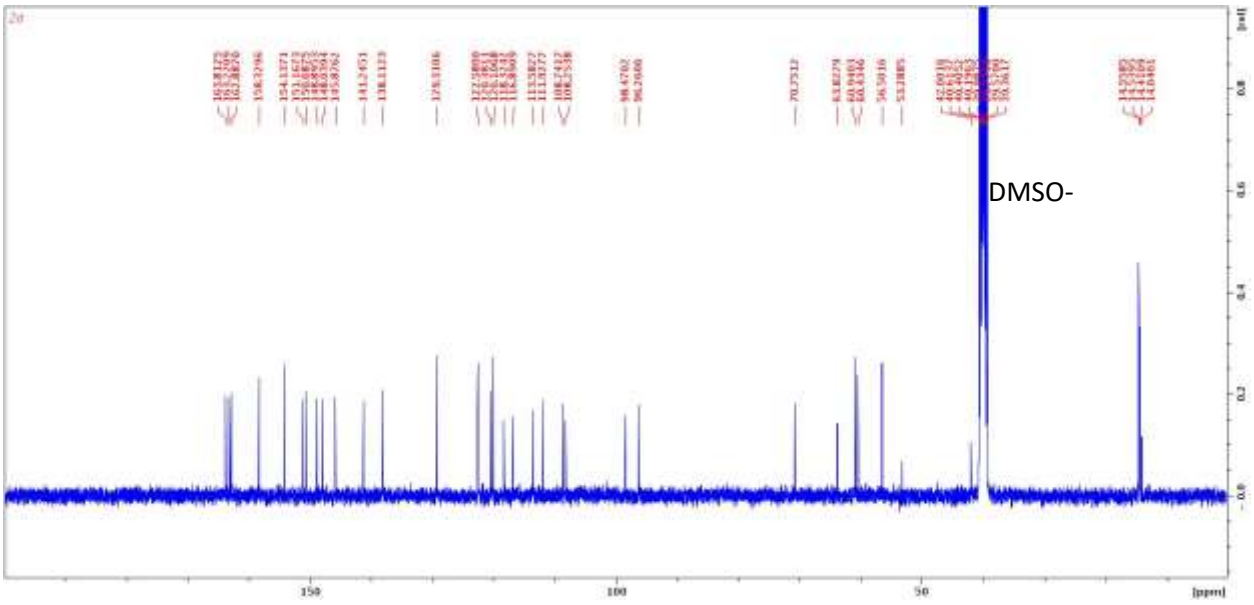
DMSO-

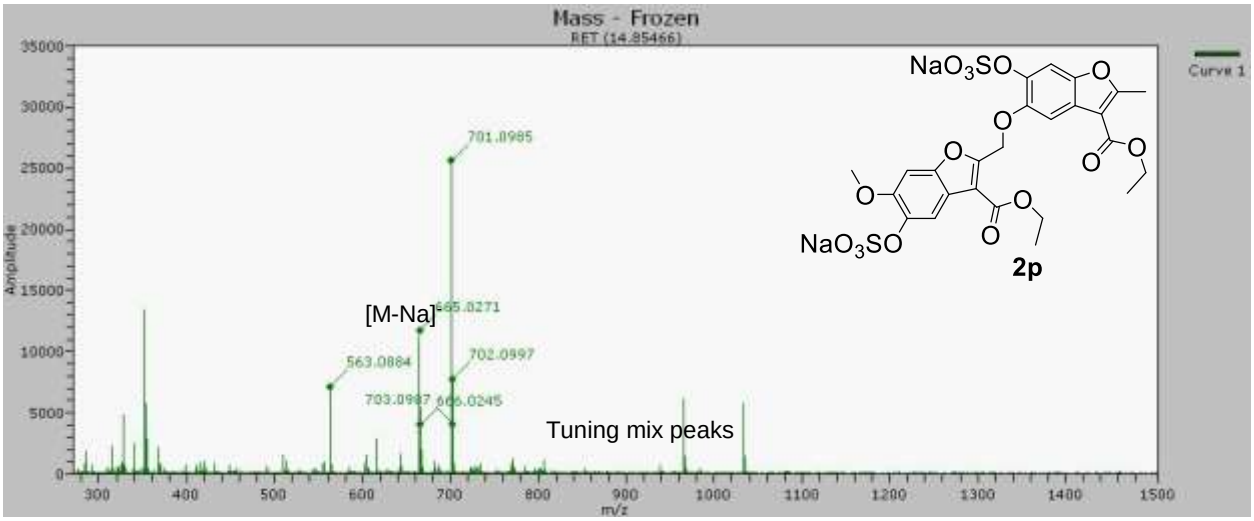
Mass - Frozen
RET (14.85466)
Curve 1
Amplitude
m/z
701.0985
[M-Na]
665.0271
563.0884
702.0997
703.0987
666.0245
Tuning mix peaks
NaO3SO
NaO3SO
2p

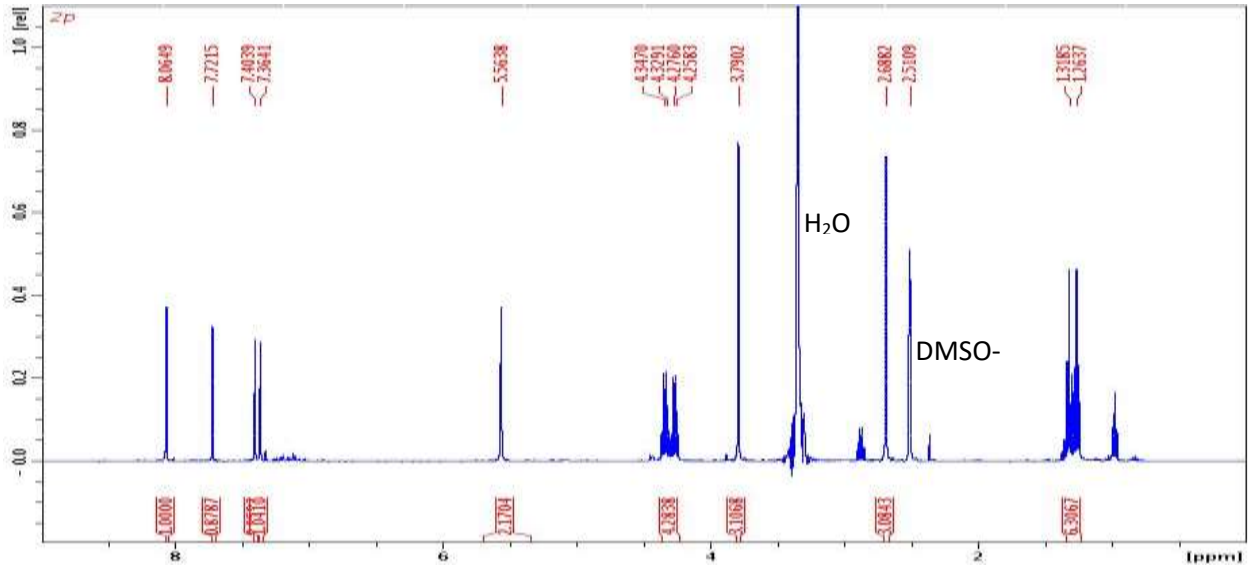
H2O
DMSO-
ppm

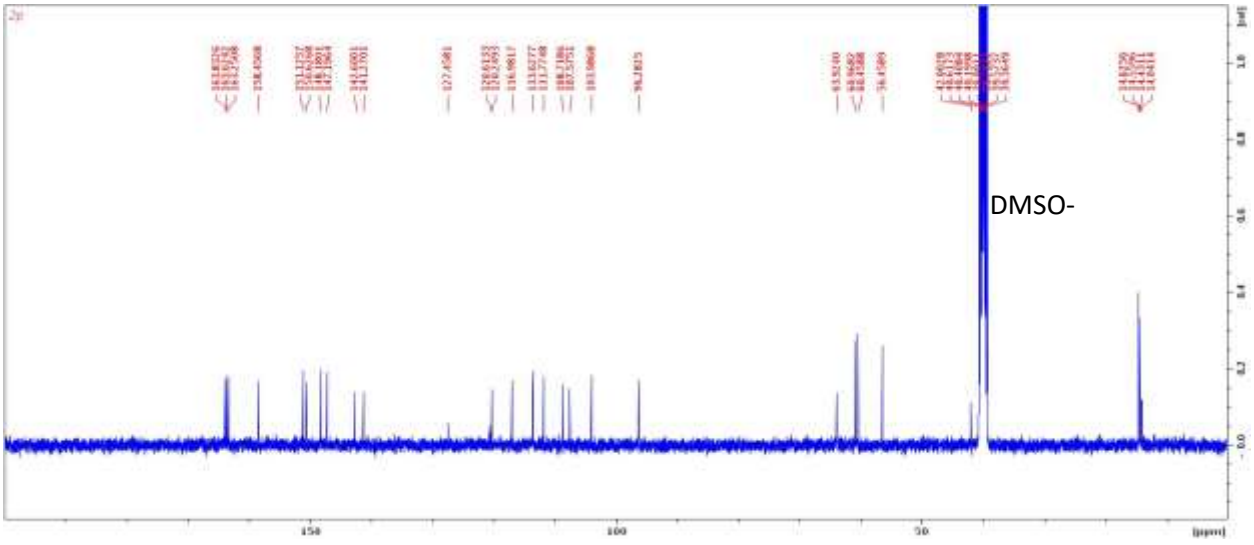
DMSO-
ppm

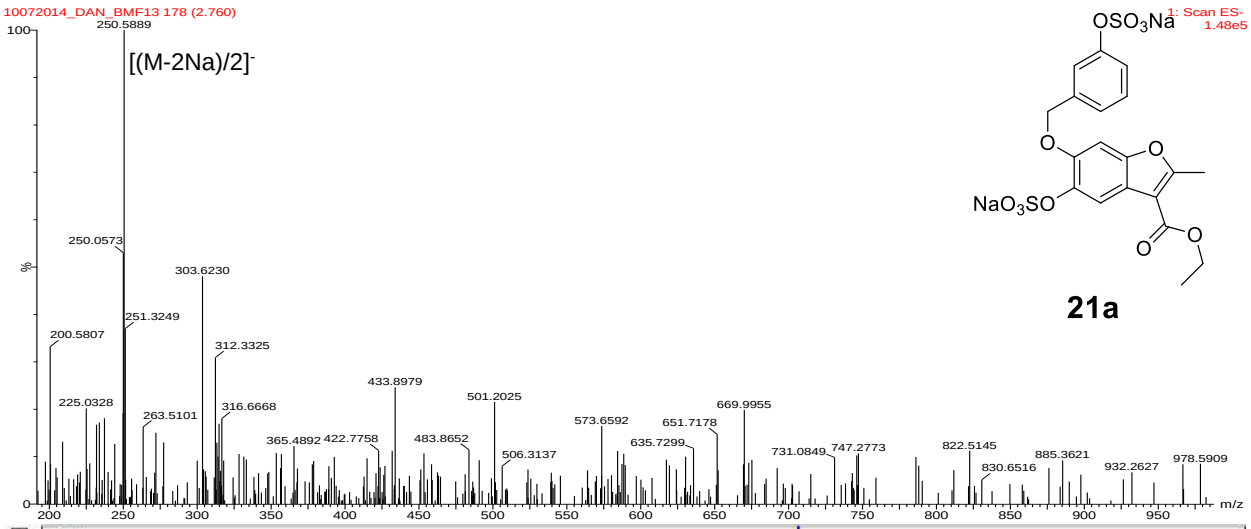
10072014_DAN_BMF13 178 (2.760)
1: Scan ES-
1.48e5
[(M-2Na)/2]-
250.5889
250.0573
303.6230
251.3249
200.5807
312.3325
225.0328
433.8979
501.2025
263.5101
316.6668
573.6592
669.9955
651.7178
365.4892
422.7758
483.8652
635.7299
506.3137
731.0849
747.2773
822.5145
885.3621
830.6516
932.2627
978.5909
%
m/z
OSO3Na
NaO3SO
21a

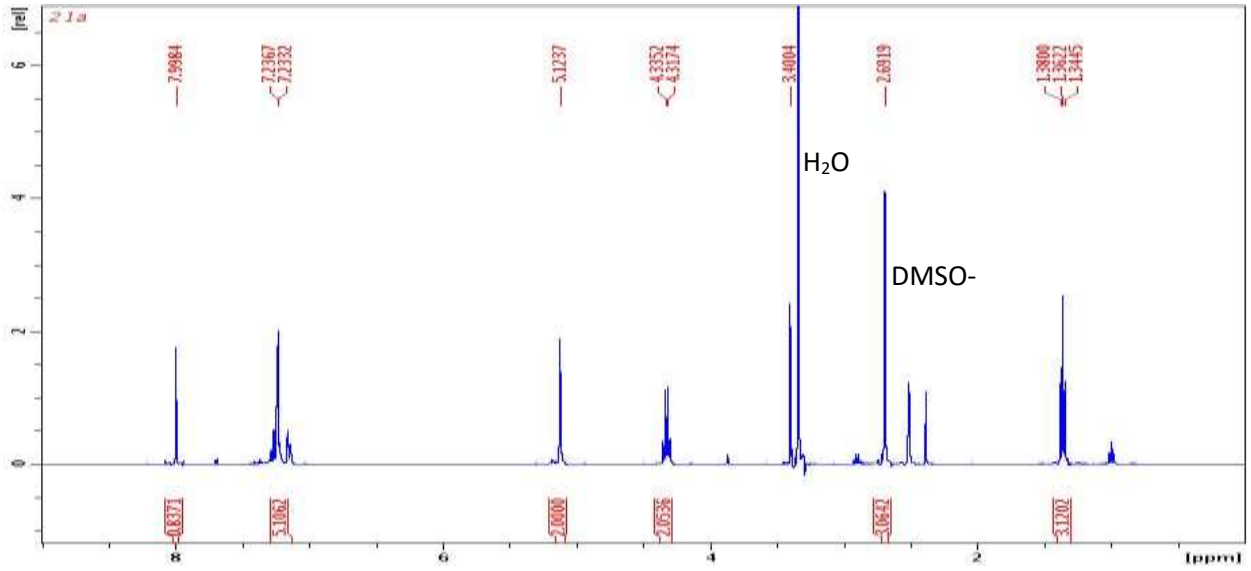
21a
H2O
DMSO-
[ppm]

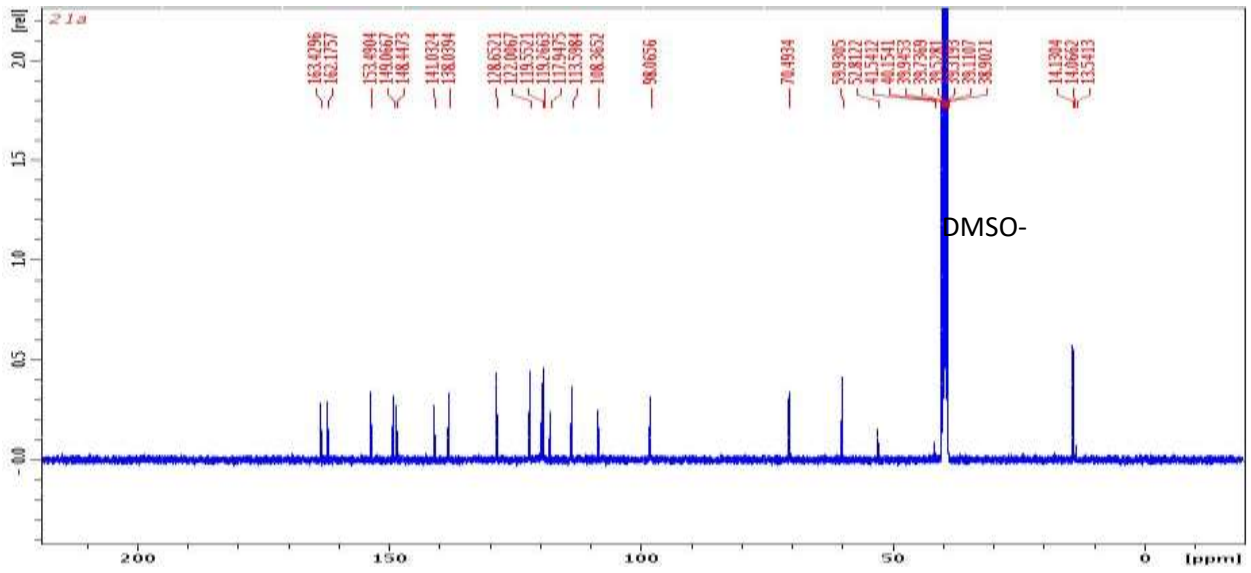
21a
DMSO-
[ppm]

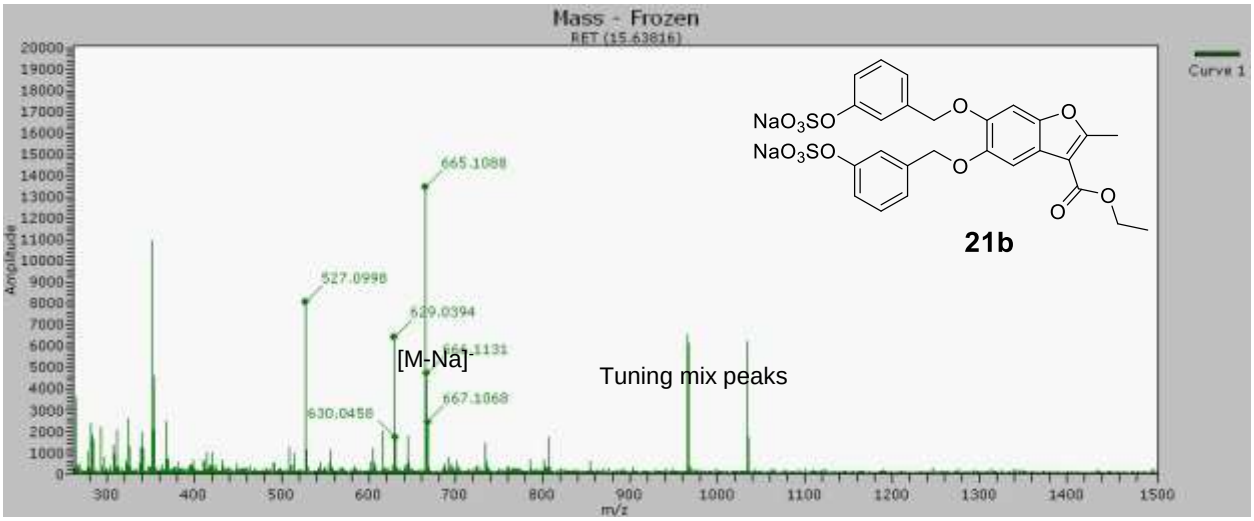
Mass - Frozen
RET (15.63816)
Curve 1
Amplitude
m/z
665.1088
527.0998
629.0394
[M-Na]
667.1068
630.0458
Tuning mix peaks
NaO3SO
NaO3SO
21b

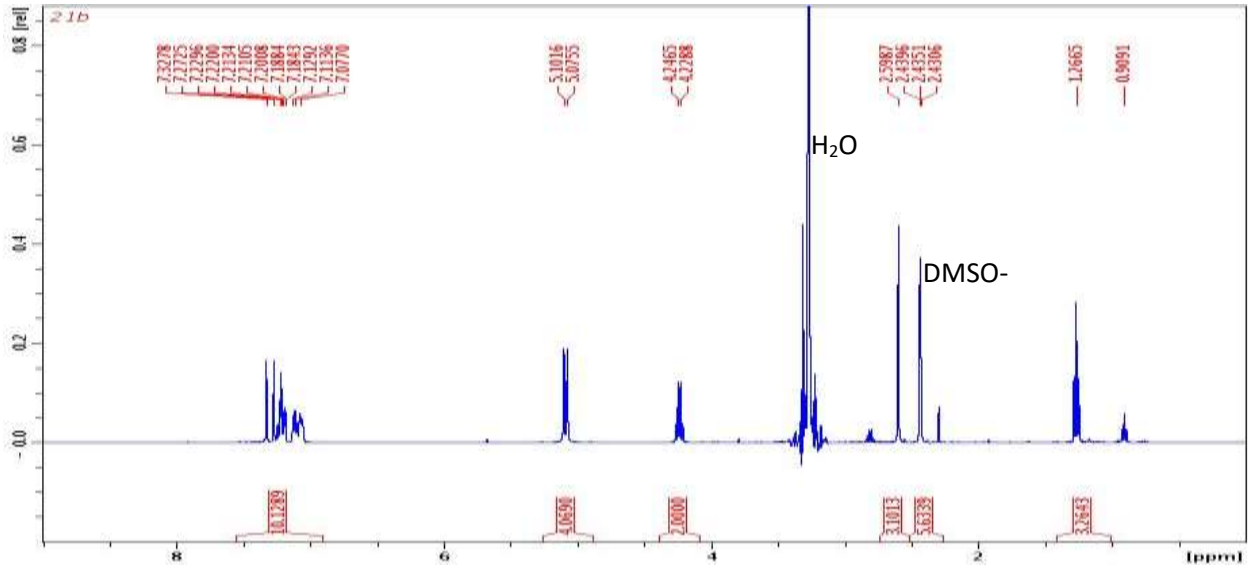
21b
H2O
DMSO-
ppm

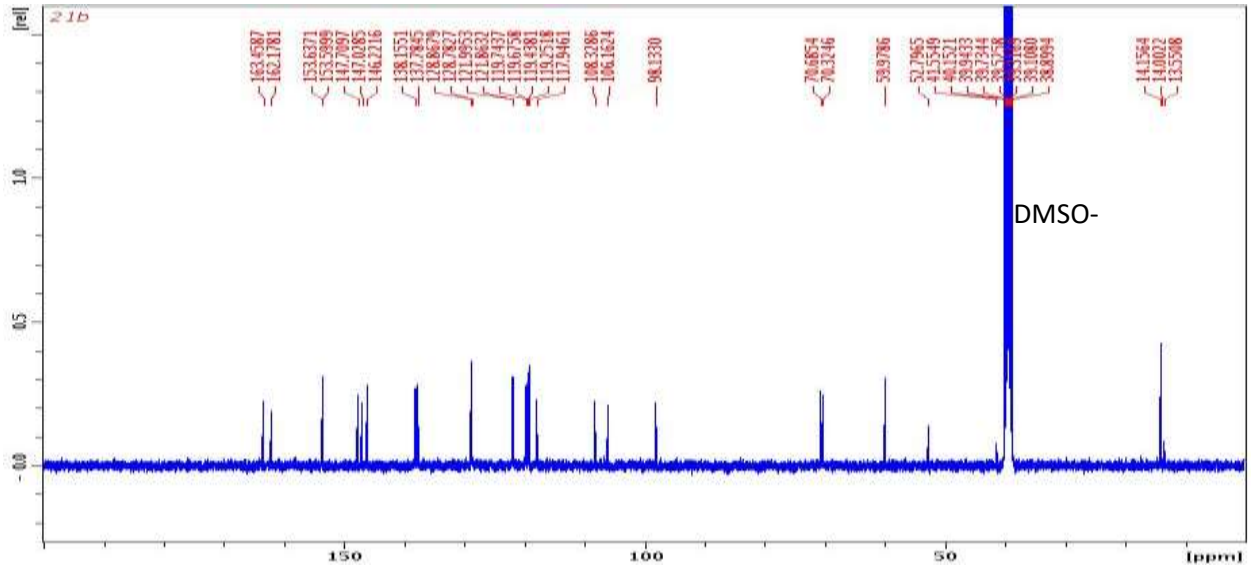
21b
DMSO-
ppm

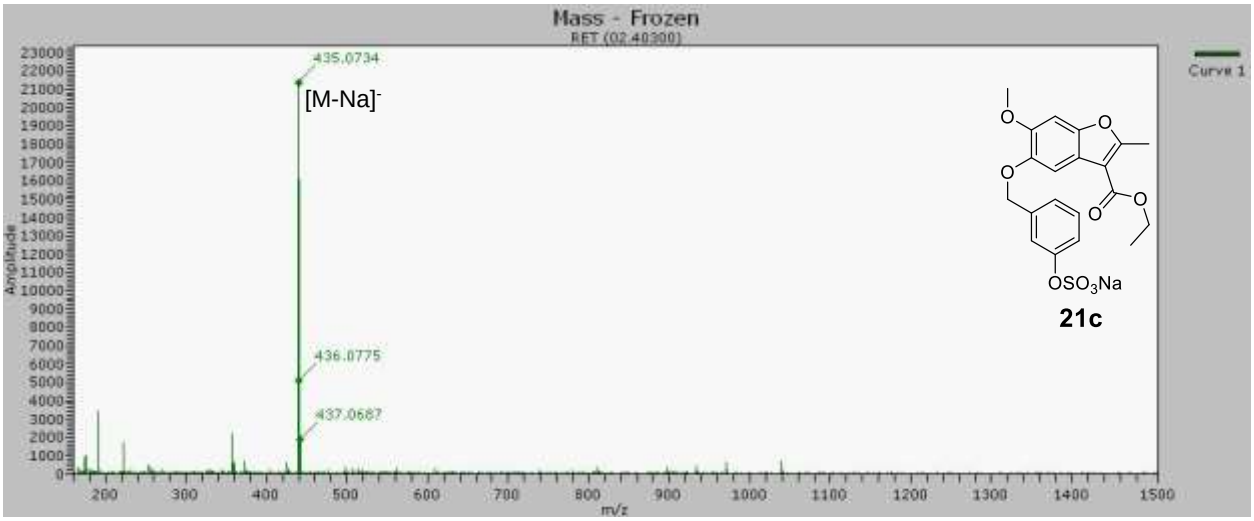
Mass - Frozen
RET (02.40300)
435.0734
[M-Na]-
436.0775
437.0687
Curve 1
Amplitude
m/z
OSO3Na
21c

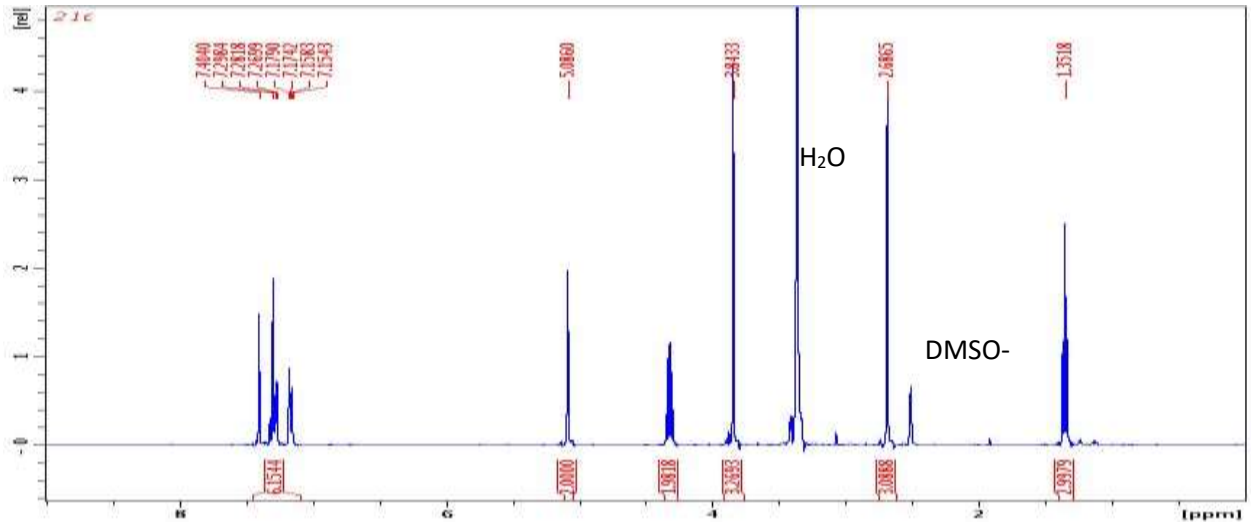
21c
H2O
DMSO-
[ppm]

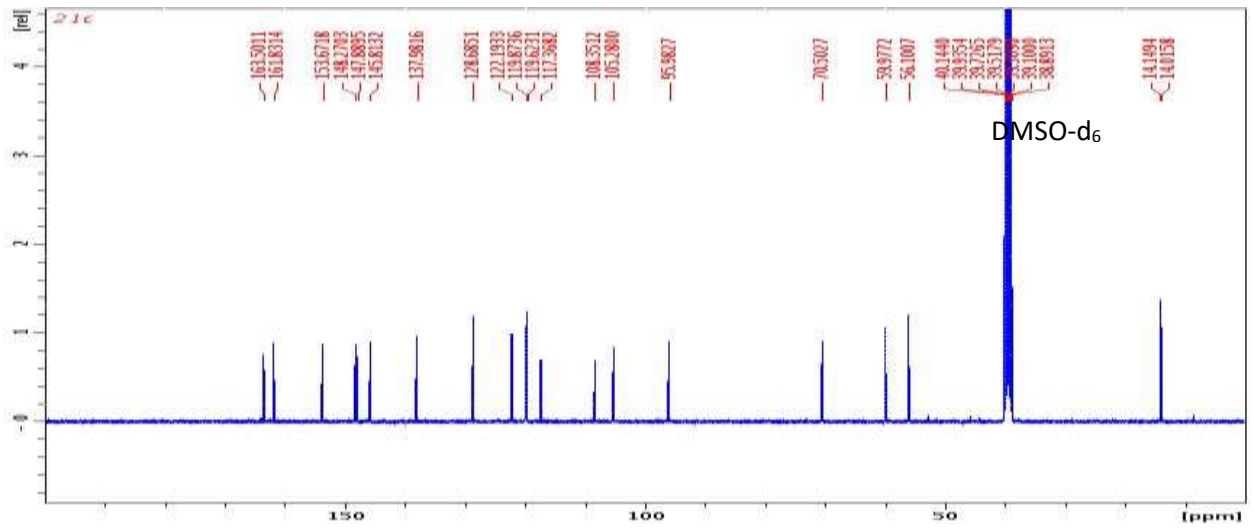
21c
DMSO-d6
[ppm]

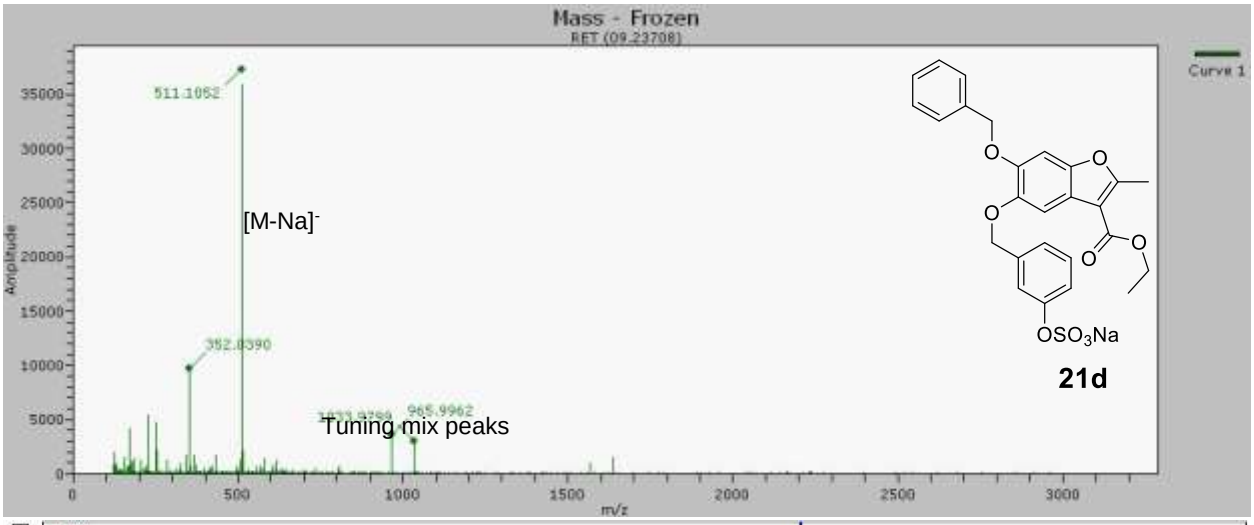
Mass - Frozen
RET (09.23708)
Curve 1
511.1052
[M-Na]-
382.0390
965.9962
Tuning mix peaks
Amplitude
m/z
OSO3Na
21d

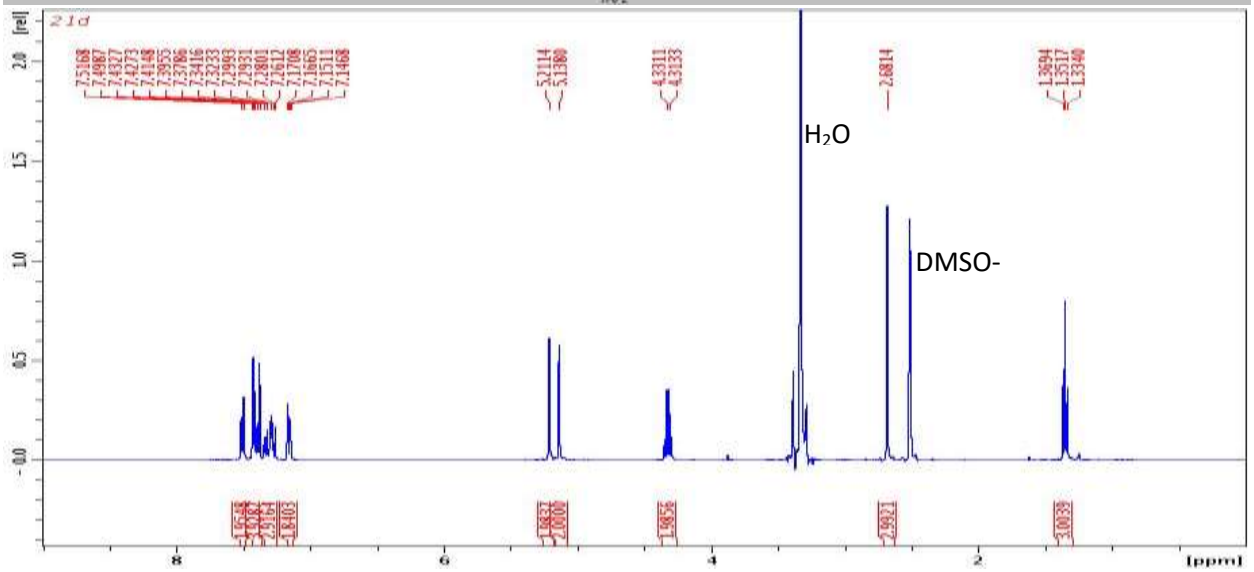
H2O
DMSO-
[ppm]

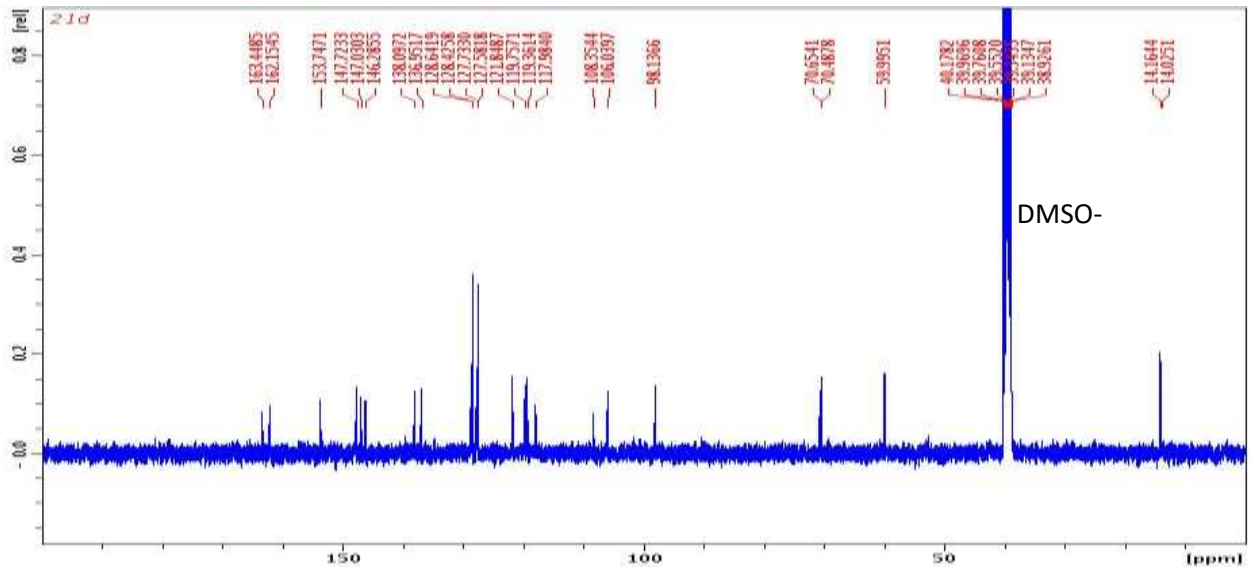
DMSO-
[ppm]

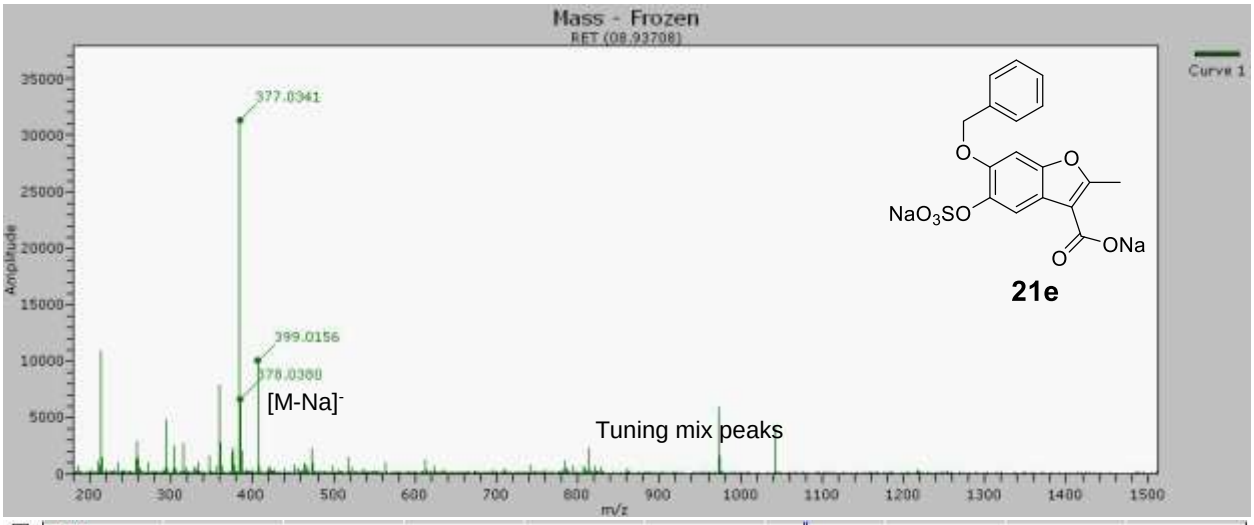
Mass - Frozen
RET (08.93708)
Curve 1
Amplitude
m/z
377.0341
399.0156
378.0380
[M-Na]-
Tuning mix peaks
NaO3SO
ONa
21e

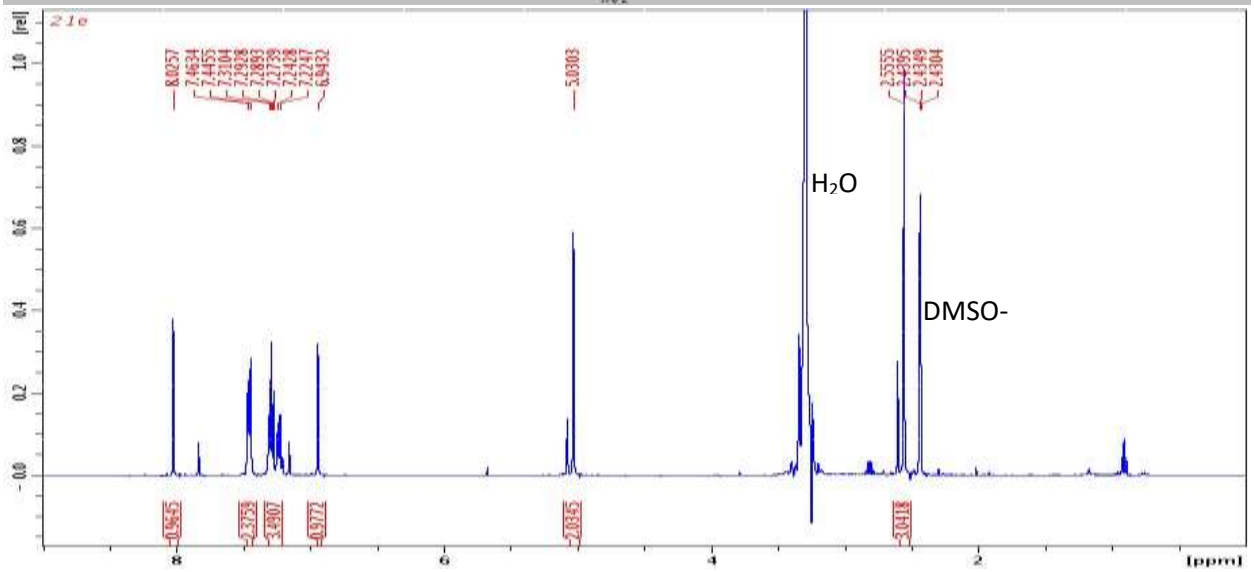
21e
[rel]
H2O
DMSO-
[ppm]

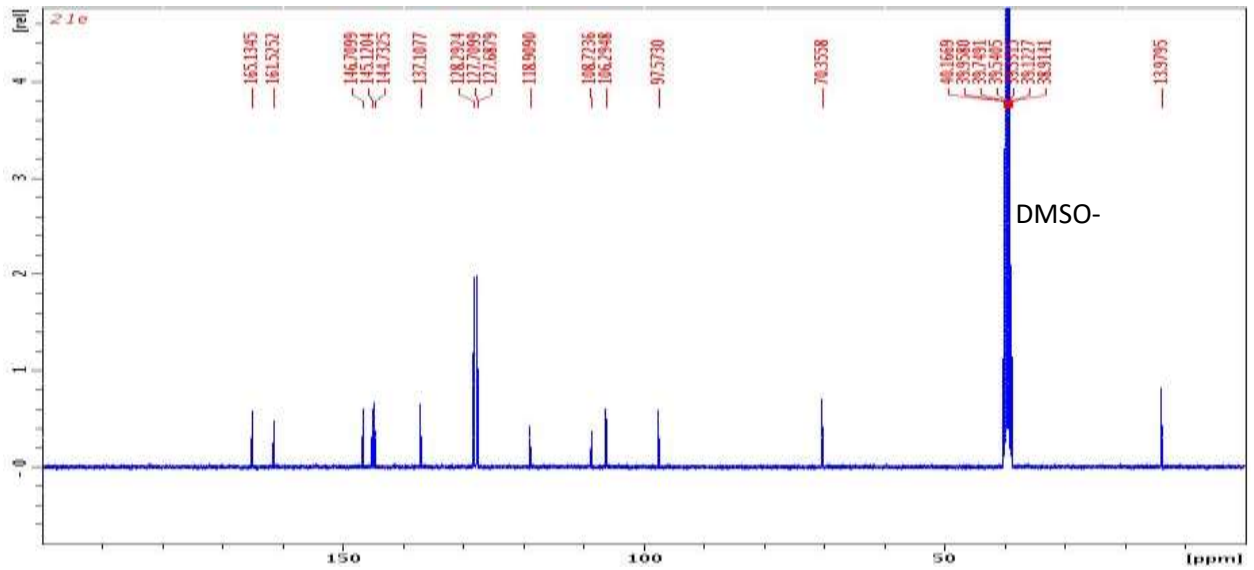
21e
[rel]
DMSO-
[ppm]

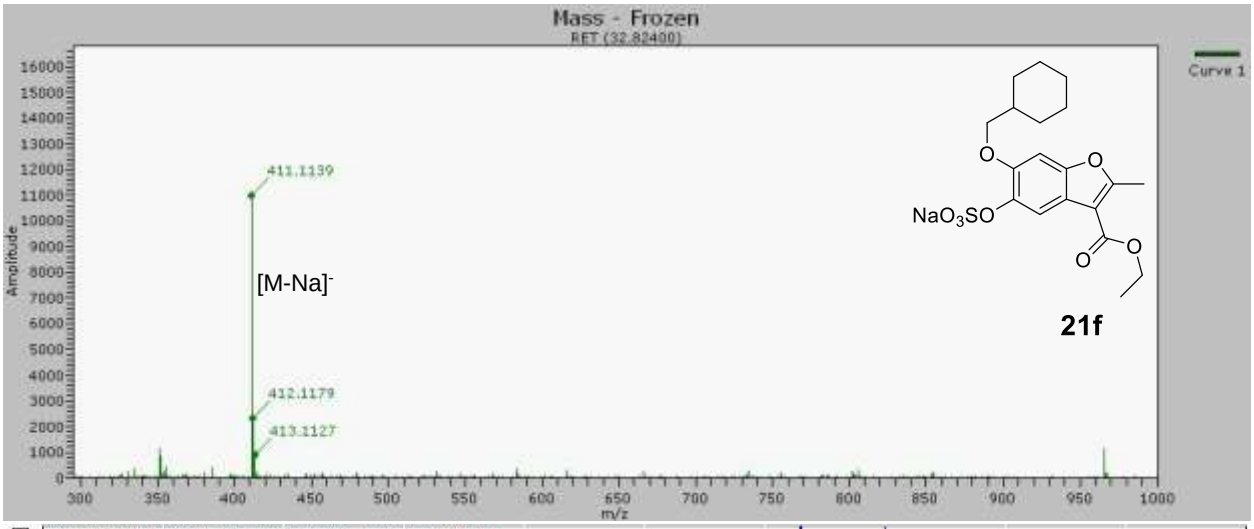
Mass - Frozen
RET (32.82400)
Curve 1
Amplitude
m/z
411.1139
412.1179
413.1127
[M-Na]-
NaO3SO
21f

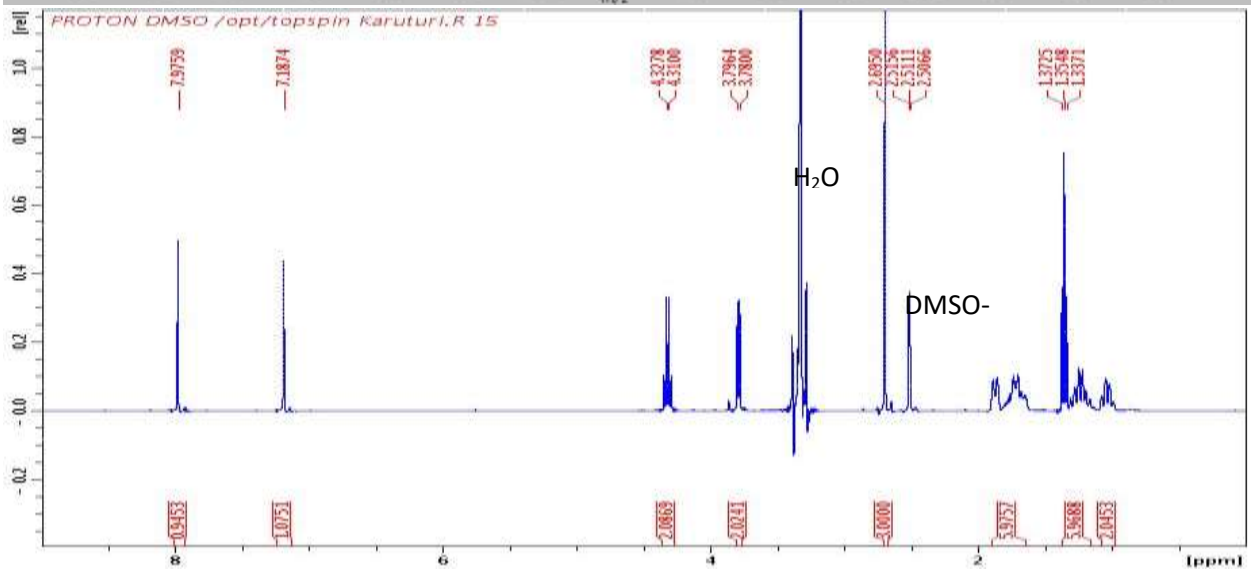
PROTON DMSO /opt/topspin Karuturi.R 15
H2O
DMSO-
[ppm]

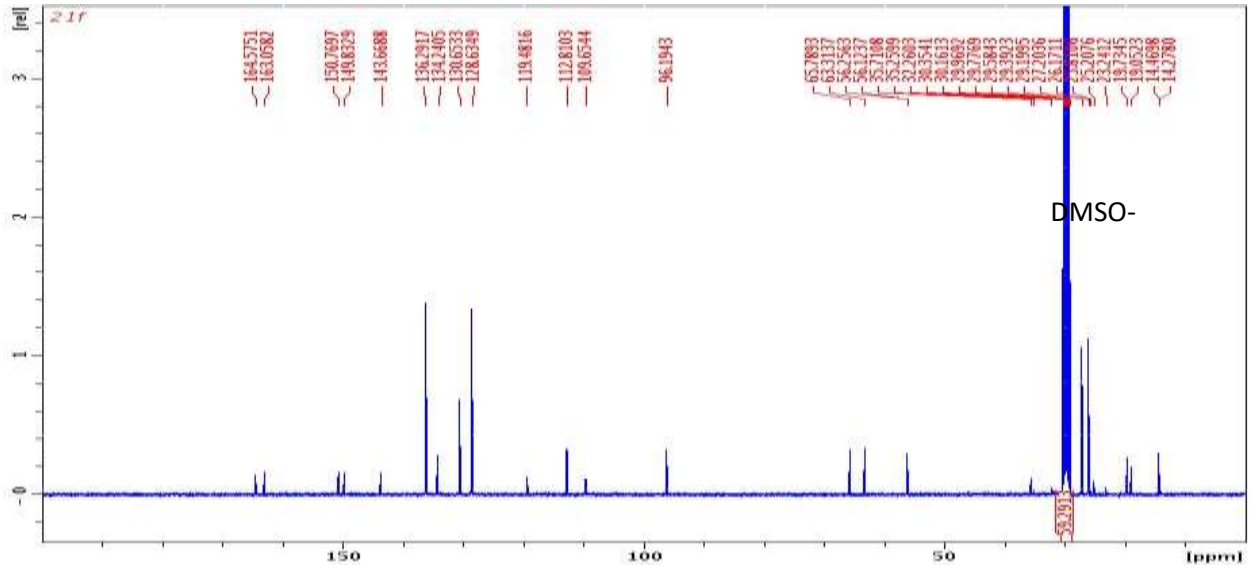
21f
DMSO-
[ppm]

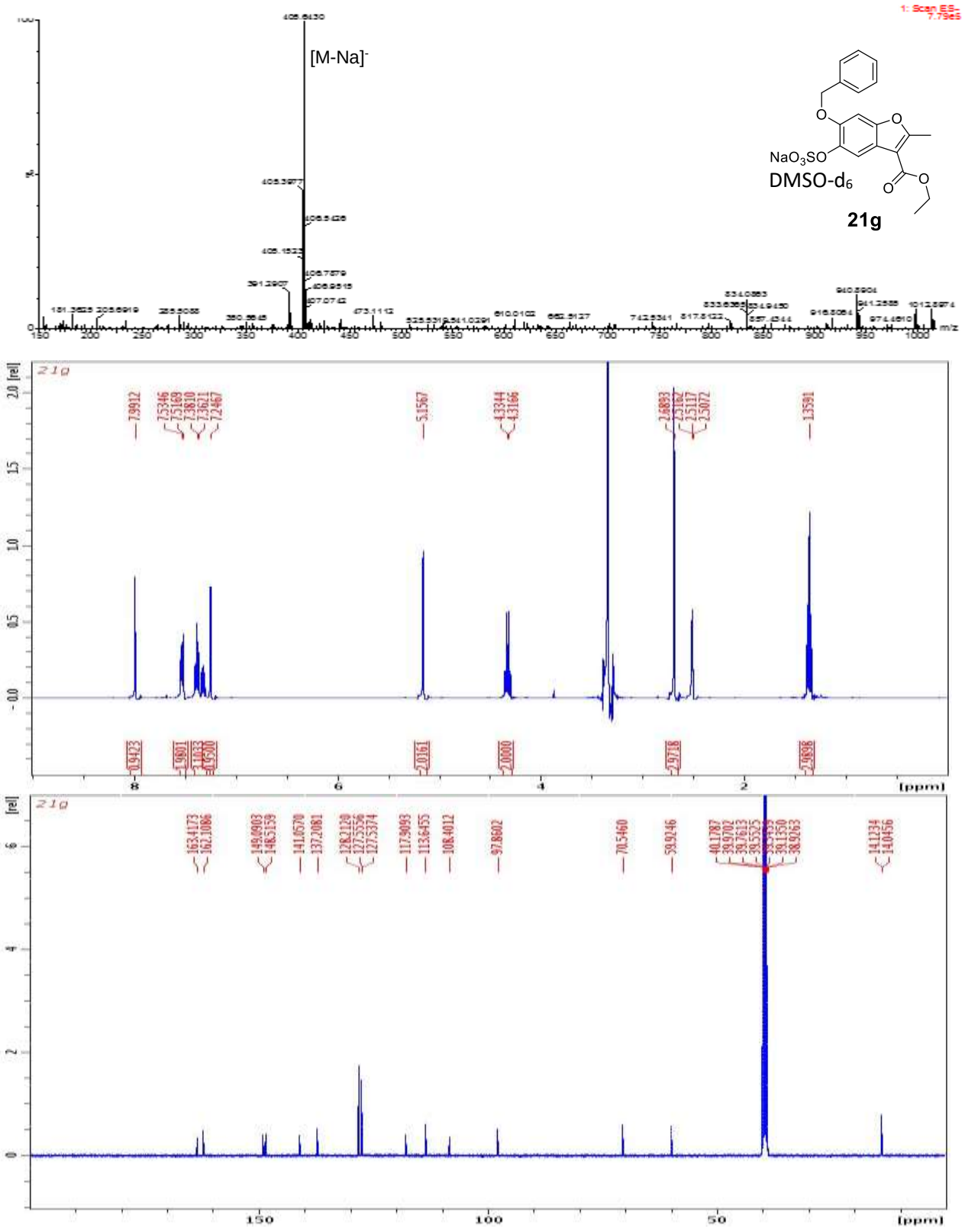
[M-Na]-
NaO3SO
DMSO-d6
21g
ppm

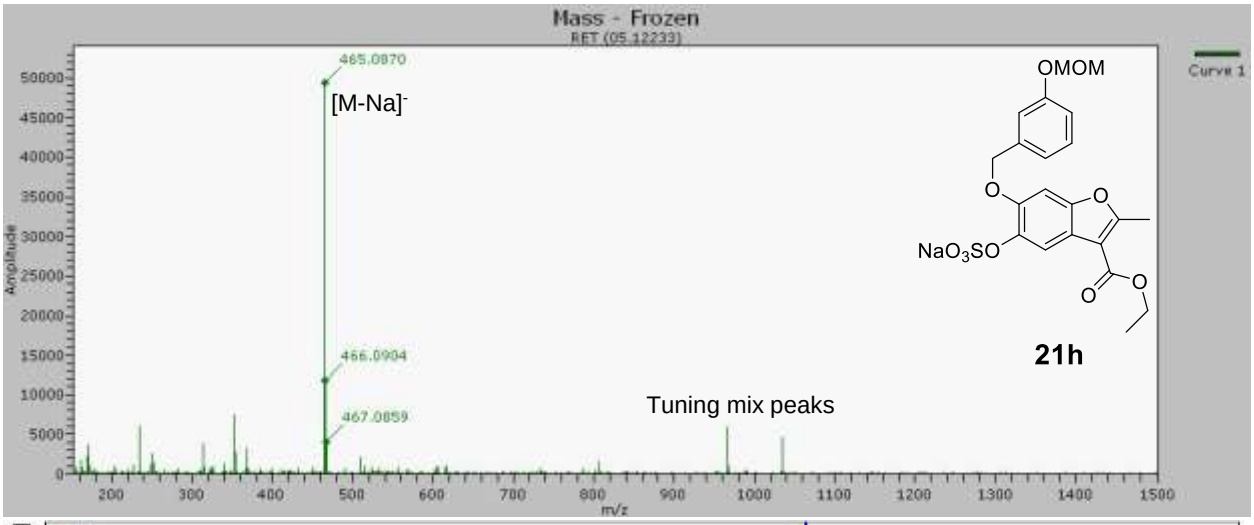
Mass - Frozen
RET (05.12233)
Curve 1
Abundance
m/z
465.0870
[M-Na]-
466.0904
467.0859
Tuning mix peaks
OMOM
NaO3SO
21h

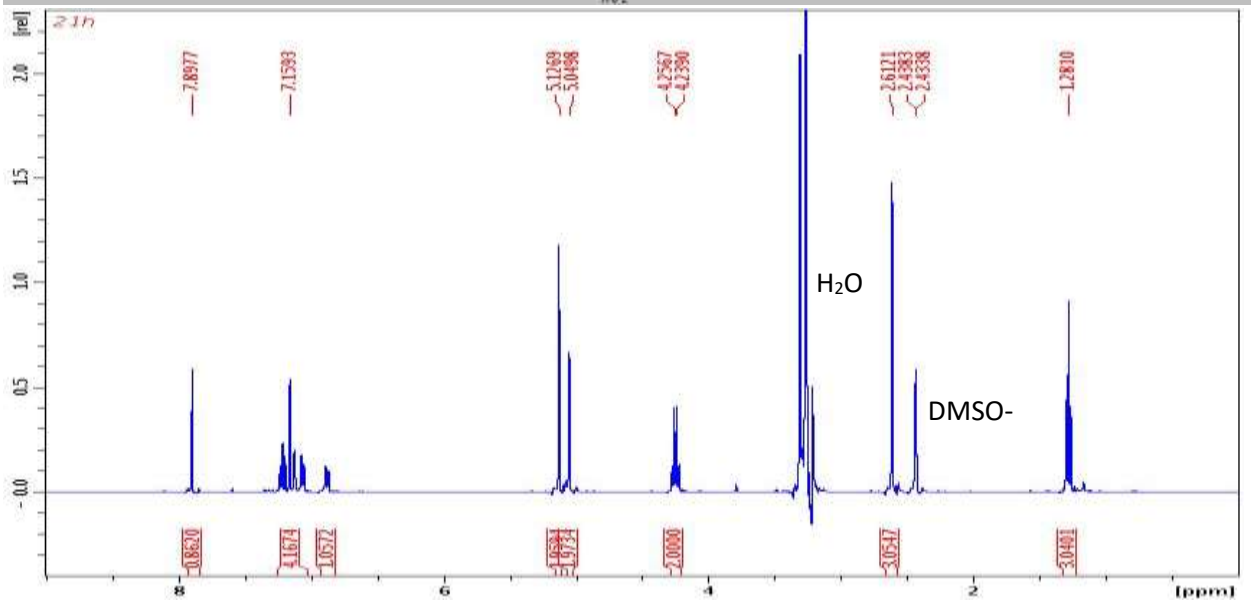
21h
H2O
DMSO-
[ppm]

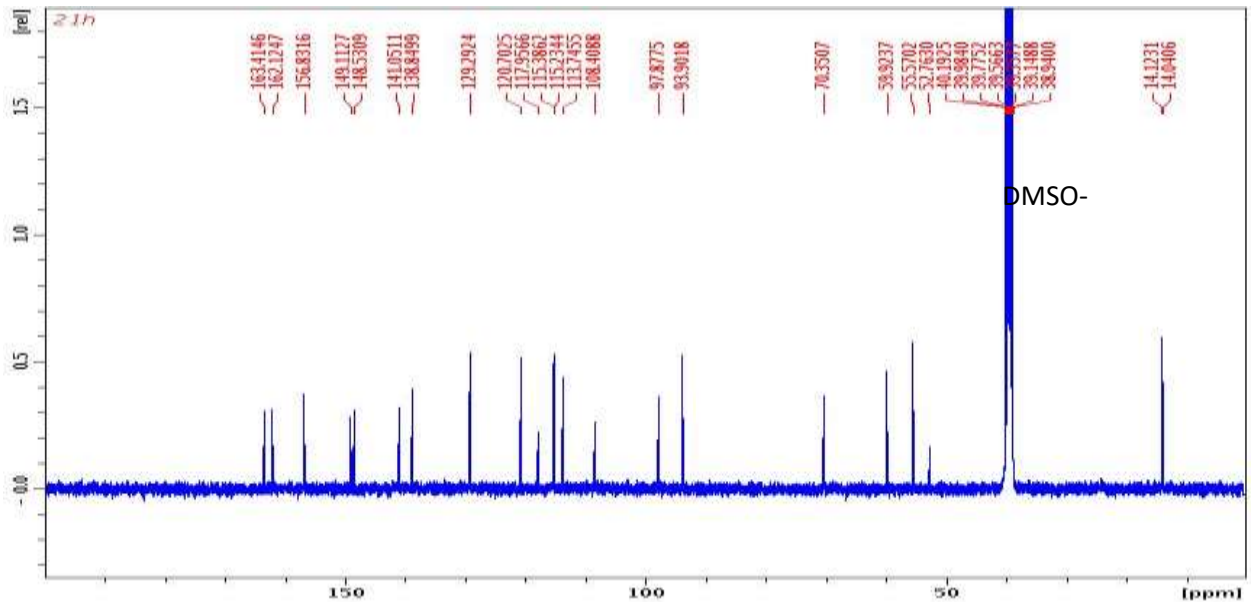
21h
DMSO-
[ppm]

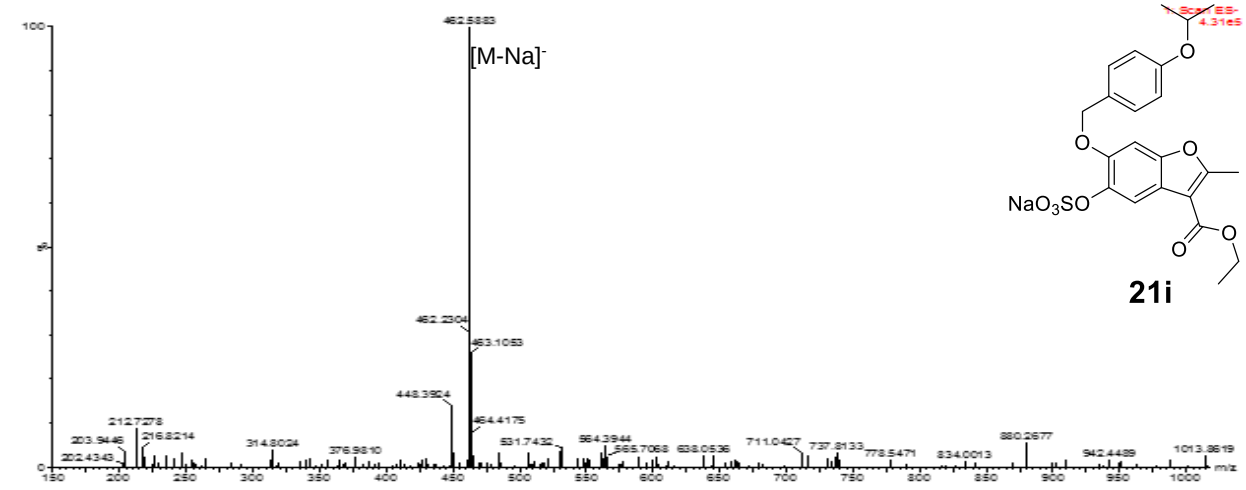
462.5883
[M-Na]-
462.2304
463.1053
448.3904
464.4175
212.7278
216.8214
203.9446
202.4343
314.8024
376.9810
531.7432
564.3944
565.7068
638.0536
711.0427
737.8133
778.5471
834.0013
880.2677
942.4489
1013.8619
m/z
NaO3SO
21i

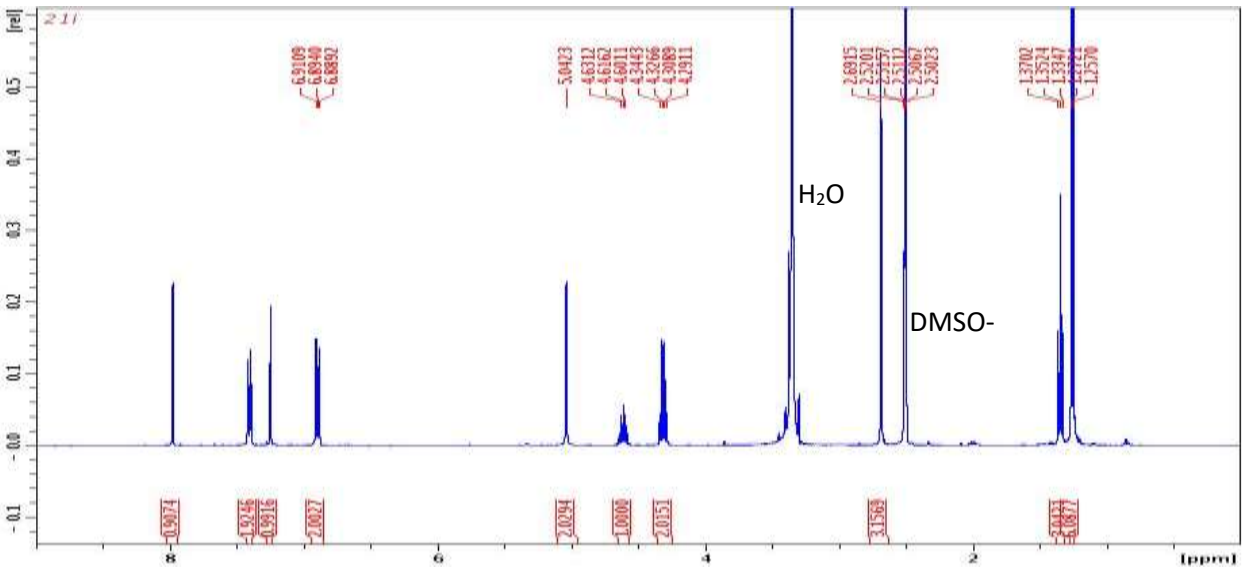
21i
[rel]
H2O
DMSO-
[ppm]

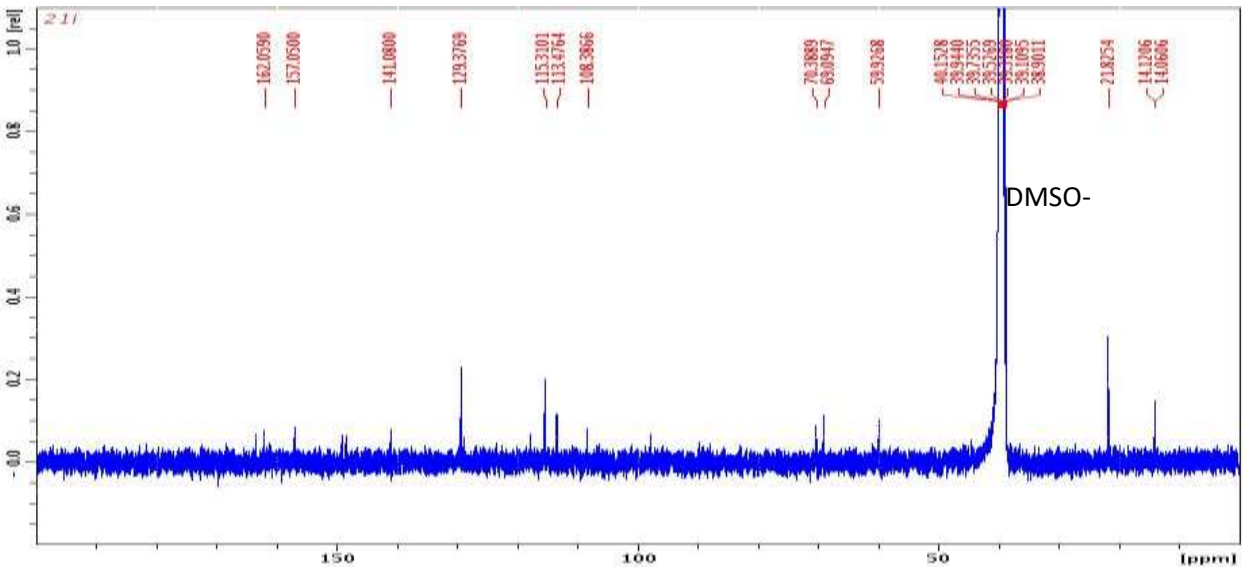
21i
[rel]
162.0590
157.0500
141.0800
129.3765
115.3301
113.4764
108.3866
70.3889
63.0947
58.9268
46.1528
39.9440
39.7555
39.5669
39.3783
39.1897
38.9011
21.8254
14.1206
14.0666
DMSO-
[ppm]

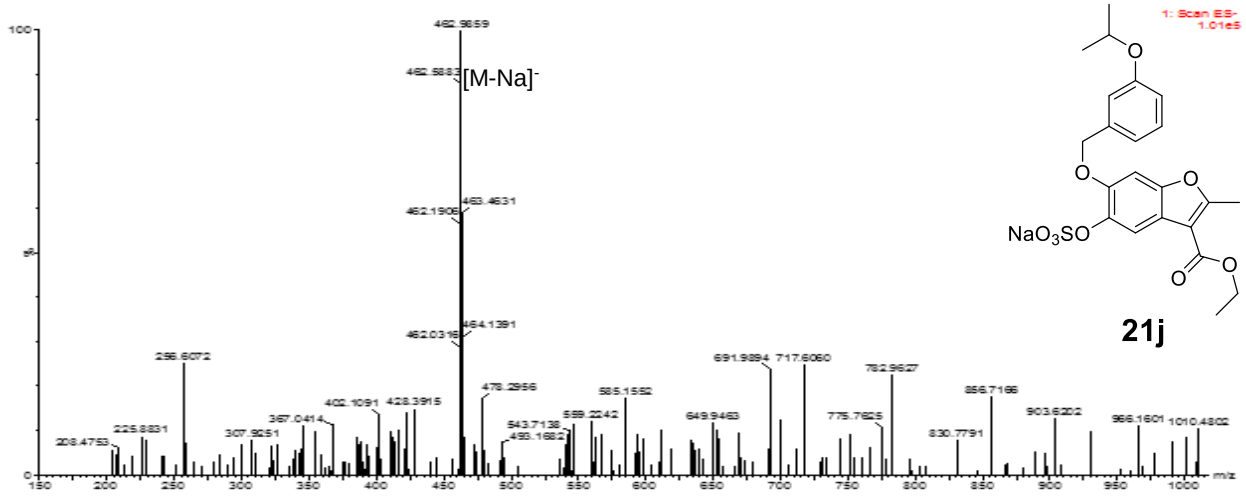
[M-Na]-
NaO3SO
21j

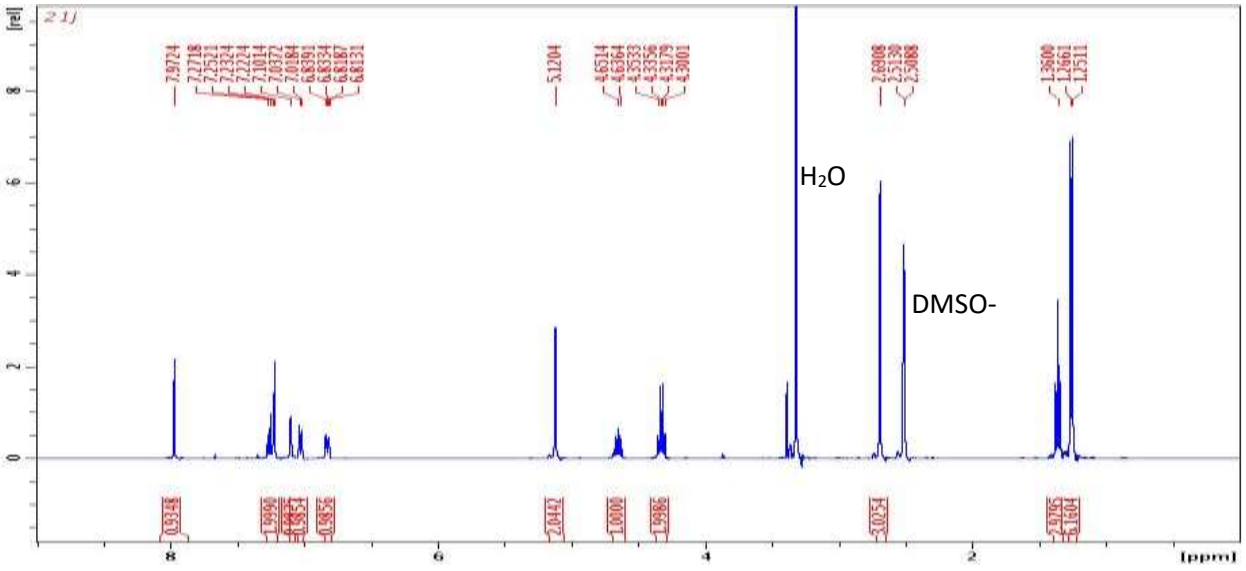
H2O
DMSO-

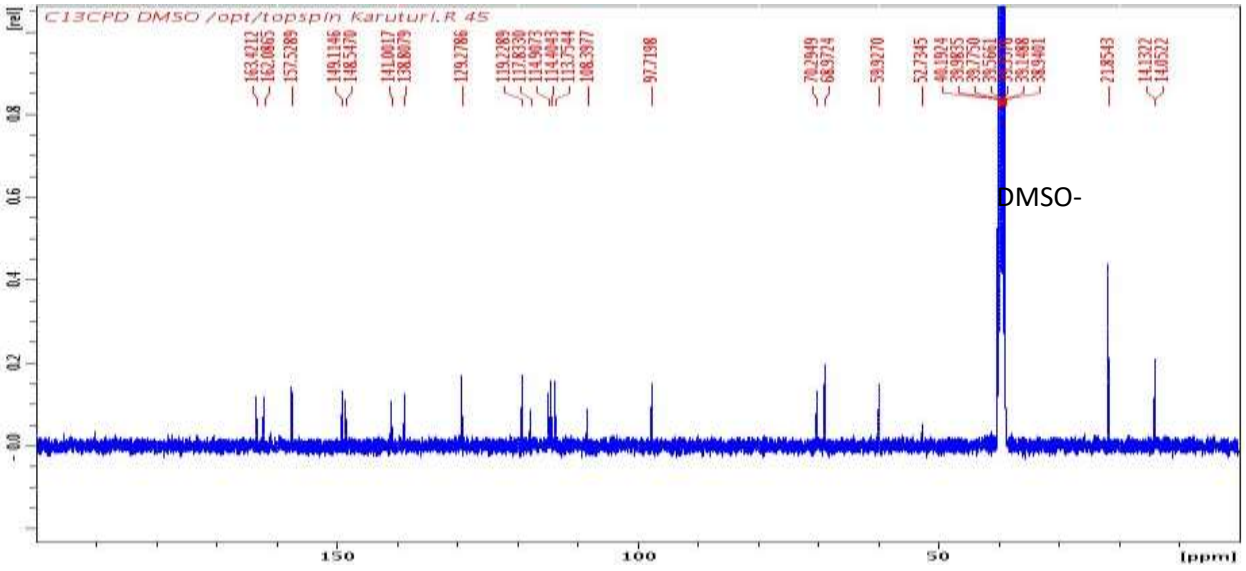
DMSO-

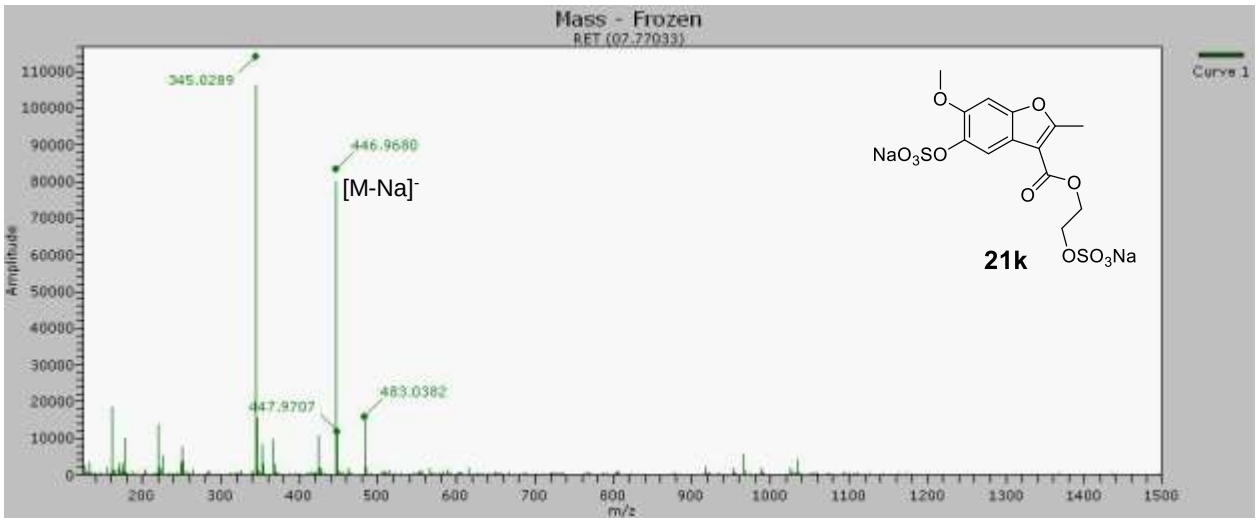
Mass - Frozen
RET (07.77033)
Curve 1
345.0289
446.9680
[M-Na]-
447.9707
483.0382
Amplitude
m/z
NaO3SO
O
O
O
O
OSO3Na
21k

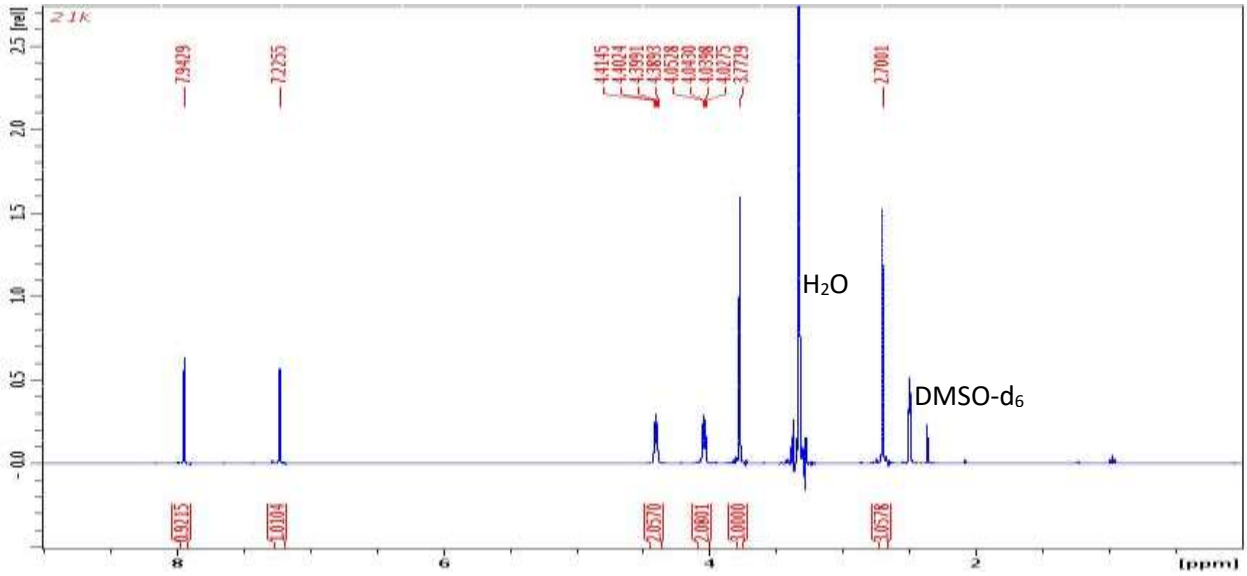
21K
H2O
DMSO-d6
[ppm]

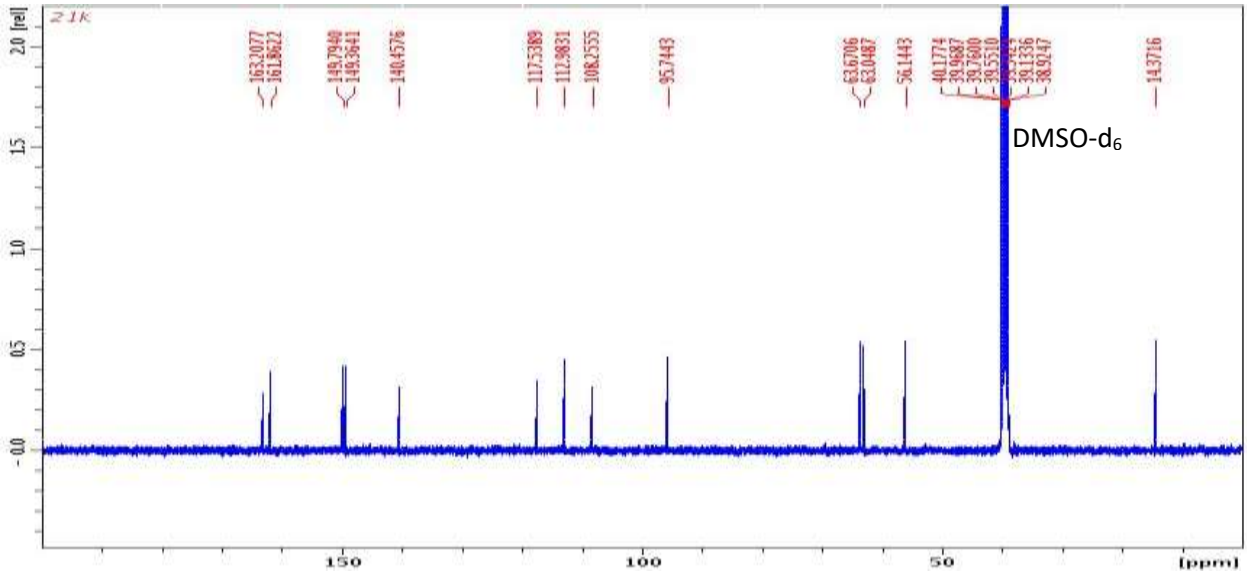
21K
DMSO-d6
[ppm]

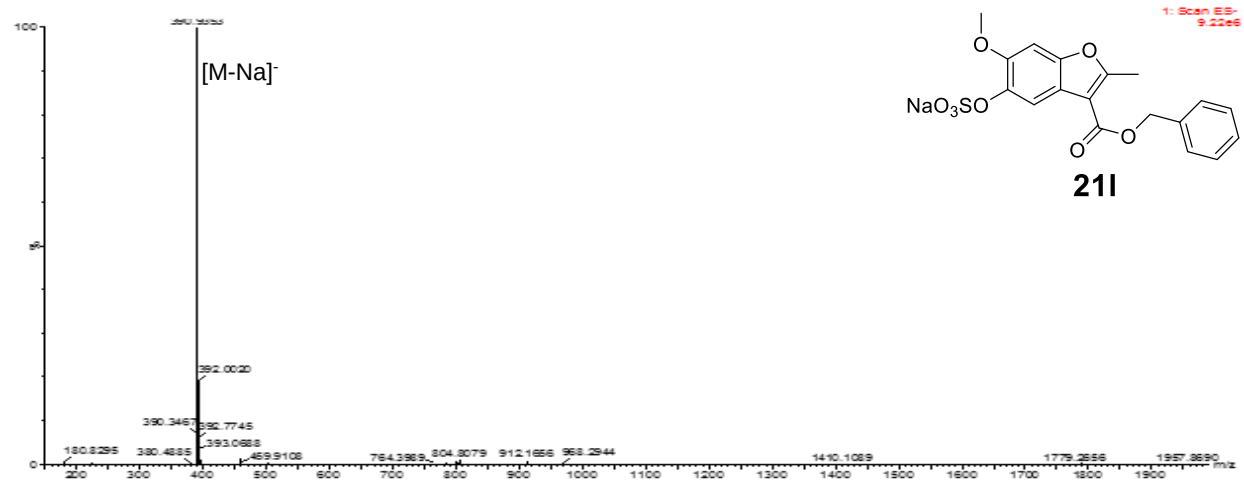

21l

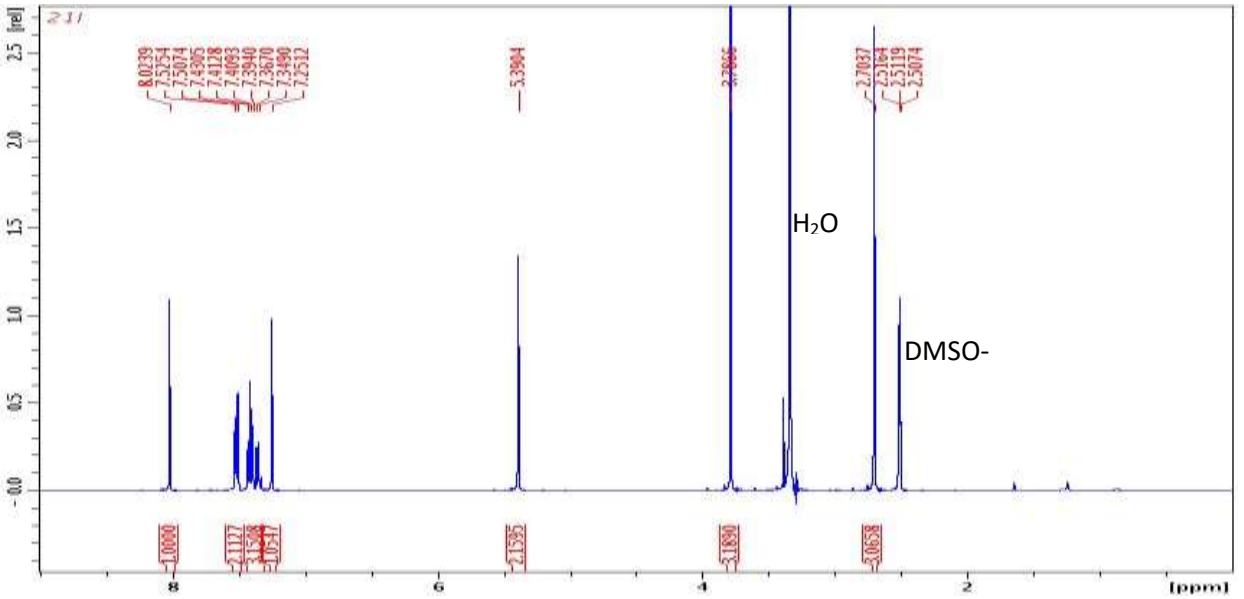

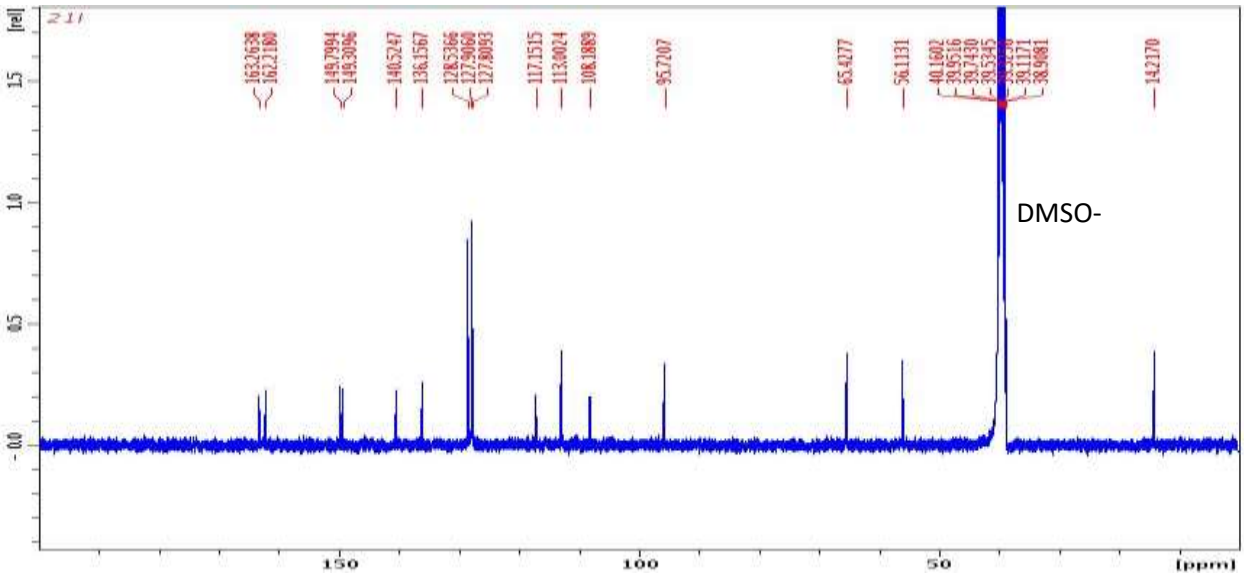

4) Spectral profiles of sulfated diflavonoids

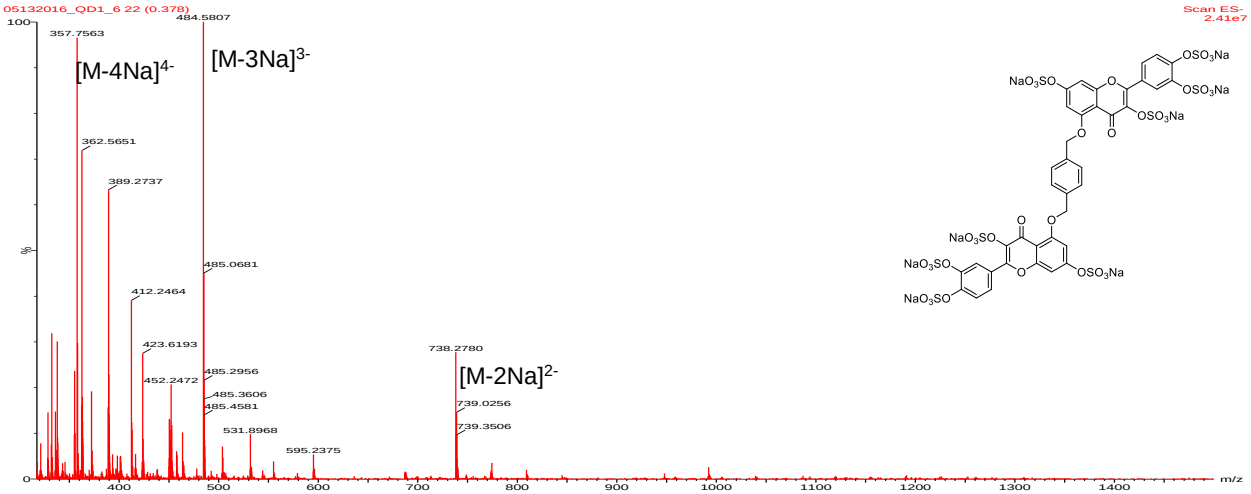

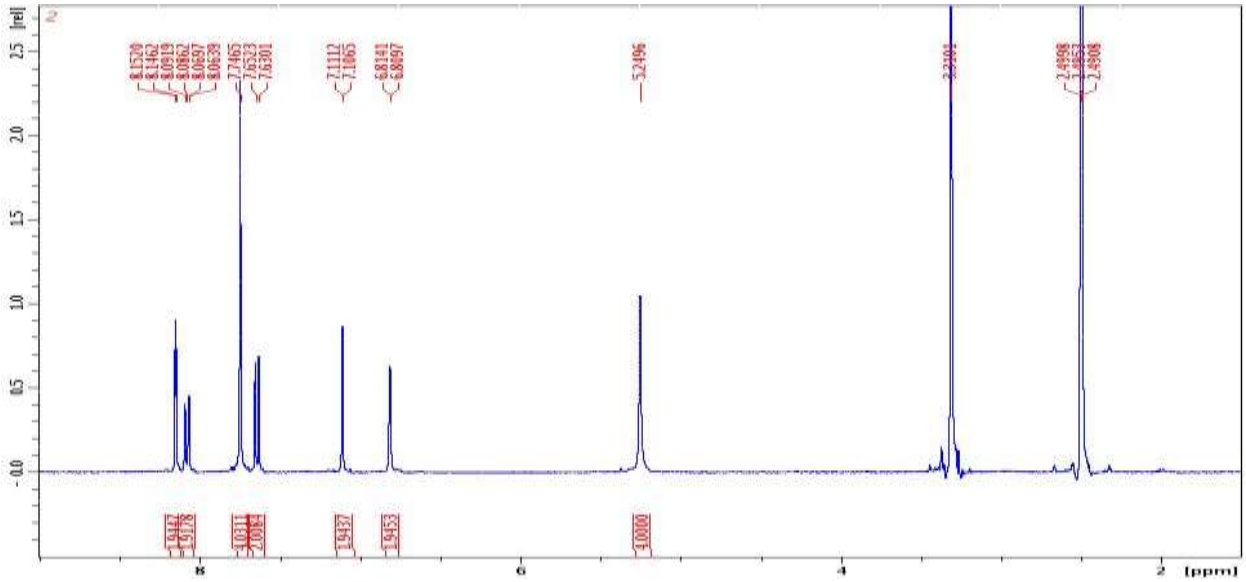

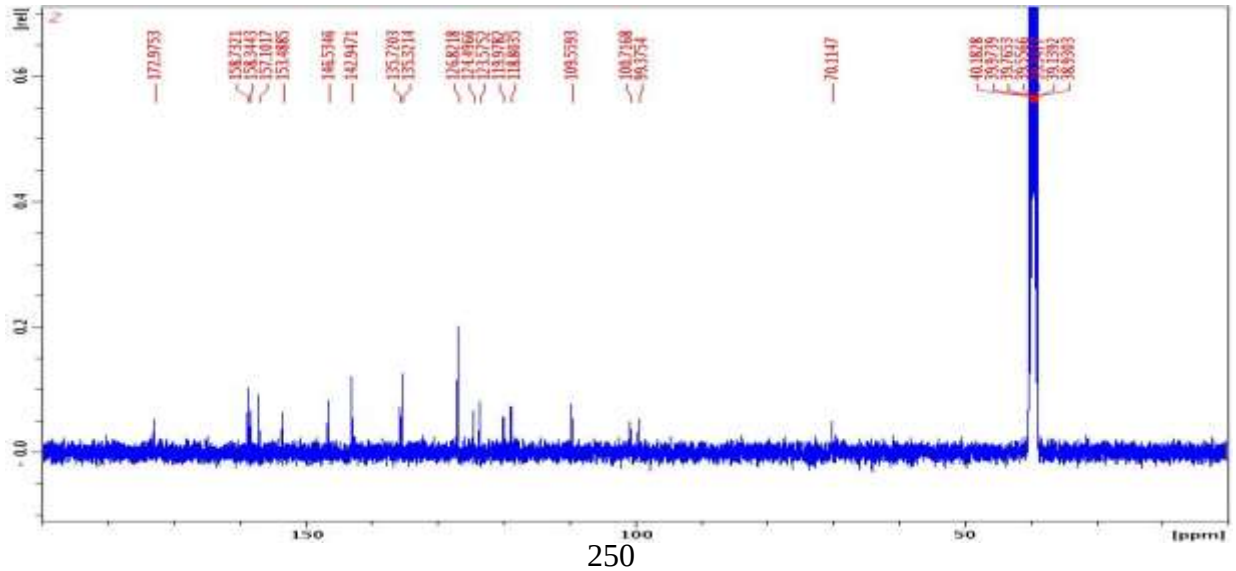


QD4_4_1 15 (0.258)
Scan ES-
8.39e6
[M-4Na]4-
[M-3Na]3-
[M-2Na]2-
NaO3SO
OSO3Na
m/z

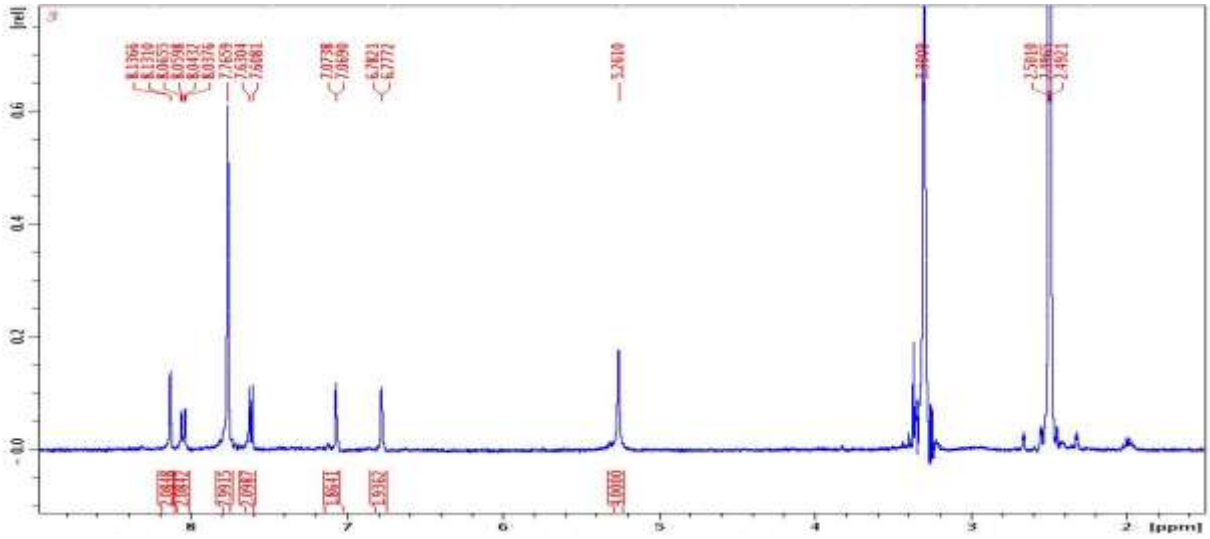
[ppm]

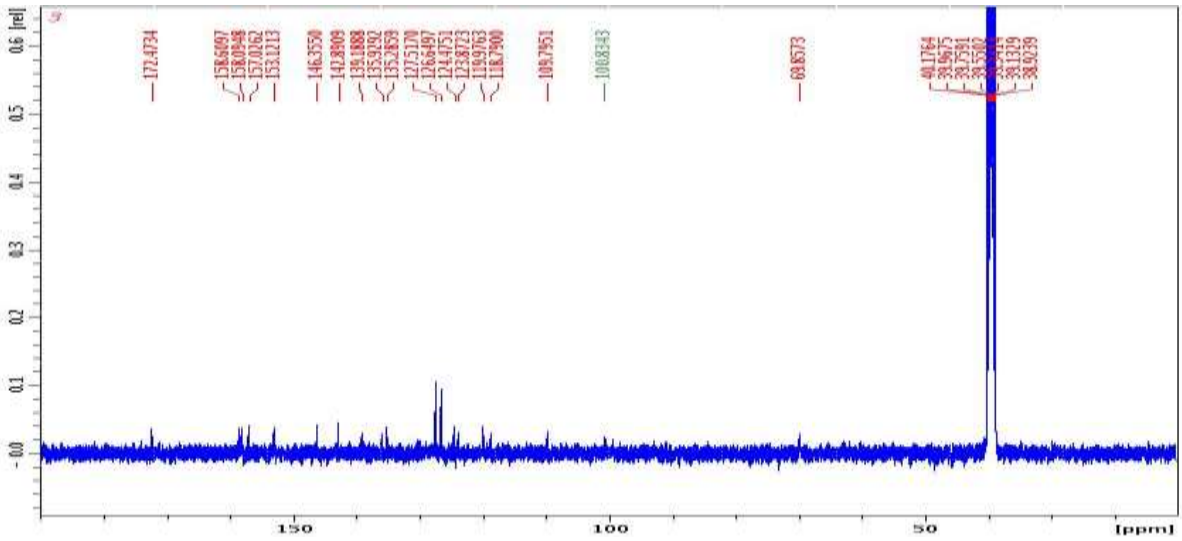
[ppm]

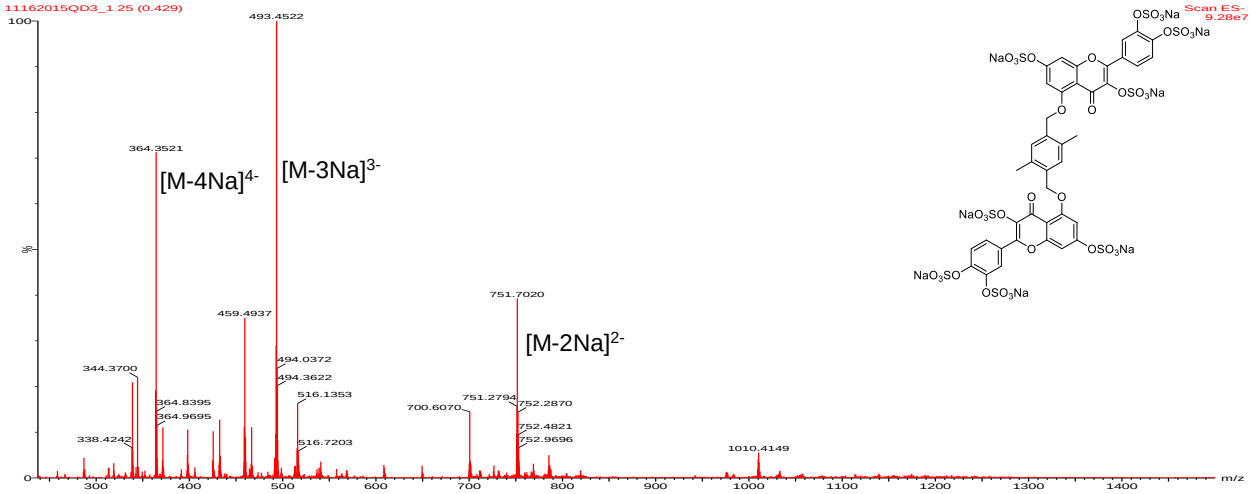
11162015QD3_1 25 (0.429)
Scan ES-
9.28e7
493.4522
364.3521
[M-4Na]4-
[M-3Na]3-
751.7020
[M-2Na]2-
459.4937
494.0372
494.3622
344.3700
516.1353
364.8395
364.9695
751.2794
752.2870
700.6070
752.4821
752.9696
338.4242
516.7203
1010.4149
m/z

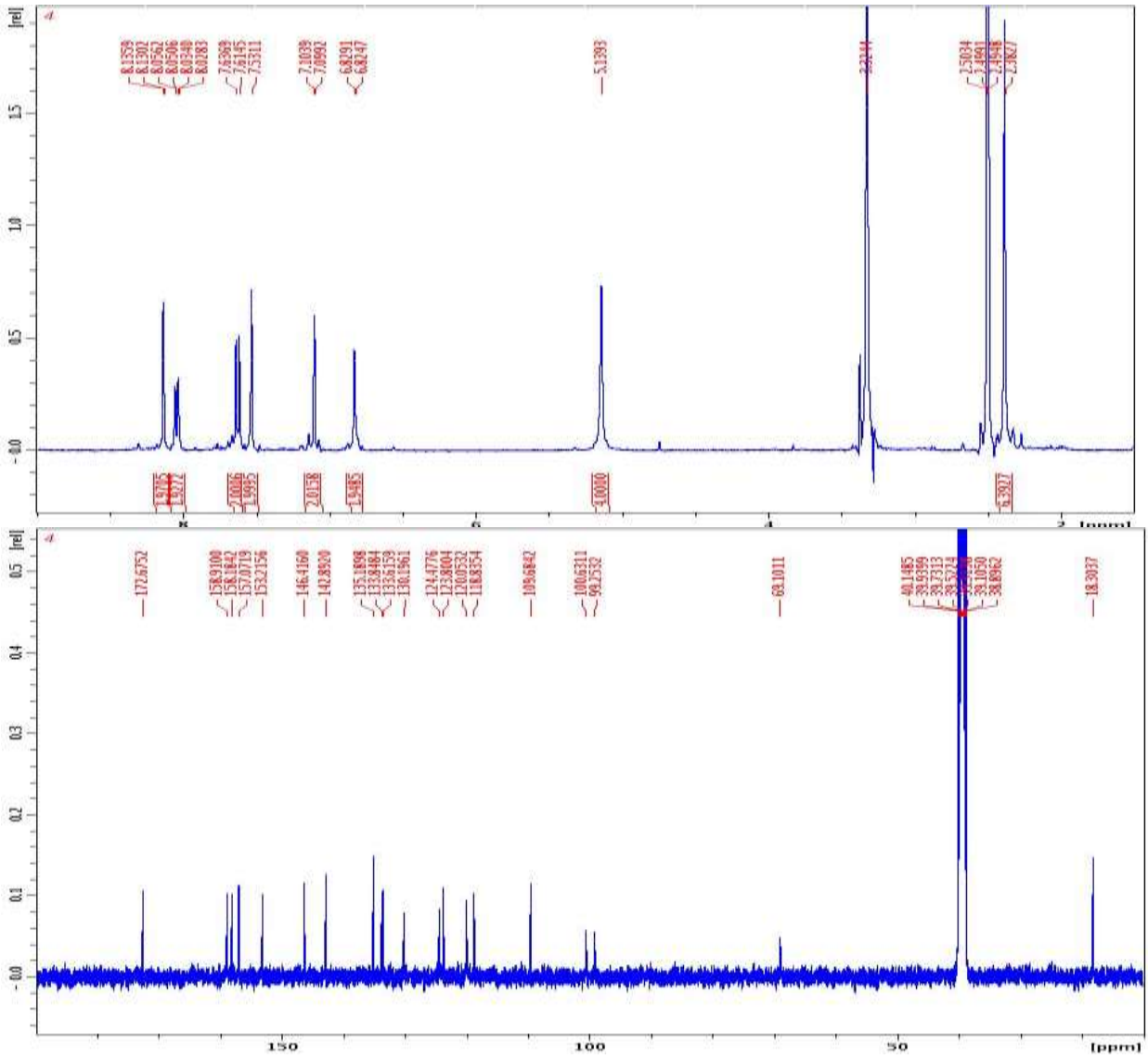

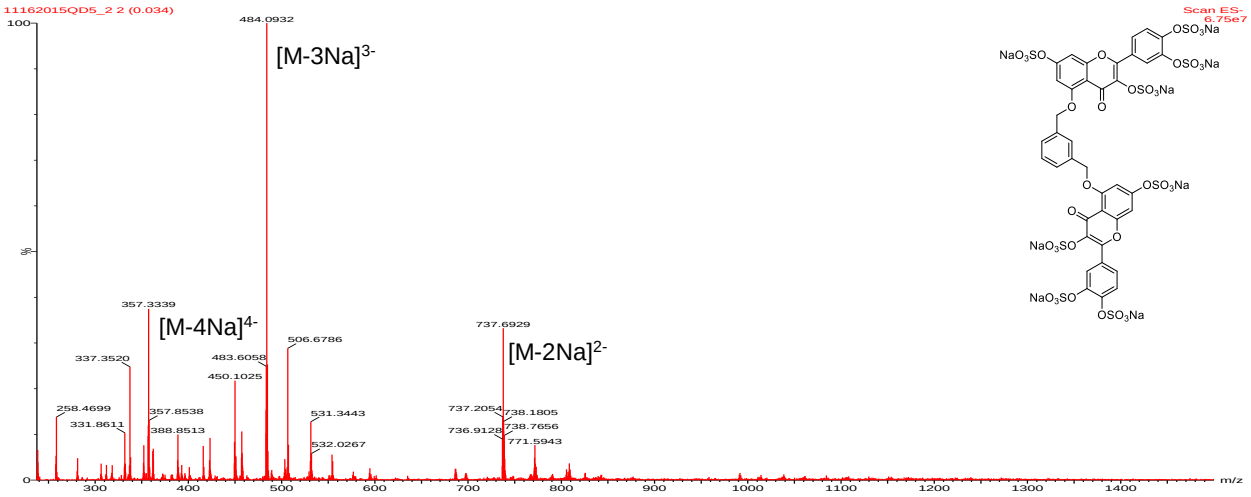
11162015QD5_2 2 (0.034)
Scan ES-
6.75e7
484.0932
[M-3Na]3-
357.3339
[M-4Na]4-
737.6929
[M-2Na]2-
506.6786
483.6058
450.1025
337.3520
258.4699
331.8611
357.8538
388.8513
531.3443
532.0267
737.2054
738.1805
736.9128
738.7656
771.5943
NaO3SO
OSO3Na
m/z

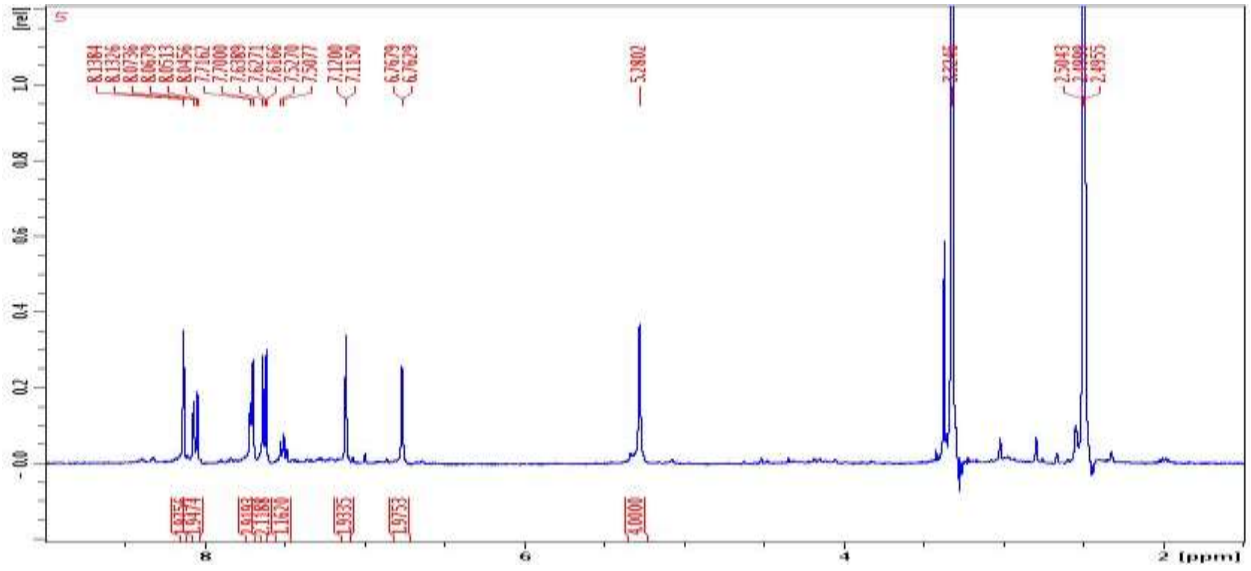
[ppm]

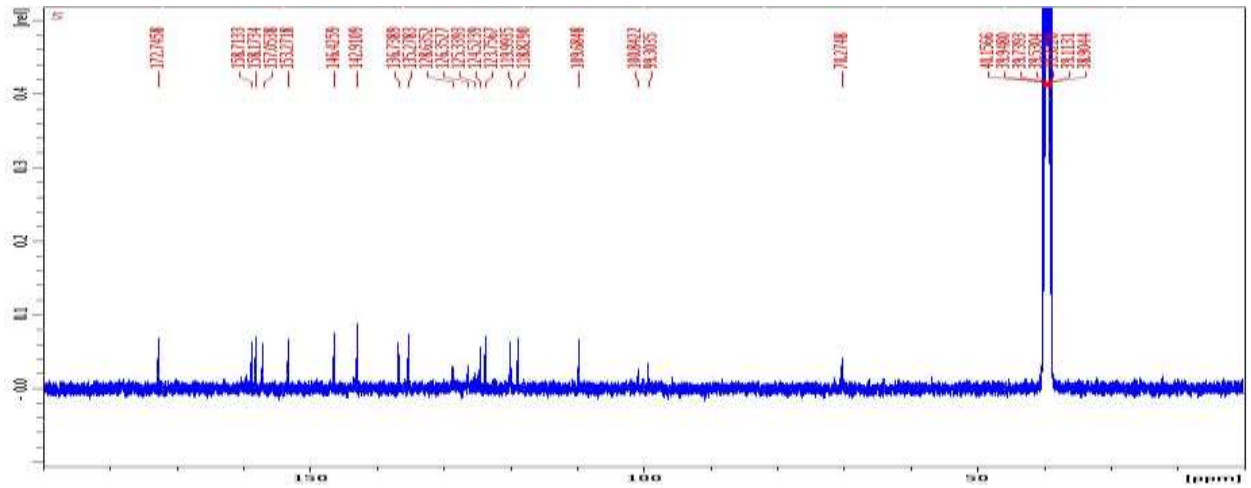
[ppm]

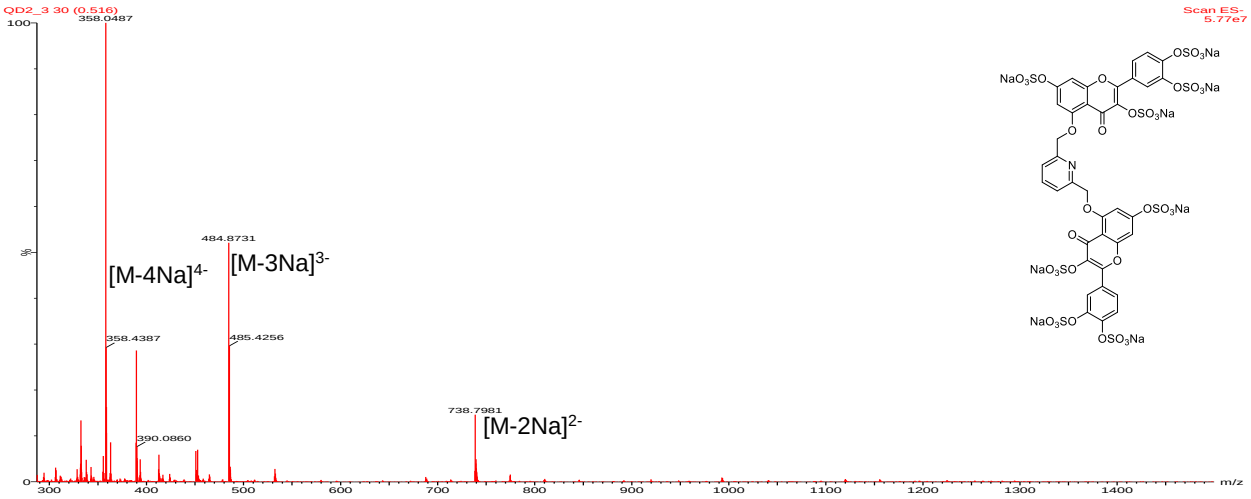
QD2_3 30 (0.516)
Scan ES-
5.77e7
358.0487
484.8731
[M-4Na]4-
[M-3Na]3-
358.4387
485.4256
738.7981
[M-2Na]2-
390.0860
m/z

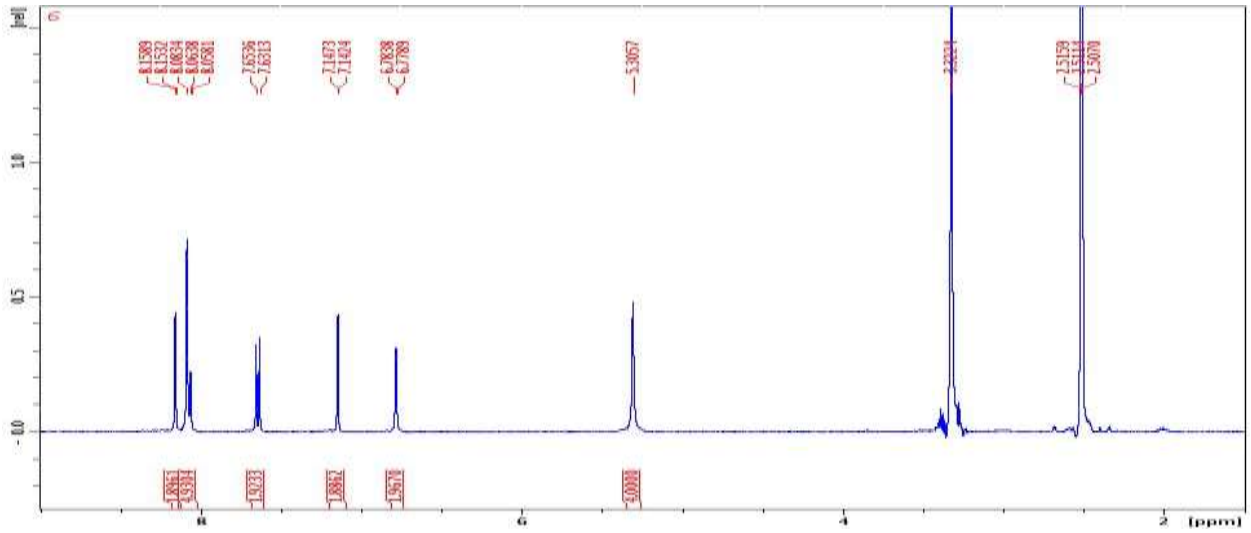
[ppm]

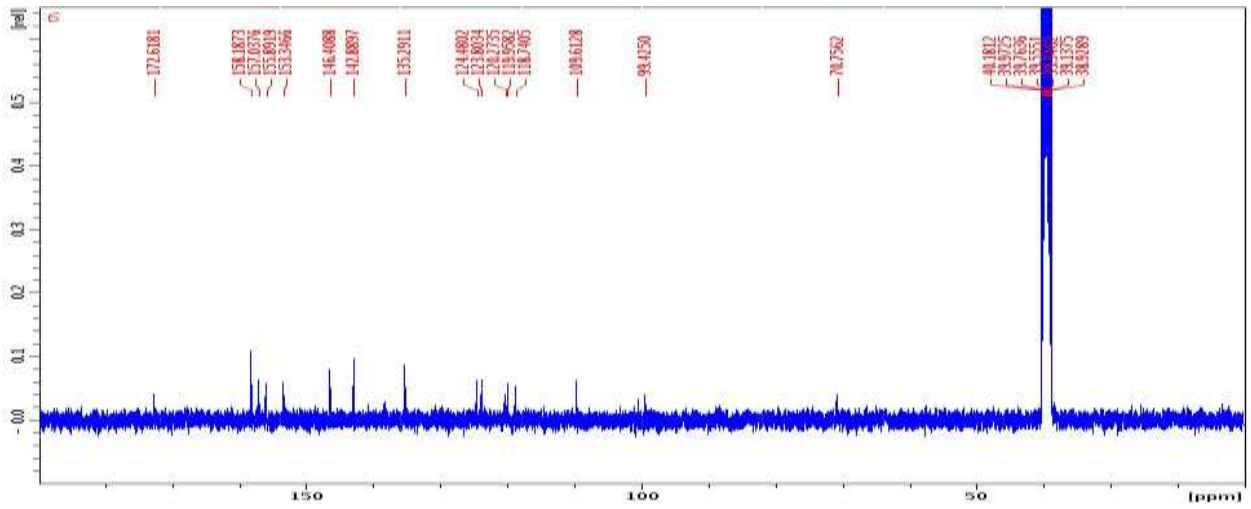
[ppm]

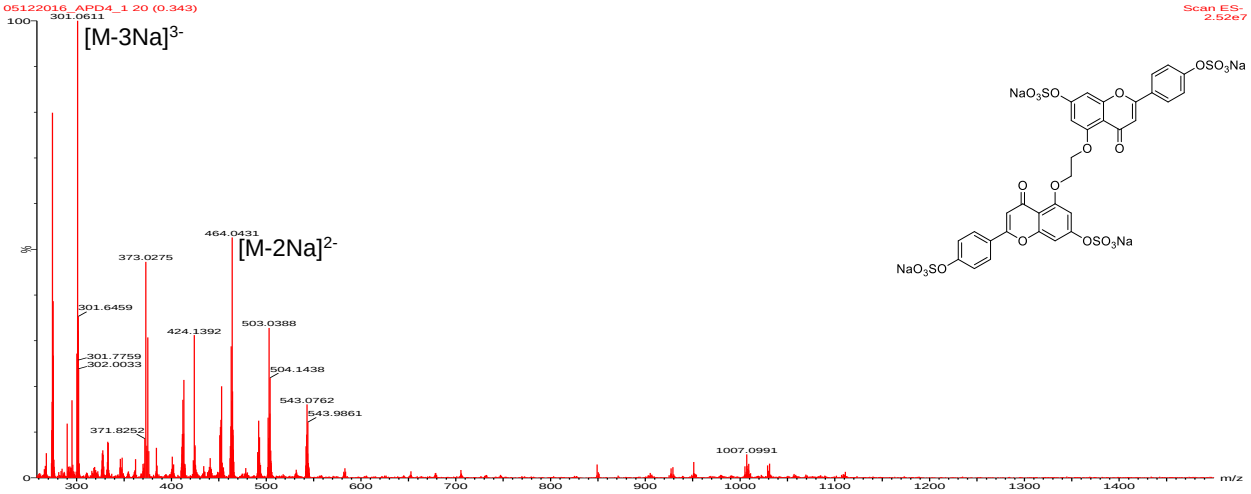
05122016_APD4_1 20 (0.343)
Scan ES-
2.52e7
[M-3Na]3-
[M-2Na]2-
301.0611
464.0431
373.0275
301.6459
424.1392
503.0388
301.7759
302.0033
504.1438
543.0762
543.9861
371.8252
1007.0991
%
m/z
NaO3SO
OSO3Na
OSO3Na
NaO3SO

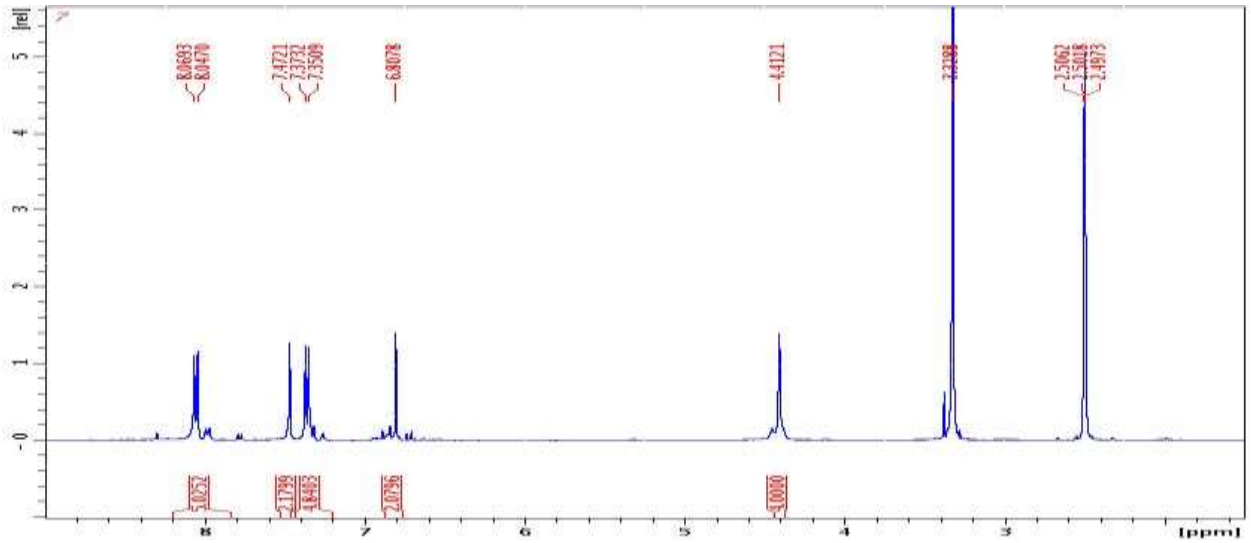
[rel]
8.0693
8.0470
7.4721
7.3732
7.3509
6.8078
4.4121
3.3398
2.5062
2.5018
2.4973
5.0252
2.1799
1.6482
2.0796
3.0000
[ppm]

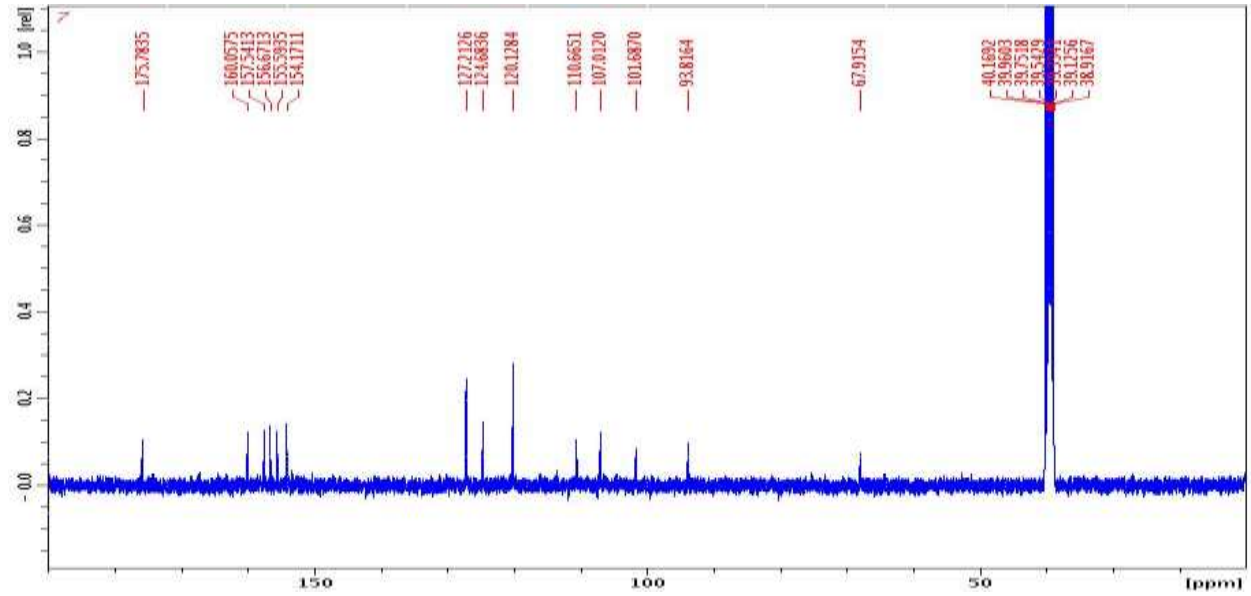
[rel]
175.7835
160.0575
157.5413
156.6713
155.5935
154.1711
127.2126
124.6836
120.1284
110.6651
107.0120
101.6870
93.8164
67.9154
40.1892
39.9683
39.7518
39.5429
38.1256
38.9167
[ppm]

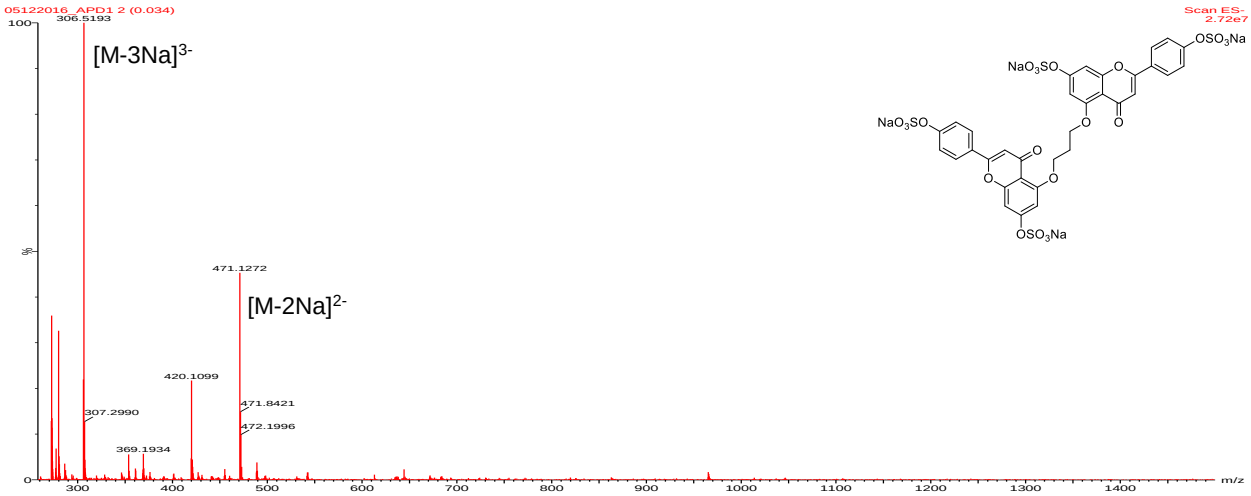
05122016_APD1 2 (0.034)
306.5193
[M-3Na]3-
471.1272
[M-2Na]2-
420.1099
307.2990
471.8421
472.1996
369.1934
m/z
Scan ES-
2.72e7
NaO3SO
OSO3Na
NaO3SO
OSO3Na

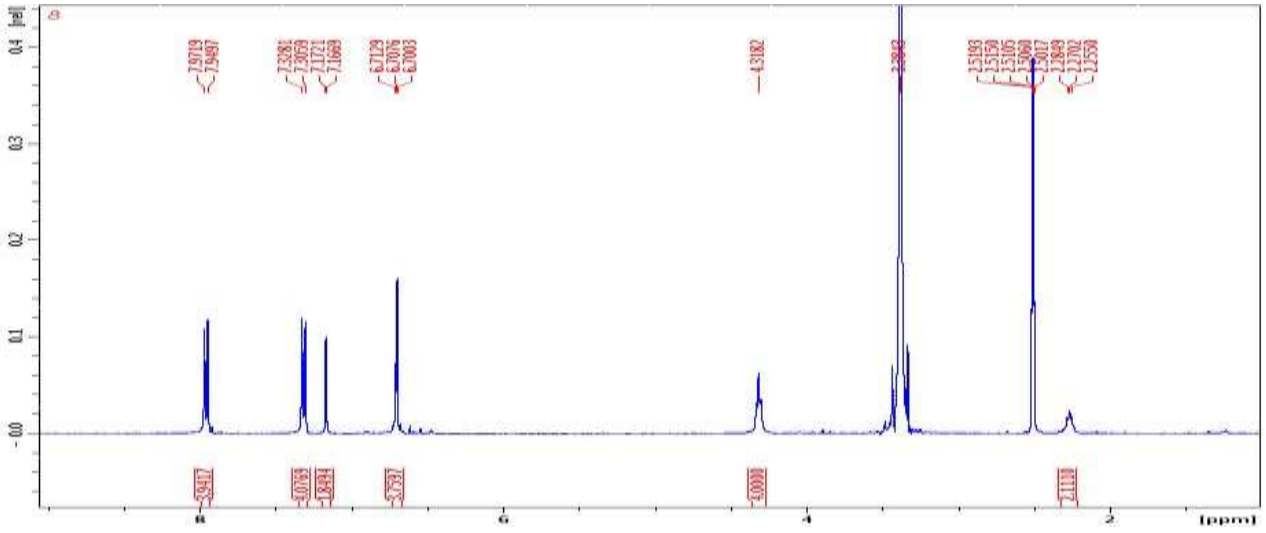
[ppm]

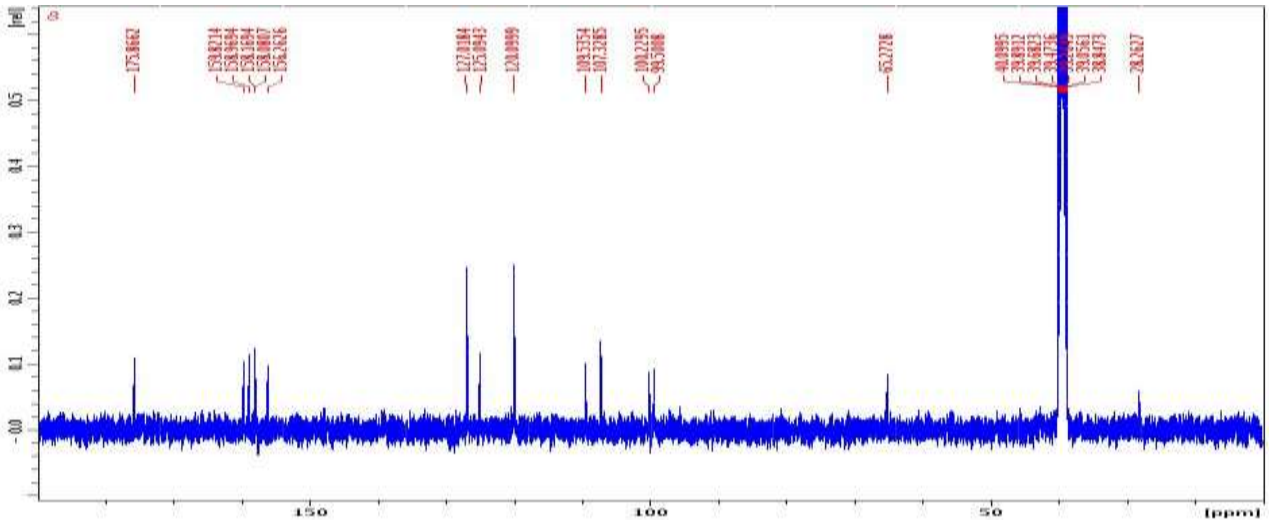
[ppm]


05132016_APD2_2 10 (0.172)
Scan ES-
6.37e7
227.7384
[M-4Na]4-
311.2627
[M-3Na]3-
478.2439
[M-2Na]2-
311.5876
311.7500
311.8800
312.0424
312.1724
427.2912
479.1862
m/z
NaO3SO
OSO3Na
OSO3Na
NaO3SO

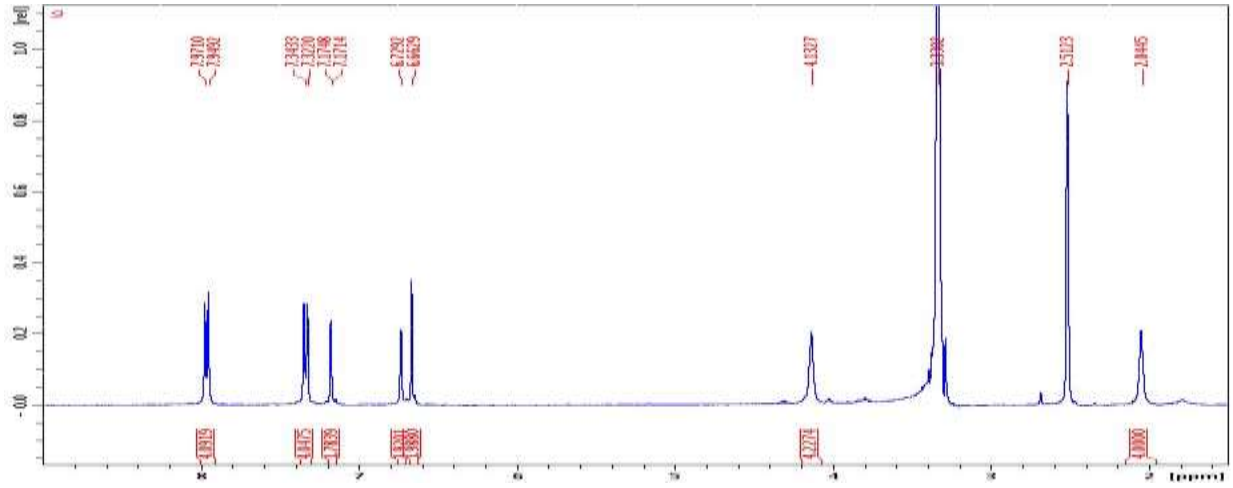
[ppm]

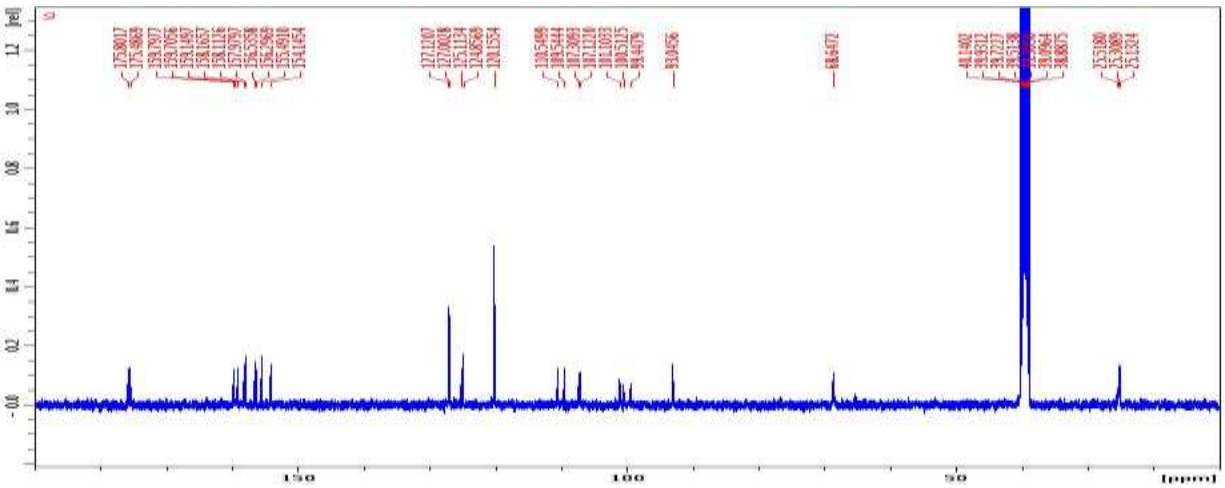
150
100
50
[ppm]


05122016_APD3_1 20 (0.343)
Scan ES-
4.46e7
100
%
0
310.5154
[M-3Na]3-
477.1390
[M-2Na]2-
310.9378
311.1002
426.1214
311.3926
477.9189
478.2763
321.1395
977.2901
300
400
500
600
700
800
900
1000
1100
1200
1300
1400
m/z
NaO3SO
OSO3Na
O
O
O
O
O
O
NaO3SO
OSO3Na

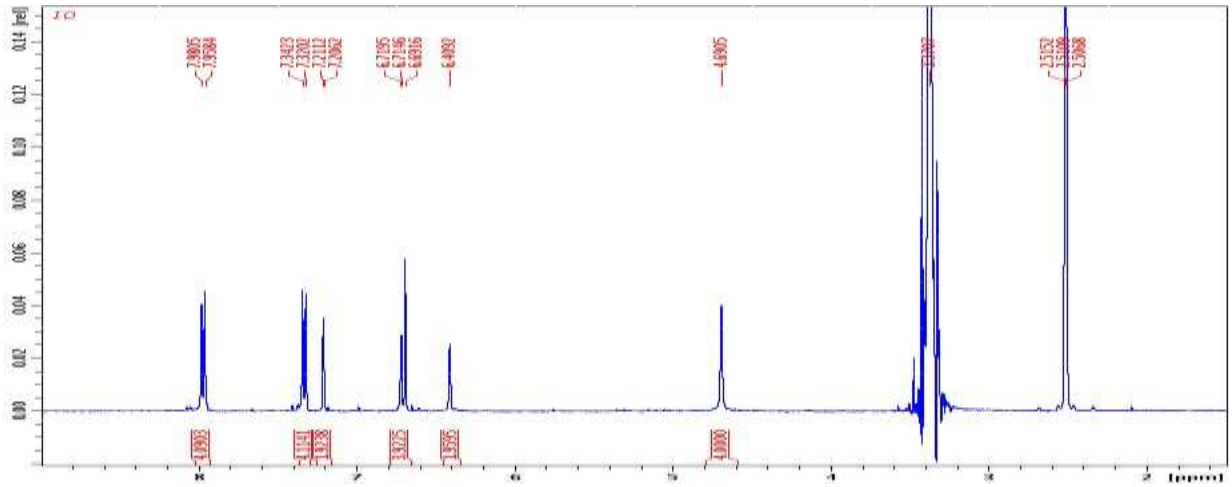

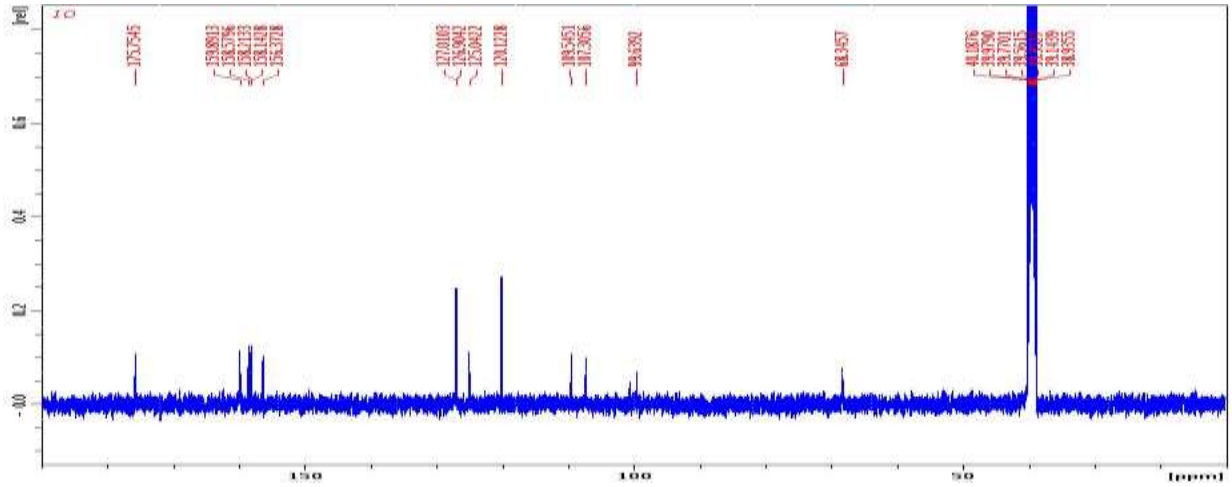

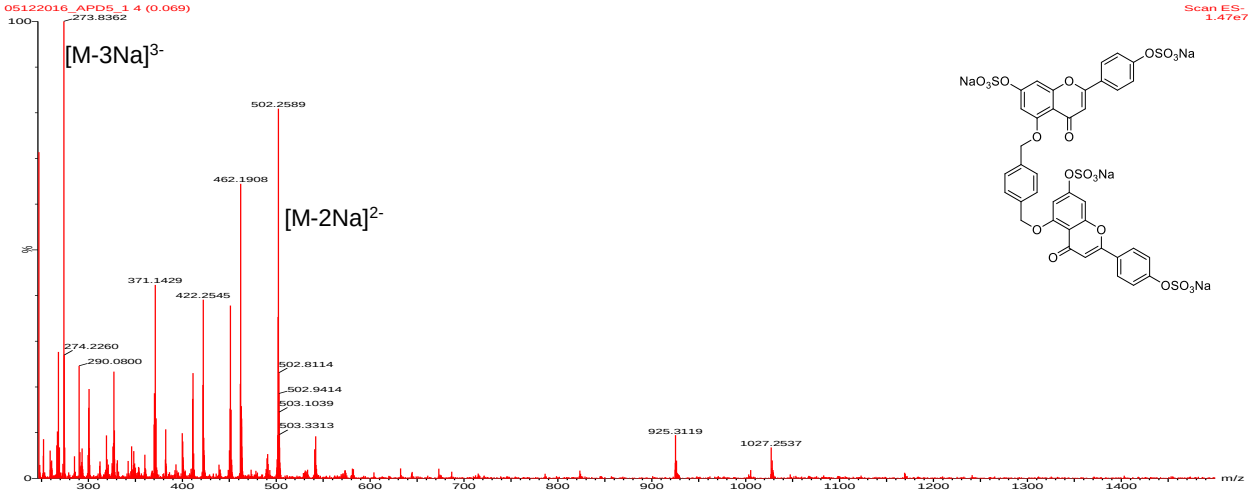
05122016_APD5_1 4 (0.069)
Scan ES-
1.47e7
[M-3Na]3-
[M-2Na]2-
273.8362
502.2589
462.1908
371.1429
422.2545
274.2260
290.0800
502.8114
502.9414
503.1039
503.3313
925.3119
1027.2537
NaO3SO
OSO3Na
OSO3Na
OSO3Na
m/z

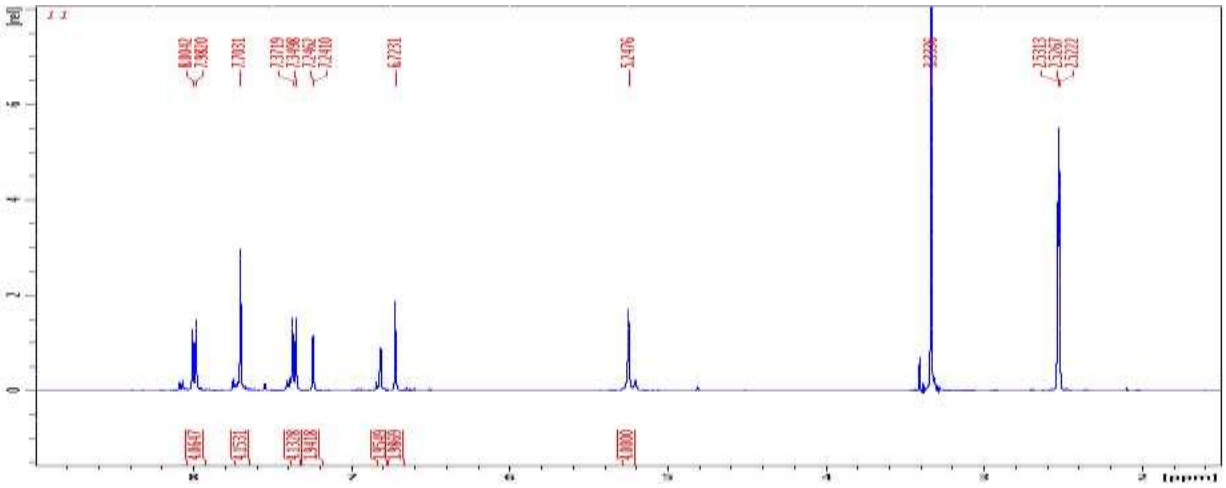
[ppm]

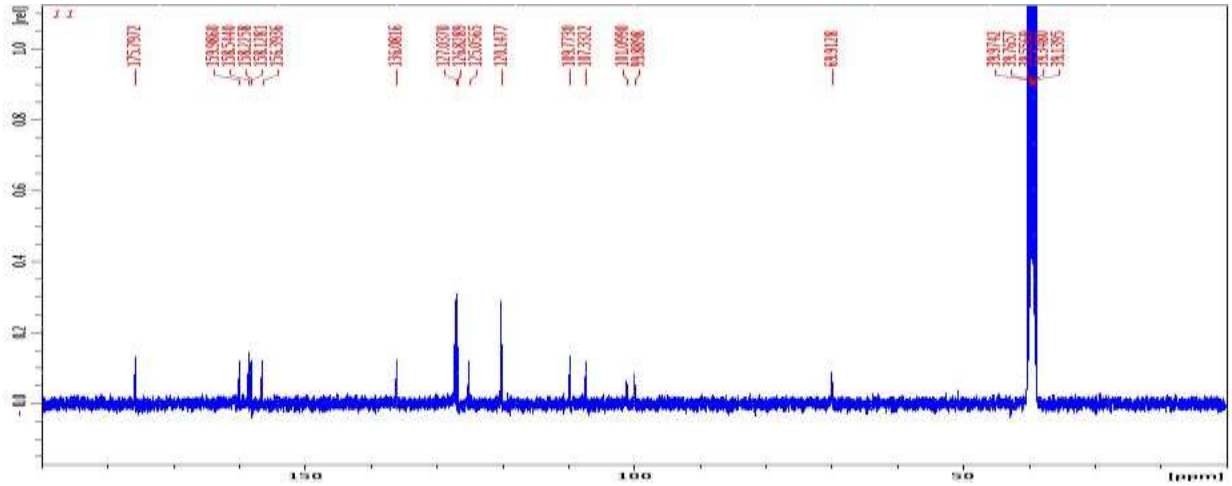
[ppm]

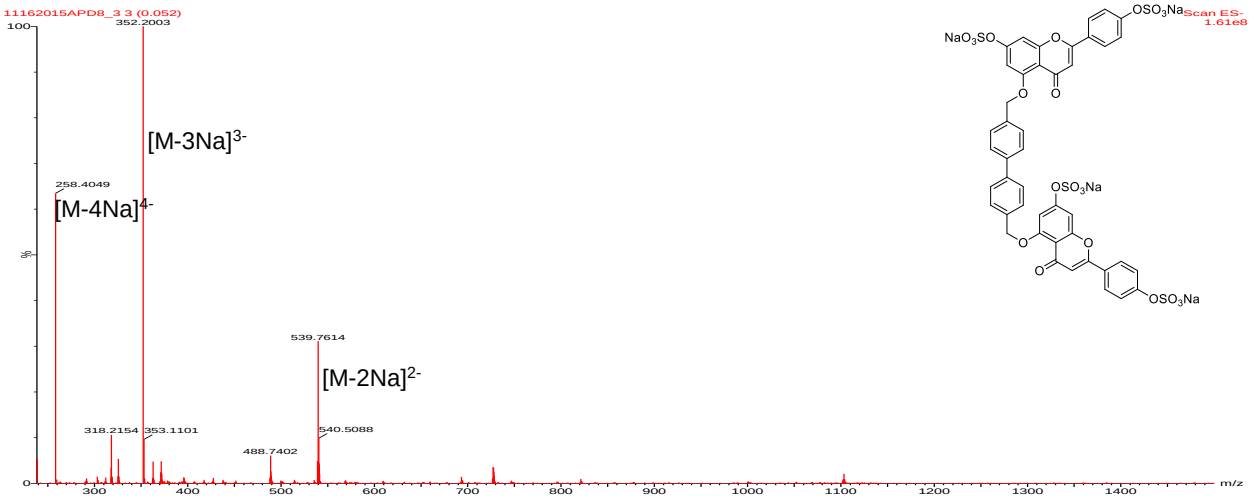
11162015APD8_3.3 (0.052)
352.2003
[M-3Na]3-
258.4049
[M-4Na]4-
539.7614
[M-2Na]2-
318.2154
353.1101
540.5088
488.7402
Scan ES-
1.61e8
NaO3SO
OSO3Na
OSO3Na
OSO3Na
m/z

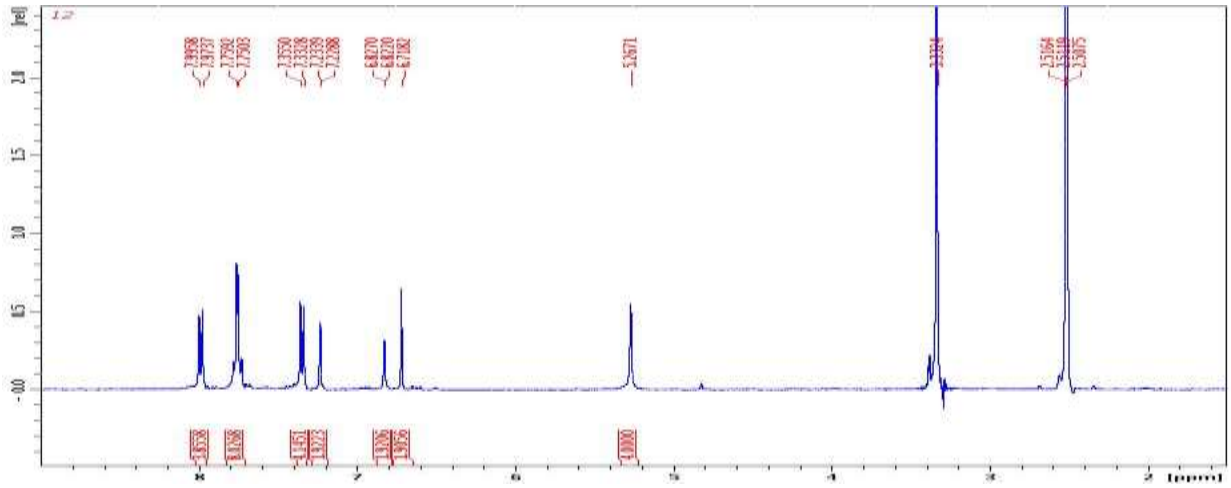

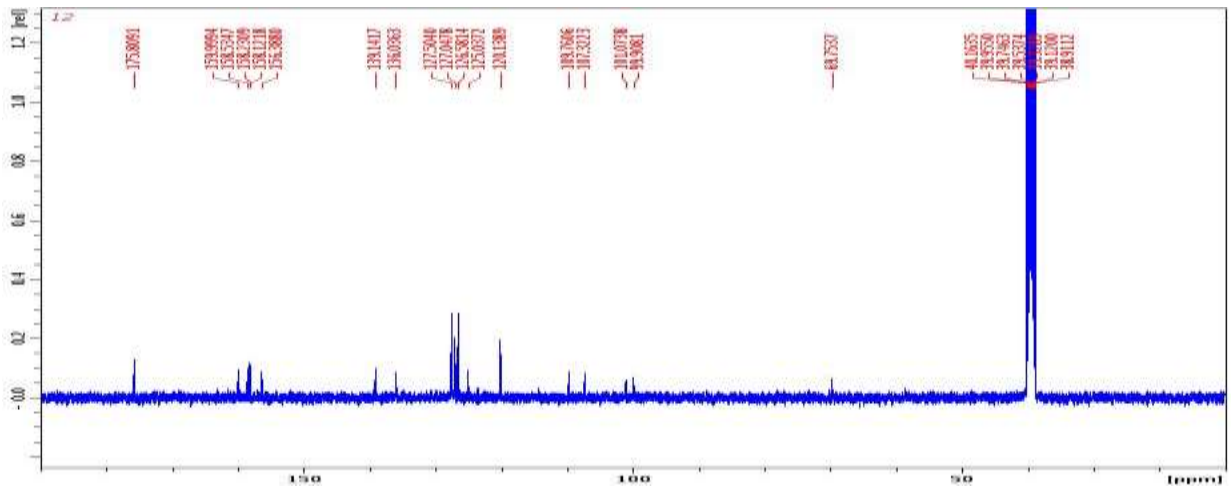


10202015APD7SO4 1 (0.017)
Scan ES-
8.06e7
336.1568
[M-3Na]3-
336.8315
337.2439
371.8444
464.7086
515.8131
516.3005
[M-2Na]2-
NaO3SO
OSO3Na
OSO3Na
OSO3Na
m/z

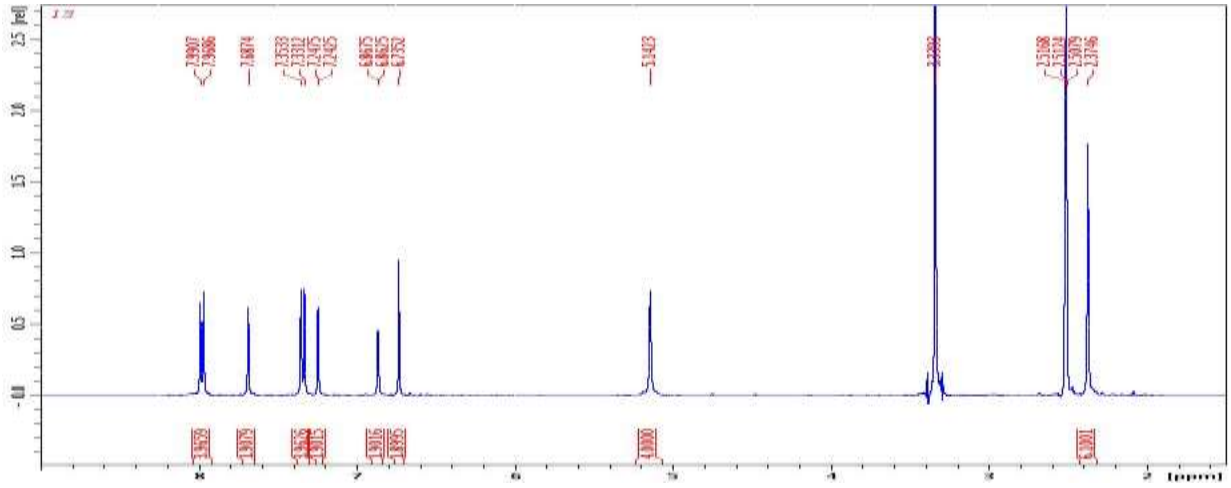
[ppm]

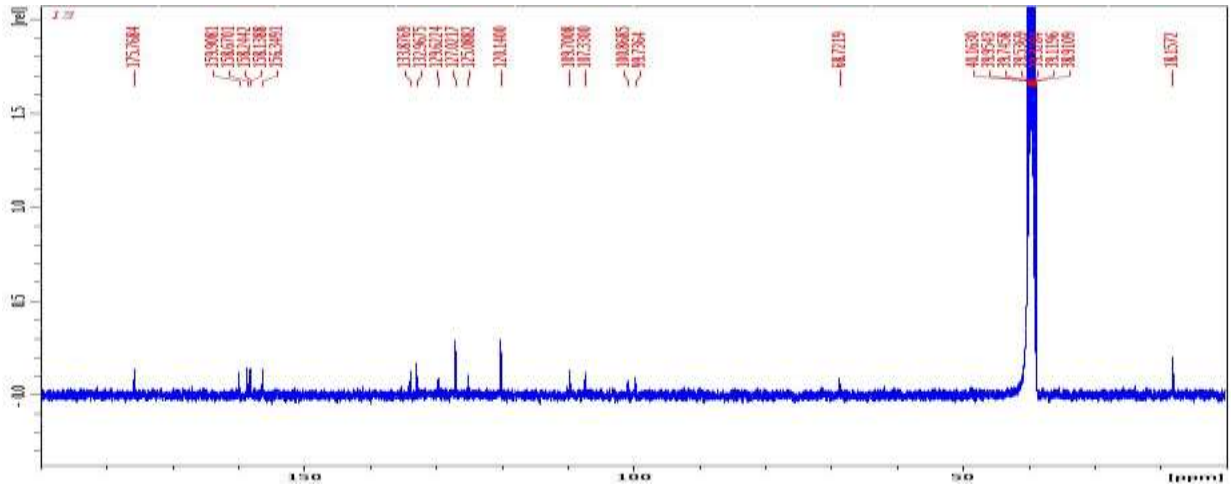
[ppm]

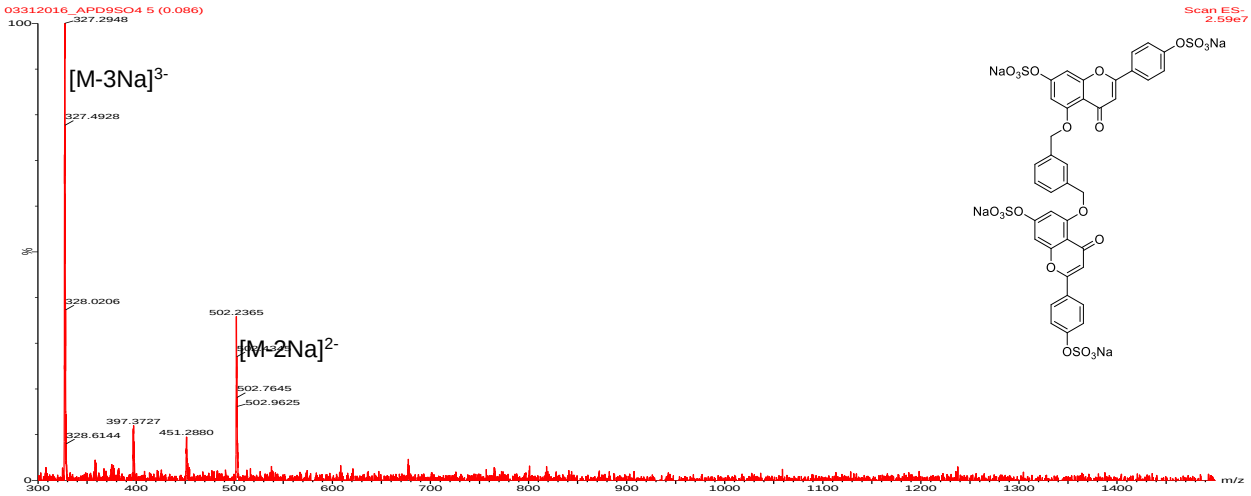
03312016_APD9SO4 5 (0.086)
Scan ES-
2.59e7
[M-3Na]3-
[M-2Na]2-
327.2948
327.4928
328.0206
502.2365
502.7645
502.9625
397.3727
451.2880
328.6144
NaO3SO
OSO3Na
m/z

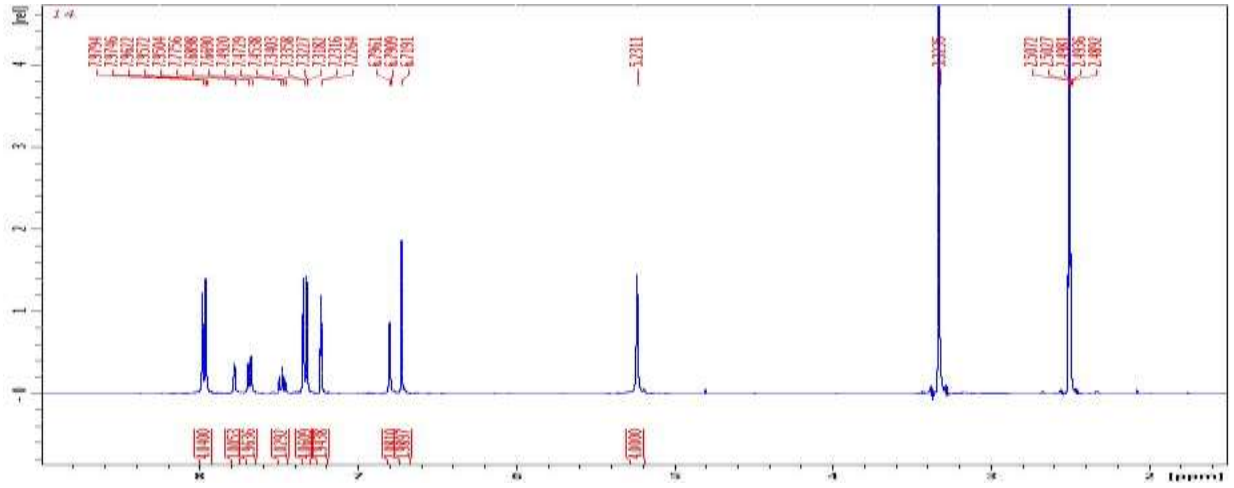

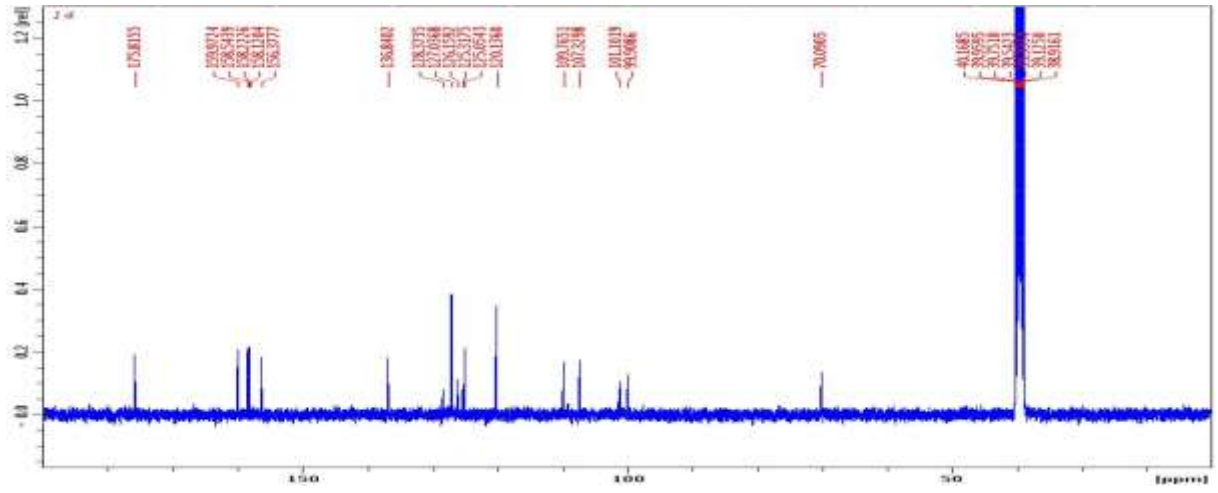


10082015APD6FINAL_1 3 (0.052)
Scan ES-
7.58e7
[M-3Na]3-
[M-2Na]2-
NaO3SO
OSO3Na
N
O
327.6100
502.3524
397.2993
328.0224
503.1023
501.8275
358.3488
451.2862
503.5147
607.6812
677.6190
1027.9930
1027.5428
1028.5557
1028.8932
m/z

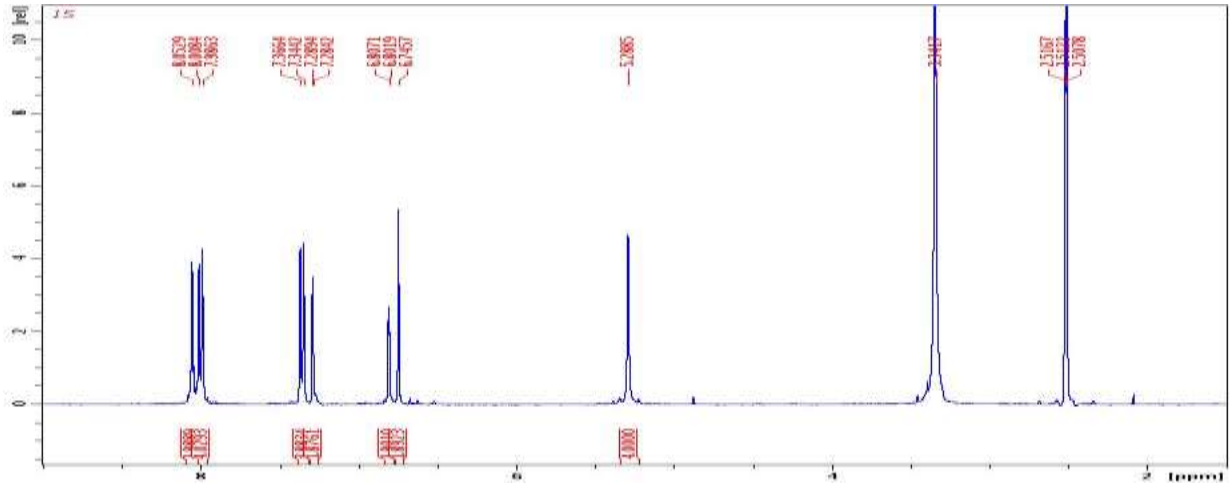
[ppm]

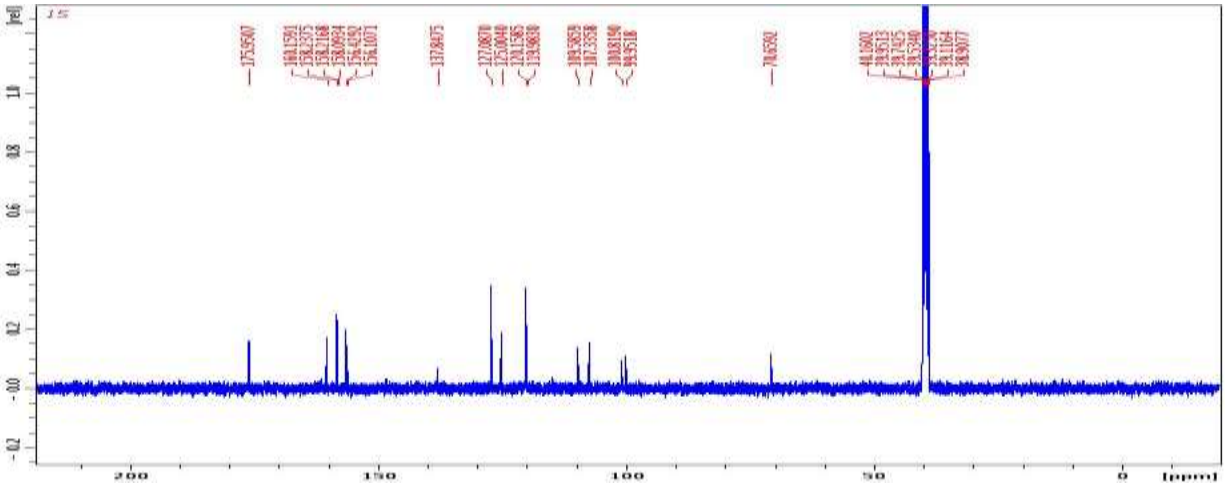
[ppm]

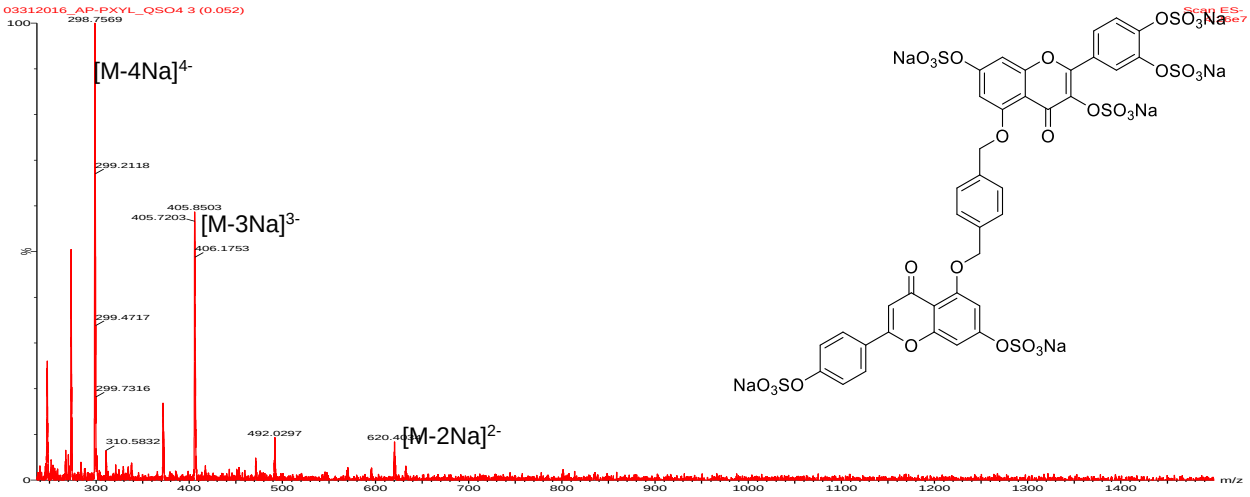
03312016_AP-PXYL_QSO4 3 (0.052)
298.7569
[M-4Na]4-
299.2118
405.8503
405.7203
[M-3Na]3-
406.1753
299.4717
299.7316
310.5832
492.0297
620.4084
[M-2Na]2-
m/z
NaO3SO
OSO3Na
OSO3Na
OSO3Na
OSO3Na
NaO3SO

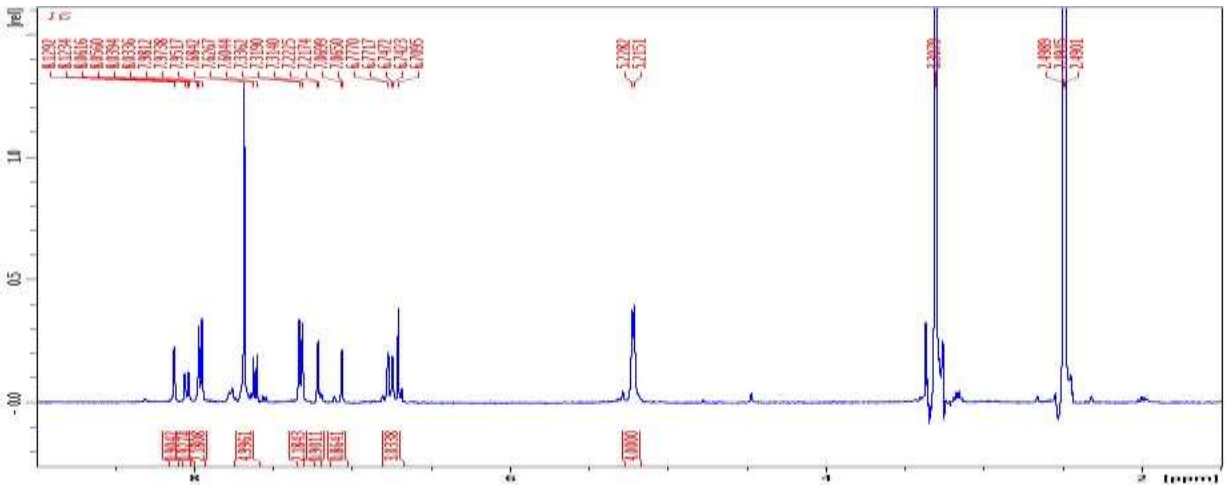

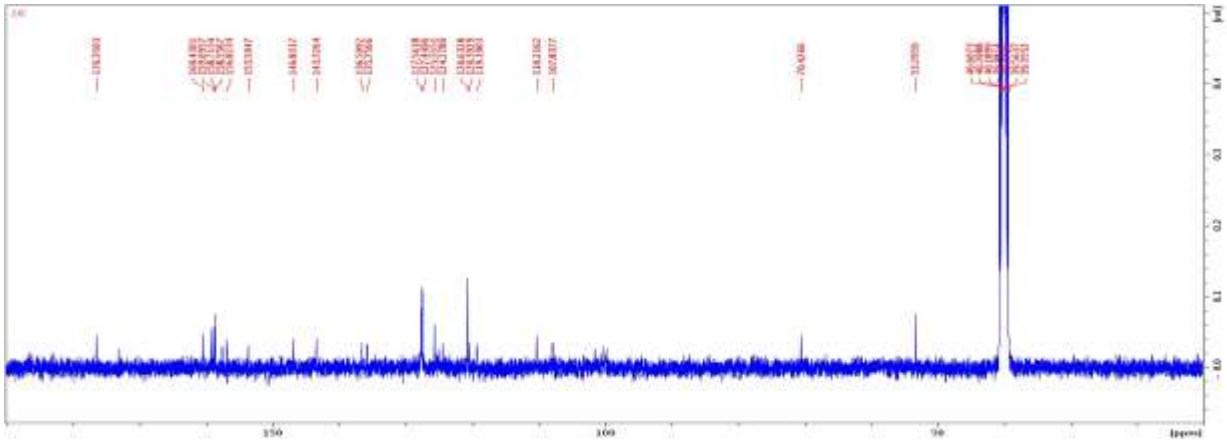

5) UPLC profiles of Sulfated diflavonoids

23a

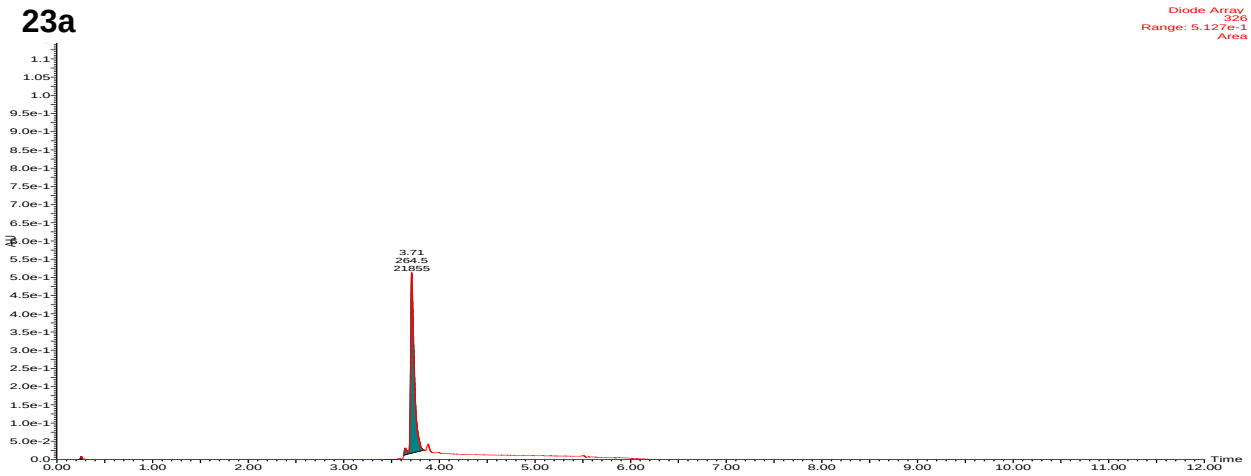

23b

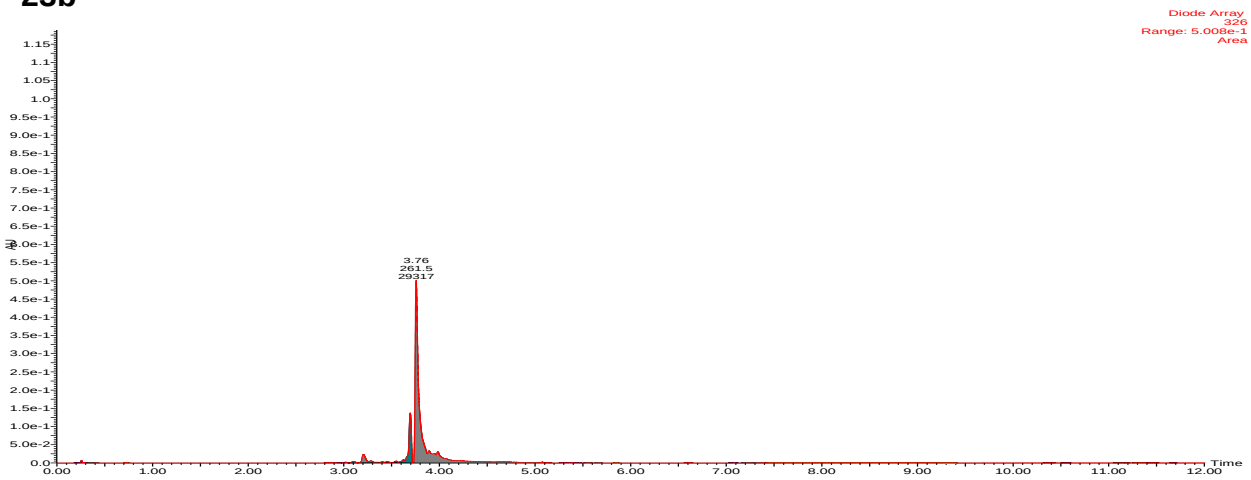

23c

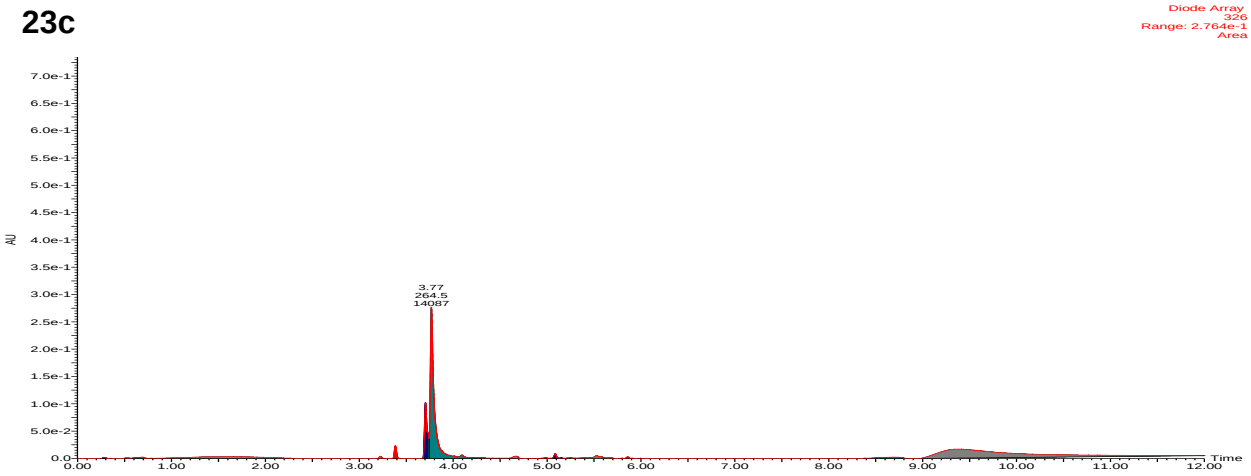

23d

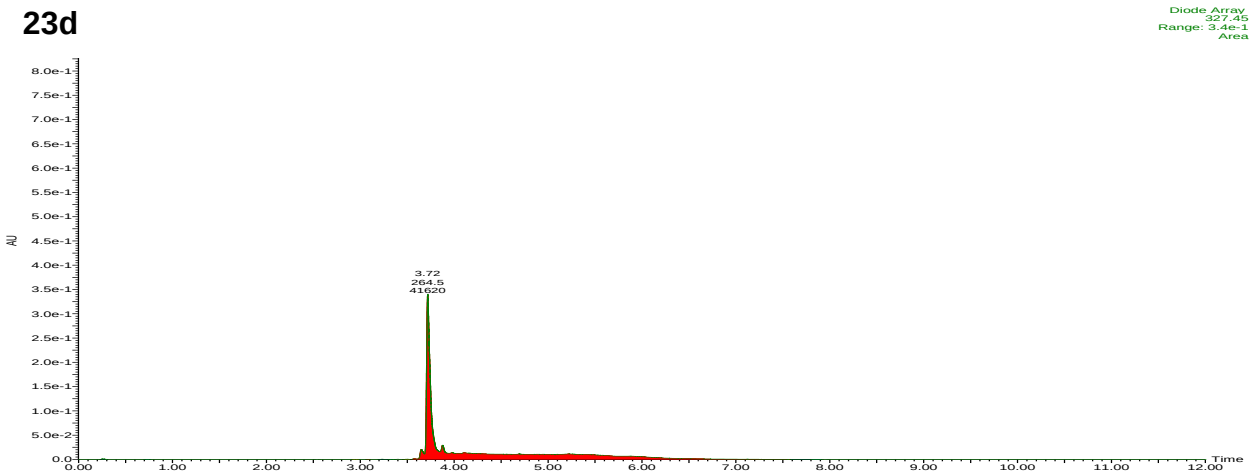
Diode Array
327.45
Range: 3.4e-1
Area
AU
3.72
264.5
41620
Time

23e

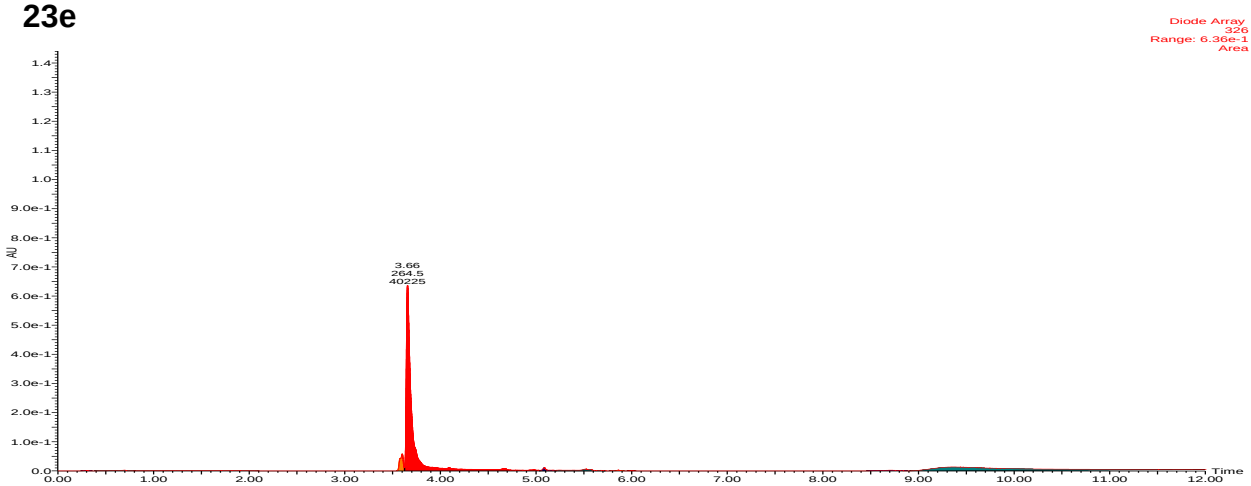
Diode Array
326
Range: 6.36e-1
Area
AU
3.66
264.5
40225
Time

23g

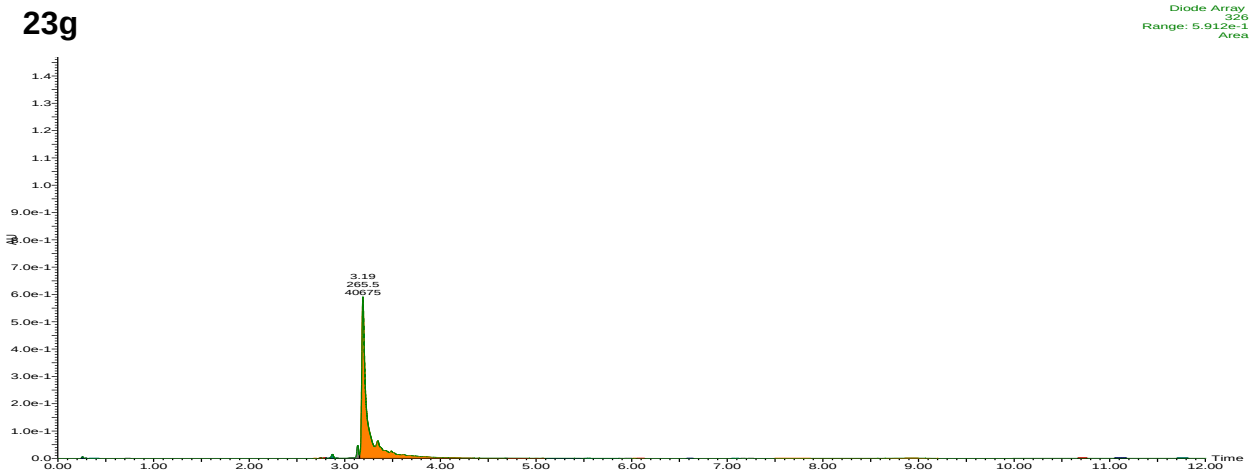
Diode Array
326
Range: 5.912e-1
Area
AU
3.19
265.5
40675
Time

23h

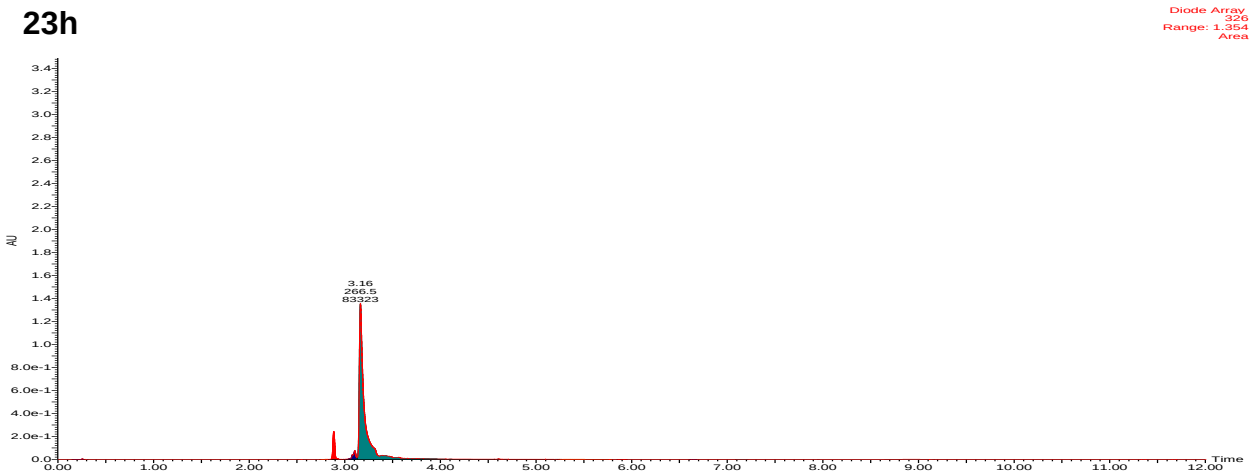
Diode Array
326
Range: 1.354
Area
AU
3.16
266.5
83323
Time

23i

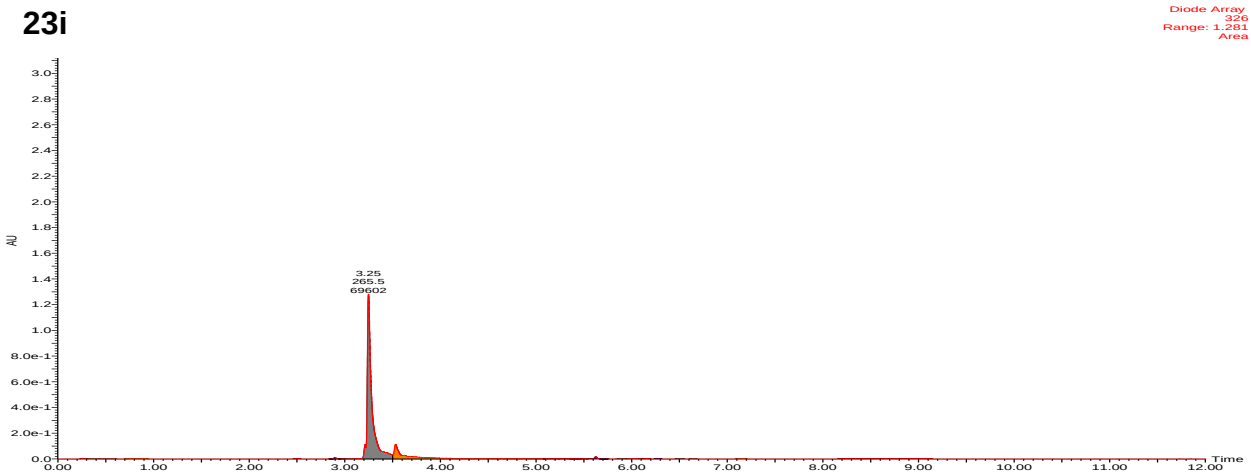
Diode Array
326
Range: 1.281
Area
AU
3.25
265.5
69602
Time

23j

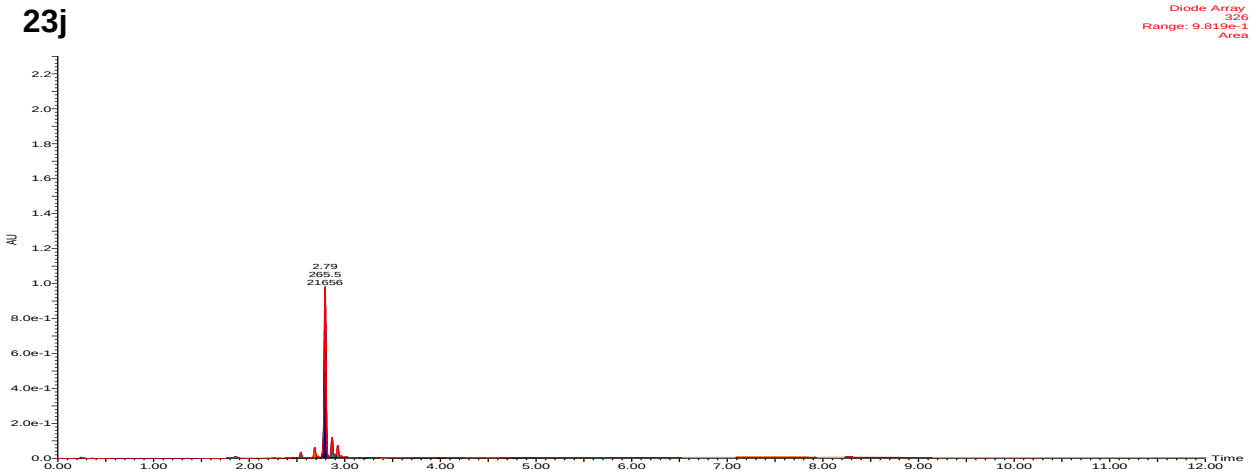
Diode Array
326
Range: 9.819e-1
Area
AU
2.79
265.5
21656
Time

23k

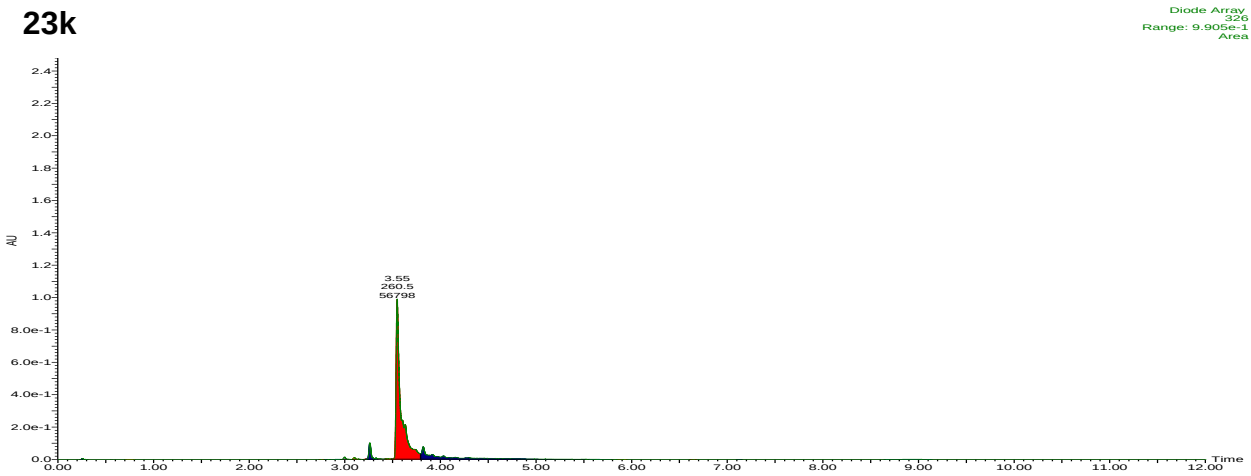
Diode Array
326
Range: 9.905e-1
Area
AU
Time
3.55
260.5
56798

23l

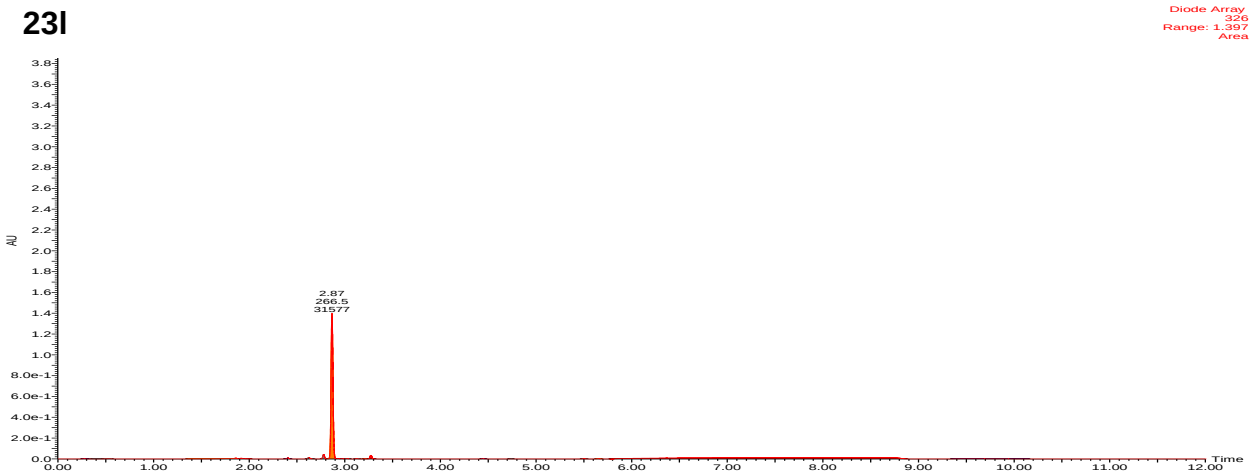
Diode Array
326
Range: 1.397
Area
AU
Time
2.87
266.5
31577

23m

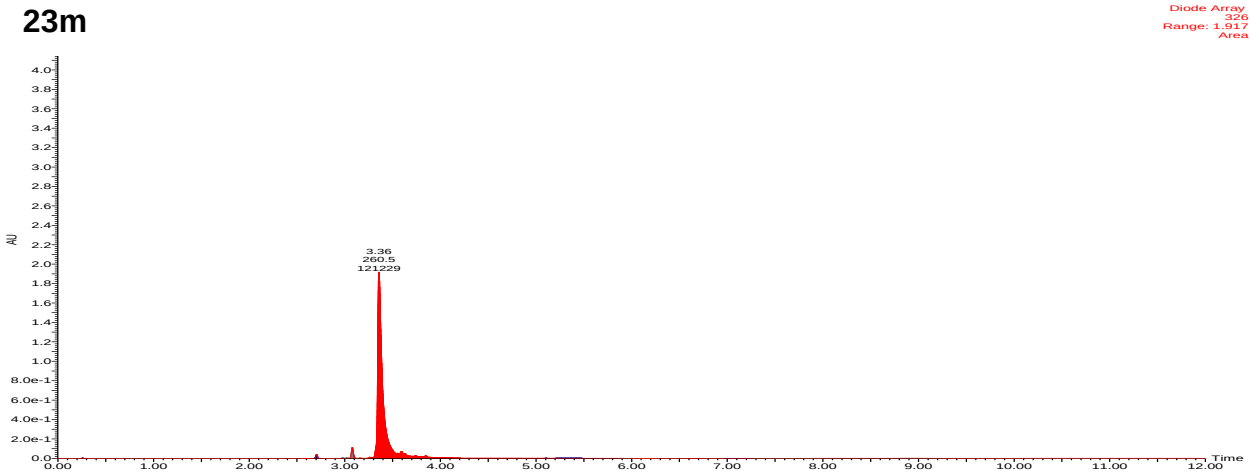
Diode Array
326
Range: 1.917
Area
AU
Time
3.36
260.5
121229

23n

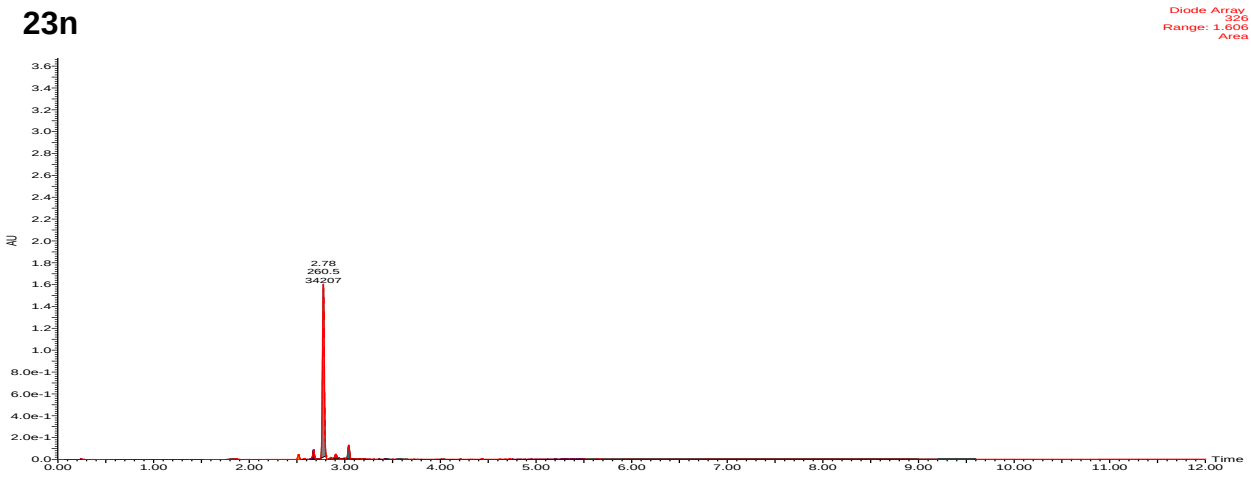

6) NMR of Enoxaparin and 2-O,3-O-desulfated Enoxaparin (ODSE)

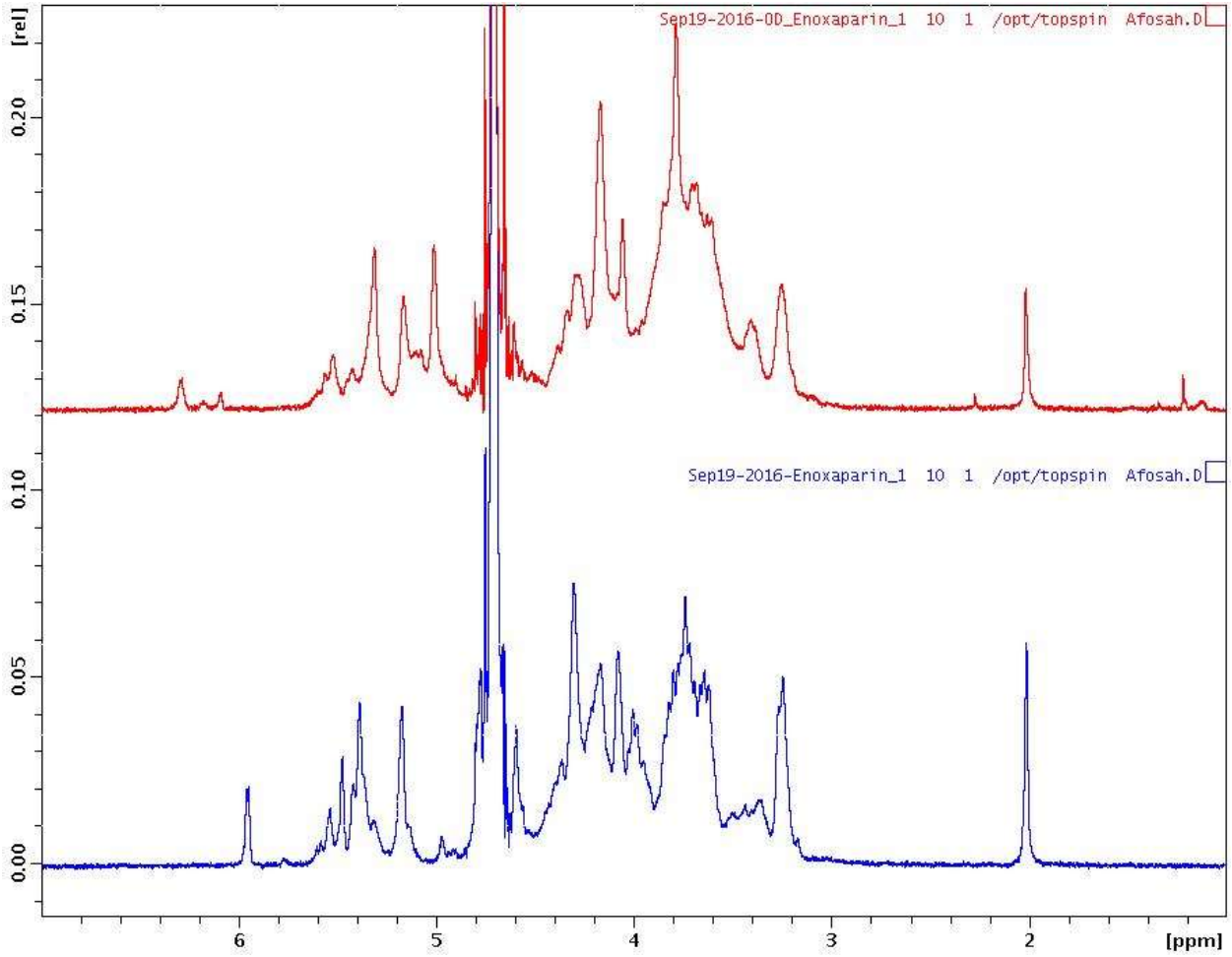

Vita

Daniel Afosah was born in Accra, Ghana on December 22, 1984 to Ms. Comfort Akoma Somuah, and the late Ebenezer Daniel Afosah. He graduated from the Presbyterian Boys' Senior High School, Accra, Ghana in 2002. He proceeded to receive his Bachelor of Pharmacy, and Master of Science in Pharmaceutical Analysis and Quality Control degrees from the Kwame Nkrumah University of Science and Technology, Kumasi, Ghana, in 2007 and 2010, respectively. He then worked as a quality control pharmacist at Ernest Chemists Limited, Ghana, and a regulatory officer at the Food and Drugs Authority, Ghana, before pursuing a PhD in Medicinal Chemistry at Virginia Commonwealth University in 2012.